SAN/1108-8/2

CENTRAL RECEIVER SOLAR THERMAL POWER SYSTEM

PHASE 1. CDRL ITEM 2

Pilot Plant Preliminary Design Report

Volume 3, Book 1. Collector Subsystem

By
Raymon W. Hallet, Jr.
Robert L. Gervais

Date Published—November 1977

Work Performed Under Contract No. EY-76-C-03-1108

McConnell Douglas Astronautics Company
Huntington Beach, California

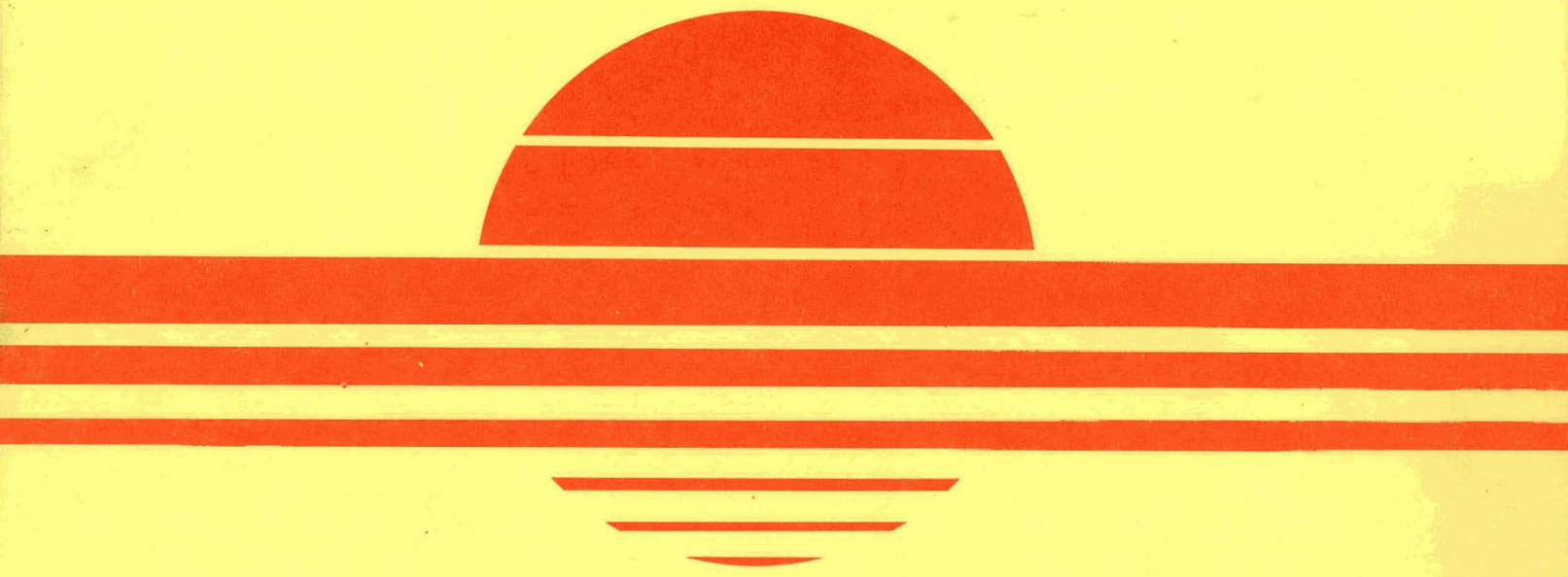

U.S. Department of Energy

Solar Energy

DISCLAIMER

NOTICE

MDC-G-6776(Vol.3)(Bk.1)

SAN/1108-8/2
Distribution Category UC-62

CENTRAL RECEIVER SOLAR THERMAL POWER SYSTEM PHASE 1

CDRL ITEM 2
Pilot Plant
Preliminary Design Report

VOLUME III, BOOK 1
Collector Subsystem

Raymon W. Hallet, Jr. and Robert L. Gervais

Date Published – October 1977

Prepared for the U.S. Department of Energy
Under Contract No. EY-76-C-03-1108

MCDONNELL DOUGLAS ASTRONAUTICS COMPANY
5301 Bolsa Avenue
Huntington Beach, California 92647

PREFACE

This report is submitted by the McDonnell Douglas Astronautics Company to the Department of Energy under Contract EY-76-C-03-1108 as the final documentation of CDRL Item 2. This Preliminary Design Report summarizes the analyses, design, test, production, planning, and cost efforts performed between 1 July 1975 and 1 May 1977. The report is submitted in seven volumes, as follows:

Volume I, Executive Overview

Volume II, System Description and System Analysis

Volume III, Book 1, Collector Subsystem

Book 2, Collector Subsystem

Volume IV, Receiver Subsystem

Volume V, Thermal Storage Subsystem

Volume VI, Electrical Power Generation/Master Control Subsystems and Balance of Plant

Volume VII, Book 1, Pilot Plant Cost and Commercial Plant Cost and Performance

Book 2, Pilot Plant Cost and Commercial Plant Cost and Performance

Specific efforts performed by the members of the MDAC team were as follows:

- McDonnell Douglas Astronautics Company
  Commercial System Summary
  System Integration
  Collector Subsystem Analysis and Design
  Thermal Storage Subsystem Integration

- Rocketdyne Division of Rockwell International
  Receiver Assembly Analysis and Design
  Thermal Storage Unit Analysis and Design

- Stearns-Roger, Inc.
  Tower and Riser/Downcomer Analysis and Design
  Electrical Power Generation Subsystem Analysis and Design

- University of Houston
  Collector Field Optimization

- Sheldahl, Inc.
  Heliostat Reflective Surface Development

- West Associates
  Utility Consultation on Pilot Plant and Commercial System Concepts

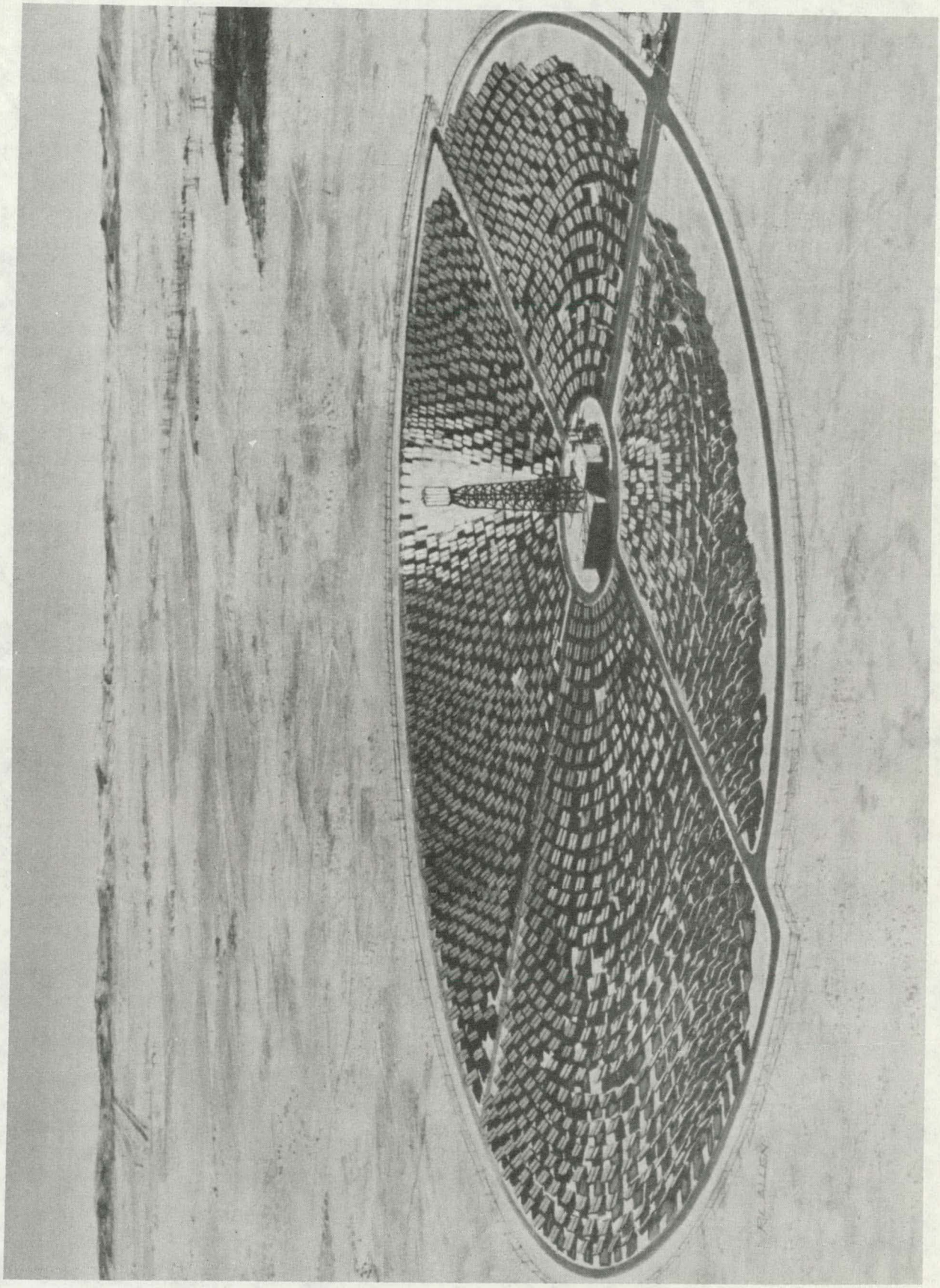

CONTENTS

Section 1
INTRODUCTION AND SUMMARY

The central receiver system consists of a field of heliostats, a central receiver, a thermal storage unit, an electrical power generation system, and balance of plant. This volume discusses the collector field geometry, requirements and configuration. The development of the collector system and subsystems are discussed and the selection rationale outlined. System safety and availability are covered. Finally, the plans for collector portion of the central receiver system are reviewed.

1.1 COLLECTOR FIELD GEOMETRY

The collector field geometries for the Commercial and Pilot Plants are developed in Volume 2. The geometries are based on optimization techniques developed by the University of Houston. The collector field geometries are reviewed in this section.

1.1.1 Collector Field Geometry, Commercial Plant

The collector field geometry for the Commercial Plant is shown in Figure 1-1. 22,914 heliostats are arranged in a radially staggered array in a field 2,415m x 1,931m (7,920 ft x 6,335 ft). The tower and balance of plant are located in the southern portion of the field. The top of the tower is at an elevation of 242m (794 ft) and the receiver centerline is at an elevation of 268m (879 ft).

1.1.2 Collector Field Geometry, Pilot Plant

The collector field geometry for the Pilot Plant system reflects the geometric relationships anticipated for a Commercial system. The most critical of these parameters include the heliostat locations relative to the tower, heliostat-receiver "look" angles, and interheliostat spacing. Optimization studies carried out with respect to the Commercial system indicated the

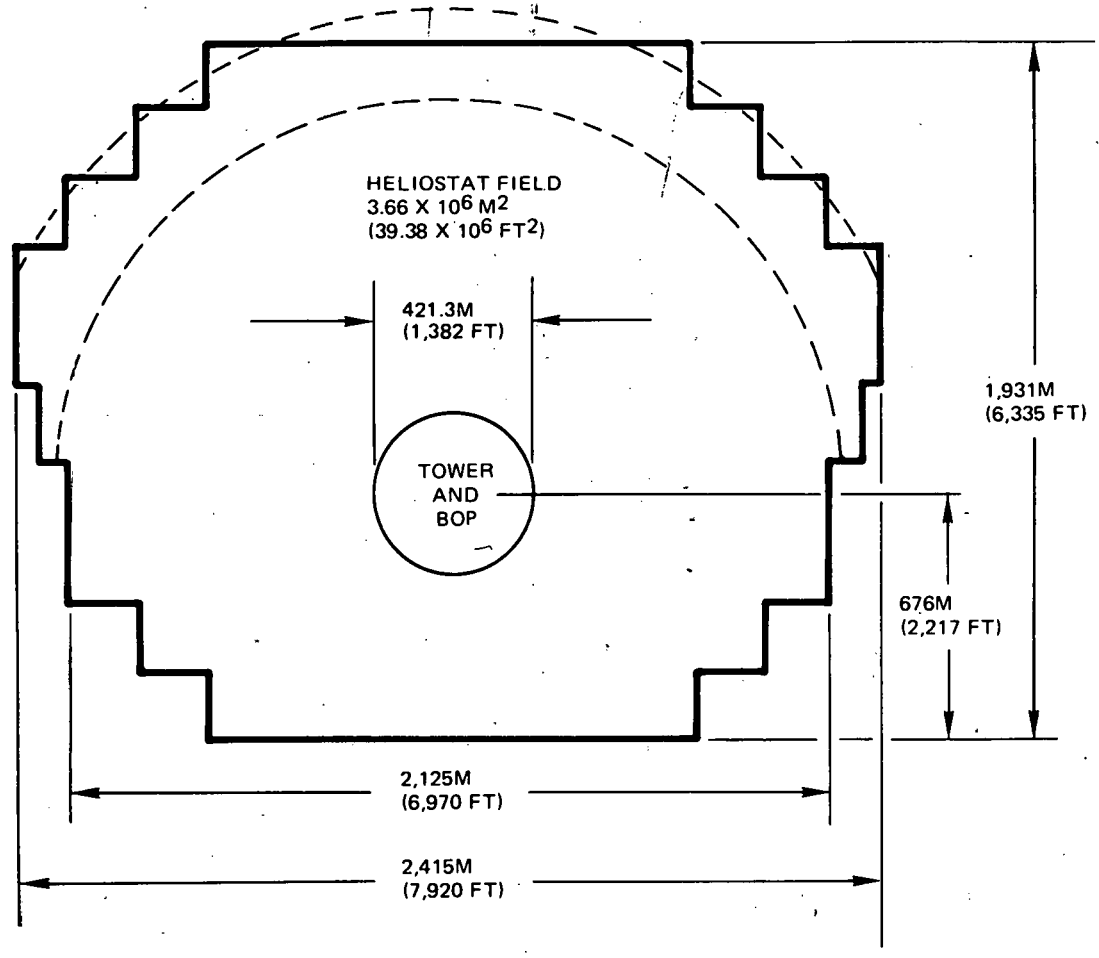

- RADIAL STAGGER ARRAY
- OPTIMUM ANNUAL ENERGY TRIM (BASED ON EARLY COMMERCIAL SYSTEM)
- RECEIVER CENTERLINE ELEVATION 268M (879 FT)
- TOWER TOP ELEVATION 242M (794 FT)
- GLASS AREA 869,586 M^2 (9.36 X 10^6 FT^2)
- NUMBER OF HELIOSTATS 22,914

Figure 1-1. Commercial System Field Layout

desirability of a full 360-deg collector field based on total system economic considerations. In addition, the studies indicated the superiority of a heliostat arrangement laid out along radii emanating from the tower. Finally, an optimization analysis established criteria for the packing of heliostats into the collector field and the trimming away of those portions of the field which failed to satisfy minimum cost/performance criteria.

The collector field physical characteristics are shown in Table 1-1. The collector field arrangement is indicated in Figure 1-2. The heliostats are arranged in a radial stagger array along 32 circular arcs with the inner 19 forming closed circles. The 32 arcs are grouped into six bands with each using its own uniquely defined set of radii as the basis for the staggered arrangement. This periodic redefinition of the radii is necessary to prevent the gross divergence of interheliostat spacing as one moves away from the tower. The transition between bands occurs along slip lines which are easily identified by the arcs along which heliostats have been periodically deleted. In addition, main access corridors have been included to provide regional access to the collector field as well as access to the central exclusion area which contains the tower along with the thermal storage, turbine, feedwater equipment, offices, warehouse, and maintenance facilities. The cooling towers and switch gear are located beyond the southern extreme of the collector field.

The collector field contains 1,760 heliostats with 74 field controllers providing regional heliostat control. The heliostat distance from the base of the tower varies from 62m (203 ft) for the inner circle to 368.3m (1,208 ft) for the northernmost arc.

1.2 COLLECTOR REQUIREMENTS

The collector requirements include:

- Operating requirements.
- Design requirements.
- Environmental requirements.
  - Operating
  - Survival
- Safety requirement.

Table 1-1

COLLECTOR FIELD PHYSICAL CHARACTERISTICS, PILOT PLANT

Field Arrangement	Radial Stagger/Circular Arcs
Number of Heliostats	1,760
Collector Field Area	$3.04 \times 10^5 m^2$ (75 Acres)
Glass Packing Density	
Maximum	45%
Minimum	13%
Average	23%
Central Exclusion Area	$10,387 m^2$ (2.6 Acres)
Tower Height	65m
Receiver Centerline Elevation	80m

The operating requirements are a function of (1) interfaces between the collector and the balance of the central receiver system and (2) the operating modes.

The collector reflects the sun's energy to the receiver. The receiver heats the transfer fluid and provides energy to operate the electrical power generation system and the storage units. The collector interfaces with the receiver, master control and power distribution system. The collector interfaces with the receiver through the reflected beams from the heliostats. The heliostats track the sun and direct the reflected beams so that the light falls on the receiver with a prescribed flux distribution. Spillage of light missing the receiver is minimized, consistent with overall system economics. The collector interfaces through the field controller with the master control. Ephemeris data and collector operating mode commands are sent from master control to the field controller. Collector status and malfunctions are transmitted from the field controller to the master control. The collector receives power from the distribution system to operate the electric motors and control system.

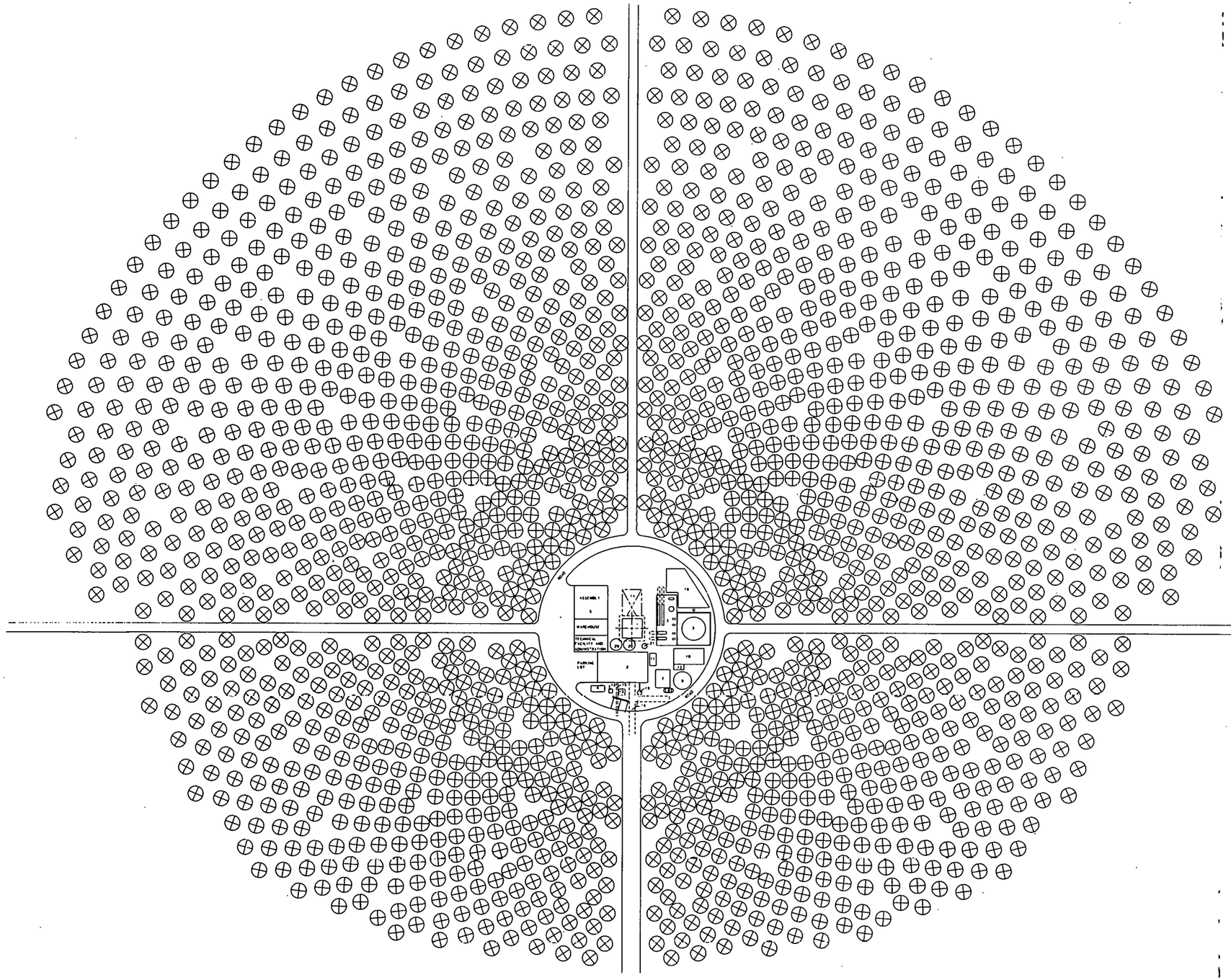

GENERAL NOTES

A POWER HOUSE AND AUXILARIES

1 RECEIVER TOWER AND FOUNDATION
2 POWER HOUSE
3 THERMAL STORAGE SUBSYSTEM
4 CONDENSATE STORAGE TANKS
5 ASSEMBLY, AS NOTED
6 DIESEL GENERATOR
7 WATER TREATING BLDG
8 ACID STORAGE TANK
9 LIME SOFTENER
10 CLEARWELL, COVERED
11 SEWAGE UNIT
12 AUX TRANSFORMER
13 MAIN TRANSFORMER
14 RECEIVER PANELS LAYDOWN AREA
15 POWER AND CONTROL CABLE TRENCH
16 BURIED PIPE LANE
17 TREATED WATER AND FIRE PUMPS
18 ROCK-FILLED CATCH BASIN
19 LUBE OIL STORAGE TANK
20 CONDENSATE STORAGE TANKS
21 FUEL OIL TANK

B SOUTH ACCESS ROAD IS 11M (36 FT) WIDE

C EAST, WEST, AND NORTH ACCESS ROADS ARE 9.5M (18FT) WIDE EACH

D ⊗ - HELIOSTAT EXCLUSION CIRCLE

Figure 1-2. MDAC 10 MW Central Receiver Collector Field Layout

The operating mode requirements are shown in Table 1-2. In the closed-loop system, the heliostats track the sun in the "normal tracking mode" by means of an optical sensor. The remaining modes of the closed-loop system and all the modes of an open-loop system use an output encoder/input shaft counter.

The collector design requirements are:

- Commercial and Pilot Plants' collectors are the same.
- Collector uses qualified components.
- Collector is compatible with the receiver.
- Heliostat is capable of inverted stowage.
- Collectors have low cost commensurate with safety, availability, reliability, and ease of maintenance.
- Heliostats have a rigid drive and structural system to prevent excessive movement under gust conditions.
- Reflectors are dimensionally stable with high optical efficiency.

Table 1-2

OPERATING MODE REQUIREMENTS

Mode	Field Controller	Master Control
Normal Tracking	Autonomous	Monitor, only
Synthetic Tracking	Track to master control requirements	Compute ephemeris or other tracking data
Command Position	Same	Direct position, eg maintenance, cleaning
Local Manual Control	Mobile test set controls	Locked out
Stowage	Stow to master control requirements	Select mode and command

The design operating environment is as follows:

A. Design wind speeds (with gusts) are:
   1. System performance at 3.5m/s (7.8 mph) at 10m elevation.
   2. Design deflection at 11.6 m/s (26 mph).
   3. Stowage initiation speed at 16.1 m/s (36 mph)

B. Temperature range = 0^{o} - 49^{o}C (32^{o} - 120^{o}F).

C. Track the sun at low insulation levels (0.3 kW/m^2).

D. 30-yr life.

The survival environment is as follows:

A. Maximum wind speed.
   1. Stowed, elevation axis aligned with wind: 40.2 m/s (90 mph).
   2. Any orientation: 22.4 m/s (50 mph).

B. Ambient air temperature: 30^{o} to 60^{o}C (-22^{o} to $+140^{o}$F).

C. Earthquake: 0.25g peak ground acceleration.

D. Precipitation.
   1. 250 Pa (5 psf) snow.
   2. 50 mm (2 in.) ice.
   3. 100 mm (4 in.) annual average rainfall.
      75 mm (3 in.) maximum 24-hr rate.
   4. 19 mm (3/4 in.) hail, any orientation, at 20 m/s (65 fps).
      25 mm (1 in.) hail stowed, at 23 m/s (75 fps).

E. Blowing dust devils, with wind speeds up to 17 m/s (40 mph).

The safety requirements are:

A. Meet OSHA, CAL-OSHA, NFPA, ANSI, and Southern California Edison requirements.

B. Control reflected beam.
   1. No unsafe beam outside exclusion area.
   2. No unsafe beam on structures or plant personnel.

C. Provide for safe stowage in the event of failure.

1.3 PRELIMINARY DESIGN COLLECTOR CONFIGURATION

The preliminary design collector configuration is shown on Figure 1-3. The inverting heliostat configuration consists of six 2.16m x 2.9m (85 in. x 114 in.) reflectors with a tracking mirror. The structural support is a main torque tube with four cross beams. The drive unit incorporates azimuth and elevation "Orbidrive" rotary units. The cylindrical pedestal supports the drive unit through a bolted interface and is in turn bolted to a precast reinforced concrete cone foundation. The control system comprises heliostat, field and master controllers using a closed-loop system. The optical sensor is mounted on a sensor pole adjacent to each heliostat.

MDAC is currently developing an open-loop control system. In the event the anticipated cost advantage of an open-loop system over a closed-loop system is verified by development and test, it is expected that MDAC will recommend an open-loop control system for the 10-MW Pilot Plant. The open-loop system may require drive systems with lower backlash characteristics than those in the preliminary design configuration. Under such circumstances, it is anticipated MDAC will recommend a "Harmonic" rotary drive in azimuth and either a "Harmonic" drive or double jacks in elevation. The kinematic problem with double jacks encountered on an earlier pitch/roll heliostat is not an issue because of the less demanding kinematics of the elevation/azimuth heliostat. "Harmonic" drives and jacks have been qualified on the octagonal heliostat and the performance has been demonstrated by the Subsystem Research Experiment (SRE) program.

The maximum mirror area should be constrained only by the minimum collector cost per unit reflector area consistent with the ability to concentrate the reflected beam on a optimum size and shape receiver. MDAC found that the collector cost per unit area decreases as the area increases for the region of interest. Constraints such as flux spillage at the receiver, available size of materials, ease of transportation, handling and assembly, and heliostat compliance (or resonant frequency) become the dominant factors limiting heliostat size. Hence, MDAC has kept the designs in the 30 to 40m^2 range, with the present design at 37.9m^2 (408.3 ft^2).

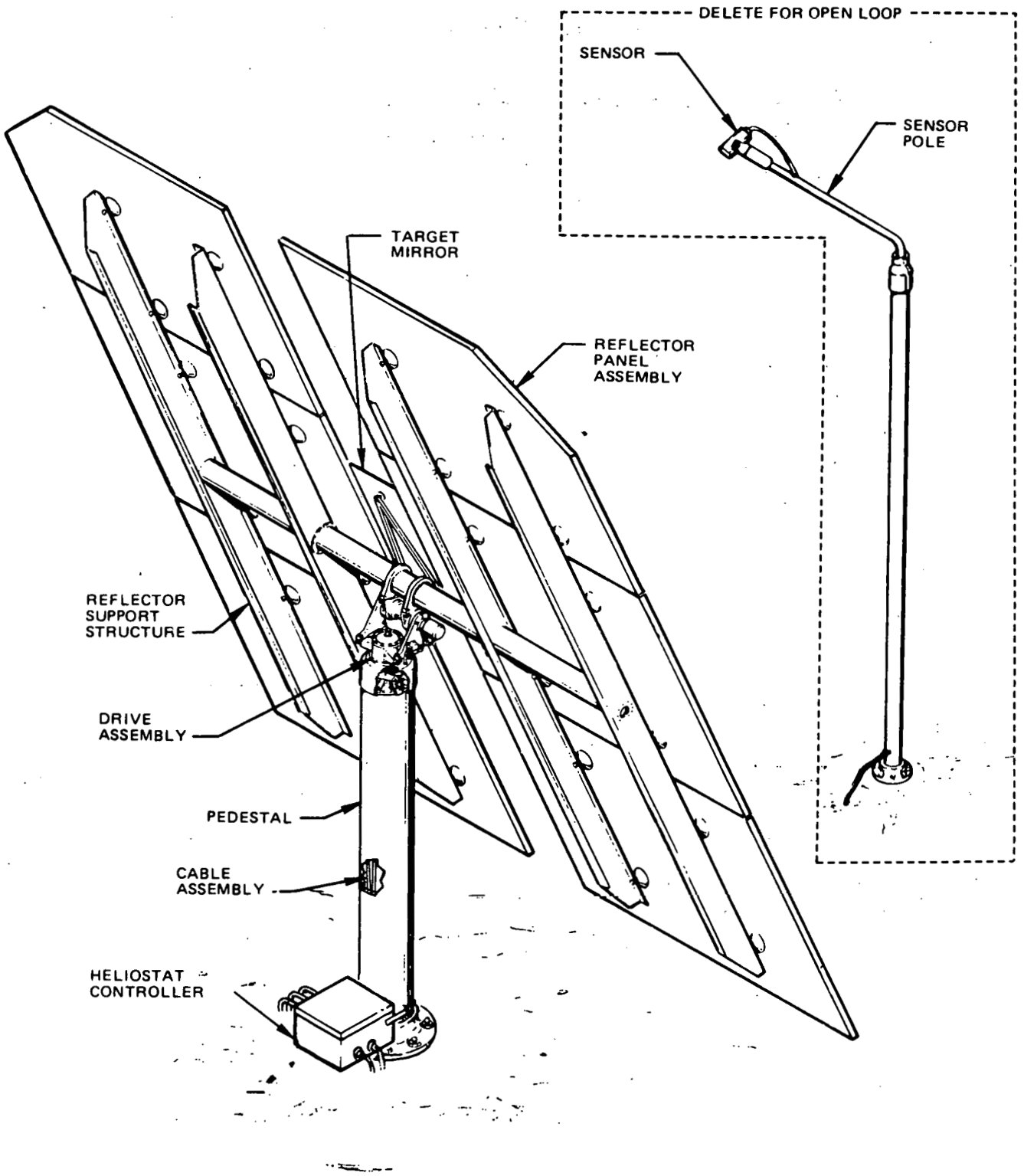

Figure 1-3. Heliostat and Sensor Pole Assembly

The inverting orthogonal design has the adaptability of being stored face down, vertical, or face up. The choice depends upon safety, dust accumulation and cleaning, and heliostat wind loads. The face-down position has the following advantages:

- Heliostat cannot reflect sunlight in a dangerous manner.
- Under light rain conditions, less dust adheres to the mirror.
- Best under high winds with blowing sand or dust, unattended fields, and for extended periods of down time.

Vertical stowage position has the following characteristics:

- Self-cleaning due to rain, heavy dew, and frost.
- Higher wind loads and potential danger of damage due to blowing sand.

Face-up stowage position has the following characteristics:

- Minimizes the loads to go face up in a rapidly rising wind.

MDAC recommends vertical stowage, where safety is not critical, for most conditions to minimize dust build up.

The details of the heliostat components are discussed in the following subsections.

1.3.1 Reflector

Each reflector panel is a flat structural sandwich. The front face is a 3.17 mm (1/8 in.) second surface mirror, and the back face is a 0.56 mm (0.022 in.) galvanized steel sheet. The faces are adhesively bonded to a 5.08 cm (2 in.) core, made from rigid extruded polystyrene foam (STYROFOAM) of 2 lb/ft^3 density. Each of the six panels measures 2.16m x 2.90m (85 in. x 114 in.). The panel edge is protected from damage by a small extension of the core and is sealed by a polyurethane weatherseal compound. At the four attachment points, the loads are transferred to the cross beams by shallow, formed, circular steel cups.

1.3.2 Structural Support

The arrangement of the support structure was selected because of its simplicity and adaptability to accommodate reflector panels of different sizes. The support structure consists of a main torque tube attached to the drive system and four channel cross beams. Each pair of cross beams supports a group of three reflector panels. The slot between these panel groups provides clearance for the central pedestal when the assembly is rotated to the face-down stowage position. Two drive attachment fittings are machined on the surfaces which mate with the drive unit and welded to the torque tube. Four ring flanges are also welded to the tube for attachment of the cross beams.

1.3.3 Drive Units

Each heliostat incorporates a drive unit which produces appropriate reflector motions for solar tracking, emergency slewing, routine reflector positioning, and stowage. The drive unit consists of azimuth and elevation drive mechanisms. These drive mechanisms are composed of motors, drive trains, position feedback transducers, reflector support bearings, and structural housings. The azimuth and elevation drive trains are schematically identical, and each is essentially a motor with two stages of reduction, capable of producing the high-torque, low-speed output needed. The input AC torque motor drives an input 45:1 reducer, whose output shaft is coupled to a 961:1 output stage reduction. Both the input and output reducers use Orbidrive cam-roller sets to achieve requisite speed reductions.

As previously mentioned, if an open-loop control system is adopted, lower backlash drive units may be required. The units would be similar to the units qualified in the SRE program.

1.3.4 Pedestal/Foundation

The pedestal is a thin-walled steel column, 50.8 cm (20 in.) in diameter and 2.74m (108 in.) long, welded at the lower end to a standard weld neck pipe flange. The upper end has a 1.9 cm (0.75 in.) thick steel plate for attachment of the drive unit. Attachment to the concrete foundation is provided by

eight 3.17 cm (1.25 in.) diameter anchor bolts equally spaced on a circle of 0.69m (27 in.) diameter. The foundation is a precast reinforced concrete, cone type spread footing, with the base 1.14m (45 in.) below ground. A central concrete column, 0.81m (32 in.) in diameter and 0.61m (24 in.) high, extends from the cone top to 7.62 cm (3 in.) above grade.

1.3.5 Sensor Pole/Foundation

The sensor pole is designed to support the tracking sensor at a location approximately on a line between the center of the heliostat and the receiver. A thin-walled tube 12.7 cm (5 in.) diameter and 3.05 mm (0.120 in.) wall, located 4.82m (190 in.) from the heliostat centerline, is used for the vertical column. A tubular steel boom 7.62 cm (3 in.) diameter x 3.05 mm (0.120 in.) wall with a 45-deg bend at the lower end is attached to the vertical column with a standard swage reducing pipe nipple. The nipple is welded to the boom and clamped to the vertical pole with four set screws to maintain a rigid position. The tracking sensor is installed on the upper end of the boom by means of a sliding mount fitting for adjustment of position along the boom. For lateral adjustment the boom swings around the pole and is locked in position by four set screws. With this scheme the booms are of five different lengths to accommodate the total field. The sensor pole foundation is 1.22 m (48 in.) in diameter and 50.8 cm (20 in.) deep.

1.3.6 Control/Electronics

The preliminary design control/electronics closed-loop control system consists of AC motors, encoders, optical sensors, and triac switches; heliostat, field and master controllers; power and data distribution systems. A block diagram for the Pilot Plant field is shown on Figure 1-4. The power distribution is accomplished by primary feeders at 2.4 kV and secondary feeders at 240V. The secondary power buses go to each heliostat. The data-distribution network encompasses the central computer, field controller, and heliostat controller. The heliostat controller receives inputs from the field controller, motor encoders, and control sensors.

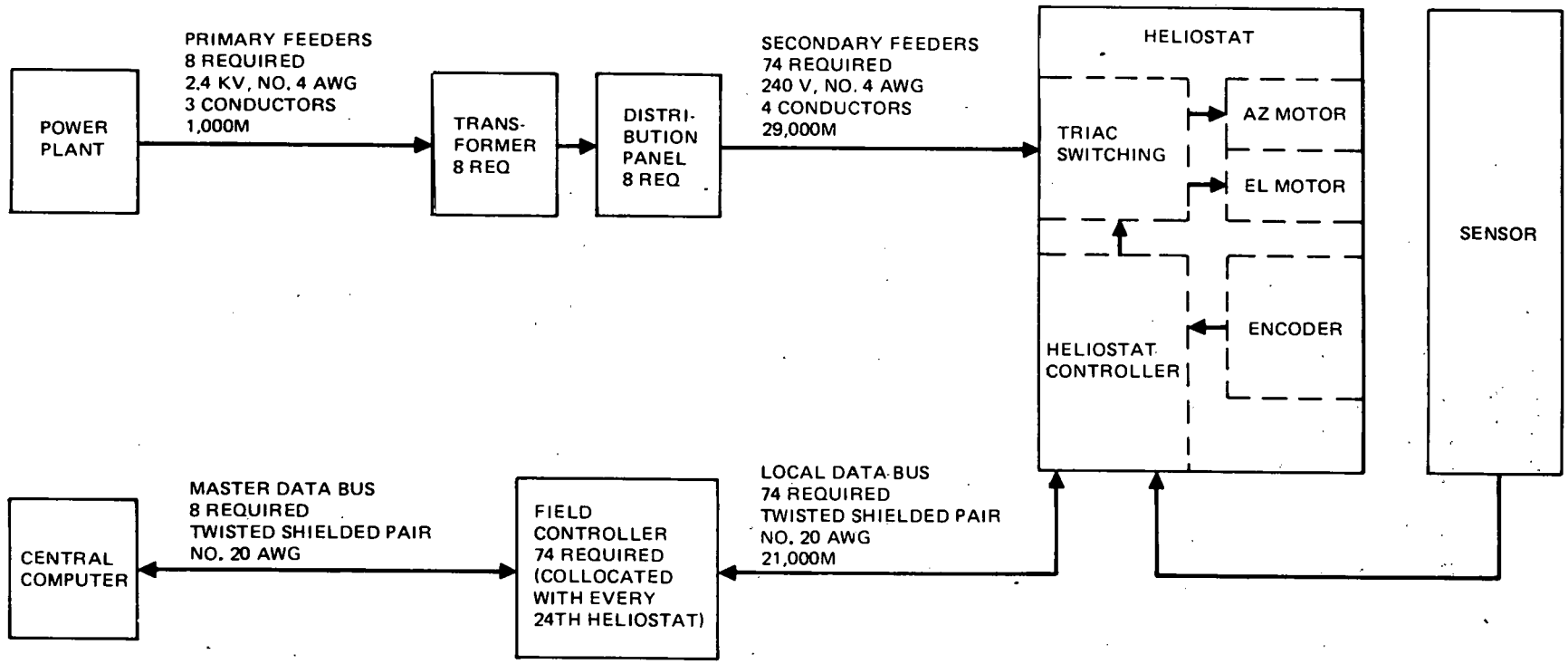

Figure 1-4. Power and Data Distribution – Collector Field Network

Control sensors are required in the system to enable the control electronics to determine the mirror attitude and to correct that attitude when required. There are two basic sets of sensors used: the tracking sensor and the position encoders. The tracking sensor is a unit associated with each individual heliostat for the purpose of fine-tracking control of the reflected beam direction toward the receiver. It is mounted on a pole between the heliostat and the receiver so that it receives the reflected beam from some part of the center mirror. The axis of the sensor is oriented to intersect the aim point on the receiver. If the reflected beam is parallel to the sensor axis a null signal is generated from the sensor. If the reflected beam is not parallel to, but within $\pm 5^{o}$ of the sensor axis, an output signal is produced proportional to the angular error. A constant error signal is produced for beam alignment errors from $\pm 5^{o}$ to $\pm 15^{o}$ to aid sun acquisition. The sensor has two orthogonal error directions lying in the plane normal to the sensor axis. When the beam is beyond the reach of the tracking sensor mirror (during stowage, slew, etc.), position encoders provide attitude information.

In the open-loop systems under development, the only difference between the open- and closed-loop hardware is the optical sensor, sensor pole, and associated hardware. These are deleted in the open-loop system.

1.3.7 Weights

The weights of the collector system, less electronics, are as follows:

	kg	lb
Reflector panels	556	1,227
Structural support	503	1,108
Drive unit	304	670
Pedestal	231	509
Total (no foundation)	1,594	3,514
Foundation	4,423	9,750
Total (with foundation)	6,017	13,264

1.4 COLLECTOR SUBSYSTEM DEVELOPMENT

The collector subsystem has undergone development since 1973. In 1974-5, MDAC conducted a heliostat model test in conjunction with the University of Houston under NSF sponsorship. Figure 1-5 shows the NSF heliostat designed, developed, and tested under this contract.

1.4.1 Noninverting Octagonal Collector

In June 1975, ERDA initiated the Phase I - Solar Thermal Power System contract with MDAC. MDAC designed, fabricated, and tested six noninverting octagonal heliostats shown in Figure 1-6. The octagonal heliostat assembly consists of eight octagonal reflectors supported by radial beams which tie into a hub. The reflectors included first-surface mirrors with acrylic coating on 0.63 cm (1/4 in.) thick float glass and second-surface laminated mirrors. The reflectors and substructure are rotated in azimuth by a "Harmonic" rotary drive and in elevation by a jack. The assembly is supported by a conical pedestal and a reinforced slab foundation. The sensor is supported by a sensor post and is connected to the field controller. The field controller is commanded by the master control.

1.4.2 Inverting Orthogonal Collector

MDAC designed, fabricated, and tested two inverting orthogonal heliostats, as shown in Figure 1-7. The orthogonal heliostat assembly consists of six rectangular reflectors supported by a central torque tube and four cross beams. The reflectors included second-surface laminated mirrors and second-surface foam sandwich mirrors. The reflectors and substructure are rotated in azimuth and elevation by "Orbidrive" rotary drives. The sensor and the electronics are identical to the octagonal heliostats.

The noninverting octagonal and inverting orthogonal heliostats underwent extensive assembly level tests (see Sections 1.4.3, 6.3.1, 6.3.2, and 6.3.3) and subsystem level tests (see Sections 1.5 and 6.4).

The configuration of the complete heliostats fabricated for test are listed in Table 1-3. The array tests were done at the Naval Weapons Center (NWC), China Lake, California.

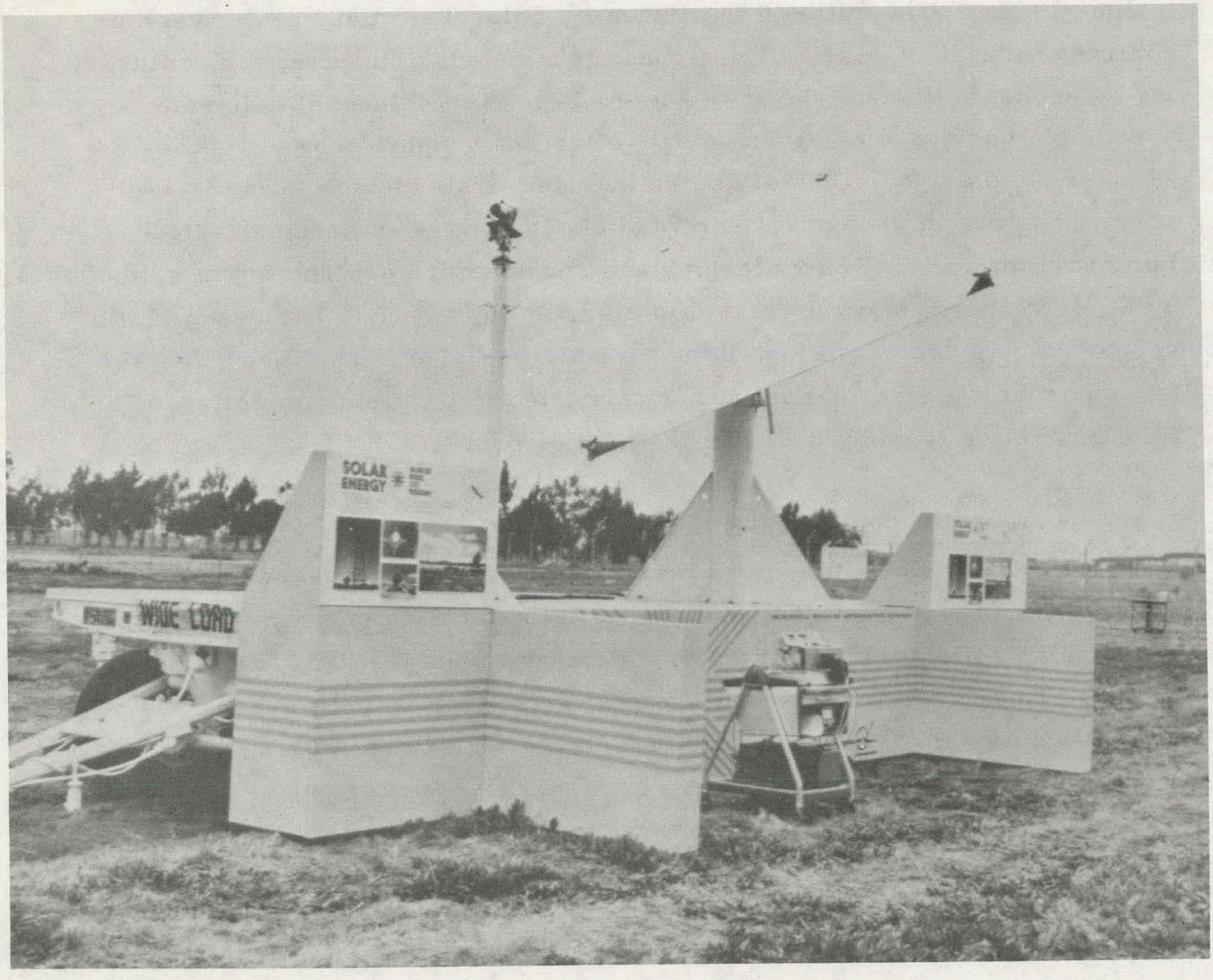

Figure 1-5. NSF Heliostat

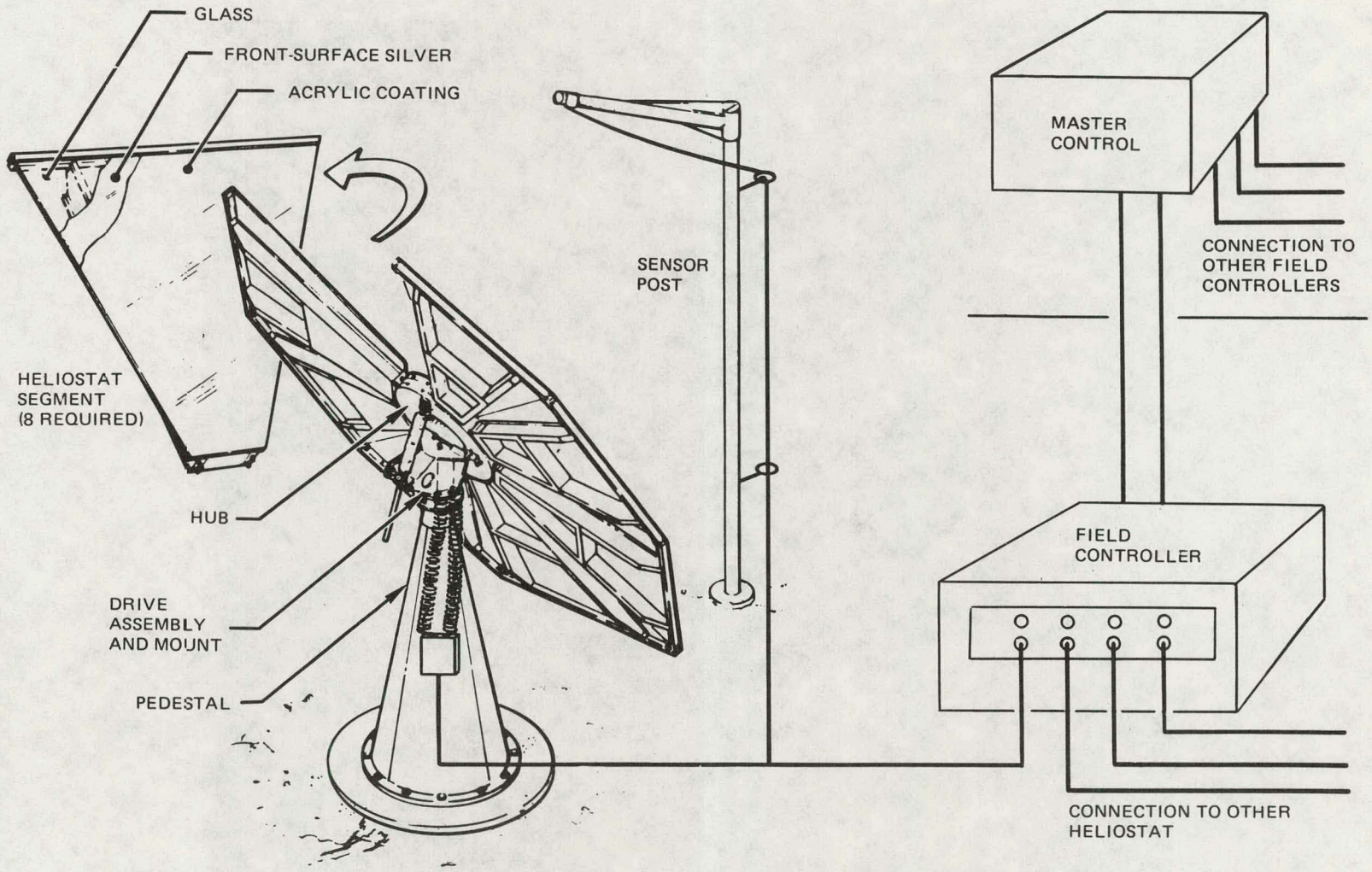

Figure 1-6. Noninverting Octagonal Collector Subsystem

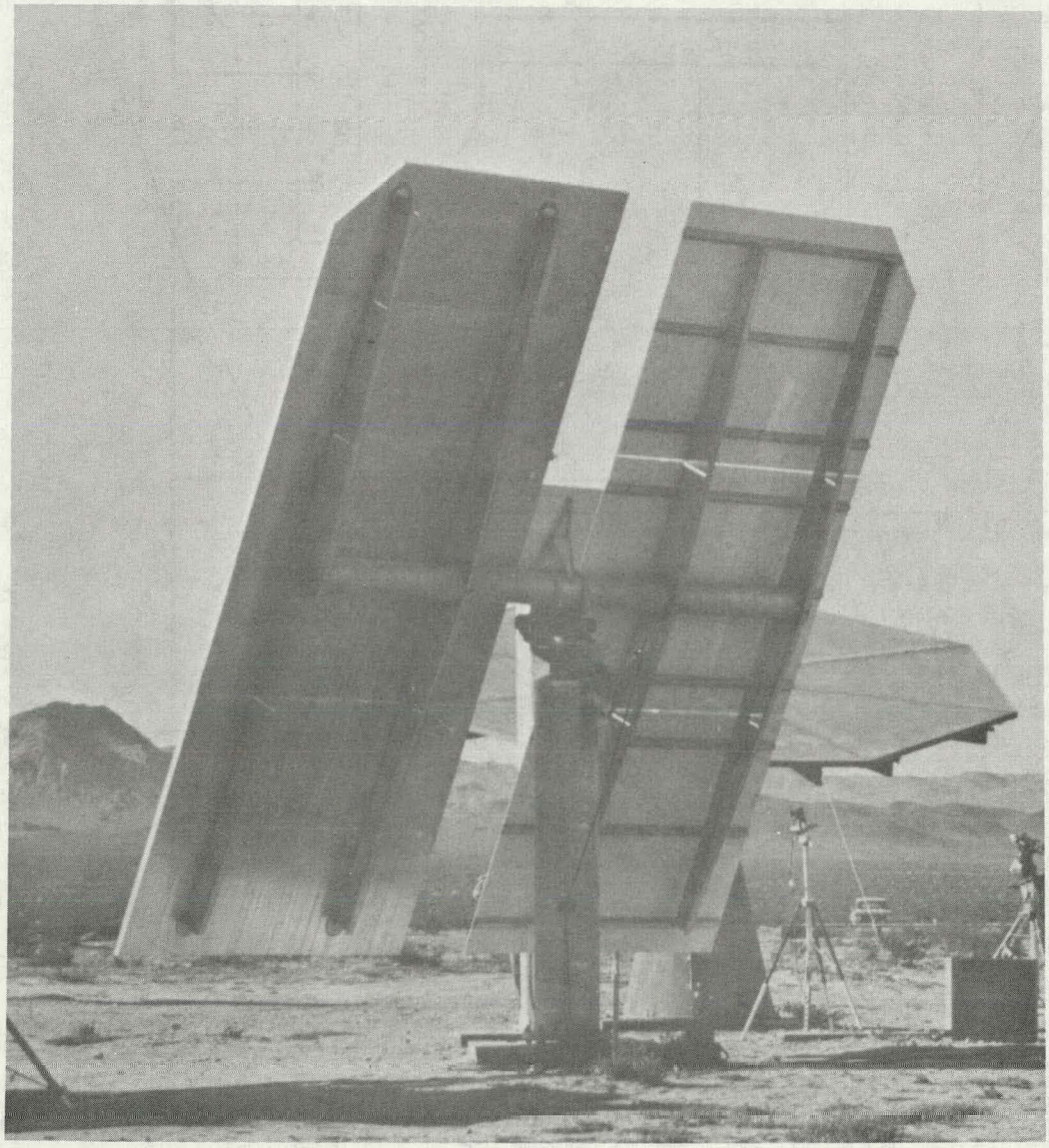

Figure 1-7. Inverted Stowage Orthogonal Heliostat

Table 1-3

HELIOSTAT HARDWARE FABRICATED

Heliostat	Reflector	Test
• Noninverting Octagonal		
H1	First Surface	Structural Test Array Test
H2	First Surface	Controls Development Test Array Test
H3	First Surface	Array Test
H4	Laminated	Array Test
H5	Laminated	Mobile Array Test
H6	Laminated	Drive Unit Life Test
• Inverting Octagonal		
IH 1, Var 1	Laminated	Controls Development Test Array Test
Var 2	1/2 Laminated 1/2 Foam Core	Array Test
1H 2	1/2 Laminated 1/2 Foam Core	Structural Test

The tests done at MDAC-Huntington Beach, CA, were: structural test, controls development, and Harmonic drive/jack life.

Tests done at Compudrive, Massachusetts were on Orbidrive life.

1.4.3 Subsystem Level Tests at NWC

A subsystem level test program was conducted at NWC for engineering performance tests, and installation, operation, and maintenance.

The heliostat array test location is shown on Figure 1-8. Five heliostats were installed on foundations 195m (640 ft) north of the two towers supporting the target. A photograph of the five heliostats is shown in Figure 1-9. The

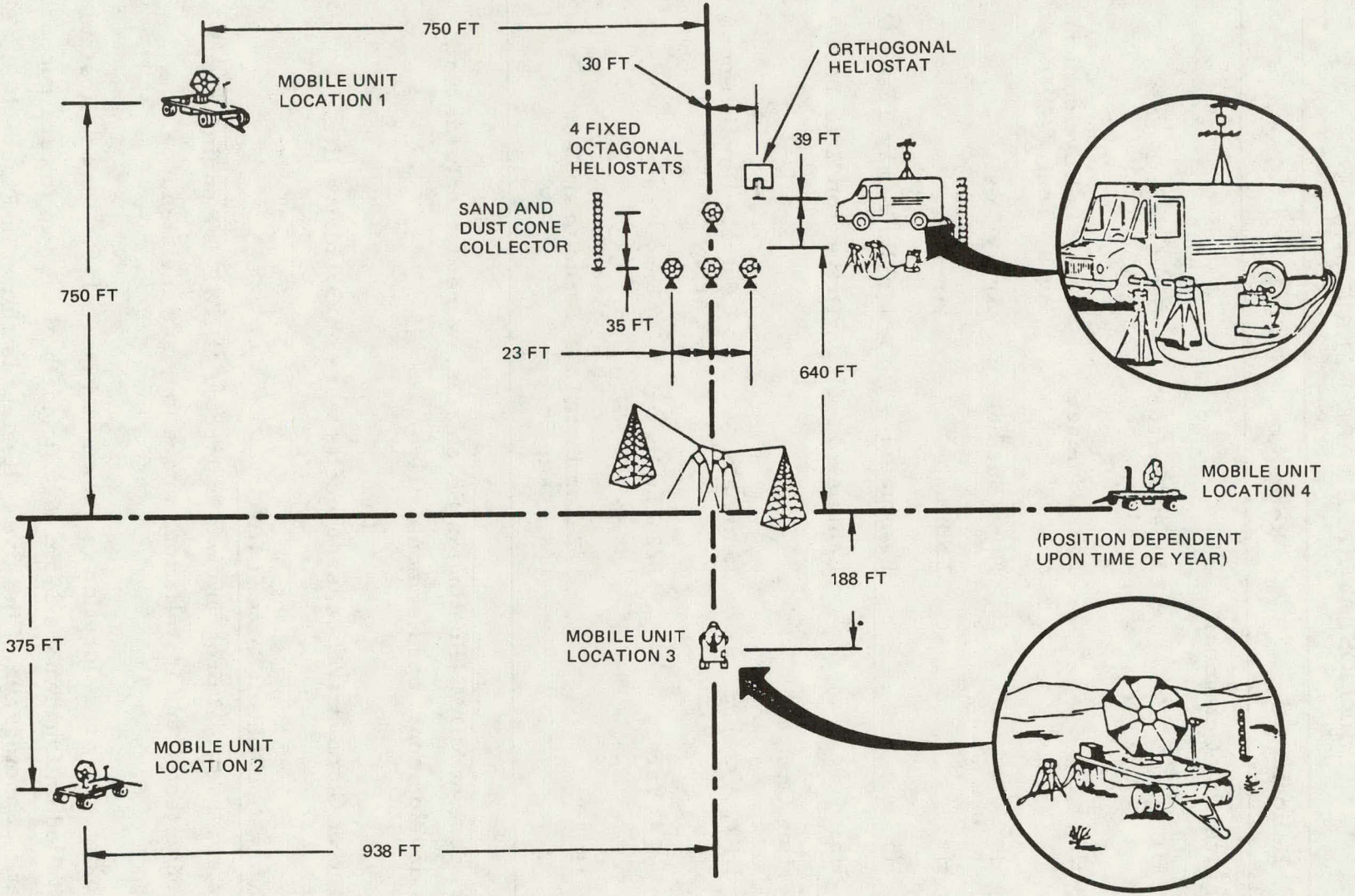

Figure 1-8. Heliostat Array Test Locations

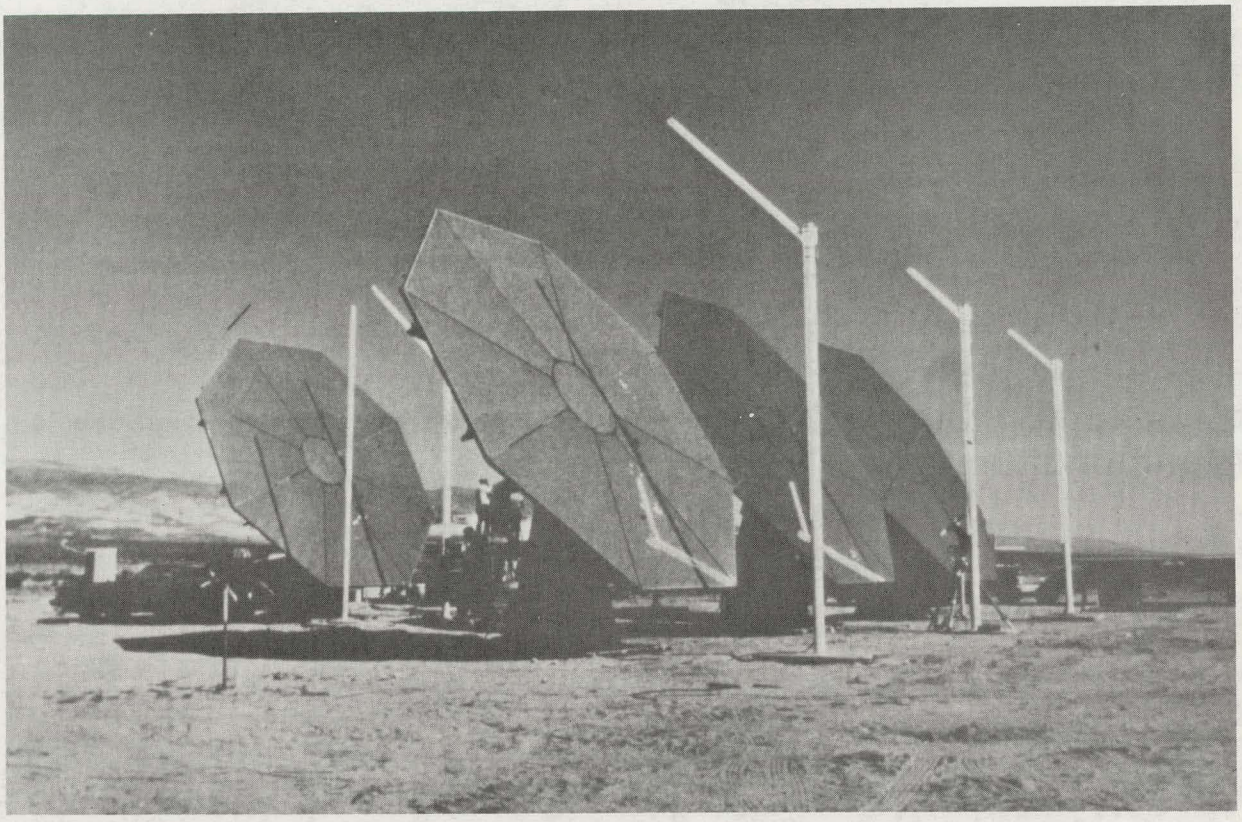

Figure 1-9. Heliostat Array at Naval Weapons Center

sixth heliostat was mounted on a trailer to permit operation from different locations in the field.

The engineering performance tests provided the following information:

- Data on the operating modes.
- Mirror reflectivity.
- Heliostat beam irradiance distribution at the target.
- Heliostat power consumption.

The operating data showed that: the heliostat and field controller were stable and the units operated satisfactorily in the following modes:

A. Sun acquisition.
B. Synthetic tracking.
C. Command position.
D. Off nominal performance (to 1/16 normal sun intensity).
E. Stowage (as applicable).
F. Multiple aim.

The algorithm for slewing through a tracking "pole" was not verified due to time constraints.

Array tracking performance was as follows:

	Typical Time Averaged Error Band (mr)	
Wind Velocity	Noninverting Octagonal with Harmonic/Jack	Inverting Orthogonal With Two Orbidrives
Calm	1/2	3/4
10 m/s	3/4	2

The mirror reflectivity was measured at regular intervals by Epply pyrheliometers. The average reduction is reflectivity due to dust accumulation between washings was:

A. Noninverting heliostat:
   1. Acrylic mirrors ~7 to 8%.
   2. Laminated mirrors 6-1/2%.
B. Inverting heliostat ~3%.

Tests performed on out-of-flatness of the laminated mirrors using two beam sensors showed as much beam error as 6 mr.

The heliostat beam irradiance distribution at the target was given by the digital image radiometer (DIR). The DIR block diagram is shown in Figure 1-10. The radiometer consists of a video camera and scanning electronics, A/D converter, NOVA 1200 computer, cassette tape storage, CRT display, video monitor, and keyboard. The radiometer and target were calibrated against thermopile pyrheliometers so that the irradiance (Watts/meter^2) as measured by the DIR is within an accuracy of 2% for any given data/point. The 3,600 data points from the DIR were recorded on tape, and processed to plot the beam intensity distribution, weighed centroid, total power, and total energy.

The beam quality of the heliostats at NWC was determined and correlated with the insolation level and reflector characteristics. Some of the significant results were as follows:

A. The DIR determines the power within 2% for full-scale heliostats.
B. The optical performance of the laminated reflectors and the acceptable sandwich core reflectors were about the same. Unacceptable sandwich core reflectors showed a decrease in performance of about 5 to 7%.

The heliostat power consumption was remarkably low. The normal tracking power was approximately 12 watts/heliostat. The power during sun acquisition was 16 to 18W. The energy to stow the inverted heliostat (180^o motion) was 65 watt hours.

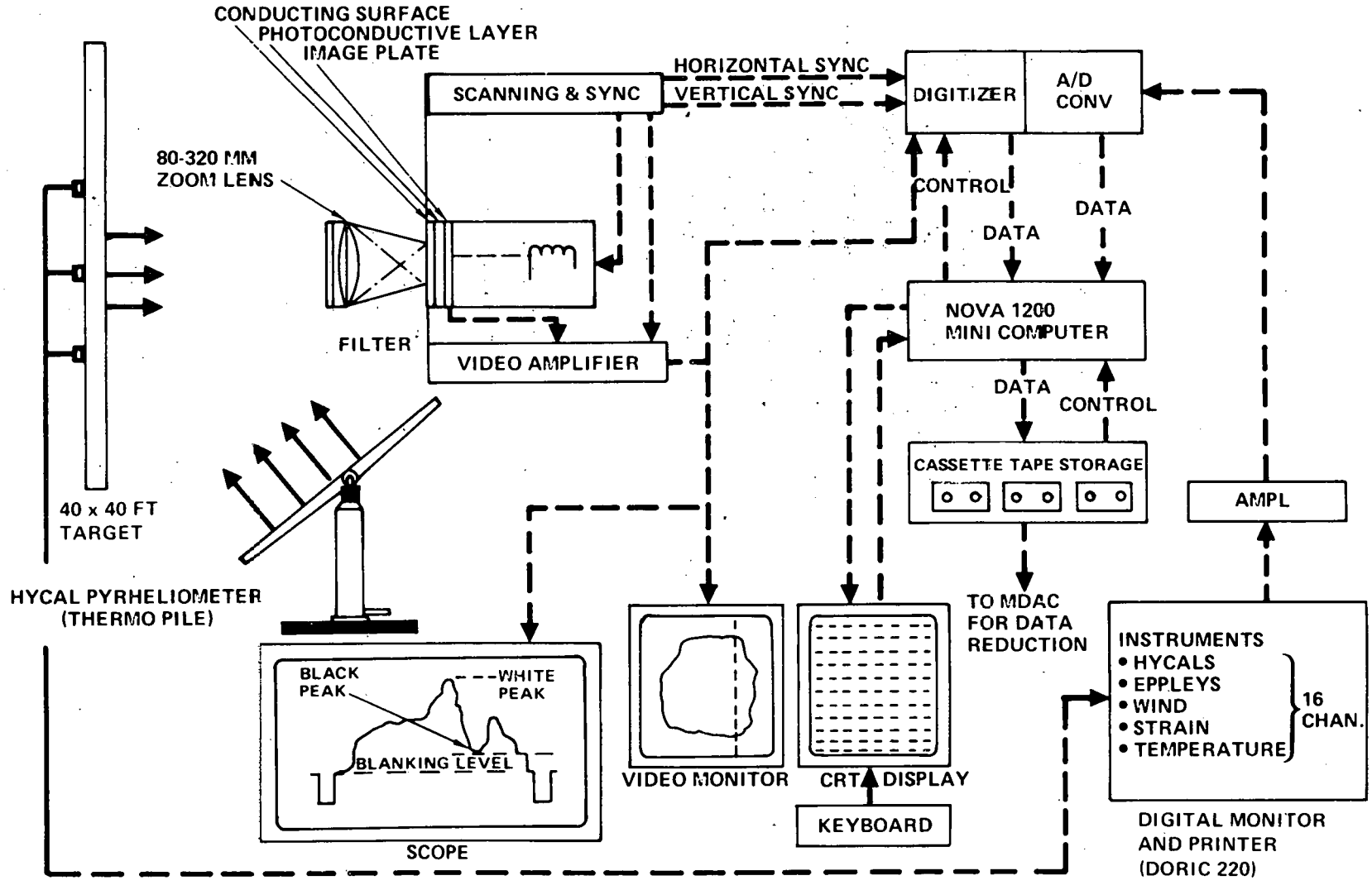

Figure 1-10. Digital Image Radiometer Block Diagram

The installation, operation, and maintenance of the heliostats provided the following significant data:

A. Installation times for future estimates.
B. Simple, rapid closed-loop sensor alignment procedures were developed.
C. Meteorological data at NWC pertinent to Pilot Plant operation. NWC is 72.4 km (45 mi) from Barstow, and has similar weather conditions.
D. The acrylic first surface reflectors showed unacceptable degradation due to pinholes, staining, and acrylic delamination.
E. The heliostat and sensor pole foundations were quite stable.
F. Validation of reflector washing requirements and timelines. Surprisingly, frost and snow turned out to be an excellent cleaner.

1.5 COLLECTOR COMPONENT DEVELOPMENT

The collector component included reflectors, structural support, drive units, pedestal, foundation, sensor pole/foundations, field controller, and master control. The component was developed by trade studies, design, fabrication, and test.

1.5.1 Reflector

The reflector development included:

A. The basic characteristics of the silver deposition, and the effect of glass chemistry and thickness.
B. Acrylic coated first-surface mirrors.
C. Laminated and foam sandwich core second-surface mirrors.

The solar reflectance efficiency of vapor and chemical deposition silver was measured at Air Mass Two. The chemically deposited silver was selected, and little difference was found between various commercial processes. Extensive testing was conducted at various acceptance angles (4 to 125 mr) with the Beckman and specular spectrophotometer over the solar spectrum and the specular photometer at 550 nm. In conjunction with other sources, data was obtained on solar transmittance and reflectivity as a function of glass thickness, chemistry (iron content), and aperture angle. The results

showed that an average reflectivity of 0.88 second surface was reasonable for vertically stowed mirrors for Pilot Plant. An average reflectivity of 0.91 for second-surface mirrors for Commercial Plant may be achieved with currently available processes.

Extensive development was conducted on first-surface mirror coatings. These included various formulations of Sheldahl type 822-12A acrylic coatings, and other coatings from Texton Plastics, Dupont, Sierracin, Owens Illinois, De Soto, and others. The Sheldahl coating was selected, and subjected to salt spray, reflectance, abrasion, and exposure tests. A number of full-scale trapezoidal panels were made and installed on noninverting octagonal heliostats. Subsequent tests showed that the first-surface mirrors are subject to pin holes, staining, and delamination of the acrylic. The conclusions are that:

- For Pilot Plant, the technology is not ready for use of first-surface mirrors using polymerized coatings.
- Cost and performance advantages indicate a desirable development area for Commercial system cost reduction.

Laminated second-surface mirrors with white mirror backing paint were developed and installed on both types of heliostats. The laminates were bonded to main beams for the octagonal configuration, and to three stiffeners attached to the cross beams for the orthogonal configuration. Problems of reliability were encountered with the grey mirror backing paint. The grey backing paint was replaced by the white backing paint, primarily due to backlighting problems. Even with white backing paint, continuous exposure to backlighting conditions over a year's time period has caused cracking of the laminate. This is considered to be too severe a test, and results are discounted. The laminates were not as flat as desired (0.060 to 0.070 in. out of flatness). No cracking of MDAC laminate glass due to the environment was observed. The cost of production of laminate reflectors is about 20% greater than the foam core sandwich (which will be discussed). All in all, the MDAC laminated mirror performance over the past 8 mo has been satisfactory.

Cost/performance trade studies of a number of different types of reflectors were made. These included sandwich, corrugations, other types of stiffened configurations. The 3.17 mm (1/8 in.) second-surface mirror, 5.08 cm (2 in. thick) Styrofoam core and 0.56 mm (0.022 in.) galvanized steel backing sheet was selected. Component tests were made to establish material, structure, and core-creep properties. Creep of the 32 kg/m^3 (2 lb/ft^3) core was not a problem. Full-scale panels 1.08m x 2.9m (42.5 in. x 114 in.), were fabricated and tested at NWC.

For both the laminated and the foam core sandwich, the following tests were conducted.

A. Flatness.
B. Thermal/backlighting.
C. Thermal cycle.
D. Thermal distortion.
E. Washing.
F. Reflectivity.
G. Exposure.
H. Salt Spray.
I. Accelerated ultraviolet.
J. Adhesive compatibility.
K. Beam creep.
L. Beam bending.
M. Hail impact.

For both configurations, the component tests indicated satisfactory performance.

To prevent glass cracking, the glass edges should not have large or sharp nicks and the transient, differential in-plane temperatures must be kept below 20°F. This can be accomplished with careful manufacturing process, edge protection, and avoidance of in-plane temperature differential.

MDAC recommends the foam sandwich reflector and believes the current development will result in efficient, low-cost reflectors. The laminated reflectors have been qualified and are a satisfactory backup.

1.5.2 Structural Support

Each heliostat incorporates a structural support for the reflectors and is attached to a drive unit on top of a pedestal and foundation.

For the octagonal heliostat, the reflectors were supported by 16 radial beams that tied to the hub. In the orthogonal heliostat, the reflectors were supported by a central torque tube and four cross beams.

Heliostat structural tests were conducted to verify the heliostat strength, deflection, and fundamental vibrational frequency. Complete heliostats of both the octagonal and inverted type were used for the structural tests. One segment or panel was given a finely distributed load. The remaining segments or panels were given concentrated loads simulating their contribution to total heliostat loading. The strain and deflection measurements were compared with predictions from analysis using a finite element computer program (NASTRAN).

Deflection levels under the simulated operational loading of 11.6 m/s (26 mph) were within 10% of the predictions from the NASTRAN model. Measured strains under the survival wind loads of 46.5 m/s (104 mph) for both the octagonal heliostat and 44.7 m/s (100 mph) for the inverted heliostat were equal to or below NASTRAN predictions. Vibrational frequencies for pitch and yaw modes were within 5 to 10% of predictions based on the NASTRAN model. The closeness between the measurements and predictions verifies the heliostat design and the validity of the model.

1.5.3 Drive Units

Each heliostat incorporates a drive unit which produces appropriate reflector motions for solar tracking, emergency slewing, routine reflector positioning, and stowage. The drive unit consists of an azimuth and elevation drive train, each comprising a motor with several stages of reduction, capable of producing the needed high-torque, low-speed output.

The requirements for the drive unit include travel, operating loads, stowage loads, backlash, minimum resonant frequency, no back drive, and 30-yr life.

For the octagonal heliostat the drive unit consisted of a "Harmonic" drive in azimuth and linear actuators in elevation. For the inverting heliostat, further trade studies were conducted in an attempt to reduce the cost of the drive unit. The studies considered Orbidrive, Harmonic drive, Helicon gears, linear actuators, spur gears, and chains. As a result of the trade studies, Orbidrive was selected for both axes due to the potentially lower cost and acceptable (1/2 mr) backlash. The Orbidrive was designed, fabricated, and tested at Compudrive Corp., and was subjected to additional testing by MDAC.

Thirty-year life cycle qualification tests were successfully completed on the Harmonic drive, Orbidrive, and linear actuators. The data included information on integrity, efficiency, backlash, slew rates, wear, and backdrive characteristics. It is significant that the test results of the backlash for the Harmonic drive and linear actuators (0 to 1/2 mr) was less than for the Orbidrive (2 mr).

The drive units and control sensors were subjected to environmental tests to verify their performance and survival during temperatures from -30°C (-22°F) to +60°C (140°F), rain to 5 cm (2 in.) per hour, icing from freezing rain, blowing dust, and hail impact up to 25 mm (1 in.).

The preliminary design configuration with closed-loop control incorporates qualified Orbidrives. In the event that anticipated cost advantage of open loop is verified by test, MDAC will probably recommend an open-loop system. This system may require drive units with less backlash. Under these circumstances, MDAC may recommend some combination of the qualified "Harmonic" drives or linear actuators. At this time, there is no significant recurring cost differential between the above systems.

1.5.4 Pedestal/Foundation

For the central pedestal concept, the thin-wall steel column is the lowest-cost solution and features simple interface attachments with the drive unit and foundation.

Trade studies were conducted by Stearns-Roger on a number of foundations. After extensive analyses, these four were chosen for further investigation:

- Precast reinforced concrete.
- Driven steel pile with lateral support.
- Steel frame with screw anchors.
- Reinforced concrete with pedestal cast in place.

Because of superior collector installation adaptability, the precast reinforced concrete foundation was selected.

1.5.5 Controls/Electronics

The controls and electronics system for the SRE consists of:

A. AC drive motors controlled by triac switches actuated by a field controller.

B. Heliostat control data provided by optical sensors in the sun tracking mode and potentiometers/limit switches in the command mode.

C. A field and master controller connected by a data distribution system.

D. Power at 240V provided by utility company transformers.

This control system was qualified in the SRE program and met all the system requirements.

The preliminary design configuration is the same as the SRE configuration with one exception. The SRE potentiometers and limit switches for sensing in the command mode have been replaced by a drive output encoder and a motor counter. This will reduce beam safety hazards by providing excellent pointing accuracy in the command mode.

To investigate the possibility of lower costs, a trade was conducted on open-loop vs closed-loop tracking for the Pilot Plant. For this trade, three general methods of control were considered:

A. Closed Loop. A sensor on a pole to obtain error signals from the reflected beam. The error signals are used to update the required orientation of the heliostat in the tracking mode.

B. Open Loop. Equations are used to calculate the position of the sun. Using the position of the sun and the receiver, the required orientation of the mirror is calculated. Commands are sent to the heliostat. The mirror orientation is measured by one or a combination of the following ways:
   1. A sensor (encoder) on the drive output.
   2. A sensor (counter) on the drive input (motor).

Error budgets were developed for each method of control as shown in Table 1-4. By the use of the "Concen" code the spillage for each control method was calculated. The cost comparison between closed-open loop system with "Orbidrive" is shown in Table 1-5. The incremental costs include electronics, spillage, and installation. The spillage costs are a result of additional heliostats to maintain the same receiver power. From this preliminary data, a 4-bit encoder on the drive output and a shaft sensor on the input was selected. The low-bit encoder on the output shaft provides a substantial increase in reliability of the system in the event a malfunction of the counter/electronics occurs. The counter is easily reset by rotating the heliostat to a discrete index on the encoder.

With this open-loop system, a further study was made on relative collector field costs. This is shown in Figure 1-11 as a function of wind velocity. The preliminary design closed-loop system with Orbidrive or the Harmonic drive indicates the potential of lower cost. In addition, the effect of reduced backlash of the Harmonic type drive system becomes significant at higher wind conditions.

Table 1-4

CLOSED/OPEN LOOP REFLECTED BEAM ACCURACY

	Error Source	Closed Loop AZ/EL (mr)	Open Loop Gimbal Sensor AZ/EL (mr)	Open Loop Shaft Sensor AZ/EL (mr)
1.	Control Dynamics	0.8/0.5	0.9/0.6	4.1/2.0
2.	Mirror Surface	2.1/2.2	2.1/2.2	2.1/2.2
3.	Command/Alignment	0.5/0.5	2.0/2.0	2.4/4.4
4.	Pedestal/Sensor Pole	0.2/1.2	1.6/1.7	1.6/1.7
5.	Beam Sensor	0.5/0.5	0/0	0/0
6.	Refraction	0/0	0.1/0.4	0.1/0.4
7.	Gravitational	0/0	0/0	0/0.3
	Total RSS	2.4/2.6	3.4/3.4	5.4/4.2

Table 1-5

CLOSED/OPEN DELTA COST COMPARISON

	Incremental Costs	Closed Loop	Open Loop Gimbal Sensor	Open Loop Shaft Sensor
1.	Electronic	$1,163,000	$1,196,000	0
2.	Spillage	0	$188,000	$592,000
3.	Installation	$208,000	0	0
	Total Incremental Cost	$1,371,000	$1,384,000	$592,000
	Differential	0	13,000	- 779,000

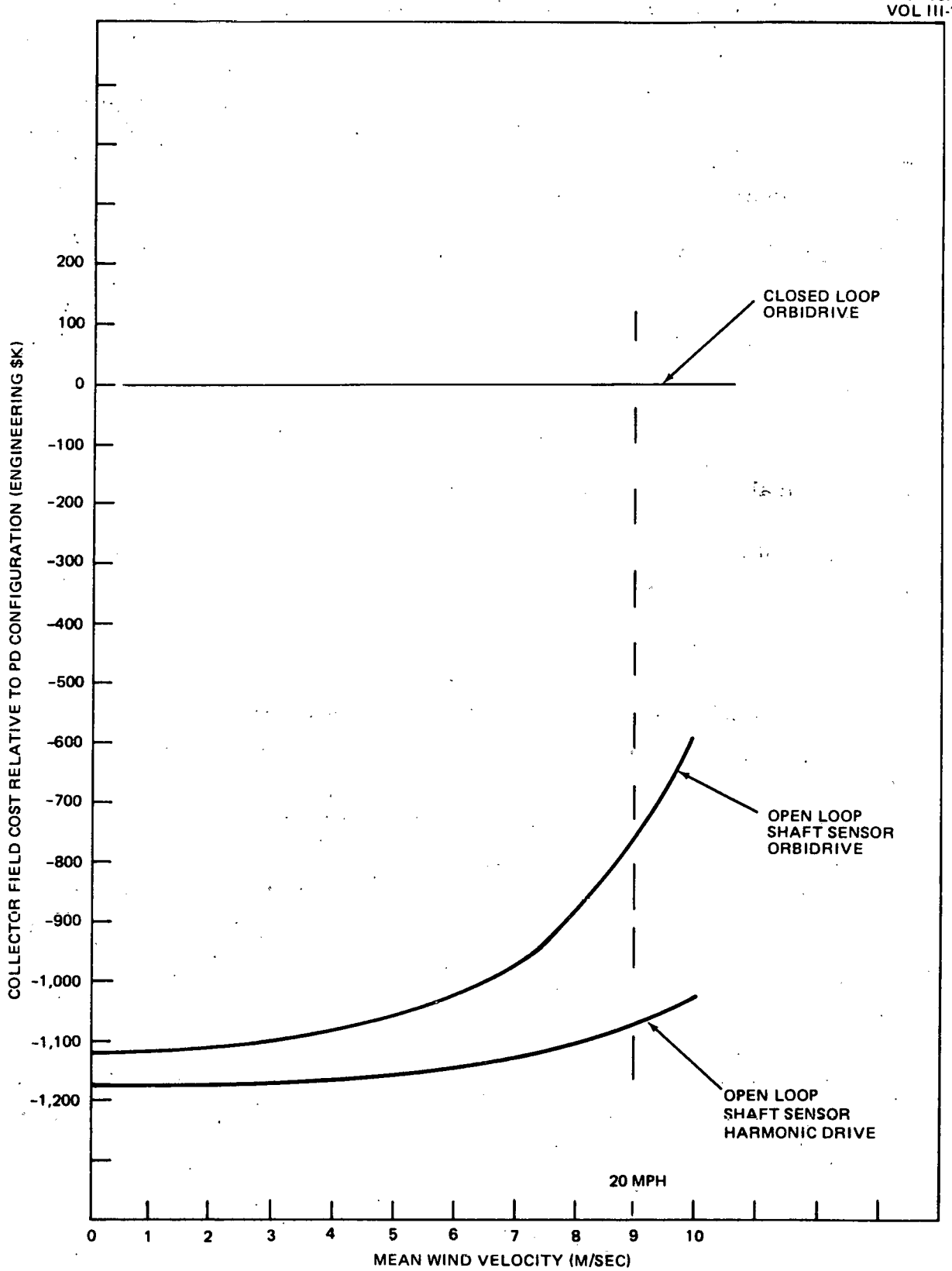

Figure 1-11. Cost Savings of Open Loop/Shaft Sensor Versus Closed Loop

Work on power and data distribution resulted in the network shown in Figure 1-4. The trenching and cabling costs are minimized by:

- Primary and secondary feeders direct to the heliostat triac switching.
- Master data buses run from the central computer to eight groups of field controllers. Local data buses run among the nine field controllers in a group and to the associated heliostat controllers. Decentralization of the controller reduces the wiring costs substantially. The preliminary design decentralized controllers are a repackaging of the SRE field controller.

1.6 RATIONALE FOR SYSTEM SELECTION

The preliminary design collector configuration is described in Section 1.3. The rationale for selection is as follows:

1.6.1 Reflector

The foam core sandwich is preferred to the stiffened laminate due to its lower cost.

1.6.2 Structural Support

The recommended configuration has satisfactory performance.

1.6.3 Drive Units

The Preliminary Design configuration is based on the qualified Orbidrive. In the event open-loop controls are recommended for Pilot Plant, consideration will be given to the qualified Harmonic drives or linear actuators due to reduced backlash.

1.6.4 Pedestal/Foundation

The cylindrical pedestal is lowest in cost. The precast reinforced concrete foundation is equivalent in cost to competitive foundations and provides more installation adaptability.

1.6.5 Sensor Pole/Foundation

The recommended configuration has satisfactory performance for the closed-loop system.

1.6.6 Control/Electronics

The preliminary baseline design was selected to provide minimum cost consistent with system reliability. The SRE design is functionally the same as the preliminary baseline design.

The preliminary design configuration is the same as the SRE configuration except for the replacement of the potentiometers and limit switches by encoders and counters. This is for beam safety considerations.

1.7 SAFETY

The safety requirements for the 10-MW Pilot Plant collector subsystem include the conventional industrial safety and the special safety problems associated with the solar thermal power plant.

The primary problem are the hazards associated with the concentrated solar beam for individual or multiple collectors. The following have been investigated:

A. The absorbed retinal irradiance due to an individual collector.
B. The probability of multiple collectors focusing at the same point.
C. The procedures to be followed in bringing the beams on or off the receiver under normal operation.
D. The procedures to be followed under a condition of heliostat failure.

The use encoders and counters in the control/electronics provides an accurate control of the heliostat beams in the synthetic tracking mode.

1.8 AVAILABILITY

An extensive collector availability analysis is described in Section 4.2.12. For the Pilot Plant, the total failures per day and per year are 1.04 and 344, respectively. The average number of heliostat outages/day is 1.32. Availability, as defined by at least 98% of the field being operational, is projected at 99.99%.

1.9 PROGRAM PLANS

Preliminary program plans have been developed for the Commercial system and generated in more detail for the Pilot Plant. For the Commercial system, the manufacturing, installation, and checkout, and operations together with the support concepts is discussed in Section 3.3. Included in this section is a summary of the rate production processes to be followed as a result of studies by A. D. Little, Inc., Cambridge, Massachusetts.

Pilot Plant Plans and schedules are discussed in Section 5. The plans include the following:

- Make or buy
- Manufacturing
- Facilities
- Quality assurance
- Packaging and transportation
- Material
- Installation, checkout, and maintenance
- Support
- Test
- Schedules

Section 2

COLLECTOR DATA LISTS

In accordance with the request for a data and information tabulation, Sandia Laboratories letter dated 11 February 1977, "Central Receiver Solar Thermal Power System Pilot Plant Preliminary Design Report (PDR) Requirements," the following section has been assembled. Tables are presented for all data items, reference is given to the paragraph(s) where the data item is discussed in detail, and for convenience, key information for each data item has been removed from the body of the report and reproduced in this section. This section essentially serves as an index for the kind of data to be found and for the location of the data development in this volume.

2.1 DESIGN CHARACTERISTICS

Collector subsystem design characteristics are listed in Table 2-1. Key data associated with the characteristics are given in Tables 2-2 through 2-7 and Figures 2-1 through 2-6.

Table 2-1
DATA LIST, DESIGN CHARACTERISTICS

	Design Characteristic	Pilot Plant		Commercial Plant		SRE	
		Overview (Figure or Table)	Discussion (Paragraph)	Overview (Figure or Table)	Discussion (Paragraph)	Overview (Figure or Table)	Discussion (Paragraph)
1.	Field Geometry	F2-1, F2-2	4.2.1	F2-3	3.2.1	-	N/A
2.	Field Layout	F2-1, F2-2	4.2.1 Appendix B	F2-3	3.2.1	-	N/A
3.	Field Oversizing to Allow For Dirt on Mirrors, Reliability, Etc.	T2-2	4.2.1	-	N/A	-	N/A
4.	Beam Pointing Accuracy and Error Budget vs Environmental Effects	T2-3	4.2.6	T2-4	3.1.1	T2-3	6.4.2
5.	Heliostat Beam Quality and Error Budget vs Environmental Effects	T2-3	4.2.6	T2-4	3.1.1	T2-3	6.4.2
6.	Heliostat Weight Breakdown	T2-5	4.2, 4.3.6	-	N/A	T2-5	6.4.2
7.	Heliostat Parts Count	T2-6	-	-	N/A	T2-7	-
8.	Foundation and Field Wiring	F2-4, F2-5, F2-6	4.2.5 4.2.10	-	N/A	-	N/A
9.	Nonstandard Parts	T2-6	-	-	N/A	-	N/A
10.	Single Source Parts	T2-6	-	-	N/A	-	N/A
11.	Longlead Items	T2-6	-	-	N/A	-	N/A
12.	Parts Having High Infant Mortality Rates	T2-6	Vol 2 Para 4.10	-	N/A	-	N/A

Table 2-2

FIELD OVERSIZING

Pilot Plant Field Oversizing For:	
Dirt on Mirrors	50 Heliostats
Beam Attenuation	33 Heliostats
Access Raods	12 Heliostats
Field Controller Outage	24 Heliostats
Heliostat Outage	5 Heliostats
Heliostats in Singularity	16 Heliostats

Table 2-3

CLOSED-LOOP TRACKING ACCURACY AND SPILLAGE

	Error Source	Accuracy (mr) Az/El** σ(rms)	Ind. of Wind and Ref Temp	% Spillage (μ)* Winds (M/S) 0	3.5	8	12	Temperature (°C) 0	15	28	35
1.	Tower/Receiver	0.4/0.2	0.1	0	0	0.1	0.2			0.1	
2.	Surface Waviness	1.2/1.2	0.6	0	0	0	0	0	0	0	0
3.	Specular Dispersion	0.8/0.8	0.5	0	0	0	0	0	0	0	0
4.	Surface Bending										
	A. Gravity	0.5/0.5	0.4	0	0	0	0	0	0	0	0
	B. Winds	0.6/0.8	0	0	0	0.2	0.5	0	0	0	0
	C. Temperature	0.6/0.8	0	0	0	0	0	2.6	1.2	0	0
5.	Mirror Alignment	1.0/1.0	0.6	0	0	0	0	0	0	0	0
6.	Control Dynamics	0.8/0.5	0.3	0	0	0.2	0.4	0	0	0	0
7.	Sensor	0.8/1.4	0.4	0	0	0.2	0.5			0.2	

*Note: Spillage does not have a normal distribution
**SRE data has been used to establish these numbers.

Table 2-4

CLOSED-LOOP REFLECTED BEAM ACCURACY
FOR COMMERCIAL PLANT

	Error Source	Azimuth rms (mr)	Elevation rms (mr)
1.	Tower/Receiver	0.9	0.2
2.	Surface Waviness	1.2	1.2
3.	Specular Dispersion	0.8	0.8
4.	Surface Bending*		
	A. Gravity	0.5	0.5
	B. Winds	0.6	0.8
	C. Temperature ($60^{\circ}F$)	0.6	0.8
5.	Mirror Alignment	1.0	1.0
6.	Control Dynamics	0.8	0.5
7.	Sensor	0.8	1.4
	RSS Total	2.5	2.6

*Errors shown are estimates based on Pilot Plant data.
The magnitudes will be updated to reflect the Commercial system.

Table 2-5

HELIOSTAT WEIGHT BREAKDOWN

Collector Element	Pilot Plant	SRE Inverting Heliostat
Reflector (Foam Core Sandwich)	1,227 lb	1,063 lb*
Reflector Structural Support	1,108 lb	889 lb
Drive Unit	670 lb	670 lb
Pedestal	509 lb	509 lb
Total (without foundation)	3,514 lb	3,131 lb
Heliostat Foundation	2.5 yd^3	3.71 yd^3
Beam Sensor Post	159 lb	159 lb
Beam Sensor Foundation	0.78 yd^3	0.78 yd^3

*For SRE inverting heliostat with 1/8 in. + 1/8 in. laminated mirror, the weight is 1,744 lb.

Table 2-6

HELIOSTAT PARTS COUNT, PILOT PLANT

Subassembly	Purchased Parts*	Fabricated Parts	Fasteners	Comments
Reflector Panel	7/Panel 42/Heliostat	4/Panel 24/Heliostat	4/Panel 24/Heliostat	Mirror Glass is Nonstandard
Tracking Mirror	1/Heliostat	9/Heliostat	12/Heliostat	Laminated Mirror and Mirror Glass Nonstandard
Support Structure	1/Heliostat	10/Heliostat	4/Heliostat	
Drive Unit	28/Heliostat	15/Heliostat	55/Heliostat	Drive Assemblies (4 Parts) are Nonstandard. Motors Have Shown Some Infant Mortality.
Pedestal	2/Heliostat	1/Heliostat	-	-
Foundations (Heliostat and Sensor Pole)	-	2/Heliostat	12/Heliostat	-
Beam Sensor	5/Heliostat	4/Heliostat	-	Thick Film Detector and Housing are Nonstandard Parts
Sensor Pole/Mount	7/Heliostat	1/Heliostat	10/Heliostat	-
Heliostat Cabling	4/Heliostat	3/Heliostat	6/Heliostat	-
**Heliostat Controller	60/Heliostat	5/Heliostat	11/Heliostat	Heliostat Controller Will Receive Burn-in Tests to Uncover Components Susceptible to Infant Mortality.
Heliostat Sensor-Elec	82/Heliostat	3/Heliostat	-	
(***Field Controller)	(169/Field Controller)	(1/Field Controller)	-	
Total Parts	239/Heliostat	81/Heliostat	132/Heliostat	

*At present, no single source or long-leadtime components are planned for heliostat usage.
**Includes piece parts, resistors, capacitors, etc.
***Shown for reference, 24 heliostats/field controller.

Table 2-7

HELIOSTAT PARTS COUNT, SRE

Subassembly	Purchased Parts*	Fabricated Parts	Fasteners
Reflector Panel	4/Panel 48/Heliostat	4/Panel 48/Heliostat	4/Panel 48/Heliostat
Tracking Mirror	1/Heliostat	9/Heliostat	12/Heliostat
Support Structure	1/Heliostat	18/Heliostat	68/Heliostat
Drive Unit	28/Heliostat	18/Heliostat	55/Heliostat
Pedestal	1/Heliostat	3/Heliostat	-
Foundations (Heliostat and Sensor Pole)	-	2/Heliostat	12/Heliostat
Beam Sensor	5/Heliostat	4/Heliostat	-
Sensor Pole/Mount	1/Heliostat	2/Heliostat	7/Heliostat
Heliostat Cabling	4/Heliostat	3/Heliostat	6/Heliostat
Heliostat Controller	-	-	-
Heliostat Sensor-Elec	47/Heliostat	2/Heliostat	-
Field Controller	(497/Field Controller)	(4/Heliostat)	
Total Parts	145/Heliostat	113/Heliostat	212/Heliostat

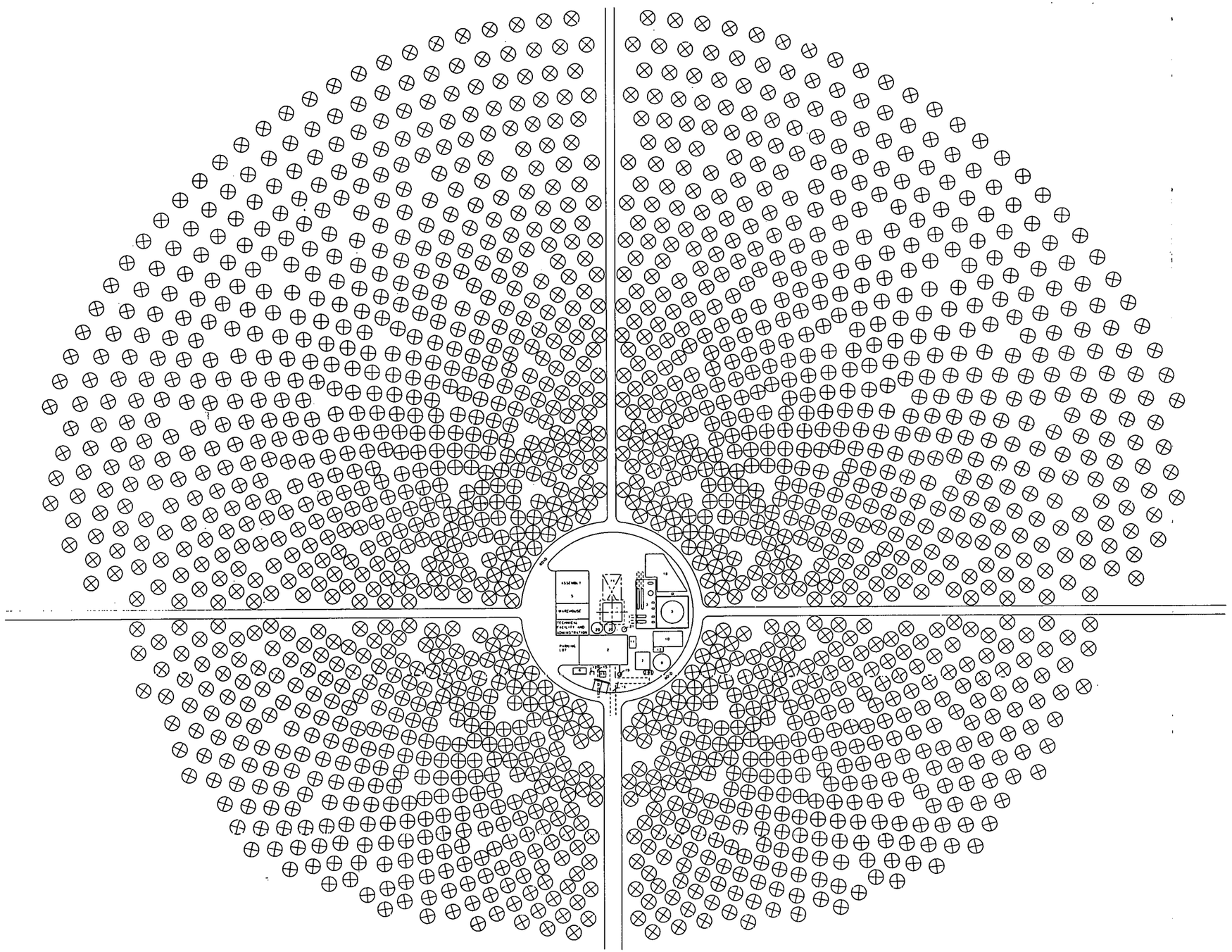

N

0 20 40 60
METERS

GENERAL NOTES

A POWER HOUSE AND AUXILARIES

1 RECEIVER TOWER AND FOUNDATION
2 POWER HOUSE
3 THERMAL STORAGE SUBSYSTEM
4 CONDENSATE STORAGE TANKS
5 ASSEMBLY, AS NOTED
6 DIESEL GENERATOR
7 WATER TREATING BLDG
8 ACID STORAGE TANK
9 LIME SOFTENER
10 CLEARWELL, COVERED
11 SEWAGE UNIT
12 AUX TRANSFORMER
13 MAIN TRANSFORMER
14 RECEIVER PANELS LAYDOWN AREA
15 POWER AND CONTROL CABLE TRENCH
16 BURIED PIPE LANE
17 TREATED WATER AND FIRE PUMPS
18 ROCK-FILLED CATCH BASIN
19 LUBE OIL STORAGE TANK
20 CONDENSATE STORAGE TANKS
21 FUEL OIL TANK

B SOUTH ACCESS ROAD IS 11M (36 FT) WIDE

C EAST, WEST, AND NORTH ACCESS ROADS ARE 5.5M (18FT) WIDE EACH

D ⊗ - HELIOSTAT EXCLUSION CIRCLE

Figure 2-1. MDAC 10 MW Central Receiver Collector Field Layout

HELIOSTAT LOCATION SUMMARY
REPORT FOR CIRCLE NO. 1*

NO.	LOCATION (METERS) (X,Y)	NO.	LOCATION (METERS) (X,Y)
1.	17.74,59.41	14.	-17.74,59.41
2.	28.82,54.89	15.	-28.82,54.89
3.	38.84,48.33	16.	-38.84,48.33
4.	47.4,39.96	17.	-47.4,39.96
5.	54.2,30.11	18.	-54.2,30.11
6.	58.97,19.13	19.	-58.97,19.13
7.	61.55,7.44	20.	-61.55,7.44
8.	59.81,-16.33	21.	-59.81,-16.33
9.	55.56,-27.52	22.	-55.56,-27.52
10.	49.23,-37.69	23.	-49.23,-37.69
11.	41.07,-46.45	24.	-41.07,-46.45
12.	31.38,-53.47	25.	-31.38,-53.47
13.	20.51,-58.51	26.	-20.51,-58.51

*APPENDIX B CONTAINS THE HELIOSTAT LOCATION DATA FOR CIRCLES 1-32 (1760 HELIOSTATS)

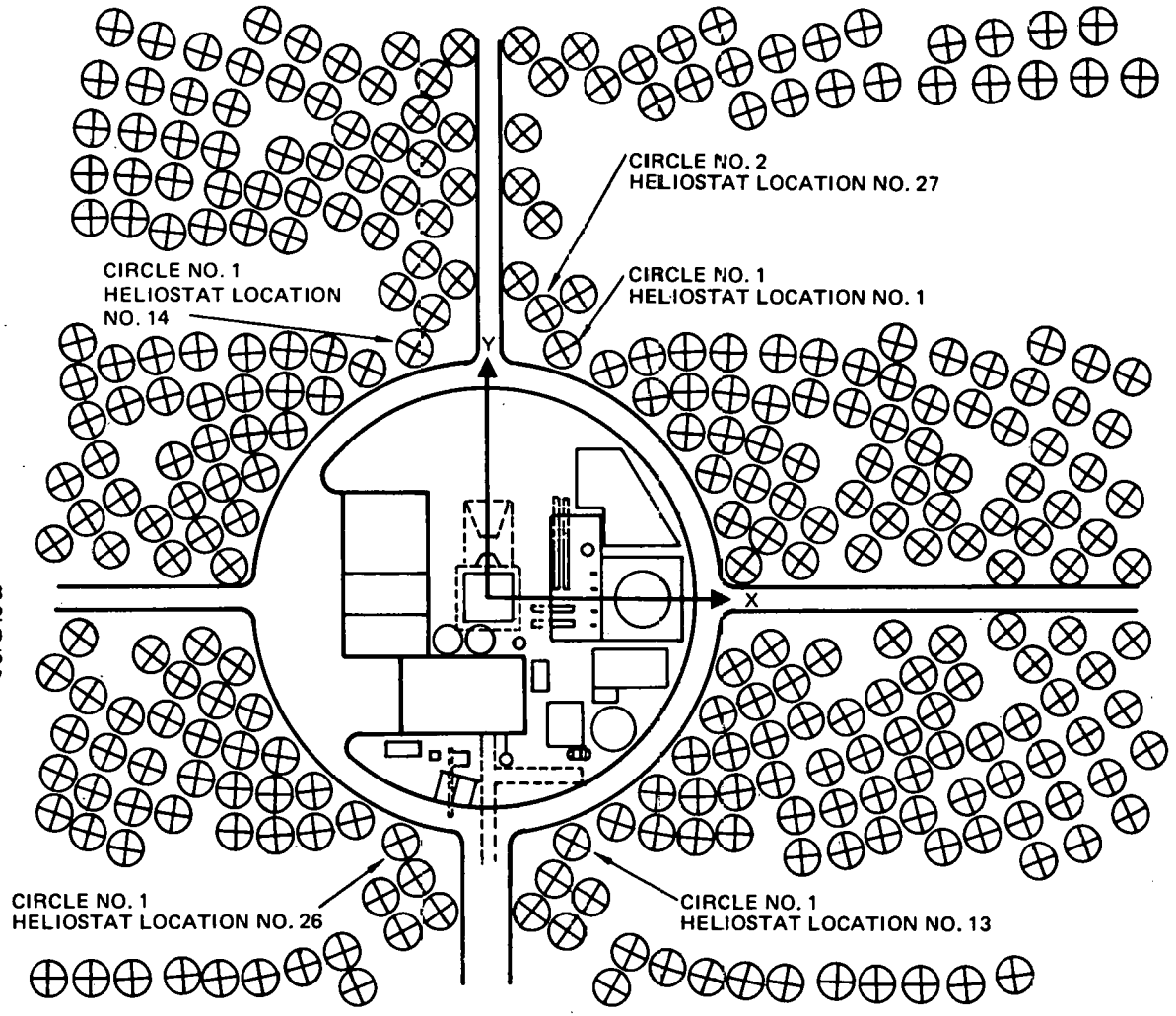

Figure 2-2. Collector Field Layout

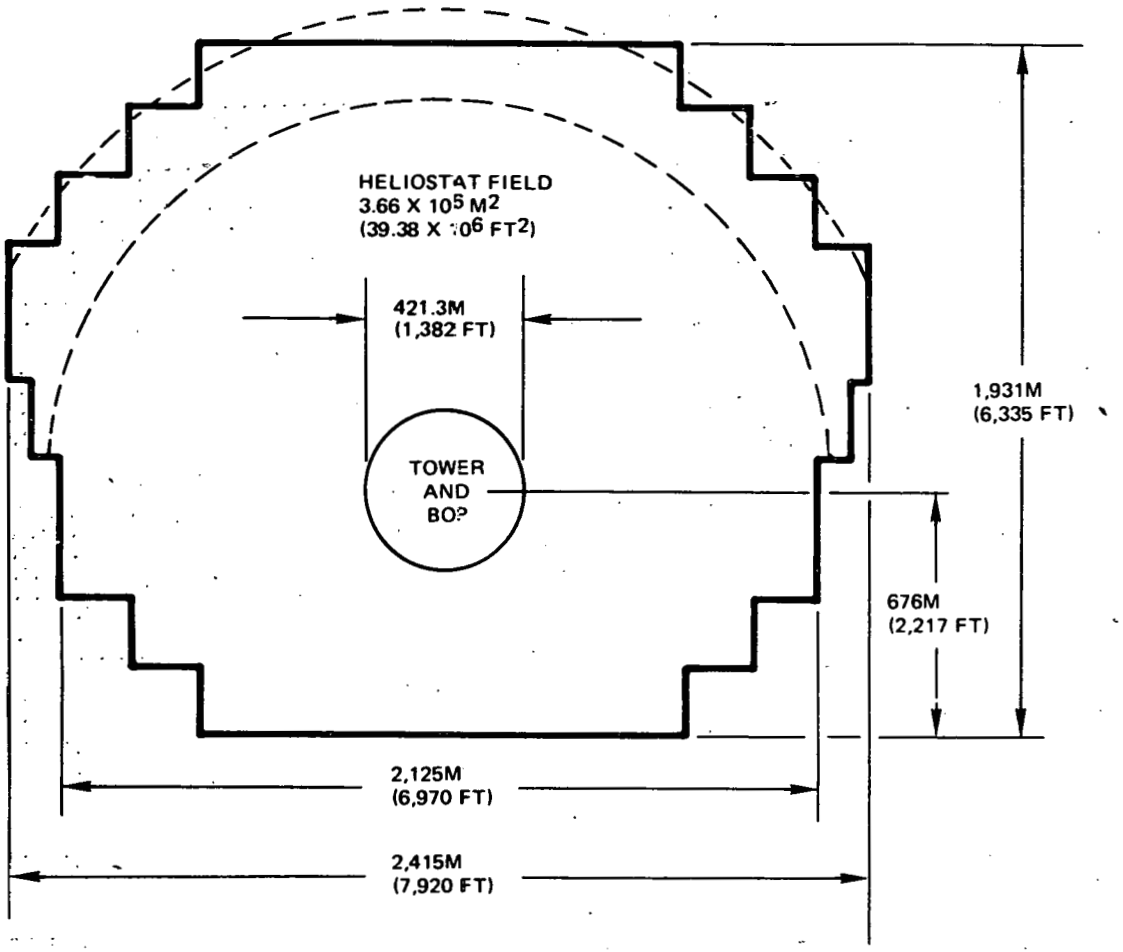

- RADIAL STAGGER ARRAY
- OPTIMUM ANNUAL ENERGY TRIM (BASED ON EARLY COMMERCIAL SYSTEM)
- RECEIVER CENTERLINE ELEVATION 268M (879 FT)
- TOWER TOP ELEVATION 242M (794 FT)
- GLASS AREA 869,586 M^2 (9.36×10^6 FT^2)
- NUMBER OF HELIOSTATS 22,914

Figure 2-3. Commercial System Field Layout

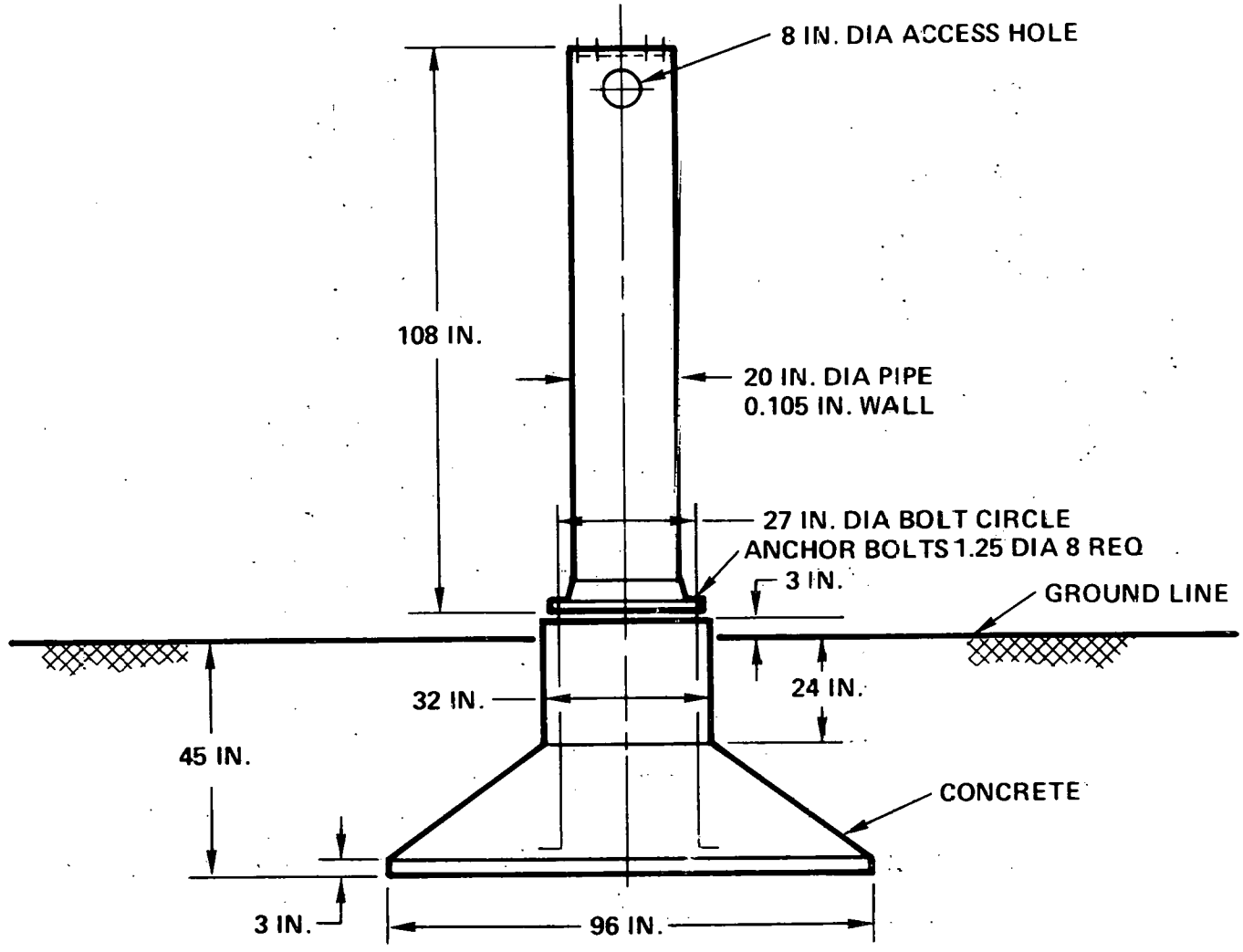

Figure 2-4. Pedestal/Foundation

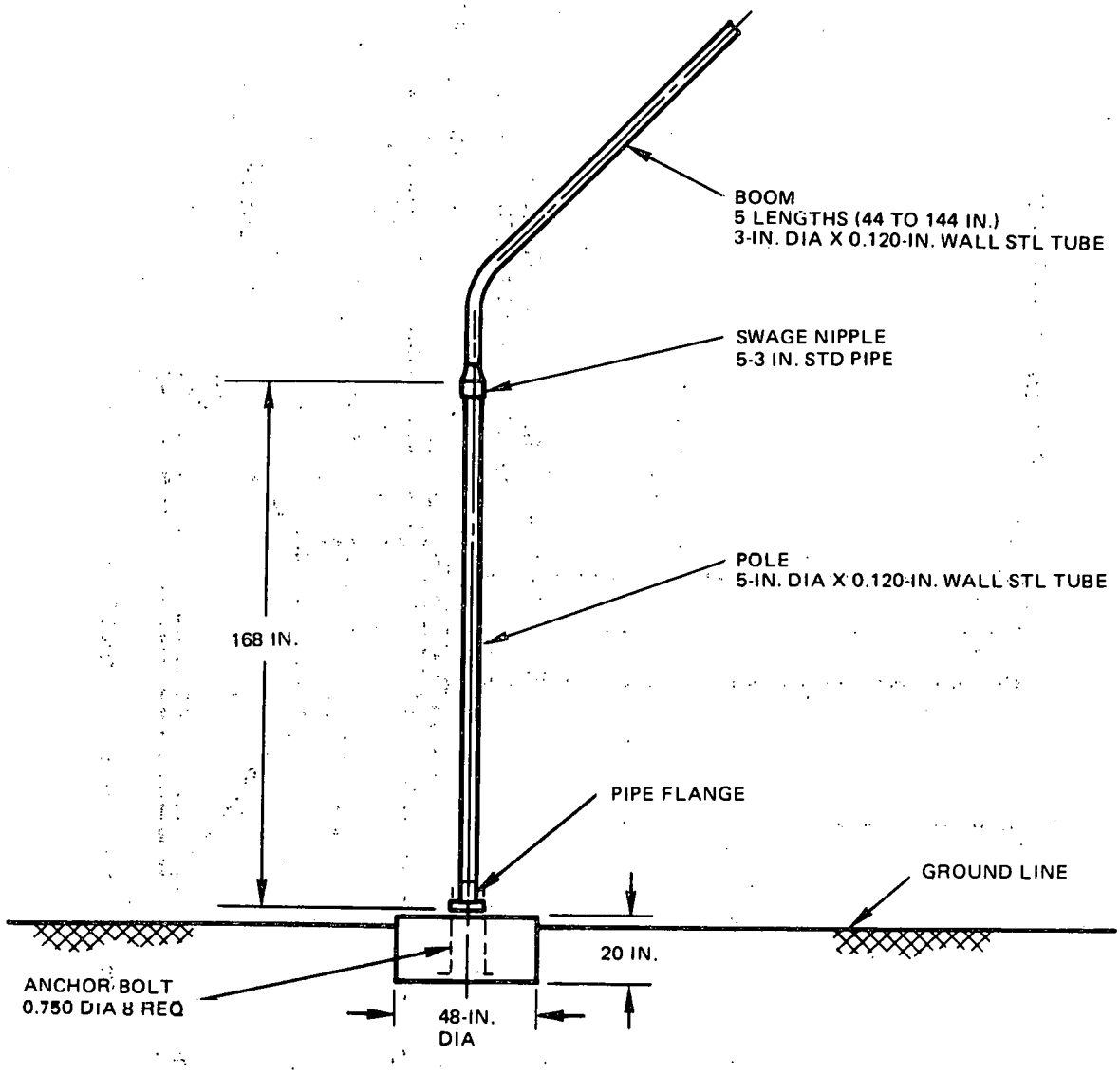

Figure 2-5. Sensor Pole

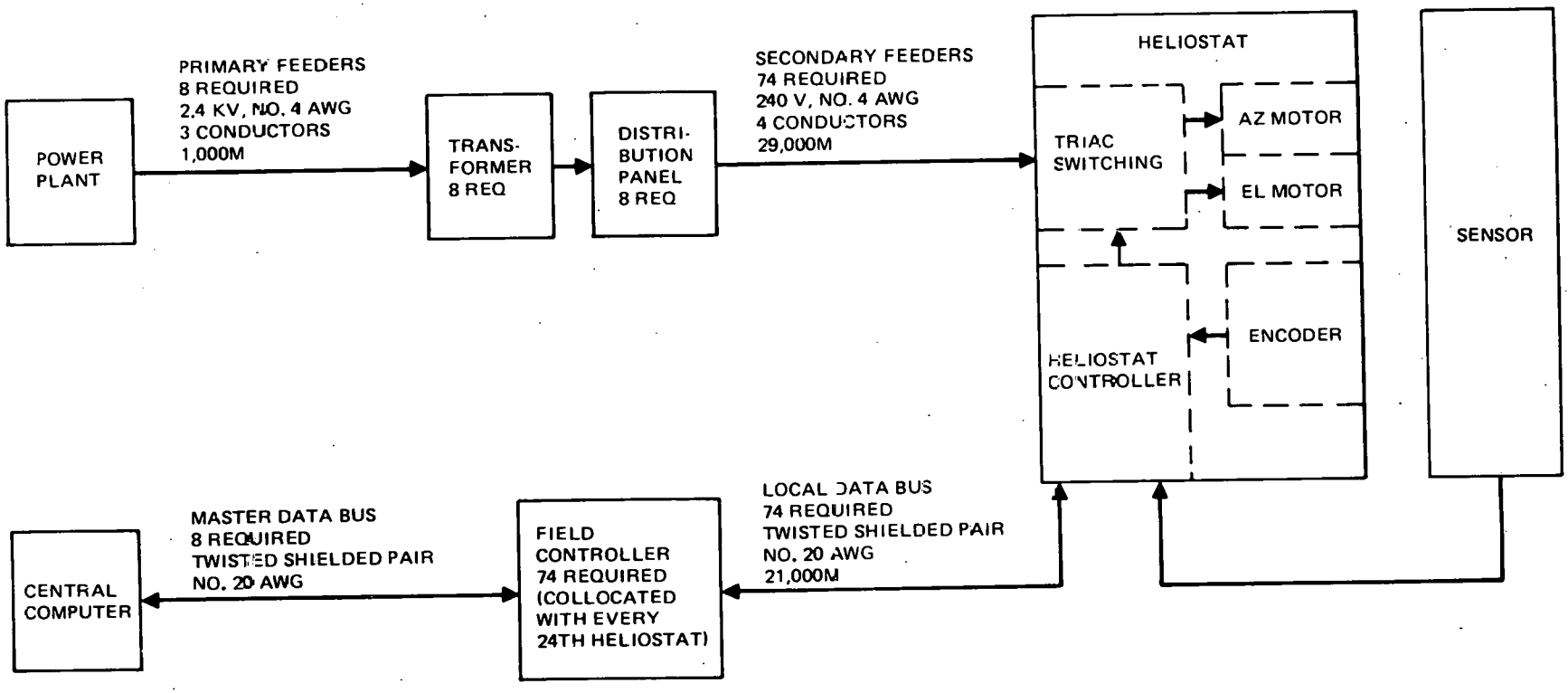

Figure 2-6. Power and Data Distribution — Collector Field Network

2.2 OPERATING CHARACTERISTICS

Collector subsystem operating characteristics are listed in Table 2-8. Key data associated with the characteristics are given in Tables 2-9 through 2-13 and Figures 2-7 through 2-9.

Table 2-8

DATA LIST, OPERATING CHARACTERISTICS

Operating Characteristic	Pilot Plant		Commercial Plant		SRE	
	Overview (Figure or Table)	Discussion (Paragraph)	Overview (Figure or Table)	Discussion (Paragraph)	Overview (Figure or Table)	Discussion (Paragraph)
1. Power Required For Track, Slew, and Emergency Shutdown	T2-9	3.1.4	-	N/A	-	N/A
2. Heliostat Operating Modes	T2-10	4.1.5	T2-10	3.1.5	-	N/A
3. Control System Details and Characteristics	F2-7	4.2.8	F2-7	3.2.3	F2-7	6.2.4
4. Operation and Survival vs Environmental Conditions	T2-11, T2-12	4.1.2	-	N/A	-	Previously Reported
5. Heliostat Focusing and Alignment Procedure	F2-8	5.2.1.2	F2-8	3.3.2.5	-	N/A
6. Maintenance Required	T2-13	5.2.3	-	N/A	-	N/A
7. Mirror Cleaning Method	F2-9	4.2.13	-	N/A	-	N/A

Table 2-9

COLLECTOR FIELD POWER REQUIREMENTS

Operating Condition	Power Required/ Heliostat	Power Required/ Field	Comments
Tracking	15W	~30 KW	
Slew	230W	~400 KW	Az and El will be Slewed Separately. El Will be Slewed First, Az Will be Slewed Only if Necessary
Emergency Shutdown	230W	~235 KW	Approximately 1,000 Heliostats Will be Slewed (In One Axis) At a Time, Outer Heliostats First

Table 2-10

COLLECTOR OPERATING MODES

Mode	Field Controller/ Heliostat Controller	Master Control
Normal Track	Autonomous Operation with Beam Sensor	Provides Reference Data on Gimbal Axis Position
Synthetic Track	Tracks to Gimbal Axis Positions Supplied by Master Control	Provides Gimbal Axis Positions Based On Solar Ephemeris or Tracking Points For Beam Safety
Command Position	Same	Provides Gimbal Axis Positions Based on Master Control Mode, e.g., Stowage, Cleaning, Maintenance, etc.
Local Control at Field Controller	Mobil Test Set Controls Heliostats Through Field Controller	Locked Out
Local Control at Heliostat Controller	Mobile Test Set Controls Heliostat Through Heliostat Controller	Locked Out

Table 2-11

SURVIVAL ENVIRONMENTAL CONDITIONS

Environment	Requirement	Source
Gravity	1 g	--
Ambient Air Temperature	$-30^{o}C$ to $60^{o}C$ ($-22^{o}F$ to $140^{o}F$)	Dept of Energy
Winds:		
1. Maximum Wind Speed Stowed	40.2 m/s (90 mph) with $\pm 10^{0}$ angle of attack	Dept of Energy
2. Align Elevation Axis with Mean Wind Vector	For γ = angle from elevation axis: $\gamma = \pm 25^{o}$ No Damage Any γ No Catastrophic Failures	MDAC
3. Wind Profile	Use Power Law Velocity Profile: $V_Z = V_{10M} \left(\frac{Z}{10m}\right)^{0.15}$	Dept of Energy
Earthquake	0.25g peak (see horizontal and vertical response spectra in Section 3.1.2)	MDAC
Snow/Ice	250Pa (5 psf) snow load 50 mm (2 in.) ice load	Dept of Energy
Hail	Survive at any orientation: 19 mm (3/4 in) at 20 m/s (65 fps) Survive at stowed position: 25 mm (1 in) at 23 m/s (75 fps)	Dept of Energy
Rain	Average annual rainfall = 100 mm (4 in)	Dept of Energy
Dust Devils	With wind speeds up to 17 m/s (40 mph)	Dept of Energy

Table 2-12

OPERATIONAL ENVIRONMENTAL CONDITIONS

Environment	Requirement	Source
Gravity	1 g	--
Ambient Air Temperature	0° to 49°C (32°F to 120°F)	MDAC
Winds:		
1. Wind Speed	11.6 m/s (26 mph) includes 1.3 gust factor	MDAC
2. Wind Speed Frequency	Speed (m/s) / Frequency (%): 0-2 / 29; 2-4 / 21; 4-6 / 19; 6-8 / 14; 8-10 / 8; 10-12 / 5; 12-14 / 3; >14 / <1	Dept of Energy
3. Stowage Initiation Speed	16.1 m/s (36 mph)	MDAC
4. Wind Rise Rate During Stowage	0.01 m/s^2 (1.3 mph/min). Heliostat shall withstand, without catastrophic failure, a maximum wind of 22.4 m/s (50 mph) from any direction.	Dept of Energy
5. Wind Profile	Use Power Law Velocity Profile: $V_Z = V_{10m} (\frac{Z}{10m})^{0.15}$ where: V_Z = mean wind velocity at height Z; V_{10m} = reference wind velocity at height of 10m; 0.15 = power law exponent for flat open country	Dept of Energy

Table 2-13

MAINTENANCE SIGNIFICANT ITEM LIST

Component	Corrective Maintenance	Scheduled Maintenance
Field Controller	Remove and replace on failure. Minor repair on-site. Major repair and overhaul at MDAC.	None
Heliostat Controller	Remove and replace on failure. Minor repair on-site. Major repair and overall at MDAC.	None
Elevation and Azimuth Drive Assemblies	Remove and replace on failure. Repair and overhaul at MDAC.	Lubrication
Elevation and Azimuth Drive Motor and Reducer	Remove and replace on failure. Repair at manufacturer.	None
Elevation and Azimuth Shaft Encoder	Remove and replace on failure. Repair at manufacturer.	None
Elevation and Azimuth Shaft Turn Pick-off	Remove and replace on failure. Repair at MDAC.	None
Pedestal J-Box	Remove and replace detail parts on failure. Remove and replace box for major damage.	None
Pedestal	Structural repair. Remove and replace for major damage.	None
Reflector Panel	Remove and replace. Discard. Clean (in addition to scheduled requirements due to severe weather conditions).	Clean
Reflection Structure	Structural repair. Remove and replace for major damage.	None
Beam Sensor	Remove and replace on failure. Repair at MDAC	None
Sensor Pole	Structural repair. Remove and replace for major damage.	None
Field Cables	Electrical repair. Remove and replace for major damage.	None
Power Distribution Panel	Remove and replace detail parts. Replace panel for major damage.	None
Power Transmission	Remove and replace on failure.	None
Test Support Station	Remove and repair components on failure. Repair components at MDAC.	Calibrate test equipment, inspect, clean, adjust and lubricate CRT/keyboard, tape reader, and recorder

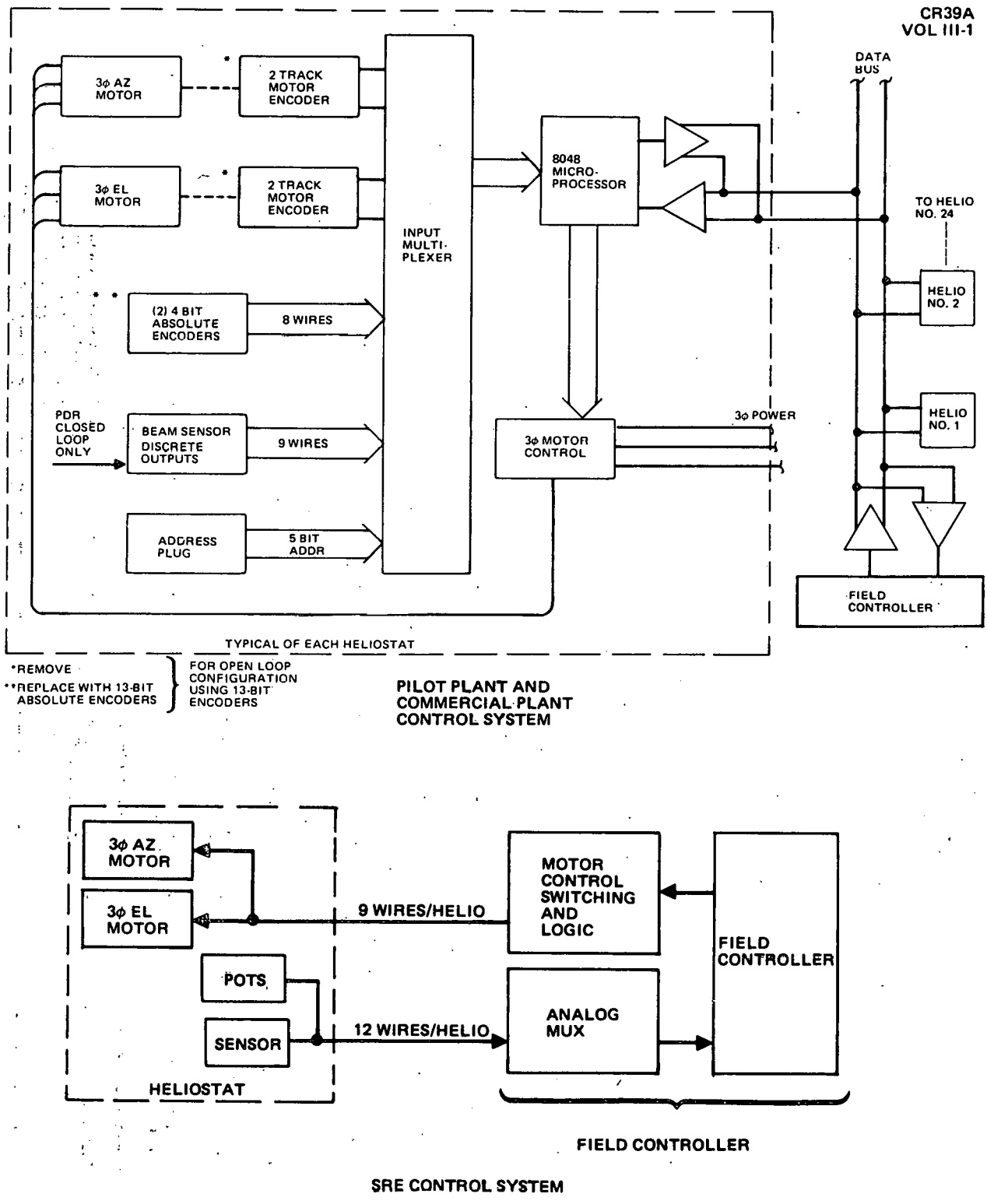

Figure 2-7. Control System Details

PROCEDURE

- SENSOR MOUNTED ON POLE AT PRESCRIBED LOCATION AND ORIENTED ALONG LINE-OF-SIGHT TO RECEIVER ±5 DEG
- HELIOSTAT(S) COMMANDED TO NEAR-TRACK ANGLE VIA MASTER CONTROL/FIELD CONTROLLER
- WORKMAN ON MOBILE LADDER ADJUSTS KNURLED VERNIER ALIGNMENT SCREWS WHILE HELIOSTAT IS ON NORMAL TRACK, AND OBSERVES BEAM MOVEMENT ONTO TARGET
- SPRING-BOLT TIGHTENED AND FINAL ADJUSTMENTS MADE TO ALIGNMENT SCREWS
- HELIOSTAT COMMANDED TO STOWAGE POSITION (RADIO LINK TO MASTER CONTROL)

EVALUATION

- TOTAL TIME ~ 3-6 MIN, 1 MAN TO ADJUST, 1 MAN TO DRIVE MOBILE LADDER
- ALIGNMENT ACCURACY LIMITED BY WORKMAN'S ABILITY TO JUDGE BEAM POSITION ON TARGET. CAN EASILY ADJUST TO WITHIN ± 0.5 FT AT 650 FT, OR ± 0.77 MR, FOR CLEARLY DEFINED EDGE OF BEAM. ALIGNMENT ERROR OF THE ORDER OF ± 1-1.5 MR FOR MORE DIFFUSE BEAM

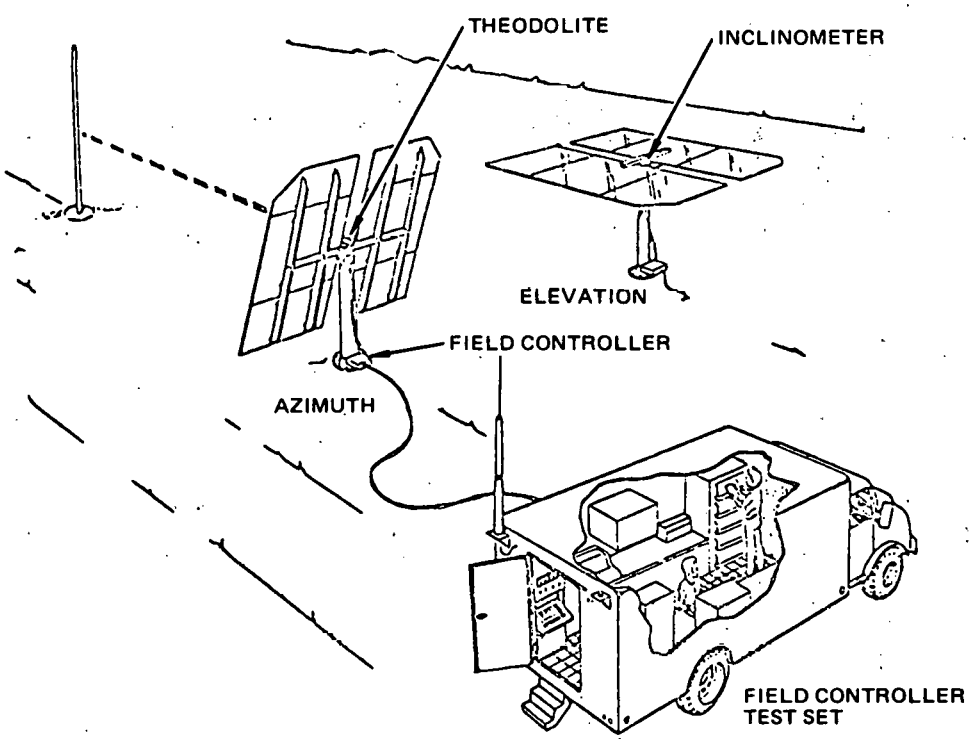

Figure 2-8. Heliostat Referencing

A. WASH WITH CHEMICAL CLEANING SOLUTION

B. RINSE WITH DEIONIZED WATER

C. APPLICATION BY TANKER TRUCK MOUNTED MULTIPLE ARRAY PRESSURE SPRAY NOZZLES

D. WASH AND RINSE SOLUTION RUN-OFF CAPTURED FOR APPROVED DISPOSAL

E. ACCOMPLISH AS SCHEDULED MAINTENANCE AT 30 DAY INTERVALS

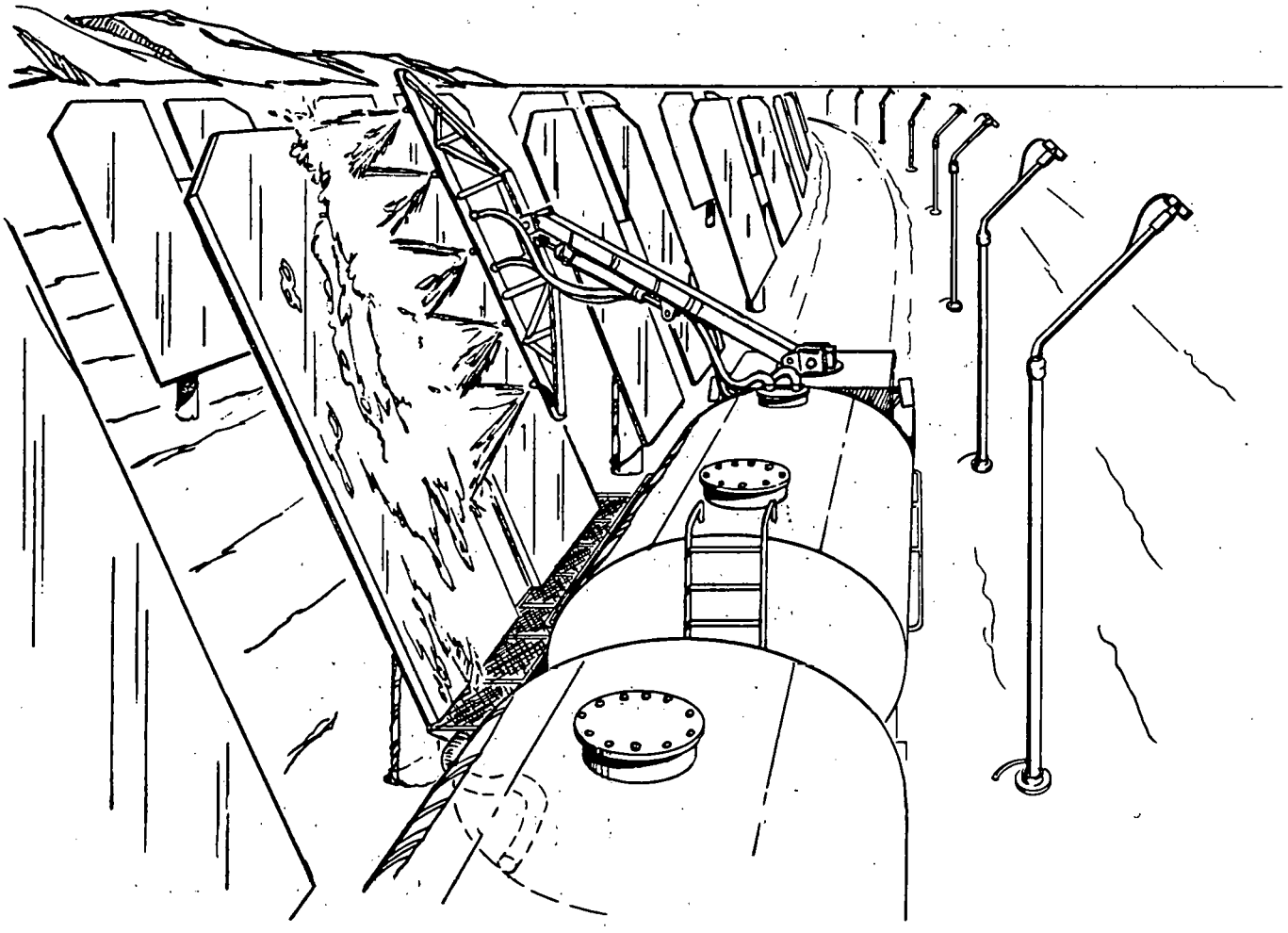

Figure 2-9. Mirror Cleaning Method

THIS PAGE

WAS INTENTIONALLY

LEFT BLANK

2.3 DESIGN DISCUSSIONS

Collector subsystem design discussions items are listed in Table 2-14. Key data associated with the items are given in Table 2-15 through 2-18 and Figure 2-10.

Table 2-14

DATA LIST, DESIGN DISCUSSIONS

	Design Discussion	Pilot Plant		Commercial Plant		SRE	
		Overview (Figure or Table)	Discussion (Paragraph)	Overview (Figure or Table)	Discussion (Paragraph)	Overview (Figure or Table)	Discussion (Paragraph)
1.	Define Mirror Requirements	T2-15	4.2.2	T2-15	4.2.2	T2-15	4.2.2
2.	Discuss Mirror Assembly Details	F2-10	5.1.2.1	F2-10	5.1.2.1	-	N/A
3.	Provide Data on Degradation Rates of Mirrors, Seals, Paint, Motors, Drains, etc.	T2-16	4.2	-	N/A	T2-16	6.4.4
4.	Discuss Method for Safe Control of Reflected Light	T2-17	4.2.11	T2-17	3.1.3	-	N/A
5.	Discuss Fail-Safe Features	T2-17	4.2.11	-	N/A	-	N/A
6.	Discuss Availability	T2-18	4.2.12	-	N/A	-	N/A

Table 2-15

MIRROR REQUIREMENTS

Requirement	Required Value	Expected Value
Reflectivity	0.88	0.91
Specularity (% in 4 mr Cone)	0.99	0.99
Hail Capability		
Any Orientation	19 mm (3/4 in.)	19 mm (3/4 in.)
Stowed	25 mm (1 in.)	>25 mm (1 in.)
Flatness (Standard Deviation)	1.0 mr	1.0 mr
Durability	Units Must Survive Desert Environment for 30 Years Without Significant Permanent Degradation (1% Reflectivity) and Maintain Structural Integrity	

Table 2-16

DEGRADATION DATA

Hardware	Degradation Observed During SRE*
Mirrors	• Reflectivity: Variable and Dependent on Weather Conditions
	• Pin Holes (Sheldahl Acrylic Reflector)
Mirror Edge Seals	• Streaking and Surface Contamination; Water-washed Material From Edge Sealant onto Glass
	• No Deterioration After Exposure to Desert Environment and 500-Hr Salt Spray Test
Paints, Finishes, and Galvanizing	• No Degradation Observed
Motors	• One Burnout: Under Investigation Suspect Water Contamination
J-Boxes, Beam Sensor, Couplings, Pots	• Minor Rust, Dust and Loosening Problems
Cables	• No Degradation Observed

*SRE observed degradations especially those as a result of wind, dust, water, rust, etc will be circumvented by design in the Pilot Plant design.

Table 2-17

FAILSAFE PROCEDURES

Failure Type	Safing Procedure
Loss of EPGS Power	1. Switch to Network Power
	2. Switch to EPGS Auxiliary Power
Loss of Master Control	1. Switch to Backup Master Control
	2. Enter Manual Command from Master Control
Loss of Primary or Secondary Feeder Circuit in Field	Stow with Mobile Test Set Until Repaired
Loss of Control Data Link in Field	Stow with Mobile Test Set Until Repaired
Disabled Heliostat	1. Drive to Stowage with Mobile Test Set Power Supply (Drill Motor)
	2. Opacify with Mirror Opacifier Solution

Table 2-18
COLLECTOR AVAILABILITY ANALYSIS

Item	Component	MTBF (Hr)	MTTR (Hr)	Pilot Plant		Commercial	
				Failures Per Yr	Unavailable Hr/Yr	Failures Per Yr	Unavailable Hr/Yr
1	Transformer	$1.2(10^6)$	7.96	0.02	0.16	0.27	2.15
2	Power Cables to Transformers	$9.3(10^6)$	3.11	0.003	0.009	0.04	0.23
3	Distribution Panels	$2.9(10^5)$	1.51	0.09	0.14	1.2	1.8
4	Field Controllers	$1.2(10^5)$	1.29	2.10	2.7	27.1	35
5	Cables to Field Controllers	$9.3(10^6)$	3.11	0.03	0.09	0.33	1.03
6	Field Controller Junction Box	$2.9(10^5)$	1.84	0.81	1.49	10.8	20
7	Heliostat Controller	$2.1(10^5)$	1.04	27.5	28.6	359	373
8	Cables to Heliostat	$9.3(10^6)$	1.50	1.22	1.80	16.0	24
9	Heliostat Circuit Breaker	$5.7(10^5)$	1.66	10	16.6	129	214
10	Azimuth Drive Motor	$5(10^5)$	2.15	11.6	25.0	151	325
11	Elevation Drive Motor	$5(10^5)$	1.54	11.6	17.9	151	233
12	Azimuth Position Sensor	$8.3(10^5)$	1.62	7.0	11.4	91	147
13	Elevation Position Sensor	$8.3(10^5)$	1.10	7.0	7.7	91	100
14	Azimuth RPM Counter	$7.4(10^5)$	1.33	7.8	10.4	102	136
15	Elevation RPM Counter	$7.4(10^5)$	1.05	7.8	8.2	102	107
16	Azimuth Primary Compudrive	$9.6(10^4)$	2.15	60	129	786	1690
17	Azimuth Secondary Compudrive	$1.3(10^5)$	2.68	44	118	575	1540
18	Elevation Primary Compudrive	$9.6(10^4)$	1.54	60	92	786	1211
19	Elevation Secondary Compudrive	$1.3\ (10^5)$	2.43	44	107	575	1396
20	Sun Sensor	$2(10^6)$	1.12	3	3.36	38	42
21	Mirror Panels	$1(10^6)$	1.12	35	39.2	454	508
22	Pedestal	$10(10^6)$	1.49	0.58	0.86	7.56	11.3
23	Reflector Structure	$2(10^6)$	2.96	2.9	8.58	38	112
24	Sun Sensor Pedestal	$10(10^6)$	1.01	0.58	0.59	7.6	7.6
	Total Failures Per Year			344.63		4498.90	
	Total Failures Per Day			1.04		13.63	
	Total Heliostat Outages Per Day			1.32		17.30	

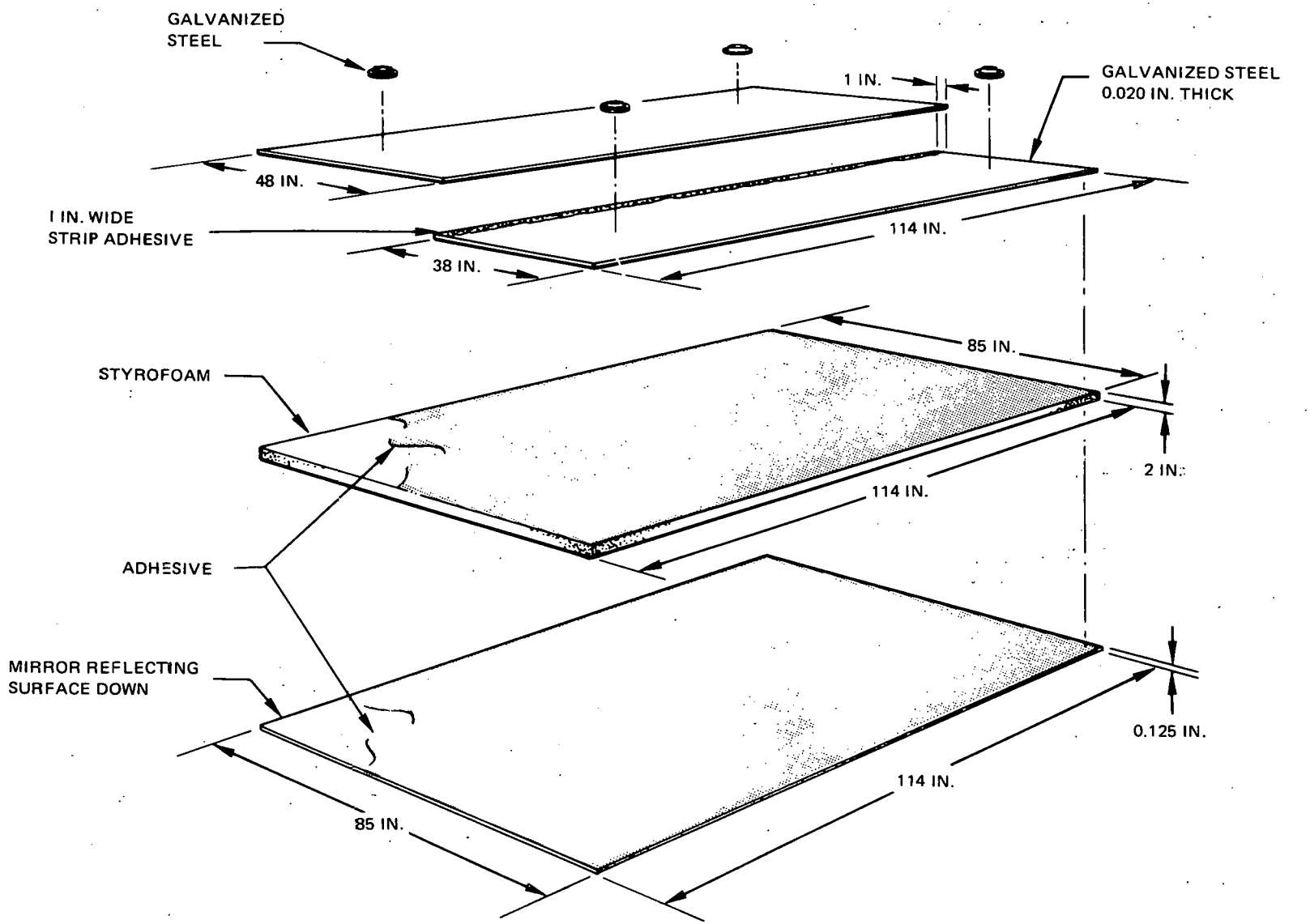

Figure 2-10. Reflector Panel Assembly

Section 3
COMMERCIAL COLLECTOR DEFINITION

The ultimate goal of the central receiver program is to provide an economically acceptable alternative to conventional electrical power. Since the collector comprises the majority of the solar portion of a central receiver Power Plant, MDAC has emphasized the Commercial system design and cost projections. The Commercial system design and requirements both flow down to the Pilot Plant and take precedence over designs and requirements strictly for Pilot Plant.

The collector subsystem for both the Commercial and Pilot Plants was described in Section 1. The discussions of Sections 3 and 4 will focus on the trade studies, analyses, and data which have led to the preliminary design.

3.1 COMMERCIAL SUBSYSTEM REQUIREMENTS

The commercial subsystem requirements are as follows:

- Performance, including the error budget and drive rates (Section 3.1.1).
- Environmental, including operational wind speeds, stowage wind speeds, temperatures and earthquake ground motion histories (Section 3.1.2).
- Safety, including applicable OSHA regulations and beam safety requirements (Section 3.1.3).
- Electronic interface requirements for the heliostat, field controller, and master control (Section 3.1.4).
- Operating, for normal and synthetic tracking; command position, stowage, and maintenance (Section 3.1.5).
- Stowage, dependent upon the environment and wind conditions (Section 3.1.6).

3.1.1 Performance Requirements

The heliostat should reflect the sunlight with combined beam and tracking errors of less than 5 mr standard deviation and concentrate the maximum cost-effective fraction of the sun's light on the receiver in the prescribed distribution. Since the heliostat is the same for the Commercial and Pilot Plant, the accuracy of the reflected beam should be basically the same as the Pilot Plant. The exception to this is the error caused by tower movement and surface bending. An error budget for the Commercial system is given in Table 3-1 for closed-loop tracking. The discussion of each error source is presented in Section 4.2.6. The numbers shown for surface bending are the same as for the Pilot Plant. It should be noted that since the receiver size and the ranges differ from the Pilot Plant, the numbers will change when the analysis is completed.

Computer simulations indicate that for normal tracking, azimuth and elevation rates throughout the field will not exceed 0.26 rad (15 deg) per hour except in a narrow singularity band in the southern portion of the field as depicted in Figure 3-1. The heliostats within this band will experience a temporary degradation of tracking accuracy while driving near singularities, but will regain their normal tracking accuracy within a minute after the high azimuth rate demand has subsided. Current drive unit capabilities are 12 deg per minute in both azimuth and elevation. These rates are adequate to satisfy design requirements during stowage for weather. Although the procedure for emergency defocus has not been defined, the maximum rate capabilities should be adequate to meet this requirement.

The heliostat fundamental vibration frequencies shall be greater than 1 Hz to preclude dynamic coupling with the controls system and minimize wind-induced vibrations. The heliostat and sensor pole shall not undergo flutter or divergence for survival winds up to 40.3 m/s (90 mph).

Table 3-1

CLOSED-LOOP REFLECTED BEAM ACCURACY
FOR COMMERCIAL PLANT

Error Source	Azimuth rms (mr)	Elevation rms (mr)
Tower/Receiver	0.9	0.2
Surface Waviness	1.0	1.0
Specular Dispersion	0.8	0.8
Surface Bending*		
Gravity	0.7	0.7
Winds	0.6	0.8
Temperature (60°F)	0.7	1.0
Mirror Alignment	1.0	1.0
Control Dynamics	0.8	0.8
Sensor	0.7	1.2
RSS Total	2.4	2.6

*Errors shown are estimates based on Pilot Plant data.
The magnitudes will be updated to reflect the Commercial system.

3.1.2 Environmental Requirements

This subsection discusses only the four environmental requirements stipulated by MDAC and their rationales: operational wind speed, stowage wind speed, operational temperature range, and earthquake. The following environmental requirements were given in the ERDA specification (Ref: 3.1.2-A and 3.1.2-B) and previously itemized in Tables 2-11 and 2-12: wind speed frequency, wind rise rate, survival wind, wind profile, survival temperature range, rain, hail, snow/ice loads, and dust devils.

Reference 3.1.2-A TWX from A.C. Skinrood, Sandia Laboratories, "Clarification of ERDA Letter-Pilot Plant Site Parameters," 11/9/76.

Reference 3.1.2-B Letter from A.C. Skinrood, 1/14/77.

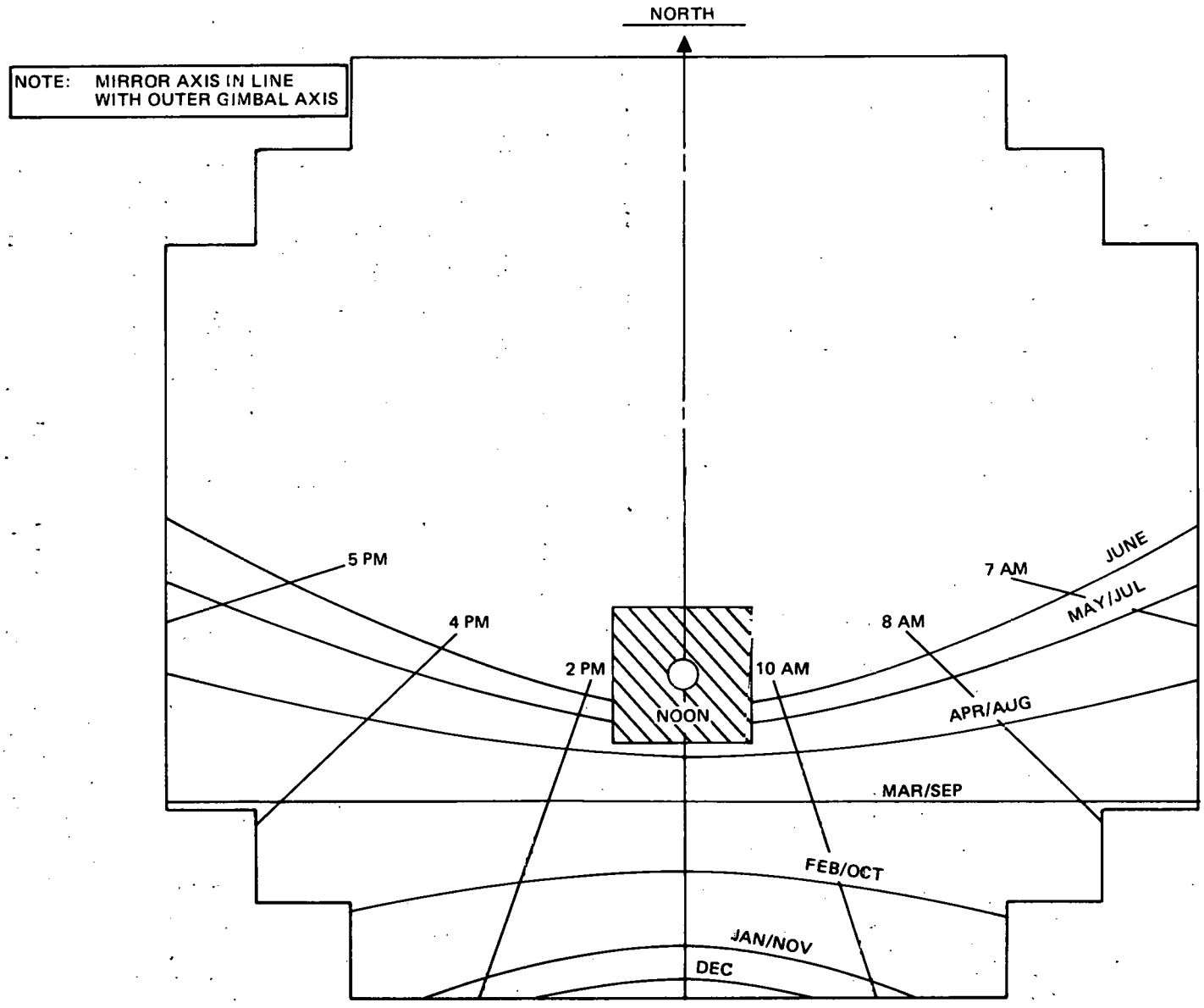

Figure 3-1. LOCI of Pole Positions for Azimuth/Elevation Gimbal

3.1.2.1 Operational Wind Speed Derivation

The operational wind speed of 11.6 m/s (26 mph) was derived to minimize the overall cost of electricity production. A detailed study was made of weather data from 12 southwestern desert military installations. The data were procured from the National Climatic Center in Ashville, North Carolina, and cover 16 to 32 years of continuous observation. The locations of the stations are shown in Table 3-2, together with the time span of observations and the site elevations.

The wind speed frequency of occurrence for NWC and the composite of the 12 stations are shown in Figure 3-2. These stations show an infrequent occurrence of wind speeds in excess of 14 m/s (30 mph).

The higher wind velocities usually result from the passage of frontal systems and may, therefore, be statistically correlated with cloudiness. In addition, the higher wind velocities are certain to be statistically correlated with haze from atmospheric dust. Hence, one should expect that shutting down the collector due to high winds at a wind speed of 14 m/s will lead to an extremely small loss of solar direct beam insolation, rather than the 1 to 2% indicated by Figure 3-2. The Aerospace Corporation performed such an analysis for Inyokern and Edwards Air Force Base for the years 1962 and 1963 (Reference 3.1.2-C). The resulting correlation is shown in Figure 3-3. The figure shows the percent of the total annual direct beam insolation which is not collected as a result of shutting down the collector field at a specific wind speed as a function of the wind speed. As expected, there is no reason to continue to operate the collector for wind speeds beyond 14 m/s. In the past, MDAC has used the single-point design wind speed of 11.6 m/s (26 mph) at which we meet our operational performance requirements. To calculate the beam errors, the worst combination of wind, temperature, and gravity was used. This approach led to a conservative design and questions as to the actual mirror performance. Another single-point design approach is to use a representative desert environment (like for Inyokern) of a 3.5 m/s (8 mph) wind speed and a temperature of 28°C (82.6°F)

Ref. 3.1.2-C: Aerospace Corporation report ATR-74(7417-16), Solar Thermal Conversion Mission Analysis, Vol 1, January 1975.

Table 3-2

WEATHER STATIONS

Station	Location	Years Observation	Elevation (m)
1. Naval Weapons Center	Indian Wells Valley, CA	20	760
2. Edwards AFB	Western Mojave Desert, near Mojave, CA	19	770
3. George AFB	Western Mojave Desert, near Victorville, CA	17	960
4. Yuma	Arizona, SW corner adjacent to California border	24	65
5. Luke AFB	Phoenix, AZ, SW central portion	28	370
6. Williams AFB	Chandler, AZ ~45 km ESE of Phoenix	26	460
7. Tucson	South central Arizona	24	85
8. Fort Huachuca	SE Arizona near Mexican border, ~100 km SE of Tucson	16	1,570
9. Kirtland AFB	Albuquerque, NM, west central NM	32	1,780
10. Holloman AFB	Alamogordo, NM, south central NM	21	1,360
11. Walker AFB	Roswell, NM, SE New Mexico	26	1,220
12. Cannon AFB	Clovis, NM, east central NM adjacent to Texas border	21	1,430

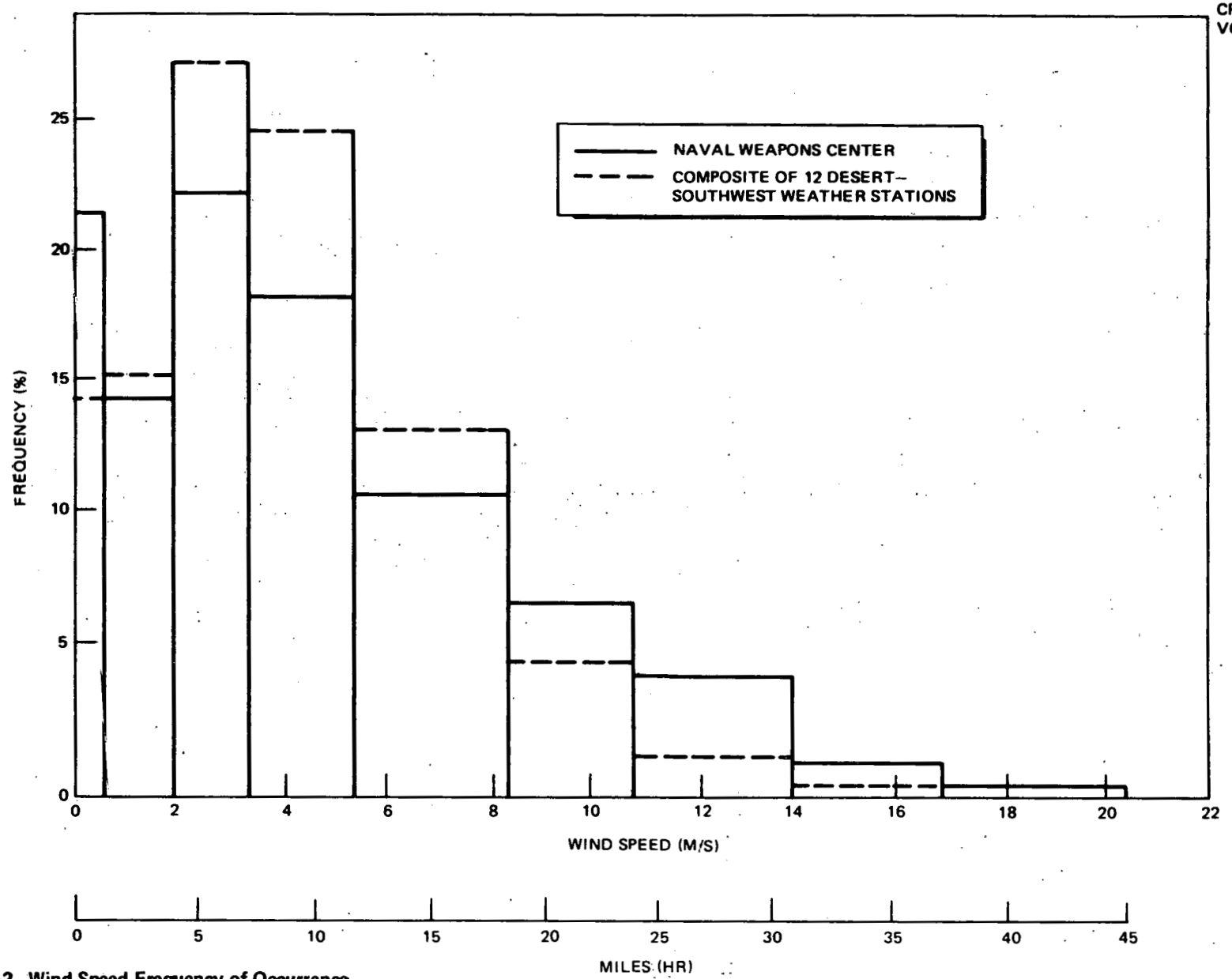

Figure 3-2. Wind Speed Frequency of Occurrence

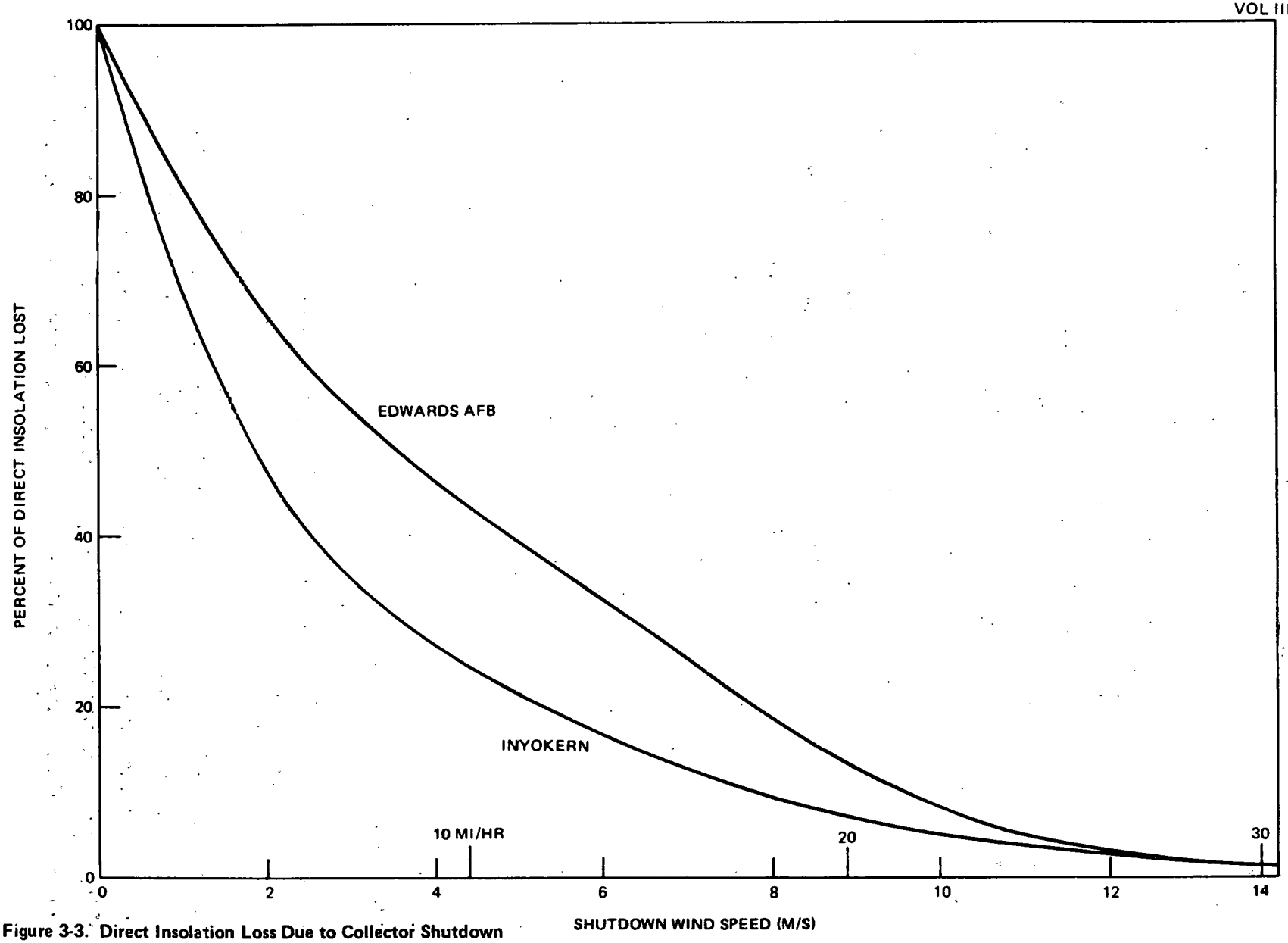

Figure 3-3. Direct Insolation Loss Due to Collector Shutdown

A better approach is to use a wind speed frequency histogram (such as given in Table 2-12) and calculate the annual power loss at the receiver. Section 4.2.6 gives preliminary MDAC results of such power loss calculations due to various effects such as wind and temperature.

3.1.2.2 Stowage Wind Speed Derivation

The stowage initiation speed is 16.1 m/s (36 mph), based on a tradeoff between loss of direct beam insolation and heliostat cost. Figure 3-4 shows the percentage of direct beam insolation lost as a function of stowage initiation wind speed (or shutdown wind speed).

The value of a percent of direct beam insolation loss is increased by the fact that the entire plant is shut down by the heliostat shutdown; i.e., 1% direct insolation loss corresponds to 1% loss of total annual energy. The collector is 60% of the total plant cost, so a 1% loss of direct beam insolation results in an effective 1.67% equivalent cost increase for the collector. The cost impact based on preliminary design baseline report costs is $0.01 \times 126.5 \times 10^6 + 23,800 = \$53$/heliostat or $13¢/ft^2$.

The loss of operating revenue associated with the cost impact may be estimated at 18% of capital cost, or $2.35¢/ft^2$/year/percent of loss of direct beam insolation. This value is traded against the heliostat cost for different initiation of stowage wind speeds.

The cost of the drive unit depends primarily on the torque loads encountered during stowage. The annual cost of the drive unit equivalent to the loss of revenue is found by assuming an 18% levelized fixed charge. Hence, the annual cost is the drive unit cost times 0.18 and divided by the reflector area, $38.0 m^2$ ($408.3 ft^2$).

The annualized drive unit cost is added to the cost of the loss of revenue resulting from the loss of direct beam insolation. The minimum of this sum represents the optimum wind speed for initiation of stowage. The dependence of the total cost on wind speed is shown in Figure 3-5 for Naval Weapons Center, Williams AFB, and the average of 12 desert southwest stations.

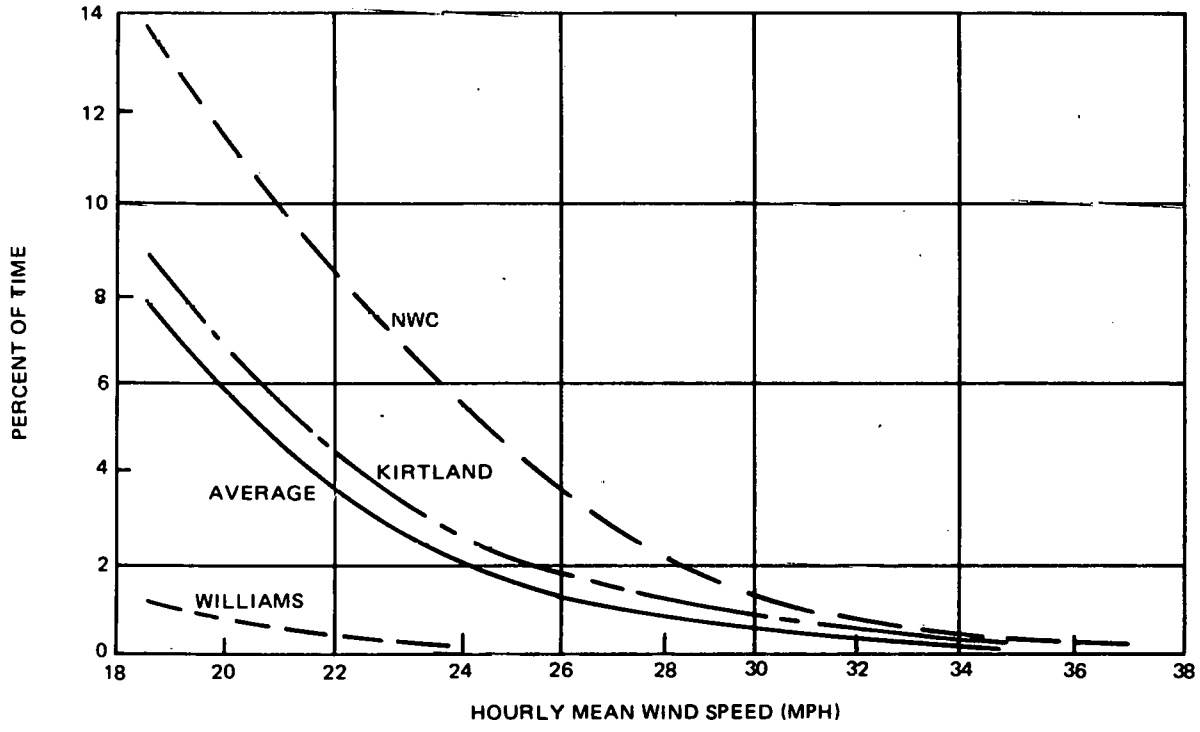

Figure 3-4. Loss of Operating Time for Shutdown Wind Speeds

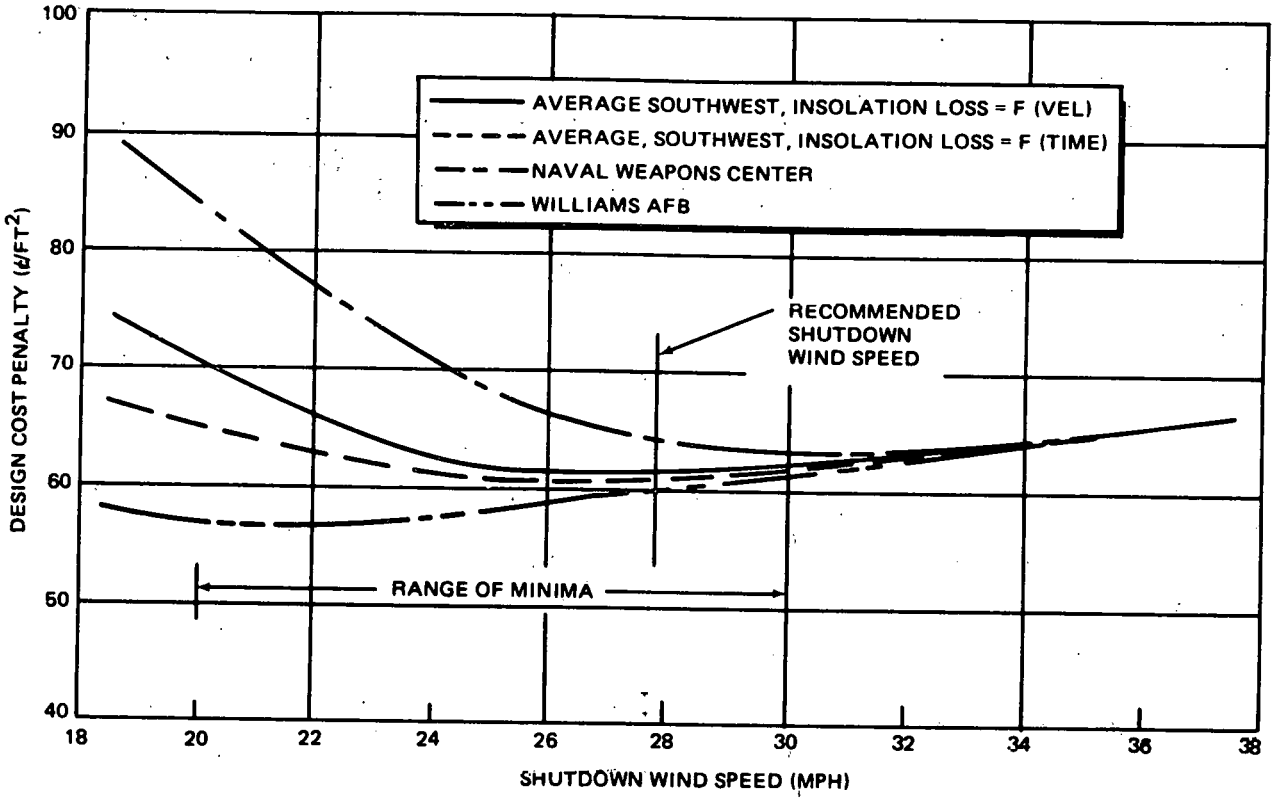

Figure 3-5. Design Cost Dependence on Shutdown Wind Speed

Both assumptions of the correlation of direct beam insolation with wind speed are shown for the average curve.

The curves of Figure 3-5 show rather broad minima and reflect the site dependence expected. However, a representative wind speed for shutdown can be selected in the range from 8.9 m/s (20 mph) to 14.3 m/s (32 mph) without unduly penalizing the design at any site. MDAC has selected 12.4 m/s (27.7 mph) as a nominal design point. The peak wind-gust speed for stowage initiation is 16.1 m/s (36 mph).

3.1.2.3 Operational Temperature Rationale

A study of temperature data from several sites in the southwestern US indicates that the average daylight temperatures are not as extreme as -20°C to 60°C (-4°F to 140°F), the original specified requirement. Figure 3-6 shows the mean daylight temperatures for the hot and cold extremes. Based on these data, an ambient air temperature range from 0°C to 49°C (32°F to 120°F) was selected for operating the heliostats.

3.1.2.4 Earthquake

The earthquake environment is described in Table 3-3 and Figures 3-7 and 3-8. The environment is given in terms of response spectra and ground motion histories for soft rock or firm sediment. If the subsystem is located on hard rock, the above environment may be reduced by 33%. If the subsystem is located on soft sediment, the above environment will be increased by 50%. The response spectra or ground motion histories were used as input to the analytical model of the soil and heliostat or sensor pole in both vertical and horizontal directions to assess earthquake-induced loads. The MDAC heliostats were analyzed for a level of 0.33g peak, slightly higher than the 0.25 g specified in Table 2-11.

3.1.3 Safety Provisions

The safety requirements or criteria for the 10MW Commercial collector subsystem include the conventional industrial safety and the special safety problems associated with a solar thermal power plant.

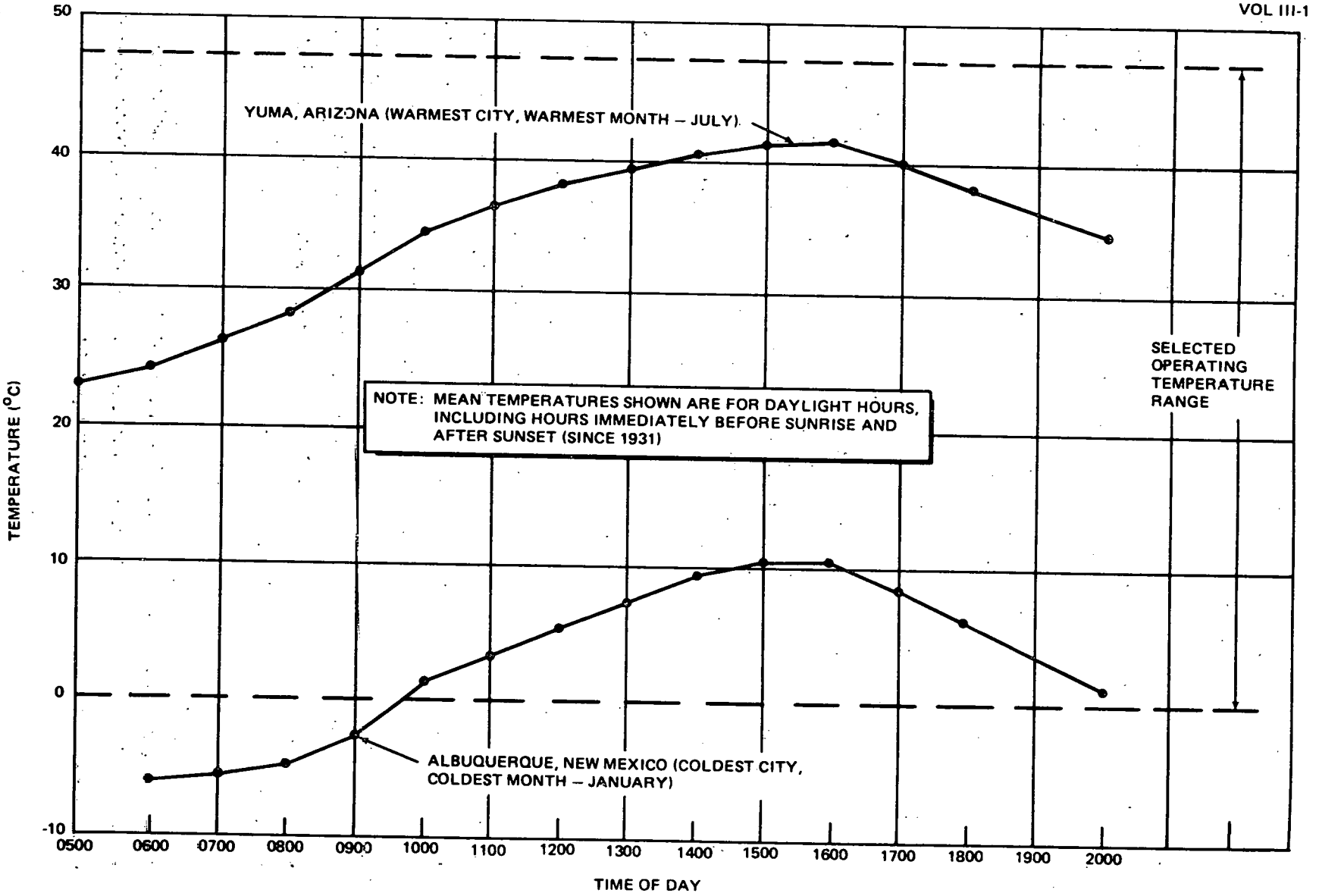

Figure 3-6. Rationale for Operating Temperature Range of Collector Subsystem

Table 3-3

EARTHQUAKE HORIZONTAL GROUND MOTION HISTORIES

Location	Year	Component	Scale Factor*
El Centro	1940	NS	1.0
El Centro	1934	EW	1.4
Olympia	1949	N10W	1.4
Taft	1952	S69E	1.7

*Each ground motion history is to be multiplied by the indicated scale factor.

The applicable Federal OSHA and the California OSHA regulations will apply as discussed in Volume II, Section 4.10.3. In addition, other safety codes such as Sections 70 (National Electric Code) and Section 78 (Lightning Protection Code) of the National Fire Protection Association (NFPA) and the American National Standards Institute (ANSI) Code No. ANSI-C2, the National Electrical Safety Code, are also applicable.

Specific potential safety problems unique to a solar thermal plant include the fact that the heliostats are under either remote control from the central computer or in a closed-loop mode and, therefore, can move in a vertical or azimuthal direction without notice. Therefore, when maintenance is being performed on an individual heliostat, the heliostat must be in a local manual control and the remote control and the closed-loop control must be locked out in a positive manner.

There are many specific safety design criterion that will be applied to the electrical and electronic components of the heliostat and field controllers, including criterion on cables and connectors, test points, controls, insulations, circuit breakers, and grounding. These criteria would be listed in detail in a Safety Design Criteria document.

The major safety problem associated with the collector subsystem is the concentrated solar beam from individual or multiple heliostats. The potential

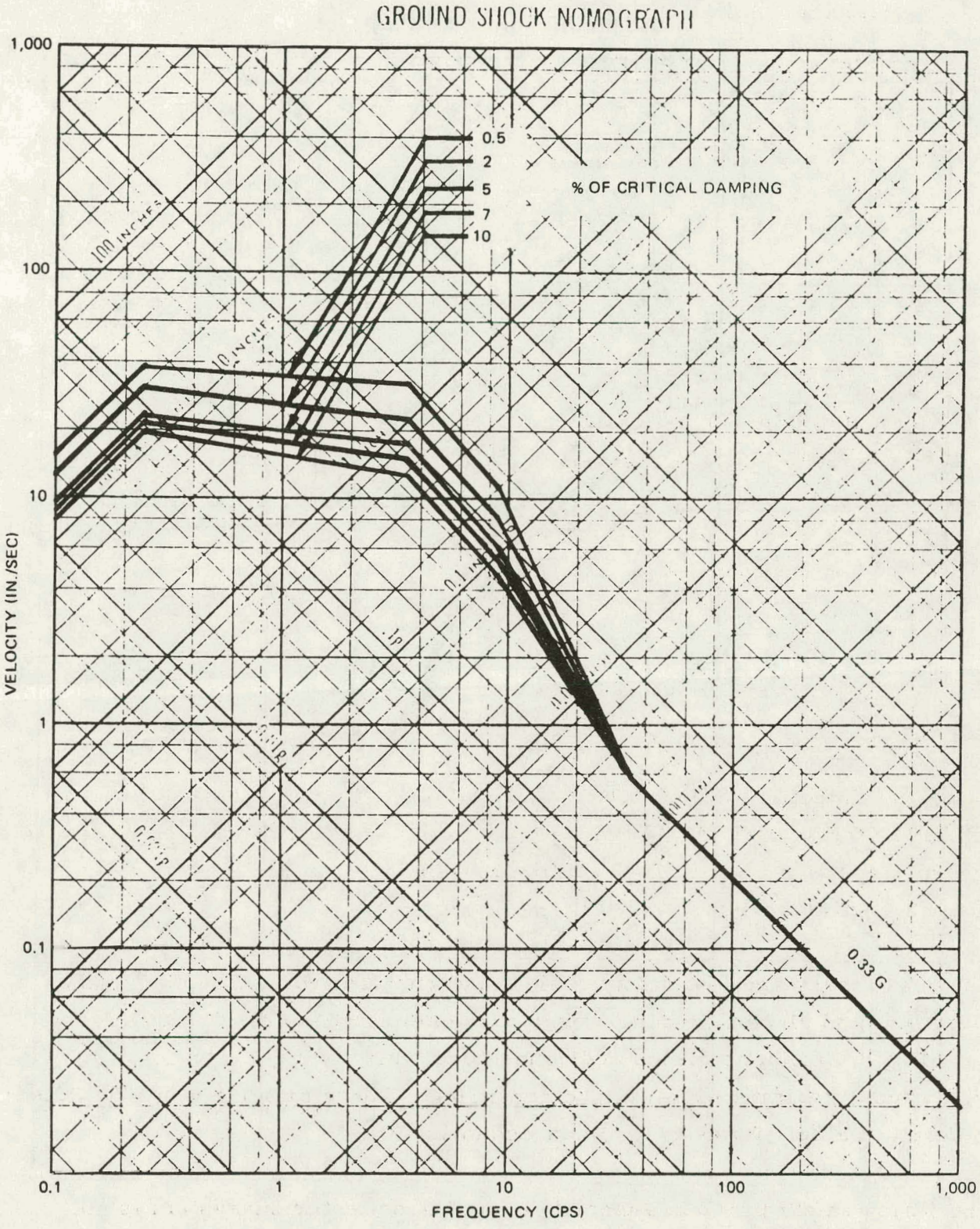

Figure 3-7. Earthquake Horizontal Response Spectra

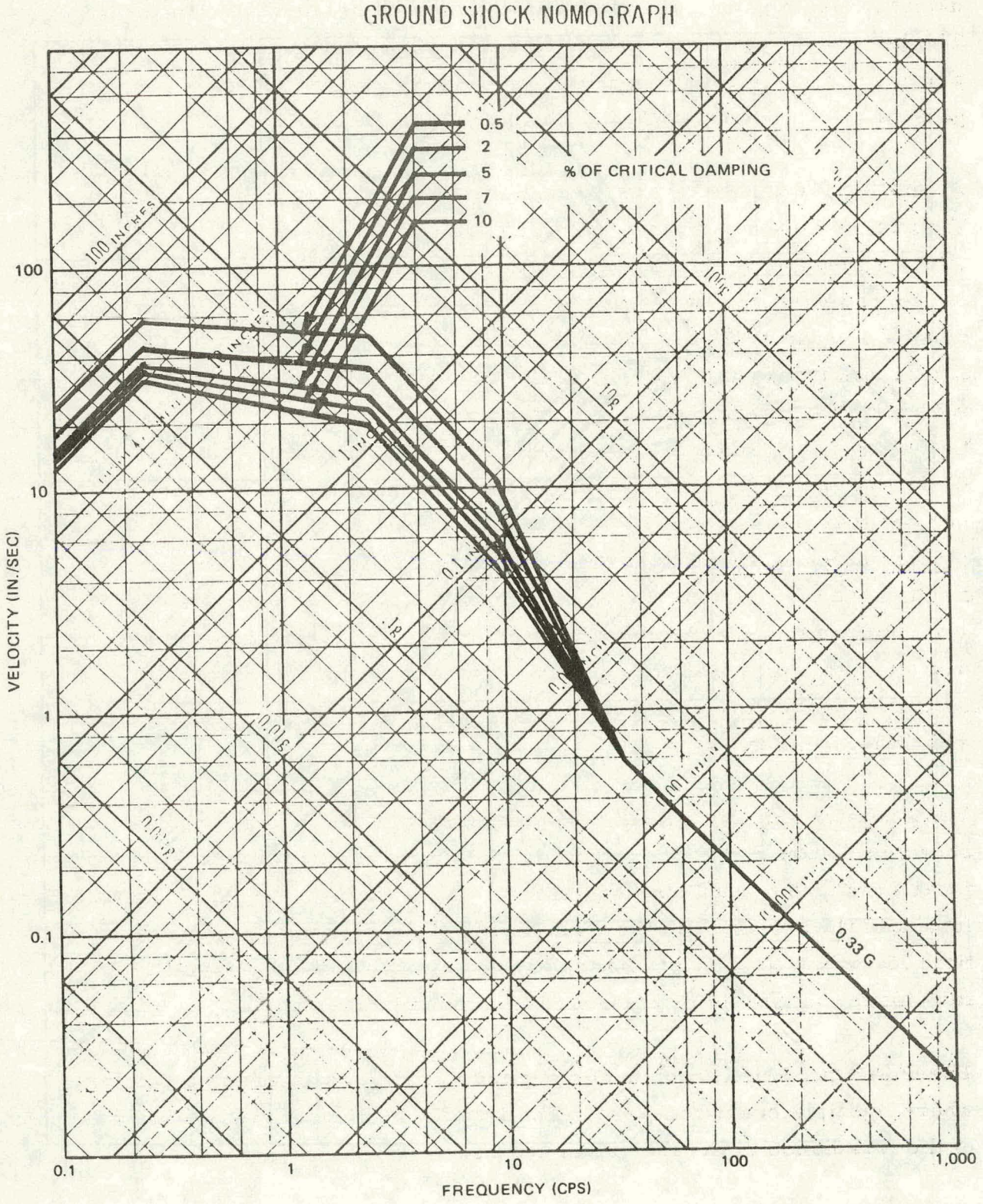

Figure 3-8. Earthquake Vertical Response Spectra

hazards from these beams include injury to the eyes and skin of personnel, damage to equipment, distraction due to eye glare, and possible brush fires. The hazards to personnel can be to personnel on the ground (both operating personnel and the general public) and to members of the public in aircraft, gliders, etc above the collector field.

A detailed discussion on the damage mechanism to personnel is given in Volume II, Section 4.10.3. The discussion in Volume II showed that the damage mechanism to the eye is retinal burns caused by a temperature rise on the retina. The amount of temperature rise is a function of the power density and the size of the retinal image. For example, the incident retinal irradiance (power density) due to the sun is a maximum of about 7.9 W/cm^2 with a retinal image size of 158 micrometers. These retinal parameters due to looking at the sun can be dangerous but the normal inherent mechanisms of the eye (blink reflex, etc) protect the eye and allow us to live safely in our one-sun atmosphere. The incident retinal irradiance which results from a person looking at the reflection of the sun in the MDAC Commercial heliostat is the irradiance of the sun reduced by the reflectance of the heliostat mirror, or about 7.22 W/cm^2. The retinal image size will be the same as the image size for the sun. Therefore, the solar beam from an individual MDAC Commercial heliostat is of a lesser magnitude than the sun and therefore is safe.

The potential skin damage is also discussed in Volume II and the results are shown in Figure 3-9. The maximum theoretical skin irradiance (at the focal point) from one Commercial heliostat is about 0.1 W/cm^2, or a little less than the irradiance of the sun as shown on Figure 3-9. The threshold time for injury at this irradiance varies strongly from individual to individual, but should be measured in many minutes.

There is a potential problem if equipment or personnel are in a position where multiple beam converge. The irradiance of multiple beams is the sum of the irradiance of the individual beams.

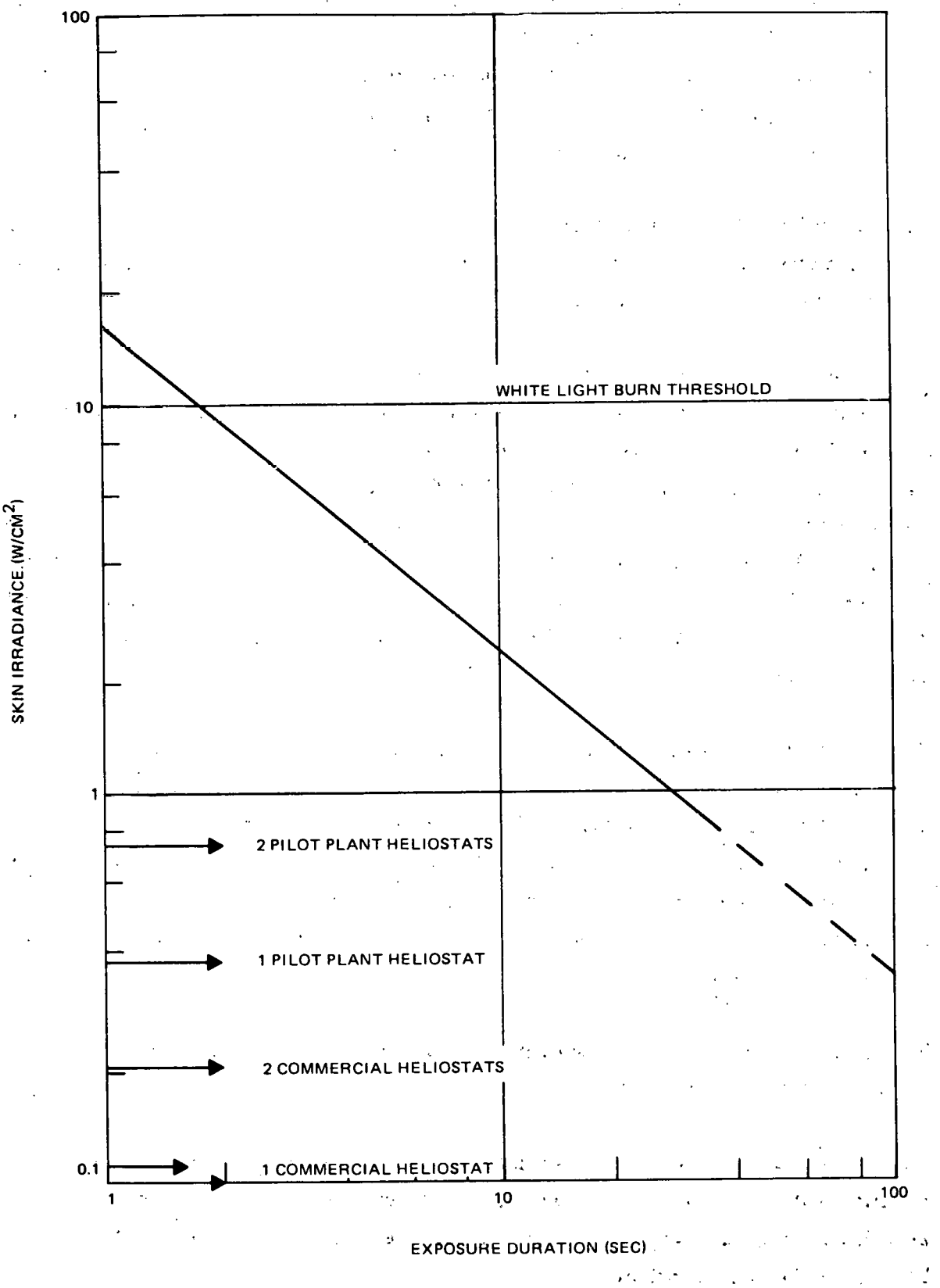

Figure 3-9. Pig Skin Injury Data

The potential problems include:

A. Personnel or equipment situated at a point on the ground where multiple beams intercept

B. The possibility that an aircraft (or glider or balloon) will appear at a point above the collector field and intercept the solar beam from a number of heliostats.

Either or both of these can occur during normal operations as the heliostat field is activated or deactivated, during heliostat storage operations, or as a result of heliostat failures.

When the collector field is activated in the morning (or after a cloud passage) and deactivated in the evening, the heliostats will be controlled by the master control in such a way that the focus point of the several heliostats will move in a controlled and safe manner. For example, the focus point can be designated as a point on the ground (in a personnel exclusion area) and then moved to the receiver on a path which does not intercept any equipment. This should preclude any hazards to personnel equipment (on brush) on the ground. However, there will be a volume of airspace where a potential hazard will exist.

The potential problem is during heliostat storage. If the heliostats are stored face down, there is no possibility of a reflection of the sun. The only possibility of a potential problem when the heliostats are stored in a vertical position is when the sun is at a zero degrees elevation and at that time the irradiance is very low. A study of storage in a face-up position showed that the maximum solar irradiance, under any condition, from one heliostat is 0.1 W/cm^2 or about 1 sun.

The effect of one heliostat with this solar magnification was shown to be safe in the discussion above.

As stated above, there is no established criteria for the maximum permissible exposure (MPE) to visible light. In lieu of a specific criteria or standard, it would appear that the airspace above the collector field should be safe under all conditions.

It is possible for a heliostat failure condition to produce a situation where two or more heliostats will have a common focus point. The failure probability for one heliostat is about 5.9 (10^{-5}) per hour as discussed in Section 4.2.12. The longest repair time for any heliostat is about three hr (Table 4-33). If two heliostats are about 10 heliostats apart, we can assume that they are independent from a retina image standpoint. This means that there are about 64 heliostats which would be dependent. The probability of two simultaneous failures (within the repair time) is about 7 (10^{-5}). This must be multiplied by the probability that both heliostats would fail in such a way that both beams are pointed at the same spot (1×10^{-5}) and the probability that someone would be in this spot at that time. It can be seen that this probability is at least less than 7×10^{-12} and thus extremely low.

The analysis has shown that there are no hazards to ground-based personnel which cannot be controlled by proper procedures and that there are no hazards above about 1,000 ft. Both conclusions are subject to further analysis and the acceptance of an MPE for visible light. Redundancy field power and control wiring is not required because of the low probability of injury due to multiple failures.

3.1.4 Interface Requirements

The collector subsystem interfaces directly with the receiver subsystem, via the reflected solar beam, with the EPGS subsystem, for electric power required, and with the Master Control. The collector subsystems mirrors will reflect the solar beam toward the receiver with an average reflectivity of 88%. The beam-pointing errors will be as discussed in Section 3.1.1.

Table 3-4 indicates the electric power required from the EPGS subsystem (or from the auxiliary power system, if required, in an emergency) to operate the collector field. During collector field slew in face of a high wind-rise condition, azimuth and elevation axes will be operated separately, elevation first. Thus, only half of the total field drive motors will operate at one time in the worst case. During emergency slew (operating on auxiliary power) approximately 1/4 of the heliostats will be slewed at one time.

Table 3-4

COLLECTOR FIELD POWER REQUIREMENTS

Operating Condition	Power Required/ Heliostat (Watts)	Power Required/ Field (kW)
Tracking	15	30
Slew	230	5,230
Emergency Shutdown	230	1,625

The interface with the master control system is a digital data link overboard line. The master control computer and the field controllers are the communicators over this link. Section 4.2.8 discusses this interface in further detail.

3.1.5 Operations and Operating Mode Requirements

The collector subsystem must be subject to system control for safe and effective operation. An operation time line through a day will serve to illustrate the required collector modes. The time line shown in Figure 3-10 is not typical of a particular day, but is synthesized to include all operating modes.

In the predawn hours, a portion of the collector is steered to a position for cleaning. Cleaning will normally be accomplished in the early morning while winds are usually low to prevent overspray soiling freshly cleaned surfaces and keep dust from the wet surfaces of the cleaned mirrors. In addition, the cooler temperatures will prevent excessively rapid drying of the surfaces between application of the cleaning solution and rinsing. By cleaning a portion of the field in the early morning, the complete field is available for operation throughout the day.

As the sun rises to about 10 deg above the horizon, the heliostats are brought to a position for sun acquisition (synthetic tracking). In regions of the collector field where shadowing of the tracking mirror occurs, alternate heliostats will be brought on track to maximize the energy collected. As soon as the beam sensors acquire the sun, the heliostats will be released to begin normal tracking.

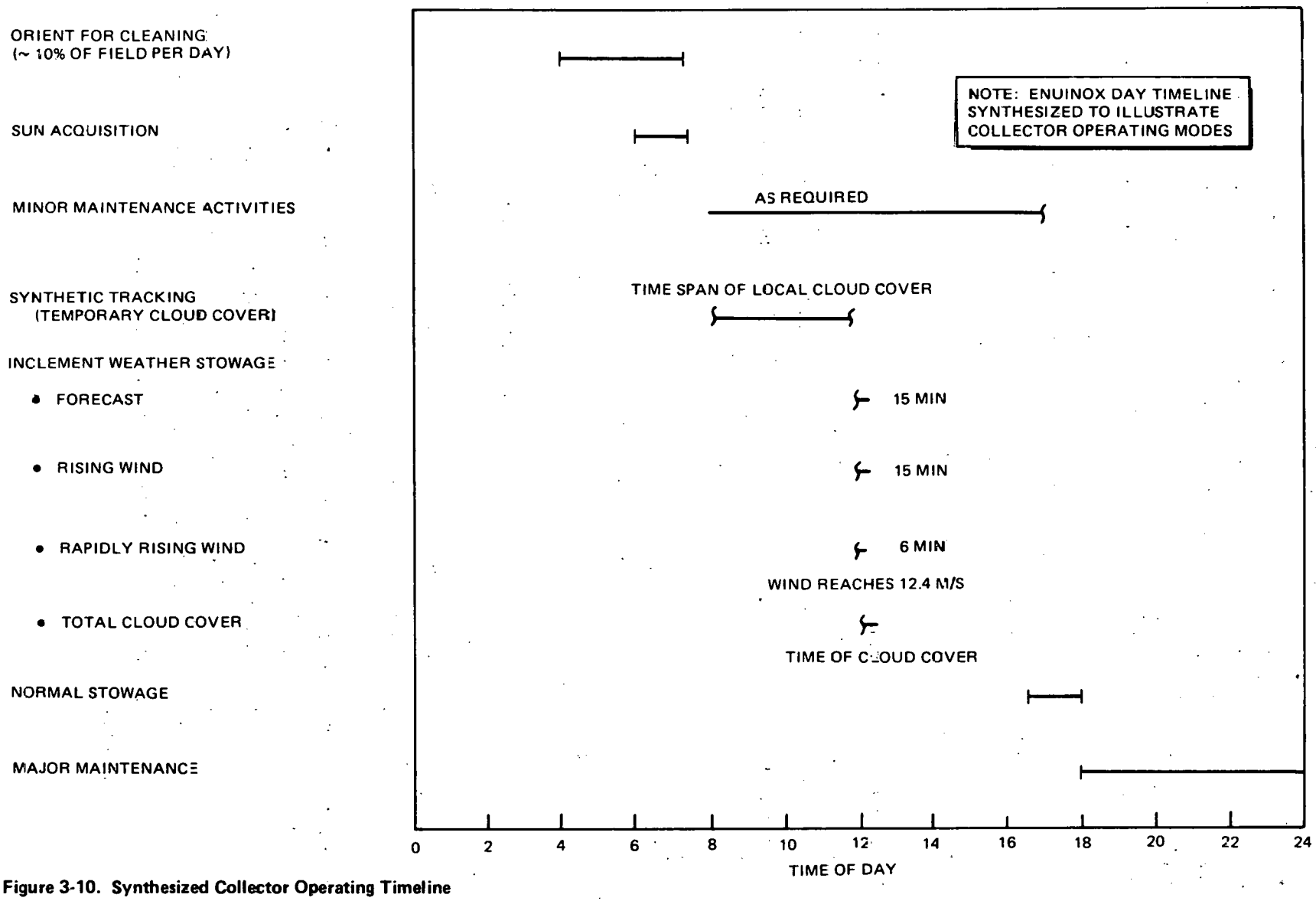

Figure 3-10. Synthesized Collector Operating Timeline

Those heliostats which require scheduled or unscheduled maintenance are released from tracking and, if possible, steered by command from master control to suitable positions for the required maintenance procedure. In the event that a heliostat or field controller is disabled, a van containing the collector test set and an auxiliary power supply is able to position the heliostats and make all repairs not requireing disassembly of the heliostat.

During periods of temporary cloud cover, the heliostats are returned to synthetic tracking. When the sun reappears, the heliostats can return to target in less than a minute. The fast response of the external receiver does not require controlled return to normal tracking.

If the wind should rise to peak gust speeds of 16.1 m/s (36 mph), horizontal stowage will be initiated. The stowage will normally be commanded on the basis of weather predictions. If a severe wind storm is forecast or the wind is rising slowly (the normal condition), the heliostats will be stowed face down. If the wind is rising rapidly and stowage has not been initiated because of a forecasted storm (rare occurrence), the heliostats may be stowed face up until it is safe to invert them. Face-up stowage must be accomplished without causing an unsafe reflected beam in the surrounding airspace or within the confines of the plant.

As the sun goes down on a normal day, shadowing of the tracking mirror will occur in some portions of the field. Alternate heliostats are stowed to keep the collector field power level as high as possible. When the sun reaches about 10-deg elevation, all heliostats are stowed.

The following collector modes are identified in the above timelines:

A. Normal Tracking. The beam sensor has acquired the sun and the heliostat is tracking independent of master control.

B. Synthetic Tracking. The collector field is tracking the sun or any other moving point under the command of the master control. Gimbal axis position transducers are used to provide closed loop control.

C. Individual Command Control. Individual heliostats or groups of heliostats are oriented by command from master control (either automatic or operator-initiated), for maximum collector field power at low sun angles, or for cleaning or other maintenance procedures.

D. Local Manual Control. The heliostats are controlled from the mobile test van to stow in the event of power distribution failure or controller failure, to assist in maintenance or repair diagnostic procedures, or for repair/replacement of faulty parts.

E. Stowage. As described in Section 3.1.6, multiple stowage positions are available and may be commanded automatically or by the operator from master control or manually initiated from the mobile test van.

3.1.6 Stowage Requirements

MDAC has considered the interaction between stowage and other system and subsystem requirements to develop the stowage requirements. The choice to be considered is whether to provide the capability of face-down or inverted stowage.

Face-down stowage must inherently increase the heliostat cost. The 180 deg of reflector rotation about the elevation axis requires a rotary actuator which is more expensive than a linear actuator which is satisfactory for face-up stowage. Clearance for inverting must be provided at the expense of longer load paths and a heavier and more compliant structure. The drive unit must go through more total motion because inverting is always the longest path to horizontal stowage; hence, the drive unit must be designed for greater life and wear.

It is most unlikely that the greater cost of inverted stowage could be justified on the basis of lower cleaning costs. MDAC estimates that the present value of the capital equipment, labor, and materials necessary to clean the entire collector field every 2 wk for 30 yr is about $50 per heliostat.

The beam safety impact was discussed in Section 3.1.3 and clearly favors face-down stowage.

Periods of major maintenance on the power plant or receiver may require the collector to be stowed for up to 2 wk. If face-up stowage were used for 2 wk, cleaning would be required. Vertical stowage would be undesirable for this time period, because the system master control and plant operator must be available to stow the collector field horizontally in the event of high winds.

Other factors explored include drive unit impacts which favor face-up or vertical stowage, and systems impacts which are negligible.

For the above reasons, MDAC has assumed a requirement to stow face down. The normal stowage position will be vertical for three reasons. First, normal dust buildup and hail capability are about equal between vertical and face down stowage. Second, cleaning of the mirror by environmental effects such as frost, heavy dew, and rain is greatly enhanced by vertical stowage and higher average performance will result from vertical stowage. Moreover, rain and heavy dew tend to wash dirt from the back of the mirror and structure to the front when stowed face down, and significant mirror soiling results. Only under conditions of light rain is face-down stowage preferred. Third, drive unit wear and system energy consumption are minimized by vertical stowage.

Face-down stowage is used for extended periods of plant shutdown, high winds, light rain or hail, and malfunctioning heliostats until repaired. Only during rapid, unforecast, wind rise will face-up stowage be employed.

When winds rise above 31 m/s (70 mph), the heliostats will be oriented with their elevations axes parallel to the mean wind vector to minimize elevation drive unit loads.

3.2 COMMERCIAL SUBSYSTEM DESIGN

The commercial subsystem design includes:

- The field geometry optimization (Section 3.2.1)
- The heliostat configuration and subsystem trades. Trades include the reflector, substructure, drive units, pedestal/foundation and sensor pole/foundation (Section 3.2.2).
- The electrical/electronic trades. These include the relationship between the heliostat, field and master controllers; open-vs closed-loop control, the power and data distribution system, and AC vs DC motor power (Section 3.2.3).
- The reliability and availability of the components (Section 3.2.4).

The Commercial field geometry and field geometry optimization are discussed in Section 3.2.1. The Commercial and Pilot Plant heliostats and electronics are conceptually identical. To avoid duplication, the design details are discussed in Section 4 and only identified and referenced in Section 3.

3.2.1 Field Geometry Definition

The collector field geometry defined for the Commercial system was developed through an extensive cost and performance optimization study by the University of Houston. The goal of the effort was to determine the field configuration and heliostat spacing that produce the lowest cost per unit of annual energy. In reality, the annual energy number used to normalize the collector field cost should be busbar electrical energy. Such an approach to optimization of the collector field cost would be difficult because it would have to include assumptions related to the thermal storage subsystem design and duty cycle, the turbine generator, and the capacity displacement credit. Instead, the approach used in optimizing the collector field considered the receiver as a source of thermal energy which in turn is sold to the utility system; therefore, the cost of thermal energy at the base of the tower is used as a suitable normalizing parameter for the optimization figure of merit.

In carrying out the optimization effort, a series of parameters are assumed to be inputs for the analysis. These parameters include an astronomical model, including sun location and atmospheric effects (or specified

insolation level), the heliostat configuration and mounting system, and the basic receiver size/geometry. Although it would appear that the receiver size should be allowed to vary as part of the optimization methodology, a fixed envelope size is assumed to facilitate the convergence of the collector field analysis effort to an optimized solution. The receiver size selected was determined on the basis of extensive analysis carried out over the past four years related to the collector field/receiver interaction. As a result, a receiver size was selected which is compatible with the anticipated thermal power redirected from the collector field. In general, the desire to minimize the receiver surface area is limited by the receiver's ability to withstand the local peak heat flux. As the receiver size is reduced, the peak heat flux intensity increases which compromises receiver life.

The optimization activity starts by breaking down a large collector field, which includes the tower and receiver, into a series of computational cells (typically an 11 x 11 matrix). A representative heliostat is placed at the center of each cell and serves as the basis for evaluating all heliostats in the cell. The optimization procedure goes through a series of steps which begins by determining an ideal figure of merit for each of the test heliostats assuming no neighbors exist and then modifies the figure of merit to reflect the influence of neighboring heliostats which is a function of heliostat arrangement and packing density. Implicit in the figure of merit are the influences of all cost and performance considerations which can be allocated to the individual heliostats. These factors include:

A. Shading and blocking of adjacent heliostats
B. Guidance error model.
    1. Slope errors of reflectors.
    2. Aiming error of sensors (due to misaim and to mechanical flexion).
    3. Tracking errors.
C. Abberation model for canted heliostats.
D. Heliostat aim strategy.

E. Cost model.
   1. Heliostats (including guidance, etc).
   2. Tower.
   3. Receiver.
   4. Plumbing in tower.
   5. Land for heliostat
   6. Wiring for heliostat.

F. Energy loss model.
   1. Mirror reflection and receiver absorption.
   2. Absorptivity vs angle of incidence.
   3. Reradiation and convection by receiver.
   4. Atmospheric losses between heliostat and receiver.
   5. Interception losses at receiver.

In addition, a series of external constraints are also imposed on the optimization analyses. These factors include:

Mechanical clearance for heliostats and access ways.

Flux limits for receiver.

Flux gradient limits for receiver.

Panel power minimum.

To serve as a starting point for the collector field optimization effort, an initial estimate of the ground coverage required by each heliostat is made. A computer code entitled LOSS was developed for this purpose. The program calculates the MWH/m^2 of lost energy due to a single neighbor as a function of distance from the representative heliostat for each cell. Figure 3-11 shows the resulting contours of constant performance loss for two typical cell locations in the field. Cell 1, 1 corresponds to the computational cell at the extreme northwest corner of the field. Cell 5, 5 corresponds to a cell slightly to the north and west of the tower. Superimposed over each of the two performance plots are two candidate heliostat arrangements shown by an "X" and "O". With this layout information, it is possible to determine the appropriate arrangement of heliostats for each cell by determining the arrangement which gives maximum density for a constant loss fraction. In all, four optional arrangement schemes are considered for each cell.

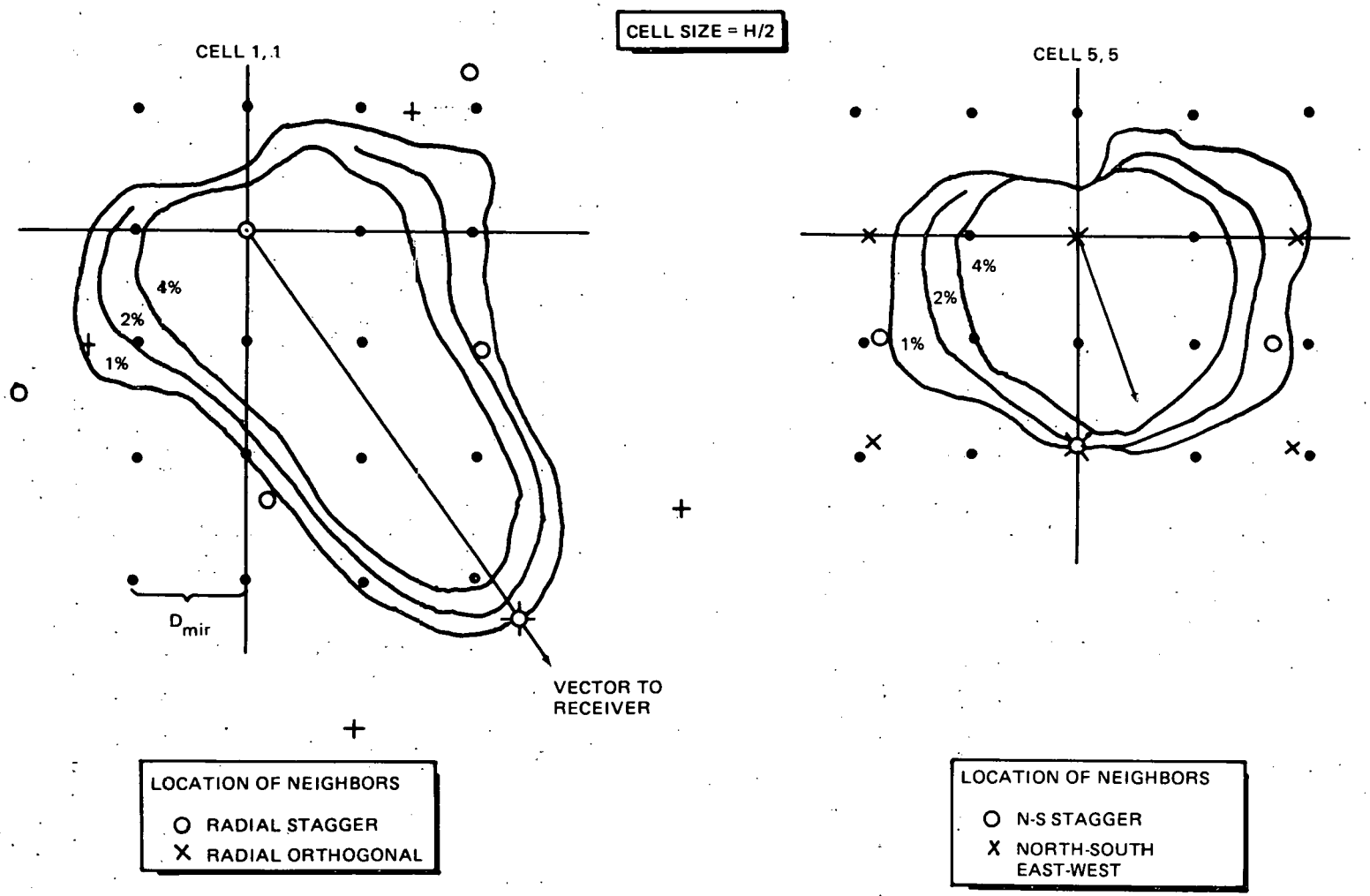

Figure 3-11. Heliostat Loss Footprints Annual Shading and Blocking Loss

The results of the LOSS analysis indicated the general superiority of the radial stagger heliostat arrangement. A summary of the "percentage of advantage" (i.e., higher ground coverage) for the radial stagger arrangement as compared to the next best alternative is shown in Table 3-5 on an individual cell-by-cell basis for a simulated year's performance. Negative entries denote cells where the radial stagger arrangement is inferior to other alternatives. The occurrence of large negatives in the southern field suggests that it might need special treatment, but this is not confirmed by the Pilot Plant study which assumed radial stagger throughout. The complications and unaccounted losses associated with chaotic cell boundaries and varying cell configurations were avoided by using the radial staggered array throughout the final Commercial and Pilot Plant studies.

Table 3-5

PERCENT OF ADVANTAGE FOR RADIAL STAGGER

		J = 1	2	3	4	5	6
I =	1	6.7	2.9	-3.0	-5.1	13.3	0.0
	2	6.5	12.2	1.2	2.9	13.5	0.0
	3	5.0	-0.6	-5.3	1.3	16.2	0.0
	4	-1.0	-6.8	-7.1	3.5	8.8	0.0
	5	5.9	1.0	-1.1	2.8	2.0	10.0
	6	6.8	4.3	-5.5	-7.2	-10.8	5.2
	7	11.6	12.2	7.6	6.5	-4.3	0.0
	8	12.8	3.8	3.0	-11.8	5.1	Tower
	9	-6.6	-1.5	-6.5	-12.8	4.8	0.0
	10	5.8	-18.6	-11.1	-14.3	-0.006	0.0
	11	11.0	-4.9	-10.5	-11.1	7.7	0.0

(Note that J = 1 to 6 is the West Half Field)

The actual optimization analysis is carried out by the University of Houston with a computer code called RCELL. To carry out the analysis, data for the performance and cost factors must be included. The guidance error model assumed includes:

A.	Flexure:	2.88 mr,	(1σ).
B.	Guidance:	$\pm$.6 mr,	(flat top).
C.	Alignment:	2.5 mr,	(1σ).

All Gaussian distributions are truncated at 2σ. The analysis for the Commercial system collector field assumed noncanted heliostats employing a three-vertical-aimpoint strategy. The cost model was for the most part based on cost estimates presented in the PDBR with some more recent considerations added. A summary of the cost model assumed follows:

Heliostat	$\$100/m^2$	(early commercial)
Tower	\$8M	(for 330m height)
Receiver	\$10M	
Piping	\$3.1M	
Land and site preparation	$\$1.08/m^2$	
Allocated wiring	$\$3.20/m^2$	

Additional factors contained in the model included minor reflectance and receiver absorptance (as a function of incident beam angle), radiation and convection losses from the receiver surface, and receiver spillage.

An additional factor which was not originally included in the optimization analysis (the effect is currently being included into the programs) involves atmospheric attenuation. An attenuation model has been developed using the computer code LOWTRAN 2* to predict the impact of atmospheric effects on optical beam transmission between the collector field and the receiver. The impact has been determined for three aerosol models assuming a subarctic

*Selby, J. E. A. and McClatche, R. A. (1972) Atmospheric Transmittance from 0.25 to 28.5 μm: Computer Code LOWTRAN 3, Air Force Cambridge Research Laboratories, Report AFCRL-72-0745

winter atmosphere which would be appropriate, from a moisture standpoint, for the assumed Barstow site. The results of the analysis are shown in Figure 3-12. The aerosol models are (1) no aerosol extinction, (2) 50-km visibility, and (3) 23-km visibility. For the assumed Barstow site, a normal visibility in excess of 50 km would be expected. The bars at the bottom of the figure represent the interval of interest for both the Pilot Plant and the Commercial system. Assuming the 50-km visibility limit, attenuation factors from 0.93 to 0.98 would be appropriate for a Commercial system collector field while values from 0.97 to 0.99 would be appropriate for the Pilot Plant. The above values corresponded to an 80 deg sun elevation angle. For lower sun elevation angles, the atmospheric transmittance between the collector field and receiver increases slightly because there is less of the blue portion of the spectrum incident on the heliostats initially, and therefore, less will be scattered from the reflected beam resulting in a higher transmittance level. For a 20 deg sun elevation angle, the improvement would be ~1.5% at 1,000m and 0.5% at 300m.

The net effect of this attenuation is currently being included in the computer codes and will influence the overall Commercial system design. A complete reanalysis of the Commercial system is planned, including both this effect as well as the latest system cost data when they become available. It should be pointed out that optimization refinements carried out subsequent to the design freeze for the Commercial system indicated that a somewhat larger collector field would be appropriate for the selected Commercial system tower height. At least in a qualitative sense, the inclusion of atmospheric attenuation effects, which preferentially penalize the remote heliostats, will have the effect of shrinking the collector field back to the current design point size.

Using the various cost and performance models which have been identified in conjunction with the RCELL optimization code, the code is used in an iterative fashion to define the optimum heliostat packing for each cell and identify the cells to be deleted from the collector field. Initial inputs for the program include estimated heliostat densities for each cell and an initial guess at figure of merit. The computation proceeds by adding or subtracting glass to each cell as dictated by the assumed figure of merit,

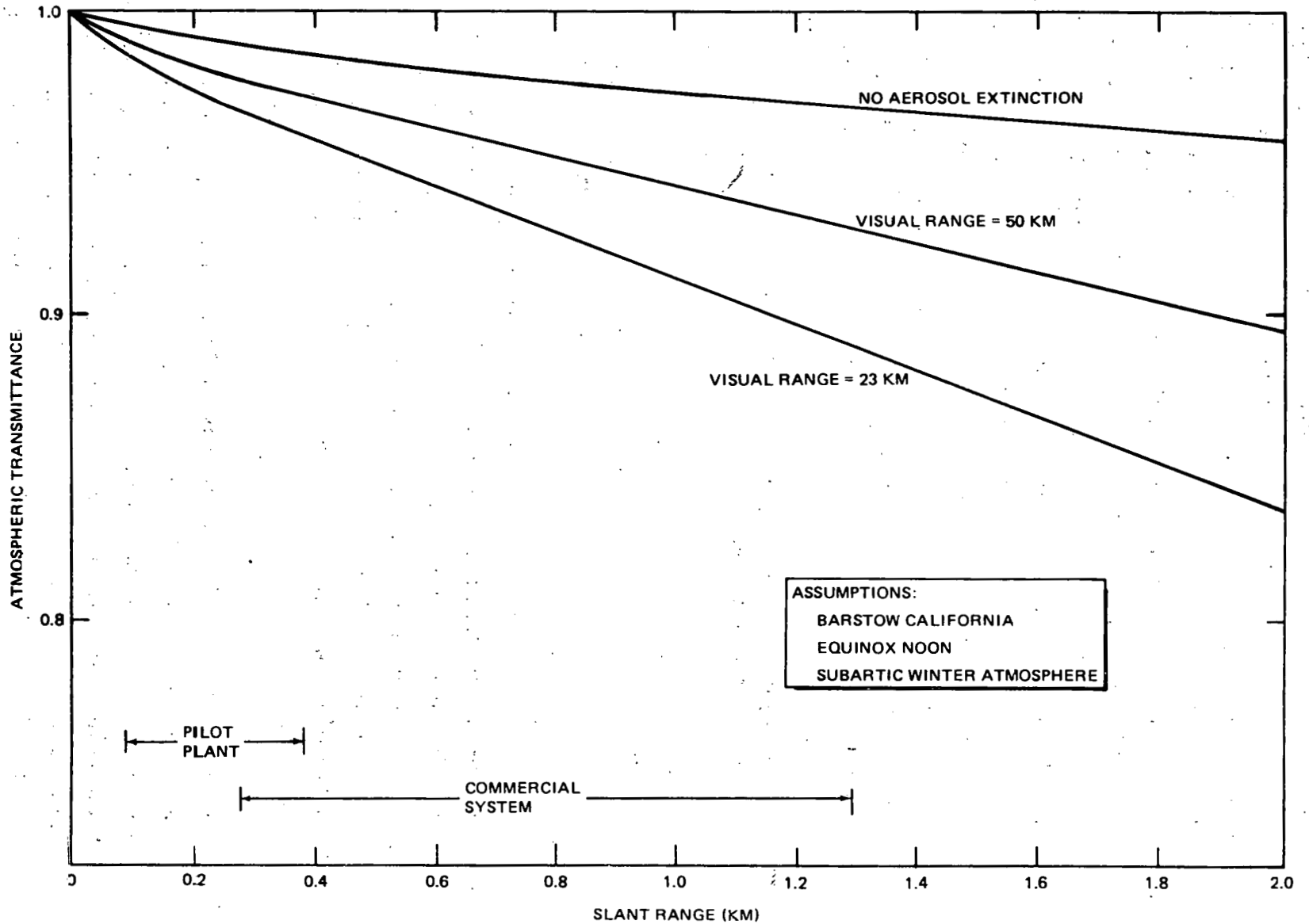

Figure 3-12. Effects of Aerosol Extinction on Transmittance from Heliostat to Receiver

ordering the cells sequentially by decreasing performance, calculating a new figure of merit, and trimming away ineffective cells from the field. Using the revised figure of merit and glass coverage densities (for each cell) as inputs, the process is repeated on an iterative basis until convergence is reached (generally 2-3 iterations).

The field trim which results from this analysis and serves as the basis for the Pilot Plant system is shown in Figure 3-13. The heliostats in each cell are assumed to be layed out in a radial stagger arrangement. The glass coverage fractions for each cell, which are symmetric in the east-west direction, are shown in Table 3-6.

Additional information pertaining to the University of Houston optimization procedure is contained in Volume II, Section 3.3 and Appendixes C and D.

3.2.2 Heliostat Definition

The heliostat design for the Pilot Plant is basically the same as for the Commercial Plant. Section 4.2 gives design characteristics for each component of the heliostat assembly: reflector, structural support, drive unit, pedestal/foundation, and control sensors. For the Commercial Plant, the manufacturing processes will be the same, but the degree of automation and vertical integration will be increased.

A single, central pedestal has been selected because it is efficient structurally. The drive unit is placed at the top of the pedestal, where drive moments are minimal, leading to additional cost reduction in the drive unit. The drive unit should use elevation/azimuth drive axes, which gives lower operational design loads than a pitch/roll drive unit. Face-down stowage capability will permit resolution of some unsettled issues during Pilot Plant operation, such as dust buildup, beam performance, plant operations, and beam safety.

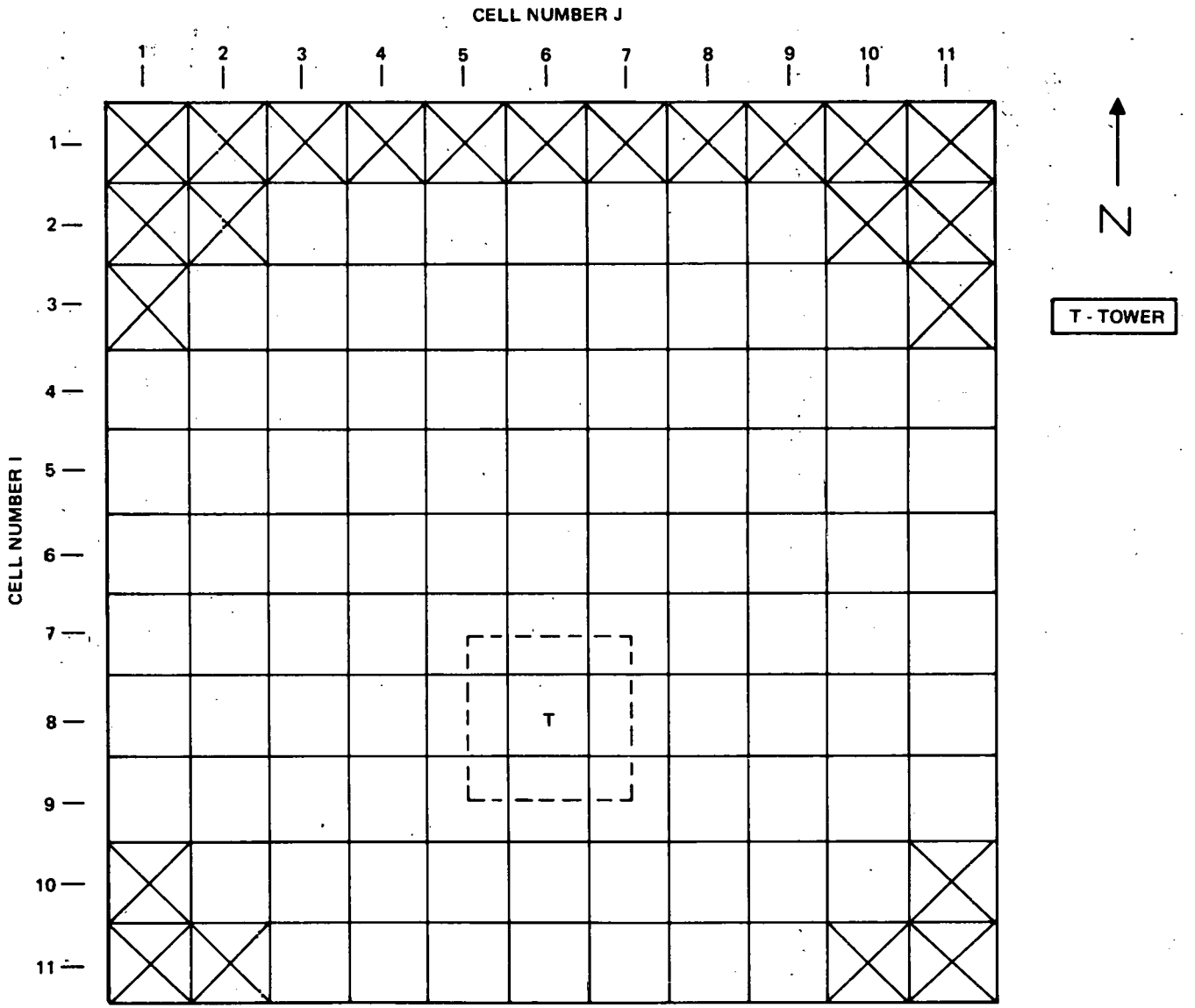

Figure 3-13. Commercial System Collector Field Showing Computational Cell Matrix and Deleted Cells

Table 3-6

CELL-BY-CELL GLASS COVERAGE FRACTION (WEST SIDE ONLY)

CELL NUMBER

	(1)	(2)	(3)	(4)	(5)	(6)
(1)	-	-	-	-	-	-
(2)	-	-	0.141	0.156	0.158	0.169
(3)	-	0.146	0.168	0.185	0.193	0.198
(4)	0.145	0.169	0.198	0.214	0.243	0.228
(5)	0.157	0.189	0.222	0.262	0.294	0.278
(6)	0.178	0.222	0.253	0.296	0.344	0.374
(7)	0.183	0.234	0.277	0.342	0.385	0.405
(8)	0.186	0.232	0.290	0.370	0.419	Tower
(9)	0.131	0.185	0.223	0.298	0.402	0.432
(10)	-	0.182	0.237	0.298	0.327	0.363
(11)	-	-	0.234	0.226	0.241	0.267

The average fractional ground coverage is 0.235.

3.2.3 Controls and Electronics

The controls and electronics for the Commercial system are the same as for the Pilot Plant system except for the obvious effects of scale. There will be, as in Pilot Plant, one heliostat controller per heliostat; one field controller per 24 heliostats (a total of 955); one primary distribution transformer per 220 heliostats (a total of 105). The heliostat controller and field controller are discussed in Section 4.2.8, the heliostat electrical design in Section 4.2.9, and Section 4.2.10 discusses the cable network and lightning protection.

3.2.4 Availability

The availability calculations for the Commercial system collector subsystem are similar to that reported in detail in Section 4.2.12 for the Pilot Plant. The major difference between the two analyses is that the Pilot Plant has 1,760 heliostats, 74 field controllers, and 8 field power transformers. The Commercial collector field has 22,914 heliostats, 955 field controllers, and 104 field power transformers. It was assumed that the component MTBF and MTTR are the same for the Pilot Plant and the Commercial

versions of the heliostat. Therefore, the only difference in the results is the failures per year and the component unavailable hours per year. The results are shown in Table 3-7, which indicates that the expected failure rate for the collector field is 4,498 per year or 13.6 per day. The expected number of heliostat outages (considering failures of heliostats, field controllers, and power transformers) is 5,709 per year or 17.3 per day.

The contribution of the collector subsystem to the overall system unavailability is zero for the Commercial system. The definition of a forced outage (see Vol. II, Section 4.1.0) states that a loss in system power of less than 2% is not charged as a forced outage or charged against the availability calculation. The loss of a power transformer would cause a loss of about 1% of the total field, and it is expected that the system will experience one loss every 218 days. A loss of a field controller will affect only 0.1% of the field and only one failure is expected every nine days. It is expected that the system will lose 13 heliostats per day, but this is only 0.06% of the field. A loss of a field controller and a power transformer at the same time would mean an outage of 257 heliostats or 1.1%. Therefore, there should not be any time when component failures will cause a loss of 2% or more of system power.

3.3 MANUFACTURING, INSTALLATION, CHECKOUT, AND OPERATIONS

The fabrication and assembly operations for rate production have been investigated. The manufacturing processes for the N th Commercial, first Commercial, and Pilot Plant are shown.

The site activation activities, installation and check-out tasks and the Commercial operations scenario are outlined.

3.3.1 Commercial Plant Manufacturing Summary for Collector Assembly (Heliostat)

This section summarizes a conceptual plan for a Commercial Plant operation for the manufacture of the heliostat. This plan was developed by MDAC with the assistance of the Arthur D. Little Company. The plan contains a

Table 3-7

COLLECTOR AVAILABILITY ANALYSIS

Item	Component	MTBF (hr)	MTTR (hr)	Pilot Plant Failures Per Yr	Pilot Plant Unavailable Hr/Yr	Commercial Failures Per Yr	Commercial Unavailable Hr/Yr
1	Transformer	$1.2(10^6)$	7.96	0.02	0.16	0.27	2.15
2	Power Cables to Transformers	$9.3(10^6)$	3.11	0.003	0.009	0.04	0.23
3	Distribution Panels	$2.9(10^5)$	1.51	0.09	0.14	1.2	1.8
4	Field Controllers	$1.2(10^5)$	1.29	2.10	2.7	27.1	35
5	Cables to Field Controllers	$9.3(10^6)$	3.11	0.03	0.09	0.33	1.03
6	Field Controller Junction Box	$2.9(10^5)$	1.84	0.81	1.49	10.8	20
7	Heliostat Controller	$2.1(10^5)$	1.04	27.5	28.6	359	373
8	Cables to Heliostat	$9.3(10^6)$	1.50	1.22	1.80	16.0	24
9	Heliostat Circuit Breaker	$5.9(10^5)$	1.66	10	16.6	129	214
10	Azimuth Drive Motor	$5(10^5)$	3.15	11.6	25.0	151	325
11	Elevation Drive Motor	$5(10^5)$	1.54	11.6	17.9	151	233
12	Azimuth Position Sensor	$8.3(10^5)$	1.62	7.0	11.4	91	147
13	Elevation Position Sensor	$8.3(10^5)$	1.10	7.0	7.7	91	100
14	Azimuth RPM Counter	$7.4(10^5)$	1.33	7.8	10.4	102	136
15	Elevation RPM Counter	$7.4(10^5)$	1.05	7.8	8.2	102	107
16	Azimuth Primary Compudrive	$9.6(10^4)$	2.15	60	129	786	1690
17	Azimuth Secondary Compudrive	$1.3(10^5)$	2.68	44	118	575	1540
18	Elevation Primary Compudrive	$9.6(10^4)$	1.54	60	92	786	1211
19	Elevation Secondary Compudrive	$1.3(10^5)$	2.43	44	107	575	1396
20	Sun Sensor	$2(10^6)$	1.12	3	3.36	38	42
21	Mirror Panels	$1(10^6)$	1.12	35	39.2	454	508
22	Pedestal	$10(10^6)$	1.49	0.58	0.86	7.56	11.3
23	Reflector Structure	$2(10^6)$	2.96	2.9	8.58	38	112
24	Sun Sensor Pedestal	$10(10^6)$	1.01	0.58	0.59	7.6	7.6
	Total Failures Per Year			344.63		4498.90	
	Total Failures Per Day			1.04		13.63	
	Total Heliostat Outages Per Day			1.32		17.30	

discussion and description of the manufacturing concept which uses a main manufacturing plant for details and subassemblies and a site plant for final assembly. This plan was sized for a steady-state condition for production of 60,000 heliostats per year at the main manufacturing plant with an initial startup rate of 15,000 heliostats per year. These rates provide capacity to produce heliostats in support of initial Commercial powerplants, build to a steady-state production, and provide for further growth either through plant expansion or additional plants. Production of 60,000 heliostats per year at the main manufacturing plant located in the Southwest supports multiple site plants also in the southwest. Site plants are sized to the requirements of the size of powerplant being serviced; however, basic sizing has been assumed to be a site which requires 21,400 heliostats to be installed over a period of 18 mo.

3.3.1.1 Main Manufacturing Plant

The main manufacturing plant (Figure 3-14) measures approximately 500 by 900 ft and represents 450,000 ft^2 of manufacturing and coverered storage space. This plant size does not include space requirements for offices, which may total an additional 40,000 ft^2. The plant is designed for operation on a 5-day, 2-shift basis, which allows for production contraction to 30,000 (one shift), if required. The plant is designed to fabricate and assemble heliostat subassemblies to the point at which they can be shipped to the site plant location(s) for final assembly and transfer to the installation site.

Basically, the manufacturing plant consists of four fabrication/assembly areas as follows:

- Reflector surface assembly area.
- Support components fabrication/finish area.
- Machine/drive assembly area.
- Electrical/electronics assembly area.

To support the assembly/fabrication areas, storage areas for in-process materials and finished goods are established near the appropriate work locations.

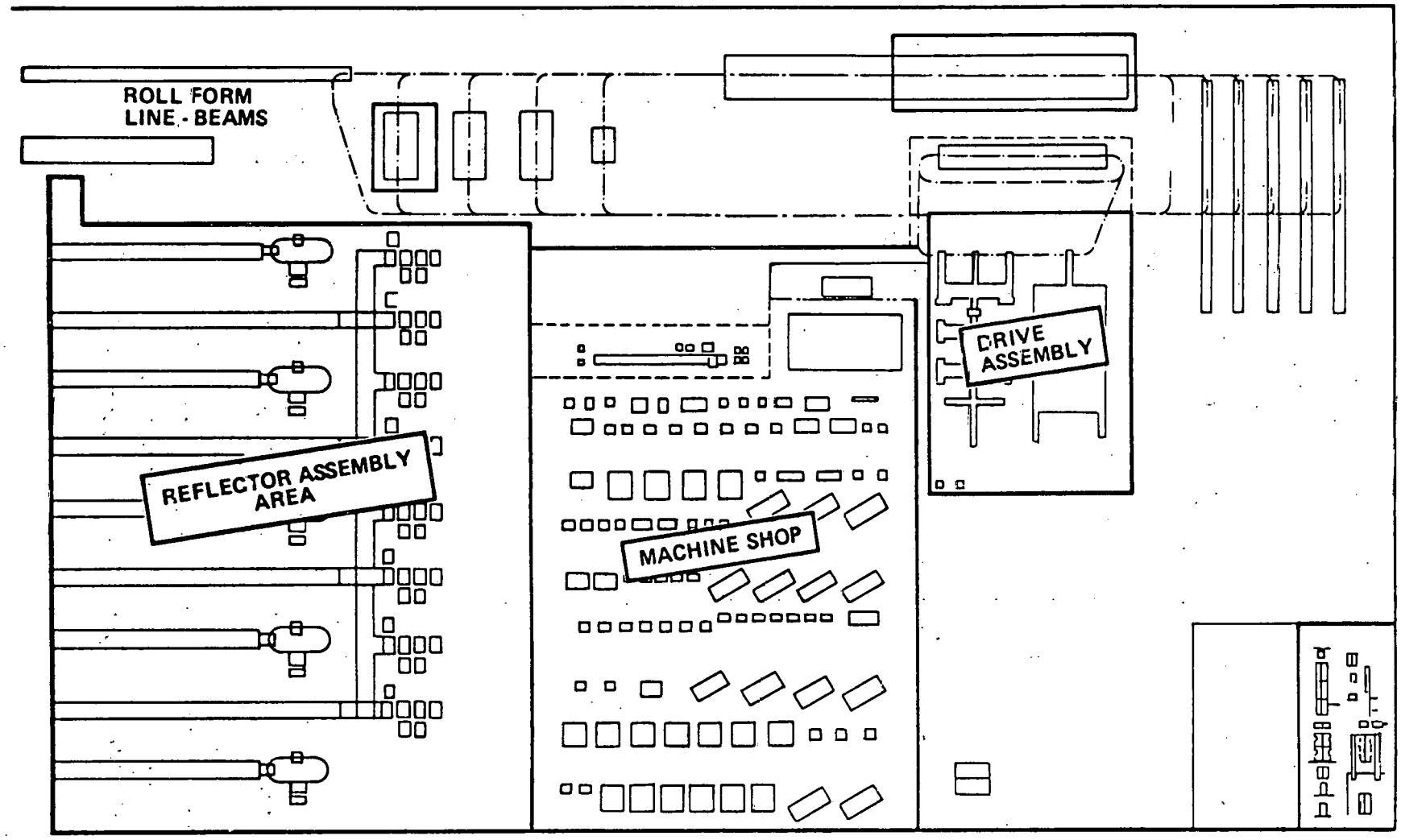

Figure 3-14. Main Manufacturing Plant

Reflector Surface Assembly Area

The reflector assembly area operations are as follows:

- Fabrication of 114 in. x 85 in. backsheets from galvanized sheet metal in coil form.
- Lamination of foam core and backsheet. Curing of the bonding adhesive is accomplished in compression conveyors, which also transfer these foam/steel sheets to the final lamination stations.
- Lamination of foam/steel sheets with mirrored glass. A similar cure process in compression conveyors in transit to edge sealing stations and packaging.

Glass handling is accomplished by automatic equipment which moves glass shipping frames from the receiving area to the work stations, where each glass panel is mechanically removed from the shipping frame. Transfer from work stations to compression conveyor is by means of air-cushion conveyors. Transfer from the end of the compression conveyor to shipping frames is accomplished by vacuum transfer monorail.

Support Components

This portion of the plant has approximately 135,000 ft^2 (900 ft x 150 ft) for:

- 60,000 torque tubes.
- 240,000 cross beams.
- 60,000 pedestals.

Operations carried out in the area include:

- Fabrication of cross beams.
- Welding of pads to cross beams, collars to torque tube, collar and base to pedestal.
- Finishing line comprised of a wheelabrator, vapor degreaser, wash, dry, dip prime, dry tunnel, finish paint, and final dry.

Parts are picked up at the various stations and carried through the finish line operations to the packaging/shipping stations. At these locations the parts are off-loaded, palletized as necessary, and shipped.

Machine Shop/Drive Assembly

The machine shop (66,000 ft^2) and drive assembly (17,000 ft^2) areas provide necessary operations to produce 60,000 drive units for the heliostats. All machining operations required on drive unit castings and steel stock components are included. The machining operations are divided into five areas, each equipped and dedicated to produce a specific part or group of parts.

The drive assembly area consists of work stations for assembling sequentially the azimuth and elevation drive housings, which are then brought together for painting, final assembly, and testing. Transfer between the assembly area and the paint line is accomplished by continuous monorail which also carries the drive units through the paint line.

Electrical/Electronic Assembly

This area occupies approximately 6,000 ft^2 (Figure 3-15) for:

- 60,000 heliostat controllers.
- 2,500 field-processors.
- 60,000 sensors.

Assembly operations are such that only one shift is necessary, which permits extension of work schedule to partial second or full second shift, if necessary.

Assembly is manual with the exception of the wave solder operation following P/C board component stuffing.

Also included is a wire harness fabrication operation at which all wiring required in the control enclosures as well as between the enclosures and the drive units are manufactured.

3.3.1.2 Site Manufacturing Plant

Each site plant measures 240 ft x 320 ft or a total of 76,000 ft^2 (Figure 3-16). The nominal assembly capacity of each site plant is 60 heliostat units per day, 14,300 units per year or 21,400 units in an 18-mo assembly period. Each site plant will be located adjacent to the installation site to reduce the final transport requirement for fully assembled heliostats.

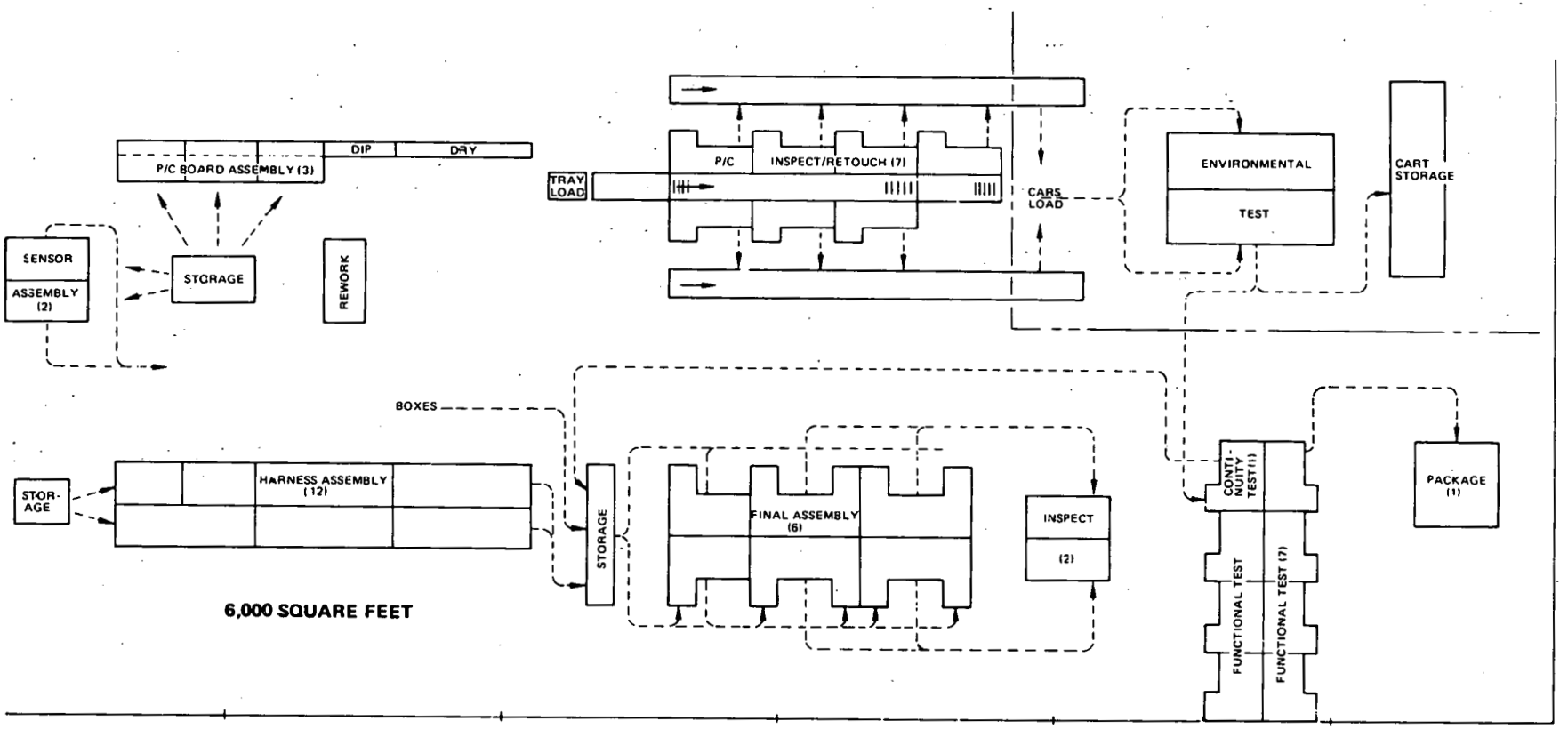

Figure 3-15. Electrical/Electronics Assembly Area

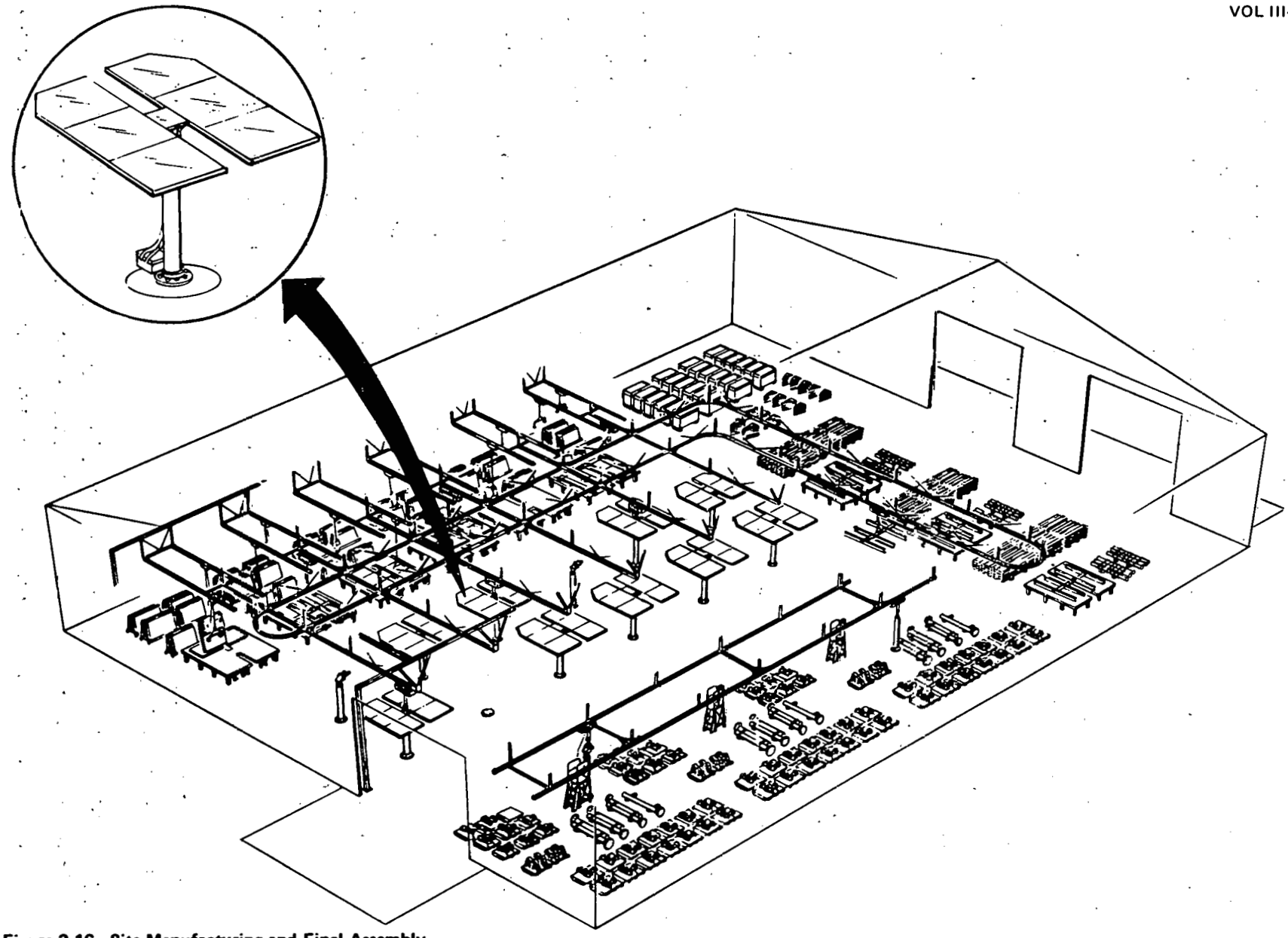

Figure 3-16. Site Manufacturing and Final Assembly

Based on the construction nature of the installation work, the site plant will be designed to operate on one shift; the same shift as is worked by the installation and construction crews. If a decision is made to operate the site plant on two shifts, the assembly capacity, size or storage requirements of this plant will be affected.

Four basic assembly operations take place in the site plant. They include:

A. Assembly of the cross beams to the torque tube.
B. Assembly of the cross beams and torque tube to the reflective panels.
C. Assembly of the drive units and wiring harnesses to the pedestal.
D. Assembly of the reflective array and supports to the drive and pedestal.

Assembly of the Cross Beams to the Torque Tube

The cross beams and torque tubes are assembled on work tables. The four cross beams are loosely assembled onto the torque tube. The pads on the cross beams are then positioned on scribed spots on the work table and locked down. The torque tube is rotated until the centrally mounted collars lock into a given position in a holding jig at the center of the table. When the entire assembly has been locked up, the yokes of the beams will be impulse-welded to the flange and ends of the torque tube. After welding, the assembly will be hoisted from the work table on a monorail and either stored in the overhead or moved to a reflective array assembly work table.

Assembly of the Cross Beams and Torque Tube to the Reflective Panels

This assembly area consists of work tables which are used to bond the assembly. Operators at these stations remove the reflective panels from their shipping A-frames at stations immediately adjacent to the work tables and lay them on the work surface in predetermined positions. Mechanical aids are provided for the movement of the panels and their exact positioning on the work tables. One of the torque tube-beam assemblies is then positioned over the work surface and panels, and the two structures mated and locked together.

Assembly of the Drive Units and Wiring Harnesses to the Pedestal

This assembly activity (Figure 3-17) consists of the following steps:

- Transport of the pedestals and drive assemblies to the work station.
- Mounting of the drive unit to the top ring of the pedestal.

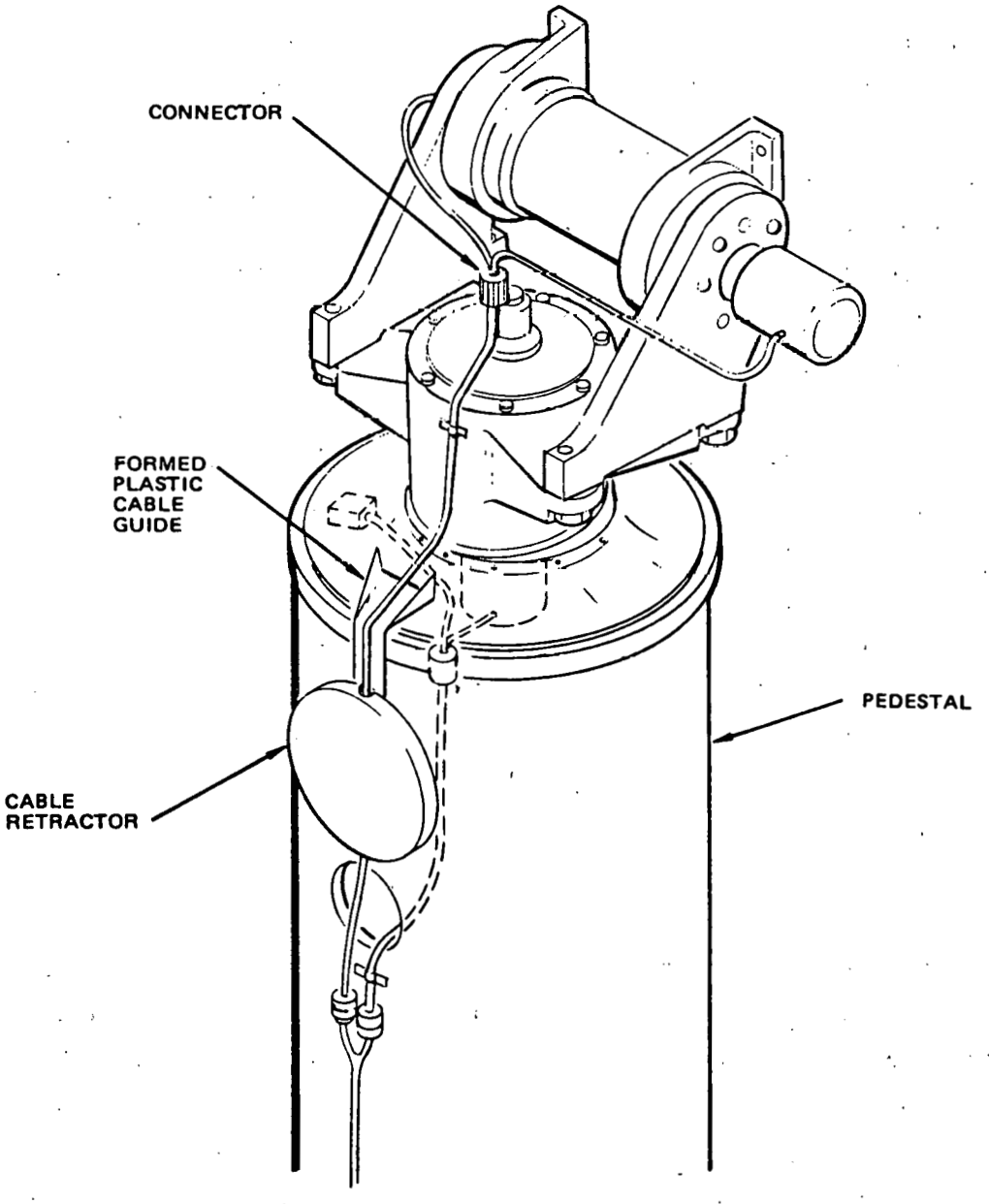

Figure 3-17. Elevation Drive Motor Power and Control Wiring

- Mounting of the drive cable retractor and junction box.
- Attachment of cable clamps to the pedestal and shaft housing.
- Connection of the complete wiring harness.
- Powered check of both drive elements.
- Assembly and sealing of the drive rain shields.
- Transport of the subassembly to the final assembly station.

Assembly of the Reflective Array and Supports to the Drive and Pedestal

The last operation within the site plant occurs at six final assembly stations. Three additional crews at the six stations perform the following final steps in the heliostat assembly process:

- Obtain, transport, and rotate a reflective array and structure from one of the array assembly work tables and position it over a pedestal and drive subassembly at the final assembly station.
- Mate the torque tube collars with the elevation drive mounting feet and mount the array to the drive.
- Mount the sensor reflector and its supports.
- Touch up painting of the completed heliostat.
- Transport of the heliostat to a holding position for movement to the site on a special vehicle.

None of the activities in the site plant require special fabricating or assembly equipment.

The preceding section has discussed the manufacturing, concepts, and processes envisioned in the steady-state or the Nth Commercial Plant, with yearly production capacity of 60,000 or more heliostats. The first Commercial Plant, with a capacity of approximately 21,000 heliostats per year, would incorporate some of the automated techniques of the Nth plant where these prove cost-effective and retain some of the Pilot Plant processes where increased automation is not cost-effective. For instance, automatic welding of the pedestal back and top plate would be similar to if not identical to the Nth plant process. On the other hand, printed circuit board component assembly would use optically aided manual insertion as planned for the Pilot Plant.

3.3.2 Installation Scenario

Before initiation of collector installation activities, a number of site activation tasks will have been completed. Those pertinent to collector installation and checkout (I&C) would be site grading, roadway construction, and installation of heliostat and sensor pole foundations. Erection of the heliostat final assembly site plant must also precede installation.

Final assembly of the heliostats takes place in a site at the site boundary to avoid cost and difficulties inherent in over-the-road transportation of the assembled reflector.

After completion of I&C, a system test verifies that all subsystems are properly interfaced, and that system performance requirements are satisfied. Normal plant operation is then initiated.

Installation and checkout, system test, and plant operation will all require logistical support. Support concepts are presented in Section 3.3.3 for I&C and plant operations. System test support concepts are identical to those for plant operations. To clarify what is considered to be encompassed within system or logistical support, the major elements of a support system are as follows:

- Transportation, handling, packaging.
- Maintenance analysis.
- Supply support.
- Support equipment.
- Training.
- Technical documentation.
- Field service.
- Facilities.

To properly frame the relationship among collector installation and checkout, collector subsystem support, and other phases of the program, Figure 3-18 is presented. A significant segment of the support system will be allocated to collector subsystem support both during I&C and plant operations. Explanations of the blocks shown on Figure 3-18 are given in the following subsections and in Section 3.3.3.

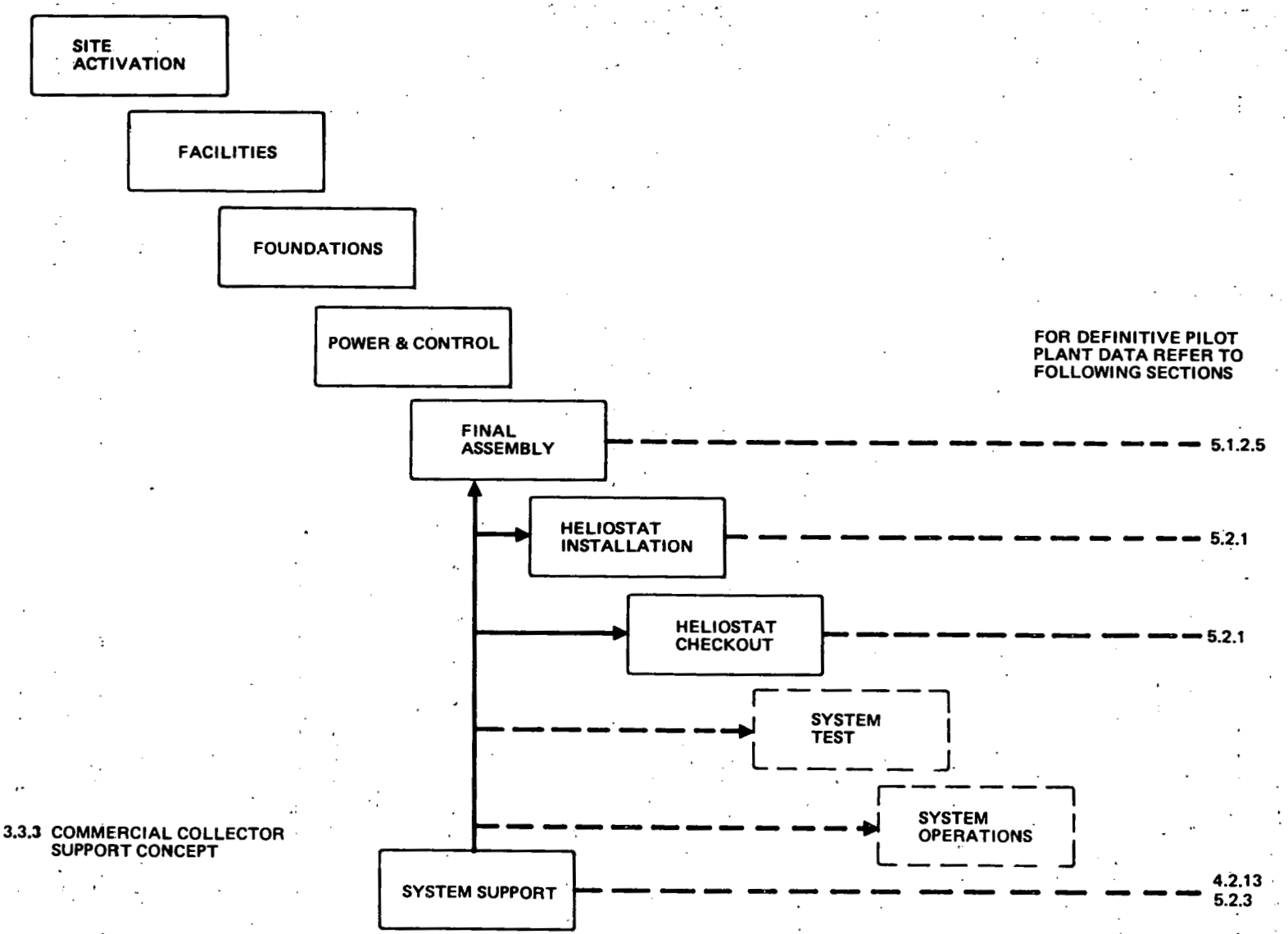

3.3.3 COMMERCIAL COLLECTOR SUPPORT CONCEPT

Figure 3-18. Collector Subsystem Installation and Logistics Structure

3.3.2.1 Site Activation

In the context used here, site activation encompasses the preparatory work done by the general contractor; e.g., grading, road building, facilities constructions, utility connections, etc. General contractor tasks which are considered prerequisites to collector I&C are site grading, preparation of access roads, preparation of foundations for heliostats and sensor poles, installation of power transformers and power distribution panels, and laying power and control cables.

3.3.2.2 Facilities

Permanent and temporary facilities will be required for collector subsystem assembly, installation, and test operations. A temporary site plant for housing the heliostat assembly operations will be erected near the field installation site to minimize transportation problems. A permanent building will be required for installation and testing operations. This building will be converted into a repair depot and supply storage facility during Commercial operations.

The quantity of vehicles and handling equipment will be augmented for installation and testing operations. Parking and storage of vehicles and equipment should not be a problem; however, servicing and storage of maintenance materials will require additional facilities. Operating two or three shifts for servicing and repair, along with contracting for services with local garages, will minimize facilities requirements.

Open storage of some subsystem components may be feasible in the desert. If not, temporary sheds may be required. Field controllers, sensors, mounts, and cable assemblies will be stored in the permanent environmentally controlled installation facility mentioned above. Delivery rates of these items will be matched with installation rates.

3.3.2.3 Power and Control

During site activation, the general contractor will install power transformers and power distribution panels in the field as required to provide operating

power to the field of heliostats. He will also dig necessary trenches and lay both power and control cables to interconnect the prime power to the transformers, operating power from the transformers to the distribution panels, and on to the heliostats, and from the central control room to the field controllers. During I&C, cable connections of the heliostats will be made by I&C crews.

3.3.2.4 Final Assembly

Each heliostat is completely assembled for installation in a final assembly site plant. The site plant is to be located adjacent to the installation site to reduce the final transport requirements for fully assembled heliostats. Based on the construction nature of the installation work, the site plant will operate on one shift; the same shift as is worked by the installation and construction crews. If a decision is made to operate the site plant on two shifts, the assembly capacity, size or storage requirements of this plant will be affected.

Four basic assembly operations in the site plant are as follows:

A. Assembly of the cross beams to the torque tube.
B. Assembly of the cross beams and torque tube to the reflective panels.
C. Assembly of the drive units and wiring harnesses to the pedestal.
D. Assembly of the reflective array and supports to the drive and pedestal.

3.3.2.5 Heliostat Installation

Current planning defines the Commercial Plant as a scaled version of the Pilot Plant. Consequently, this scenario of the methods and resources applied to the installation of a Commercial collector field reflects data developed for the scheduled 10-MW Pilot Plant to be constructed at Barstow. Because of variations in the installation and checkout periods between the Commercial and Pilot Plants, scaling cannot be based on the difference in the quantity of heliostats between the Commercial and Pilot Plants. The scaling up from Pilot Plant to Commercial Plant has been done on the difference in installation rates applicable to the two programs.

Nonrecurring costs for the Commercial Plant should be minimal for the following reasons:

A. Support equipment design completed during Pilot Plant development.
B. Installation procedures developed and validated during Pilot Plant development.
C. Training courses and aids developed and perfected by use in training Pilot Plant installation personnel.

Preparation costs for Commercial Plant collector installation would, of course, be higher than for the Pilot Plant. These costs are driven by (1) the quantity of equipment shipped to site and erected, (2) the number of installation personnel hired, processed, and trained, and (3) the facilities required to support installation and checkout activities. The planned approach of hiring a large percent of the installation personnel at the site location should keep travel and subsistance costs low.

Material costs for support of the installation and checkout program would increase for the Commercial Plant; however, these costs would be controlled by judicious selection of spare items. High-cost items, such as reflectors, reflector panels, and electronic controllers, would not be procured as spares. When the need for this type of a spare develops, it will be diverted from the production line. Following this action, a replacement item would be ordered for delivery to production. This concept reduces investment in spares while ensuring schedule compliance.

The following sections identify, in gross terms, the resources required for installation and checkout of the Commercial Plant. They include the rationale for the resource loading.

Schedule

Installation and checkout time periods used to develop this report were extracted from the schedule shown in Figure 3-19.

Rates

The rate at which heliostats are installed must match the rate at which they are assembled. This final assembly is done on-site in a dedicated facility, which obviates any need for intermediate transportation from the assembly

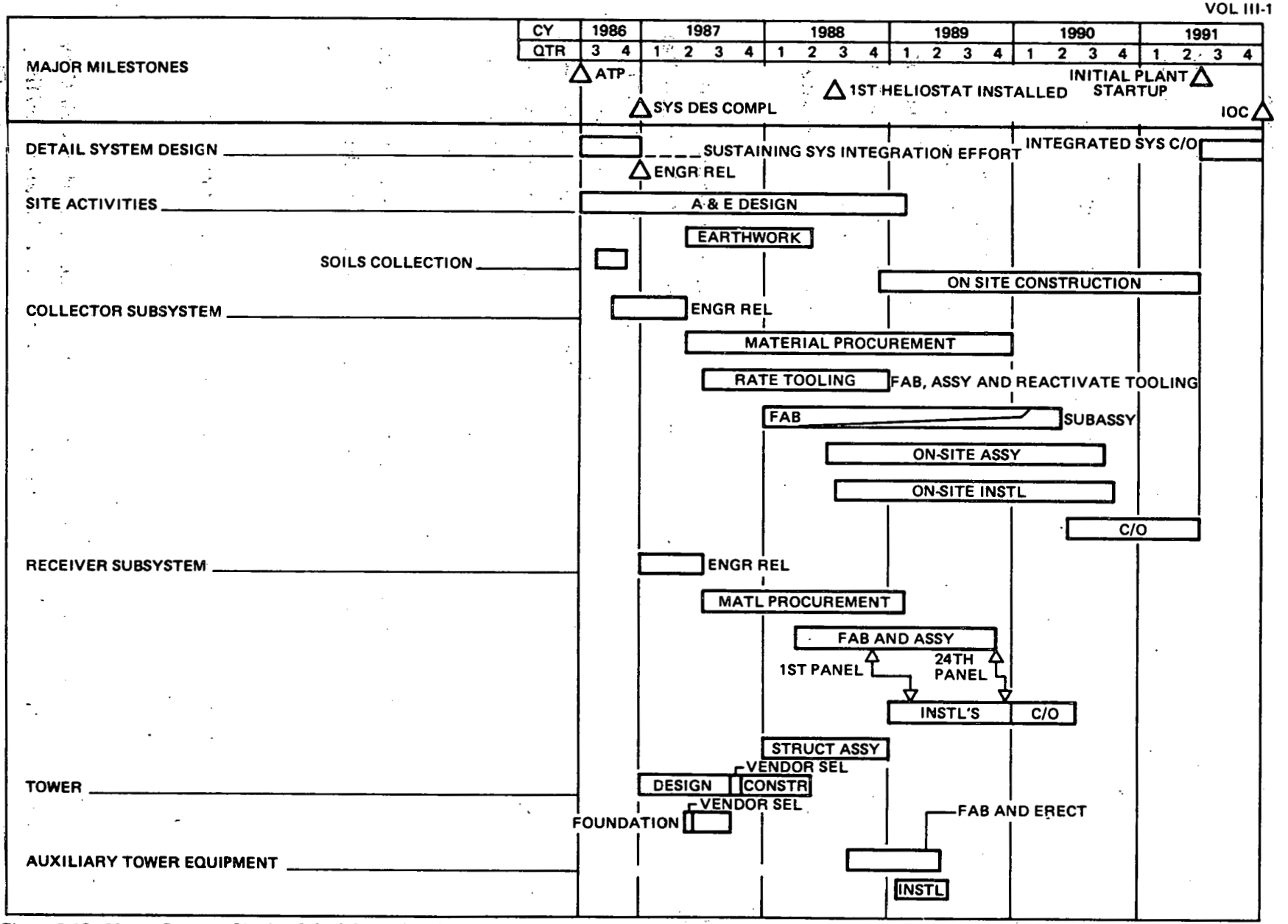

Figure 3-19. Master Program Phasing Schedule — First Commercial Plant

area to the site. The final assembly rate, and therefore, the installation rate, was developed by calculations using the quantity of heliostats, 22,914, and the time period scheduled for assembly, 2.34 years:

2.34 yr x 52 wks = 121.68 or 122 wks

122 wk - (1 wk startup + 1 wk shutdown + 5 wk holidays) = 115 wk

22.914 Hel ÷ 115 wks = 199.25 Hel/wk rate

199.25 Hel/wk ÷ 5 days = 39.85 or 40 Hel/day rate

Based on the preceding calculations, the average installation rate for heliostats was established at 40 per day. This rate assumes a five-day, eight-hr work shift and compensates for holidays. Schedule slips would be corrected by working extended days and extended week shifts. It should be noted that this rate is four times the Pilot Plant rate, 10 per day.

The checkout rate for heliostats is expressed in number of cells (24 heliostats) per day. The rate is a function of the number of cells and the checkout time period, calculates as follows:

22,914 Hel ÷ 24 = 954.75 or 955 cells

955 cells ÷ 32 wk = 29.84 or 30 cells/wk rate

Installation Tasks

The discrete tasks performed to accomplish the installation and checkout of a heliostat are described in this section. The descriptions provided are for Pilot Plant installation and checkout tasks as presently planned. They are directly transferable to the Commercial Plant, however, improvement in methods and equipment based on Pilot Plant experience is expected.

The sequence in which the tasks are performed for a single heliostat is shown in Figure 3-20. During field installation, the tasks are actually performed in parallel. The sequence starts with the foundations completely installed. Tasks are as follows.

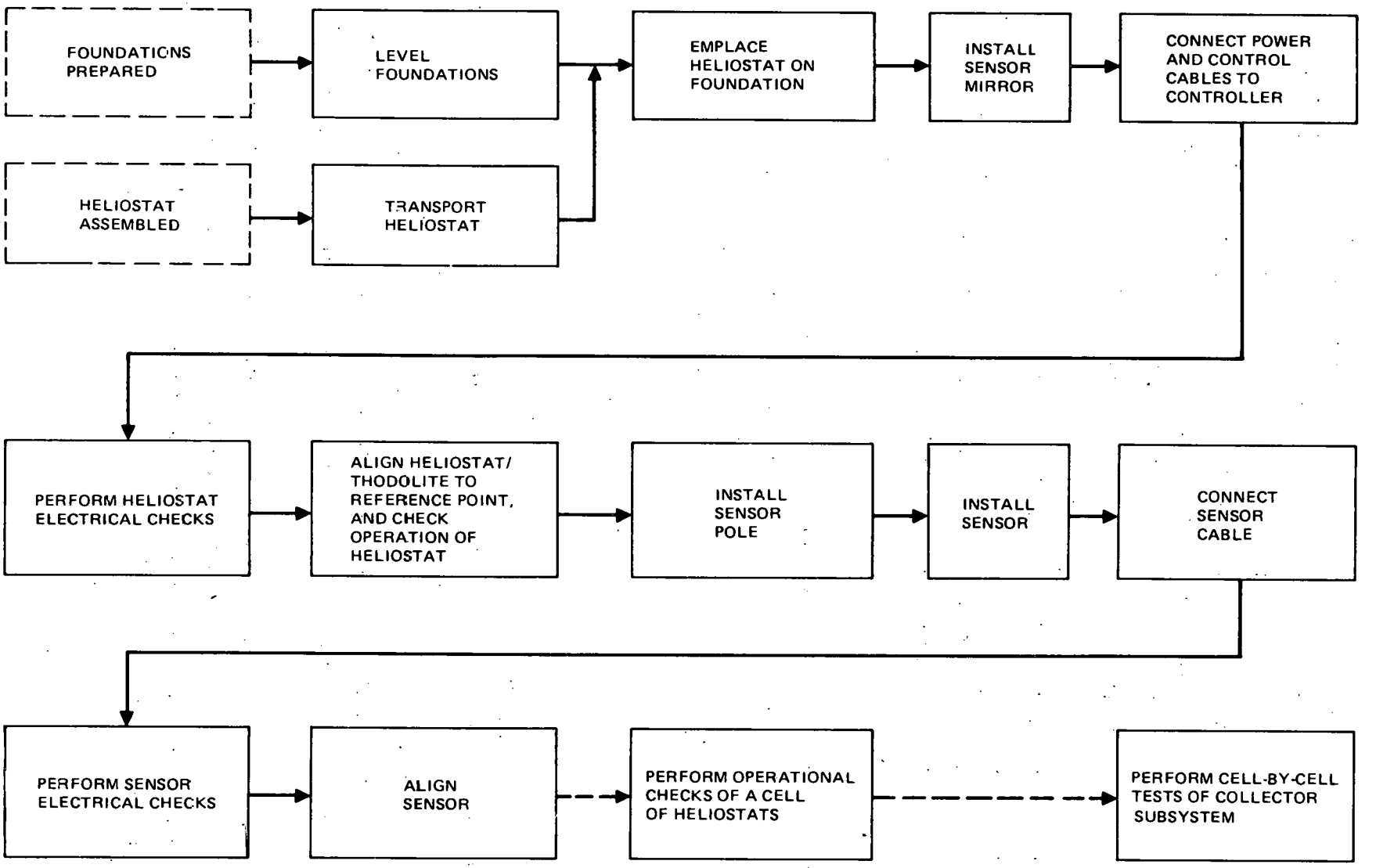

Figure 3-20. Heliostat Installation Sequence (Closed-Loop System)

Level Foundation to Heliostat Interface. Three leveling nuts on each foundation are adjusted to a plane in two axes using a pedestal leveling fixture and an inclinometer. Once a level plane is established, the three leveling nuts are secured with locking nuts.

Transport Heliostat to Foundation. The heliostat, consisting of reflector panels, drive units, pedestal, and controller will be assembled and wired in the assembly building on site. A heliostat handling fixture, specially adapted to a forklift, is mated to the completely assembled heliostat. The heliostat is lifted clear of its assembly fixture by the forklift and is then carried to the assigned foundation.

Emplace Heliostat on Foundation. Once the heliostat is positioned over the foundation, the pedestal restraining strap is released. This leaves the heliostat suspended from the forklift adapter lifting eye, free to be guided onto the foundation anchor bolts. As soon as the lower pedestal flange comes to rest on the three leveled nuts, retaining nuts are installed on the same three anchor bolts. At this point the handling fixture is disengaged from the heliostat and is dispatched to pick up another heliostat. Next, the other five nuts under the pedestal flange are positioned against the under surface of the flange. After installing the additional five retaining nuts, all eight retaining nuts are torqued using a reactionless power torque wrench.

Install Sensor Mirror. The small sensor mirror, which was removed from the heliostat to provide access for the forklift adapter hoist, is reinstalled.

Connect Power and Control Cables. Once the heliostat mechanical installation crew had completed installation of the heliostat, an electrician crew connects the power and control cables into the electronic junction box of the base of the pedestal. Cable laying is done earlier in the program by the general contractor.

Perform Heliostat Electrical Checks. As part of the electrical hookup, the electrician crew runs electrical checks such as megger, continuity, polarity, etc.

Align Heliostat and Run Operational Checks. During these checks, azimuth reference of the heliostat is aligned (Figure 3-21) by mounting a theodolite on the reflector surface and sighting a known reference point on a previously installed flagpole, 25 to 30 ft high. The azimuth encoder is adjusted at this time. Elevation reference is aligned by driving the heliostat reflector horizontal to the ground, mounting an inclinometer, and adjusting the elevation encoder to a level condition. Concurrently, other heliostats are operationally checked. A programmed series of commands is fed into the heliostat controller which will cause the heliostat to be driven to preset limits of travel in both azimuth and elevation.

Install Sensor Pole. The sensor pole is installed, leveled, and secured.

Install Sensor. The sensor mount and sensor are installed on the sensor pole, and the sensor is roughly aligned on the receiver.

Connect Sensor Cable. Necessary conduit is installed and the sensor cable is installed between the sensor and the controller.

Perform Sensor Electric Checks. As part of the sensor electrical hookup the electrician crew runs electrical checks for continuity, AGC, polarity, etc.

Align Sensor. After the electrical hookup and checkout tasks are completed and verified, the sensor is aligned on the receiver panel. Since this is a closed-loop tracking system, tracking accuracy is dependent on the accuracy with which the sensor is aligned.

One technician, riding in a cherry picker (Figure 3-22), directs another technician at the mobile field test station in driving the heliostat in elevation and azimuth until the reflected spot is on the receiver panel. Directions are transmitted by walkie-talkie radio sets. When the reflected spot is on the receiver panel, the field controller is commanded to track. While tracking is in progress, the technician in the cherry picker adjusts the sensor to align the reflected spot with the designated aim point on the receiver. The sensor is then locked.

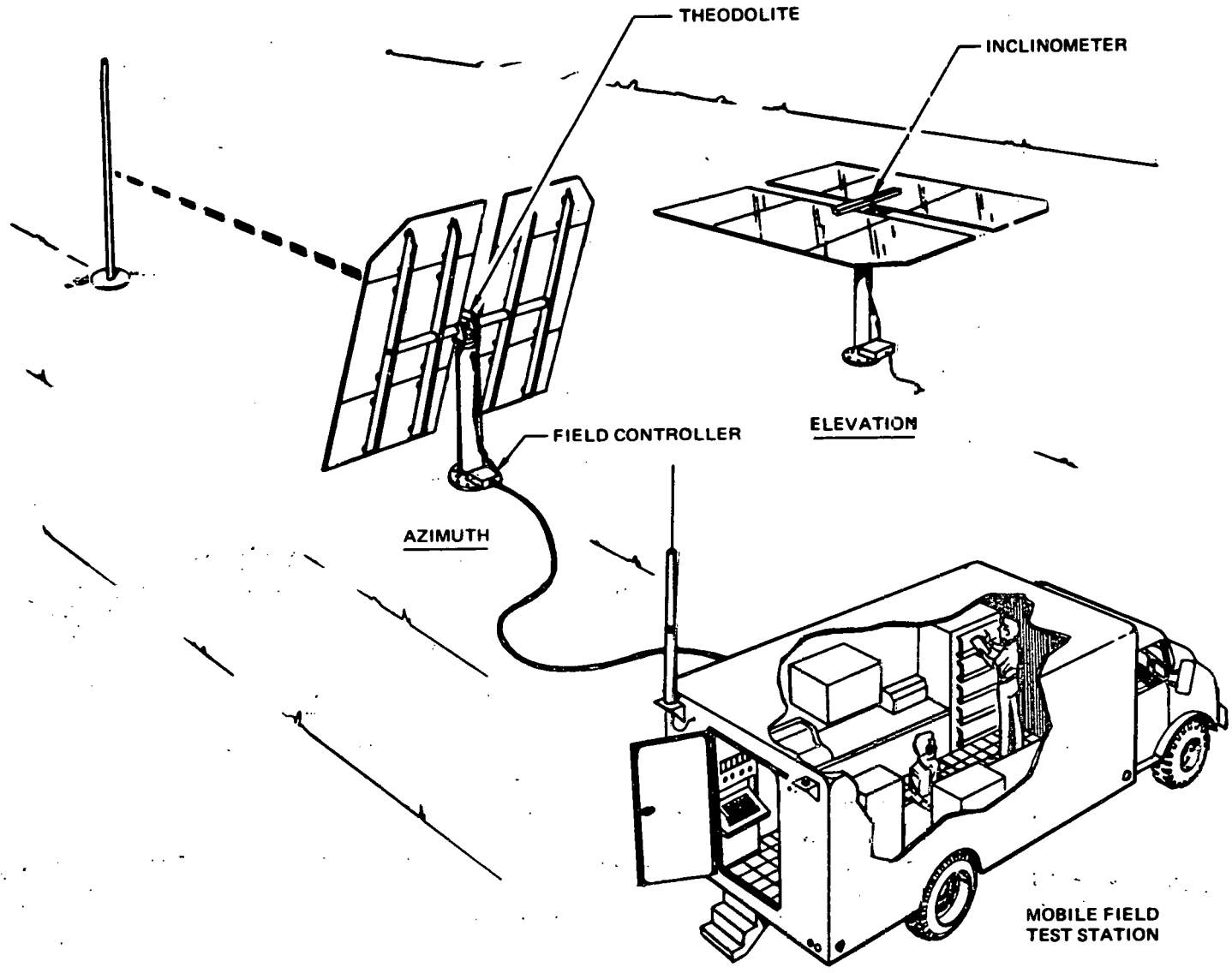

Figure 3-21. Heliostat Referencing

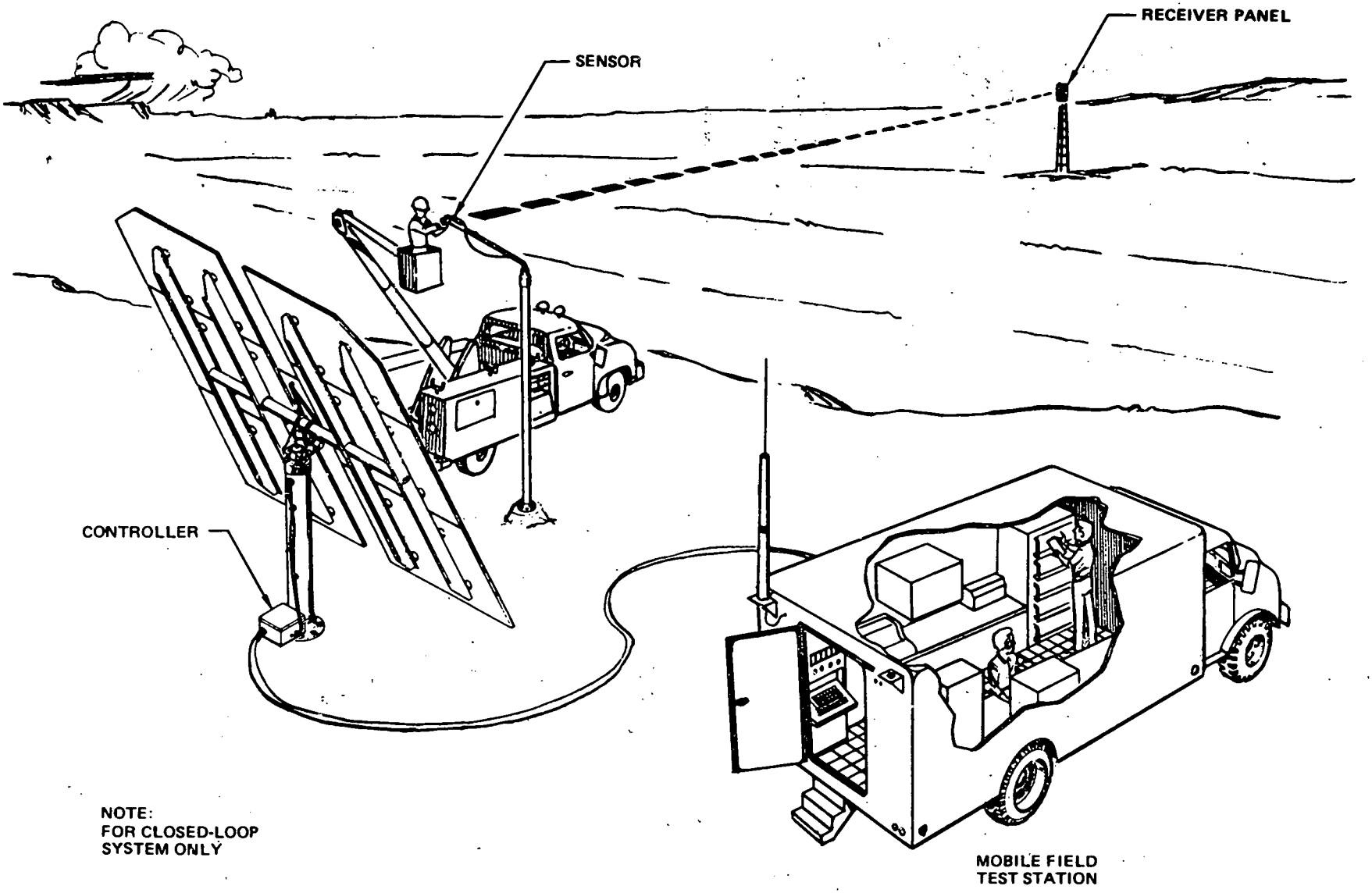

Figure 3-22. Heliostat Sensor Alignment

3.3.2.6 Heliostat Checkout Tasks

Perform Compatibility Checkout. After installing heliostats, verification tests and checkouts are performed to ensure the compatibility of a field controller and a cell of heliostats. The mobile field test station is connected to the field controller, and the cell of heliostats is commanded to individually acquire sun, normal track, synthetic track, slew off receiver, wash position inverted position, and stow position. This test verifies that each heliostat in a cell is properly interfaced with the field controller.

Perform Cell Operational Checkout. The final collector subsystem test of the installation phase takes place prior to Pilot Plant system testing. During this activity, it will be necessary to have water flowing through the receiver panel. Cell-by-cell tests of tracking, slew-off, and stowage actions are performed (Figure 3-23). Stringent safety precautions must be enforced to preclude personnel injury from reflected beams.

3.3.2.7 Resource Requirements

Using the quotient of the difference in installation rates as a rate factor; i.e.:

$$\frac{40 \text{ Hel/day}}{10 \text{ Hel/day}} = 4$$

a rough estimate of the resources needed to accomplish a Commercial Plant collector installation is presented in this section.

Support Equipment

Estimated support equipment requirements are shown in Table 3-8. It is probable that the quantities shown could be reduced somewhat by in-depth planning and scheduling. Pilot Plant experience will undoubtedly impact both quantities and design of support equipment.

Personnel

The estimate of personnel requirements was developed in the same manner as that for support equipment, and the same statements regarding planning, scheduling, and Pilot Plant experience apply here.

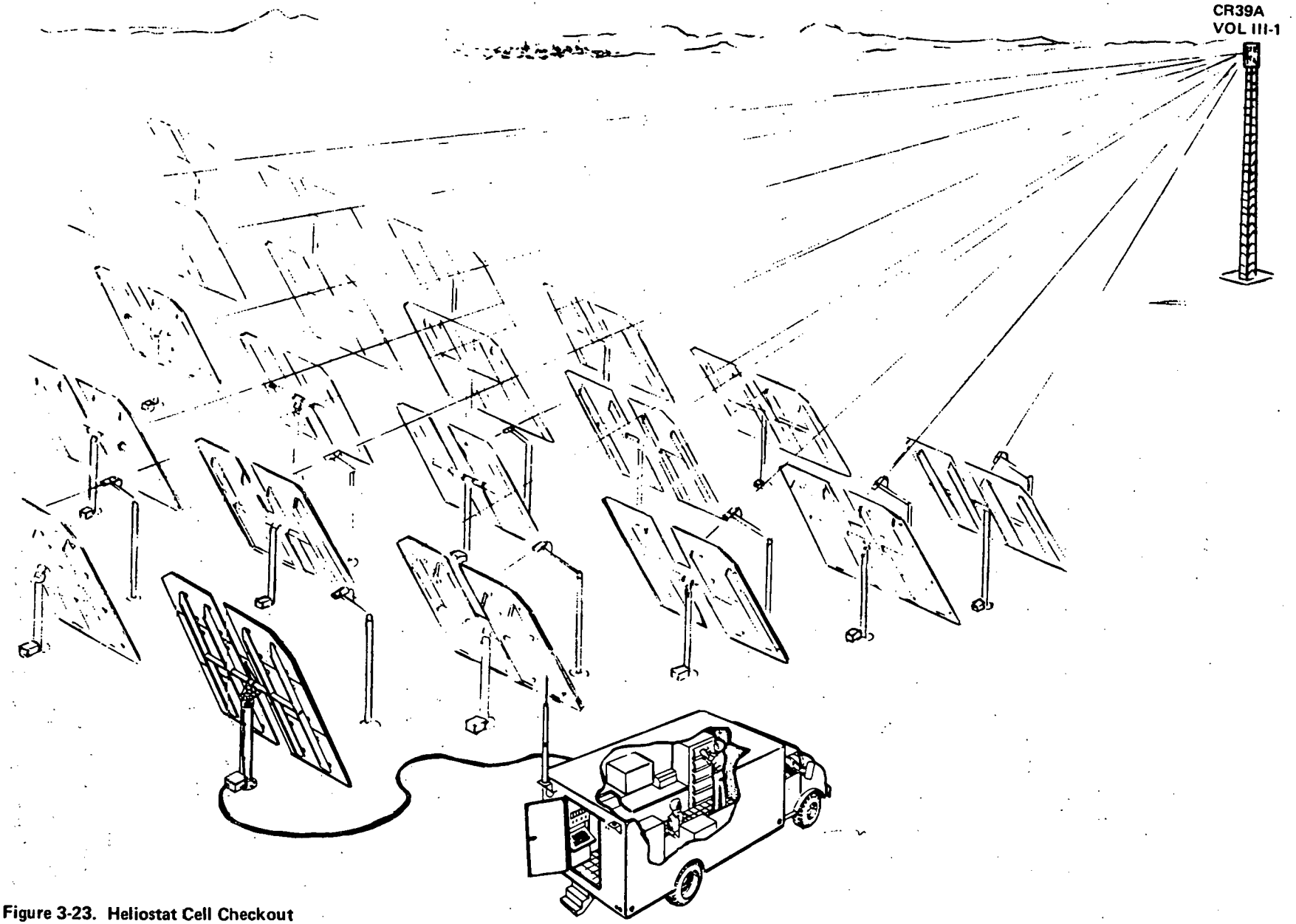

Figure 3-23. Heliostat Cell Checkout

Table 3-8

SCALE-UP OF SUPPORT EQUIPMENT

Nomenclature	Pilot Plant Qty	Rate Factor	Commercial Plant Qty
Heliostat Handling Fixture	2	4	8
Handling Sling, Heliostat Mirrors	2	NA	4
Mobile Workstand (Cherry Picker)	2	4	8
Pedestal Leveling Fixture	2	NA	4
Power Torque Wrench	2	4	8
Forklift	1	4	4
Multimeter-Volt Ohmmeter	6	NA	10
Digital Voltmeter	6	NA	10
Pickup Truck, Modified to Incorporate Workstand in Truck Bed	2	4	8
Mobile Crane	1	4	8
Walkie-Talkie Communication Sets	4	NA	10
Inclinometer	2	4	8
Theodolite	2	NA	4
Mobile Field Test Station	2	4	8

NA - Not applicable, maintenance equipment is used to support I&C

While the Commercial Plant requirements for support equipment shown in Table 3-8 are finite, the personnel requirements shown in Table 3-9 cannot be translated into cost directly. Precise scheduling for each task is essential to estimating the actual manhours required to perform the task. Figure 3-24 shows the period of performance for each major task.

Facilities

Two types of facilities are required during Commercial Plant collector installations: (1) office and storage space during the full installation period, and (2) classrooms for presenting training courses to installation and checkout personnel at the beginning of the period, and operating and maintenance personnel near the end of installation and checkout activities.

The first requirement will be satisfied by incorporating adequate floor space and furnishings into the final assembly building.

Table 3-9

SCALE-UP OF PERSONNEL

Task	Pilot Plant Qty	Rate Factor	Commercial Plant Qty
Supervision	1	4	4
Level Foundation	1 2-man crew	4	4 2-man crew
Transport Heliostat	2 2-man crew	4	8 2-man crew
Emplace Heliostat and Install Sensor Mirror	1 4-man crew	4	4 4-man crew
Connect Cables to Heliostat	1 1-man crew	4	4 1-man crew
Perform Heliostat Electrical Checks	1 2-man crew	4	4 2-man crew
Align Heliostat and Run Operational Checks	1 3-man crew	4	4 3-man crew
Install Sensor Pole	1 3-man crew	4	4 3-man crew
Install Sensor	1 2-man crew	4	4 2-man crew
Connect Sensor Cables and Make Electrical Checks	1 3-man crew	4	4 3-man crew
Align Sensor	1 4-man crew	4	4 4-man crew
Perform Compatibility and Cell Operational Checkout	2 4-man crew	NA	3 4-man crew

NA - Rate factor not applicable

Space for conducting training courses will probably be rented near the site.

Training Material and Installation Procedures

Both training courses and aids, and installation procedures developed for and perfected during the Pilot Plant program will be available for Commercial Plant program use.

Spares

Only a minimal quantity of low-cost spare items would be required as an initial buy. Higher-cost items, such as electronic controllers, reflector panels, etc, would be discrepant components. Repair or procurement of replacement parts would be accomplished within the production system.

3.3.2.8 System Test

The next phase of the program following I&C of the subsystems is a system test to verify that all interfaces among the subsystems have been correctly

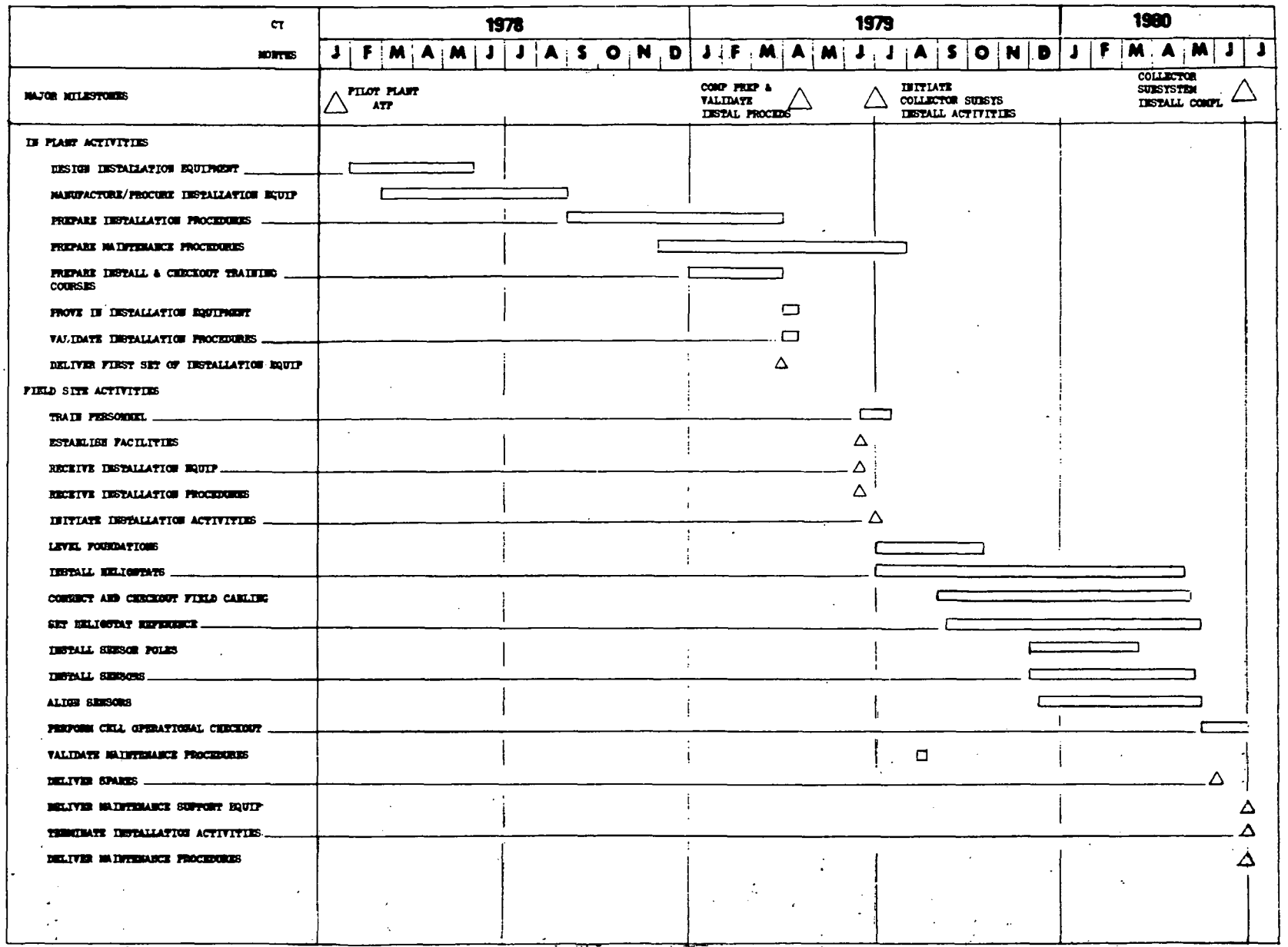

Figure 3-24. Collector Subsystem — Field Site Installation and Checkout Schedule (Closed Loop)

made, and that the system output matches the system specification values. During this six-month period the support system described in Section 3.3.3 will be implemented and refined to accommodate changes resulting from field experience.

3.3.2.9 System Operations

After system test has proven the Commercial Plant's operational capability, normal plant operations are started. These operations are planned to continue for 30 yr, and will be supported and maintained in accordance with the system support concepts provided in Section 3.3.3. Cost-saving improvements in the support system will develop over the years until an optimized support operation is attained.

3.3.3 Commercial/Collector Subsystem Support Concepts

Concepts covering support requirements for a 100-MW Commercial solar thermal power system were developed by using system requirements as a baseline, and by identifying site activation installation and test requirements, and subsequent power generation operations. These concepts are subject to change depending on knowledge and experience gained during operation of the Pilot Plant.

3.3.3.1 Installation and Checkout Operations

Planning and preparation for the 100-MW Commercial Plant will be based on experience gained during installation and checkout of the 10-MW Pilot Plant. All necessary scheduling, ordering of equipment and materials, and hiring of personnel will be accomplished with sufficient lead time to effect a smooth operating capability at the onset of site activation.

Transportation, Handling, and Packaging

The quantity of material that must be brought to site for assembly and installation of 22,914 heliostats probably justifies construction of a railroad spur to the site. After selection of the Commercial Plant location, a tradeoff study will consider the cost of the spur and the cost of trans-shipping the material from the nearest rail siding by truck.

Facilities

Facilities mentioned in Section 3.3.2.2 will be used to support I&C operations.

Support Equipment (Table 3-8)

Two categories of support equipment, with some commonality, will be used during I&C operations. One category will be the plant operations and maintenance support equipment (special tools and test equipment); the other category will be the specialized I&C equipment. This design and use of both categories will have been used, tested, improved as necessary, and certified during Pilot Plant I&C. One complement of operations support equipment will be provided at site. The mix and quantity of specialized I&C equipment will be dependent on installation rates which must be met to comply with I&C schedules.

Specialized I&C equipment could be leased or purchased. The cost-effective choice will have to be determined, considering such factors as degree of specialization, amoritization period, availability, and others.

Maintenance

Maintenance activities during installation and checkout of the collector subsystem will be responsive to:

- Protecting installed equipment from environmental effects.
- Repairing damaged equipment during installation and checkout operations.
- Discovering discrepant items.

Periodic maintenance will be scheduled for inspection and recertification of support equipment, inspection of installed equipment, and operations such as washing reflector surfaces and lubricating mechanical equipment.

Corrective maintenance will be accomplished by removal and replacement of damaged or discrepant items. Repair of items will be accomplished at site or at the appropriate manufacturer's facility.

Spares Supply

Approved quantities of consumables and low-cost spares and repair parts, as defined by maintenance data analyses, will be acquired and delivered to support installation and checkout operations and maintenance tasks.

High-cost spares, such as reflector panels and field controllers, will not be acquired. As the need arises for this type of spare, the item will be diverted from the production line. Then a spare will be ordered and turned over to the production line as a replacement. This concept reduces investment in high-cost spares and ensures installation and checkout scheduled completions.

The approved quantities of spares and repair parts needed to support equipment unique to I&C tasks, i.e., equipment not used after I&C will be acquired and delivered to site as required to support I&C operations.

Technical Documentation

The performance of I&C, operations, maintenance, and turnover tasks will be controlled by technical documentation emanating from MDAC, MDAC subcontractors, Government agencies, and commercial agencies. Applicable regulations, procedures, plans, manuals and specifications will be identified, with effective dates, in the site activation plan. Production and installation drawings, with effective change identification, will be identified on a job drawing list or lists. Except for post Pilot Plant changes and additions, the technical documentation made applicable to the Commercial Plant will have been used and verified during Pilot Plant I&C. Critical technical documents will be controlled so that all changes receive program Office review and approval prior to issuance.

3.3.3.2 Commercial Operation

The customer will assume responsibility for operations and maintenance of the Commercial Plant at the end of I&C. Support concepts could be totally implemented and carried over into the Commercial operations phase. MDAC could furnish technical support to the customer until full operations and maintenance capabilities are established.

Preliminary analysis of a Commercial Plant operational requirements provides a bias toward a concept of maximum repair at the operating site. This concept is reinforced by the remoteness of the site and the expected operating life of the plant. It appears that this concept could be further expanded to include the support of several individual plants by a single maintenance and supply depot. The feasibility and application of such a concept would be dependent on many variables, each of which would require

detailed study. Also a limiting factor would be the acceptable response time for correction of a single point failure occurring at the most remote plant. The functional concepts presented in the following subsections will be applied to the degree feasible during Pilot Plant operations for verification expansion, and improvement.

Transportation Handling and Packaging

At the present level of analysis, the categories of transportation requirements identified are:

A. Intrasite. Movement of personnel, equipment, parts, and tools to and from the areas where maintenance activities take place.

B. Intersite/External. Movement of replenishment material to site and repairable items to and from repair locations.

At this time, the concept for supporting Category A is the establishment and maintenance of a site motor pool with sufficient numbers and types of vehicles to handle estimated workloads.

While use could be made of the site motor pool vehicles in support of Category B, the present concept is to use commercial transportation facilities. These would include truck, rail, and air transport as appropriate for points of origin or destination, and for the urgency of the requirements.

Spares and repair parts shipped to site by the manufacturers should be packaged and preserved to provide a minimum storage of 2 yr. Proper packaging control would be effected by citing the appropriate commercial and special packaging and preservation specifications on purchase orders released to suppliers. Preparing repairable items for shipment to repair facilities would be done in the receiving and shipping facilities.

The distribution and storage center which was set up during site activation will remain active to perform receiving, shipping, material handling, transportation, and traffic management functions.

Facilities

Although facilities criteria have not been developed for a Commercial Plant, the following are considered basic requirements for adequate support of the

operating modules. It is postulated that support facilities should be centralized to effect economies in investment and operating costs.

A. Prime Module. The prime module is defined as the 100-MW power generating module, probably the first to be constructed, selected to be the maintenance and supply depot for all of the area modules. With the present visibility of Commercial Plant operations, the following are considered basic requirements for support facilities:
   1. A motor pool including, servicing, repair, and petroleum, oil, and lubricant storage facilities.
   2. A shipping and receiving dock, including installed handling equipment, and packaging and crating tooling.
   3. A repair and maintenance building, including installed machine shop, welding shop, and test equipment.
   4. A central warehouse and stockroom, including a controlled tool crib.
   5. Washing and toilet facilities for maintenance personnel, including an adequate number of lockers for storing personal possessions.
   6. A food and drink dispensing facility, probably a cafeteria.
   7. A medical care facility that meets OSHA specifications.

B. Satellite Module. A satellite module is defined as any 100-MW power generating module dependent on a prime module for maintenance and supply support. Although a satellite module is supported by the prime module, the following are considered to be requirements for support facilities at each satellite module:
   1. A stockroom and controlled tool crib.
   2. An instrument repair and calibration room.
   3. Washing and toilet facilities for maintenance personnel, including an adequate number of lockers for storing personal possessions.
   4. A medical facility that meets OSHA specifications
   5. A food and drink dispensing facility.

Support Equipment

The support equipment required for corrective and scheduled maintenance tasks is listed in Table 3-10.

Table 3-10

REQUIRED SUPPORT EQUIPMENT

Mobile Workstand (Cherry Picker)	Beam Sensor Alignment
Mobile Crane	Heliostat Hoisting
Forklift	Miscellaneous Heavy Equipment Handling
Hoisting Slings - General Purpose	Heliostats and Miscellaneous Equipment Hoisting
Pick-up Truck	General Purpose
Inclinometer	Pedestal Leveling
Mobile Communications Set	Field Communications
Theodolite	Heliostat Alignment
Hoisting Sling - Heliostate Mirror	Mirror Panel Replacement
Pedestal Leveling Fixture	Pedestal Leveling
Reflector Washing Equipment	Heliostat Reflector Cleaning
Collector Field Test Station	Subsystem and Component Level Fault Isolation and Test

Equipment Maintenance

The basic corrective and scheduled maintenance tasks for the collector subsystem have been determined by a hardware analysis to identify maintenance-significant components. Maintenance-significant components are defined as hardware items for which a discrete maintenance action is required based on the maintenance concept. These maintenance actions result from equipment failures or may be scheduled actions such as cleaning or lubrication to prevent equipment deterioration and/or to sustain performance characteristics. Table 3-11 lists the maintenance significant components and provides a brief description of the required maintenance actions.

Table 3-11

MAINTENANCE-SIGNIFICANT ITEMS

Component	Corrective Maintenance	Scheduled Maintenance
Field Controller	Remove and replace on failure. Minor repair on-site.	None
Heliostat Controller	Remove and replace on failure. Minor repair on-site.	None
Elevation and Azimuth Drive Assemblies	Remove and replace on failure.	Lubrication
Elevation and Azimuth Drive Motor and Reducer	Remove and replace on failure.	None
Elevation and Azimuth Shaft Encoder	Remove and replace on failure.	None
Elevation and Azimuth Shaft Turn Pickoff	Remove and replace on failure.	None
Pedestal J-Box	Remove and replace detail parts on failure. Remove and replace box for major damage.	None
Pedestal	Structural repair. Remove and replace for major damage.	None
Reflector Panel	Remove and replace. Discard. Clean (In addition to scheduled requirements due to severe weather conditions.)	Clean
Reflection Structure	Structural repair. Remove and replace for major damage.	None
Beam Sensor	Remove and replace on failure.	None
Sensor Pole	Structural repair. Remove and replace for major damage.	None
Field Cables	Electrical repair. Remove and replace for major damage.	None
Power Distribution Panel	Remove and replace detail parts. Replace panel for major damage.	None
Power Transmission	Remove and replace on failure.	None
Test support station	Remove and repair components on failure.	Calibrate test equipment, inspect, clean, adjust and lubricate CRT/ keyboard, tape reader, and recorder

Scheduled Maintenance

The scheduled maintenance actions for subsystem operating equipment consists of periodic cleaning of mirror surfaces to maintain required reflectivity, lubrication of elevation and azimuth drive units, and an annual damage and corrosion-control inspection. Scheduled maintenance for maintenance support equipment includes test equipment calibration and servicing and load test recertification for handling and hoisting equipment. Tasks and frequency requirements are identified in Table 3-12.

Corrective Maintenance

Corrective maintenance actions unique to the collector subsystem are listed in Table 3-13. Critical alignments and adjustments are necessary following removal and replacement of heliostat components and sensors. Descriptions of critical alignments and adjustments are in the paragraph on Installation Tasks.

Table 3-12

SCHEDULED MAINTENANCE REQUIREMENTS

Component	System Quantity	Task	Frequency
Subsystem Equipment			
Heliostat Reflectors	22,914	Clean	30 Days
Heliostat Drive Units	45,828	Lubricate	Annual
Heliostat Assembly/Field	22,914	Inspect	Annual
Support Equipment			
Handling Sling - Mirror	8	Load Cert.	Annual
Mobile-Field Test Station	8		
Printers, CRT/Keyboard Tape Reader, Recorder, Digital Eye System		Insrt and Service	30 Days
Multimeter, Oscilloscope, Digital Counter, Mfgr.		Calibrate	6 Mo

Table 3-13

CORRECTIVE MAINTENANCE
MAINTENANCE MANHOURS PER MAINTENANCE TASK

Item	Component/Task	*EMT	Elect Tech	Mech Tech	Opt Tech	Crane Oper	Forklift Oper	Rigger	Trnchr Oper	C-Picker Oper
1	Field Controller (F/C)									
	Remove/Replace	1.36	1.36	1.36	1.36					
	Repair	0.66	0.66	0.66	0.66					
2	Heliostat Controller (H/C)									
	Remove/Replace	1.10	1.10	1.10	1.10					
	Repair	0.53	0.53	0.53	0.53					
3	Azimuth Drive Assembly									
	Remove/Replace	2.68	2.68	5.36		1.93	1.93	3.86		
4	Elevation Drive Assembly									
	Remove/Replace	2.43	2.43	4.86		1.68	1.68	3.36		
5	Elevation Dr Motor and 1st Stage Drive									
	Remove/Replace	1.54	1.54	3.08						
6	Az Dr Motor and 1st Stage Drive									
	Remove/Replace	2.15	2.15	4.30						
7	Elevation Shaft Encoder									
	Remove/Replace	1.10	1.10	1.10						
8	Az Shaft Encoder									
	Remove/Replace	1.62	1.62	1.62						
9	Elevation Shaft Turn Pickoff									
	Remove/Replace	1.05	1.05	1.05						
10	Az Shaft Turn Pickoff									
	Remove/Replace	1.33	1.33	1.33						
11	Pedestal J-Box (with F/C)									
	Remove/Replace	4.00	4.00	4.00						
	Repair	1.60	3.20							
12	Pedestal J-Box (with H/C)									
	Remove/Replace	3.50	3.50	3.50						
	Repair	1.45	2.90							
13	Pedestal									
	Remove/Replace	1.57	1.57	3.14	0.30	1.47	1.47	2.94		
	Repair	0.80		1.60						
14	Reflector Panel									
	Remove/Replace	1.12	1.12	2.24		1.12		2.24		
15	Reflector Structure									
	Remove/Replace	5.04	5.04	10.08		4.00		8.00		
	Repair	0.88		1.76						
16	Beam Sensor									
	Remove/Replace	1.12	1.12	1.12	1.12					1.12
17	Sensor Pole									
	Remove/Replace	1.01	1.01	2.02	0.25		0.76			0.60
18	Pedestal Cables									
	Remove/Replace	1.66	3.32							
	Repair	1.45	2.90							
19	Field Cables									
	Remove/Replace	6.05	12.10	6.05					3.00	
	Repair	2.13	4.26							
20	Distribution Panel									
	Remove/Replace	4.03	4.03	4.03			0.50			
	Repair	1.23	1.23	1.23						
21	Transformer									
	Remove/Replace	8.55	8.55	12.60			2.00			
	Repair	2.68	2.68	2.68						

*EMT = Elapsed Maintenance Time

Supply

The preliminary supply support concept is responsive to the basic concept of having a centralized maintenance and supply depot located at the selected prime power plant module. The bulk of spares and repair parts would be received, stocked, and issued there, with only selected spares and repair parts stored for use at the satellite modules.

The selection and positioning of spares, repair parts, and consumables will depend on the levels of repair determined by the support requirements analysis and the following criteria:

A. The mean-time-between-maintenance-actions provided by the maintainability analyses will be the departure point for spares determinations. The quantities and mix will be such that there is a 90% probability of a part being available on demand.

B. Pipeline quantities will be determined on the basis of system location demand rate and repair cycle times. Resupply methods, distribution, and location of system stocks will be determined after site selection.

C. Long-leadtime supply items will be procured or released early enough to be on site 30 days prior to initial operation. Other items will be procured or released leadtime away to minimize obsolescence due to design changes, except for those items for which significant cost savings can be achieved through acquisition concurrent with production.

Technical Documentation

Maintenance procedures will have been prepared and used during Pilot Plant operations. Instructions will define preventive and corrective maintenance, fault detection, inspection, alignment, lubrication, and repair requirements.

Instructions will be updated, to reflect equipment modifications and procedural improvements.

Training

A training program developed for Pilot Plant operations will include courses and pertaining to collector subsystem requirements for tasks, maintenance, and skills, and will be presented to personnel selected for site operations.

Primary method will be on-the-job/on-equipment training with supervision by a knowledgeable training engineer.

The training program will be time-phased to ensure a smooth and effective operation at the onset of site activation.

Section 4

PILOT PLANT COLLECTOR DEFINITION

The Pilot Plant collector subsystem has been designed to be the best representation of the best Commercial Plant collector possible, consistent with production volume and plant size. The collector subsystems for both the Commercial and Pilot Plants were described in Section 1.1 and the Commercial collection in Section 3. The Pilot Plant collector described in this section is the result of flowdown of the Commercial collector design and requirements, results from the collector Subsystem Research Experiments (SRE), and lower-level trades considering Pilot Plant peculiar requirements and available materials and technology.

4.1 PILOT PLANT COLLECTOR REQUIREMENTS

The Pilot Plant collector requirements are in general identical to those for the Commercial Plant. This section summarizes requirements with the source (Commercial Plant flowdown or Pilot Plant peculiar) identified.

4.1.1 Performance Requirements

The Pilot Plant reflector should reflect the sun's light with an average specular reflectivity of 0.88. This requirement is based on available, suitable materials for the Pilot Plant.

The heliostat should reflect the sunlight with combined beam and tracking errors of less than 3 mr standard deviation, and concentrate the maximum cost-effective fraction of the sun's light on the receiver in the prescribed distribution. This requirement flows down from the Commercial plant.

The heliostat slew rates about the drive unit axes should be greater than 12 deg/min to permit rapid stowage during a rising wind. Other slew rate requirements such as emergency defocus from the receiver, sun acquisition from stowage, and orientation for maintenance result in lower rate requirements. These requirements flow down from the Commercial Plant.

The heliostat fundamental vibration frequencies shall be greater than 1 Hz to preclude dynamic coupling with the controls system and minimize wind-induced vibrations. The heliostat and sensor pole shall not undergo flutter or divergence for survival winds up to 40.3 m/s (90 mph). These requirements also stem from the Commercial Plant requirements.

4.1.2 Environmental Requirements

The heliostat shall withstand winds with peak gust speeds up to 40.3 m/s (90 mph) in the stowed position without damage. The heliostat shall also withstand winds up to 22.4 m/s (50 mph) in any orientation without damage. These wind speeds are flowdown requirements from the Commercial Plant. The heliostats and controls system shall withstand temperatures from -30°C (-22°F) to +49°C (120°F) without damage and shall be able to operate.

The heliostats and controls shall withstand ice loads up to 50 mm (2 in.), snow loads up to 250 Pa (5 psf), rain up to 50 mm per hour (2 in./hr), and blowing dust up to 10^{-5} Hz/m^2sec (10^{-5} gm/m^2sec) without damage.

The reflective surface shall survive hailstones up to 19 mm (3/4 in.) at 20 m/s (65 fps) in any orientation and 25 mm (1 in.) at 23 m/s (75 fps) in preferred orientations without damage. Earthquakes with peak ground accelerations up to 0.25g shall also be survived without damage.

All of the above requirements flow down from the Commercial collector requirements.

4.1.3 Safety Requirements

The heliostats must always be controlled such that no unsafe combinations of beam intensity, irradiance, and retinal image size may exist outside of a prescribed exclusion area in the airspace surrounding the Pilot Plant. Heliostat beams falling on the ground or on structures within the Pilot Plant boundaries will similarly be controlled to preclude personnel hazards and possible damage to structures. Prescribed safety equipment may be considered in determining hazardous light levels within the Pilot Plant. While this requirement flows down from the Commercial Plant, the details which result will be somewhat different because of different focal lengths of the two systems.

Applicable Federal and State OSHA regulations will apply. In addition, other safety codes such as National Fire Protection Association (NFPA) and American National Standards Institute (ANSI) requirements will be observed, as in the Commercial Plant. The collector field shall be capable of being safely stowed in the event of (1) primary power source (EPGS) failure, (2) loss of power at a critical point in the distribution network, (3) loss of communications with the system Master Control, (4) failure of a field controller, or (5) failure of a heliostat. The collector field shall be capable of indicating to the system master control the operational status of all critical components implied above and signaling to the system master control any failures of those components to respond to command.

4.1.4 Interface Requirements

The Pilot Plant collector will simulate and demonstrate all Commercial Plant collector subsystem interfaces. The Pilot Plant will draw operating power from the EPGS. While voltages need not be the same, the principle of primary and secondary feeder cables interfacing at a stepdown transformer will be demonstrated. Primary control of the collector field will be through a communications interface with the system Master Control. The collector field shall concentrate the sun's light on the receiver in the manner prescribed in Section 4.1.1.

4.1.5 Operating Modes

The Pilot Plant collector subsystem will be capable of simulating and demonstrating all of the commercial collector subsystem operating modes. These modes include (1) normal tracking, wherein the heliostats track the sun autonomously, (2) synthetic tracking, wherein the heliostats track any moving point in the sky and to any moving target point within an allowed range of motion under the direction of the system master control, (3) command positioning, wherein the heliostats assume a directed position for stowage, cleaning, other maintenance, etc, (4) local manual control at the field controller, and (5) local manual control at the heliostat controller.

4.1.6 Stowage

The Pilot Plant shall be capable of executing and demonstrating the potential Commercial Plant stowage positions. These positions are (1) vertical stowage, wherein the heliostat is oriented with its reflective surface vertical to within ± 15°; (2) inverted stowage wherein the heliostat is oriented with its reflective surface horizontal to within ± 2° and face down, (3) face-up stowage wherein the heliostat is oriented with its inflective surface horizontal to within ± 2° and face up.

During vertical stowage, the heliostat may be rotated to any azimuth orientation. The system Master Control and power supplies must be available to permit horizontal stowage (face-up or inverted) in the event of high winds, blowing sand and dust, light rain, etc. During horizontal stowage, the heliostat may also be rotated to prefered azimuth orientations. If these orientations are to be used to reduce the peak drive unit loads, system Master Control and system power must be available and ensured during high winds and failure to achieve the preferred orientation must result, at most, in damage limited to the drive unit elements suffering degraded performance.

4.1.7 Production and Support

The Pilot Plant collector field will be designed to facilitate economic production and installations. The production and installation methods employed must aid in meeting the Pilot Plant goal of "indicating economic feasibility of a Commercial Plant" through a design, production technique, and installation method which will provide economic data for the Commercial Plant.

The support concept of the Pilot Plant should likewise simulate that of the Commercial Plant to provide economic data on operating costs. The collector should be designed to facilitate cleaning and other scheduled and unscheduled maintenance activities.

4.2 PILOT PLANT COLLECTOR DESIGN

The Pilot Plant collector design flows down from the requirements in Section 4.1. The Pilot Plant collector field simulates as closely as possible the characteristics of the Commercial system collector field (Section 4.2.1). The collector design is discussed in Sections 4.2.2 through 4.2.10. The design covers:

- Reflector.
- Structural support.
- Drive unit.
- Pedestal/foundation.
- Closed- and open-loop control.
- Controls sensors.
- Field controller.
- Heliostat electronics.
- Collector field wiring.

The safety, availability, and support concepts are covered in Sections 4.2.11 through 4.2.13.

4.2.1 Pilot Plant Collector Field Layout

The principal objective in defining the Pilot Plant collector field is to simulate as closely as possible the characteristics of the Commercial system collector field. This simulation objective includes both the heliostat packing characteristics and the relative geometry between the heliostats and the receiver.

In making the transition to the Pilot Plant collector field, it is seen that the cellwise approach, used to analyze the Commercial system, is of questionable worth in the Pilot Plant because each cell contains only a few heliostats (typically 10 to 30) with most interacting with the cell boundaries. Thus, preserving the cellwise approach to the layout would produce a large number of discontinuities and local compromises in the layout required to transition between cells.

The Commercial optimized collector field laid out in the radial staggered arrangement is so nearly circular (see Appendix D, Volume II) that it

seems appropriate to assume that the Pilot Plant could be laid out along unbroken circular rows. The next issue which must be addressed is how the radial stagger arrangement can best be fitted into the circular field layout. The stagger requires adjacent circles to have the same number of heliostats, so that the inner circles become progressively compressed, until an unacceptable density occurs. Consequently, the field has to be split into circular zones. The zone boundary allows for a decompression via lessening the number of heliostats per circle in the inner zone. Six zones are required for the Pilot Plant.

The transitions required between the zones could be accomplished by opening circular gaps between adjacent layout circles at the interface or by using a series of exact ratios for reducing the heliostat density. By using the gap approach, a significant portion of effective ground area is unusable which forces the heliostats that would normally be placed in those areas to more remote and less effective locations in the field. The exact ratio approach minimizes the existence of such wasteful gaps and thus appears to be a superior approach.

A series of studies produced the following results regarding the rationing down in numbers of heliostats in adjacent circles:

A. 3/2 provides excess decompression, resulting in wasted space.
B. 4/3 provides an intermediate very satisfactory situation.
C. 5/4 provides too little decompression, resulting in many zones.

The 4/3 reduction leads to the situation shown in Figure 4-1. The outer three heliostat circles represent the normal radial stagger arrangement. With the third circle, it is assumed that the compression is becoming too severe so that a subsequent expansion in the layout is necessary. This third circle forms the slip plane which would correspond to the inner circle of one of the field layout zones. The expansion in the figure is accommodated by opening up the inner circle angular spacing by 4/3 over what was previously used. This results in a periodic lining up of heliostats in adjacent layout circles at the slip plane interface. This effect can be seen at the center of the third and fourth layout circles in the figure. Since a great deal of

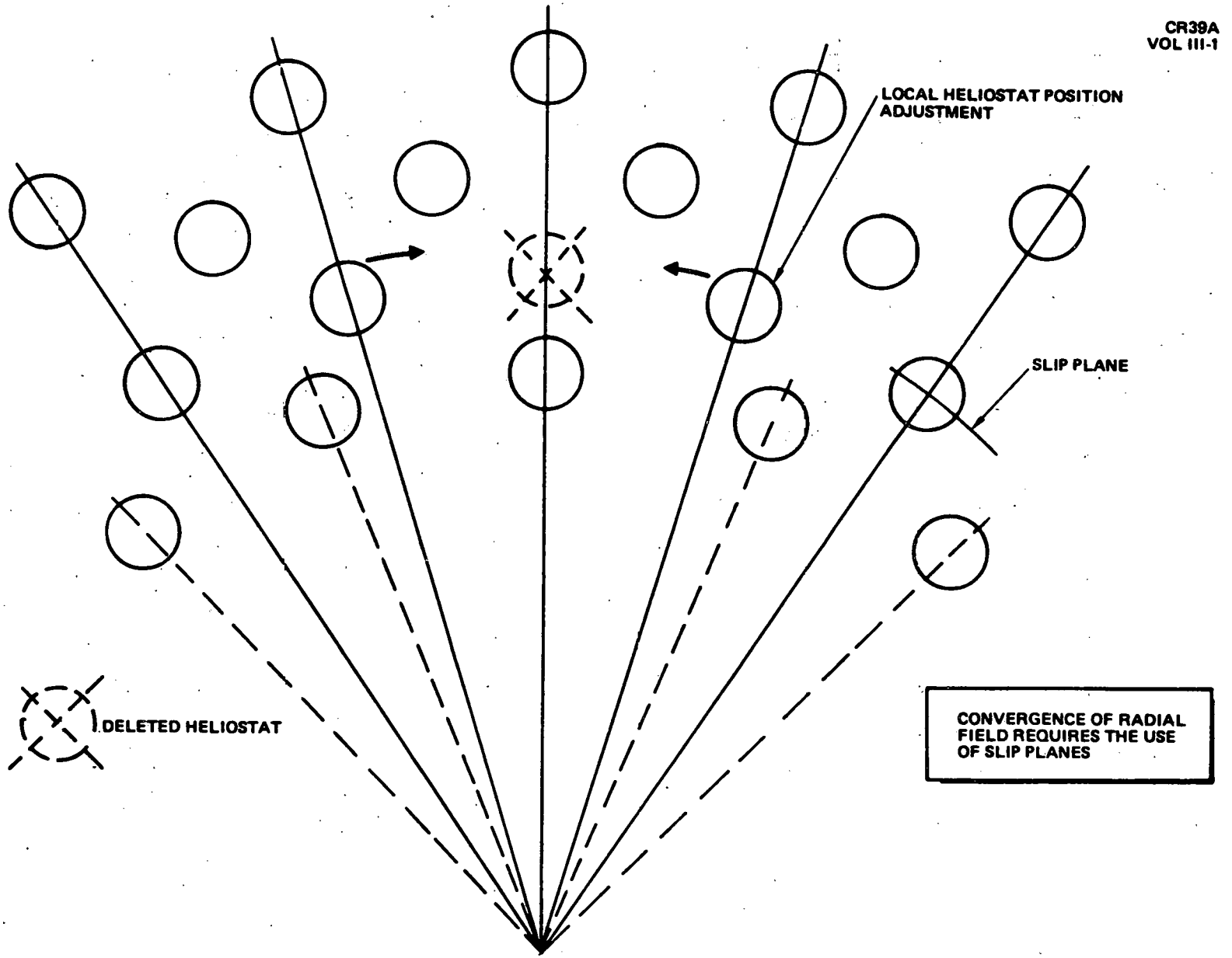

Figure 4-1. Radial Field Characteristic

blocking and shadowing would occur between these aligned heliostats, the more remote heliostat is deleted from the collector field as indicated in the figure. Heliostats on the same layout circle and immediately adjacent to the deleted heliostat are shifted somewhat into the void area to improve their optical performance. The degree of shift is limited by blocking and shadowing conditions with heliostats behind the one being shifted.

The resulting heliostat field layout which has been developed for the Pilot Plant was shown in Figure 1-2. As seen, the ideal circular field has been broken into quadrants by access roads. This has resulted in the displacement of some heliostats to more remote/less favorable locations. In all, 1,760 heliostats are included in the design, as follows:

	Required Heliostats
Minimum number required (ideal scaled collector field)	1,703
Impact of displacement for roads	+ 12
Field controller outage (1)	+ 24
Individual heliostat outages (5)	+ 5
Heliostats passing through control singularity	+ 16
Total	1,760

A heliostat reflectivity of 0.88 is assumed for this sizing analysis which would be representative of an average unwashed value. The outage assumption used in arriving at the total heliostat requirement is conservative in that the daily heliostat failure rate of 1 to 2 is more appropriate. If no failures are experienced at the winter 2 PM design point, an additional 1% degradation in heliostat reflectivity could be tolerated without impacting the system's ability to satisfy the design point point power level.

Before leaving the discussion on the overall Pilot Plant configuration, it is of interest to compare the fidelity of the Pilot Plant with the model Commercial system. Factors to be compared include the heliostat fields, the central receivers, and the total system perfomances. The Pilot Plant and the Commercial system use the same basic heliostat, so that Pilot Plant construction will contribute to the mass production experience for the heliostats

which will go into the ultimate commercial system. However, in order to maintain concentration with 7.8% as many heliostats, the Pilot Plant concept calls for canted heliostats. Six rectangular flat segments are used, canted to focus on the receiver. One might expect that this will lead to Pilot Plant concentration ratios of 46.8% of that for the Commercial system (6 x 7.8%). However, aim strategies are used to ensure that the incident heat flux on the receiver is compatible with its cooling capability. Peak heat fluxes of 0.3 MW/m^2 (0.184 $Btu)/_{sec-in^2}$) and 0.85 MW/m^2 (0.52 $Btu/_{sec-in^2}$) are the limiting design values for the Pilot Plant and Commercial system, respectively. The overall concentration ratio (glass area to receiver surface area) for the Commercial system is 638.5, while the corresponding Pilot Plant level value is 243.

A comparison of the ground coverage densities between the two systems is presented in Figure 4-2. The heliostat locations for the commercial system have been transformed to equivalent Pilot Plant field locations which are expressed in terms of layout circle number. The four lines for the Commercial system refer to the four indicated sectors of the field. In this way, a comparison with the complete Commercial system can be seen. Superimposed on this figure are the six solid lines which represent the equivalent ground coverage for the six Pilot Plant circular groups or zones. It is seen that a good agreement exists between the two systems except near the inner portion of the field, where locally higher coverage values occur for the Pilot Plant. Part of the reason for this is that the Pilot Plant field data that is available for every circle far exceeds the level of resolution possible for the commercial system which is defined in a gross cellwise manner. As a result, similar local effects would be anticipated for the Commercial system although they do not appear on the curve.

A comparison of local heliostat performance or "brightness" between the two systems is shown in Figure 4-3. The saw tooth pattern for the Pilot Plant is caused by the six layout zones which periodically compress and expand, causing the fluctuations in performance. It is seen that good overall agreement exists to the north and northeast directions from the tower while some discrepancies occur toward the south and southeast. Part of this effect

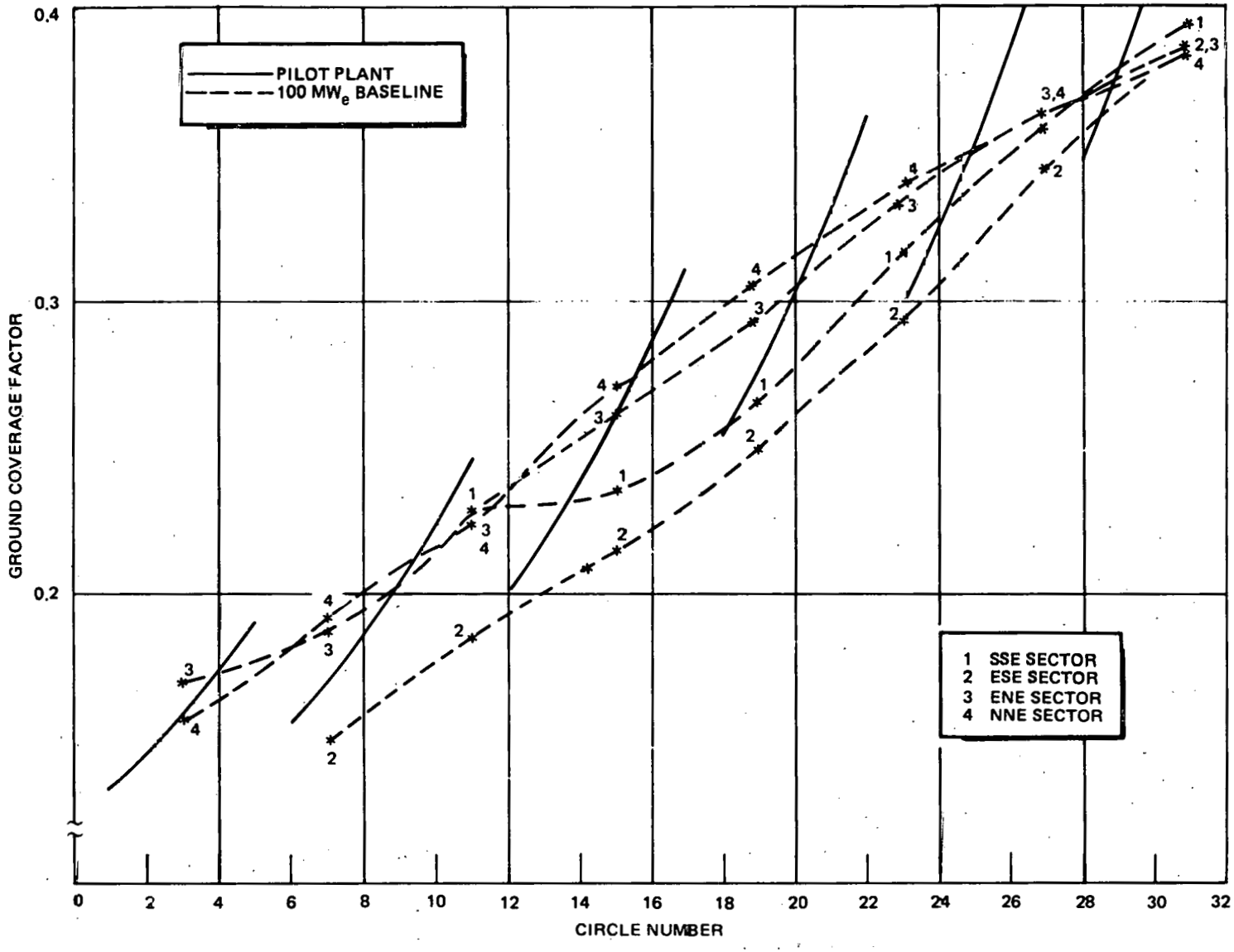

Figure 4-2. Ground Coverage Factor Comparison

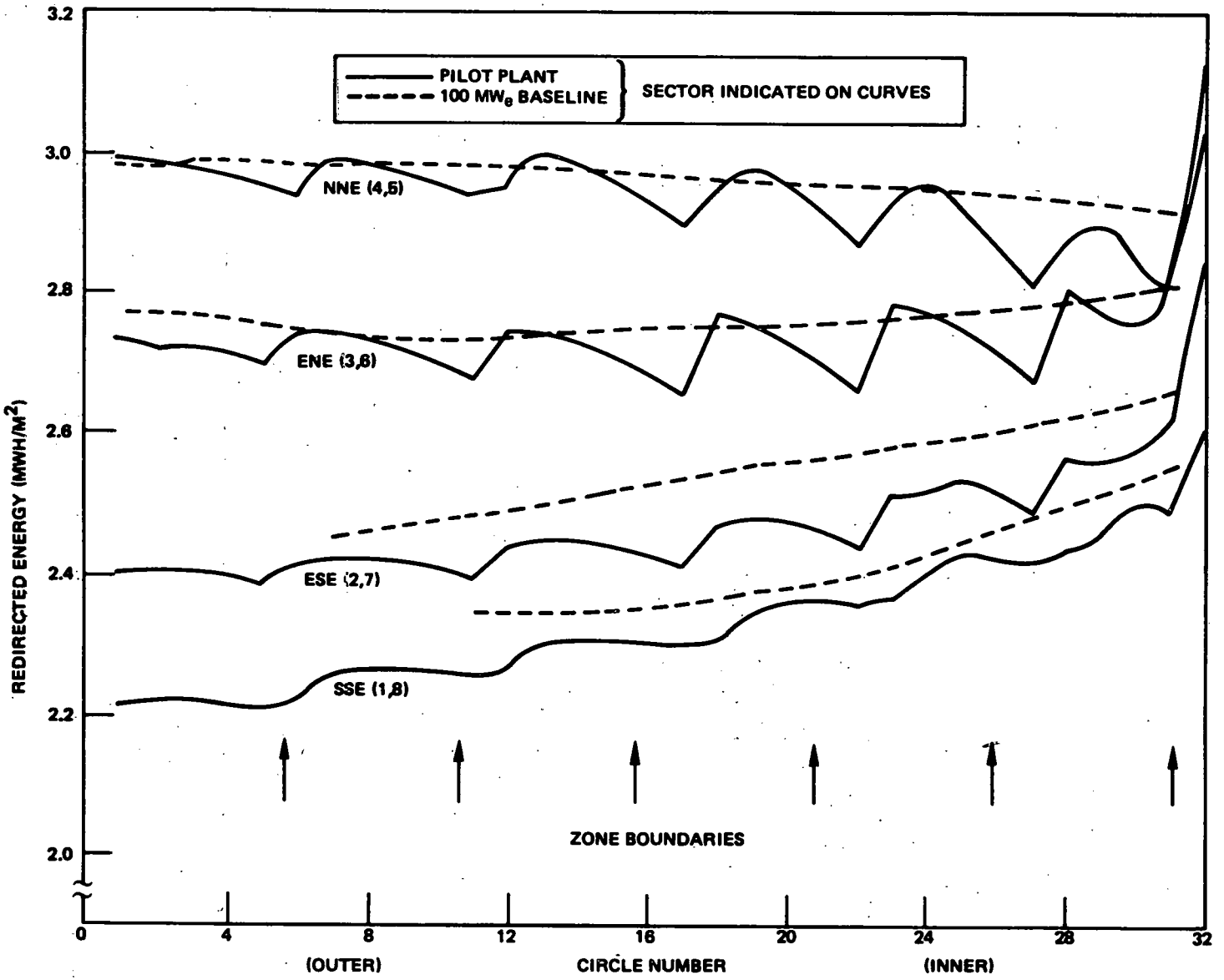

Figure 4-3. Annual Performance Comparison

is due to the north-south staggered pattern which was originally assumed for the south field of the commercial system. Unfortunately, changes in the computer codes during this period make it difficult to generate exactly comparable performance data for the 100-MWe radial staggered southern field. Every indication is that that correlation is appreciably better than the one shown here. In particular, note the expanded scale on the chart, the largest difference in redirected energy is about 4%. Thus, the variation of "brightness" in the 100-MWe baseline is well preserved in the Pilot Plant.

Preservation of this "brightness" and of the ground coverage is essential if the receiver in the Pilot Plant is to experience spatial and temporal flux variations which are representative of those which will be encountered in the Commercial system. Consequently, it is believed that the Pilot Plant will give a true representation of all the important behaviour and problems which will occur in the Commercial Plant. Further, all the various concerns of access, mechanical limits, and heliostat interactions which will occur in the Commercial system will be revealed in this Pilot Plant configuration.

4.2.2 Reflector Design/Performance

This section describes in detail the selection of the MDAC reflector panel design and rationale. First, a discussion of the mirror type, glass thickness, iron content, and reflectivity is given. Data are presented to support our choice of reflector design for the Pilot Plant, 1/8-in. float glass with 0.05% iron content and 91% reflectivity. Second, the development of the MDAC second surface reflector panel is traced, beginning with descriptions of a laminated mirror and a foam-core sandwich reflector. A detailed comparison between the two reflector panel types is then shown, listing the advantages and disadvantages of each, and ending with the rationale for MDAC's choice of the foam-core sandwich as the Pilot Plant design. Third, various design details of the reflector panel are given, such as panel dimension selection, panel description, edge seal, and weights of materials.

4.2.2.1 Selection of Glass Thickness/Iron Content

The theoretical total efficiency of silver is 98.7%*. The specular reflectance efficiency at 4 mr of commercially applied chemically deposited silver was measured to be 92.8% (Table 4-1). However, difficulty in stabilizing the signal and reducing background noise level at the 4-mr aperture opening have made this measurement suspect. The reflectance efficiency measurements at 8 and 16 mr are probably more representative.

Various chemical silvering processes were next measured to determine whether there are differences in the reflectance among the various commercial processes. No appreciable differences in reflectance efficiency were found between the different commercial silvering process (Table 4-2), or for varying silver thickness for the Mirrolab Process from 0.65 to 1.29 g/m^2 (60 to 120 mg/ft^2) (Table 4-3). Consequently, any nationally used chemical silvering process such as Mirrolab, London Laboratory, Hilemn, or Peacock Process at a minimum silver thickness of 0.75 g/m^2 (70 mg/ft^2) will probably provide the necessary reflectance efficiency.

The dependence of solar transmittance through glass with varying iron content and glass thickness has been observed by R. Surowiec of Ford Motor Glass Company (see Figure 4-4). This was also observed by MDAC when both sheet and float glass with varying iron content and glass thickness were mirrored. The resultant reflectance efficiencies were measured (Table 4-4) and are plotted on Figure 4-5, where the strong dependency of reflectance efficiency with iron oxide content and glass thickness can be seen. Plotted also are the expected reflectivity data converted from Surowiec's solar transmittance data. The measured reflectance data was in good agreement with the predicted reflectance data for glass with iron content in excess of 0.07% by weight.

Although the total reflectance efficiency of glass at a thickness of 3.2 mm (1/8 in.) with an iron oxide content of 0.05% by weight is around 91 to 93% (Table 4-4), the specular component is lower. A typical curve for sheet

*R. Kingslake (ed.). Applied Optics and Optical Engineering, Academic Press, 1965, p. 313

Table 4-1

SOLAR REFLECTANCE EFFICIENCY OF SILVER AT AIR MASS TWO

Mirroring Process	Silver Deposition	Exposure (Days)	Acceptance Angle (mr)	Solar Reflectance Efficiency at the Following Wavelengths (Nanometers)										Average Value Over Solar Spectrum
				426	498	561	623	691	774	860	1008	1208	1594	
Theoretical (Kingslake)	Vapor			96.3	97.9	98.4	98.7	98.9	99.1	99.2	99.4	99.4	99.4	98.7
Liberty Mirror	Vapor	Protected by top coat	125	93.0	95.5	95.5	96.0	96.5	97.5	97.5	98.0	98.0	98.5	96.6
				98.0	97.5	96.5	97.0	97.0	97.0	96.5	97.0	97.5	97.0	97.1
Mirrolab	Chemical	1 (stored in nitrogen for 88 days)	125	97.0	98.0	98.5	98.5	99.0	98.0	98.0	98.5	98.0	98.0	98.3
			16	89.1	93.7	94.5	96.2	95.5	92.6	93.3	95.7	96.7	--	94.1
			8	88.2	92.9	93.8	95.5	94.8	92.0	93.3	95.7	95.6	--	93.5
			4	87.2	91.4	93.0	93.8	94.4	91.5	93.3	95.7	94.6	--	92.8
London Laboratory	Chemical	7	125	80.0	92.0	96.5	98.0	99.0	99.0	99.0	99.0	98.5	99.0	96.0
PPG Industries	Chemical	42	125	89.0	93.8	96.0	96.5	97.0	97.0	96.8	97.0	96.7	97.1	95.7
			125	87.5	92.5	94.0	95.2	96.4	96.5	96.0	96.8	96.5	97.0	94.8

Table 4-2

SPECULAR REFLECTANCE EFFICIENCY OF VARIOUS SILVERING PROCESS
USING 6.5 mm (1/4 IN.) THICK FORMED GLASS

Silvering Process		Specimen Number	Silver Thickness Grams/m^2	Values at Various Acceptance Angles (mr)			
				Over Solar Spectrum Using Beckman	At Wavelength of 550 Nanometer Using Specular Photometer		
				125 mr	125 mr	8 mr	4 mr
Peacock Laboratory		55-3	1.35 (125 mg/ft^2)	85.0	93.5	91.0	62.0
London Laboratory	2 part	51-5	0.86 (80 mg/ft^2)	84.3	91.0	90.0	88.5
	3 part	56-4	0.84 (78 mg/ft^2)	84.5	93.0	92.5	85.0
Hilemn		57-1	0.82 (76 mg/ft^2)	84.1	92.5	91.5	79.0
Mirrolab		60-1	1.01 (94 mg/ft^2)	85.3	92.5	90.0	59.5

Table 4-3

SOLAR REFLECTANCE EFFICIENCY AS FUNCTION OF SILVER THICKNESS FOR MIRROLAB PROCESS

Type Glass and Thickness (mm)	Specimen Number	Silver Deposition in Milligrams Per Square Decimeter	Reflectance Efficiency at Various Acceptance Angles (mr)						
			Beckman Spectrophotometer (Over Solar Spectrum)	Specular Photometer (550 nm)			Specular Spectrophotometer (Over Solar Spectrum)		
			125 mr	16 mr	8 mr	4 mr	16 mr	8 mr	4 mr
Fourco Sheet Glass 6.5 mm (1/4 in.)	58-4	6.5 (60 mg/ft^2)	83.7	91.5	90.0	81.0			
	59-3	8.6 (80 mg/ft^2)	84.1	91.5	91.0	89.0			
	60-1	10.1 (94 mg/ft^2)	85.3	92.5	90.0	59.5			
	61-3	10.8 (100 mg/ft^2)	83.1	90.0	88.0	82.0			
	62-1	12.9 (120 mg/ft^2)	84.7	92.0	90.5	85.5			
ASG Industries Float Glass 2.4 mm (3/32 in.)	87-1	6.5 (60 mg/ft^2)	85.0	92.0	92.0	91.0			
	88-1	8.6 (80 mg/ft^2)	85.0	93.0	92.0	92.0			
	89-1	10.1 (94 mg/ft^2)	86.0	93.0	92.0	88.0	83.6	83.2	77.2
	90-1	10.8 (100 mg/ft^2)	85.0	93.0	93.0	93.0			
	91-1	12.9 (120 mg/ft^2)	85.0	92.0	92.0	92.0			

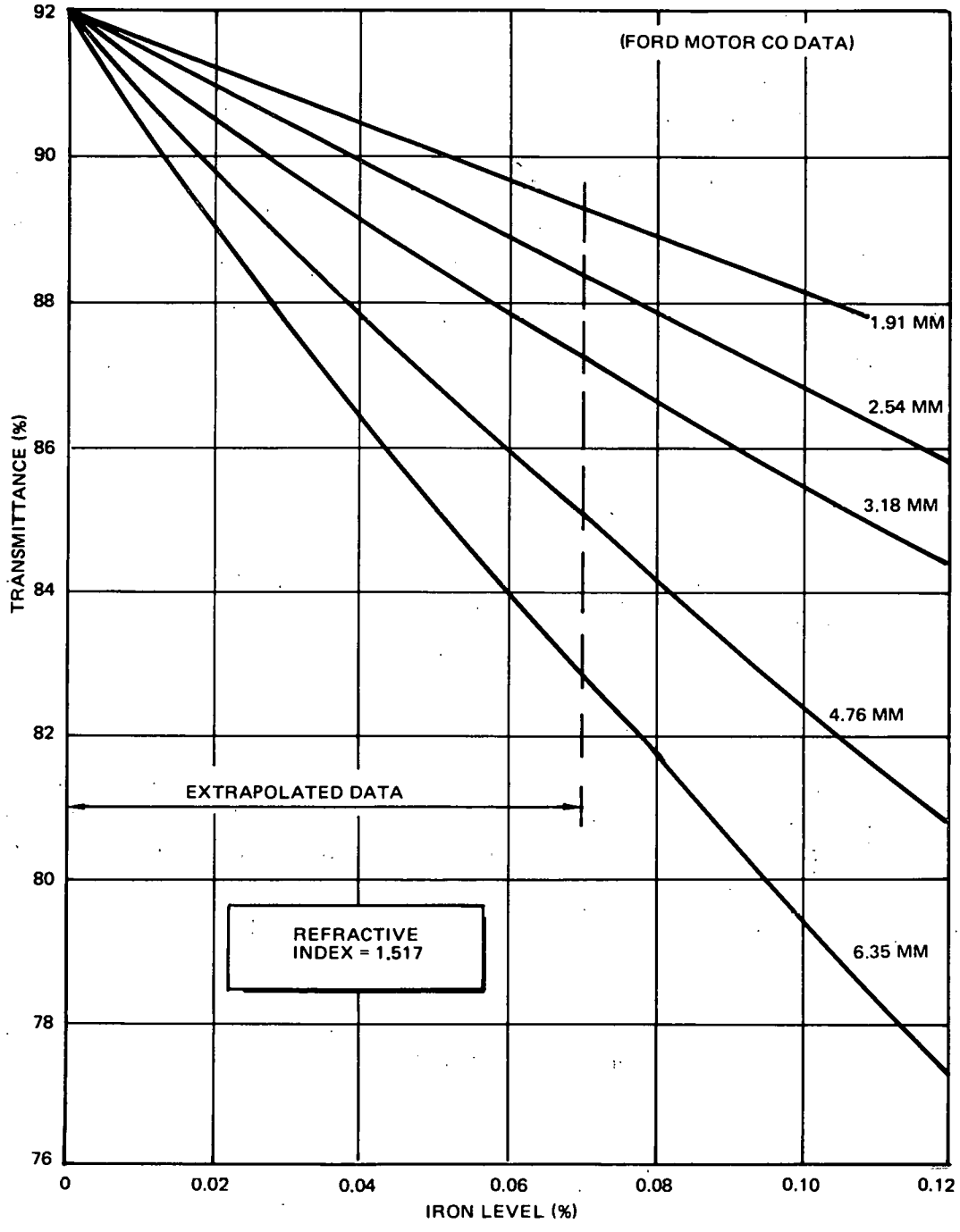

Figure 4-4. Solar Transmittance as a Function of Iron Level.

Table 4-4 (Page 1 of 2)

REFLECTANCE MEASUREMENTS OF SECOND-SURFACE GLASS MIRRORS

Glass (Wt % Iron Oxide)	Mirror Manufacturer and Silvering Process Used	Thickness in Millimeters (In.)	Specimen Number	Values at Various Acceptance Angles (mr)						
				Over Solar Spectrum Using Beckman	At Wavelength of 550 Nanometer Using Specular Photometer			Over Solar Spectrum Using Specular Spectrophotometer		
				125 mr	16 mr	8 mr	4 mr	16 mr	8 mr	4 mr
		2.4 (0.093)	See Table 4-3							
ASG Industries Float (0.10-0.13)	Binswanger Mirror Co. Mirrolab Process	3.2 (0.125)	Lot No. 2	83.7	92.0	91.0	90.5	81.6	82.1	78.5
			B-1	84.2	92.0	92.0	86.0	83.1	83.1	78.8
			B-2	83.7	92.0	92.0	89.5	82.3	82.3	75.9
			B-3	84.8	92.5	92.0	87.5	84.8	84.8	80.9
		4.8 (0.188)	Lot No. 1	77.9	88.0	88.0	81.5	76.0	76.0	71.8
	Buchmin Ind. Mirrolab Process	6.4 (0.250)	64-22	71.1	88.0	88.0	88.0	71.0	71.0	66.0
			52-2	85.7	96.5	96.0	96.0			
		2.4 (0.093)	52-3	85.7	94.5	94.5	94.0			
			52-4	85.9	94.0	93.5	93.0			
Ford Motor Float (0.09-1.0)	Buchmin Ind. Mirrolab Process		52-5	86.0	96.0	95.0	95.0			
			52-6	86.1	93.0	93.0	93.0			
		3.2 (0.125)	65-X	83.3	91.0	91.0	86.0	81.9	81.9	78.0
			65-22	83.2	91.0	91.0	88.0	81.0	81.0	76.0
		6.4 (0.250)	6-001	70.7	89.0	88.5	88.5			
			6-002	70.7	89.0	88.5	88.5			
LOF Float (0.12)	Tyre Bros. London Lab. Process	2.5 (0.100)	29-3	82.4	93.0	92.0	92.0			
		6.4 (0.250)	30-1	64.7	81.0	79.0	75.0			
Guardian Ind. Float (0.10)	Buchmin Ind. Mirrolab Process	3.2 (0.125)	66-3	82.5	93.5	92.5	92.0			

Table 4-4 (Page 2 of 2)

REFLECTANCE MEASUREMENTS OF SECOND-SURFACE GLASS MIRRORS

Glass (Wt. % Iron Oxide)	Mirror Manufacturer and Silvering Process Used	Thickness in Millimeters (In.)	Specimen Number	Values at Various Acceptance Angles (mr): Over Solar Spectrum Using Beckman	At Wavelength of 550 Nanometer Using Specular Photometer			Over Solar Spectrum Using Specular Spectrophotometer		
				125 mr	16 mr	8 mr	4 mr	16 mr	8 mr	4 mr
PPG Industries 0.05 Float	Buchmin Industries Mirrorlab Process	3.2 (0.125)	1	92	95	95	95	90	89	81
			2	92	95	95	95	89	88	81
			3	92	95	95	95	90	89	84
0.07		2.4 (0.093)	111-1	88				87	86	82
			111-2	87				87	86	81
0.10		3.2 (0.125)	86-1	83.5				83.3	82.8	77.1
ASC Ind. Lustra Sheet (0.05-0.06)	Buchmin Ind. Mirrorlab Process	2.4 (0.093)	110-1	94				93	92	86
			110-2	94				92	92	88
		3.2 (0.125)	65-3	91.4	95.5	95.0	93.5			
			65-13	93.5	94.5	94.0	93.5			
			65-15	93.5	94.5	94.5	93.5			
			65-16	94.3	95.0	95.0	94.0	92.0	93.0	87
	Gardner Mirror Co. & Process		67-3	91.9	95.5	94.5	94.0			
Fourco Sheet (0.06)	Tyre Bros. 2 Part London Lab. Process	2.3 (0.090)	32-3	93.1	95.0	94.0	90.0			
			50-2	90.4	96.0	96.0	94.0			
			50-3	90.3	97.0	96.0	96.0			
			50-4	90.7	96.5	96.5	96.0			
			50-5	90.3	95.0	95.0	92.0			
		6.4 (0.250)	33-3	86.8	89.0	87.0	88.0			
			51-2	83.9	94.0	94.0	88.0			
			51-3	84.4	93.0	92.0	88.0			
			51-4	84.5	93.0	93.0	91.0			
			51-5	84.3	91.0	90.0	88.5			

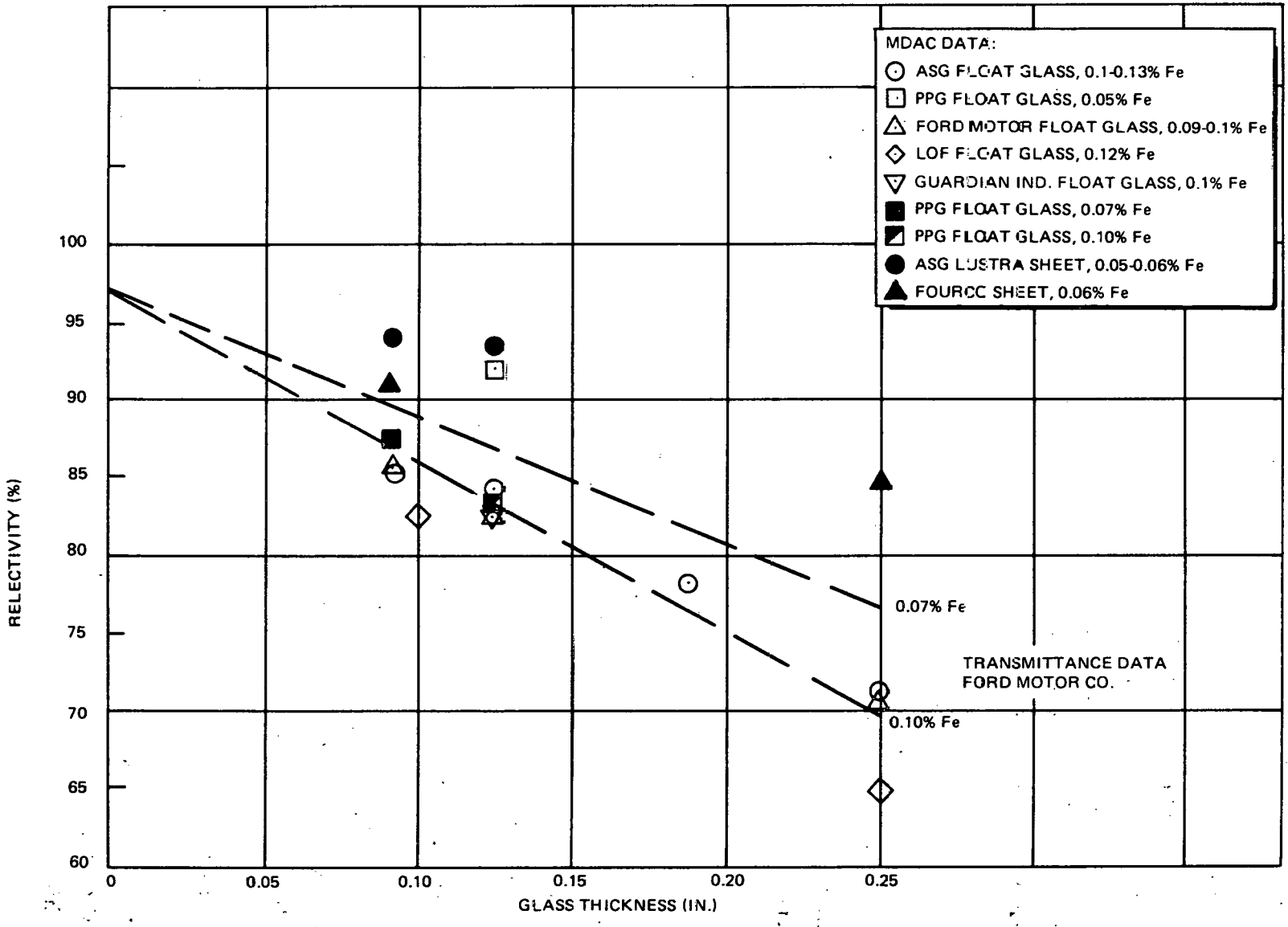

Figure 4-5. Effect of Iron Content and Glass Thickness on Reflectivity

and float glass is given in Figure 4-6. The 4-mr data have been deleted because of apparent experimental error. Data by Dr. Pettit of Sandia, (Albuquerque) are included to show typical behavior in the narrow-angle region.

Dr. Pettit also measured the degradation of specular reflectivity due to mirror soiling. Figure 4-7 shows some of Pettit's early data, as yet unpublished. The clean mirror reflectivity is 91.5 at 500-nm wavelength. The mirrors were maintained at a constant orientation, as indicated. The vertically stored mirror shows the least degradation, probably because of the cleaning effect of dew, frost and rain. The face-up stored mirror shows the greatest degradation because the above factors will tend to cake the dirt rather than clean. The face-down stowage accumulated dust which degraded the specular reflectivity of the mirrors more than the total reflectivity. Data from the MDAC tests at China Lake are also indicated on Figure 4-7. The clean mirror reflectivity is 0.87. Data at 17 mr averaged over the solar spectrum are shown as a range for face-up and face-down stowage. The range in these data reflects the effect of varying environmental conditions including rain, dew, dust, and frost. Based on these data, degradation of specular reflectivity is estimated at 3%. The degradation of specular reflectivity for an operating plant will depend on the site, meteorological conditions, and the operating orientation of the mirror in addition to the stowage position. Therefore, any estimates of the reflectivity reduction due to mirror soiling based on the above data are speculative.

Evaluation of the leading candidates for the mirror glass for Pilot Plant (Table 4-5) would result in the selection of 3.2-mm (1/8-in.) thick 0.05% Fe oxide PPG float. It has a total measured reflectance efficiency of 92% which would result in an expected average specular reflectivity of 87% to 88%. The glass is commercially available in large sizes and, being float glass, past measurements indicate that it would be flatter and have less residual stresses than sheet glass.

For the Commercial Plant, the total reflectance efficiency of glass mirrors would be 94% and the average specular reflectance would be 91%. This can be achieved by producing float glass with lower iron oxide content and by

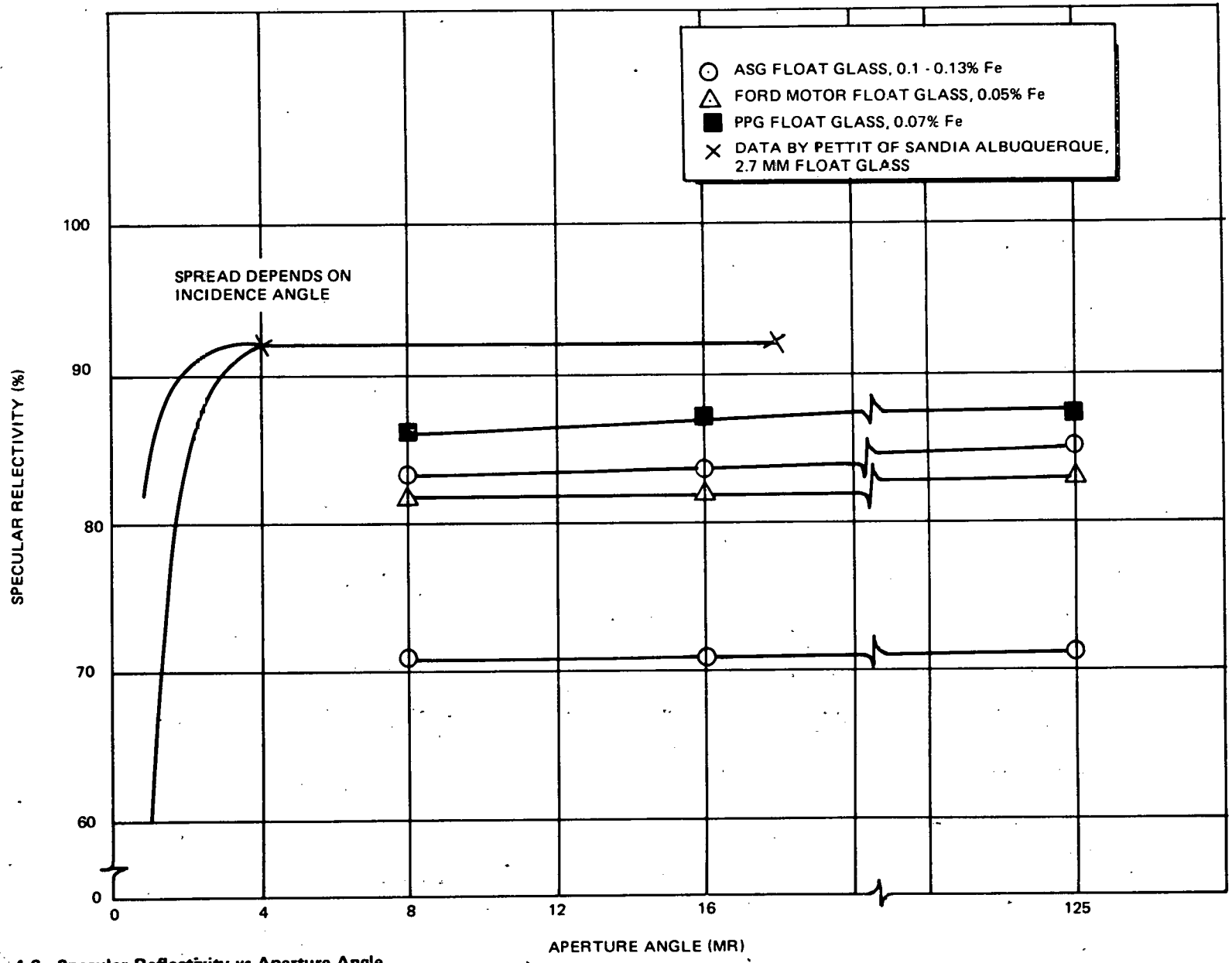

Figure 4-6. Specular Reflectivity vs Aperture Angle

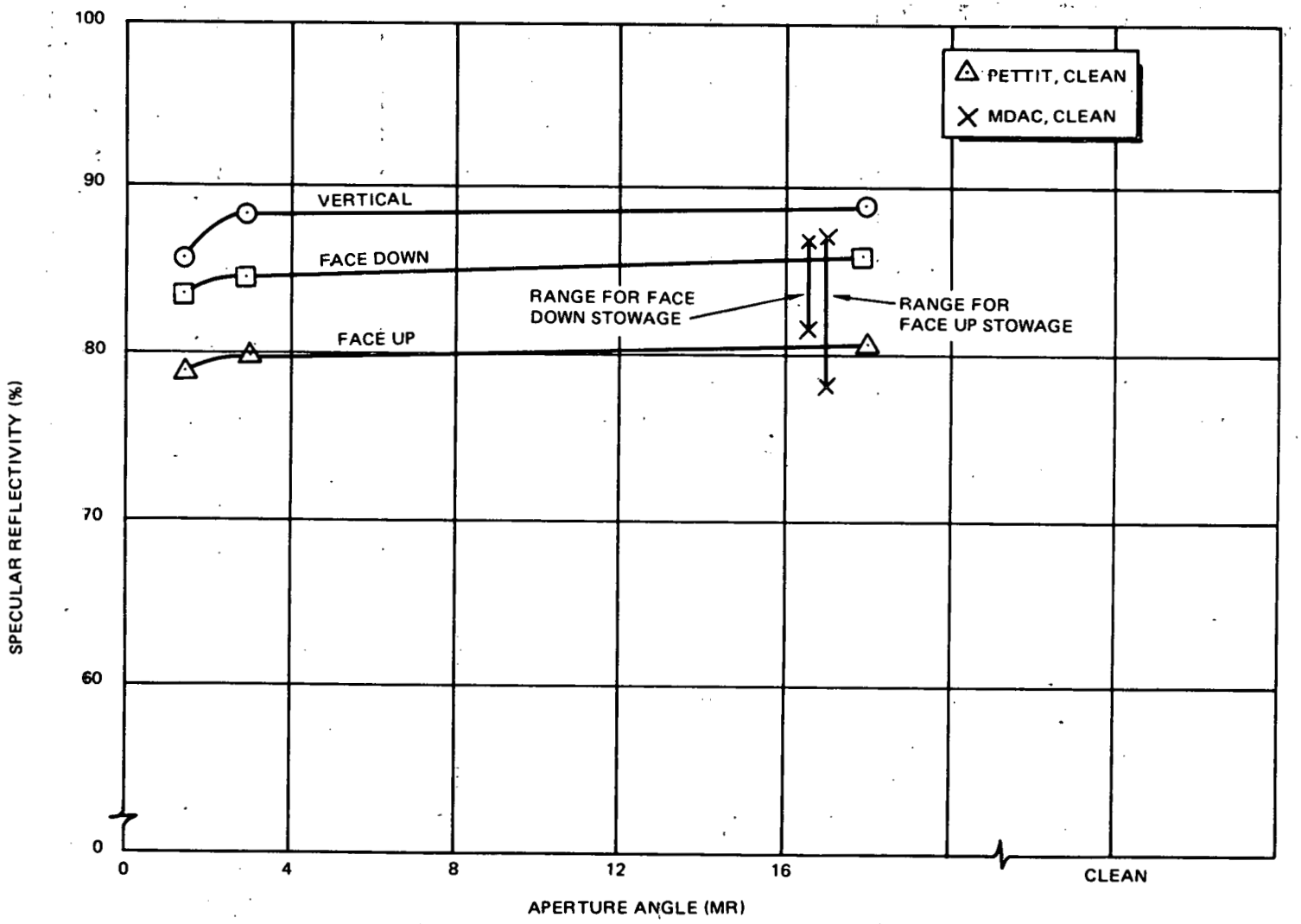

Figure 4-7. Effect of Dirt and Reflector Orientation on Specular Reflectivity

Table 4-5

PROPERTIES OF CANDIDATE MIRRCRS FOR PILOT PLANT

Glass	Thickness (mm)	Iron Oxide Content (Wt %)	Total Reflectance Efficiency (Air Mass 2)	Cost in Cents Per Square Decimeter (Cents/ft^2) Initial	Effective	Hail Impact	Cracking
PPG Low Iron Float	3.2	0.05	91 ± 1	10.2 (95) current (35) potential	0.5 (5)	OK	OK
Clear Float	2.4	0.07	88 ± 1*	3.8 (35)	3.8 (35)	Marginal	Marginal
Ford Motor Float	2.4	0.10	86 ± 1	3.8 (35)	3.8 (35)	OK Laminated	OK Laminated
SRE ASG Industries Float	3.2	0.10	84 ± 1	3.8 (35)	3.8 (35)	OK	OK
ASG Industries Sheet	2.4	0.05	93 ± 1	3.8 (35)	3.8 (35)	Problem	Problem

Notes: *Expected efficiency based upon extrapolation of similar mirrors.
Final confirmation based on actual measurements will be required.

changing the FeO/Fe_2O_3 ratio. Because the Commercial Plant would require a large volume of float glass, more float glass manufacturers would be interested in melting low iron float. If so, tanks which had been used only for melting clear float (0.07% by weight Fe oxide) could be used which could result in float glass with iron oxide content less than 0.05%. In addition, the iron in float glass is present as a mixture of FeO and Fe_2O_3 and increased transmission efficiency can be achieved by changing the mixture to result in Fe_2O_3 only being present because the latter compound has greater transmission properties. This can be achieved by operating the float line in a slightly oxidizing atmosphere. Since these techniques are currently available, glass mirrors for the Commercial Plant can be made available with a total reflectance efficiency of at least 94% and an average specular reflectivity of 91% between cleanings.

4.2.2.2 Reflector Development

The development of the MDAC reflector panel has gone through several cycles. The octagonal heliostat was first conceived with a 1/4-in. float glass front-surface mirror with an acrylic protective coating. As a backup to this, MDAC planned to use either a 1/8 + 1/8 in. or 3/32 + 3/16 in. float glass laminated second-surface mirror. Both the front-surface mirror and laminated second-surface mirror underwent preliminary environmental tests. In this preliminary test program and the SRE program, it became apparent that the front-surface mirrors could not survive the desert environment. Therefore, the second-surface laminated mirrors were chosen as the reflector for the inverting heliostat. Further investigation of laminated mirrors revealed that they were expensive because of the laminating process. A second surface mirror development program was thus begun to develop an efficient, cost-effective, second-surface mirror reflector. Results of trade and cost studies early in the program indicated a foam-core sandwich reflector showed adequate structural properties and low cost. The foam-core sandwich reflectors were built and tested on the inverted heliostat in the SRE program along with the laminated reflectors. In addition, both reflectors underwent a series of component-level tests.

4.2.2.3 Laminated Reflector Design

The laminated second surface mirror reflector was the baseline reflector for the inverted heliostat. Figure 4-8 shows the laminated reflector panel. It consists of a 1/8-in. float glass second-surface mirror laminated to a 1/8-in. float glass substrate. Three galvanized steel hat-section stiffeners are bonded to the 1/8-in. glass substrate. The reflector panel is attached at six loactions to the cross beams.

The design of the laminated reflector panels began during the design phase of the inverted heliostat. A 1/8- in. + 1/8-in. laminated mirror was chosen to match the stiffness of the old 1/4-in. front-surface mirror. Hat-section dimensions and location were selected based on preliminary analyses and previously acceptable spans for 1/4-in. glass. The heliostat reflector panels and supporting structure were modeled on the NASTRAN structural analysis program. Five of the panels were modeled in a coarse grid and one panel was modeled in a fine grid. The fine grid panel was used to determine reflector slopes due to operational wind, gravity, and temperature loadings. Minor changes to hat-section dimensions and location were made to yield a reflector capable of meeting design requirements. The laminated reflector panel dimensions of 85 in. x 114 in. were determined by available glass size and division of the heliostat into six equal panels while keeping in mind the need for a square heliostat with a 28-in. slot for inverting.

4.2.2.4 Foam Core Sandwich Reflector

Figure 4-9 shows the details of the foam-core sandwich reflector. The 1/8-in. float glass second-surface mirror is bonded to a 2-in. thick Styrofoam IB core, which is bonded to a 0.022-in. thick galvanized steel backface sheet. The edges of the foam and mirror are weathersealed. Four formed galvanized steel cups are bonded to the steel backface sheet to provide for attachment of the reflector to the crossbeams.

Face Sheets

To develop an efficient low-cost reflector it is desirable to use the required mirror also as a structural member. With the second-surface float glass mirror established as the front face, an investigation into an appropriate

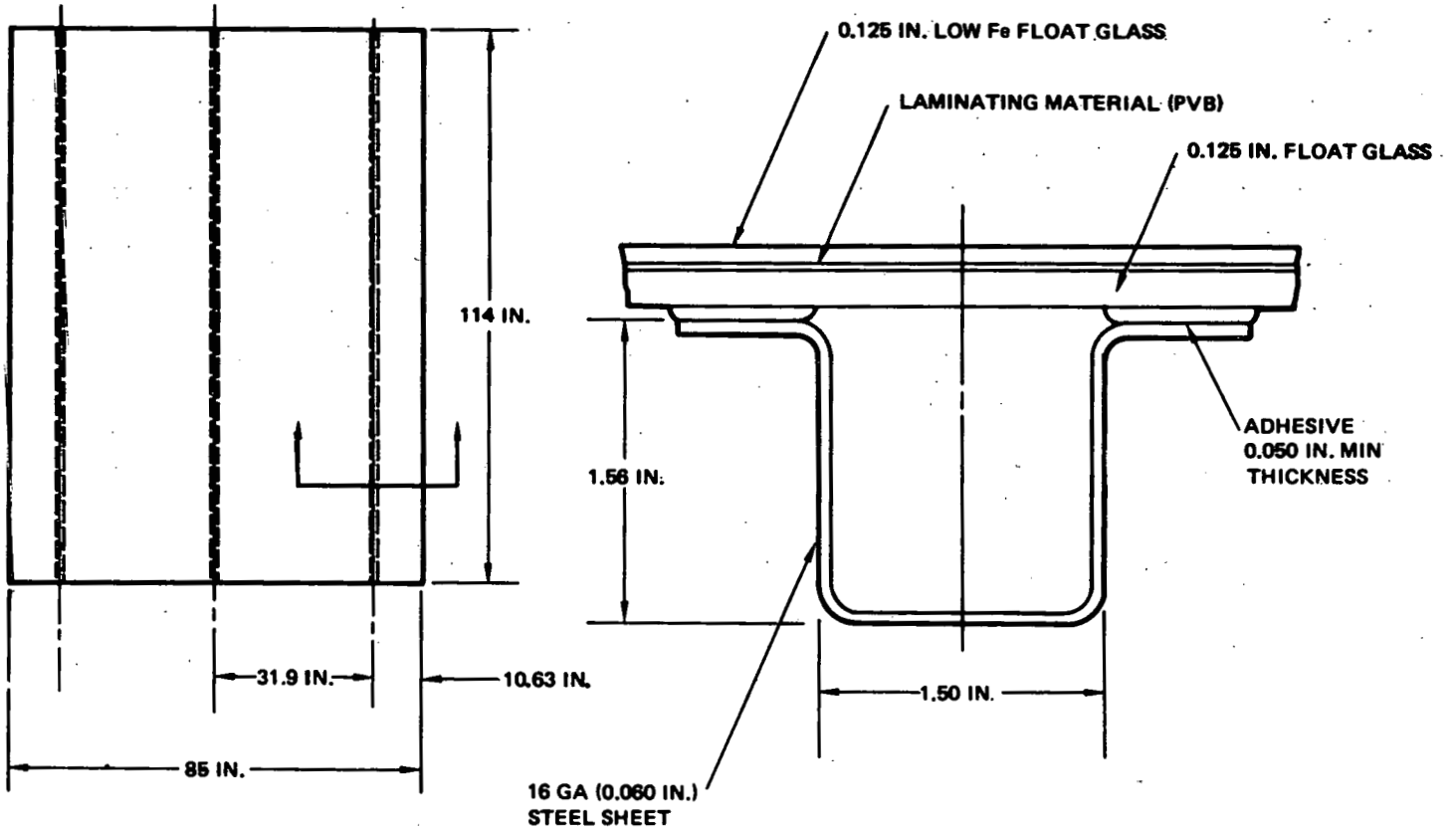

Figure 4-8. Laminated Reflector

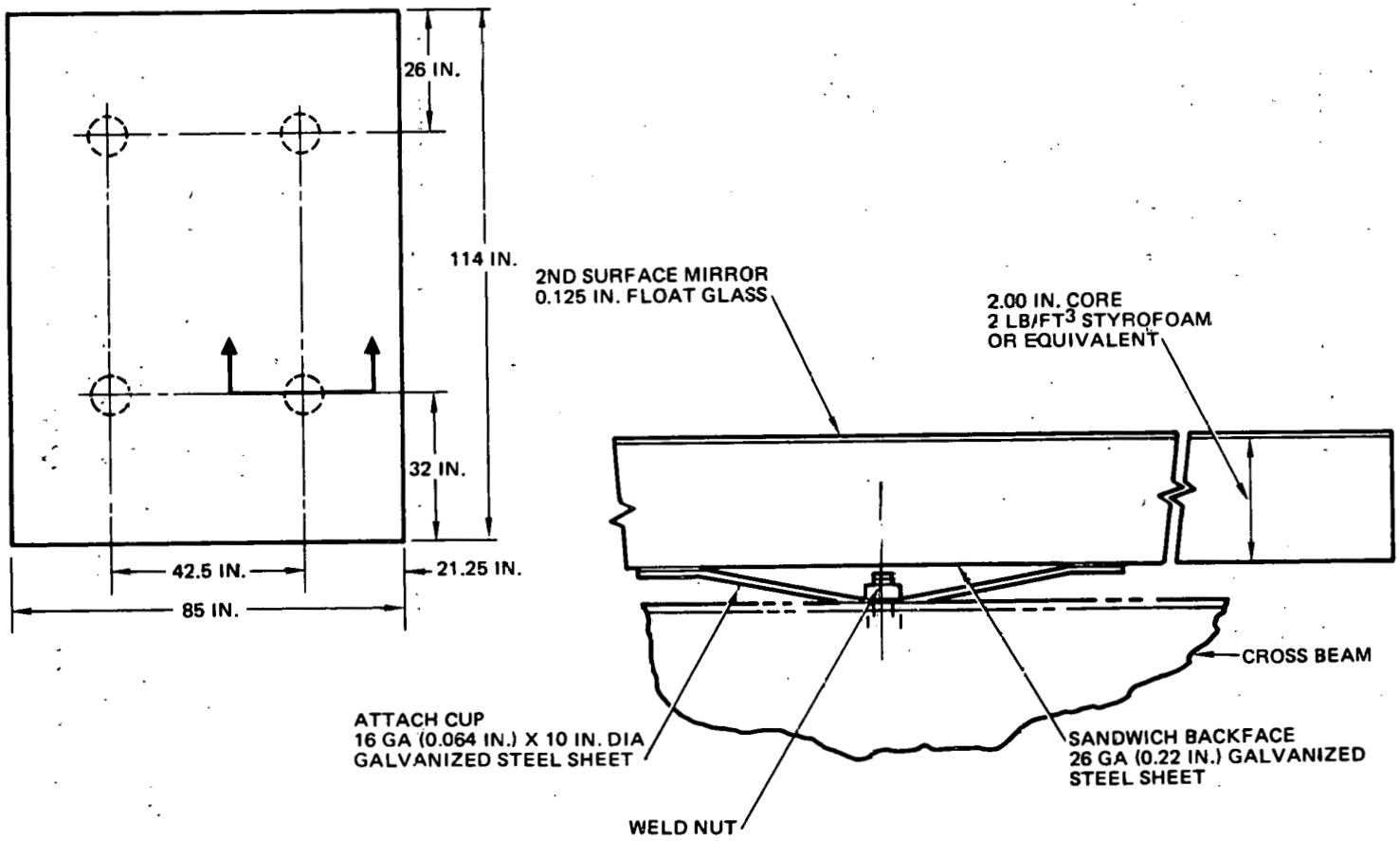

Figure 4-9. Heliostat Sandwich Reflector

backface sheet was begun. The requirements of the backface sheet were high modulus, low cost, weatherability, and a coefficient of thermal expansion as close to that of glass as possible. Many materials were considered; galvanized steel and tempered hardboard (Masonite) were the most promising. The major advantages of galvanized sheet steel are its high modulus (stiffness) and outstanding weatherability. The major advantages of tempered hardboard are low initial cost and excellent match of coefficient of thermal expansion. The average coefficient of thermal expansion of float glass in the range of 30°F to 100°F is $3.9 \times 10^{-6}/°F$ compared with tempered hard board of $4.0 \times 10^{-6}/°F$. The galvanized steel was selected because of its far superior long-term weatherability.

Core Type

The selection of the core material was the next step in the de sign. The major requirements of a core material were adequate shear stiffness and low cost. Numerous materials were considered: aluminum honeycomb, paper honeycomb, polystyrene foams, polyurethene foams, foam glass, and formed plastics such as "Hale Core" and "Quadricore." All materials considered, except the expandable bead polystyrene foam, could meet the stiffness requirements, with paper honeycomb and extruded polystyrene foam (Styrofoam) being the lowest in cost. Further investigation showed that the paper honeycomb may absorb water after a period of time and thereby degrade its structural properties. Therefore, the extruded polystyrene foam was chosen, mainly because of its low cost and adequacy to fulfill the remaining requirements.

Extruded polystyrene foam is manufactured in the United States only by the Dow Chemical Company. The Dow brand name for their extruded polystyrene foam is Styrofoam. Styrofoam comes in several types and many sizes. After testing and evaluating three types of Styrofoam (IB, SM, HD300), Styrofoam IB was selected because of its good flatness when compared to the other types. Along with the selection of the foam type was the selection of the foam thickness.

Foam Thickness

The thickness of the Styrofoam core was determined by stiffness and thermal distortion requirements. The stiffness of the core was determined by equating maximum total deflection (shear plus bending) of the foam core panel for a given uniform loading to the maximum deflection of a laminated mirror panel for the same loading. This resulted in a core thickness of about 1.8 in. Therefore, IB foam of 2-in. thickness was selected and analyzed for thermal distortion. For a 30°F change in temperature from the assumed bonding temperature of 70°F (i.e., over the range of 40°F to 100°F), a maximum slope error due to temperature of 1.71 mr was calculated. (No temperature gradient was assumed across the panel thickness.) This was within the error budget allocated for temperature distortion. Thus, a 2-in. foam thickness was established. The thickness provided the required stiffness and face sheet separation to restrain thermal distortion. Both deflection and thermal distortion vary inversely with core thickness. Thus, if the core thickness was increased 50% to 3 in., there would be a corresponding decrease in deflections. The panel dimensions of 85 in. x 114 in. were kept the same as those of the laminated reflector.

4.2.2.5 Comparison of Laminated and Foam-Core Reflectors

Both the laminated reflector and the foam-core sandwich reflector have advantages and disadvantages over the other. Table 4-6 and the following paragraphs compare the two reflectors over important criteria. The comparisons are for the SRE reflector configuration. The major change between the SRE and Pilot Plant configuration is an increase in the mirror thickness of the foam-core sandwich from 3/32 in. to 1/8 in. This change may affect the comparisons and is so noted in the following discussion:

A. Performance. Similar performance was observed between the laminated and foam-core sandwich reflectors.

B. Flatness. The laminated reflector has greater long wavelength deformation but this does not seem to degrade performance.

Table 4-6 (Page 1 of 2)

COMPARISON OF LAMINATED AND FOAM-CORE REFLECTORS

Criteria	Laminated 1/8 in. + 1/8 in., 0.1% Iron	Foam-Core Sandwich 3/32 in., 0.07% Iron
Performance	Similar specular reflectivity	
Flatness		
Long wavelength deflection	0.100 in. in 30 in.	0.035 in. in 30 in.
Short wavelength rippling	Minor	0.004 in. in 3 in.
Stiffness and Strength	Structural test results show adequate stiffness and strength.	Structural test results show adequate stiffness and strength.
Thermal Distortion	Max. predicted slope ≈1.2 mr for 30°F ΔT. Currently being tested.	Max. predicted slope ≈1.7 mr for 30°F ΔT. Measured 1.5 to 2 times predicted. Currently being retested.
Crack Susceptibility Due to		
Edge flaw	No cracks noticed.	2 cracks due to thermal stresses.
Thermal cycle	Not tested.	No cracks with properly prepared edges.
Backlighting	No cracks at NWC. Both white and gray backing paint mirrors cracked - test may be overly severe.	No cracking due to backlighting.
Hail Resistance	Not tested at MDAC; other tests show survived 3/4 in. at 65 fps.	Survived 3/4 in. at 65 fps on front.
Thermal Cycling	Currently being tested.	Initial edge flaw turned into crack. Panel otherwise survived and remained flat after test.

Table 4-6 (Page 2 of 2)

COMPARISON OF LAMINATED AND FOAM CORE REFLECTORS

Criteria	Laminated 1/8 in. + 1/8 in., 0.1% Iron	Foam-Core Sandwich 3/32 in., 0.07% Iron
Edge Sealing	Edge sealing required to protect laminate bond.	Polyurethane, butyl, or silicone weather seal compound required.
Mirror Edge Condition	Need to "blunt" to prevent injury.	Need to protect to prevent "flaws."
Cost	About 20% more.	
Creep	Currently being tested, may be important.	Tests show a possible additional 0.6-mr slope due to creep over 30 yr.
Mirror Backing Paint Protection	Exposed to sunlight.	Completely protected.

C. Thermal Distortion. Measured data showed from 1.5 to twice the deflections predicted due to thermal distortion. Further tests were performed to determine the coefficient of thermal expansion (α) for the mirrored glass and galvanized steel. The measured values of α were $3.9 \times 10^{-6}/^{\circ}F$ for mirrored glass and $6.4 \times 10^{-6}/^{\circ}F$ for galvanized steel, compared with $4.8 \times 10^{-6}/^{\circ}F$ and $6.8 \times 10^{-6}/^{\circ}F$ for glass and steel, respectively, as originally obtained from manufacturer data and textbook sources. These differences should not cause the factor of two discrepancy in the thermal distortion test. This test will be repeated for the foam-sandwich core and the laminated reflector will also be tested for thermal distortion.

D. Crack Susceptibility. No cracks have been observed for the laminated reflectors at NWC whereas slight cracking has occurred on the foam core panels at NWC and Huntington Beach. Backlighting may cause cracking of the laminated reflector. One solution to

this may be to paint the backside of the reflector white. MDAC is performing additional backlighting tests of the laminated reflector to determine if cracking is a significant problem.

E. Hail Resistance. No hail cracking problems are anticipated for the laminated reflector for the 3/4-in. diameter hailstones at 65 fps. Test results indicate a change of 1/8-in. mirror thickness yields a 1-in. hail capability for the foam-core reflector. However, for larger diameter and higher velocity hailstones, the foam-core reflector has more capability because, once inverted, it has a steel backface sheet exposed to the hail.

F. Thermal Cycle. Both reflectors have adequate resistance to thermal cycle degradation.

G. Mirror Edge Condition. The condition of the mirror edge appears to be more important for the foam-core reflector. It is anticipated that solution of cracking problem will determine what mirror edge conditions are required for the foam core reflector.

H. Cost. The cost of laminated reflector is about 20% greater than that of foam core. This increased cost is due to the expensive laminating process and this laminating cost is not expected to decrease with increased volume.

Summary

In summary, the foam-core reflector has advantages over the laminated reflector in cost, hail resistance, mirror-backing protection, and cracking due to backlighting. Thus MDAC believes the foam-core reflector is the more cost-effective reflector and proposes this reflector for Pilot Plant.

4.2.2.6 Reflector Panel Dimensions

The baseline heliostat reflective surface is composed of six separately mounted sandwich panels 85 x 114 in. in size. This size is an optimistic projection from the 42.5 x 114 in. size so far produced, its feasibility being contingent upon development of techniques for handling thin glass. Laminated panels 85 x 114 in. have been produced. The optimum panel size for a heliostat reflector system approximately 21 ft on a side will be the most cost-effective of the options defined in Figure 4-10 and Table 4-7.

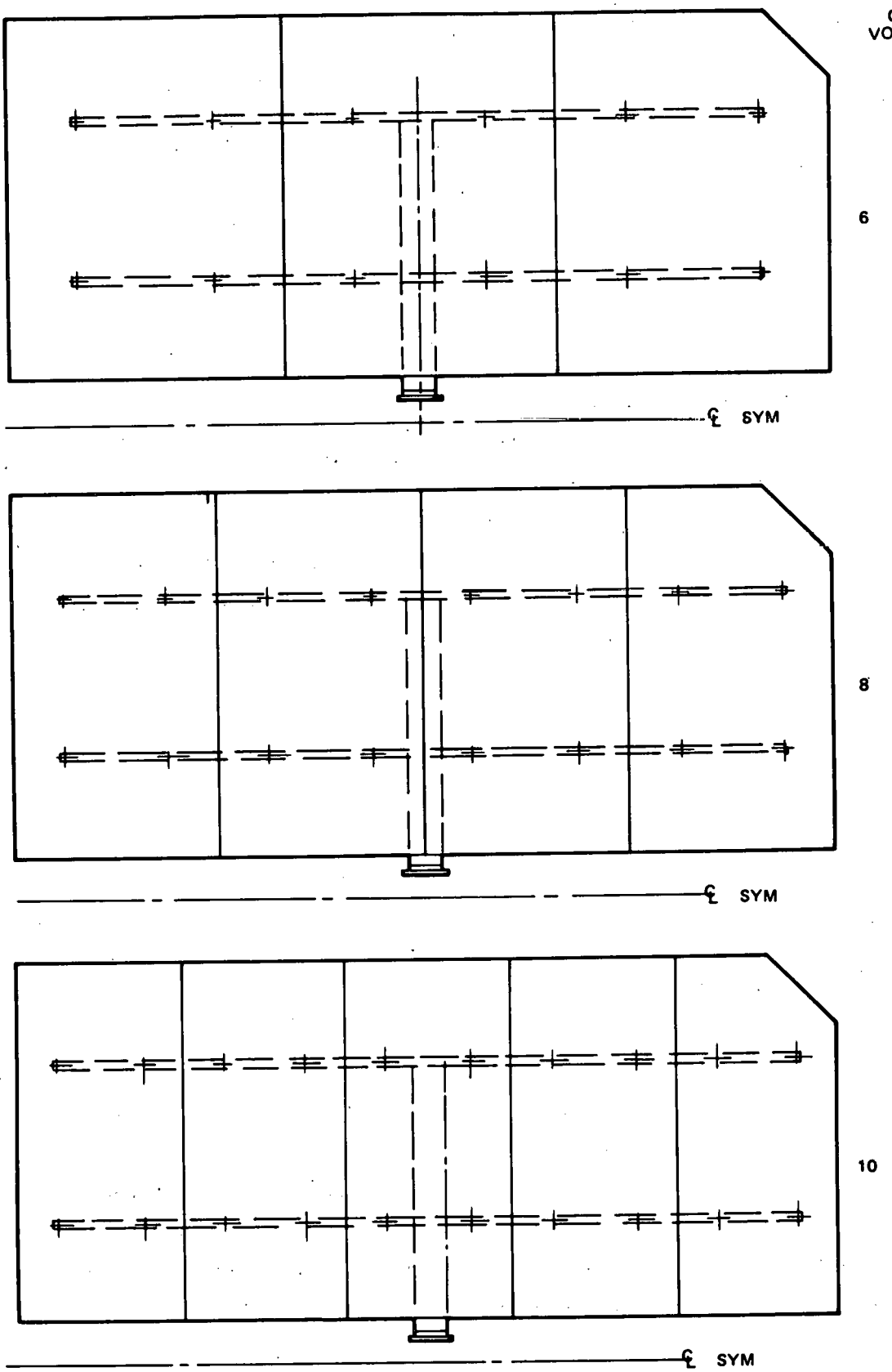

Figure 4-10. Sandwich Reflector Variations

Table 4-7

SANDWICH REFLECTOR COMPARISON

No. Of Panels Per Heliostat	Panel Size (In. x In.)	No. Of Attachments /Heliostat	Overall Width (In.)	Crossbeam Length (In.)
6	85 x 114	24	256.0	215.5
8	63.75 x 114	32	256.5	226.63
10	51 x 114	40	257.0	233.5
*12	42.5 x 114	48	257.5	238.25

*SRE size - 6 per crossbeam pair. Not shown on accompanying sheet.

The thinnest obtainable glass is desired to minimize the transmission loss of a second-surface mirror. However, thin glass, because of handling difficulties not yet resolved, is expected to limit panel size. Large panel size is expected to reduce the handling and assembly costs and also to permit slightly shorter crossbeams in the supporting structure.

Panel size is also influenced by focusing requirements. All the flat panels must be canted so that the centroid of a projected spot from each one falls on the heliostat aiming axis. The resulting image size is determined by the initial panel size and the spread of the sun's reflected image. For Pilot Plant, the 85 x 114 panel image is adequately small to remain on the target at maximum slant range.

In the baseline case, focusing for all heliostats is accomplished to the same specification by building the substructure with an outboard crossbeam higher than the inboard one. A standard shim washer is then placed under each outboard attachment point of each of the outboard reflector panels, four altogether. For a slant range of 376m the outboard crossbeam is installed 0.134 in. higher than the inboard crossbeam, and the shim height at the beam ends is 0.123 in. (Figure 4-11).

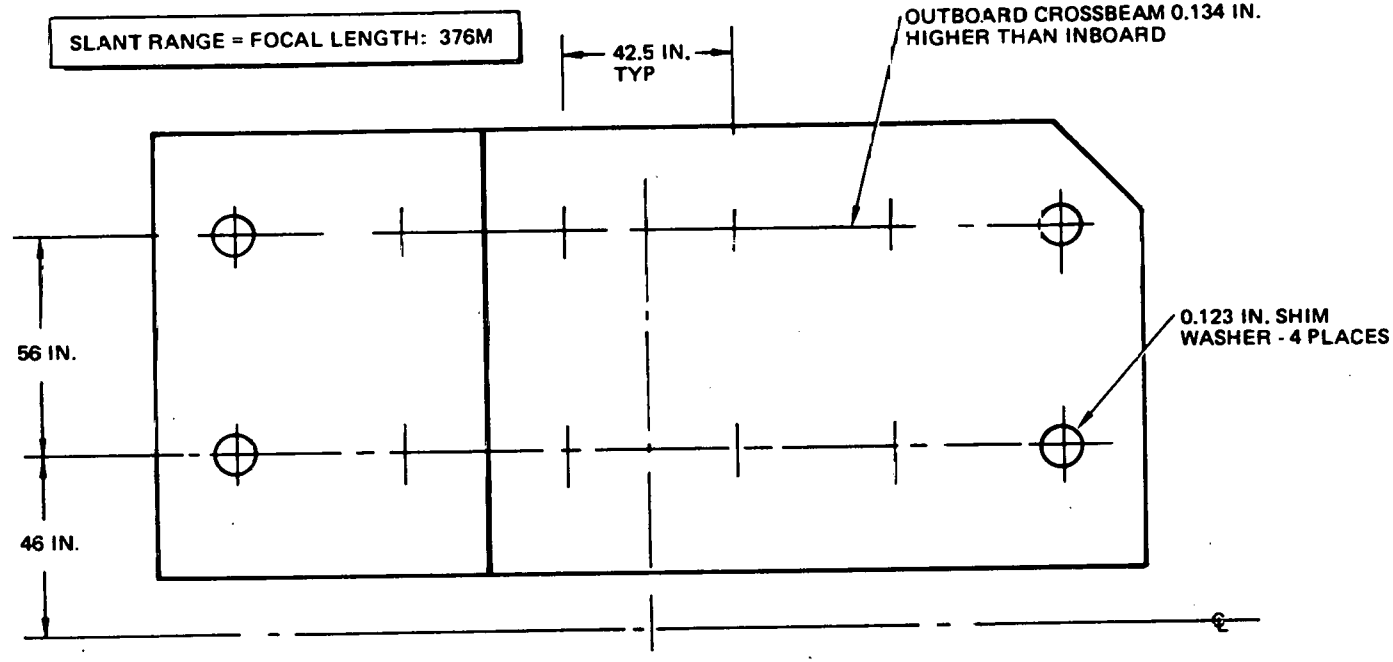

Figure 4-11. Heliostat Focusing

4.2.2.7 Reflector Panel Description

Each reflector panel is a flat structural sandwich, the front surface a thin (0.125 in.) second-surface mirror, the back face a 26-ga (0.22 in.) galvanized steel sheet. The faces are adhesively bonded to a 2-in. core, presently made from polystyrene rigid foam of 2 lb/ft^3 density. The baseline mirror is 0.125 in. PPG float glass, with 0.05% iron oxide content and 91% reflectance. An alternate is 0.093-in. float glass, with 0.07% iron oxide content and 89% reflectance.

At the four attachment points, the concentrated reaction load is spread to an acceptably low intensity by shallow formed steel cups. A tool fixture holds the mounting face accurately in a plane parallel to the mirror face, any variations in thickness or flatness of the panel back being compensated by variable thickness of the bondline between the cups and the back sheet.

Seals

The exposed edges of each mirror sandwich panel are subject to degradation due to weathering. The two primary approaches for protecting the panel edges are either to apply a coating of a protective material over the edge or to apply a protective member such as a film, extrusion, or tape around the edge.

The first candidate edge sealer was PRC's Rubber Calk 210, a nonsagging polyurethane sealant. This product has had considerable usage for calking and sealing of vertical and horizontal joints and openings in buildings, precast facings, and other areas where a watertight seal is required and structural movement is encountered.

Initial evaluation of this product showed it to cure up to a flexible, tacky, rubbery material. As a matter of fact, it would be desirable to eliminate the tackiness after cure.

Sandwich panels, 5 in. x 5 in., consisting of mirror-Styrofoam IB galvanized steel, bonded with a polyurethane adhesive, and edges sealed with Rubber Calk 210 were fabricated. One batch of specimens was taken to Fort Irwin

for desert exposure; a second batch subjected to 500 hr of salt spray exposure. Visual and tactile examination of the Rubber Calk 210 coating on the specimens subjected to the salt spray test showed no appearance of degradation or deterioration of the sealant.

Weights of Materials

The typical 85 x 114 in. reflector panel weighs about 200 lb, as follows:

1/8-in. glass		110.3 lb
Foam		22.4 lb
Galvanized steel sheet:	Steel	52.5 lb
	Zinc	8.5 lb
Four attachment cups		5.7 lb
		199.4 lb

If the panel has one corner clipped, it weighs 195 lb. The tracking mirror in the center weighs about 38.9 lb, including the mounting bracket and channel frame.

4.2.3 Reflector Structural Support

The support structure proposed for a Pilot Plant heliostat consists of a main torque tube attached to the drive system and four channel crossbeams, each pair of crossbeams supporting three reflector panels. The slot between these panel groups provides clearance for the central pedestal post when the assembly is rotated to the face-down stowage position.

The supporting structure arrangement was selected because it is compatible with face-down stowage, and because its simplicity was expected to reduce cost. The last expectation has been verified by cost analysis showing approximately 5% lower cost per square foot than the previous radial baseline design for Pilot Plant quantities.

The support structure assembly consists of 11 parts: a main torque tube, two drive attachment fittings, four crossbeam attachment flanges, and four single-piece crossbeams. These elements are arranged as shown in Figure 4-12.

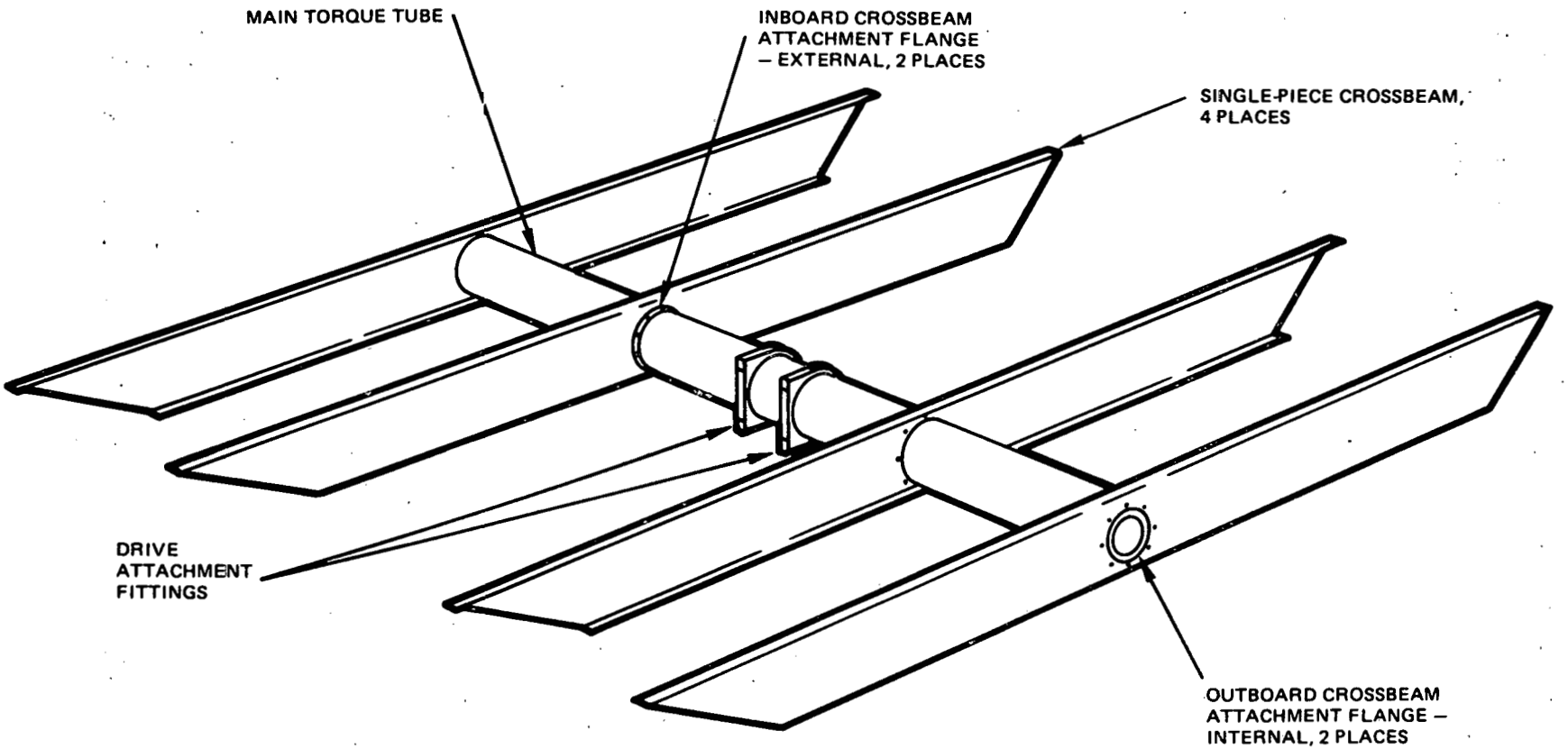

Figure 4-12. Reflective Surface Supporting Structure

The torque tube, a nominal 10-in. standard low carbon steel pipe, has an outside diameter of 10.75 in. with a 0.25-in.-wall thickness. It is 206.25 in. long. The two drive attachment fittings, flame cut from 2-in. low carbon steel plate, are machined on the surfaces which mate with the drive unit and are welded to the pipe. Also welded to the torque tube are four ring flanges for attachment of the crossbeams. Because the crossbeams are single units, the outboard attachment flange must be inside the torque tube to allow the inboard crossbeam to pass over the torque tube on assembly. The arrangement of these joints is shown in Figures 4-13 and 4-14. The crossbeams are constant section channels of 11 ga (0.123 in.) galvanized low-carbon steel sheet, 14 in. deep and 215.50 in. long.

The reflector substructure is attached to the drive system with four 0.75-in. diameter bolts. The geometry is that depicted in Figure 4-15.

All changes from the SRE test heliostat design stem from the substitution of single-piece, full-length, full-depth crossbeams for the previous tapered half-beams. This design has been changed to reduce cost and because, with more tooling, it is considered possible to hold the tops of the crossbeams straight, ensuring an accurate interface plane for attachment of the reflector panels.

This change permits a much lighter attachment between crossbeams and torque tube because all balanced moments remain within the crossbeam structure. They are not transferred from one half-beam into the splice flange and from there into the opposing half-beam. A further consequence of the change is a reduction in the load carried by the attachment flanges and a reduction in their thickness from 0.375 in. to 0.188 in. The attachment pattern itself, 6 spotwelds instead of 12 heavily torqued bolts, is less expensive. The spotwelds will all be made simultaneously in a manufacturing setup which provides a separate spot-welding head for each spot.

Because the inboard crossbeams must be slipped over the torque tube end to reach the attachment flange, the outboard flange must be inside the torque tube. Consequently, the joints are different, but they are equally simple.

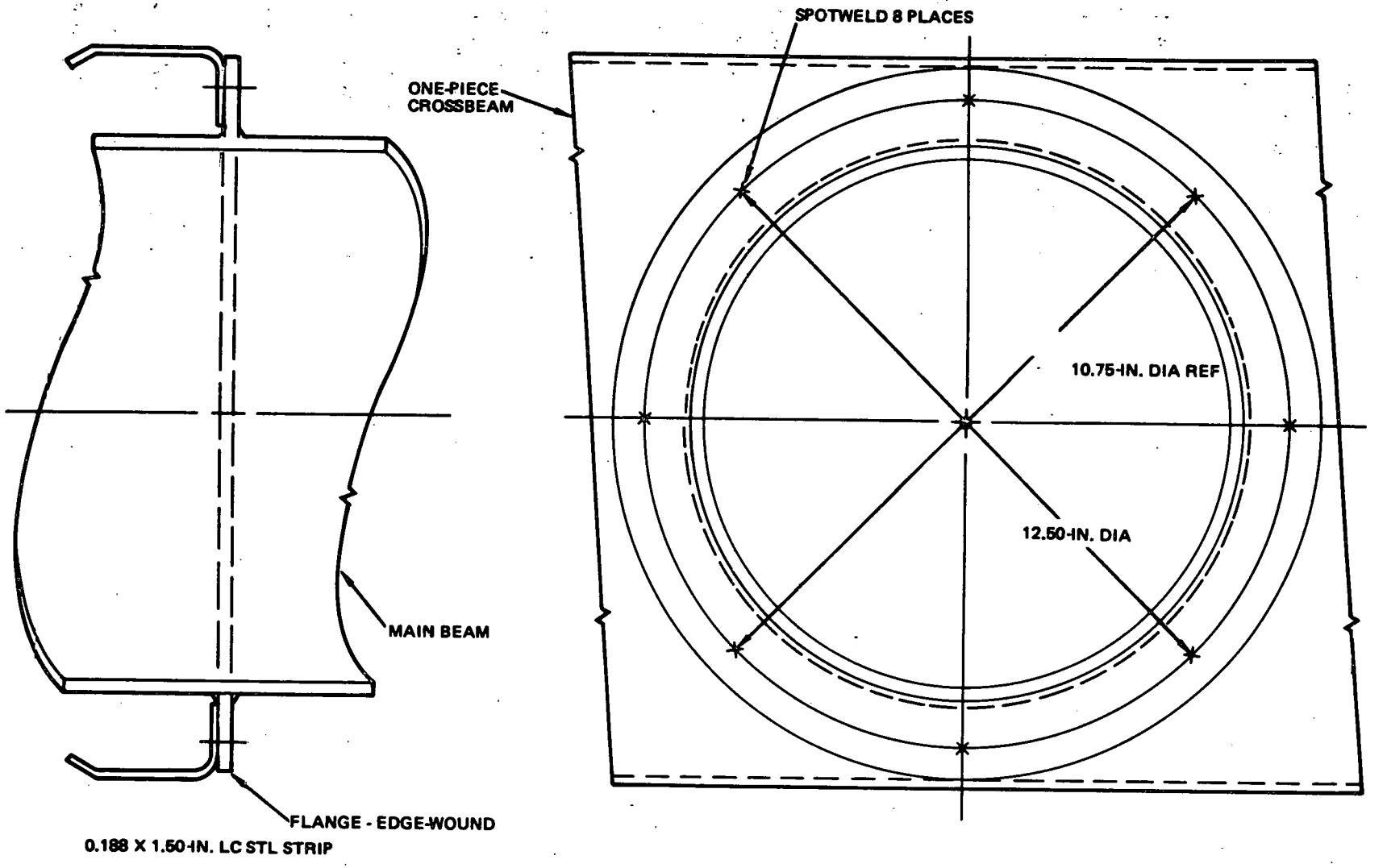

Figure 4-13. Inverted Heliostat Inboard Crossbeam Joint

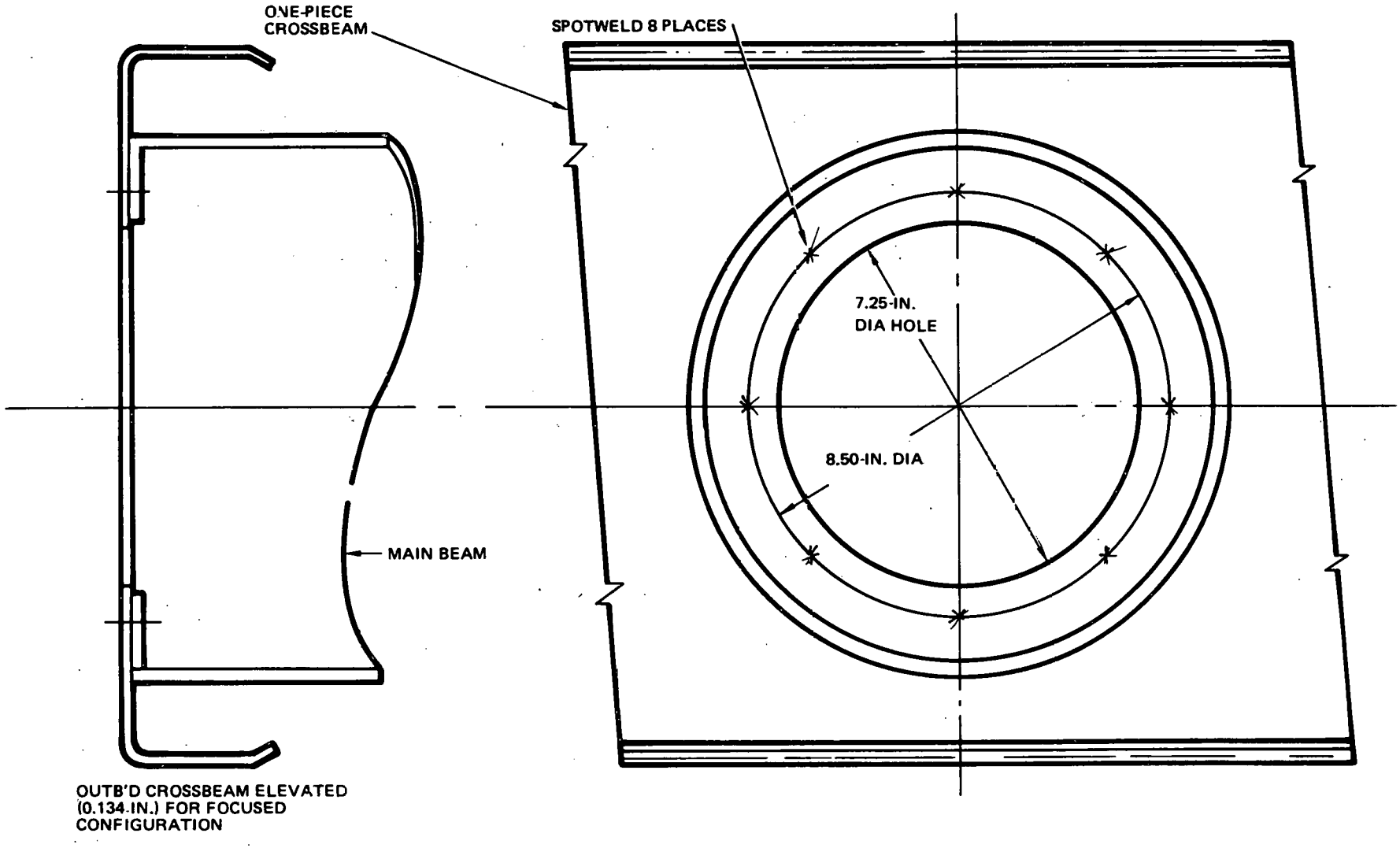

Figure 4-14. Inverted Heliostat Outboard Crossbeam Joint

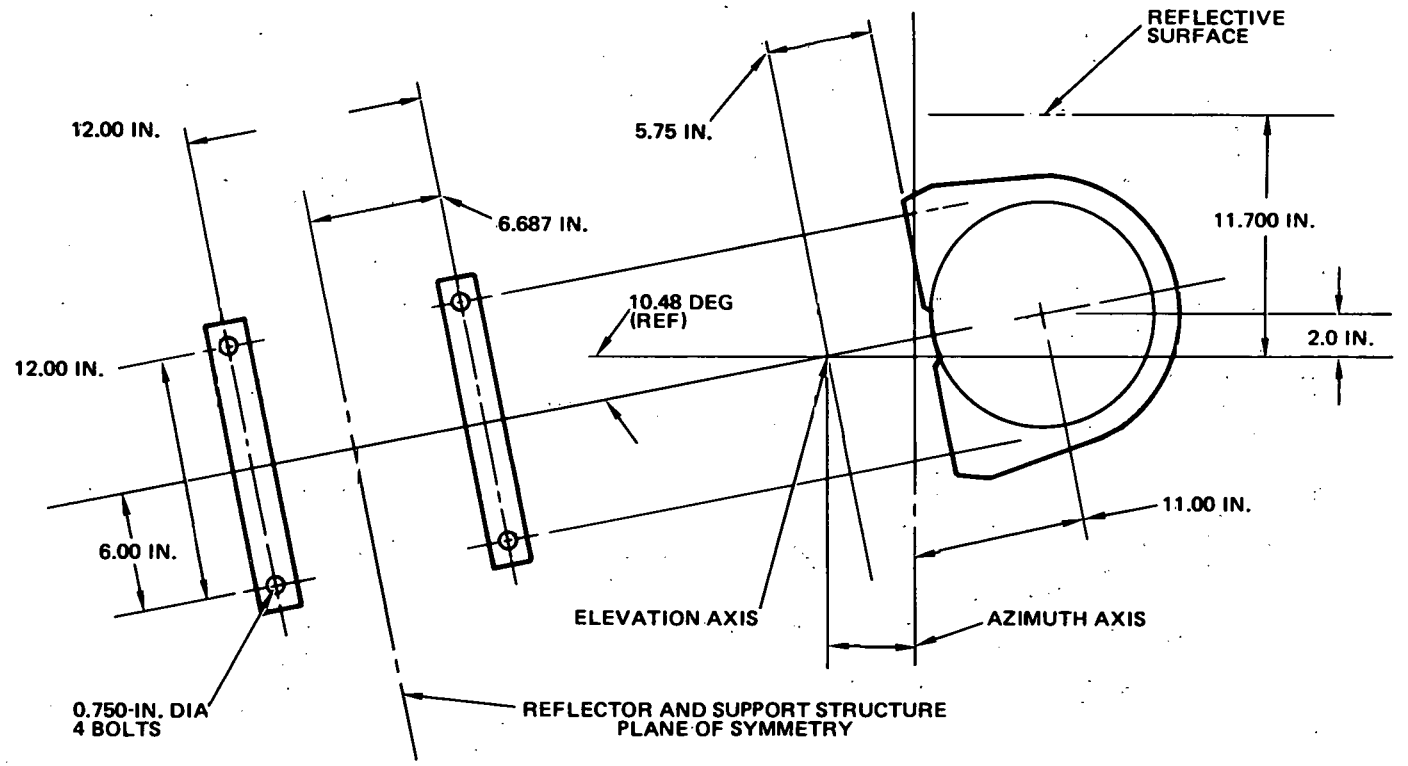

Figure 4-15. Reflector Support Structure Attachment Interface

Most of the heliostat steel hardware were galvanized with a zinc coating, made from galvanized sheet from the mill or hot-dip galvanized. Table 4-8 identifies the finish for the major structural components.

Hot-dip zinc galvanized coatings per ASTM Specification A123-73 were applied where permanence of protection was the prime consideration and other design requirements could be subordinated. It is the experience of electrical power companies that such finishes can last 25 yr in desert exposures. The design effort required to provide correct-size modules for galvanizing and compatibility throughout the structure with the galvanizing process will greatly reduce long-term maintenance.

Table 4-8
HELIOSTAT PAINTS AND FINISHES

Component	Paint/Finish
Reflector Substructure	
Torque Tube	Hot-dip galvanized
Crossbeams	Galvanized sheet from mill
Drive Unit	
Meehanite Ductliron Casting Parts	No finish
Exterior Steel Parts	Hot-dip galvanized
Pedestal	Hot-dip galvanized
Sensor Pole	DeSoto, Inc., No. 513-703 Primer plus U. S. Paint, Lacquer, and Chemical Co. No. AA92-W-2A Topcoat

The sensor pole finish coating presented a situation where low thermal energy absorption to keep the structure temperature low (and hence defocusing structural deflection low) became an additional concern. A catalized No. 513-703 chromated epoxy, yellow primer (from De Soto, Inc., Berkeley, California), top-coated with two-part, nonyellowing, di-isocyanate cured, white polyurethane, No. AA92-W-2A from US Paint, Lacquer, and Chemical Co., St. Louis, Missouri, was used. This is the most durable

finish system found to date for a similar purpose on the top surfaces of jet transport aircraft. The finish can be expected to be intact and retaining gloss after 4 yr.

The heliostat structural support weighs about 1,108 lb, as follows:

Torque Tube:	Steel	552.5 lb
	Zinc	33.0 lb
Crossbeams:	Steel	509.8 lb
	Zinc	13.0 lb
		1,108.3 lb

4.2.4 Drive Unit Design and Performance

Each heliostat incorporates a drive unit which produces appropriate reflector motions for solar tracking, emergency slewing, routine reflector positioning, and stowage. The unit consists of an azimuth and elevation drive train, each comprising a motor with several stages of reduction, capable of producing the high-torque, low-speed output needed. In addition, the unit serves as the structural support for the reflector and its substrate. The kinematic and structural requirements imposed on the drive unit make it a key cost element of the heliostat.

In the discussion which follows, the process will be described whereby the currently recommended drive unit design featuring "Orbidrive" speed reducers was selected as the most cost-effective for the proposed Pilot Plant application. Tests on the recommended Orbidrive configuration will be shown to confirm the technical adequacy of the proposed design.

4.2.4.1 Drive Unit Performance Requirements

Specific performance requirements for the drive unit are summarized in Table 4-9. The azimuth travel requirement of ±270 degrees stems from earlier computer simulations of heliostat motions for the pilot plant field, while the requisite limits of elevation motion are dictated by designing for inverted reflector stowage. The elevation "safe" load occurs during stowage at the most adverse yaw angle with a wind velocity of 44.7 m/s (100 mph).* The drive unit is designed to survive this most adverse condition, even

*Recently, the stowage wind velocity requirement was relaxed to 40.2 m/s (90 mph) for Pilot Plant. Thus, the drive unit requirements and design specified in this volume incorporate a measure of conservatism potentially permitting further cost reductions during the Pilot Plant design phase.

Table 4-9

DRIVE UNIT REQUIREMENTS

			Azimuth	Elevation
• Travel			±270°	0° to 180°
• Operating Loads				
Breakout			7,345 nm (65,000 in.-lb)	7,345 nm (65,000 in.-lb)
While Stowing			*	9,605 nm (85,000 in.-lb)
• Stowage Loads (Reflector Horizontal, $\alpha = \pm 10^{\circ}$)				
Condition	Wind Velocity	Elevation Axis Position		
Normal	44.7 m/s (100 mph)**	±25° from Wind	5,085 nm (54,000 in.-lb)	15,029 nm (133,000 in.-lb)
Normal	31.3 m/s (70 mph)	Random	*	15,029 nm (133,000 in.-lb)
Safe	44.7 m/s (100 mph)**	Random	7,345 nm (65,000 in.-lb)	28,250 nm (250,000 in.-lb)
• Backlash			0.5 mr max	0.5 mr max
• Stiffness (Minimum Resonant Frequence)			1 Hz	1 Hz
• No Back-Drive Under Specified Loads			7,345 nm (65,000 in.-lb)	28,250 nm (250,000 in.-lb)
• Life			30 yr	30 yr

*Noncritical

**This requirement was recently changed to 40.2 m/s (90 mph) for Pilot Plant. Thus, the drive unit requirements and design specified in this volume incorporate a measure of conservatism potentially permitting further cost reductions during the Pilot Plant design phase.

though it is planned to align the elevation axis with the wind during high winds, producing the more benign "normal load" maximum specified. The heliostat is designed to perform without degradation after exposure to the normal load condition. The safe stowage and operating loads of Table 4-9 are the same for the azimuth drive, representing the maximum occurring during stowage, since the azimuth drive must be capable of moving the elevation axis to its preferred orientation under maximum winds. The azimuth and elevation requirements specified in Table 4-9 are appropriate for the proposed Pilot Plant design, selected to satisfy the most demanding anticipated stowage scenario.

4.2.4.2 Drive Unit Tradeoffs

Considerable effort was expended in exploring alternative drive unit designs to achieve the most cost-effective approach. Some of the more promising concepts considered are described in this section. Each drive train is identified by the type of output reduction stage employed, because this is the principal factor influencing drive unit cost. The drives which have been given the most consideration are described in Figure 4-16 and are compared by the matrix of Table 4-10. Drive selection was based mainly on initial cost, since all of the drives were felt to be qualifiable in terms of meeting collector performance requirements. At the time of drive unit selection for the inverting heliostat in mid-1976, cost estimates for the leading two azimuth drive contenders favored the Orbidrive of Figure 4-17 by about $500 per heliostat over the octagonal helistat's harmonic drive described in Section 6.2.2.4. This incentive was judged sufficient to justify the additional development effort anticipated in using the less-seasoned Orbidrive.

The principal elevation drive contenders for the inverting heliostat were the Orbidrive of Figure 4-17 and a concept employing dual linear actuators as shown in Figure 4-18. The harmonic drive of Figure 4-19 was not a serious elevation drive candidate at this time because of its already noted higher cost. The dual linear actuator approach had been rejected in an earlier pitch/roll heliostat study because of clearance problems in achieving requisite actuator motions. However, the more benign kinematics of the elevation/azimuth heliostat imposed no such constraint. The inverting heliostat actuators shown in Figure 4-20 differ from the octagonal heliostat's single linear actuator described in Section 6.2.2.4, primarily in their employment of a housed screw to eliminate the need for a separate protective boot. Since the

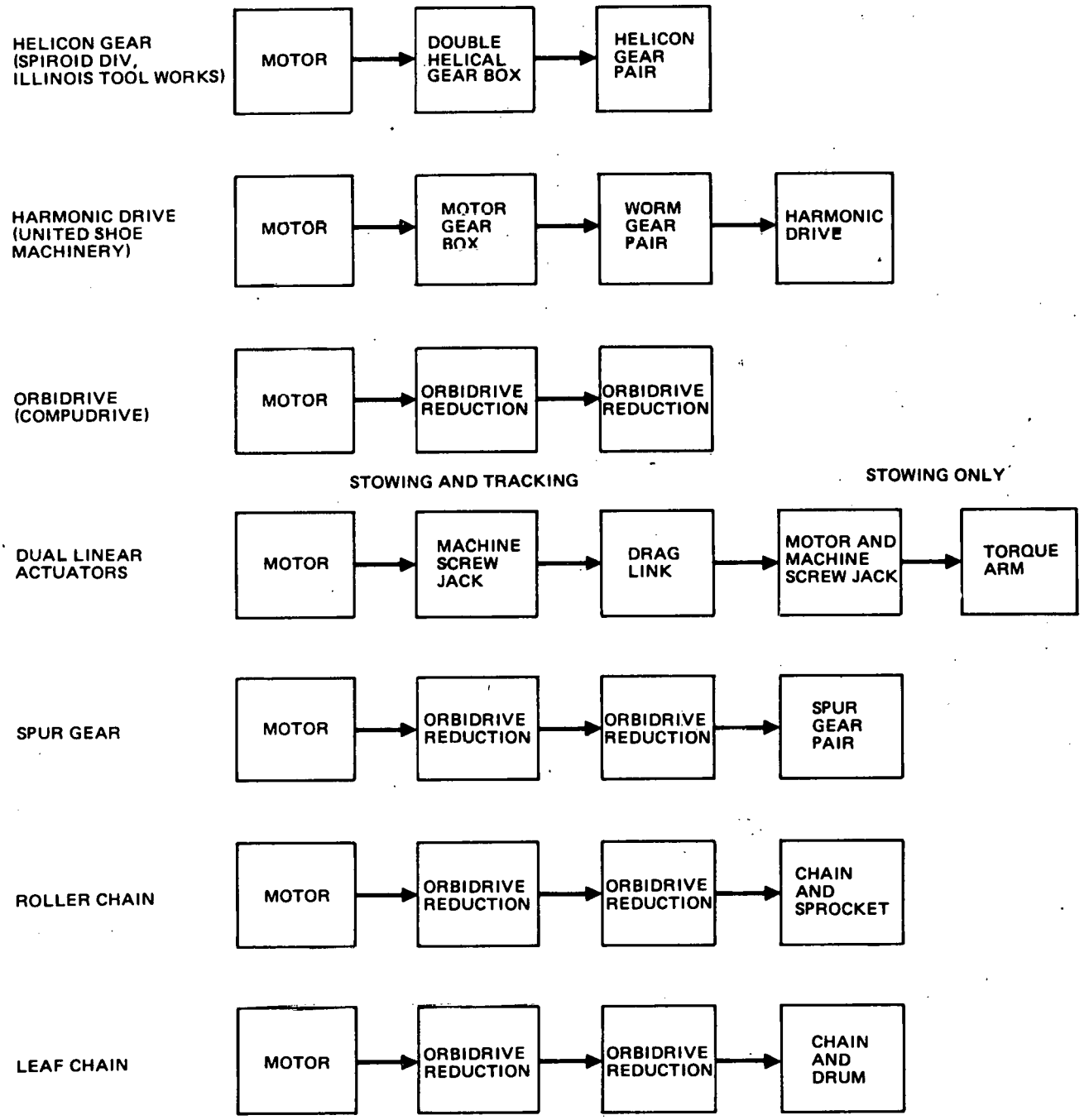

Figure 4-16. Alternate Drive Systems

Table 4-10
DRIVE UNIT TRADES

	Azimuth Axis				Elevation Axis						
	Requirement	Helicon Gear	Harmonic Drive	Orbidrive	Requirement	Linear Actuators	Roller Chain	Leaf Chain	Orbidrive	Spur Gear	Harmonic Drive
Cost Factor*		1.28	1.00	.84-1.03		1.09 Rom	**	**	1.00	**	1.12 Rom
Maintenance Characteristics		Good	Good	Good		Good	Poor	Poor	Good	Good	Good
Qualification Status		No	Yes	Yes		No	No	No	Yes	No	No
Backlash (mr)	≤0.5	1.25 (was ≥ 0.5) ***	1.0 Hysteresis ***	2 (was ≤ 0.5) ***	≤ 0.5	0.5	2 (was < 0.5) ***	2 (was ≤ 0.5) ***	2 (was ≤ 0.5) ***	1.5 (was ≤ 0.5) ***	1.0 Hysteresis ***
Stiffness NM/Degree (in.-lb/degree)	>17,850 (158,000)	>17,850 (158,000)	65,750 (582,000)	22,600 (200,000)	>17,850 (158,000)	43,050 (381,000)	>17,400 (154,000)	>17,400 (154,000)	22,600 (200,000)	>17,400 (154,000)	65,750 (582,000)
Static Efficiency	> 7.9%	7.2%	> 7.9%	> 7.9%	> 7.9%	> 7.9%	> 7.7%	> 7.7%	> 7.7%	> 7.7%	> 7.9%
Dynamic Efficiency		12.4%	28%	16% (was 22%) ***		18%	16% (was 22%) ***	16% (was 22%) ***	16% (was 22%) ***	16% (was 22%) ***	28%
Size of Output Element MM (in.)		391 (15.4) Dia	254 (10) Dia	191 (7.5) Dia Cam		498 (19.6) Lever Arm	508 (20) Dia Drum	312 (12.3) Pitch Dia	191 (7.5) Cam	508 (20) Pitch Dia	254 (10) Dia
Output Stage Reduction Ratio		47.5:1	242:1	961:1		1970:1	6.85:1	1.26:1	961:1	5:1	242:1
Total Reduction Ratio		70,400:1	108,900:1	43,245:1	<43,245:1 Stow	<53,523:1 Track <26,761:1 Stow	<43,245:1	<43,245:1	<43,245:1	<43,245:1	43,245:1
Motor Rating w (hp)		18.6 $\left(\frac{1}{4}\right)$	12.4 $\left(\frac{1}{6}\right)$ 30:1 Gearhead	18.6 $\left(\frac{1}{4}\right)$		24.9 $\left(\frac{1}{3}\right)$ 30:1 Gearhead	18.6 $\left(\frac{1}{4}\right)$	18.6 $\left(\frac{1}{4}\right)$	18.6 $\left(\frac{1}{4}\right)$	18.6 $\left(\frac{1}{4}\right)$	18.6 $\left(\frac{1}{4}\right)$
Slew Rate		8.69°/min	5.62°/min	14.15°/min		22.87°/min Stow	14.15°/min	14.15°/min	14.15°/min	14.15°/min	14.15°/min

*Based on supplier bids.
**Qualitative evaluation indicated these designs too costly.
***Estimated value at time of tradeoff study.

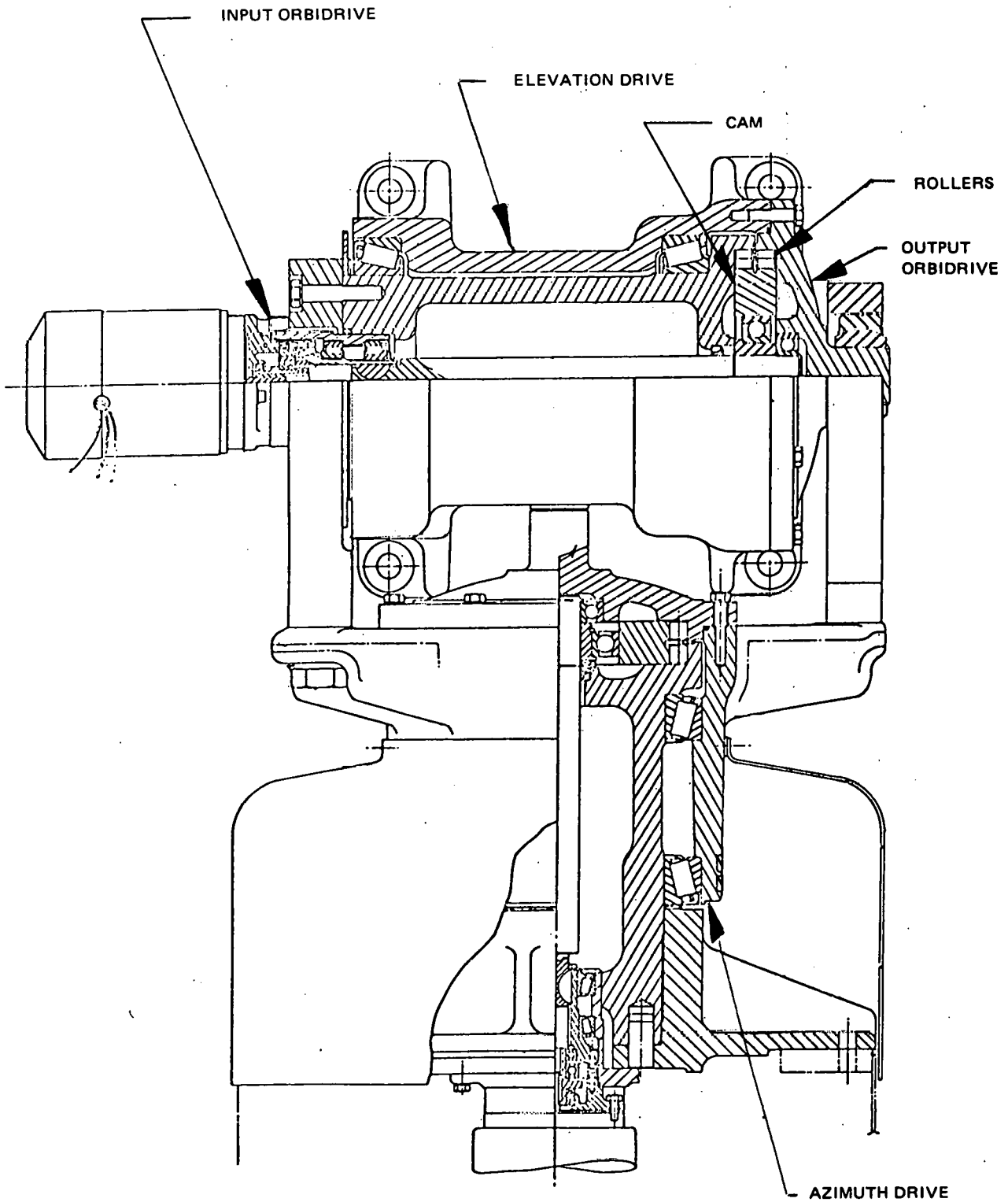

Figure 4-17. Orbidrive Configuration

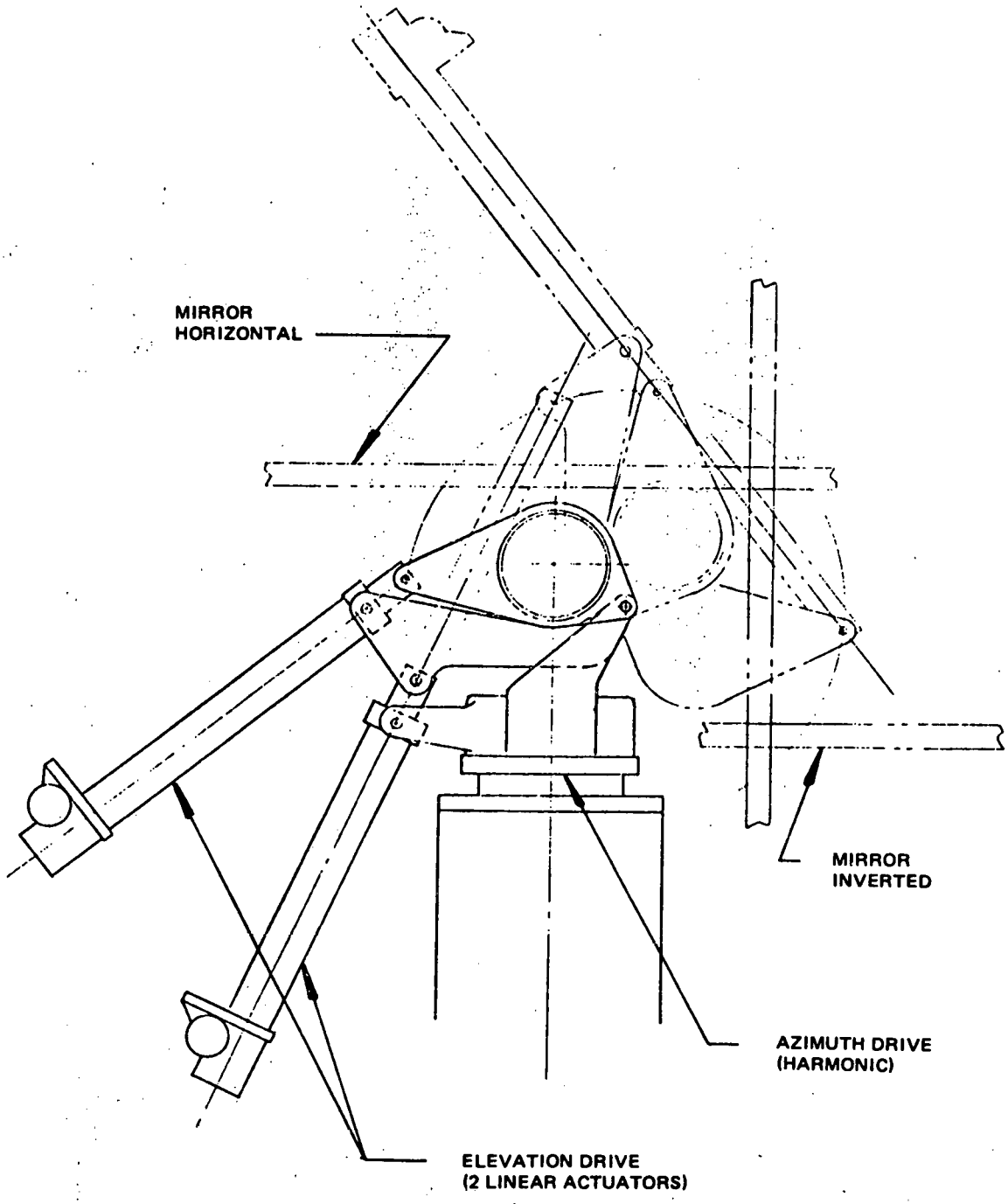

Figure 4-18. Dual Linear Actuator/Harmonic Drive Configuration

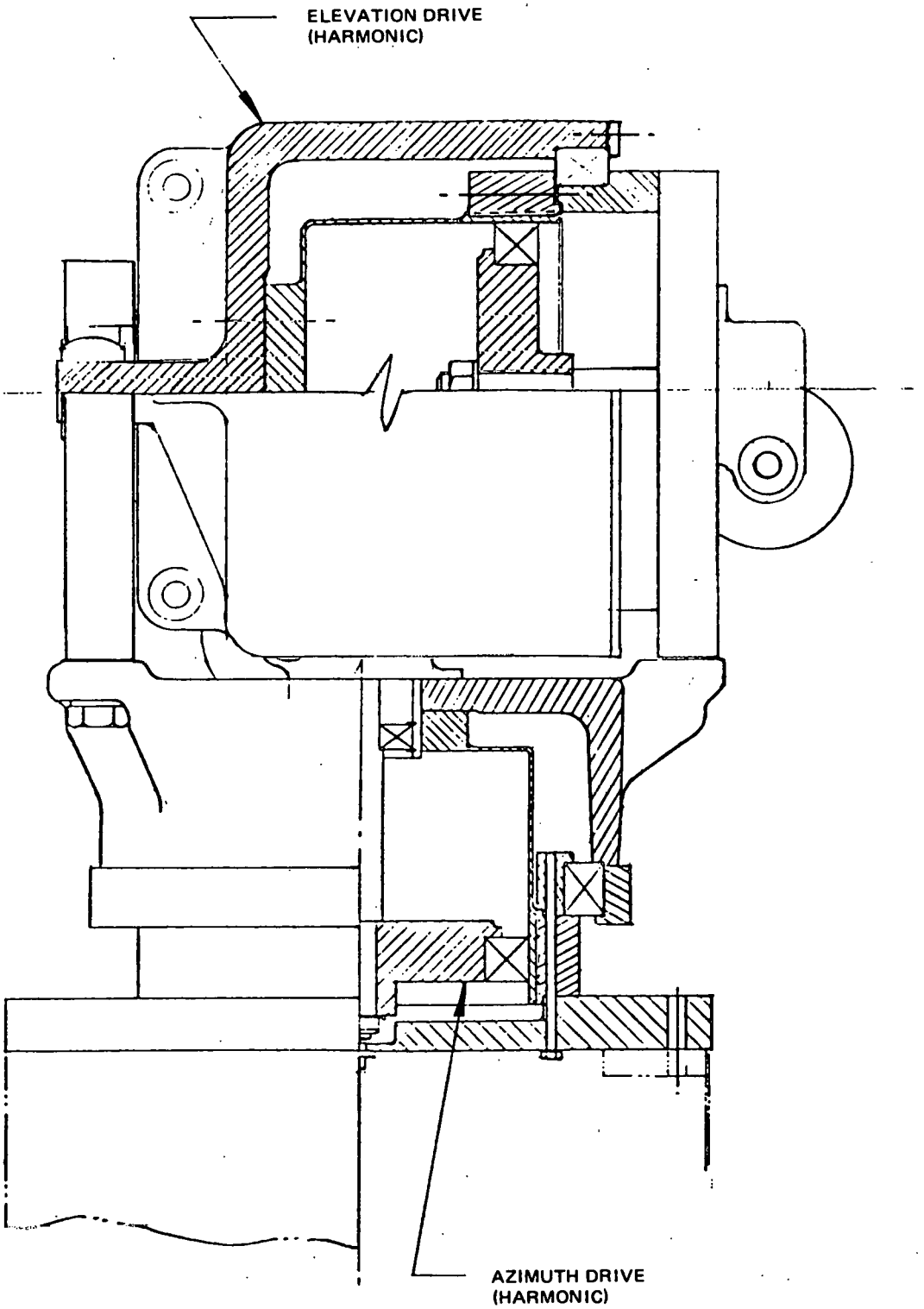

Figure 4-19. Harmonic/Harmonic Drive Configuration

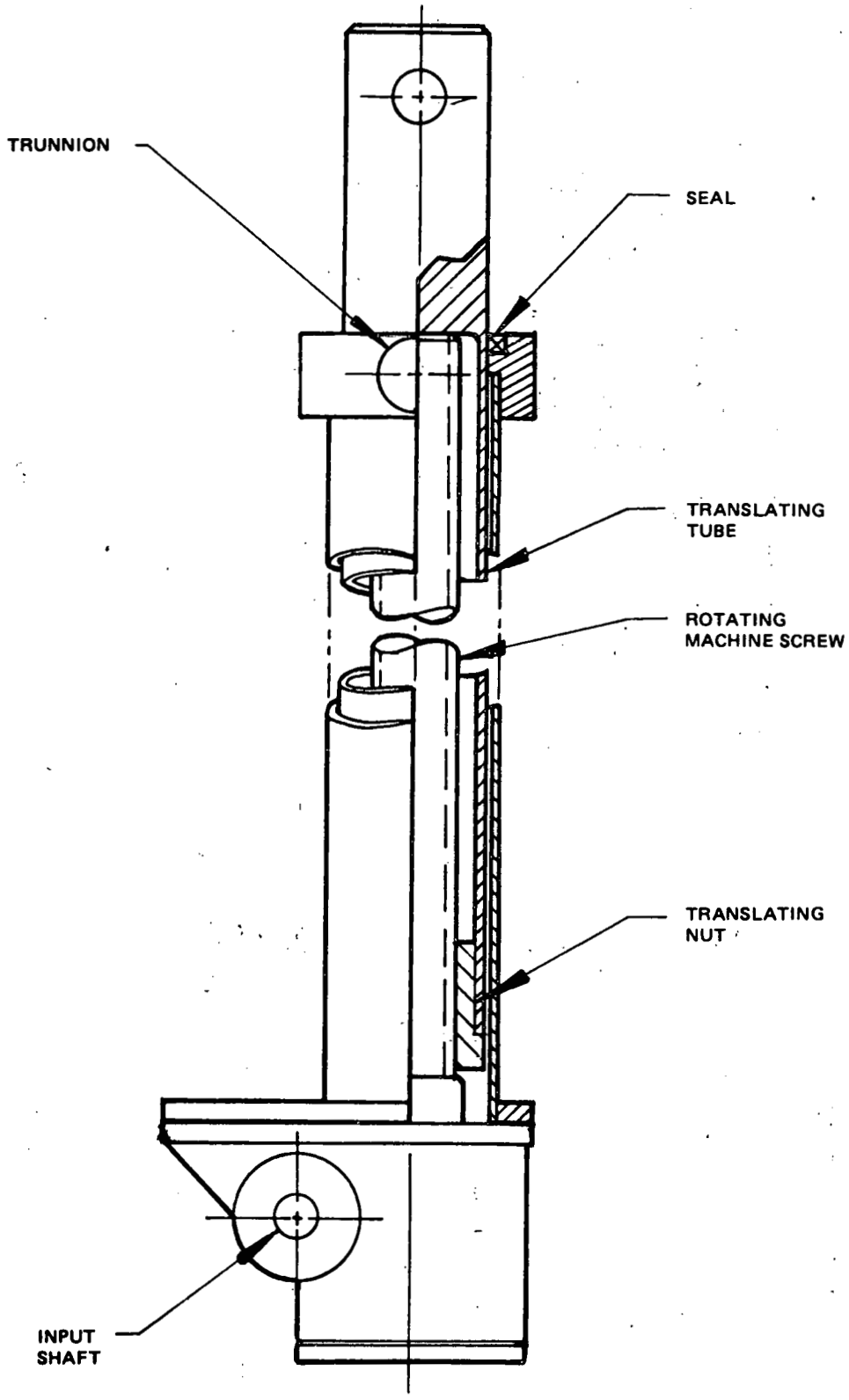

Figure 4-20. Linear Actuator

dual linear actuator concept and Orbidrive concept were estimated to cost about the same, it was decided to use the Orbidrive for elevation in the interest of drive commonality and because the more compact Orbidrive is less exposed to the elements. Orbidrive seasoning was not an issue in selecting the elevation drive, since the additional development entailed had already been assumed for azimuth.

4.2.4.3 Selection of Drive Unit Motor and Speed Reducer Characteristics
The following sections describe the process whereby the many factors influencing drive train design were collated to produce a cost-optimal configuration.

Orbidrive Output Stage Parameters

To prevent back-driving by external loads, the output stage reduction must be sufficiently high that its back-drive torque efficiency is always negative for torques up to the survival load. The present design's output reduction ratio of 961:1 was conservatively selected on the basis of available experimental data to satisfy that requirement.

The three most critical factors involving sizing of the output Orbidrives are static load capacity, torsional stiffness, and fatigue life. The output Orbidrive must be sufficiently large to limit the Hertz stress acting between cam and rollers to 2757.9 MPa (400,000 psi) under maximum static load, to maintain heliostat resonant frequencies above 1 Hz, and to provide a cam-roller fatigue life equivalent to 10,000 output shaft revolutions while exposed to representative shaft loads. Table 4-9 shows that the elevation drive is more critical with regard to stowage load, while the azimuth drive's torsional stiffness must be higher to provide the required resonant frequency because of the heliostat's higher azimuth moment of inertia. The higher average loading of the elevation drive, together with its large daily rotation, make the elevation drive more critical life-wise. An 18.10-cm (7-1/8 in.) diameter cam was determined to just satisfy the elevation static load constraint and to adequately provide the requisite cam-roller life. This size cam was calculated to produce an elevation resonant frequency of 2.4 Hz, but an azimuth frequency of 1.6 Hz. It was decided to use the 18.10 cm (7-1/8 in.) cam size for the azimuth drive to allow a reasonable margin between the calculated and required frequency, and to permit exploitation of parts commonality advantages.

Input Reducer and Motor Characteristics

A computer program was generated to assess the interactions of time/displacement-dependent aerodynamic and gravitational loads with load-dependent motor and drive train characteristics to support selection of motors and input reducers, and to permit evaluation of dynamic loading and fatigue life consumed for various operating and stowage scenarios. The computer program stores heliostat wind-tunnel test data, adapts the data to the particular heliostat geometry of interest, and calculates aerodynamic forces and moments at specified heliostat locations for transformed reflector pitch, yaw, and roll angles of attack, and for altitude and time-dependent wind mean and gust velocities. Gravitational moments, varying with elevation angle, are summed algebraically with aerodynamic loads to produce net drive moments. Drive train forward and backward torque efficiencies convert net drive moments to equivalent motor loads, which are related to input speed through tabular motor torque-speed characteristics stored within the computer and adjusted for motor drive voltage. Fatigue life consumption is expressed for convenience in terms of equivalent output shaft rotation at 2,825 nm (25,000 in.-lb).

The computer program was first used to compare the Bodine R4-D and R5-D motors as candidates for this drive application. Both are 42-frame polyphase motors, wound to provide maximum torque at zero speed. However, the R5-D motor has approximately twice the stall torque of the R4-D, achieved by increasing the motor length 7% and the weight 18%. The computer program was used to determine maximum required breakout torques for both the azimuth and elevation drive trains, based on stowage initiation at 16.1 m/s (36 mph). Drive reductions were selected for the R4-D and R5-D motors to produce the needed breakout torques. Computer simulations were made with these motor-drive train combinations to obtain drive unit torque/deflection time histories and sizing for a variety of potential stowage scenarios.

Computer simulations indicated that the maximum elevation tracking torque requirement of 7345 nm (65,000 in.-lb) occurs with the reflector horizontal 10° assumed wind angle of attack and with the maximum tracking wind velocity of 16.1 m/s (36 mph) occurring at zero yaw angle of attack. The

maximum azimuth tracking torque requirement was found to be only about half that for elevation. However, the maximum azimuth torque under adverse stowage conditions with 44.7 m/s (100 mph) was found to reach 7,345 nm (65,000 in.-lb). The azimuth reduction was sized to permit driving from this adverse condition to the normal stowage region.

Inverted stowage was simulated for the two motor-drive train combinations, producing the worst-case elevation torque/deflection traces of Figure 4-21. The maximum elevation torque for the smaller R4-D motor is seen to be nearly twice that for the R5-D motor, necessitating some increase in drive unit cam size to accommodate the higher loads.

If the operational groundrules are relaxed to allow face-up stowage in a rising wind, the more benign elevation loads of Figure 4-22 result, permitting the R4-D motor to be employed without any increase in drive unit cam size. The maximum elevation torque produced during face-up stowage with the R4-D motor is shown to be no worse than that encountered during inverted stowage with the R5-D motor.

An alternative change in the stowage groundrules entails rotating the elevation axis into the wind before inverting the reflector. Figure 4-23 summarizes the elevation torques for two variations of this stowage scheme using the R4-D motor. In the first case, the elevation axis is rotated in azimuth the shortest distance possible (a maximum of 90 deg) into alignment with the wind, producing an acceptable maximum elevation torque during inversion of 13,334 nm (118,000 in.-lb). The second case shown in Figure 4-23 describes the situation in which cable limitations require the elevation axis to be rotated in azimuth "the long way around" (180 deg maximum) into alignment with the wind. For this case, the elevation torque during inversion exceeds that encountered for stowage with random wind azimuth (see Figure 4-21), thus offering no advantage for this stowage scheme.

On the basis of the above described motor tradeoff study it was decided to select the R5-D motor and its companion 45:1 input reducer, permitting maximum operational flexibility. The drive unit is designed such that the R4-D motor and its appropriate input reducer can be substituted easily if warranted, permitting a modest cost reduction to be realized.

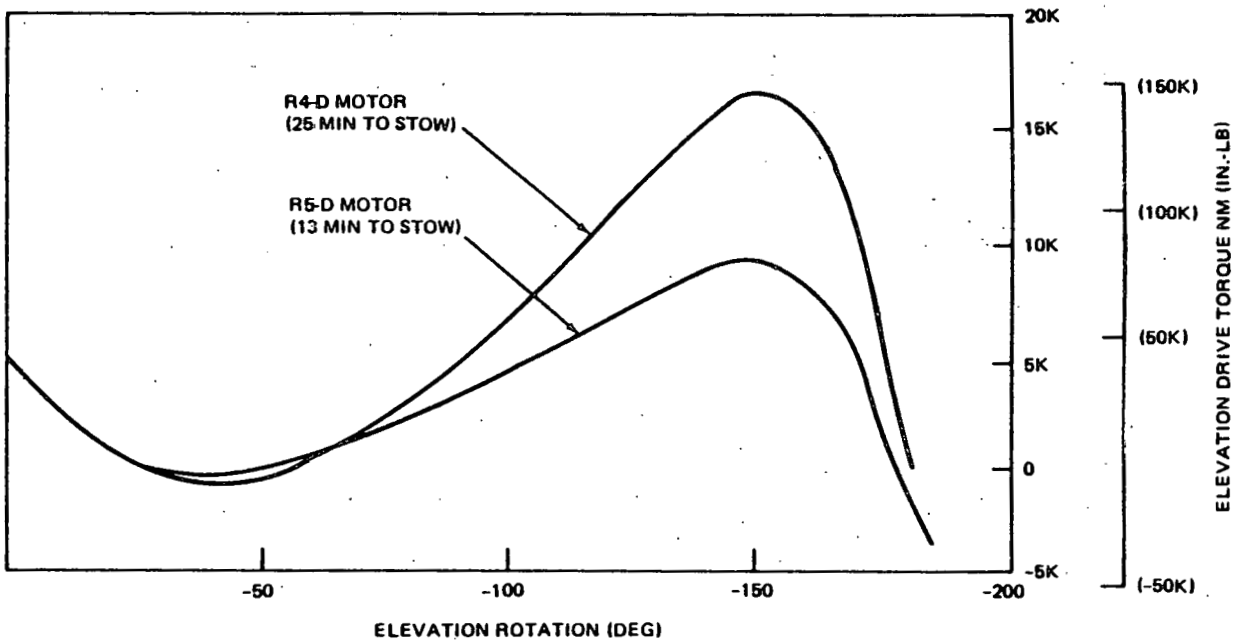

Figure 4-21. Elevation Drive Loads While Stowing Face Down

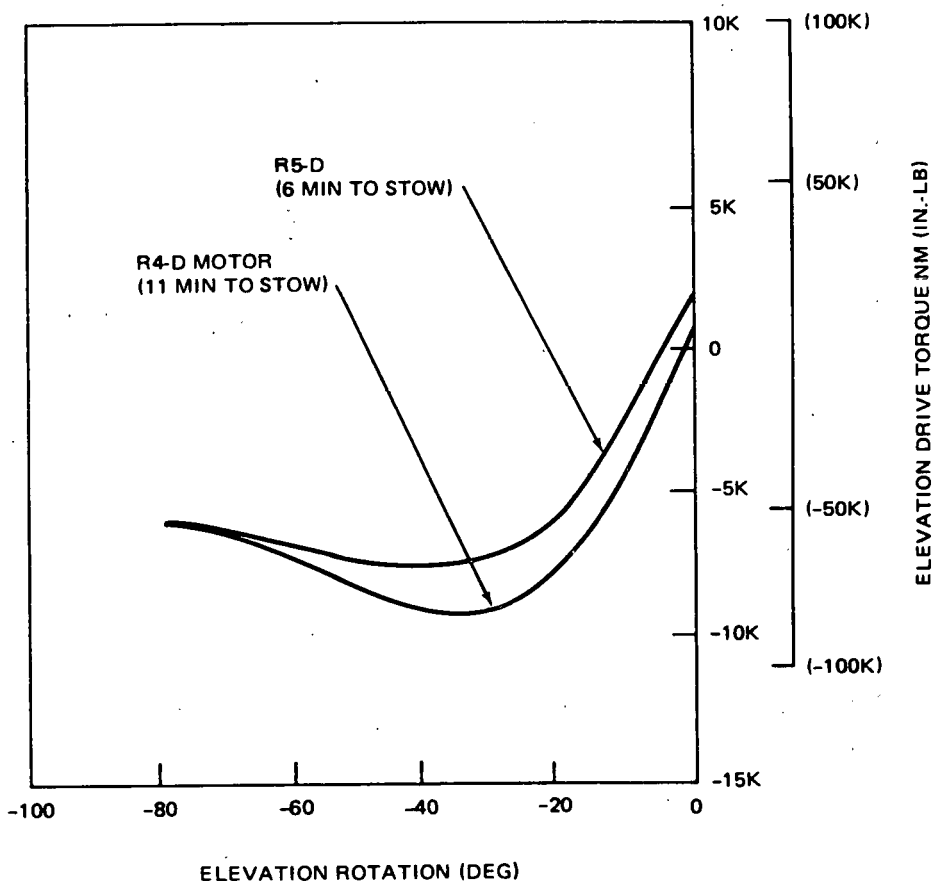

Figure 4-22. Elevation Drive Loads While Stowing Face Up

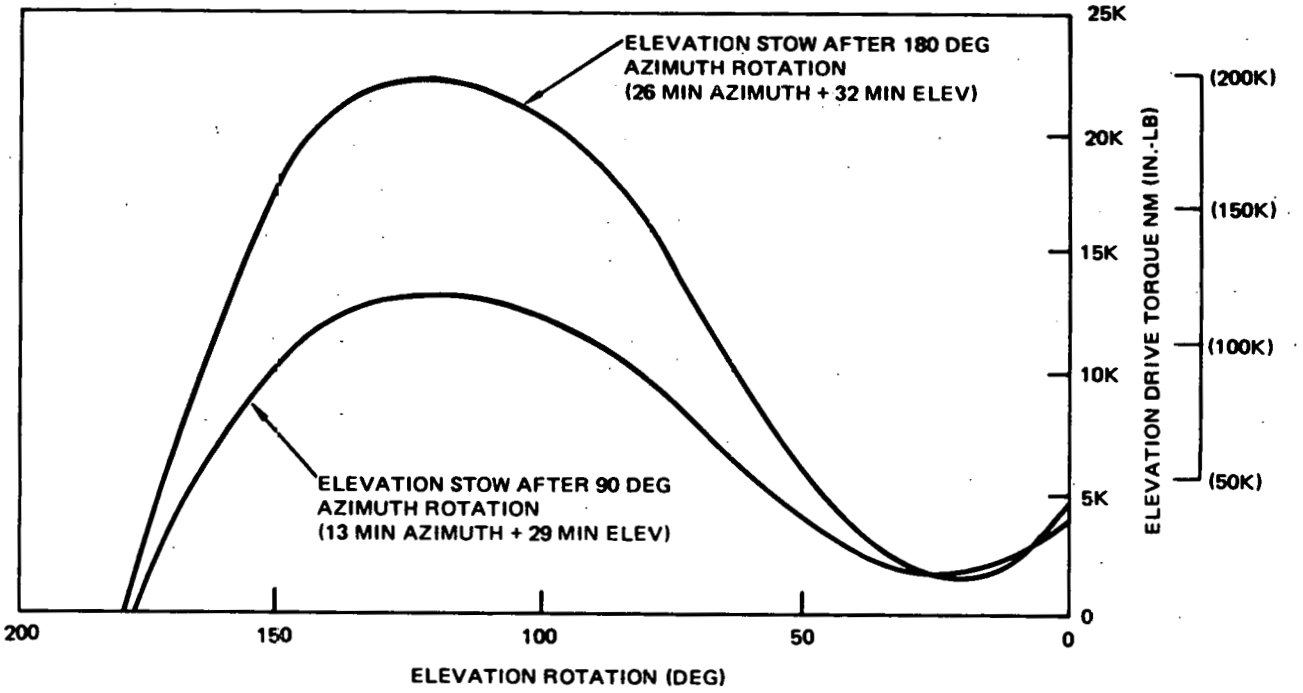

Figure 4-23. Elevation Drive Loads with R4-D Motor Stowing Face Down After First Rotating Elevation Axis Into Wind ± 25 Deg

4.2.4.4 Drive Unit Hardware Description

Each heliostat incorporates azimuth and elevation drive mechanisms to produce movement of the reflective surface about its axes of rotation. The drive mechanims are composed of motors, drive trains, position feedback transducers, reflector support bearings, and structural housings. The azimuth and elevation drive trains are schematically identical as depicted by Figure 4-24. The 230V, 3-phase, 42-frame, 4-pole AC torque motor drives an input 45:1 reducer, whose output shaft is coupled to a 961:1 output stage reduction.

Both the input and output reducers employ Orbidrive cam-roller sets to achieve requisite speed reductions. Figure 4-25 schematically shows the functional parts of a typical Orbidrive. The reaction and output cams are integrally machined as a common piece, which is fitted to the input shaft's eccentric, causing the reaction cam to orbit within the rollers of the reaction disc when the input shaft is rotated. Since there is one less reaction cam lobe than the number of reaction disc rollers, the cam indexes one roller for each cam orbit. In a similar fashion, the number of rollers on the output disc is one less than the number of output cam lobes, so that the output disc indexes one roller in the opposite direction relative to the output cam for each orbit. The differential motion of the output disc relative to the reaction disc can thus be extremely small per input shaft revolution, providing the high-speed reduction desired.

The principal structural elements of the drive unit are shown in Figure 4-26. The main reflector support beam is bolted to the four attachment points on the elevation drive housing. The housing's Orbidrive-coupled elevation shaft is bolted to the shaft support, and housing reaction loads are carried through a spherical bearing in the housing support. The elevation housing and shaft supports are bolted to the azimuth drive housing, which is coupled through a second Orbidrive to the azimuth drive shaft/base. The base is mounted to the heliostat support pedestal.

The complete drive unit assembly is shown in Figure 4-27. For clarity, only the elevation drive elements have been specifically identified. The azimuth drive employs identical motor, input reducer, output reducer cam and output disc, and even the same Timken support bearings.

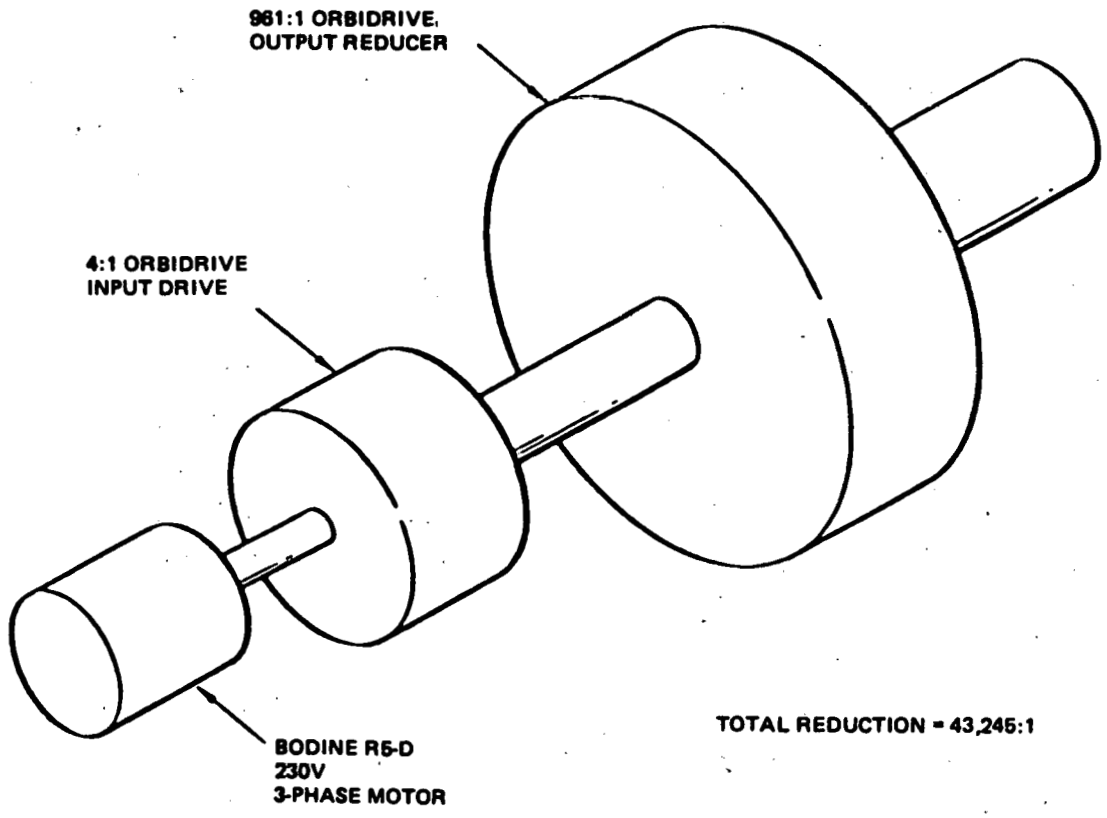

Figure 4-24. Azimuth/Elevation Drive Schematic

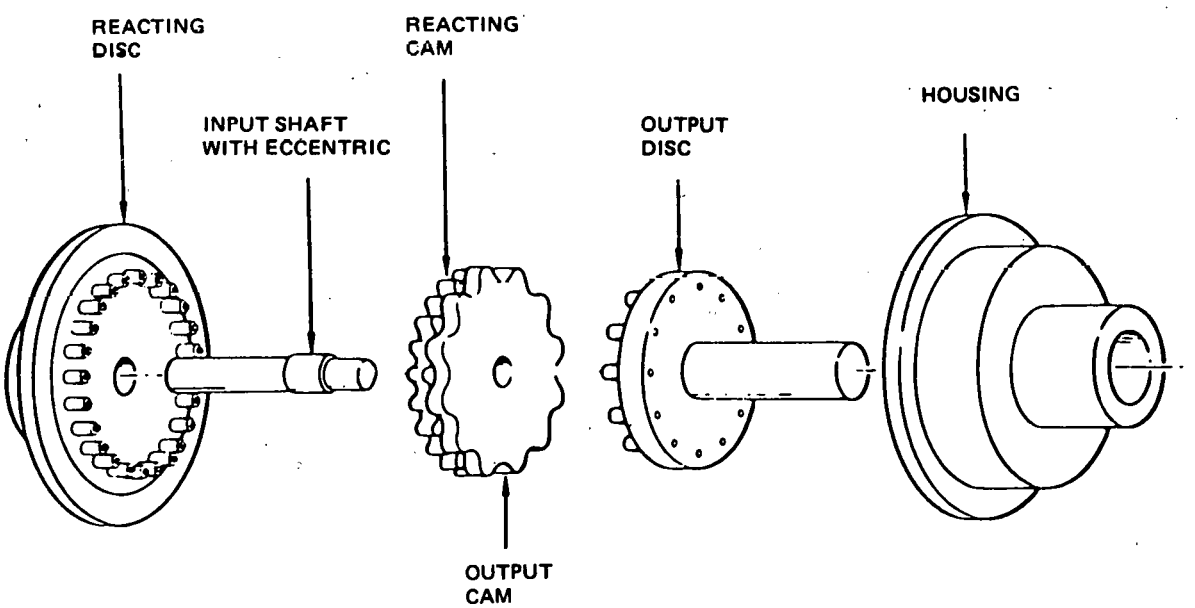

Figure 4-25. Orbidrive Operating Principle

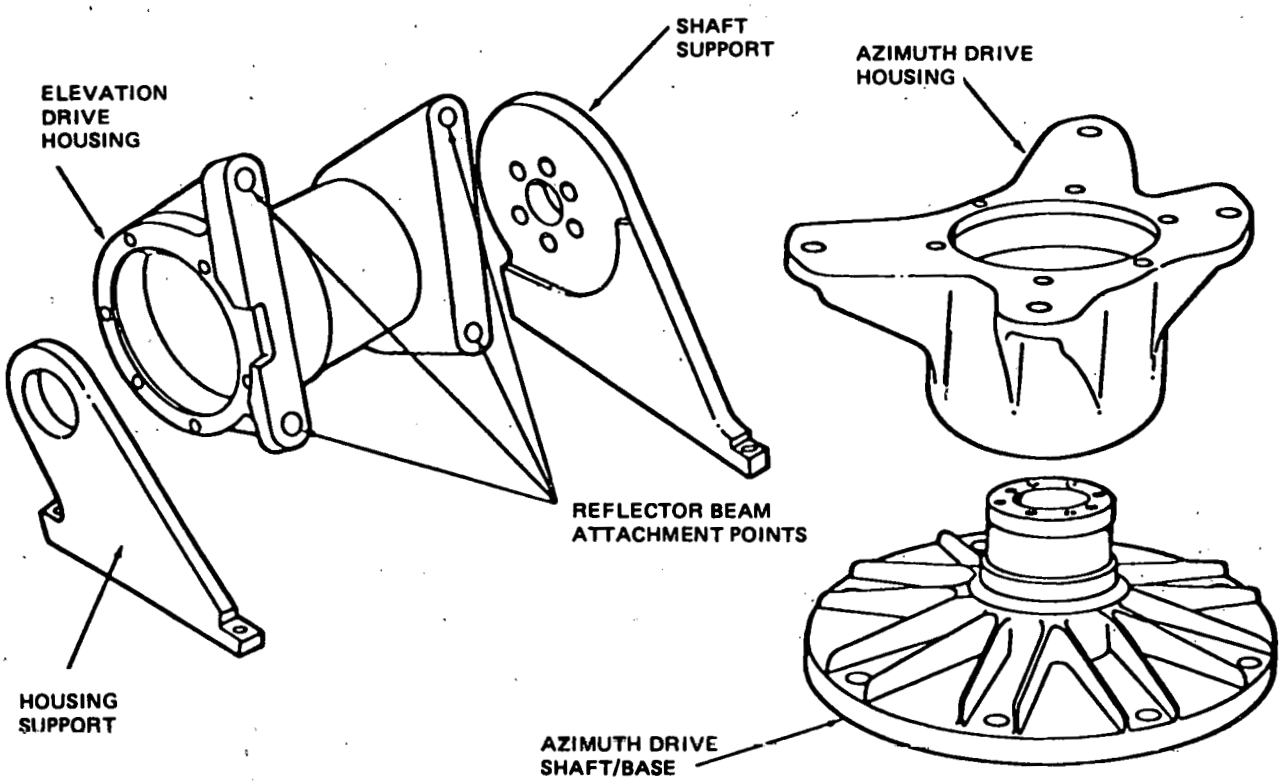

Figure 4-26. Drive Unit Structural Elements

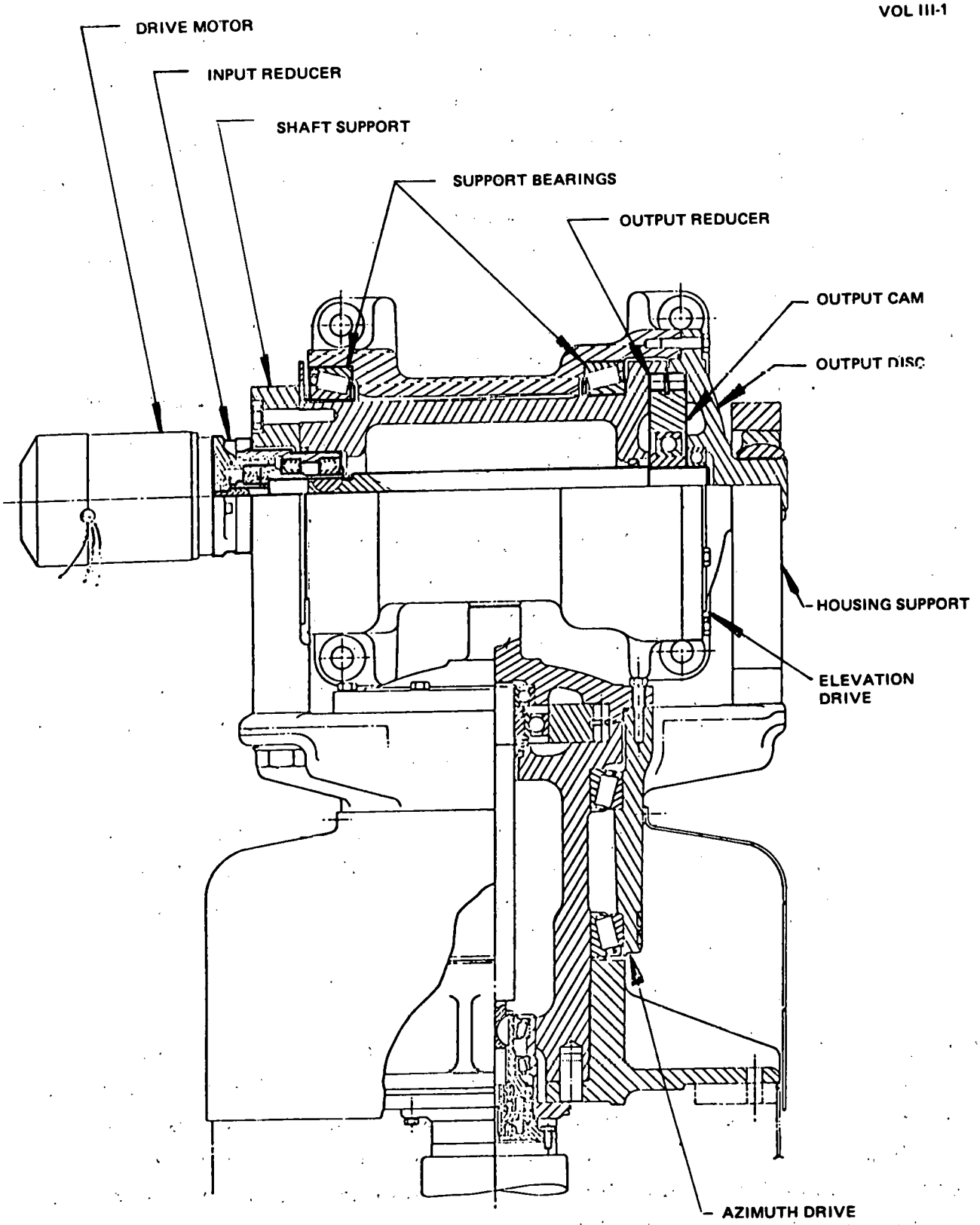

Figure 4-27. Orbidrive/Orbidrive Drive Unit Assembly

4.2.4.5 Drive Unit Design Summary

Table 4-11 summarizes performance characteristics of the proposed Pilot Plant drive unit and describes the key factors leading to their selection. The output reduction ratio was made sufficiently high to prevent back-driving under maximum stowage loads, and to minimize requisite size (and hence cost) of the input reducer. The elevation input reduction ratio was selected in conjunction with the drive motor to produce the maximum needed breakout torque. The same size input reducer was retained for the azimuth drive in the interest of parts commonality.

Cam size of the elevation output Orbidrive reducer was chosen to assure adequate fatigue life and static load capacity, while needed stiffness prevented the use of a smaller azimuth output cam. Fatigue criteria alone dictated elevation input reducer cam size.

The elevation motor was sized in conjunction with the input reducer to achieve requisite breakout torque, while driving the reflector fast enough during stowage to avoid having to increase output stage cam size beyond that required by fatigue and static load conditions. The azimuth motor was made the same size as the elevation motor in the interest of parts commonality and to provide maximum flexibility for satisfying defocusing and safety criteria which are not yet completely resolved.

The 2.0-mr output reducer backlash specified in Table 4-11 represents a value readily realizable with the Orbidrive concept, and demonstrated in heliostat tests to produce acceptable beam-pointing performance with the presently proposed closed-loop control scheme.

4.2.4.6 Drive Unit Test Summary

Both the inverting heliostat drive unit just described and the octagonal heliostat drive unit described in Section 6.2.3.4 were subjected to functional, environmental, fatigue, and survival load tests which qualified both the inverting heliostat's Orbidrive configuration and the octagonal heliostat's harmonic azimuth drive and linear elevation actuator. Test results for the recommended inverting heliostat drive unit are summarized in Table 4-12. Note that while this unit satisfied most of the design goals, it fell short in

Table 4-11

DRIVE UNIT CHARACTERISTICS

Item	Data	Critical Requirements
Reduction Ratio		
Input Reducer	45:1	Breakout Torque
Output Reducer	961:1	Backdrive
Overall Reduction	43245:1	
Cam Size		
Input Reducer	5.08 cm (2 in.)	Fatigue Life
Output Reducer	18.1 cm (7-1/8 in.)	Azimuth: Resonant Frequency Elevation: Stowed Load and Fatigue Life
Motor Size	Bodine 42 R5-D 42 Frame, 230 VAC, 3 Phase, 4 Pole 60 Hz	Breakout Torque Drive Rate
Drive Rate	14 deg/min	Stowing Loads
Output Dynamic Torque Efficiency	≥ 20%	Drive Rate
Output Static Torque Efficiency	≥ 12%	Breakout Torque
Output Stage Backlash	≤ 2.0 mr	Beam Accuracy

Table 4-12

ORBIDRIVE TEST OVERVIEW

Test	Requirement/Design Goal	Results
Static Load	133,000 In.-Lb - No Degradation	No Degradation
Survival Load	250,000 In.-Lb - Survive in Tact	300,000 In.-Lb
Backdrive	None to 250,000 In.-Lb	None
Stiffness	≥ 158,000 In.-Lb/Deg	> 200,000 In.-Lb/Deg
Input Dynamic Torque Efficiency	≥ 66%	≥ 66% At High Torque
Output Dynamic Torque Efficiency	≥ 34%	≥ 20% At High Torque
Output Static Torque Efficiency	≥12%	12 to 15%
Output Stage Backlash	≤0.5 mr	1.8-mr Maximum
Fatigue Life	≥323 Cycles at 70,000 In.-Lb	Qualified for 30-Yr Life

the areas of output dynamic torque efficiency and backlash. Subsequent analyses and testing revealed that the achieved performance is adequate for the proposed closed-loop scheme. Drive unit tests are described in more detail in Section 6.3.3.1.

4.2.4.7 Post-SRE Studies

Upon completion of SRE drive unit tests, the following additional efforts took place to better define the inverting heliostat drive unit for the Pilot Plant:

1. Orbidrive cost reduction/producibility study.
2. Orbidrive wear/backlash study.
3. Orbidrive grease distribution scheme definition.
4. Study to improve azimuth shaft/pedestal interface.
5. Identification of improved cable-wrap mechanism.

The first of these efforts was instituted to provide assurance that the Orbidrive elements can indeed be produced for the favorable NTE costs quoted. This study identified significant design changes needed to permit cost-effective fabrication of roller sockets to the drawing-specified positional accuracy of ±.0127 mm (0.0005 in.). However, actual measurement of acceptably performing Orbidrive hardware revealed that the sockets had actually been located within tolerances achievable with inexpensive drill jig operations, thus eliminating concern about socket fabrication costs.

The other significant area of concern identified in this study was that of cam fabrication. This concern resulted from vendor-reported difficulties with cam warpage experienced after heat treatment, necessitating considerable subsequent grinding. It appears that this difficulty can be corrected by better control of the heat-treatment process and/or by changing the cam material.

The Orbidrive wear/backlash study was instituted to predict the increase in Orbidrive backlash with life. A survey of literature relating to the type of roller/socket wear detrimental to Orbidrive backlash was used as the basis for extrapolating wear measured during fatigue testing to predict the increase in Orbidrive backlash with life. These predictions indicate that the more

critical azimuth backlash will not increase more than 0.5 mr over 30 yr, and that the elevation backlash will not increase more than 9 mr over the same period. It should be emphasized that the accelerated fatigue testing was conducted under loading extremes highly atypical of representative wear conditions, and can thus be expected to yield conservative wear predictions. These pessimistic predictions appear acceptable for the proposed closed-loop drive scheme.

The SRE inverting heliostat drive unit features grease fittings for periodic relubrication. However, some concern exists that simply injecting grease into the drive cavity may not adequately displace old grease residues from the critical roller socket areas. Therefore, the grease distribution scheme shown in Figure 4-28 was devised to assure direct feeding of new grease to the roller and socket areas.

The azimuth shaft-pedestal interface has been identified as a promising area for further drive unit cost reduction. Several potentially lower-cost schemes have been identified, and will be evaluated further during the Pilot Plant design phase.

The cable-wrap mechanism allows requisite azimuth rotation and reflector inversion to take place without tangling or chaffing of the electrical cables which service the elevation drive and are carried across the moving azimuth joint. The SRE mechanism is serviceable but somewhat bulky, and exposed to the elements. Therefore, the more compact, enclosed design shown in Figure 4-29 has been devised. This concept has been successfully tested at $10^{\circ}F$, which is below the lowest recorded temperature for the proposed Pilot Plant site. The mechanism, which allows a full ±270 deg of azimuth rotation, is protected from the environment by the indicated cover.

4.2.4.8 Drive Unit Implications of Current Open-Loop Study

MDAC is currently developing an open-loop control system which appears to offer significant cost advantages over the present closed-loop design. However, the open-loop approach may require a drive unit with less backlash than that practically achievable with the Orbidrive reducer. If the apparent cost advantages are verified by development and test, MDAC will recommend

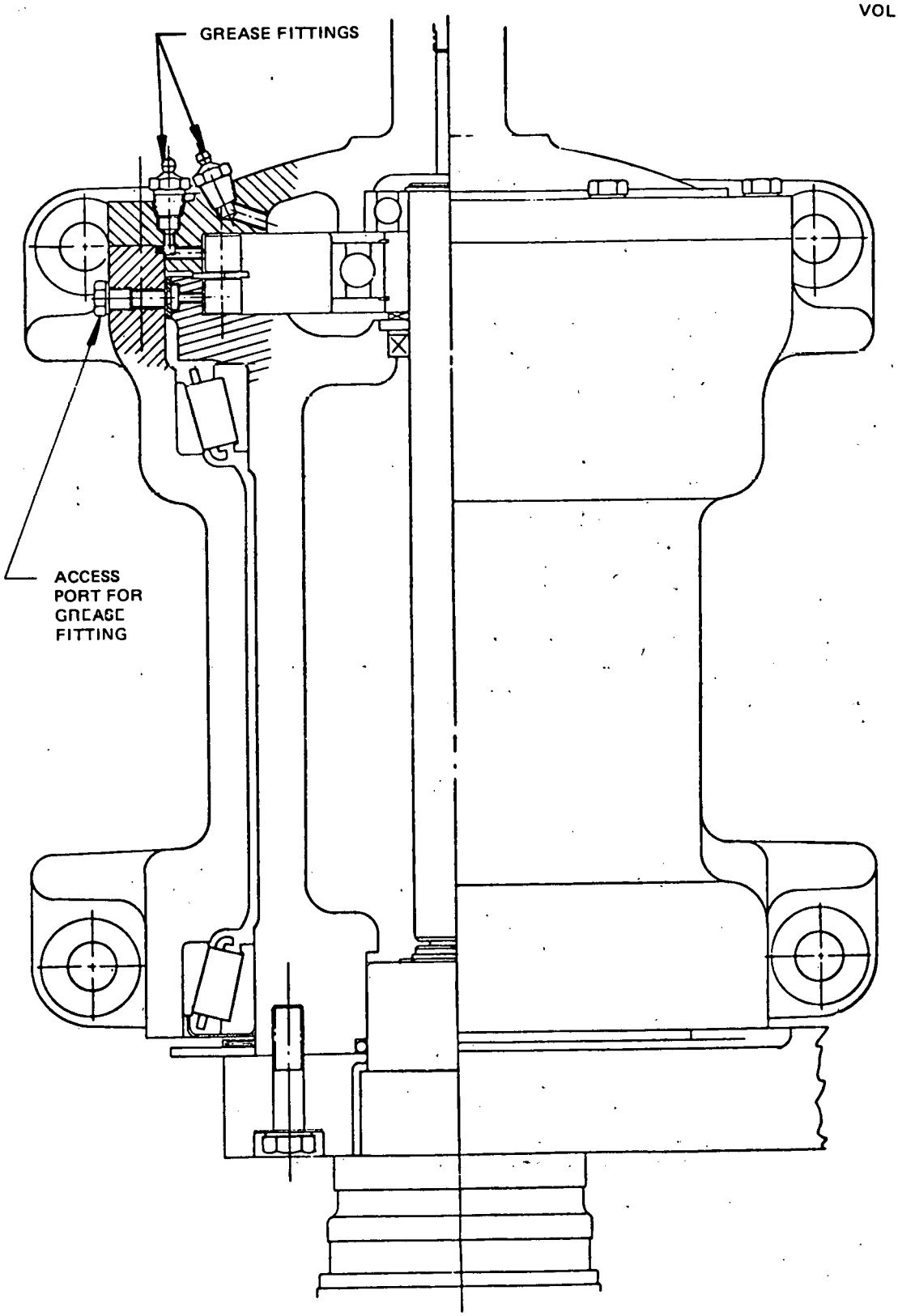

Figure 4-28. Orbidrive Grease Labyrinth

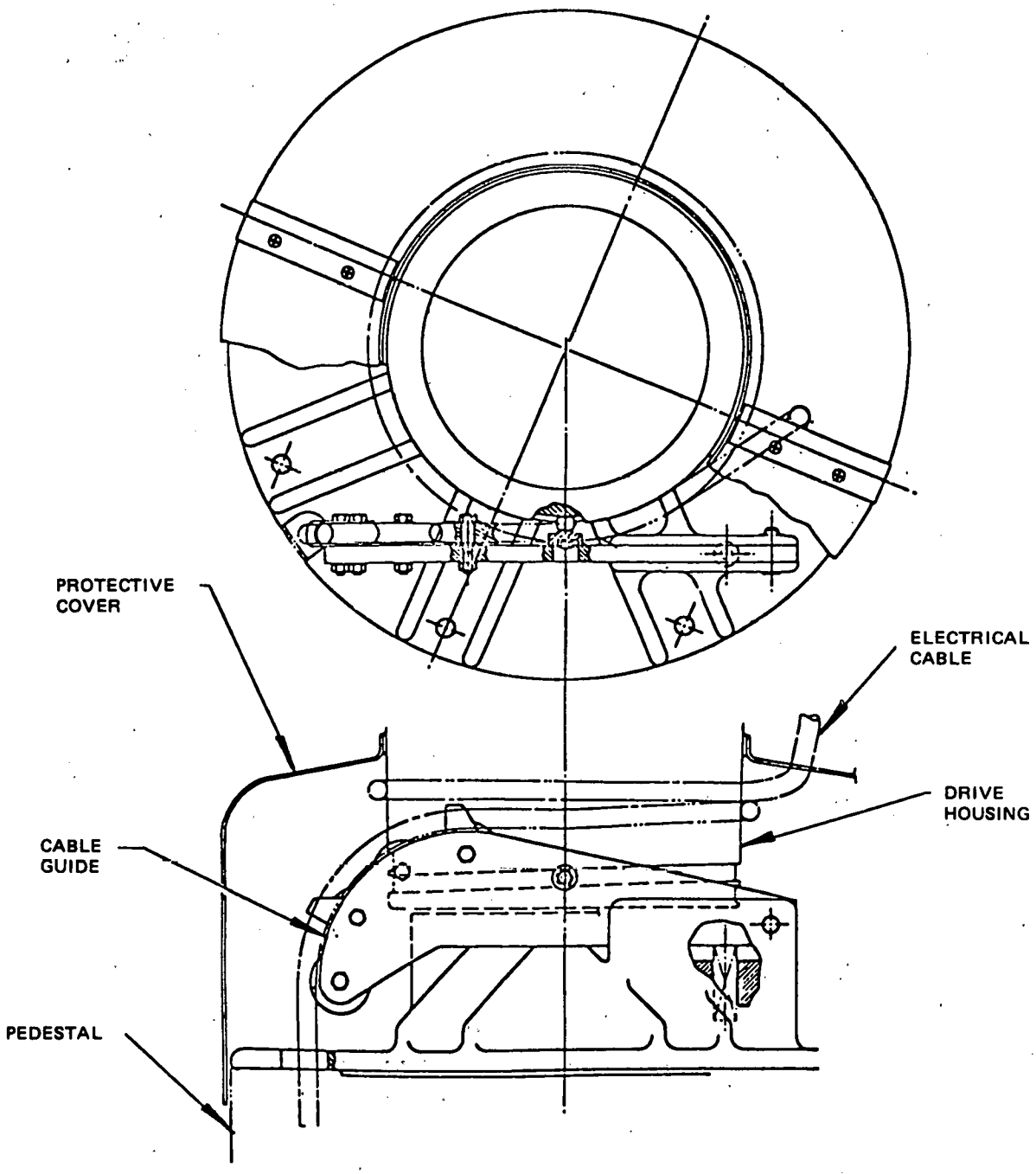

Figure 4-29. Electrical Cable Stowing

an open-loop system for the 10-MW Pilot Plant. Under these circumstances, if the need for tighter backlash is verified, it is anticipated that MDAC will recommend some combination of "Harmonic" rotary drives and jacks similar to those qualified in the SRE program.

4.2.5 Pedestal/Foundation Design/Performance

For a central pedestal concept, the thin-wall steel column is the simplest choice to transfer the heliostat loads to the foundation. For the MDAC inverted heliostat with face-down stowage, it is the cheapest solution and features simple interface attachments with the drive unit and foundation.

The reinforced precast concrete foundation is selected from among four final candidates Stearns-Roger picked from an original list of 35 foundation types. The candidate foundations were first evaluated on the basis of workability, gross quantities of materials, degree of installation difficulty, and approximate cost estimates. These 35 were then reduced to 14, which were again evaluated as to: mass, repetitive-type construction, use of standard and/or specialized equipment, production rate, and cost. After extensive analyses and comparisons, these four final foundations (Figure 4-30) were chosen:

- Precast reinforced concrete.
- Driven steel pile with lateral support.
- Steel frame with screw anchors.
- Reinforced concrete with pedestal cast in place.

The final selections were again reviewed for design, construction flow methodology, type and amount of prefabrication, composition and use of construction crews, types and amounts of specialized equipment required, and other factors which would influence the unit cost of the foundations. MDAC selected the precast reinforced concrete foundation because of the increased installation flexibility of an above-grade bolted type connection to the pedestal.

Figure 4-31 shows the pedestal/foundation. The pedestal is a 20-in. dia 0.105-in. wall steel pipe, 108 in. long. The upper end has a 0.75-in. thick plate for attachment of the drive unit. The bottom end has a standard pipe

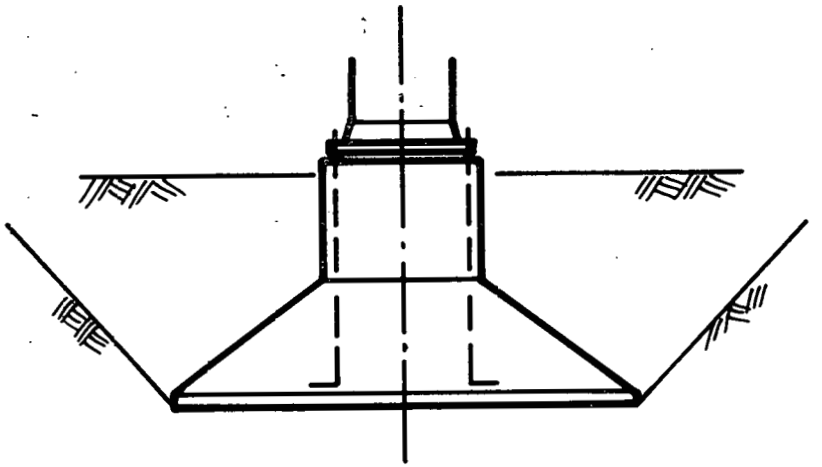

PRECAST REINFORCED CONCRETE CONE

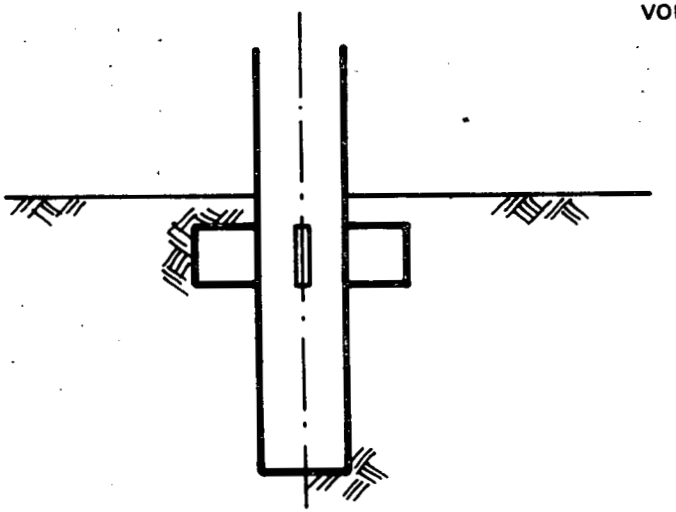

STEEL PILE WITH LATERAL RESTRAINT

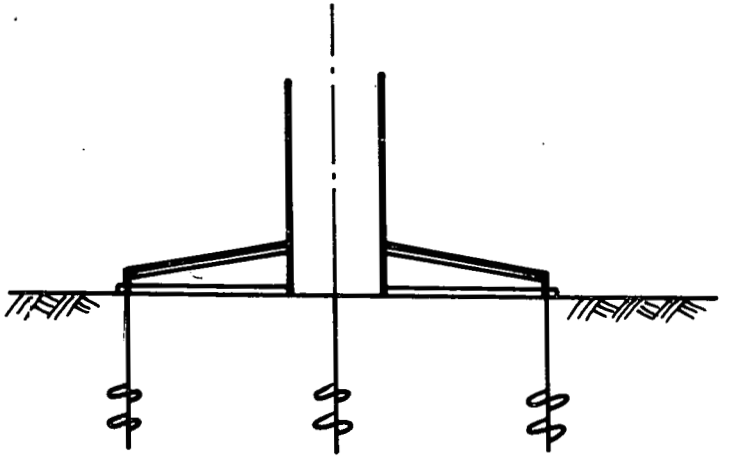

STEEL FRAME ON SCREW ANCHORS

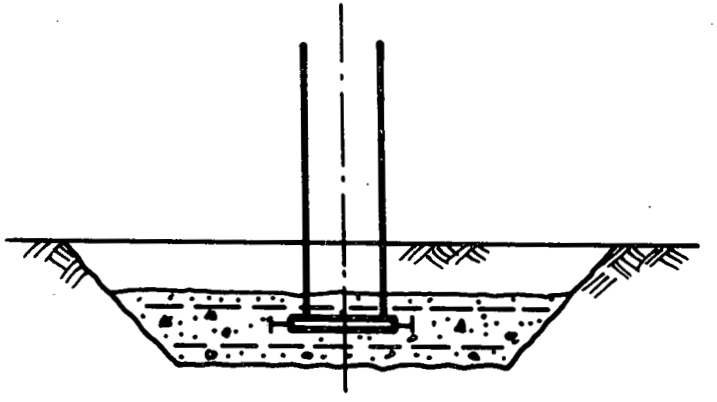

POURED-IN-PLACE REINFORCED CONCRETE SPREAD FOOTING

Figure 4-30. Four Final Foundation Types Selected By Stearns-Roger

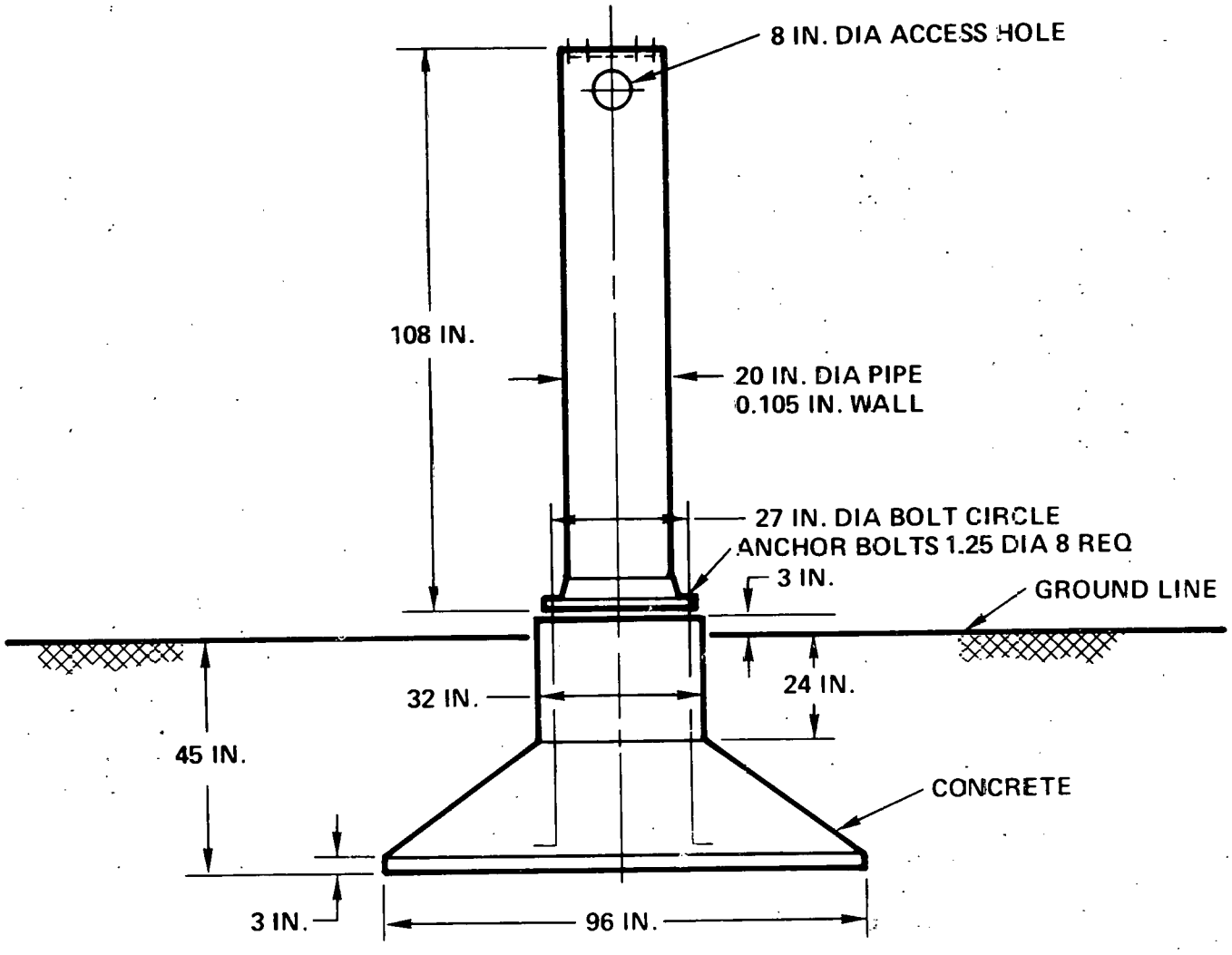

Figure 4-31. Pedestal/Foundation

flange welded to it for strengthening purposes. The pedestal is attached to the foundation by eight 1.25-in. dia anchor bolts equally spaced on a 27-in. bolt circle.

The foundation is reinforced precast concrete. Each unit would be precast offsite, shipped to the site, and stockpiled. A drill rig would dig a round excavation. After excavation, the precast units would be transported to the various installation points. To set the foundations in place, a special straddle carrier and setting machine will have to be developed to minimize risks. This machine would pick up the precast foundation, straddle the excavation, adjust and level itself over the installation point, and set the foundation into position. With the sandy type soil which exists in the area, proper bedding would be obtained by spinning and vibrating the foundation while it is being placed. Backfill of the excavation would be done by using a modified backhoe which would both fill and compact the soil. Final design of the foundation requires a comprehensive knowledge of the soil-bearing capacity. The present design is conservative, and calculations show it to have a margin of safety against overturning of greater than two.

The pedestal/foundation weighs about 10,259 lb, as follows:

Pedestal:	Steel	472.5 lb
	Zinc	36.0 lb
Foundation		9750.0 lb
		10,258.5 lb

4.2.6 Closed- and Open-Loop Control Design/Performance

The surface characteristics of the mirror and the ability to control the reflecting surface and point the reflected beam at the receiver have a direct effect upon the energy intercepted at the receiver. In this section, the error sources that reduce the performance of the heliostats will be identified, the magnitude of the errors will be determined, the rationale used and assumptions made to arrive at the error magnitudes will be discussed, and some sensitivities will be given. A major effort has been made to integrate SRE test data into this analysis.

There are several ways in which the heliostat can be controlled to reflect the sun's energy at the receiver. Three general methods of control will be considered in this section. They are:

A. Closed Loop. A sensor on a pole is used to obtain error signals of the reflected beam. The error signals are used to update the required orientation of the heliostat.

B. Open Loop. Equations are used to calculate the position of the sun. Using the position of the sun and receiver, the orientation of the mirror is calculated. Commands are sent to the heliostat. A sensor on the drive output is used to measure the achieved mirror orientation (mirror gimbal angles).

C. Open Loop. Same as B above except a sensor on the motor shaft (drive input) is used to measure the achieved mirror orientation.

Several of the error sources are independent of the control mechanizations. These error sources are given in Table 4-13. Additional error sources are given in Table 4-14 for the closed-loop mechanization, Table 4-15 for open loop with sensor on the drive output, and Table 4-16 for open loop with sensor on the motor shaft. The error magnitudes given in these tables are representative of an inverted heliostat with an Orbit drive, nominal winds of 8.94 m/s (20 mph) with gusts of 1.34 m/s (1σ) (3 mph) and temperatures of 60°F or above. The effect of a Harmonic drive will also be discussed. The remainder of this section discusses each of the error sources listed in the tables and compares the three different tracking mechanizations. It should be noted that the accuracies in the tables are for the reflected beam and not the mirror normal.

Table 4-13 (Page 1 of 2)

REFLECTED BEAM ERRORS COMMON TO BOTH CLOSED AND OPEN LOOP

Error Source	Azimuth (mr) σ(rms)	Elevation (mr) σ(rms)	Subsystem Requirement	Comment
Tower/Receiver	Near/Far*	Near/Far		
Wind and Temperature	0.4/0.2	0	Tower movement caused by design environment winds and temperature shall not move the tower in the horizontal direction more than 2 in. (1σ) or ±4 in. (95%).	Structure analysis indicates that the bending at 26 mph will be 1 in.
Foundation	0.2/0.1	0.2/01	The foundation shall be constructed in such a manner that the degree of sinkage or foundation time creep will not cause the center of the tower to move more than 1 in. (1σ) or ±2 in. (95%) in the horizontal and vertical direction between alignment periods.	
Surface Waviness	1.2	1.2	After mounting glass, slope from normal shall be less than 0.6 mr (1σ).	Based upon SRE test data.
Specular Dispersion	0.8	0.8	Before glass is mounted, 95% of reflected beam shall be within 4 mr.	Based upon SRE test data.
Surface Bending				
Gravity	0.5	0.5	Bending from gravity shall not cause slope errors more than shown in Figure 1.	Based upon a structure analysis program (NASTRAN) and solar power collection system model (CONCEN).
Winds (Static 26 mph)	0.6	0.8	Same Figure.	

*Near/Far refers to the location of the heliostat with respect to receiver

Table 4-13 (Page 2 of 2)

REFLECTED BEAM ERRORS COMMON TO BOTH CLOSED AND OPEN LOOP

Error Source	Azimuth (mr) σ(rms)	Elevation (mr) σ(rms)	Subsystem Requirement	Comment
Temperature ($60^{o} \rightarrow 104^{o}F$)	0.6	0.8	Same Figure. 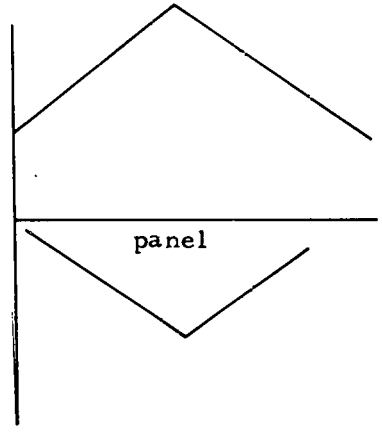	
Mirror Alignment	1.0	1.0	After mounting mirror, the normal of each mirror normal shall be within 0.5 mr (1σ) of desired normal.	
Refraction (Heliostat/Receiver)	0	0.3	Environmental	
Total (RSS)	2.1	2.2		

Table 4-14

REFLECTED BEAM ERRORS FOR CLOSED-LOOP, POLE SENSOR

Error Source	Azimuth (mr) σ(rms)	Elevation (mr) σ(rms)	Subsystem Requirement	Comment
Control System	Near/Far	Near/Far		
No Winds	0.3	0.2	Motor pulse granularity shall not be more than 2 rev/pulse.	Based upon SRE data. Includes effect of hysteresis, backlash, etc.
Signal Granularity	0.2	0.2	A/D converter shall be at least 8 bits.	
Winds	0.7	0.4	Backlash of 1 mr	Based upon SRE data and Monte Carlo simulations. Winds of 26 mph.
Sensor				
Alignment	0.5/0.2	0.5/0.2		
Foundation Movement Between Alignment	0.2	1.0	Foundation shall maintain pole in vertical direction within 1 m(σ) between alignment periods.	Based upon SRE data, has some temperature effects in data.
Movement Caused by Winds Temperature	 0.1 0.1	 0.2/0.1 0.7/0.4	Pole bending frequency shall be greater than 2 Hz. Filter shall reduce oscillation by at least a factor of 4.	May require a higher data sample rate than 2 sec.
Slope Error	0.2	0.2	The sensor slope shall be ±0.023°/V (95%) of the nominal value.	
Intercept	0.1	0.1	At 0 voltage reading, the beam error shall be less than ±0.2 mr (95%).	
Rotation	0.1	0.1	Rotation axis of sensor shall have coupling error less than 0.1 mr (1σ).	
Alignment of Sensor Mirror	0.5	0.5		
Total (RSS)	1.1/1.0	1.5/1.3		

Table 4-15

REFLECTED BEAM ERRORS FOR OPEN-LOOP, SENSOR ON DRIVE OUTPUT

Error Source	Azimuth (mr) σ(rms)	Elevation (mr) σ(rms)	Subsystem Requirement	Comment
Control System				
No Winds	0.3	0.2	Single pulse to motor shall not result in more than 2 rev.	Based upon SRE data. Includes effect of hysteresis, backlash, etc.
Signal Granularity	0.4	0.4	13-bit accuracy on drive output location.	
Winds	0.7	0.4	Compliance not less than 130,000 in-lb/deg. Backlash less than 1 mr.	Based upon SRE data and Monte Carlo simulation. Winds of 20/6 mph. $\alpha = 90^{\circ}$, $\beta = 135^{\circ}$
Refraction (Sun to Heloistat)	0.1	0.4	Software refraction model shall be accurate within 0.4 mr.	Requires software to calculate atmospheric refractions model. Error based upon radar refraction models. Could use one sun tracker.
Command (After alignment see error budget for command calculation)	2.0	2.0	Alignment method shall be accurate to less than 0.8 mr.	
Pedestal Foundation Movement between alignments	1.5	1.5	Foundation will not allow pedestal to move more than 0.75 mr (1σ) in a 4-mo period.	Based upon SRE data over 4-mo data. Questions on measurement accuracy of data.
Bending from Drive to Mirror Structure	0.3	0.6		Based upon structure analysis program (NASTRAN)
Pedestal Deflection from Winds	0.6	0.6		
Total (RSS)	2.7	2.8		

Table 4-16

REFLECTED BEAM ERRORS FOR OPEN-LOOP, SENSOR ON MOTOR SHAFT

Error Source	Azimuth (mr) σ(rms)	Elevation (mr) σ(rms)	Subsystem Requirement	Comment
Control System				
No Winds	0.8	0.8	Backlash less than 1 mr	Based upon SRE data. Includes effect of hysteresis.
Sensor Granularity	0.1	0.2	One revolution counter	
Winds	3.9	1.8	Compliance not less than 130,000 in.-lb/deg. Backlash less than 2 mr.	Based upon SRE data and Monte Carlo simulation. Winds of 20/6 mph. $\alpha = 90^{\circ}$ $\beta = 135^{\circ}$
Refraction (Sun to Heliostat)	0.1	0.4	Software refraction model shall be accurate within 0.4 mr.	Requires software to calculate atmospheric refraction model. Error based upon radar refraction models. Model would not require measurement of atmospheric conditions.
Command (After alignment see error budget for command calculation)	2.4	2.4	Alignment method shall be accurate to less than 1 mr.	
Pedestal Foundation Movement Between Alignment	1.5	1.5	Foundation will not allow pedestal to move more than 0.75 mr (1σ) in a 4-mo period.	Based upon SRE data over 4 mo. Some question as to accuracy of measurements.
Bending from Drive to Mirror Structure	0.3	0.6		
Pedestal Deflection From Winds	0.6	0.6		Based upon structure analysis program (NASTRAN).
Gravitational Moment	0	0.3	Gravitational moment shall be known within ±27% (2σ).	Software will have to calculate gravitational moment and compensate elevation command.
Total (RSS)	5.0	3.6		

4.2.6.1 Errors Common to All Mechanization

1. Tower/Receiver. The receiver is subject to movements caused by winds, temperature, and foundation settling. These movements are equivalent to a beam error. The structure analysis of the tower shows that movement of the receiver caused by winds and temperature to be less than 2 in. (1σ). Since deflections toward the heliostats would result in negligible error, it is assumed that the deflections are perpendicular to the beam (worst-case situation). The beam error in the azimuth direction for a tower height of 110m and for a near heliostat (54m) is

$$\sigma_A = \frac{2}{4823} = 0.41 \text{ mr}$$

and for a far heliostat (350m) is

$$\sigma_A = \frac{2}{12,947} = 0.15 \text{ mr}$$

The elevation error is negligible. The time between alignment periods will be such that the foundation movement will be less than 1 in. (1σ).

2. Surface Waviness. In the process of mounting the glass to the foam, the reflective surface will be deformed from a perfectly flat surface. The amount of error caused by mounting was determined by measuring the deflection at 40 equally spaced points over the surface of a number of panels. An estimate of surface slope error was obtained by taking the difference between the deflection at adjacent points and dividing by the distance between the points. This assumes that the variation in the thickness of the glass is small and that the mounting slope error does not have high-frequency content. Because of the distance between measurements, any high-frequency slope error would not be detected. The distribution of slope error is shown in Figure 4-32 for two different panels. This process also assumes no correlation between slope error and position on mirror.

Combining the statistics of the two samples results in a surface slope error of

$$\sigma_s = 0.6 \text{ mr}$$

in both the x and y direction. The beam error is approximately twice the slope error or

$$\sigma = (2)(0.6) = 1.2 \text{ mr}$$

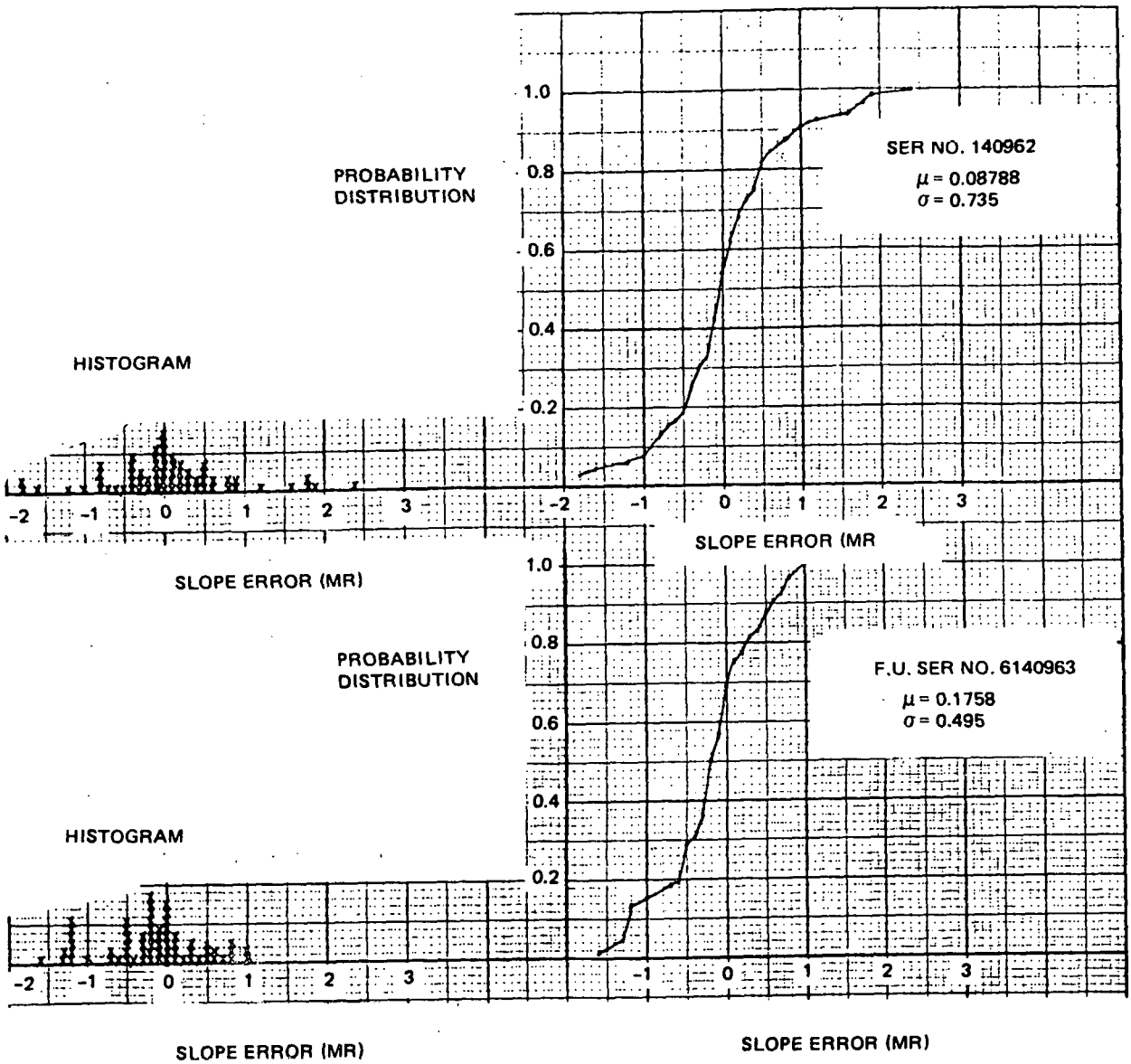

Figure 4-32. Mirror Normal Error for SRE Test Panels

3. Specular Dispersion. The energy of the reflected beam will be spread over some angle due to microscopic surface irregularities. An estimate of the specular dispersion was obtained from test data where the percent of energy within a cone angle of 4, 8, 16 mr was measured. The test data is presented in Table 4-17 for three different samples. The results indicate that, within the accuracy of the measurements, 100% of the reflected energy is within 8 mr. An estimate of the specular dispersion was obtained by taking the average of the difference in energy at 8 mr and 4 mr:

$$E\ (>4\ \text{mr}) = \frac{(83.1-78.8) + (82.3-75.9) + (84.0-80.9)}{3} = 4.87$$

and assuming that the energy is distributed according to a bivariate normal distribution, then

$$2.46\sigma = 2\ (\text{half cone angle})$$
$$\sigma = 0.81$$

It should be noted that measurements below the line shown in Table 4-17 required the use of a different instrument. After the tests were done, a problem was found with the instrument which makes the data at 4 mr questionable. This data will be updated with new test data when it becomes available. Present estimate is that a σ of 0.81 is too large for specular dispersion.

4. Surface Deviations. Environmental conditions such as gravity, winds, and temperature will cause the reflector surface to deviate from a flat surface. These deviations may cause the reflected beam to spread as it travels toward the receiver. Slope histories for each of the heliostat panels and for each environmental effect were obtained from the structural analysis program NASTRAN. The slope histories were then input into the solar power collection system computer program CONCEN (Reference R1). Total received power and flux density distribution were computed for a given sun and heliostat location. The program divides the surface of each heliostat into 121 elements and then uses the slope of each element to compute where the reflected beam will hit the receiver. The program can be used to investigate the environmental effect upon the performance of a single heliostat or a field of heliostats. A Monte Carlo method is used when the power from the total field is desired.

Table 4-17

SRE SPECULAR DISPERSION DATA

Wavelength (nm)	Cone Angle								
	Sample B-1			Sample B-2			Sample B-3		
	4 mr	8 mr	16 mr	4 mr	8 mr	16 mr	4 mr	8 mr	16 mr
426	88.5	88.5	88.5	88.5	88.5	88.5	89.3	89.3	89.3
498	93.4	93.4	93.4	92.1	92.1	92.1	93.9	93.9	93.9
561	92.5	93.6	93.6	92.5	92.5	92.5	94.2	94.2	94.2
623	90.1	89.1	89.1	88.9	88.9	88.9	91.4	91.4	91.4
691	86.7	88.3	88.3	88.3	88.3	88.3	89.1	89.1	89.1
(See Note)									
774	75.6	80.0	80.0	68.9	77.8	77.8	79.3	81.5	81.5
860	71.2	75.9	75.9	65.0	74.3	74.3	75.4	76.9	76.9
1008	65.4	69.8	69.8	60.2	69.9	69.9	67.8	72.2	72.2
1208	64.1	70.1	70.1	58.6	69.8	69.8	65.0	72.6	72.6
1594	60.9	82.6	82.6	56.1	80.7	80.7	63.6	86.4	86.4
Average	78.8	83.1	83.1	75.9	82.3	82.3	80.9	84.8	84.8

Note: Measurements below this line required a different instrument. The new instrument is believed to give erroneous data for 4 mr.

In this mode of operation, the heliostat and element are randomly selected. The received power data were generated for 10 AM on winter solstice.

The beam errors shown in the tables were determined by finding the element slope standard deviation that would result in the same power loss. This was done for 10 AM on a winter solstice day. It should be noted that the aim strategy employed in CONCEN was held constant, it is possible that some power can be gained by changing the aim strategy with beam accuracy.

A. Gravity. Gravity forces cause the frame to deflect and the reflector surface to sag between supports. This results in a spreading of the reflected beam. The effects of gravity can be reduced somewhat by additional canting of the mirror panels beyond that required for focusing. The effects of gravity are a function of the elevation angle of the heliostat. The nearest heliostats are affected the most since they are more horizontal than vertical. Gravity effects were analyzed by scaling the slope history for heliostat in the horizontal position by the appropriate scale factors for the elevation angle of each individual heliostat as determined by the computer program CONCEN. The scale factors used were as follows:

$$S.F._{G_i} = \sin(\psi_i) \qquad \psi_i = \text{elevation angle of ith heliostat}$$

The effect of gravity was incorporated into the error budget as an angular error in the reflected beam. This required the generation of the sensitivity of total received power to angular errors in the reflected beam.

The total power loss over the field because of gravity forces is 0.4%, which is equivalent to a tracking error of 0.67 mr. The angular error was assumed to be equally divided between azimuth and elevation.

$$\sigma_{az} = \frac{0.67}{\sqrt{2}} = 0.47 \text{ mr} \qquad \sigma_{ele} = \frac{0.67}{\sqrt{2}} = 0.47 \text{ mr}$$

B. Winds. Winds cause deflections in both the glass surface and support frame. Slope histories for the panels were obtained from structures for a 26-mph wind, parallel to the slot. The wind was assumed to affect all the heliostats equally over the collector field (all heliostats have the same slope history regardless of orientation). Slope histories for other velocities were obtained by applying the following scale factors:

$$S.F._v = \frac{V_d^2}{(26\ \text{mph})^2} \qquad V_d = \text{desired wind velocity}$$

When the power loss was determined for different wind velocities, it was found that less power was lost at 26 mph than at 8 mph. A preliminary investigation into this odd phenomenon resulted in the hypothesis that wind in this direction produces a concave surface as shown in Figure 4-33, which results in a focusing of the beam. Since time did not allow for verification of this hypothesis and for development of a wind model that included the effect of wind direction and different elevation angles of each heliostat, this phenomenon was neglected. Instead the statistics of the slopes over the surfaces were computed for a static wind of 26 mph. This resulted in errors of

$$\sigma_{az} = 0.6\ \text{mr} \qquad \sigma_{el} = 0.8\ \text{mr}$$

C. Temperature. The thermal expansion coefficient is different for glass than for steel. Cold temperatures cause the panels to become convex, which causes the beam to spread. Warm temperatures cause the panels to become concave, which tends to contract the beam. Slope histories for the panels were obtained for a temperature of 104°F based on a reference temperature (no surface errors) of 75°F. Slope histories for other temperatures are obtained by applying the following scale factor:

$$S.F._T = \frac{T_d - 75°F}{29°F} \qquad T_d = \text{desired temperature}$$

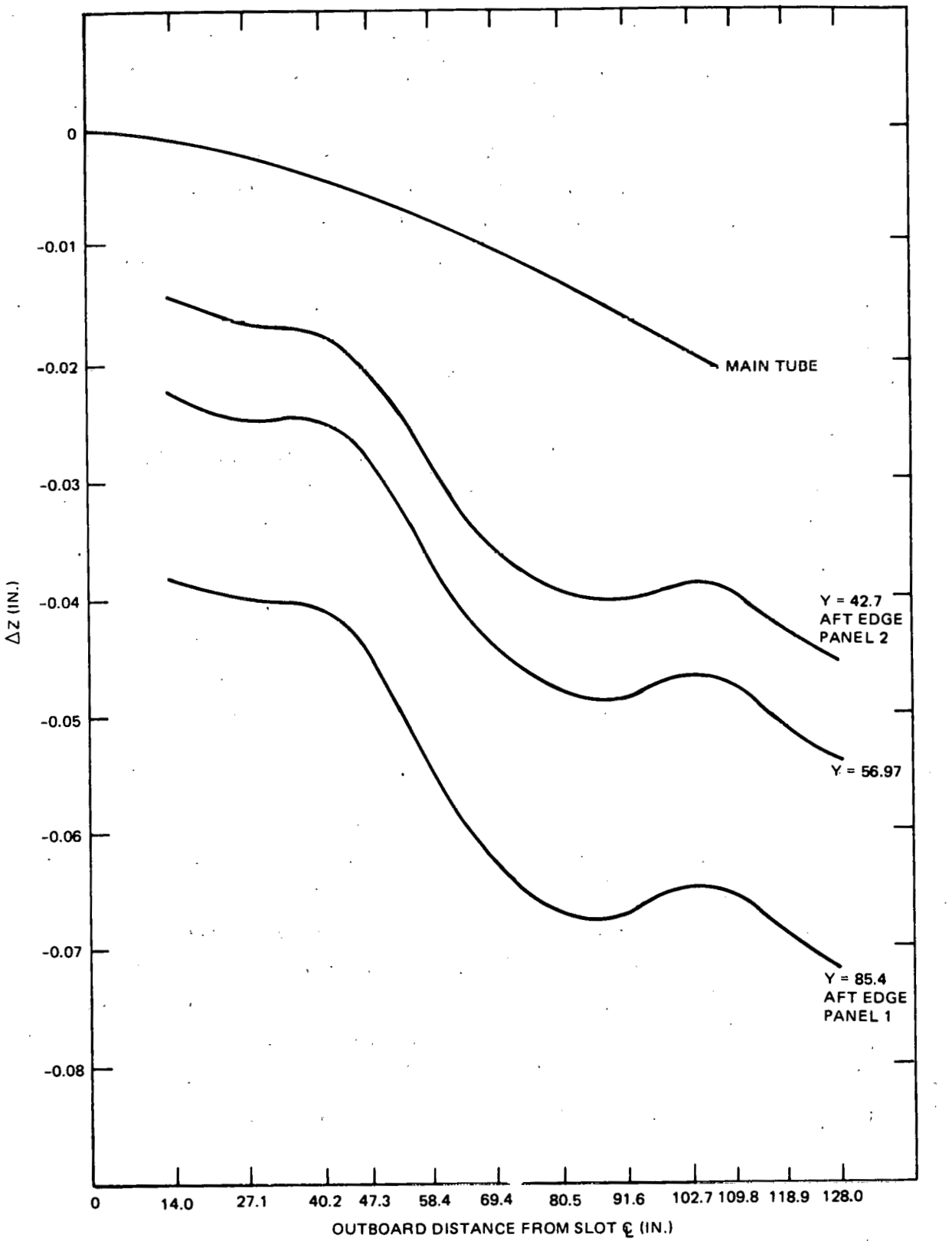

Figure 4-33. Vertical Mirror Deflections – 26 Mph Wind α = 30 Deg

The slope history for 104°F and the appropriate scale factor were input into CONCEN to determine the total power received for the desired temperature. A cooldown to 32°F from the reference temperature results in a loss in received power of 1.5%. A warmup of 104°F results in approximately the same received power (small increase) as the case where there are no surface errors. Effects of temperature could be reduced by lowering the reference temperature, thereby increasing the probability of a warming condition. The data in the error budget are for a temperature of approximately 60°F.

$$\sigma_{az} = 0.8 \qquad \sigma_{ele} = 0.6$$

If the environmental effects can be accurately modeled, the impact on power loss may be lessened with modification to the aiming strategy and the cant of the mirror panels used. The impact on the flux density over the surface of the receiver must also be determined.

5. Mirror Alignment. A requirement has been placed upon the mirror structure that will result in the normal of each mirror segment being within 0.5 mr of the heliostat normal. The following tolerances have been placed upon the mirror structure:

A. Mirror plus foam plus cups = ±0.01 in.
B. Mounting points on the same beam = ±0.011 in.
C. Corresponding mounting point on the opposite beam = ±0.0394 in.

6. Refraction. The reflected beam will experience some refraction before reaching the receiver. Based upon calculations for low-frequency electromagnetic radiation, the amount of refraction would be less than 0.05 mr for the short ranges of the Pilot Plant. Because of ground radiation, it is possible that more refraction could result. An estimate of 0.3 mr is used in this analysis. Further work will be done to define this error.

4.2.6.2 Closed-Loop Error Sources

1. Control System Errors. There are a number of error sources and dynamic effects within the control loop that cause the reflected beam to be aimed off the nominal point. The control loop is illustrated in Figure 4-34, along with effects that cause errors in the reflected beam. In order to evaluate the transfer function from the error source to the beam error, a small two-dimensional Monte Carlo simulation of the control loop was generated. The ways in which some of the major error sources were modeled are:

A. Drive Dynamics. The model of the drive unit is illustrated in Figure 4-35. It includes the effect of backlash, compliance/stiffness, and hysteresis. A comparison of the model representation and test data are shown in the same figure.

B. Wind Effect Upon Mirror Dynamics. The winds produce a moment on the mirror which, because of the dynamics of the drive unit, will produce a beam error. The wind moment model used is shown in Figure 4-36. The wind gust and variation in angle of attack are generated by passing white noise through a first-order lag. The constants (S_v, τ_v, S_β, τ_β) determine the output standard deviation and autocorrelation function.

C. Motor Dynamics. Because the motor can only be commanded to move in incremental steps, a movement quantization error is introduced. The SRE test data, shown in Figure 4-37, not only shows the relationship between the number of turns per commanded pulse but also a variation in the number of turns. Both of these effects were included in the simulation.

In order to verify that the simulation gives representative results, data from the simulation was compared to SRE test data. An example of the comparison is shown in Figure 4-38. Although there are a number of sources of beam error that are not included in the simulation, such as cross coupling, it is felt that the simulation results compare close enough to the SRE data to

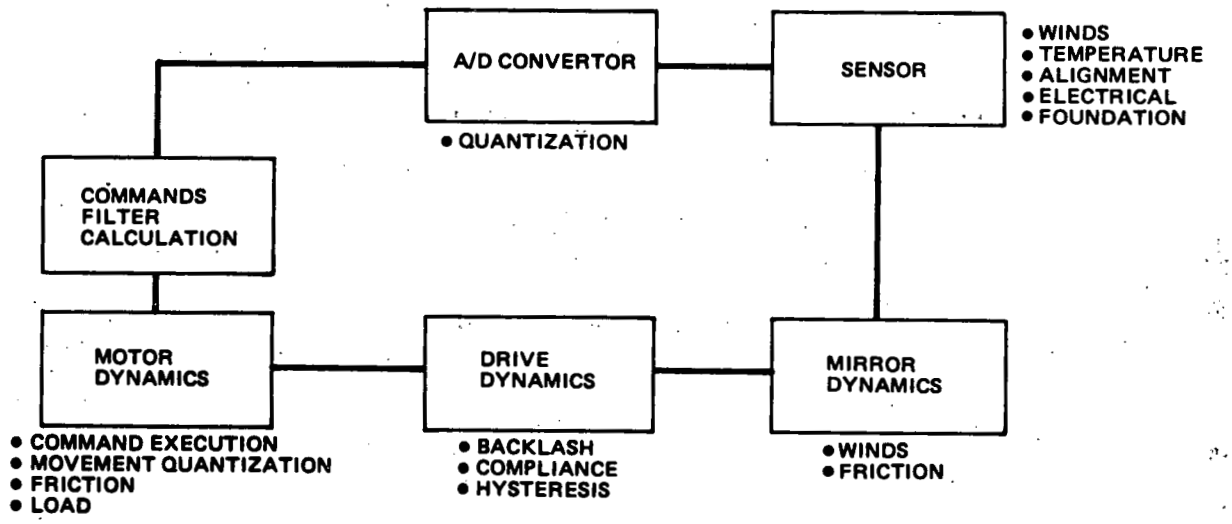

Figure 4-34. Control Loop Error Model

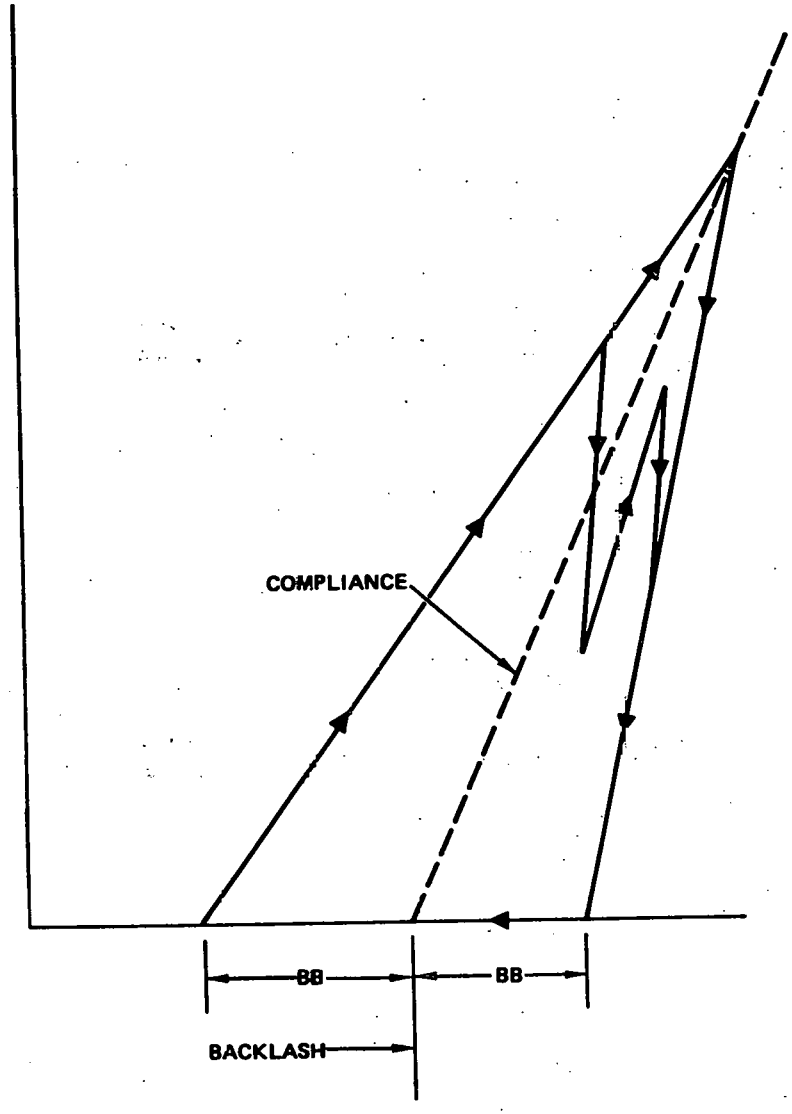

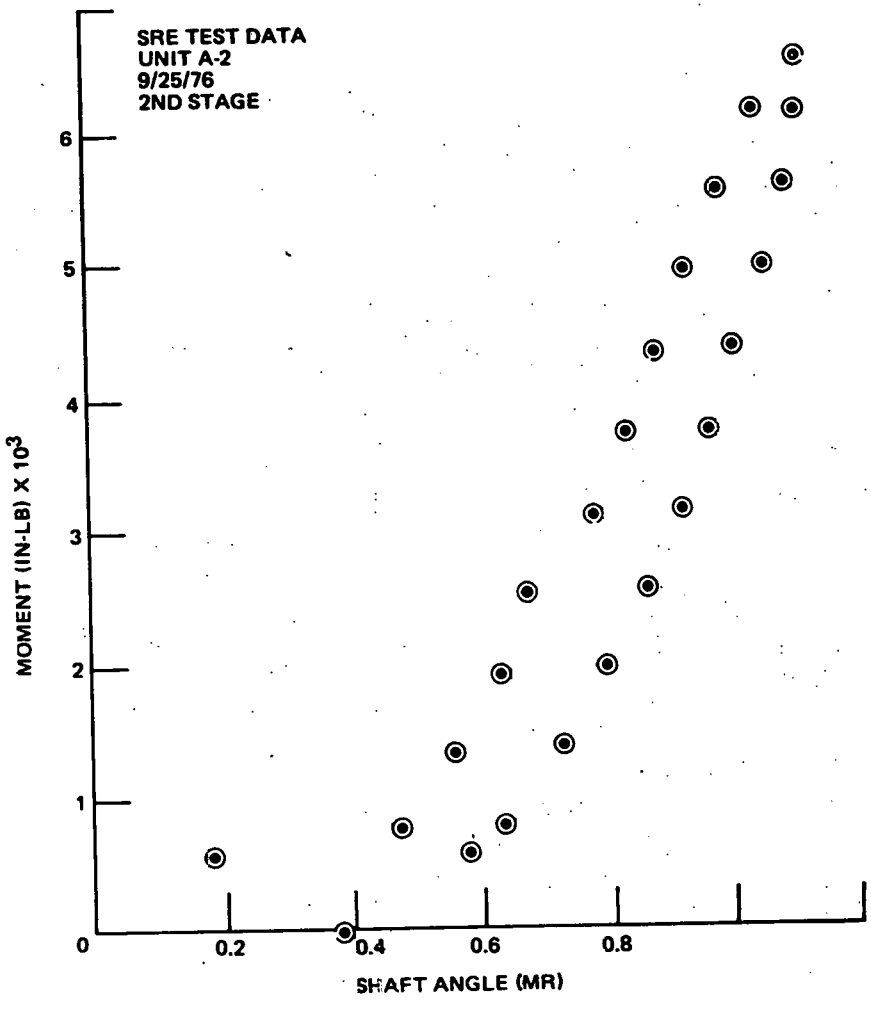

Figure 4-35. Hysteresis Model

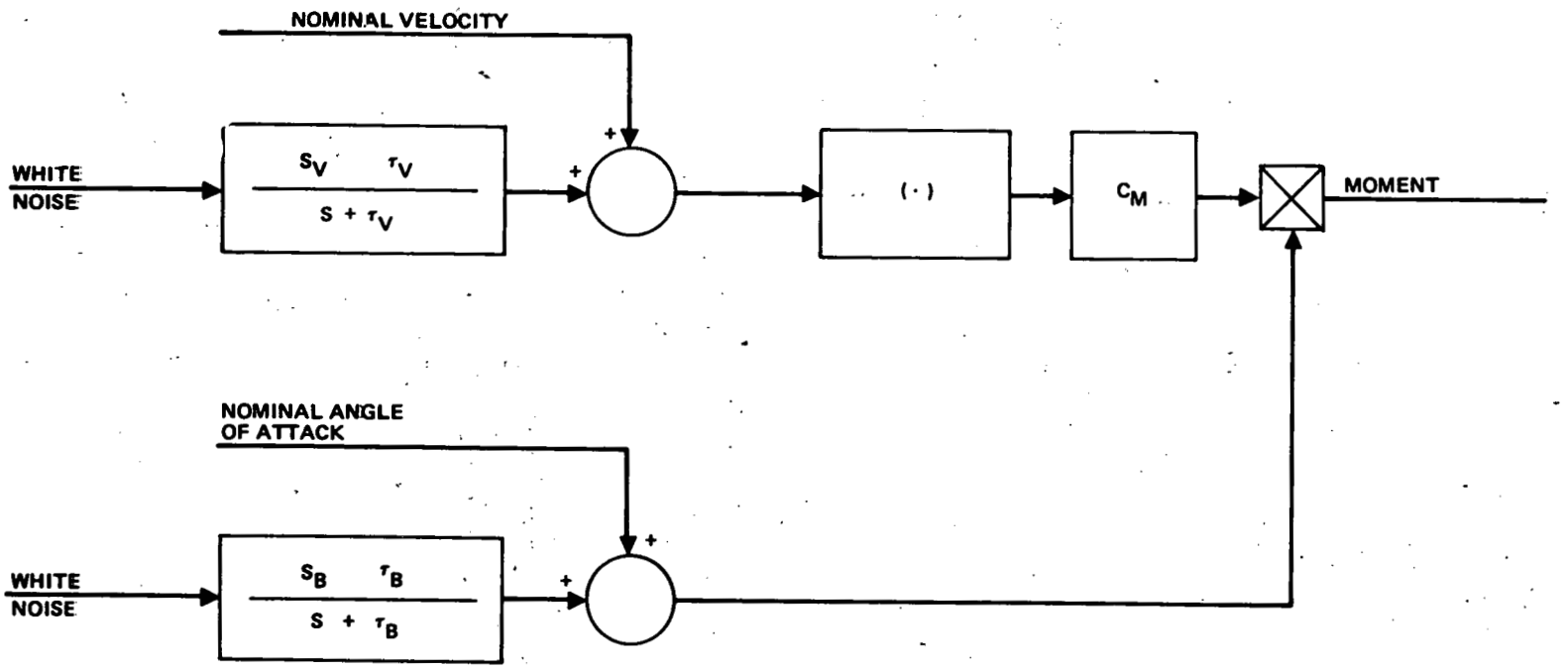

Figure 4-36. Wind Model

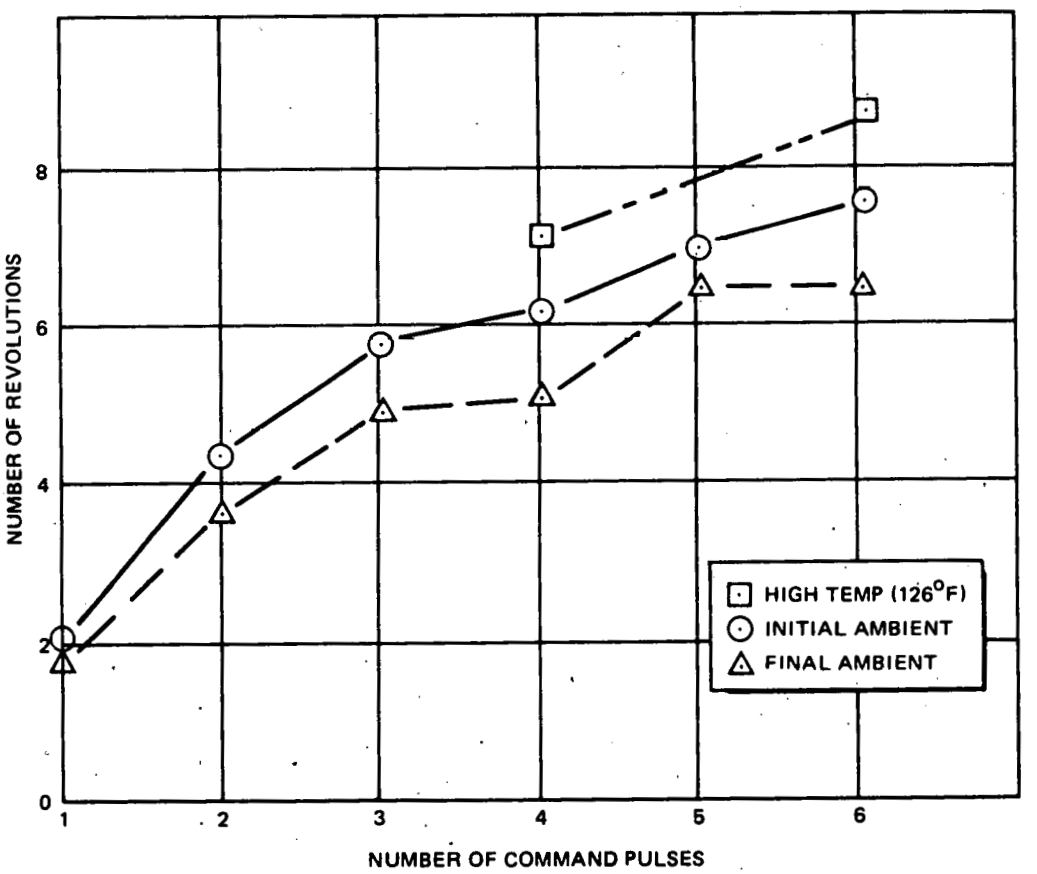

Figure 4-37. SRE Motor Tests Data

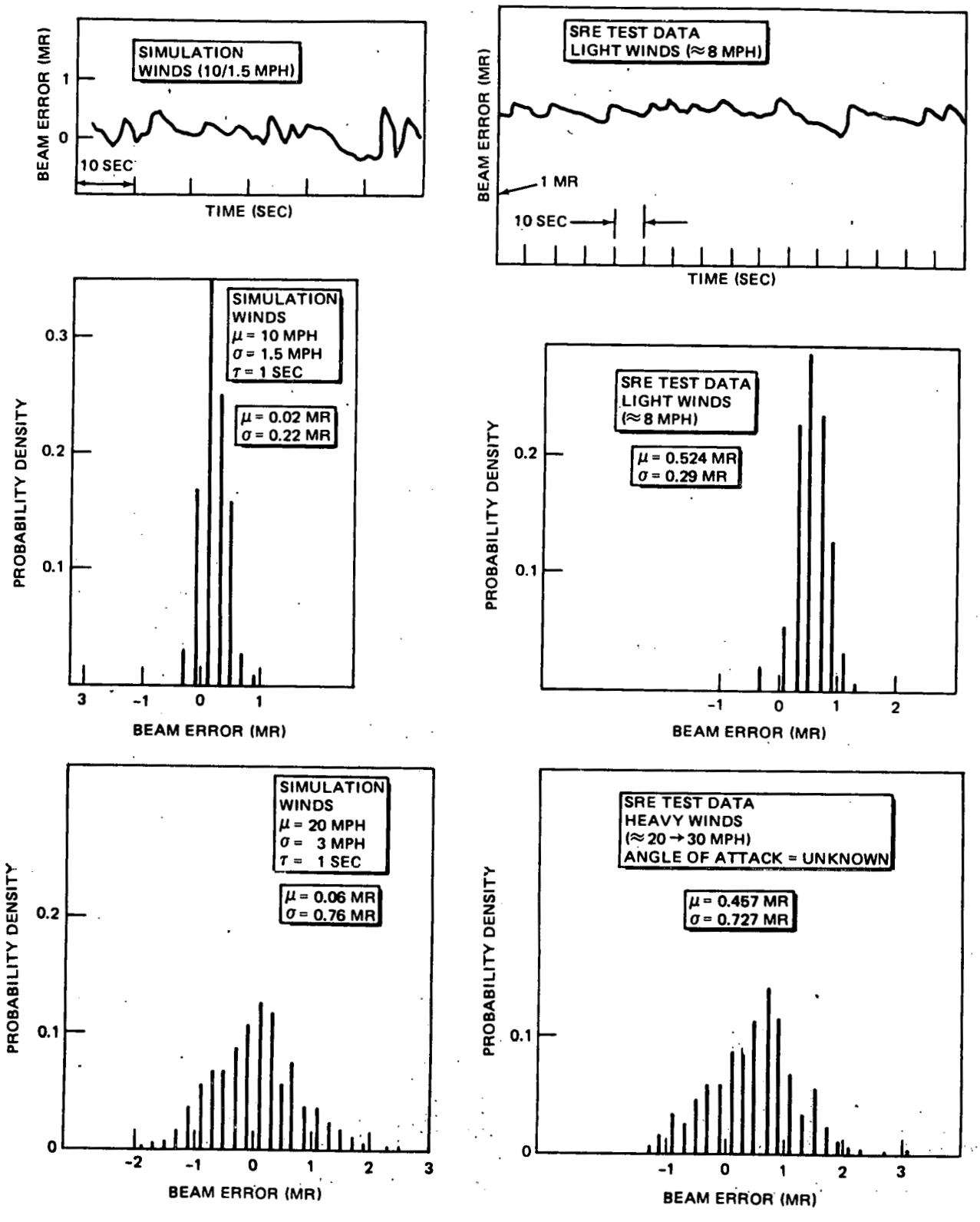

Figure 4-38. Comparison of Simulation and SRE Test Data

warrant using the simulation to investigate the sensitivity of beam error to different error sources.

One of the major concerns in the design of the heliostat has been the effect of backlash upon beam error. Tests that have been done to date (Reference R2) indicate that 0-year backlash can be obtained from 1 to 2 mr and, with time, this may grow to 2.5 to 4 mr. Using the simulation, the sensitivity to backlash was investigated. The results are shown in Figure 4-39 for two different nominal wind directions. These directions were chosen because:

- At $\beta = 135°$ and $\alpha = 90°$, the maximum aerodynamic moment is experienced. This should yield a maximum beam error because backlash would be combined with maximum compliance bending.
- At $\beta = 0°$ and $\alpha = 90°$, the moment will change signs when β changes signs. This could result in the mirror rotating from one side of the backlash to the other. The results would be a beam error proportional to the amount of backlash.

Although a large deflection error is generated at $\beta = 135°$, the deflection error has a large mean value which is a direct function of the amount of backlash, but the beam sensor is capable of detecting this value and the command logic will remove the mean value. At wind directions where the wind moment would have a constant sign (the majority of the directions), the closed-loop system is not sensitive to the amount of backlash. For the case where the wind moment can oscillate in sign, the beam error will be a direct function of the backlash, as shown in Figure 4-39. The frequency with which the wind velocity and direction change (autocorrelation time) has a direct effect upon the beam error as shown in Figure 4-40. If the gust velocity and direction are changing at a high rate (low autocorrelation time), then the mirror structure dynamics act as a filter and the beam error will be reduced. If the gust velocity and direction are changing at a low rate (high autocorrelation time), then the control loop is capable of keeping up with the mirror motion. In between these two points, the maximum beam error will occur. A value of 2 sec, which is the worst case, was used in the major part of the analysis.

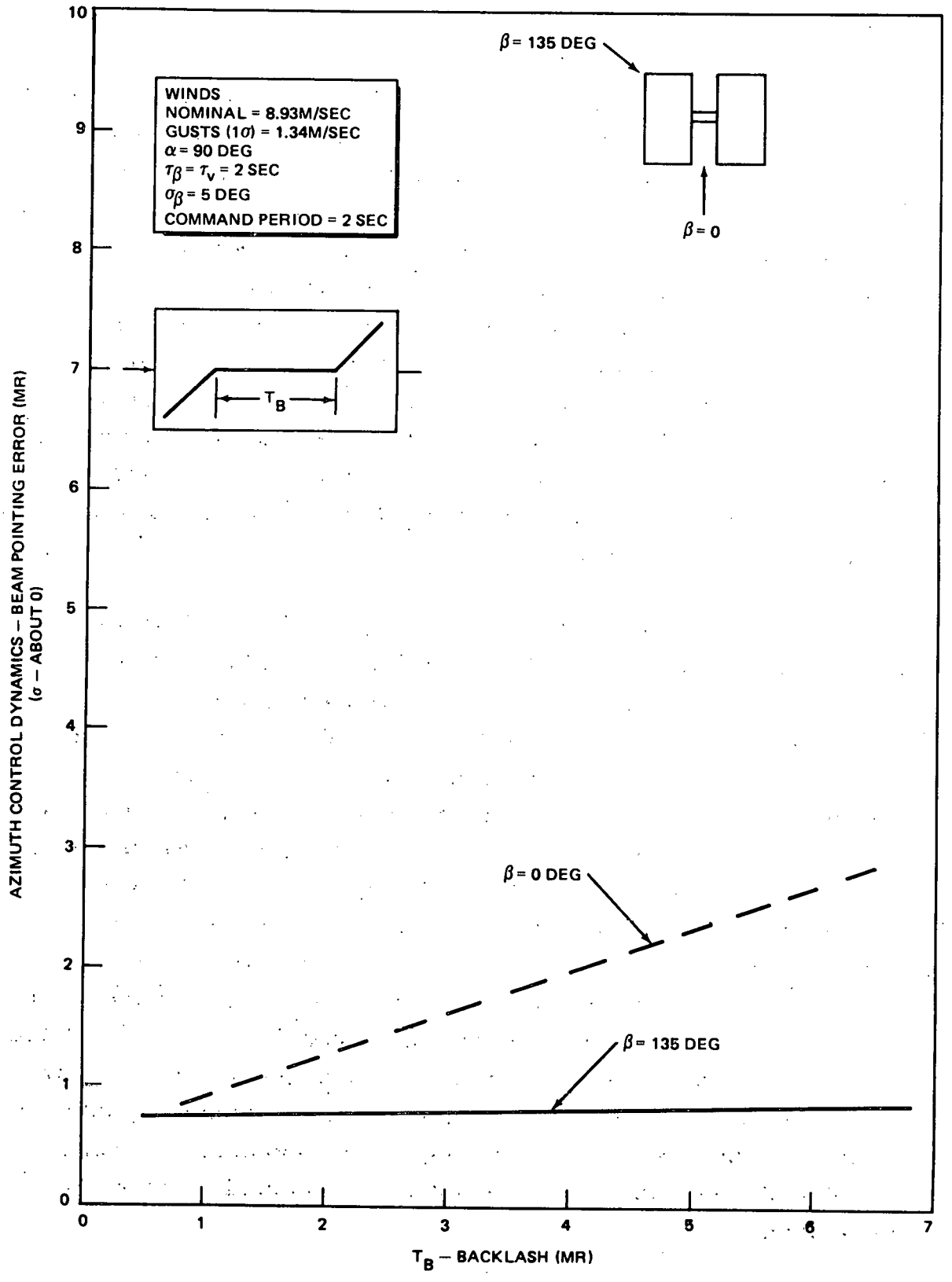

Figure 4-39. Effect of Backlash Upon Beam Error for Closed Loop – Simulation Results

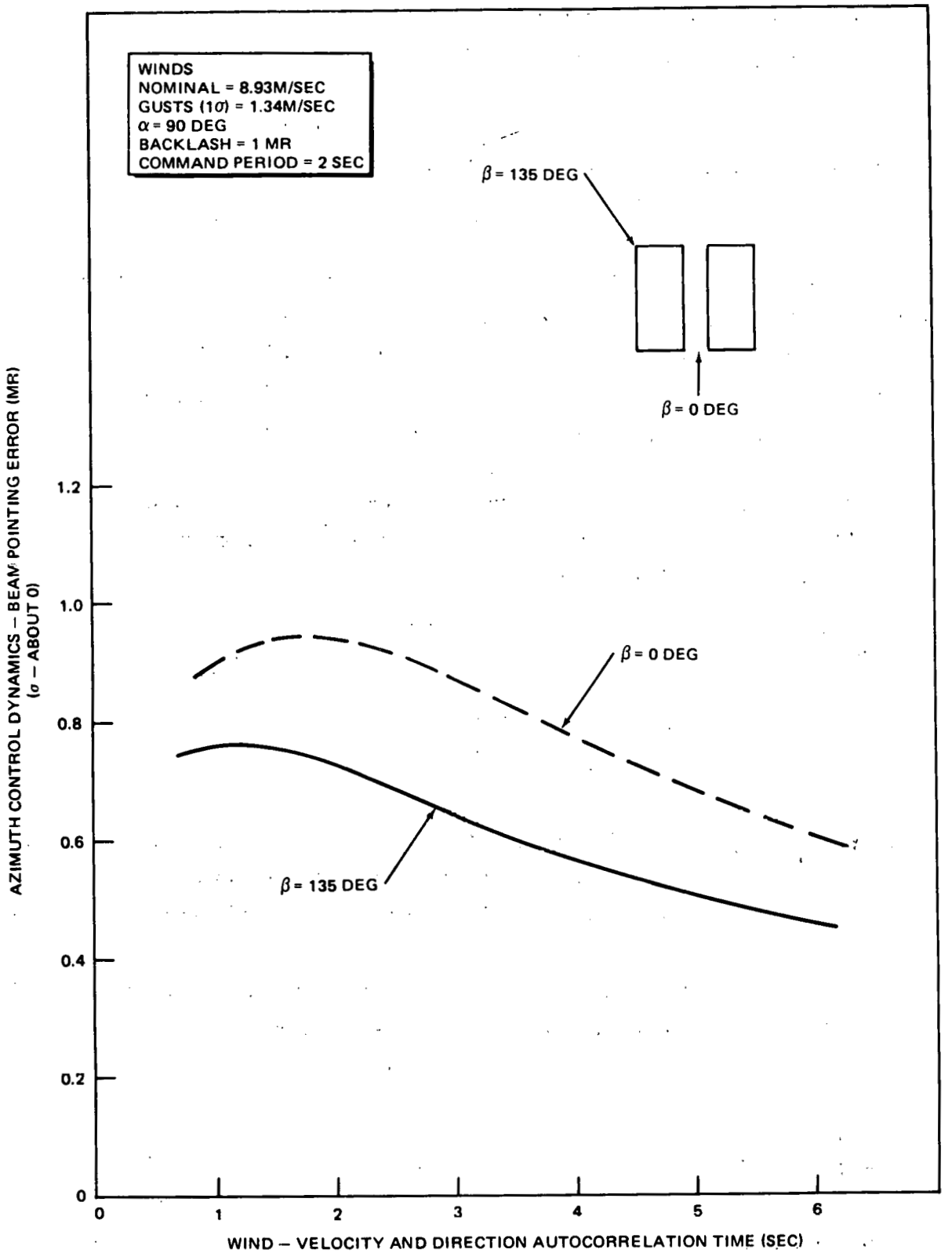

Figure 4-40. Effect of Wind Autocorrelation Time Upon Beam Error for Closed Loop – Simulation Results

The effect of backlash and winds could also be reduced by increasing the command rate, as shown in Figure 4-41. The penalty, of course, would be an increase in control power used as shown in the same figure.

The sensitivity of the closed-loop mechanization to the nominal (mean) wind velocity is shown in Figure 4-42. The standard deviation of gusts was scaled according to the mean wind velocity for this analysis.

2. Sensor. There are a number of random errors associated with the beam sensor which are not necessarily contained in the control system errors discussed above. Two of these would be slope error (Volts out per mr of beam error) and intercept error (Volts out with no beam error). The values shown in Table 4-14 are based upon the sensor specification.

The sensor pole will also have some angular movement with time as a result of the foundation settling. An estimate of the sensor pole angular movement was obtained from the SRE test data shown in Table 4-18. There is some question as to the accuracy of the measurements, but for lack of better information, an angular pole error of 1.04 mr will be used. The alignment method will reduce any mean error to a very small value. It should also be noted that this data contains some temperature effects since the temperature varied over a range of 42°F for the measurements shown.

A false beam sensor error is introduced to the control loop when the sensor pole is deflected from winds or temperature. Table 4-19 shows the type of deflections that can be expected. SRE test data indicates that pole oscillations are reduced by approximately a factor of four by the filter. Assuming that the deflections can occur in any direction with equally likely probability, then beam error caused by wind movement would be for a near heliostat

$$\sigma_E = \frac{1.25}{4\sqrt{2}} \approx 0.2 \text{ mr}$$

and for a far heliostat

$$\sigma_E = \frac{0.73}{4\sqrt{2}} \approx 0.1 \text{ mr}$$

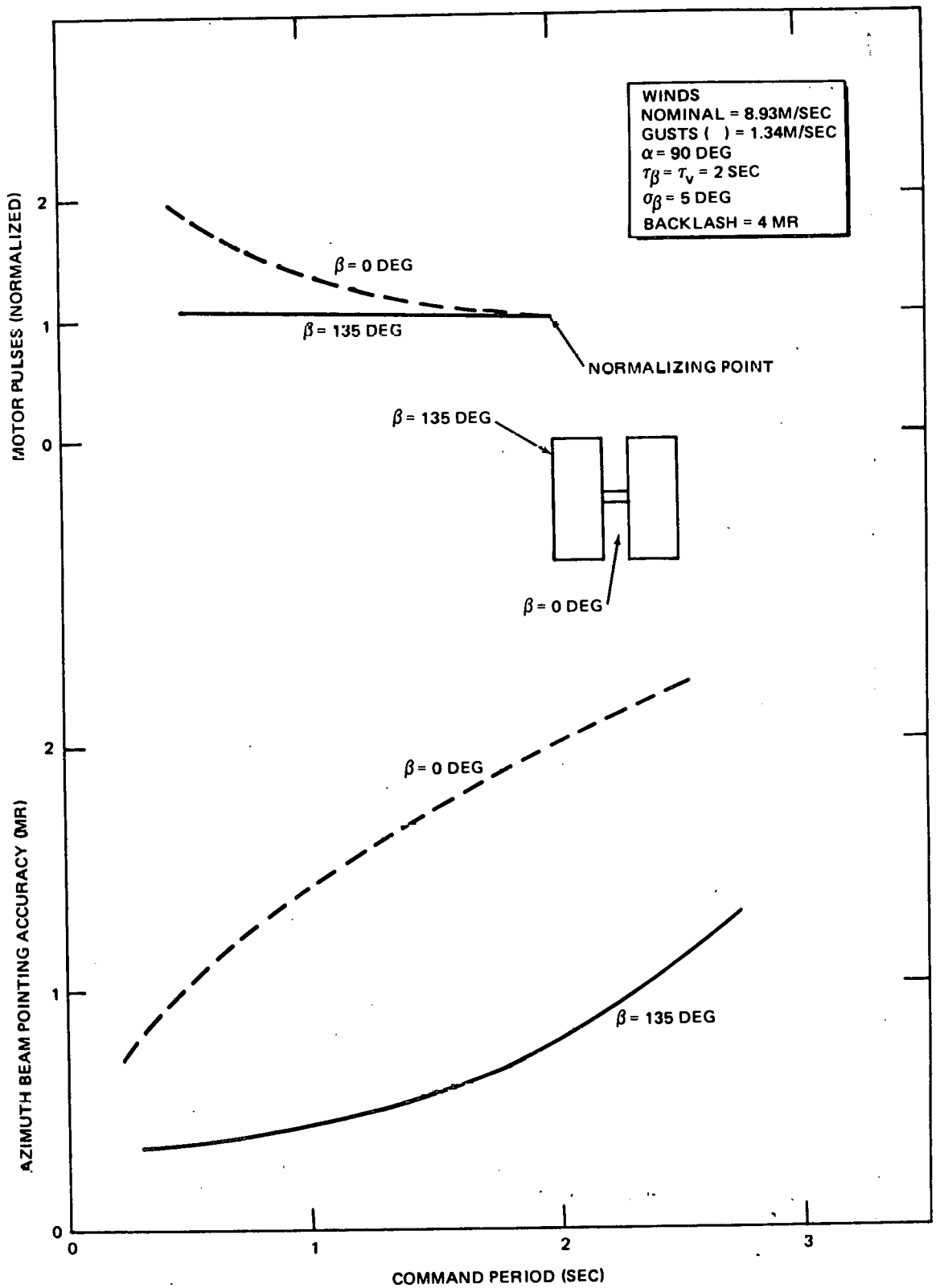

Figure 4-41. Effect of Command Period Upon Beam Error for Closed Loop Tracking – Simulation Results

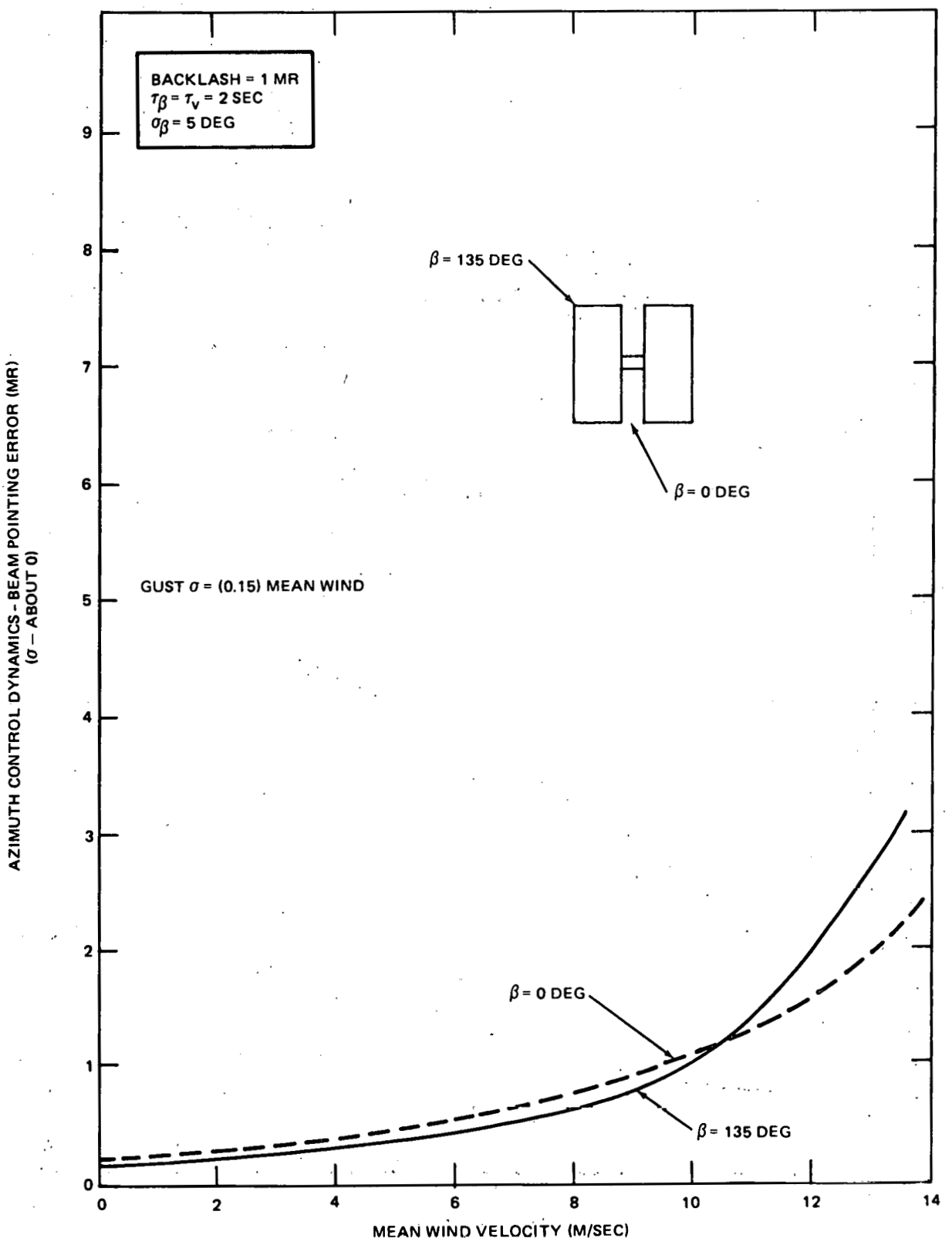

Figure 4-42. Effect of Wind Velocity Upon Beam Error for Closed Loop Tracing – Simulation Results

Table 4-18

SENSOR POLE ANGULAR MEASUREMENTS

Date	Time Hr-Min	Temp. °F	H1 N-S	H1 E-W	H2 N-S	H2 E-W	H3 N-S	H3 E-W	H4 N-S	H4 E-W	IH1 N-S	IH1 E-W	
10/15/76	9:00 AM	72.00	90°15'	29°50'	90°9'	89°50'	90°9'	89°50'	90°50'	81°58'	-	-	
12/15/76	2:00 PM	67.00	90°0'	89°51'	90°16'	89°51'	90°7'	89°36'	90°51'	89°50'	89°51'	90°21'	High Wind
12/21/76	9:30 AM	40.00	89°59'	89°53'	90°15'	89°49'	90°6'	89°33'	90°52'	89°47'	89°54'	90°20'	
12/22/76	9:00 AM	30.00	90°03'	89°49'	90°18'	89°43'	90°7'	89°33'	90°52'	89°48'	89°57'	90°22'	
1/12/77	8:30 AM	33.00	90°03'	89°51'	90°16'	89°45'	90°5'	89°36'	90°50'	89°36'	89°56'	50°20'	
1/21/77	12:20 PM	48.00	90°03'	89°52'	90°15'	89°51'	90°10'	89°37'	90°50'	89°47'	89°52'	90°19'	
Mean (Min.)			90.02'	51.2'	15.83'	48.17'	7.38'	37.5'	50.83'	47.8'	54'	20.2'	
σ(mr)			0.57	0.43	0.34	0.98	0.54	1.85	0.28	2.05	0.74	0.32 = 1.04*	

*Has some temperature effects

Table 4-19

SENSOR POLE DEFLECTIONS

	Rotations From Operational Conditions (mr)	
	Wind → 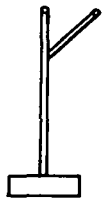	Wind → 
Effect	(mr)	(mr)
Boom Rotations from Wind	0.127	-
Pole Rotations from		
Boom	0.375	-
Wind	0.680	0.680
Base Plate Rotation	0.059	0.047
Foundation Rotation	0.007	0.006
Total Rotation from Winds	1.248	0.733
Rotation from Temperature	1.04	0.57
Total (RSS)	1.62	0.93

NOTE: Based upon structural analysis

The beam error caused by temperature movement would be for a near heliostat

$$\sigma_E = \frac{1.04}{\sqrt{2}} \approx 0.7 \text{ mr}$$

and for a far heliostat

$$\sigma_E = \frac{0.57}{\sqrt{2}} \approx 0.4 \text{ mr}$$

It is estimated that the centroid of the beam can be located to within 2 in. (1σ). The alignment error is

$$\text{Near } \sigma = \frac{2 \text{ in.}}{(54^2 + 80^2)^{1/2} \quad (3.28)(12)} = 0.5 \text{ mr}$$

$$\text{Far } \sigma = \frac{2 \text{ in.}}{(310^2 + 80^2)^{1/2} \quad (3.28)(12)} = 0.2 \text{ mr}$$

3. Alignment of Sensor Mirror. Winds and temperatures acting upon the sensor mirror and structure will produce a beam error. The error left after the initial alignment with the sun in one position will produce a different error when the sun is in another position. It is estimated that the combined effect of these errors will be less than 0.5 mr.

4.2.6.3 Open-Loop Errors with Sensor on Drive Output

1. Control Dynamics. The accuracy of this mechanization was investigated by modifying the closed-loop Monte Carlo simulation described previously. The beam sensor was removed and a device with 13-bit accuracy was added to the gimbals to obtain mirror angle feedback. The sensitivity of the mechanization to backlash is shown in Figure 4-43. The results are similar to the closed-loop mechanization.

2. Refraction. The velocity of light will vary as it traverses the atmosphere because of changes in atmospheric temperature, pressure, and composition. The amount of error that can be caused by atmospheric refraction (taken from Reference R3) is shown in Figure 4-44 for nominal atmospheric conditions. The magnitude of this error dictates that the heliostat elevation commands must be corrected for atmospheric refraction. This can be accomplished by using a single sun tracker or a simple mathematical model. Considering the variation in Refractive Modulus, it is estimated that the refractive error can be reduced to less than 0.4 mr (1σ) using a mathematical model. The above estimate is based upon radar models that have been developed.

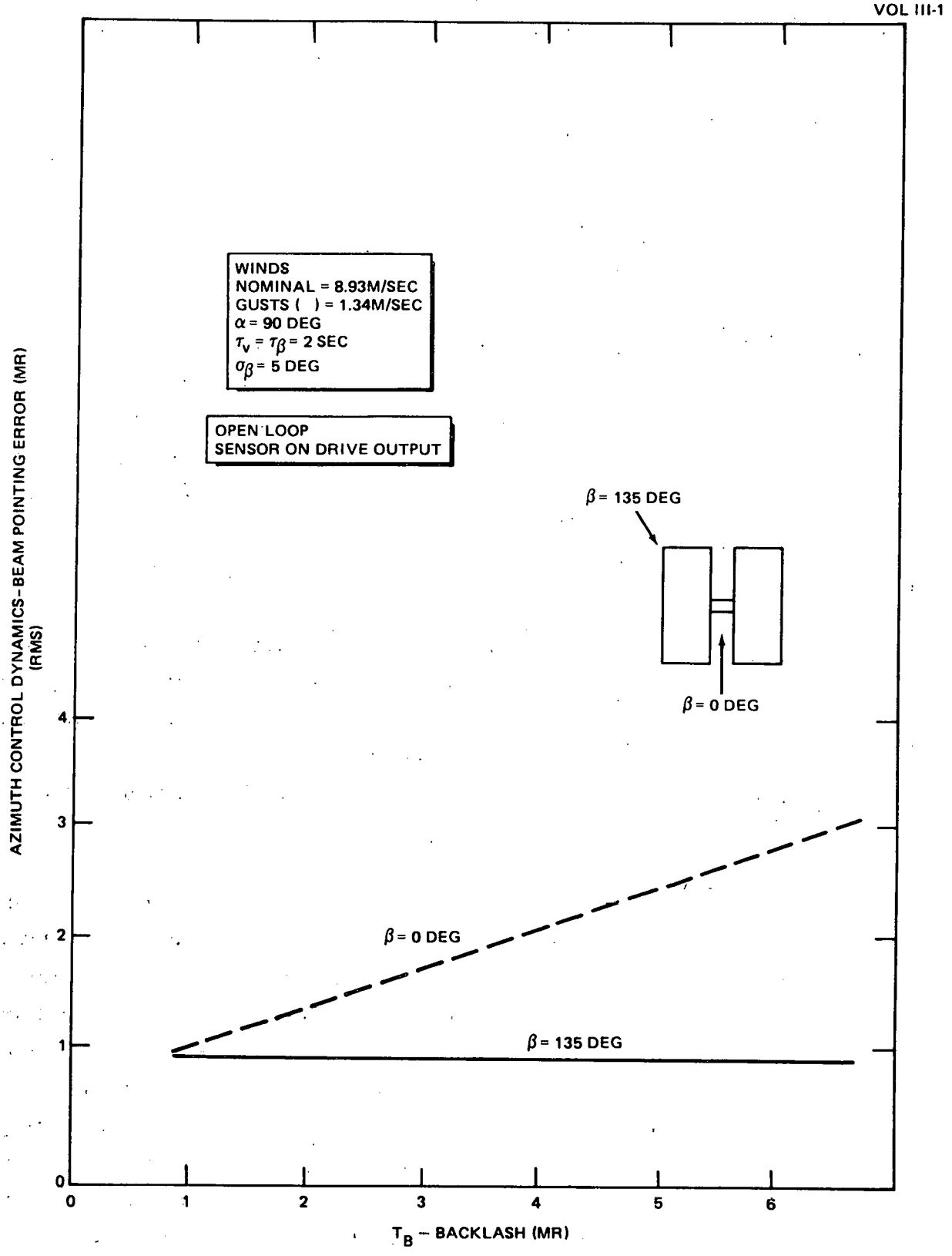

Figure 4-43. Effect of Backlash Upon Beam Error for Open Loop/Gimbal Sensor – Simulation Results

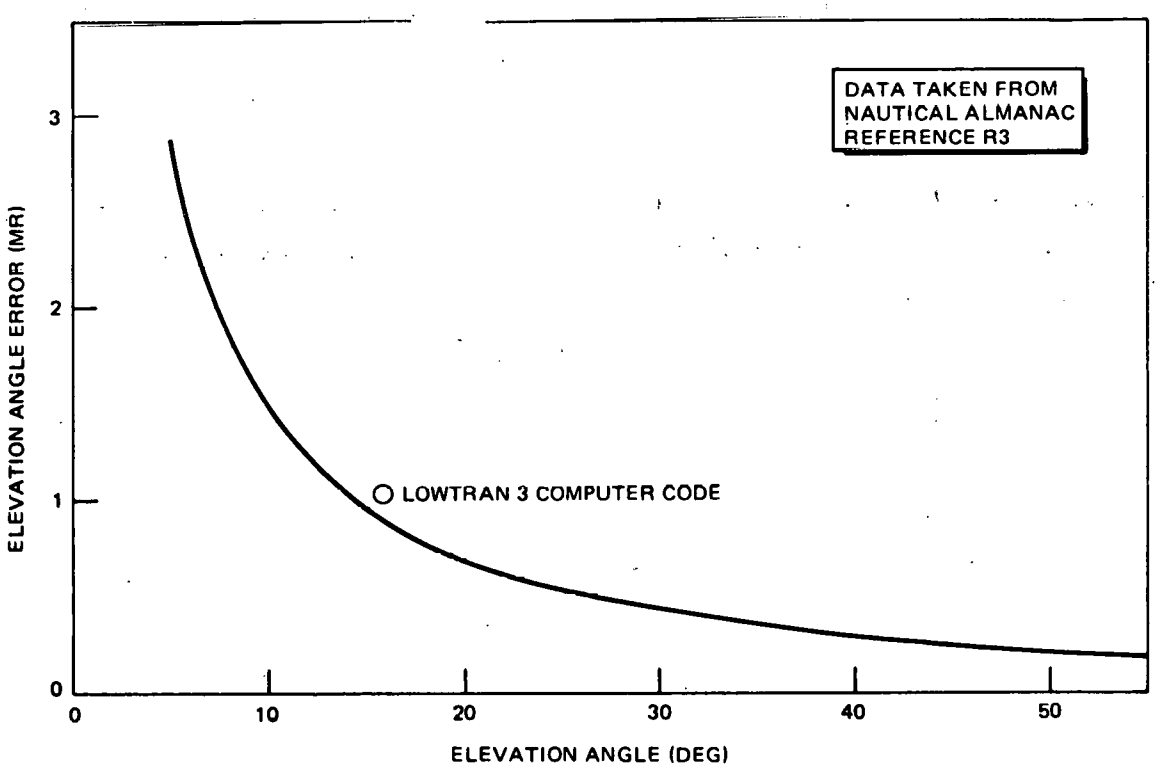

Figure 4-44. Elevation Angle Error Caused by Atmospheric Refraction

Some preliminary work on refraction has been done using the LOWTRAN 3 computer code (see Reference R4). A single point comparison with the nautical almanac data is shown in Figure 4-44.

3. Command Calculations. The primary difference between a closed-loop and an open-loop system is the method of determining commands to be given to the heliostats. In a closed-loop system, these commands are mainly computed from the feedback of an error signal. In an open-loop system, the pointing of the heliostat is accomplished by calculating commands based upon equations which give the position of the sun. In the open-loop system considered in this section, an absolute encoder on the drive output will feed back information of the actual positions of the azimuth and elevation axes. This information would be used to update the next calculated commands.

Figure 4-45 illustrates the heliostat-receiver geometry. The following equations are solved to position the heliostat so that the reflected beam is directed towards the receiver:

$$\gamma = \tan^{-1}\left[\frac{(\cos\epsilon \sin\alpha + \cos\theta \sin\beta)}{(\cos\epsilon \cos\alpha + \cos\theta \cos\beta)}\right]$$

$$\psi = \sin^{-1}\left[\frac{1}{2\cos\frac{\phi}{2}} (\sin\epsilon + \sin\theta)\right]$$

where

γ = azimuth angle of mirror normal

ψ = elevation angle of mirror normal

β = azimuth angle of receiver from heliostat

θ = elevation angle of receiver from heliostat

α = azimuth angle of sun

$$= \tan^{-1}\left[\frac{\sin h}{(\cos h \sin\rho - \tan\delta \cos\rho)}\right]$$

ϵ = elevation angle of sun

$$= \sin^{-1} (\cos\delta \cos h \cos\rho + \sin\delta \sin\rho)$$

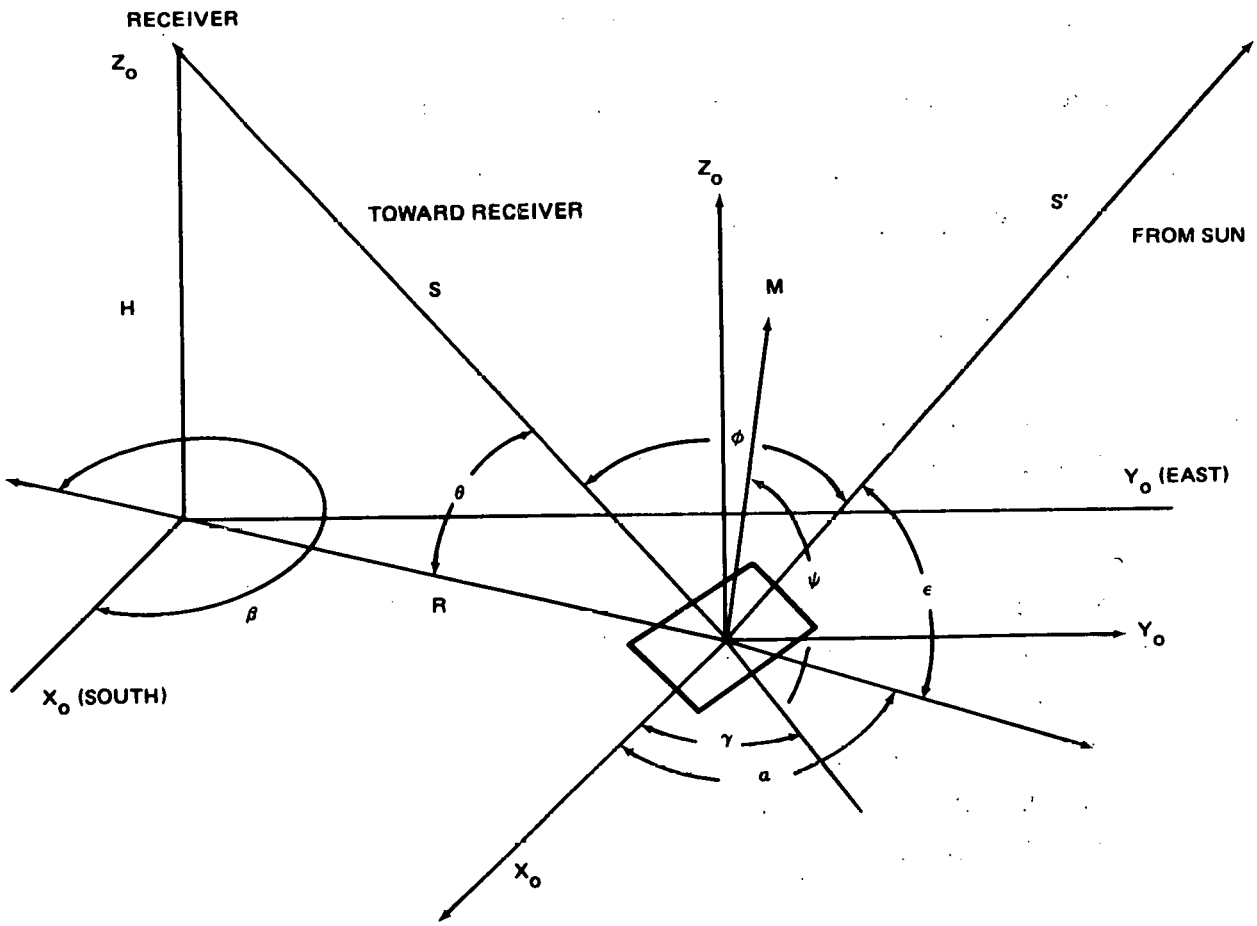

Figure 4-45. Central Receiver Heliostat Geometry

h = hour angle of sun

= 15 (12-H)

δ = declination angle of sun

$$= \sin^{-1} \left(\sin (\lambda) \sin \left(2\pi \frac{D}{365.25} \right) \right)$$

ϕ = angle between incident and reflected rays

$$= 2 \cos^{-1} \left[\frac{1}{2} \left(1 + \sin \theta \sin \epsilon + \cos \theta \cos \epsilon \cos (\alpha - \beta) \right) \right]^{1/2}$$

H = number of hours after midnight (local time)

λ = obliquity of the ecliptic

D = number of days after spring equinox

The following list of parameters are the potential contributors to errors in the calculated mirror position:

A. Location of central receiver.
   1. Latitude.
   2. Longitude.
   3. Reference line to true south.

B. Coordinates (X, Y, Z) of the heliostat relative to receiver.

C. Ephemeris data.
   1. Time of day.
   2. Longitude of sun.
   3. Declination of sun.

The sensitivity of beam-pointing error to each of these error sources was determined by perturbing the nominal value. The resulting reflected beam direction was compared to the actual receiver direction to determine a beam-pointing error. Typical beam-pointing errors as a function of the time of day are presented for the above error sources in Figure 4-46. Based upon this sensitivity data, requirements were placed on each of the error sources. These requirements are presented in Table 4-20. Discussions with surveying companies indicate that the central receiver location and the field geometry can be achieved to the required accuracy by standard surveying methods. This would include surveying to install the initial markers and a second survey after the heliostats have been installed. The requirements on the ephemeris data will result in modifications to the calculations of the hour angle and declination of the sun as used in the closed-loop synthetic tracking

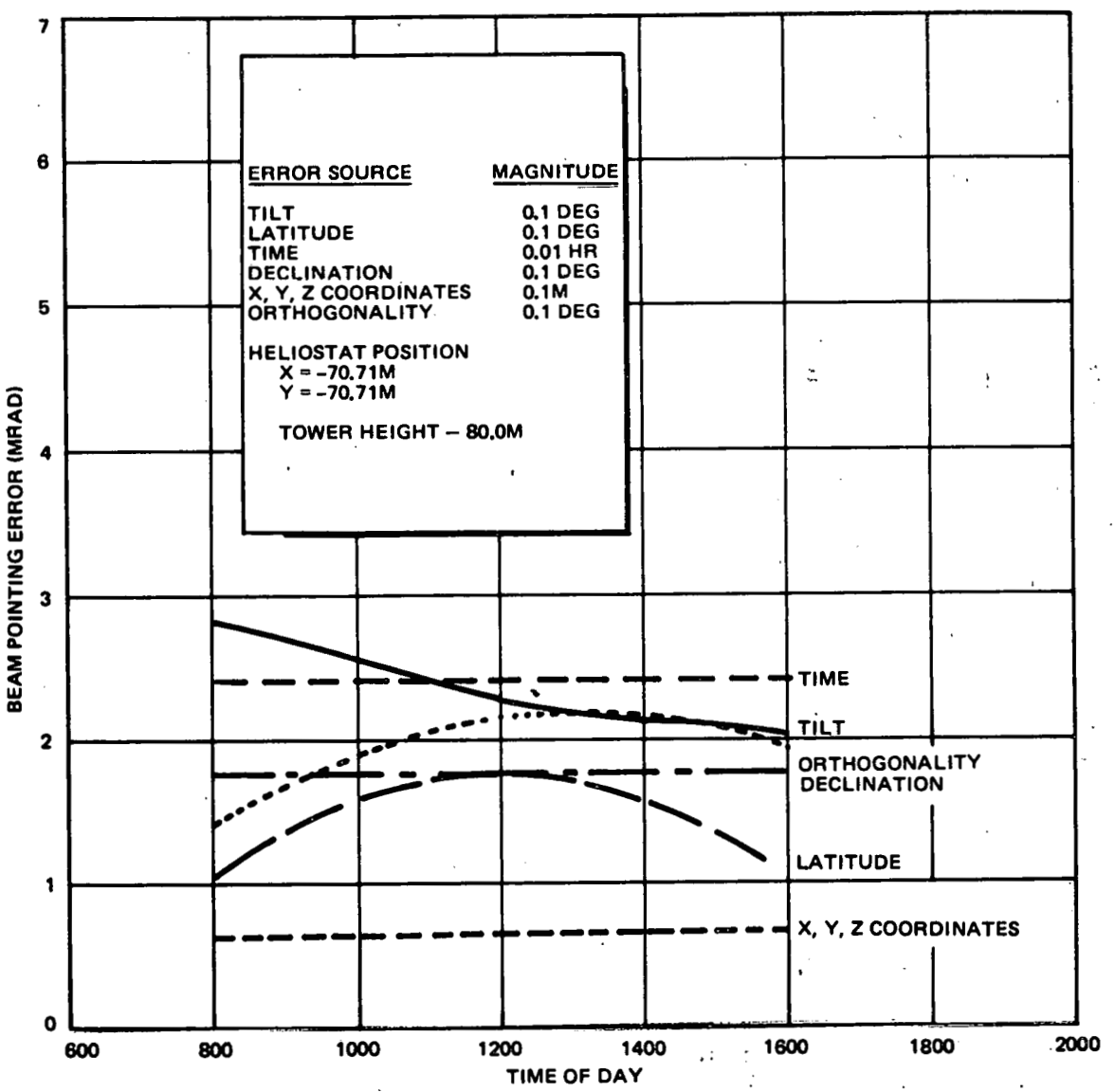

Figure 4-46. Typical Beam Pointing Errors for Command Calculation Error Sources

Table 4-20

ERROR SOURCE REQUIREMENTS

Error Sources	Tolerance (1σ)	Beam Error (Mrad) (1σ)
Surveying		
Central Receiver Location		
Latitude	0.01°	0.18
Longitude	0.01°	0.18
Heliostat Location		
Coordinates of Pivot Point of Heliostat	3 in.	0.06
Reference Line to True South	0.01°	0.18
GMT Time	1 Sec	0.07
Ephemeris Data		
Longitude and Declination of Sun	0.01°	0.18
		RSS Total 0.39 mr

mode. These changes are currently being investigated with ease of implementation in a computer algorithm and update requirements as primary considerations. The position of the sun can also be obtained from a sun tracker if one is necessary to solve the problem of refraction described previously.

There are two additional error sources that result in the heliostat not achieving its commanded mirror normal position. The first is the heliostat azimuth plane not being perpendicular to a normal to the earth. Two causes of this error would be a tilt of the heliostat pedestal and/or a misalignment of the azimuth drive unit to the pedestal due to manufacturing tolerances. The tilt of the pedestal can be determined accurately by a detailed surveying procedure. Tightening of manufacturing tolerances will also reduce this error but both procedures are costly. Since an alignment procedure is required for periodic checks, the most efficient method for reducing this error is through an automated alignment. The second error source that results in the heliostat not achieving commanded mirror normal positions is the azimuth and elevation axes not being orthogonal. This error results from manufacturing tolerances and can be reduced through an alignment procedure. The potential alignment procedures and implementation are discussed in Section 4.2.6.5.

The analysis of the alignment methods is not complete at this time but the accuracy can be estimated conservatively for a sun/heliostat/active target alignment scheme as the accuracy to which the mirror normal can be determined. Some of the errors associated with determining the mirror normal are:

A. Image Centroid. Assuming that the centroid of the reflected beam can be determined within 4 in., the accuracy of the reflected beam for a near heliostat (54m) would be

$$\sigma_N = \frac{4}{4,823} = 0.83 \text{ mr}$$

and a far heliostat would be

$$\sigma_F = \frac{4}{12,947} = 0.31 \text{ mr}$$

The uncertainty in mirror normal would be half this amount for near/far or

$$\sigma_I = 0.42/0.16 \text{ mr}$$

B. Sensor. If a 13-bit encoder is used, the sensor granularity would be

$$S_g = \frac{360^\circ}{2^{13}} = 0.77 \text{ mr}$$

Assuming this error to have a uniform distribution, the uncertainty in mirror is normal because sensor granularity is

$$\sigma_g = \frac{0.77}{\sqrt{12}} = 0.22 \text{ mr}$$

C. Surface Deviations. It will be assumed that the alignment is done when there is no, or light, winds and the temperature is near the reference temperature so that neither of these errors will contribute to the mirror normal uncertainty. Gravity will contribute the same amount or

$$\sigma_g = 0.6 \text{ mr}$$

D. Mirror Alignment. As was discussed in Section 4.2.6.1, the mirror panels will not be aligned with the heliostat normal. The requirement placed upon the structure is

$$\sigma_a = 0.5 \text{ mr}$$

E. Miscellaneous Errors. There are a number of other errors such as refraction, structure bending from sensor to mirror structure, etc. which can contribute to mirror normal error. Since these errors are mainly a function of environmental conditions – sun elevation angle, wind, etc. – it will be assumed that the alignment time can be selected to minimize their effort. It is estimated that the combined effect of these errors can be kept less than

$$\sigma_m = 0.3 \text{ mr}$$

The total mirror normal uncertainty is

σ_I	0.42/0.16
σ_g	0.22
σ_a	0.5
σ_g	0.6
σ_m	0.3
Total RSS =	0.96/0.88 mr

The total beam error as a result of mirror normal uncertainty is

$$\upsilon_n - 1.92/1.76 \text{ mr}$$

Combining these errors with the surviving errors results in a total command error of

$$\sigma_c - \overline{\sigma}_n + \overline{\sigma}_s - \overline{1.92/1.76} + \overline{0.39} = 1.96/1.80 \text{ mr}$$

4. Pedestal Foundation. The heliostat is a relatively large heavy structure sitting in a foundation in the ground. As such, unless a large costly foundation is made, the pedestal will move with time as a result of foundation settling. Foundation settling could be amplified by the large wind moments acting on the pedestal. Heliostat pedestal angular measurements were made at the test site. The measurements are given in Table 4-21. There is some question as to the accuracy of the measurements but for the lack of better information, a value of $\sigma = 0.77$ mr will be used for pedestal movement. It will be assumed that the mean angular movement can be removed with the alignment process.

Table 4-21

SRE TEST DATA
HELIOSTAT PEDESTAL ANGULAR MEASUREMENT

Date	Time Hr-Min	Temp. F	H1 N-S	H1 E-W	H2 N-S	H2 E-W	H3 N-S	H3 E-W	H4 N-S	H4 E-W	IH1 N-S	IH1 E-W
10/13/76	9:00 AM	72.00	78°10'	78°12'	77°38'	78°3'	78°27'	77°24'	78°25'	77°53'	-	-
12/15/76	2:00 PM	67.00	78°15'	78°17'	77°48'	78°5'	78°26'	77°28'	78°30'	77°58'	90°27'	89°39'
12/21/76	9:40 AM	40.00	78°12'	78°15'	66°42'	77°58'	78°28'	77°18'	78°30'	77°51'	90°30'	89°37'
12/22/76	9:00 PM	30.00	78°12'	78°17'	77°45'	78°03'	78°31'	77°20'	78°31'	77°51'	90°31'	89°37'
1/12/77	8:30 AM	33.00	78°10'	78°15'	77°43'	78°01'	78°27'	77°20'	78°27'	77°53'	90°30'	89°38'
1/21/77	12:20 PM	48.00	78°09'	78°15'	77°44'	78°03'	78°25'	77°20'	78°21'	77°58'	90°28'	89°28'
Mean (Min.) =			11.33	15.17	46.3	2.17	27.33	21.67	27.3	53.17	29.2	37.8
Standard Deviation (mr)			0.63	0.53	0.97	0.70	0.60	1.07	1.11	9.75	0.48	0.24 = 0.77

5. Bending from Absolute Sensor to Mirror Structure. It is not known exactly at this time at what point from drive output to mirror structure the sensor will measure the mirror angles. Regardless of the point of pickoff, the wind will cause some compliance bending from the sensor to the mirror structure. An estimate of this error is shown in Table 4-15.

6. Pedestal Deflection. Unlike the closed-loop process, the open loop-process is sensitive to any movement of the pivot point. Winds acting on the mirror structure produce moments on the pedestal which then result in deflection of the pivot point. Using the NASTRAN program, the deflection is estimated between 0.3 and 0.4 mr. Assuming this error can be in any direction, the beam error is

$$\sigma = \frac{(0.4)(2)}{\sqrt{2}} \approx 0.6$$

4.2.6.4 Open-Loop Errors with Sensor on Motor Shaft

1. Control System Errors. The accuracy of this mechanization was investigated by modifying the closed-loop Monte Carlo simulation described above. The beam sensor was removed and an incremental value of motor shaft was used as a feedback signal.

As might be expected, this mechanization was found to be much more sensitive to backlash and winds. The results are shown in Figure 4-47 for backlash and Figure 4-48 for mean wind velocity. The results are perhaps better understood by considering an analytical model. The beam error is made up of backlash and wind deflection. The backlash error has a uniform distribution because any position within the backlash range is equally likely. The wind-deflection error can be approximated as a triangular distribution where the peak is at the mean velocity deflection and the minimum and maximum value are at mean $\pm 2\sigma$. This model is illustrated in Figure 4-49. The total beam error is

$$x = x_t + x_w$$

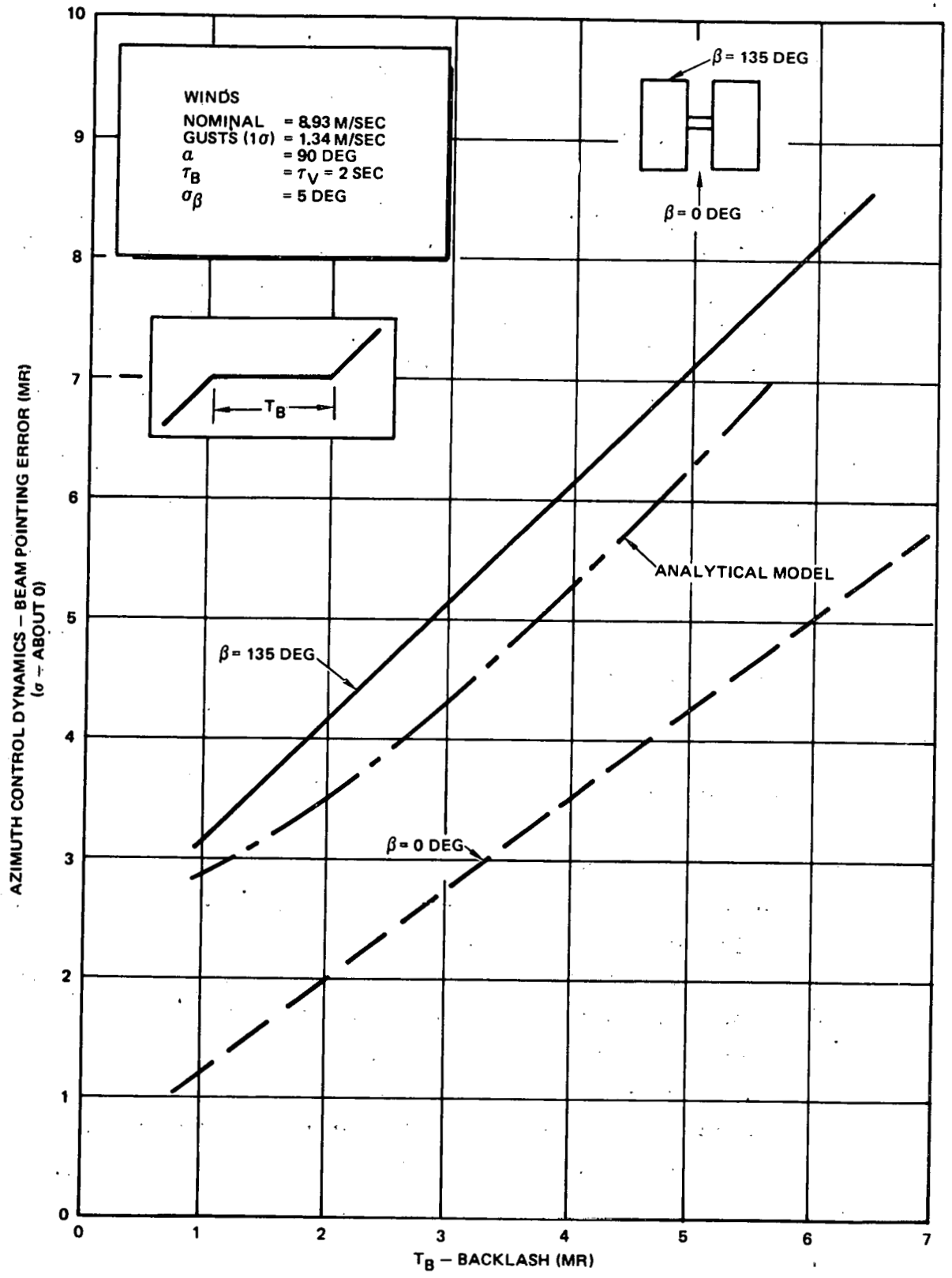

Figure 4-47. Effect of Backlash Upon Beam Error for Open Loop/Shaft Sensor – Simulation Results

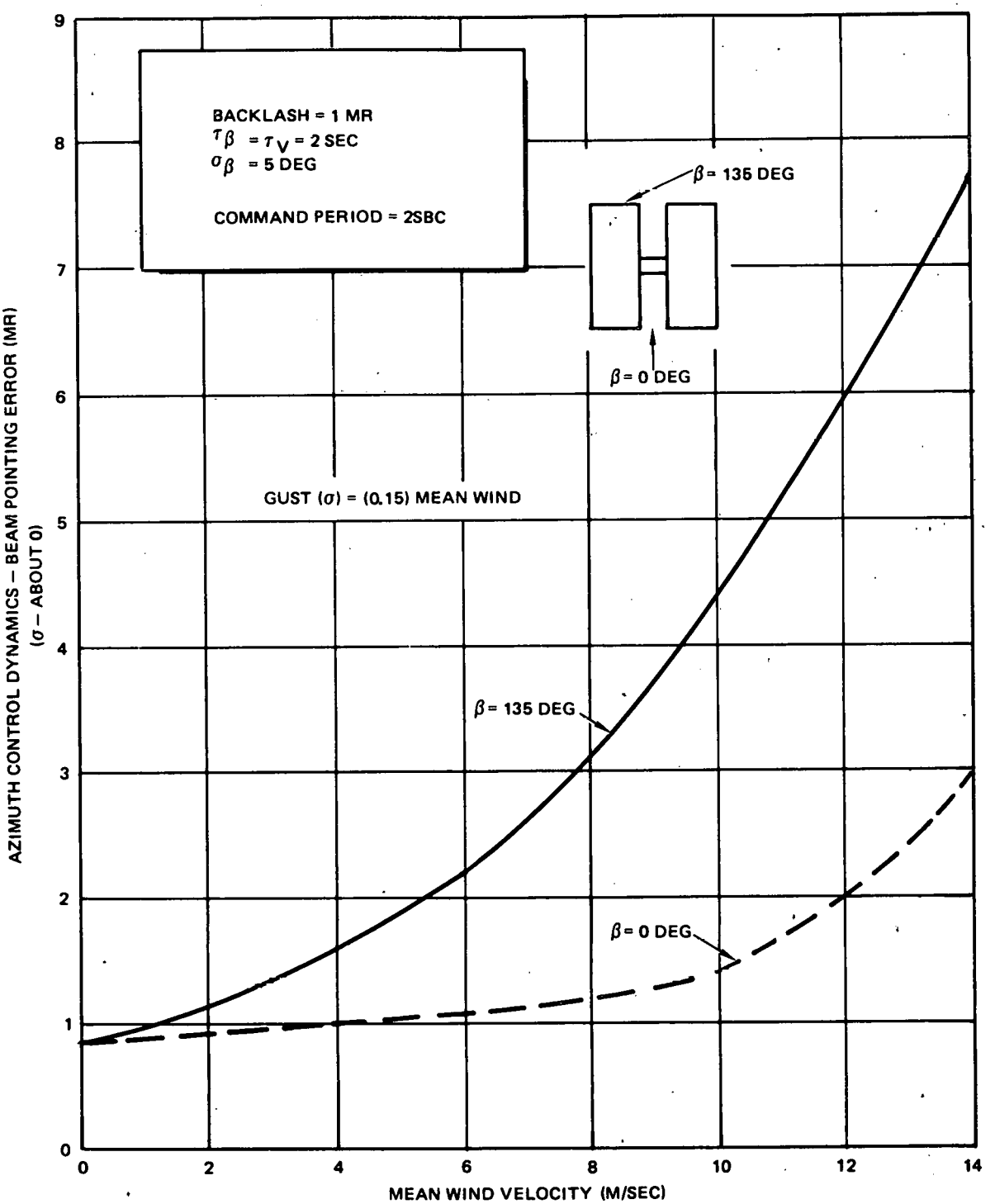

Figure 4-48. Effect of Wind Velocity Upon Beam Error for Open Loop/Shaft Sensor — Simulation Results

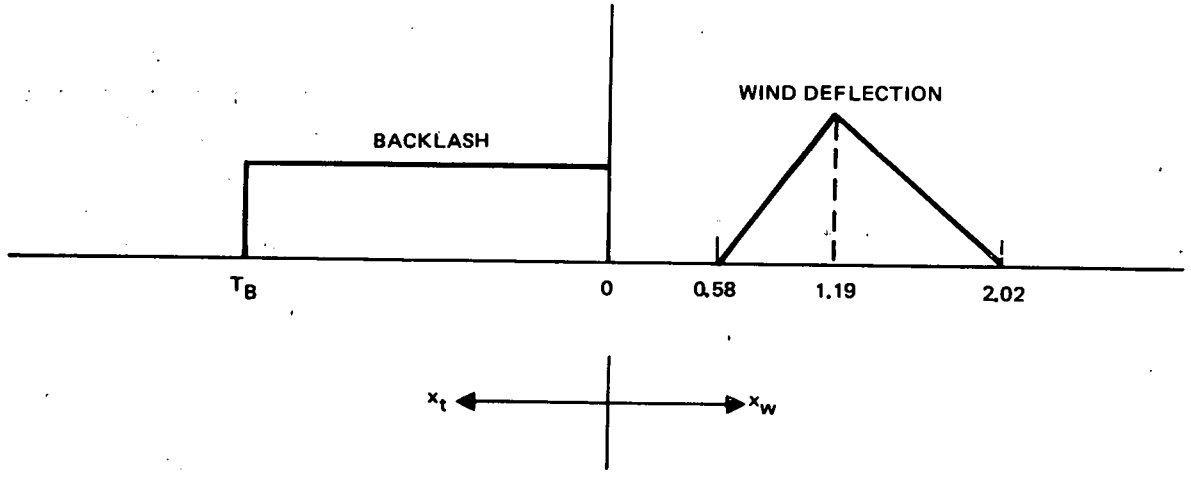

Figure 4-49. Analytical Backlash/Wind Model

The rms error is

$$\sigma^2(\text{rms}) = \sigma_t^2(\text{rms}) + \sigma_w^2(\text{rms})$$

Using the values shown in Figure 4-49, the rms error becomes

$$\sigma^2(\text{rms}) = \frac{T_B^2}{3} + (1.3)^2$$

A plot of this curve is shown in Figure 4-47. The difference between the simulation results and analytical model stems from the approximation of the distribution and the difference in autocorrelation time.

The amount of wind deflection is a direct function of the drive unit stiffness (one over compliance). The sensitivity of azimuth beam error is shown in Figure 4-50. A value of 133,000 in. -lb/deg has been used in the analysis because it is the spec value, although the test on the drive unit indicates the value may be higher.

The sensitivity to the amount of hysteresis was determined by varying the hysteresis base band (BB) in the Monte Carlo simulation. The results are shown in Figure 4-51. The bottom curve indicates the contribution of hysteresis to beam-pointing error. SRE list data indicates the base band can be somewhere between 0.1 and 0.3 mr.

The azimuth beam error for this open-loop mechanization with an Orbidrive unit that has 2 mr of backlash and a stiffness of 133,000 in. -lb/deg (a spec number) would be 4.1 mr. The severity of an error of this magnitude warrants re-evaluation of the characteristics of the drive unit. After reviewing the drive unit test (Reference R1), it was concluded that 2 mr of backlash was reasonable, but a stiffness of 133,000 in. -lb/deg was low. The test value of stiffness ranged from 145,471 in. -lb/deg to as high as 307,000 in. -lb/deg, although more hysteresis was associated with this high value of stiffness. The characteristics of the drive unit shown in Figure 4-52 were selected as being a good, yet still conservative, representation of an

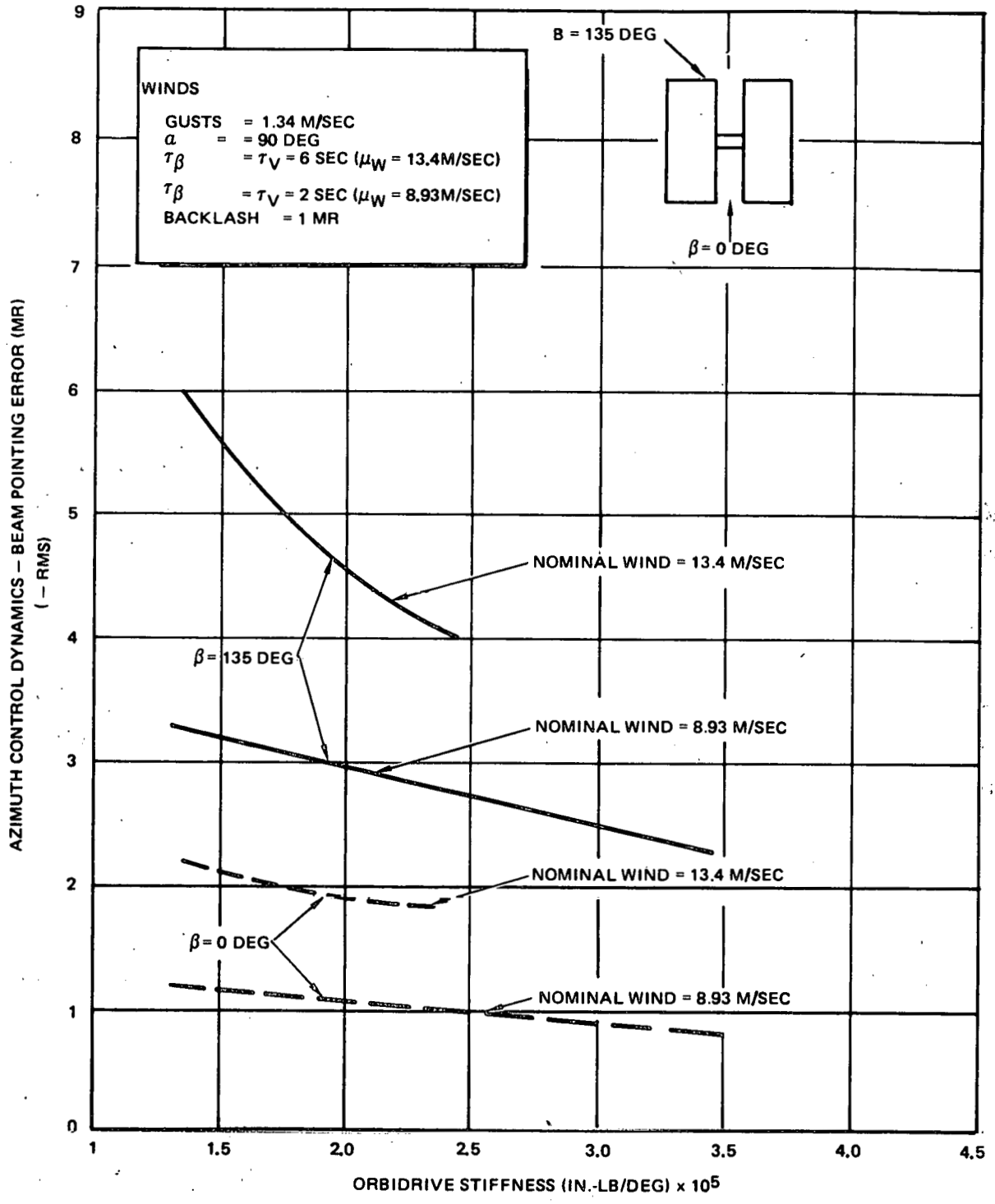

Figure 4-50. Effect of Stiffness Upon Beam Error for Open Loop/Shaft Sensor

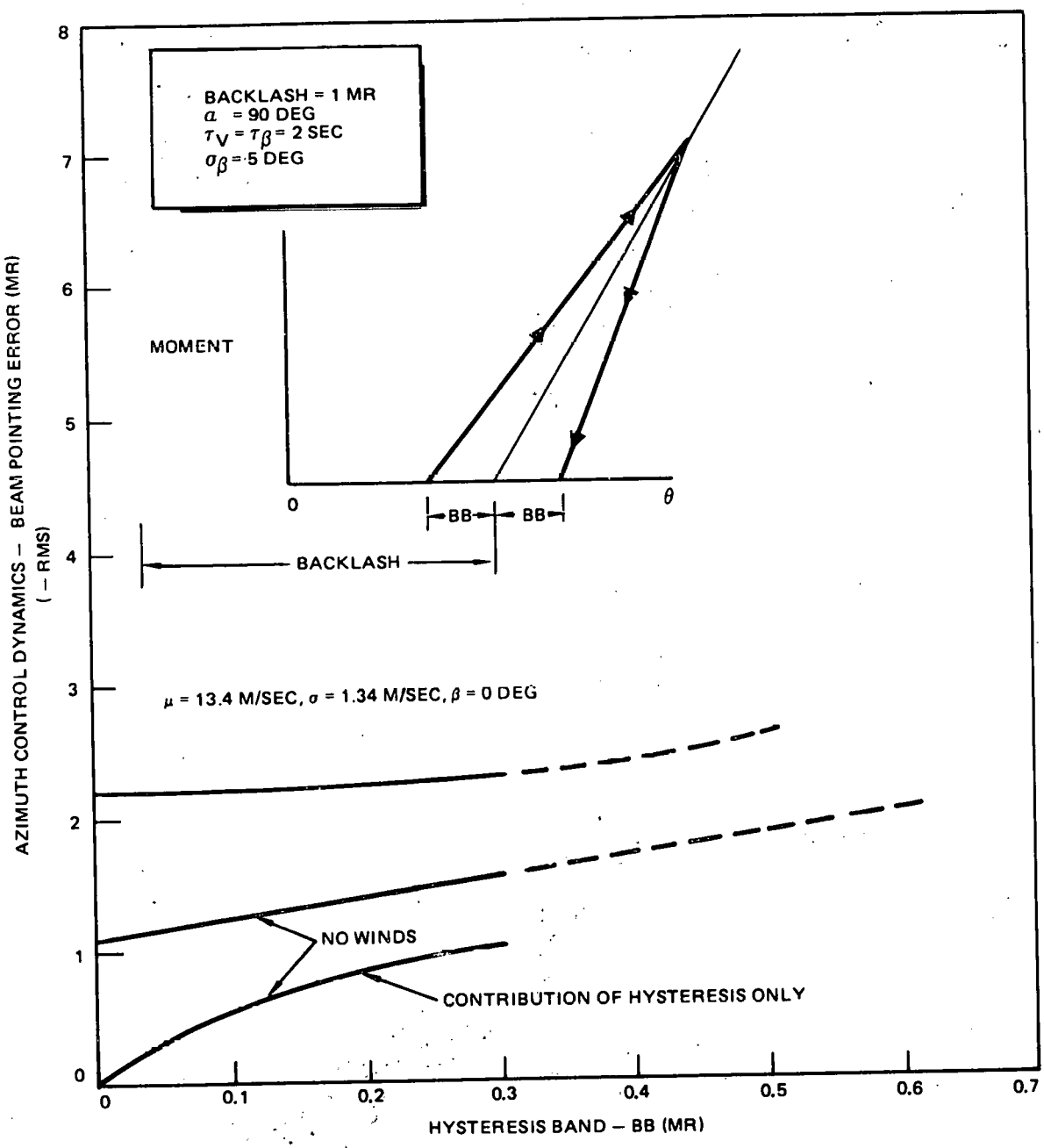

Figure 4-51. Effect of Hysteresis Upon Beam Error for Open Loop/Shaft Sensor

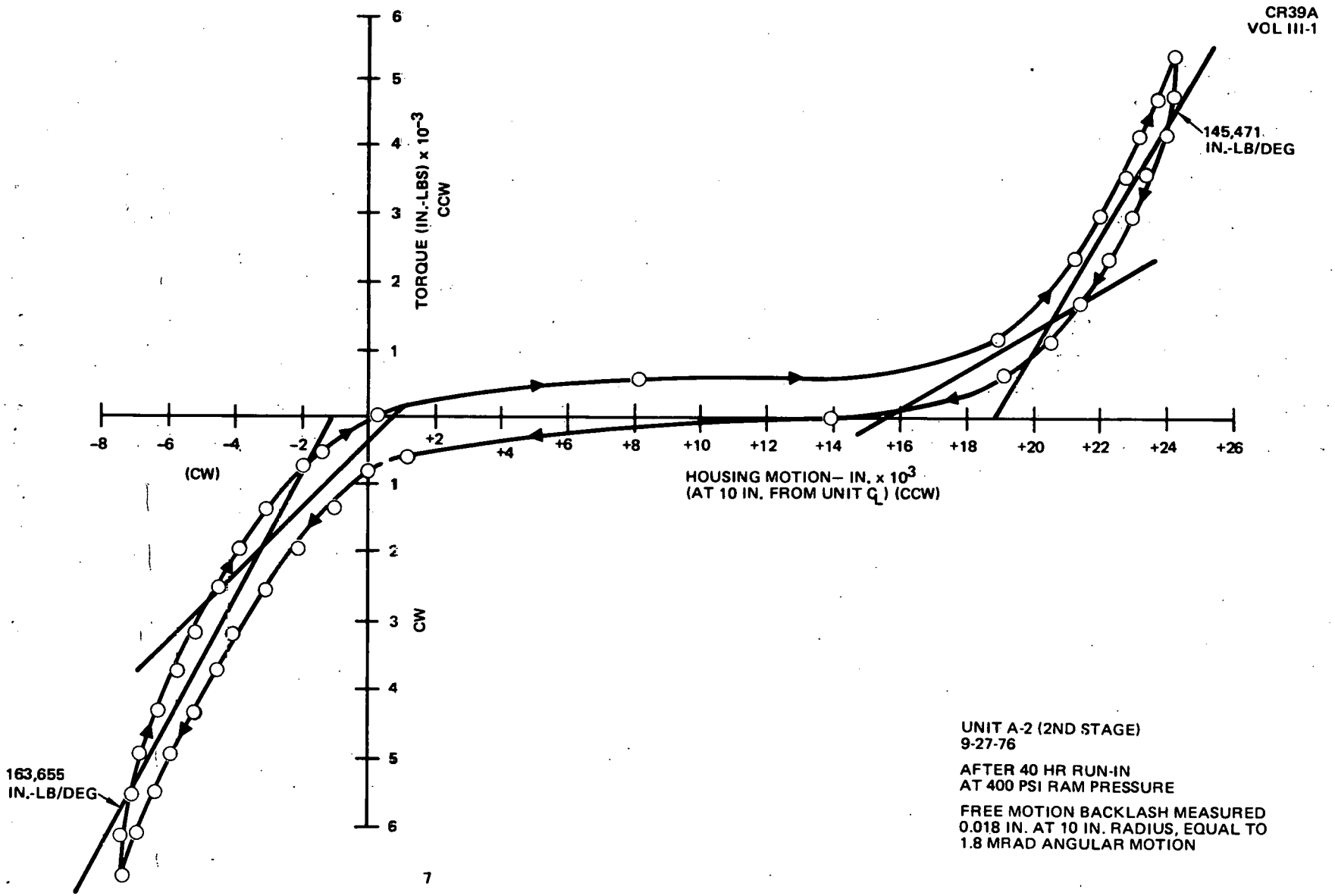

Figure 4-52. SRE Test Data for Orbidrive

Orbidrive capability. The azimuth beam error with 2 mr of backlash and a stiffness of 150,000 in. -lb/deg is 3.9 mr. For the angle of attacks considered, the elevation moment coefficient would be about half. It is estimated that the elevation error would be about half or 1.8 mr.

Because this error is still relatively large, an evaluation of a harmonic drive unit was considered. The characteristics of the harmonic drive are illustrated in Figure 4-53. The data would tend to indicate that the harmonic drive does not exhibit any backlash, but does have an inelastic effect which would result in a beam error. This test data is insufficient for the development of an error model, but after studying the harmonic drive characteristics shown in Figure 4-53, it is conceivable that harmonic drive would result in less beam error than the Orbidrive. It is estimated that harmonic drive would be approximately the same as Orbidrive with 0.5 mr of backlash which would result in an azimuth beam error of 2.75 mr and an elevation beam error of 1.27 mr.

2. Refraction. The refraction error is common between both open-loop mechanizations. The same discussion applies here as for open loop with sensor on drive output.

3. Command Calculations. The only change in the error budget presented in Table 4-15, due to the change from an absolute encoder on the drive output to an incremental encoder on the motor shaft, is in the accuracy of the alignment procedure. The alignment tolerance is increased to 1.0 mr. The additional error is due to the fact that with an encoder on the motor shaft, the output can be anywhere in the backlash and compliance.

4. Pedestal Foundation Movement. The same discussion applies here as for open loop with sensor on drive output.

5. Pedestal Deflection. The same discussion applies here as for open loop with sensor on drive output.

6. Bending from Drive to Mirror Structure. The compliance from the drive output to the mirror structure contributes to beam error. An estimate is shown in the table.

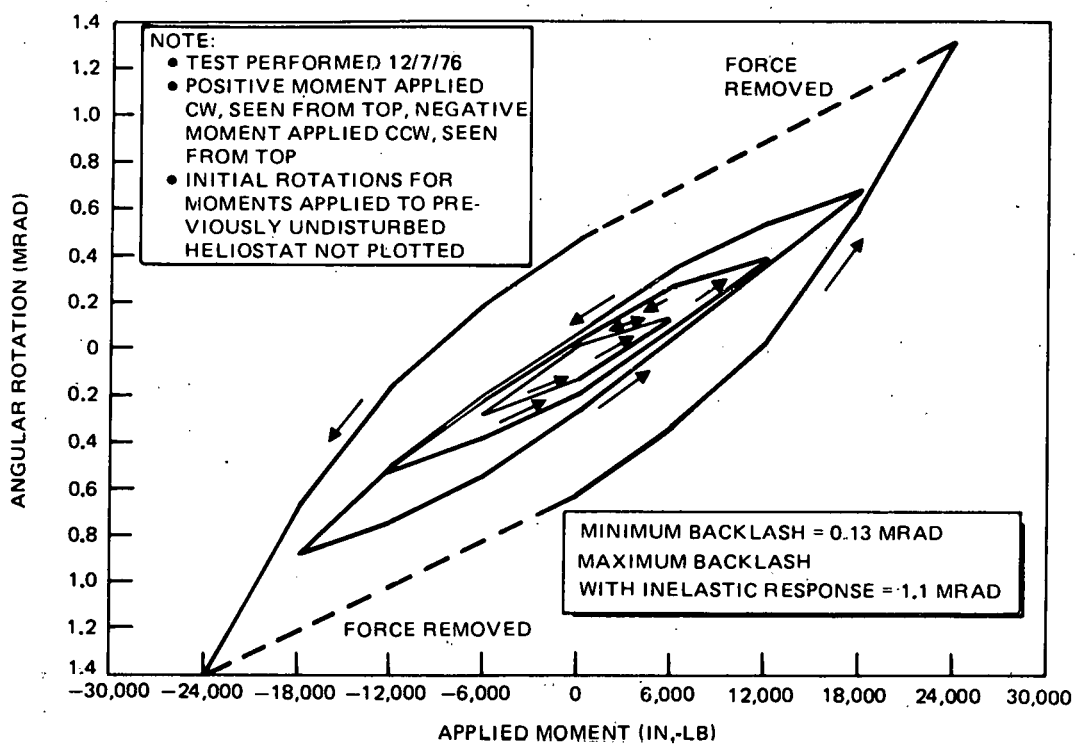

Figure 4-53. Characteristics of Harmonic Drive

7. Gravitational Moment. Gravity produces a moment in the elevation plane which acts through the compliance to produce a beam error. Since the sensor is on the motor shaft before the drive compliance, this error in elevation angle is not detected. The elevation beam error for a drive stiffness of 133,000 in.-lb/deg is shown in Figure 4-54. This error can be reduced by modeling the gravitational moment and knowing the compliance of the drive unit, the elevation angle can be modified to correct for the gravitational deflection. If the compliance of the drive unit is known to within 27% (2σ), it is estimated that the error can be reduced to 0.32 mr.

4.2.6.5 Heliostat Alignment

After the heliostat has been placed in the field, there will be a number of errors which could result in a large beam error. Some of these errors, for an open-loop mechanization, are:

A. The tilt of the azimuth plane. Depending upon the care and expense with which the pedestal is installed, there could easily be 1 to 2 deg of tilt. The azimuth drive/bearing structure could also contribute to a tilt angle.

B. The position of the heliostat pivot point with respect to the receiver. After the heliostat is installed, a position error will exist between the surveyed position and the actual position. Any tilt of the pedestal will also result in a pivot point position error. The magnitude of this error will again depend upon the care and expense with which the pedestal is installed.

C. Nonorthogonality between the elevation plane and the azimuth plane. This error stems from the structural tolerance of the rotational assembly. To reduce this error to an acceptable level will greatly increase the manufacturing costs.

D. Heliostat reference system with respect to south must be determined.

At present, a number of methods of alignment are being investigated. The cost vs accuracy study has not been completed. Some of the methods being considered are:

A. Survey the field after the heliostats have been installed, use a leveling device to determine tilt, and reflect the sun onto the receiver to obtain a reference point.

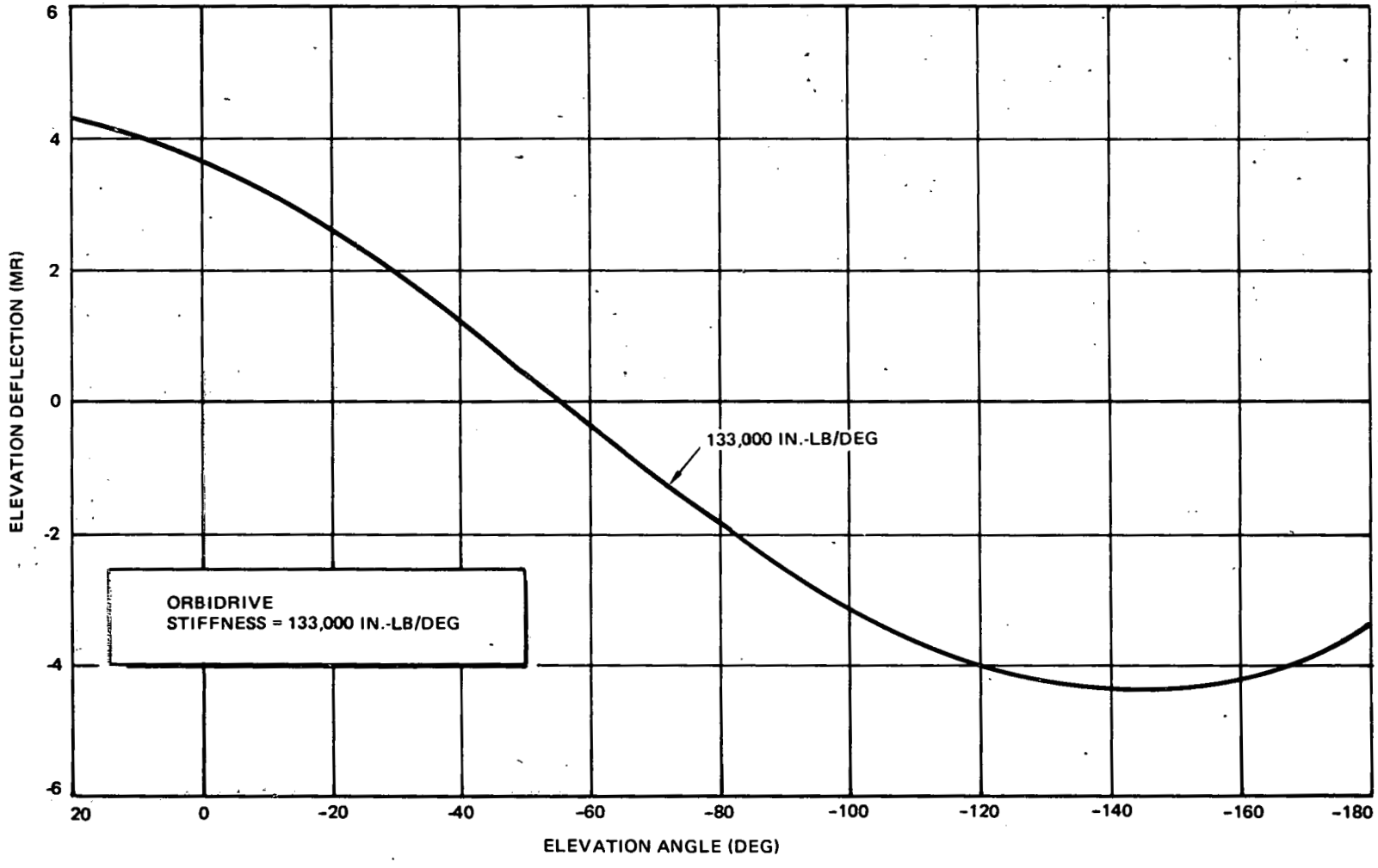

Figure 4-54. Elevation Deflection Due to Gravitational Moment

B. Use the sun, heliostat, target on tower, and a digital radiometer. The heliostat is commanded to a position which would reflect the beam at the center of the target. The difference between where the beam is commanded to be and actually points is used to calculate correction terms which would be used to adjust the heliostat commands during normal tracking.

C. Use the sun, heliostat, and active receiver on the tower. The same procedure as in B above is used to calculate command correction terms.

D. Use a laser autocollimator on the tower to survey the field.

Because of the weight of the heliostat, it seems reasonable to consider that over some period of time the heliostat pivot point will move which would result in a position and tilt error. The movement could be the result of the pedestal foundation settling or caused by an earthquake. In either case, heliostat alignment will have to be done periodically. The time period between alignments is not known at this time but it could be as short as 3 mo or as long as 2 to 5 yr.

It would seem desirable to have an alignment scheme such as Item B, C, or D above which could be done periodically without shutting down operations or requiring a lot of manhours. In addition, alignment method B and C can also be used to test heliostat performance without sending a man out in the field. Such things as dirty, cracked, or warped mirrors can be detected by examining the intensity pattern.

None of the above errors significantly affect the closed-loop mechanizations since the sensor produces error signals for the control systems which keep the beam directed at the receiver. Of course, the sensor mirror, sensor, and receiver must be aligned before this can be accomplished. Since the sensor pole orientation may change with time, periodic alignment of the sensor may be required. The alignment scheme for closed-loop could be as simple as adjusting the sensor until the image is at the desired position on the receiver or method B or C above could be implemented to do automatic alignment.

4.2.6.6 Summary

A summary comparison of the closed- and open-loop beam pointing accuracies is given in Table 4-22. The azimuth and elevation error are combined to form a single half-cone angle which contains 90% of reflected energy. The relative accuracy of the different tracking mechanization can be obtained by comparing the 90% cone angle. The amount of power lost and the total number of heliostats required to maintain a constant power at the receiver are also shown. A comparison of the advantages and disadvantages of the open- and closed-loop mechanizations is summarized in Table 4-23. Some of these are:

There have been many assumptions, conjectures, and simplifications made in the above analysis which may have a significant effect upon the results in Table 4-23. Some of these are:

A. Picking the worst angle of attack and saying it is the same for all heliostats in the field.
B. Investigation of the alignment has not been completed and the accuracy that can be obtained has not been determined at this time.
C. There is some uncertainty about the method of transferring structural deflection into beam error and power loss.
D. SRE data has been integrated into this analysis, but there is some question on some of the data as to the accuracy of the measurement device which was used to gather the data.

Taking these things into account, estimates for the range of accuracy, power loss, and additional heliostat requirements have been estimated and are shown in Table 4-24. The biggest uncertainty exists in the open-loop/shaft sensor mechanization because of the sensitivity to winds/backlash and the uncertainty in the alignment accuracy, but it has the greatest potential savings. The potential savings of this mechanization are compared to the closed-loop PD configuration in Figure 4-55. Because of the sensitivity to winds/backlash, the harmonic drive for open-loop/shaft sensor has a potential additional savings as shown in Figure 4-55. The coming testing, simulation, and analytical work will substantiate the open-loop/shaft sensor mechanization. Total cost of the open- and closed-loop tracking mechanization is discussed later.

Table 4-22

CLOSED/OPEN-LOOP COMPARISON

Beam Accuracy

Error Source	Closed Loop AZ/EL (mr)	Open Loop Gimbal Sensor AZ/EL (mr)	Open Loop Shaft Sensor AZ/EL (mr)
1. Control Dynamics	0.8/0.5	0.9/0.6	4.1/2.0
2. Mirror Surface	2.1/2.2	2.1/2.2	2.1/2.2
3. Command/Alignment	0.5/0.5	2.0/2.0	2.4/2.4
4. Pedestal/Sensor Pole	0.2/1.2	1.6/1.7	1.6/1.7
5. Beam Sensor	0.5/0.5	0/0	0/0
6. Refraction	0/0	0.1/0.4	0.1/0.4
7. Gravitational	0/0	0/0	0/0.3
Total RSS	2.4/2.6	3.4/3.4	5.4/4.2
Half Cone Angle (90%)	5.4	7.3	10.9
Power Loss (%)	1.4	2.5	5.1
Additional Heliostats (1736)	24	43	88

Table 4-23

ADVANTAGE AND DISADVANTAGE OF OPEN/CLOSED-LOOP MECHANIZATION

	Item	Closed Loop	Open Loop	
			Gimbal Sensor	Shaft Sensor
I.	Alignment	IA. Simple and Not Required to Repeat Very Often	IB. More Complicated and Required to Repeat More Often Than IA.	IC. More Complicated and Required to Repeat More Often Than IA.
II.	Backlash	IIA. Very Little Sensitivity to Backlash.	IIB. About the Same as IIA.	IIC. Very Sensitive to Backlash.
III.	Detection of Malfunction	IIIA. Detect Most Malfunctions in Control Loop.	IIIB. About the Same as IIIA.	IIIC. Detect Motor Malfunction Only.
IV.	Atmospheric Refraction	IVA. Not Sensitivity	IVB. Requires Refraction Correction From Model or Sun Tracking	IVC. Same as IVB
V.	Mechanization	VA. Requires A. Pole Sensor B. Shaft Sensor C. Gimbal Sensor	VB. Requires Good Gimbal Sensor	VC. Requires A. Shaft Sensor B. Gimbal Sensor
VI.	Computer Requirements	VIA. Low	VIB. High	VIC. High
VII.	Compliance	VIIA. Not Very Sensitive	VIIB. Same As VIIA.	VIIC. Sensitive to Compliance. Requires Known Value of Elevation Drive Compliance.

Table 4-24

ESTIMATE OF OPEN/CLOSED-LOOP ACCURACY RANGE

Item	Closed Loop	Open Loop	
		Gimbal Sensor	Shaft Sensor
Accuracy (mr)			
Azimuth (1σ)	1.8 → 2.6	2.8 → 4.0	3.0 → 6.0
Elevation (1σ)	1.8 → 2.6	2.8 → 4.0	3.0 → 6.0
Half Cone Angle (90%)	3.9 → 5.6	6.0 → 8.6	6.5 → 13.0
Power Loss (%)	1.1 → 1.6	1.7 → 3.7	1.8 → 7.4
Additional Heliostats	18 → 26	28 → 61	30 → 122

References for Section 4.2.6

R1. "Power Collection Reduction by Mirror Surface Nonflatness and Tracking Error for a Central Receiver Solar Power System." Applied Optics, Vol. 14, p. 1493, July 1975.

R2. "Final Report on Test Results of Heliostat Drive System." Compudrive Corporation. Contract No. 76721008, 28 February 1977.

R3. "The National Almanac For the Year 1974." United States Observatory, U.S. Government Printing Office.

R4. R. A. McClatchey and J. E. A. Shelby, "Atmospheric Transmittance from 0.25 to 28.5 m: Computer Code LOWTRAN 3" - Air Force Cambridge Research Laboratory, L. G. Hanscom AFB, Massachusetts, 01731, 7 June 1975.

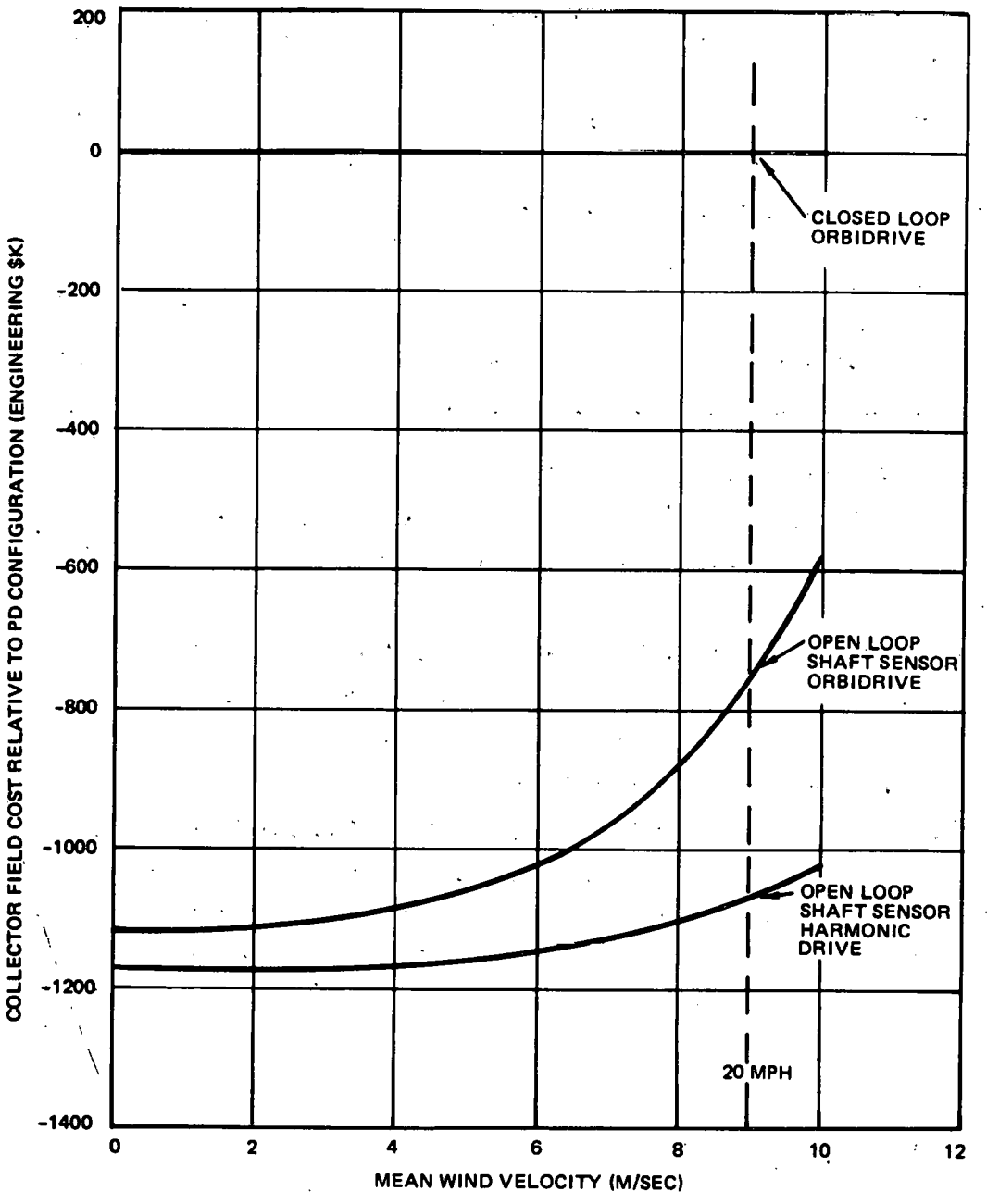

Figure 4-55. Cost Savings of Open Loop/Shaft Sensor Versus Closed Loop

4.2.7 Control Sensor Design/Performance

4.2.7.1 Open-Loop Sensors

The selection of a control sensor for the open-loop design was based on a transducer which had the required angular sensitivity and would be the most cost-effective. The candidates, along with their respective characteristics, costs, and basic electrical interface requirements, are listed in Table 4-25.

Table 4-25

CONTROL SENSOR CANDIDATES

Device	Unit Accuracy	Cost	Electrical Interface (per device)
13-Bit Absolute Encoder	0.95 mrad	$400.00	13 parallel lines and digital mux
13-Bit Incremental Encoder	0.95 mrad	$390.00	2 digital line and digital mux
[Synchro	0.85 mrad	$ 80.00	2 lines and analog mux
Synchro-Digital Converter]	2.7 mrad	$ 58.00*	plus A/D converter
Potentiometer	1.0 mrad	$350.00	1 line and analog mux plug A/D converter
1-Bit Incremental Encoder	0.15 mrad**	$ 32.00	2 lines and digital mux

* Per heliostat cost
**Output resolution through 43,000:1 reduction

The analog sensors were not cost-effective because they required an A/D converter and analog multiplexers. In addition, the unit accuracy of the synchro and high unit cost of the potentiometer made the analog sensors unattractive for this application.

The high-resolution encoders were more easily adaptable; however, the high unit cost resulted in an electronics cost nearly equal to the cost of the closed-loop electronics. The sensors would be used to measure the angular displacement of the gimbal axes, and therefore, required the high resolution.

The angular displacement of the gimbal axes can also be indirectly determined by measuring the angular displacement of the input (motor shaft) axis and knowing the gear ratio (43,000:1 reduction) of the drive mechanism.

A coarse resolution (1 bit) incremental encoder would yield a gimbal resolution of 0.15 mrad. The incremental approach requires an interface which can keep count of the total input revolutions such that the gimbal position can be determined at any time. This is the most cost-effective sensor. However, it has some drawbacks, namely its dependence on the interface to keep count of the total input revolutions and its inability to directly measure the angular movement of the gimbal. The errors resulting from the imperfections in the drive mechanism (backlash, dead space, and compliance) cannot be detected by this sensor.

4.2.7.2 Closed-Loop Sensor (Discrete Output Beam Sensor)

The closed-loop sensor characteristics are basically the same as the sensor used on SRE. One beam sensor is used with each heliostat to indicate in two coordinates the angular deviation of the beam reflected from the mirror from the desired position on the receiver. The beam sensor is mounted on a separate pole and its optical axis is boresighted to the receiver looking back at the mirror surface. If the reflected rays are not parallel with the sensor axis, error signals are generated in two orthogonal coordinates. These signals are processed and used to drive the heliostat toward a null error signal condition.

Since the sun presents an intense, slow-moving source of energy for optical tracking, it is feasible to use simple, nonscanning, trackers operating in a direct-current-coupled mode. The principal beam sensor requirements are adequate angular sensitivity, suitable control characteristics, stability, low manufacturing cost, and high reliability. A sensor meeting these requirements is the balanced-shadow concept developed for SRE shown in Figure 4-56.

The balanced-shadow sensor developed at MDAC consists of two pairs of rectangular silicon detectors arranged on the arms of a cross. A square mask is positioned and sized so that sunlight passing the mask illuminates the outer edges of each detector. Vertical baffles are located so as to isolate each detector. An imbalance in signal between opposite pairs of detectors produces an error signal. A fifth detector element at the center measures insolation to provide for automatic gain control (AGC). The output characteristics of the balanced-shadow sensor are shown in Figure 4-57.

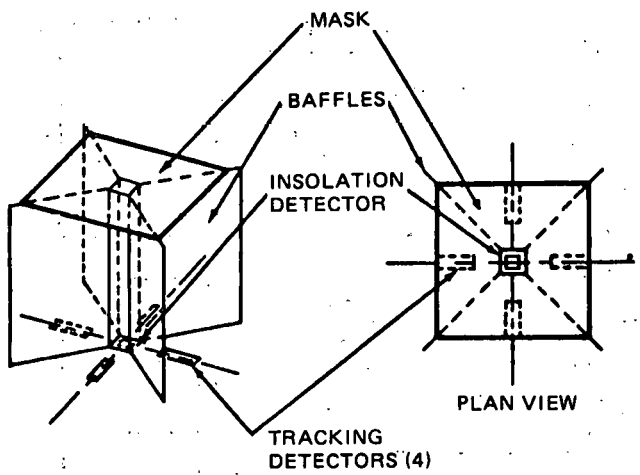

Figure 4-56. Balanced Shadow Sun Sensor

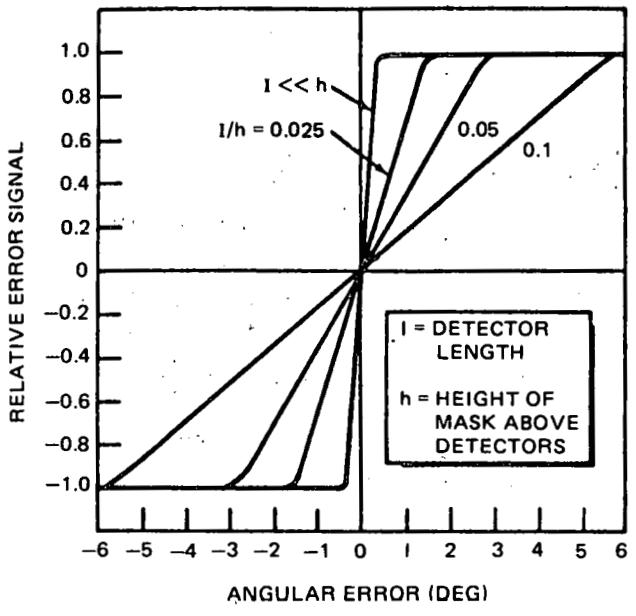

Figure 4-57. Balanced Shadow Sun Sensor Control Characteristics

The linear ranges of the beam error channels (see Figures 4-58 and 4-59) are ± 1.83 deg minimum with a nominal sensitivity of 3.1875 mr/V. The AGC channel provides a valid output over a minimum range of 1.83 deg with a nominal sensitivity of 100 w/m^2/Vdc. The full-scale outputs of the beam error channels and the AGC channel are ± 10 Vdc and -10 Vdc, respectively, when measured at a solar intensity level of 1,000 Watts/m^2. The beam sensor will function with variations in beam intensity between 250 and 1,000 Watts/m^2.

The beam error signals and AGC channel are used to create eight discrete outputs (four per axis) by using voltage comparators as shown in Figure 4-60. The AGC signal is used as the reference voltage (proportional to insolation) for the threshold detectors. Four thresholds will be selected symmetrically about the zero point on the sensor transfer characteristics. One set of thresholds will be selected to yield the required gimbal accuracy. The other set will be located near the full-scale output points and used during beam acquisition.

4.2.7.3 Sensor Pole

The sensor pole (Figure 4-61) is a two-part steel tube designed to support the tracking sensor at a location approximately on a line between the center of the heliostat and the receiver. The vertical column is connected to the variable-length boom by a swage nipple, allowing for height and lateral adjustments.

4.2.8 Field Controller Design/Performance

4.2.8.1 Controls

A trade study was conducted on several open- and closed-loop configurations, weighing their relative field cost as a function of the electronics costs, wiring costs, and the cost for additional heliostats to compensate for power losses caused by heliostat pointing errors.

A digital system using the concept of a field controller commanding a given number of heliostats, which in turn was governed by a master controller, was used as the baseline. The concept of a digital field controller/master

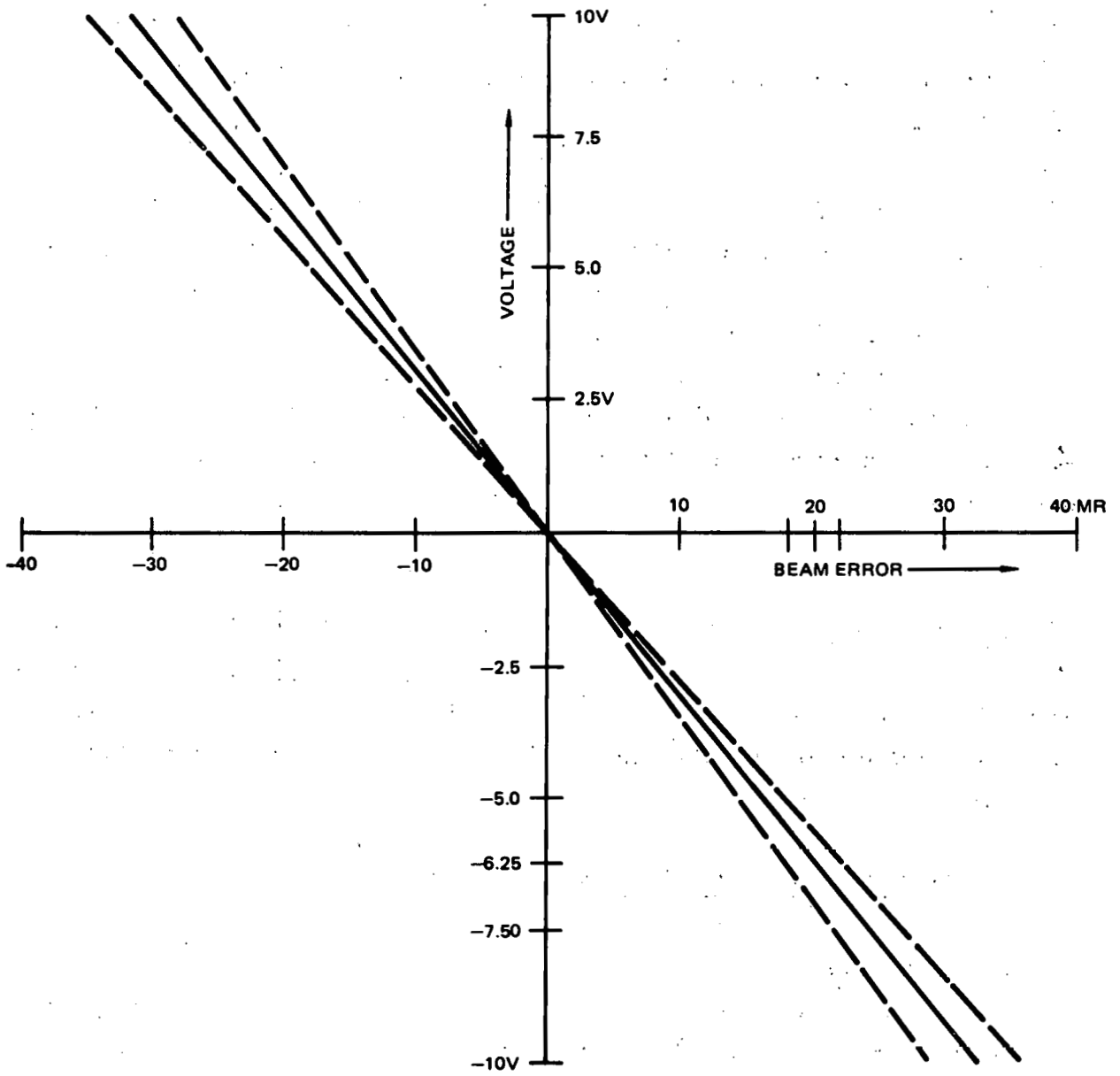

Figure 4-58. Allowable Linearity Error After Solar Intensity Correction

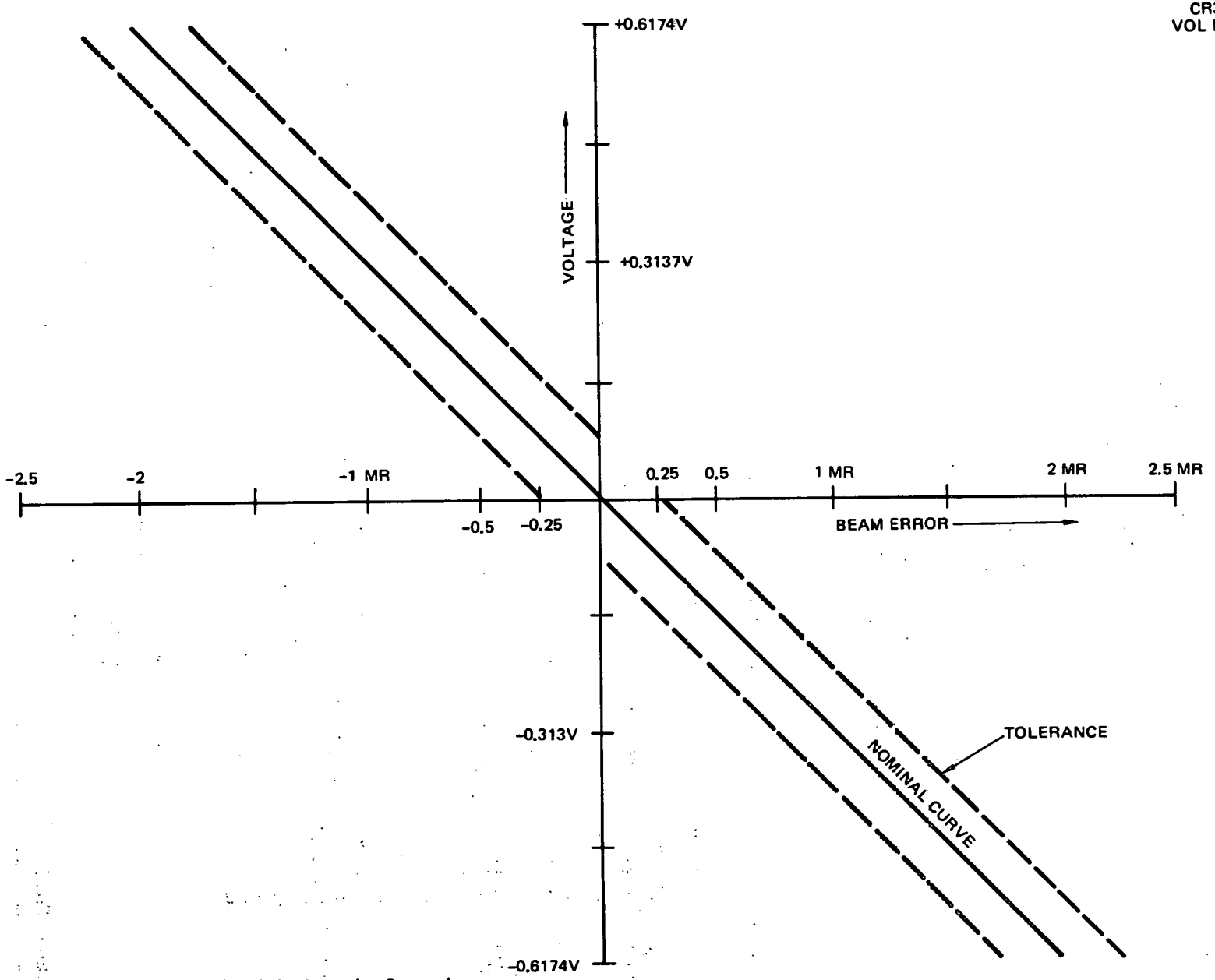

Figure 4-59. Allowable Beam Error After Solar Intensity Correction

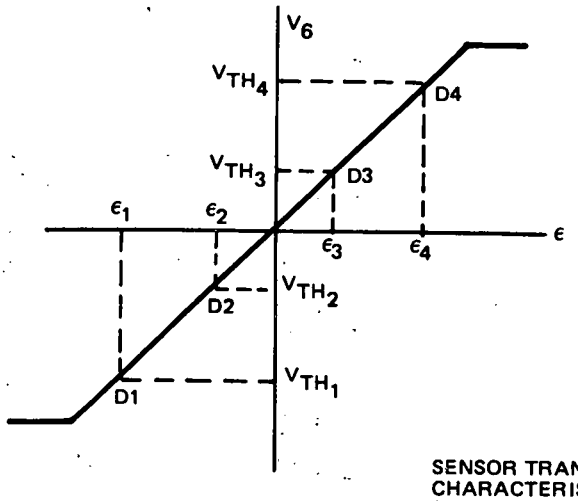

SENSOR TRANSFER
CHARACTERISTICS
(TYPICAL OF EACH AXIS)

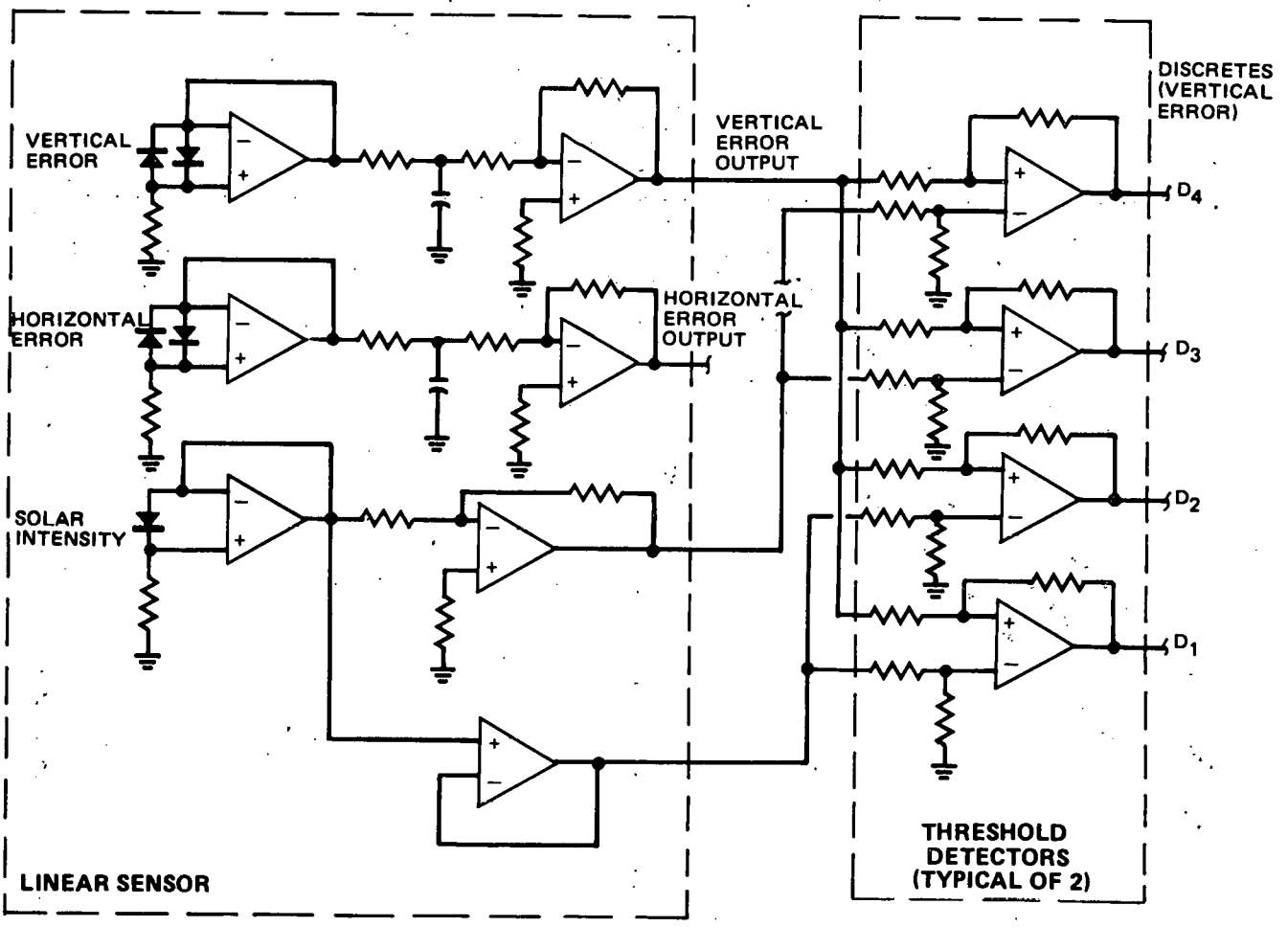

Figure 4-60. Discrete Beam Sensor

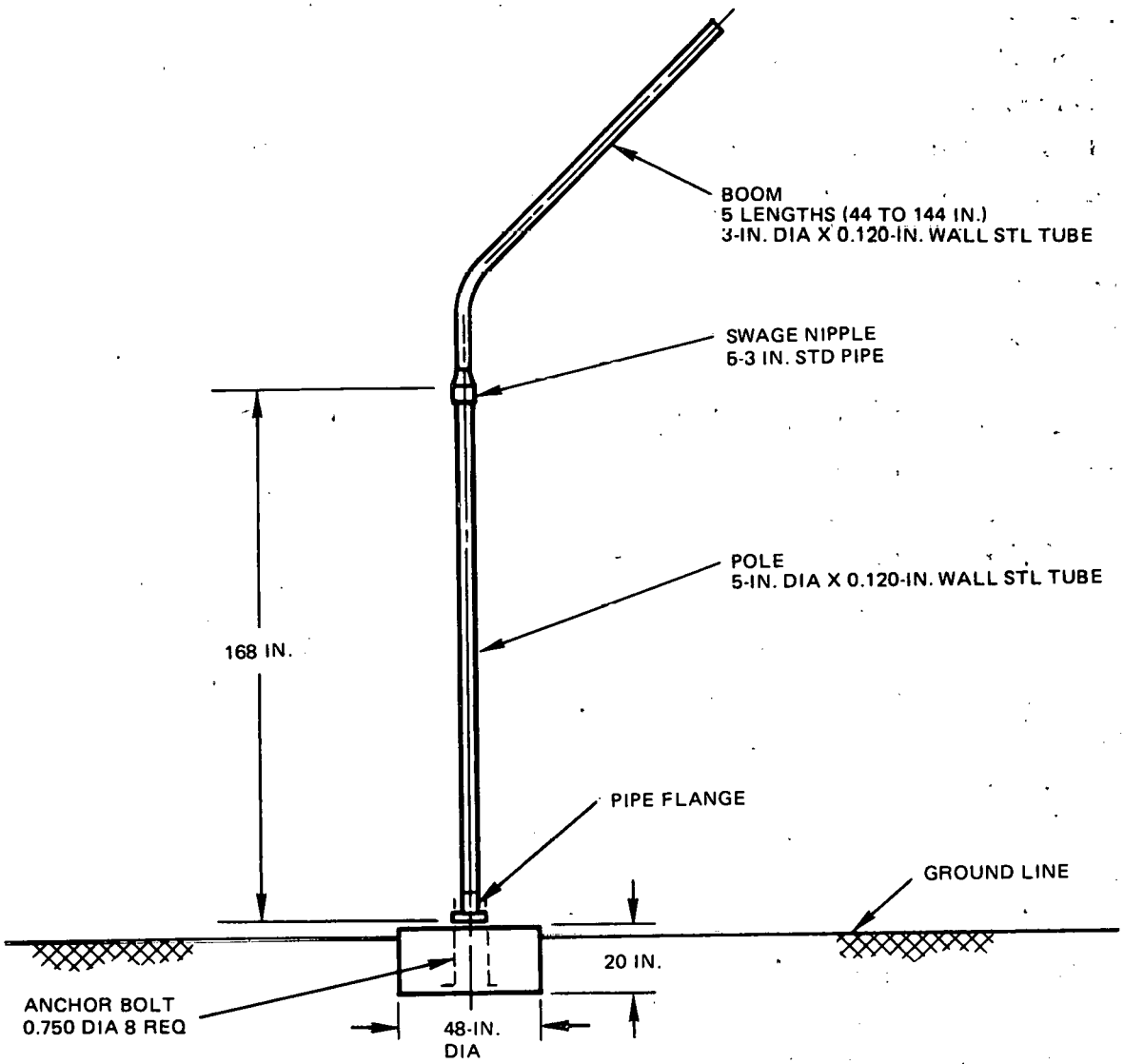

Figure 4-61. Sensor Pole

controller evolved from the trade studies weighing the cost of systems ranging from a completely centralized system to a completely decentralized system. In general, interconnection cost reduction favored decentralization, and electronic hardware cost reduction favored centralization. The reliability of a completely centralized system would suffer unless redundancy was incorporated into the design. Adding redundancy would increase the cost of the centralized system. A study of wire costs per heliostat as a function of field controller cost per heliostat showed that the optimum balance of the two configurations would be one field controller per 24 to 30 heliostats (defined as a cell). The lower limit was selected to reduce the power loss in the event of a field controller failure. The loss of a field controller does not drop the power loss below the minimum specified level.

The field controller uses sample data control techniques to accomplish its three major functions: steering, tracking, and operational monitoring. Periodic self-test routines and performance monitoring can provide fault detection and isolation.

Heliostat control is accomplished by (1) a centralized master controller exercising executive control over the field, providing system interface, and generating steering commands, (2) one decentralized field controller per 24 heliostats providing sample data-type control of each heliostat, (3) the control sensors (beam sensor or position encoders), and (4) associated communication and power grids.

Alternate analog implementations were considered. The major difficulty in analog implementation is determining a cost-effective means of performing coordinate transformation. Analog and digital machine differences are summarized in Table 4-26. In general, analog implementation yielded a less accurate and less flexible system with no appreciable cost savings.

4.2.8.2 Open-Loop Trade

A trade study was conducted on the feasibility of implementing an open-loop heliostat control system. The heliostat electronics cost could be reduced by eliminating the closed-loop beam sensor. However, the tracking inaccuracies, which increase the system power loss, increased the total

Table 4-26

ANALOG AND DIGITAL MACHINE DIFFERENCES

Condition	Analog	Digital
Cost	No significant difference Cost of field position variations not taken into account	
Coordinate transformation	Approximate; hardware differences throughout field unverified	Exact; no differences Digital adaptation of tested system
Self-test	No capability	Inherent capability, requires software only
Flexibility	Hardware modifications	Software modifications
Control	Approximations cause system to vary from overdamped to underdamped	Nearly optimum control possible throughout day
Seasons	Seasonal readjustments may be required	No changes required
Maintainability	Location sensitive; must be adjusted for field position	Module replacement

system cost. The cost increase results from the additional heliostat and accompanying electronics hardware which were added to compensate for the power loss. The other cost factors are the wiring and the electronics hardware at the heliostat and the field controller interface.

Four different configurations with varying degrees of hardware sophistication were examined. The operating mode for all configurations was the same, one field controller controlling 24 heliostats. The basic characteristics of the four configurations are shown in Table 4-27 and Figures 4-62 and 4-63.

The tracking accuracies of Configurations 1, 2, and 4 were discovered to be approximately the same (9.2 mr).* All three configurations indirectly measure angular movement of the gimbal axis knowing the angular movement of the drive input (motor shaft rotation) and the gear ratio (43,000:1) of the drive mechanism. Configuration 2 was judged to be the most acceptable because the added feature of accurately knowing the gimbal position every 22.5 deg through the 4-bit gimbal encoder (absolute encoder).

*See Section 4.2.6

Table 4-27

OPEN-LOOP CONFIGURATIONS

Configuration	Description	Feedback Electronics	Electronics Cost Per Cell ($)	Remarks
1	Stepper motor drive for control	None Required*	14,300	High stepper motor interface cost for desired speed-torque requirements
2	3ϕ motor control through a distributed processor network	(1) 4-bit gimbal encoders (2) 1-bit motor-shaft encoder	8,800	
3	Same as configuration No. 2	13-bit gimbal encoder	23,400	Costly 13-bit gimbal encoder
4	Same as configuration No. 2	1-bit motor shaft encoder*	5,900	

*These configurations have a reference detector indicating a known gimbal position on each axis.

The remaining configuration (No. 3) had a better tracking accuracy, because of the 13-bit gimbal encoder (0.77-mr resolution), but the cost saving from the increase in tracking accuracy could not offset lower system cost of Configuration 2 as shown in Table 4-28 (field size: 1,760 heliostats).

Although a sizable cost saving can be realized in the electronics hardware by the open-loop configuration, this margin is reduced by the cost of the additional heliostats required to compensate for the power loss resulting from tracking inaccuracies. However, for the field size of 1.760 heliostats it appears that a cost saving can be realized using the open-loop system configuration No. 2.

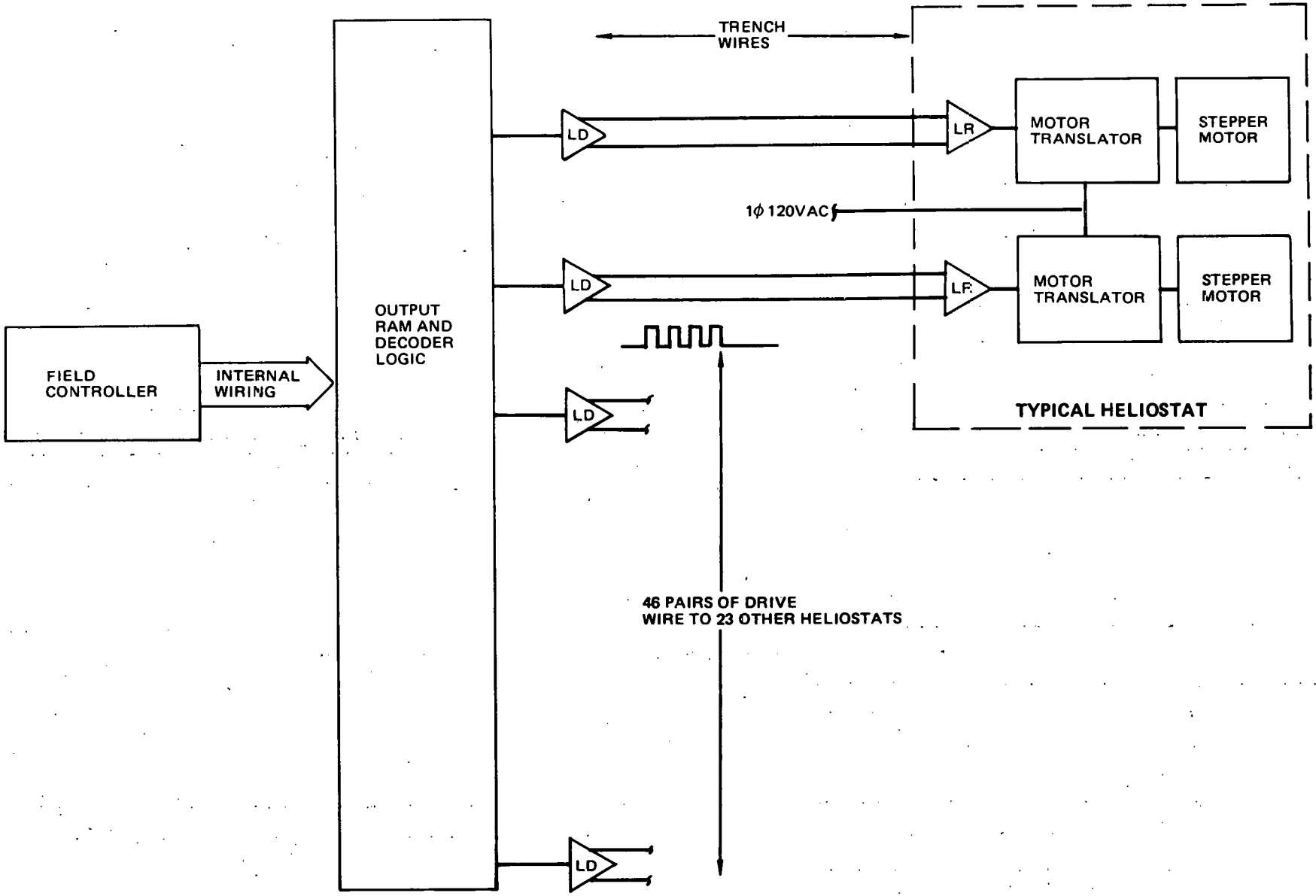

Figure 4-62. Configuration No. 1 System Diagram

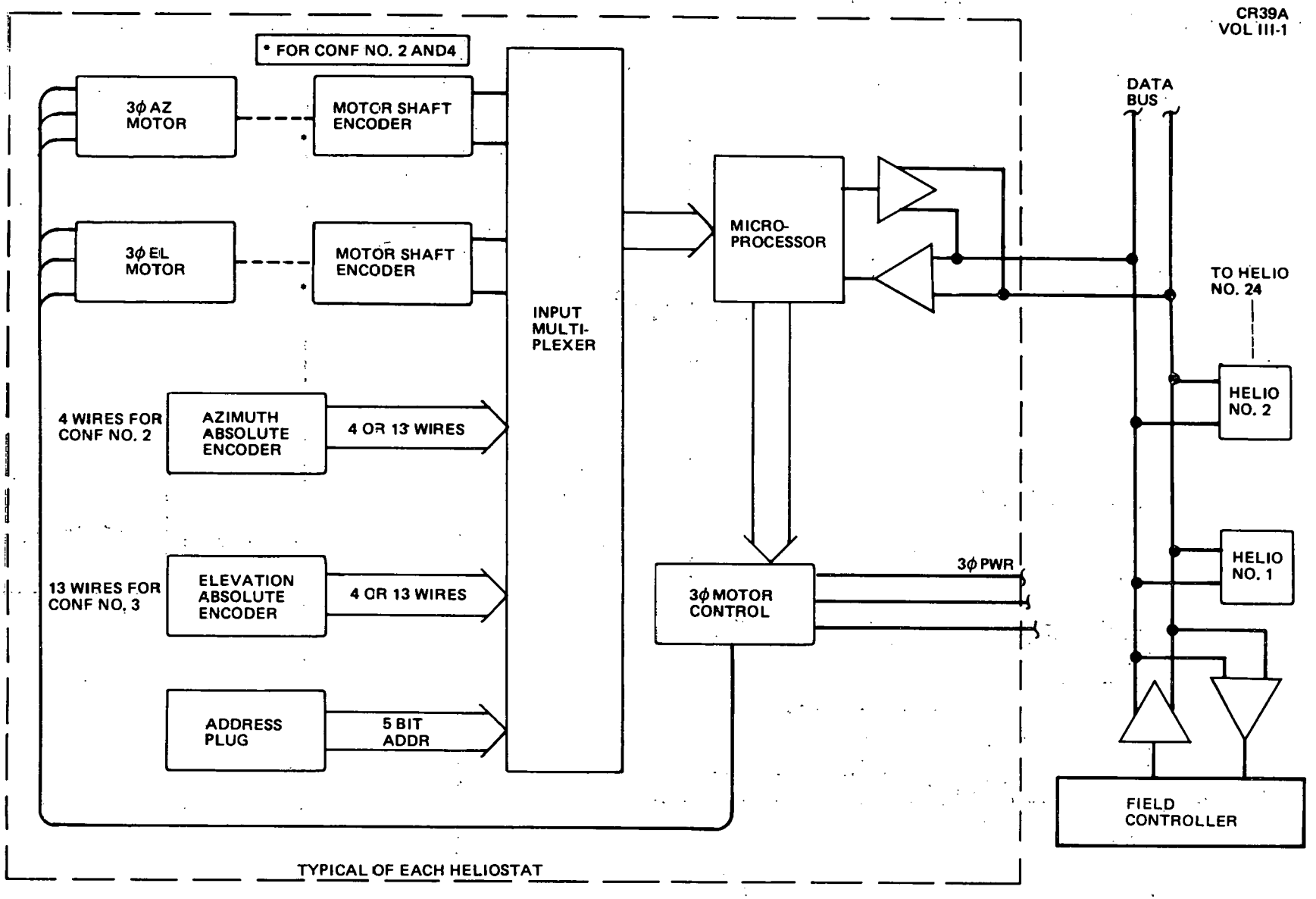

Figure 4-63. Configurations 2, 3, and 4 System Diagram

Table 4-28

RELATIVE FIELD COST COMPARISON

Configuration	Power Loss (%)	Additional Heliostat No.	Heliostat Cost($)	Electronics Cost (1,760 heliostats) Including Wiring ($)	Total($)
2	5.1	64	$592,000	0	592,000
3	2.5	19	188,000	1,196,000	1,384,000
Discrete Beam Sensor*	1.4	0	0	1,163,000	1,371,000

*Closed-loop comparison (total cost includes $208,000 installation cost not applicable to Configurations 2 and 3)

4.2.8.3 Field Controller

The field controller (F/C) serves as a communication link between the master controller (M/C) and the heliostats, provides loop-closure control for the heliostats, control to the heliostat drive motors, and fault detection for the subsystem in both the open- and closed-loop modes of control (see Figure 4-64).

The collector subsystem must be able to operate in several different modes: normal tracking, sun acquisition, normal stowage, severe storm stowage, tracking during intermittent cloud cover, and positioning for cleaning or maintenance. The modes other than normal tracking can all be characterized by gimbal axis position commands. The Master Control determines the gimbal axis positions to be assumed and commands the Field Controller

CR39A
VOL III-1

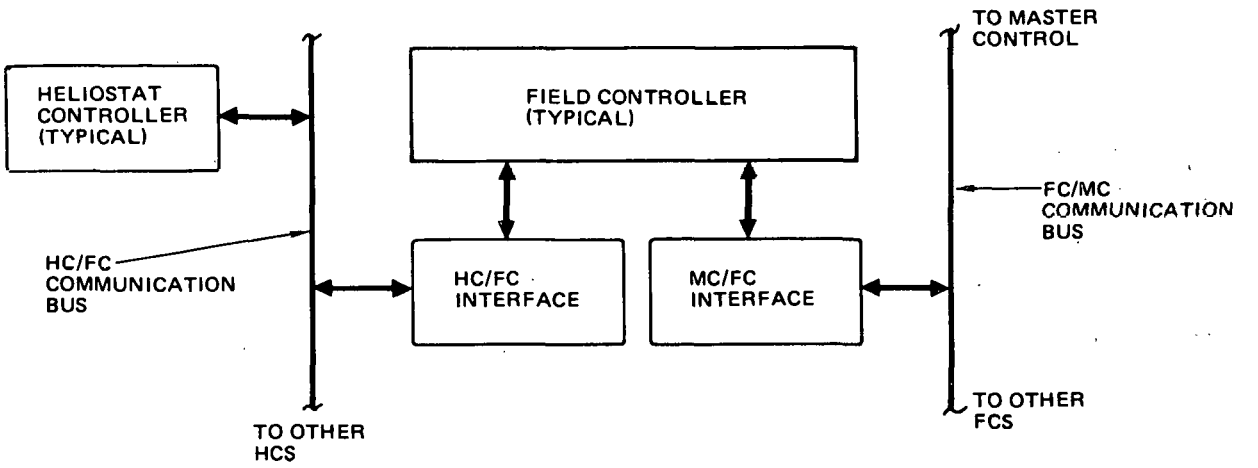

Figure 4-64. Collector Subsystem Interfaces

(via the digital communication link between Master Controller and Field Controller), to these positions. The position sensors on each heliostat provide steering to the correct orientation. During normal tracking, F/C functions autonomously, using error signals from the beam sensor to achieve closed-loop tracking or using the solar ephemeris equations to achieve open-loop tracking.

The operation of the communication system between the F/C and the M/C is similar to that of the F/C and simulated M/C used for SRE (see Section 6.2.8). The same message format can be used for Pilot Plant because it is possible to communicate with 128 F/C, each controlling up to 32 heliostats. Depending upon the communication requirements of the Pilot Plant system, it may be necessary to increase the transmission rate.

4.2.8.4 Interface Definition (Field Controller/Heliostat Controller)
The basic structure of the F/C-H/C interface for either the open-loop or closed-loop configurations is identical.

As in the case of the system configuration study, it was shown that a decentralized cell configuration reduced the interconnection cost but increased the electronics hardware cost. Again, the optimum balance was shown to be a distributed processor configuration.

This configuration (see Figure 4-65) is based upon a low-cost single-chip microprocessor located at each heliostat. The heliostat processors (heliostat controllers) communicate with the F/C through a single pair of wires which help minimize interconnection costs.

The F/C converses with each of the 24 heliostats under its control through the digital party line individually or collectively, depending upon the mode of operation. All conversations are initiated by the field controller. Each heliostat has a unique address such that the F/C can communicate with it without interference from the other heliostats.

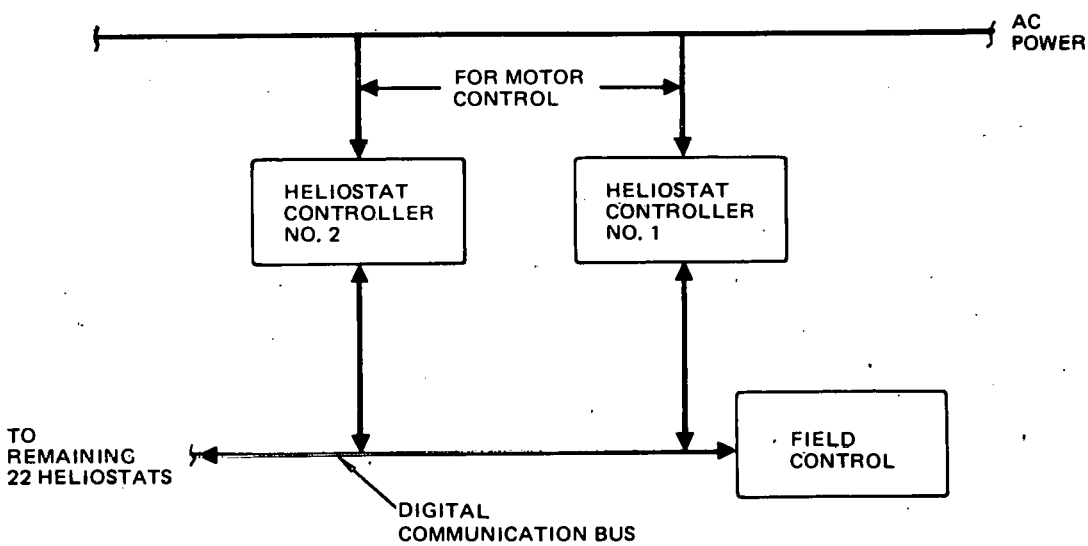

Figure 4-65. Distributed Processor

4.2.8.5 Heliostat Controller

The H/C (processor) controls the power to the motors and gathers the data from the sensors: beam sensor discretes (closed-loop configuration), motor shaft encoders, and drive output encoders (closed- and open-loop configuration). It also serves as a communication link to the field controller through which the heliostat receives its control command.

Distributed Processor Configuration

The distributed processor configuration can be applied to both the closed-loop or open-loop configurations. The hardware structure of the two configurations is nearly the same, differing only in the sensors which interface with the processor as shown in Figure 4-66.

The address plus is unique to each heliostat in the cell and enables the heliostat to recognize when it is being addressed by the F/C over the common communication buss.

The encoder signals are generated at the motor (one pulse per motor revolution) and at the output of the drive mechanism (resolution depends upon the number of encoder bits per revolution). They are used to determine gimbal position.

The H/C is capable of locally controlling the heliostat gimbal motors from instructions issued by the F/C. The motor controller translates the digital commands from the processor into motor switching commands. The mode of control for the motors is proportional bang-bang.

The communication interface is the means through which the F/C communicates with the heliostat controllers. Data exchange is through the serial transmission of a 24-bit message (3 bytes). A digital differential transceiver is used to interface with the communication buss.

Controller Operation

The processor is a single-chip microprocessor with a permanently programmed read-only memory (ROM) designed to perform its intended monitoring and controlling functions. A basic flow diagram of the H/C control program

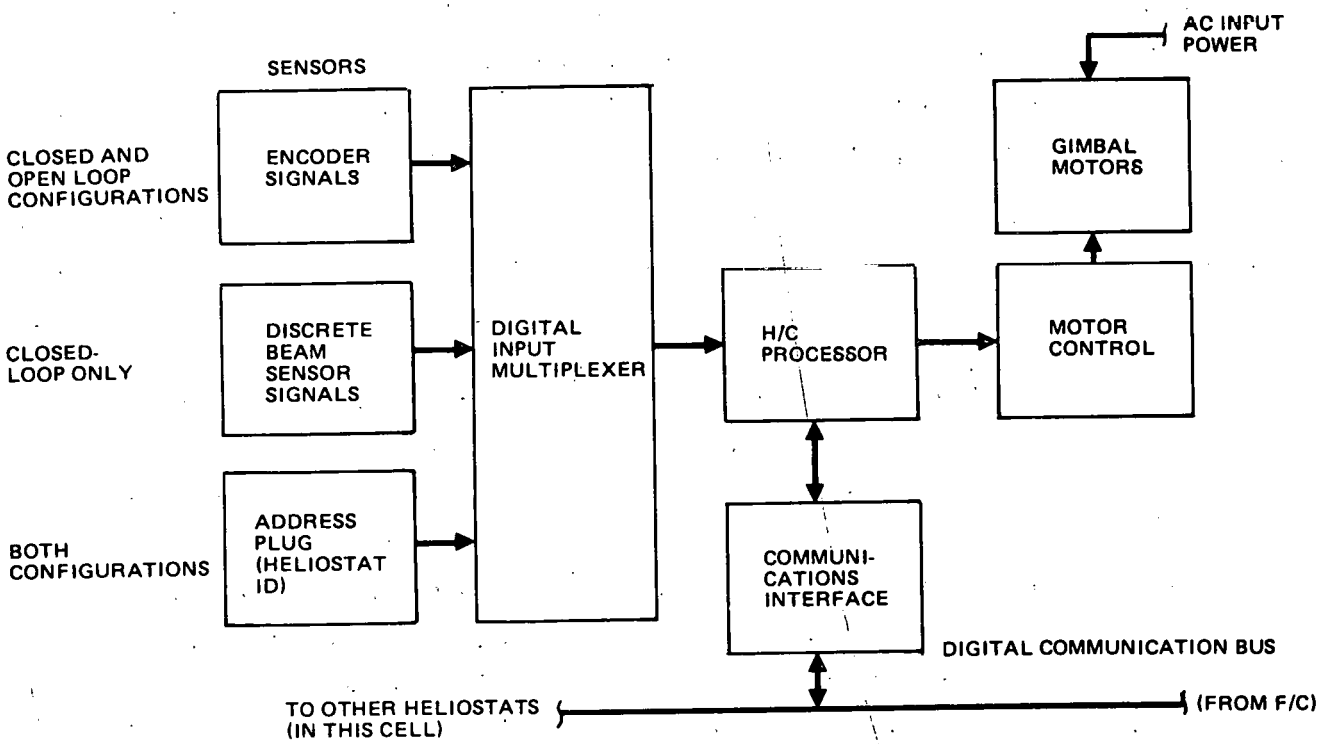

Figure 4-66. Processor Interface Structure

is shown in Figure 4-67. The processor is started by the power turn-on. It then begins the storage registers and reads its address plug such that it can communicate with the F/C.

The processor time is primarily spent gathering data from the sensors until it is pulled away from this routine by a communications interrupt. In the sensor monitoring mode, the processor addresses channel one (see Figure 4-68) of the 8-input multiplexer (i.e., A1, B1 through H1) by placing the channel one address code at Port 1 and executing a RD command. This allows the processor to read the motor encoder data, interrupt flags, and the solar intensity discretes (see Table 4-29 and 4-30 for the channel assignments and channel functions, respectively). Next, it selects Channel 2 of the multiplexer and reads the output encoder data. It continues the process of reading Channels 1 and 2 until an interrupt is received. The processor services the interrupt and returns again to the sensor-monitoring loop.

4.2.8.6 Communications Operation

The communications interrupt is generated by the UART each time a message byte (8-bit data) is received. The byte rate is 880 μsec/byte, including the formatting bits. Each message byte is stored by the H/C until the complete message (3 message bytes) is assembled. The H/C compares the address bits against its own address and responds to the message only if it is being addressed. The response is dependent on the type of command received, data request or command data. For the former case, the requested data is transmitted, and in the latter case, the message received is transmitted back to F/C to acknowledge receipt of the message.

The 3-byte message is arranged in the following order: byte 1 (5-bit address, 3-bit command type); byte 2 (azimuth data), and byte 3 (elevation data). The command codes are defined in Table 4-31.

The motor commands (CMD Code 000) for both the azimuth and elevation motors are formatted such that the most significant bit (MSB) of their respective data bytes contains the motor direction bit and the remaining

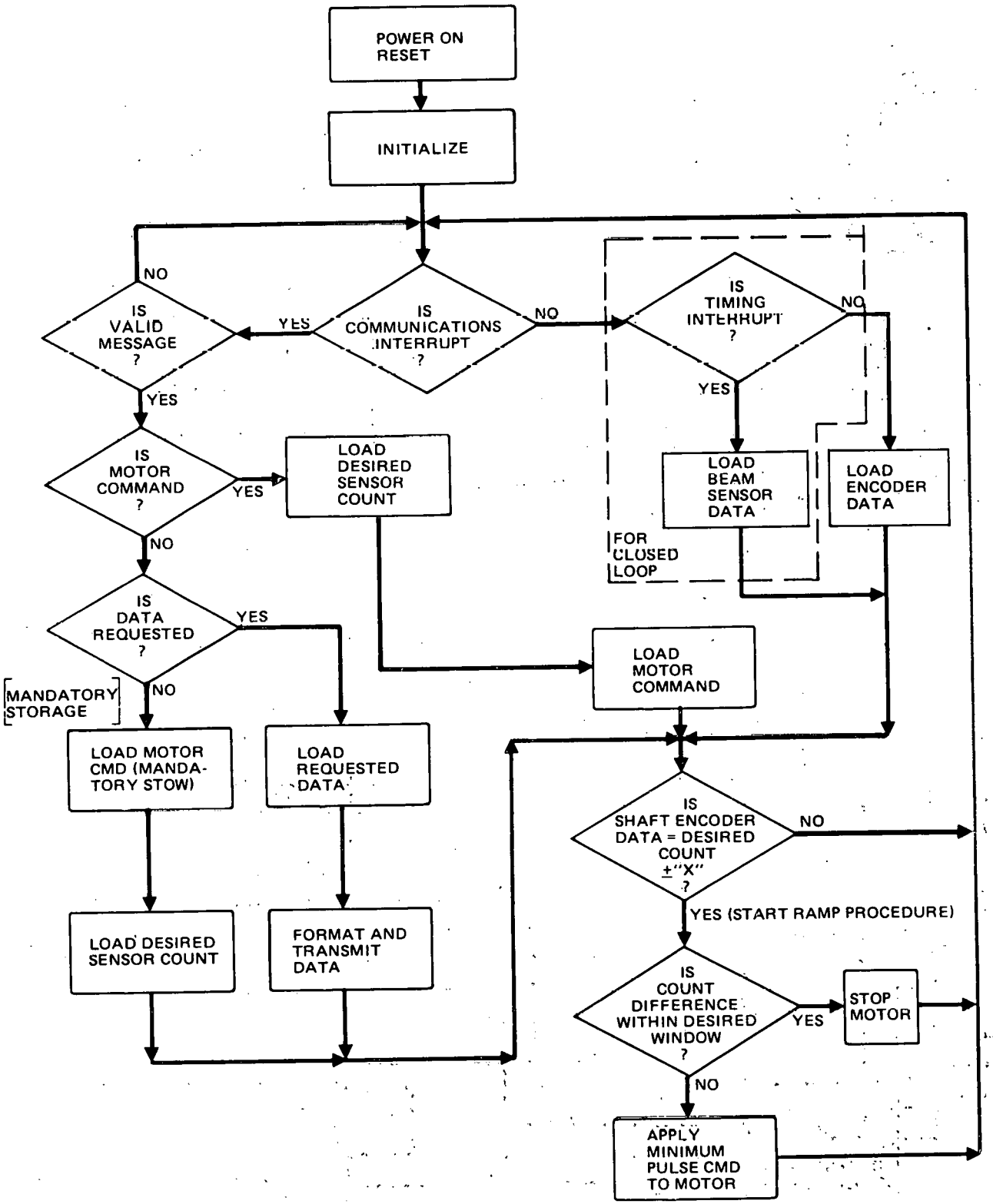

Figure 4-67. H/C Basic Flow Diagram

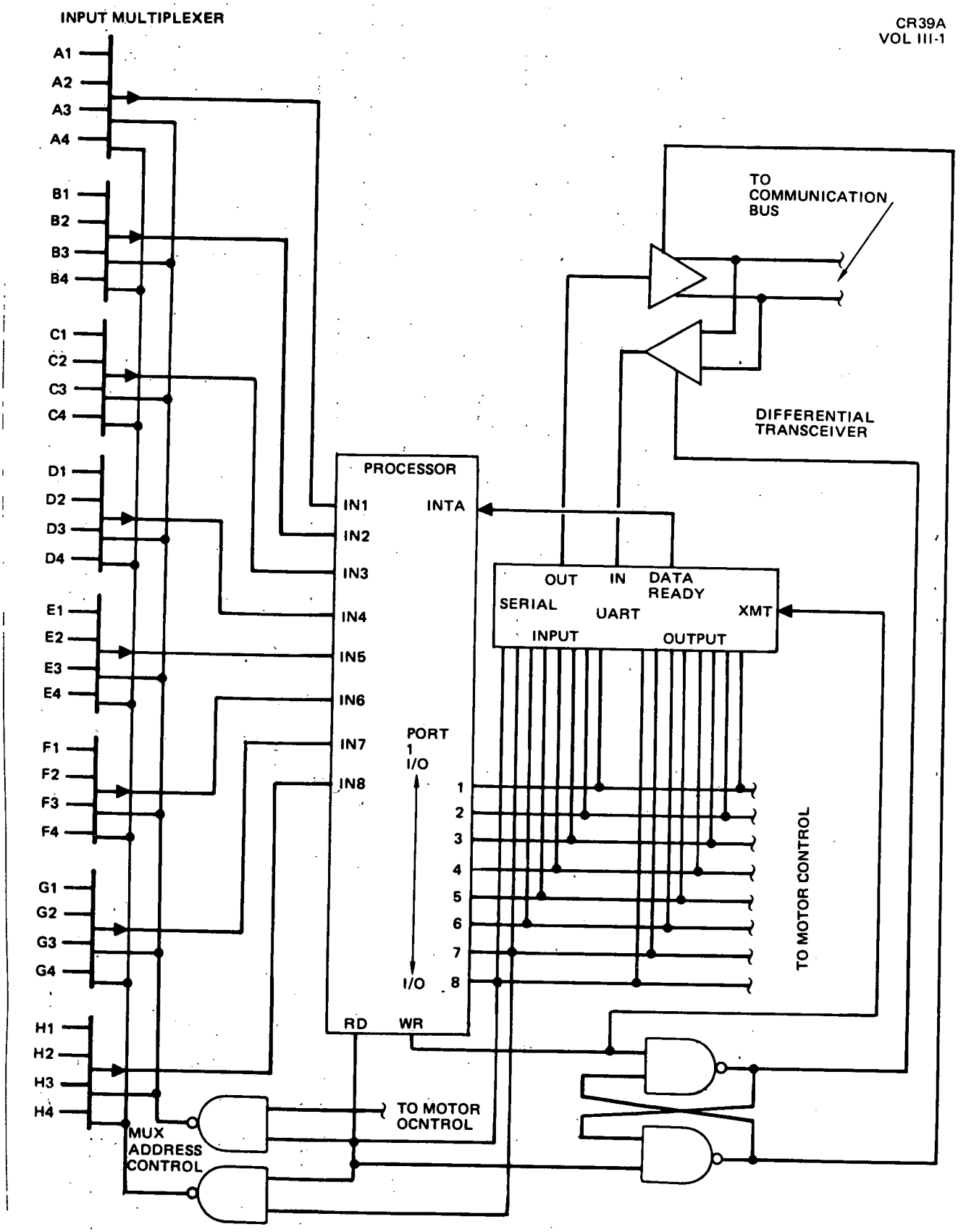

Figure 4-68. Processor and Interface Electronics

Table 4-29

INPUT MUX FUNCTIONS

Mux No. Designation	Mux Input Number 1	2		3	4	
A	Communications Interrupt (INTA)	Az Output Encoder Bit 4	D4		ADR5	
B	Motor Interrupt	Az Output Encoder Bit 3	D3		ADR4	
C	Az CW Encoder Data	Az Output Encoder Bit 2	D2	Beam* Sensor Discretes (Azimuth)	ADR3	Address Bits (H/C ID)
D	Az CCW Encoder Data	Az Output Encoder Bit 1	D1		ADR2	
E	El CW Encoder Data	El Output Encoder Bit 4	D4		ADR1	
F	El CCW Encoder Data	El Output Encoder Bit 3	D3	Beam* Sensor Discretes (Elevation	UART Transmitter Buffer Control	
G	Solar Intensity Discrete*	El Output Encoder Bit 2	D2		UART Transmitter Control	
H	UART Error Flag	El Output Encoder Bit 1	D1		Sine	

*For closed-loop configuration only

Table 4-30

CHANNEL FUNCTIONS

Mux Channel(s)	Description	Function
A1	Communications Interrupt	Flags the processor that data has been received at the data buss terminal.
B1	Motor Interrupt	Flag to indicate Phase B of the 3ϕ power input has crossed the zero voltage level. This data is used to control the duration during which a motor is turned on.
C1 - F1	Motor Encoder Data	Denotes that the motor has turned one revolution and the direction of spin.
G1	Solar Intensity Discrete	Signifies that the solar intensity at the beam sensor is above the acceptable level.
H1	UART Flag	Shows any error flags generated by UART transmission errors.
A2 - D2	Azimuth Output Encoder Bits 1-4	Indicates the horizontal position of the Orbidrive.
E2 - H2	Elevation Output Encoder Bits 1-4	Indicates the vertical position of the Orbidrive.
A3 - D3	Azimuth Beam Sensor Signals (Discretes)	Together with Channel G1, these signals indicate the angular error between the target and reflected beam.
E3 - H3	Elevation Beam Sensor Error Signals (Discretes)	
A4 - E4	Heliostat Address Bits	A 5-bit address code denoting the heliostat identification number.
F4 & G4	UART Transmitter Control	Control signals from UART indicating status of UART transmitter section.

7 bits (128 counts) of each byte contains the desired number of motor revolutions. The direction bit equal to logical one signifies that the azimuth and elevation axes should move clockwise and up, respectively.

The output encoder data request (CMD Code 001) results in the H/C loading the 4-bit absolute encoder data from the azimuth and elevation axes into bytes 2 and 3, respectively.

Table 4-31

COMMAND CODES

Command Code	Command Description	Function
000	Motor Command	Magnitude and direction of motor shaft revolutions
001	Output Encoder Data Request	4-bit azimuth and 4-bit elevation encoder data request
010	Beam Sensor Data Request (Closed-Loop Configuration Only)	4-bit horizontal and 4-bit vertical beam sensor error data and indication of solar intensity
100	Motor Shaft Encoder Data Request Byte 1 (Azimuth and Elevation)	First 8 bits of motor shaft encoder count (least significant byte)
101	Motor Shaft Encoder Data Request Byte 2 (Azimuth and Elevation)	2nd 8 bits of motor shaft encoder count
110	Motor Shaft Encoder Data Request Byte 3 (Azimuth and Elevation)	3rd 8 bits of motor shaft encoder count
111	Motor Shaft Encoder Data Request Byte 4 (Azimuth and Elevation)	4th 8 bits of motor shaft encoder count
011	Spare	

The beam sensor data request (CMD Code 010, which is applicable only to the closed-loop configuration, results in the H/C loading the 4-bit representation of the reflected beam error seen by each axes of the beam sensor into azimuth and elevation bytes. The presence of sufficient solar intensity for tracking is conveyed by a logic one in the MSB of the azimuth byte (the 4 bits of data are LSB justified).

The motor shaft encoder data requests (CMD Codes 100, 101, 110, and 111) are separated into four separate command codes because the total accumulated encoder count over 360 deg of output travel results in the requirement for 24 bits of data and one additional bit to define the direction of travel. The

encoder counts for the azimuth and elevation axes are loaded into bytes 2 and 3, respectively, with the direction bit loaded into the MSBs of the two bytes.

4.2.8.7 Communications Hardware*

A UART transmitter section converts the 8-bit parallel data from the processor interface (F/C or H/C) into an 11-bit serial word. The UART formats the eight data bits by adding a start bit (a flag to indicate the state of the serial work), stop bit (signals end of word) and a parity bit (indicates the correct parity) and transmits the word.

A UART receiver accepts the serial word and converts it into an 8-bit parallel word. The UART raises a ready flag to indicate to the processor that a word has been received. In addition, the UART also checks for parity, overflow, and framing errors which may have occurred during the transmission. A flag is raised if an error is detected.

The data ready flag generated by the UART causes an interrupt in the processor routine. The processor accepts the 8-bit message and stores it into memory. After three such interrupts, the total message has been assembled and the processor interrogates the message unless an error flag was raised by the UART. If the error was detected at the F/C UART, the F/C would repeat the message. If an error flag was detected at the H/C, the H/C would not execute the instruction or send a reply to the F/C. The absence of the reply would cause the F/C to repeat the message. Should the errors detected by the F/C UART or the absence of the replies from the H/C continue, the F/C would report this activity to the master control. Interrogative measures to correct the malfunction would be initiated by the master control.

4.2.8.8 Positioning Operation

The F/C commands the heliostat to a desired position by transmitting motor control signals in the form of the number of motor shaft revolutions required to attain the desired pointing angle.

*This description is applicable to both the F/C and H/C processor interfaces.

For the closed-loop configuration, the discrete error levels from the beam sensor are used to determine the angular error between the reflected beam and the designated target. The coordinate transformation equation for the beam sensor relative to the mirror uses these error signals to compute the angular correction. The motor commands are then determined using the transfer relation between the input (motor shaft revolution) and the output (gimbal movement) of the Orbidrive.

For the open-loop configuration, the motor shaft encoder count represents the change in gimbal position relative to a known gimbal position. The reference positions are determined from the gimbal (output) encoder data. The gimbal position information, solar ephemeris equation, and coordinate transformation determine the angular correction angle. The motor commands can then be determined from the Orbidrive transfer relation.

The 1-bit shaft encoder data (one pulse per motor revolution) and 4-bit output encoder data (bit change every 22.5 deg) from each motor and gimbal axes, respectively, are stored by the processor and transmitted to the field controller upon request. To minimize overshooting the desired position, the processor ramps the motors (software routine to "pulse" the motors to obtain a stepping effect) as the shaft encoder data approached the desired count.

4.2.8.9 Design/Changes from SRE

The basic changes in the F/C hardware from the SRE configuration to the distributed processor configuration (open and closed loop) are the removal of the analog multiplexers and the A/D converter, the 3ϕ motor controller being moved from the F/C and distributed among the individual heliostats, and the initiation of the heliostat processor. These changes resulted in a 10% cost saving in the electronics hardware. The major contributor to the cost reduction was the savings in the wiring costs from the F/C to the individual heliostats.

4.2.9 Heliostat Electrical Design Description

This section describes the design of the electrical/electronic hardware located at a heliostat. Functional operation of the heliostat hardware is discussed in Section 4.2.8.

4.2.9.1 Design Changes From SRE

There have been several significant design changes as a result of the SRE and various trade studies reported herein. The changes have involved the field controller, a heliostat controller, the addition of encoders, and the interconnecting cable network.

During SRE, the motor switching function performed by TRIACS was located in the field controller. Switched power signals were transmitted from a field controller to a number of heliostats, directly to the heliostat motors. The present configuration uses the field controller to control a number of heliostat controllers. The heliostat controllers, one per heliostat, perform the motor switching function; i.e., TRIAC switching. This arrangement reduced the amount of wire in the collector field and therefore had a significant cost-reduction effect on the collector field cable network. The network cost went down by approximately 46%. This arrangement did however add some electronics to a heliostat; the overall cost saving was still approximately 10% when all additional expenses were considered. Section 4.2.10 discusses the collector field network and tradeoffs in detail; Section 4.2.9 discusses H/C and F/C tradeoffs in detail.

In addition to these changes, an encoder has replaced the SRE potentiometers as the heliostat motor feedback element (see Section 4.2.7).

4.2.9.2 Design Descriptions

The heliostat electrical components consist of the following:

- Pedestal electrical J-box (two configurations).
- Azimuth and elevation motors.
- Azimuth and elevation encoders.
- Sensor.
- Motor/encoder cable.
- Sensor cable.
- Lightning ground rod.

A block diagram of their interconnection and physical location at a heliostat is shown in Figure 4-69. The following discusses the key hardware, namely, the pedestal electrical J-box and the heliostat cables. Encoder and sensor

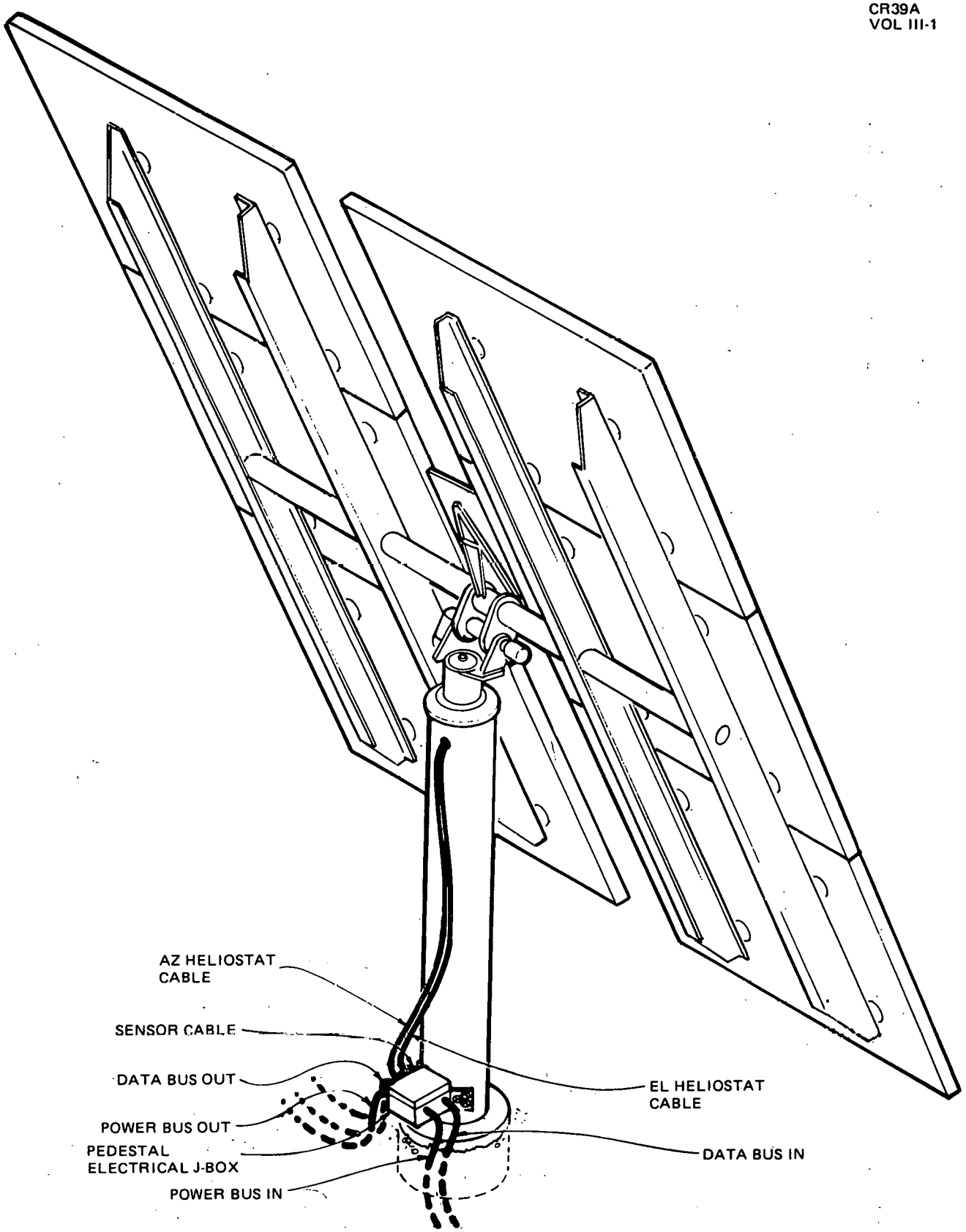

Figure 4-69. Heliostat Electrical Installation

descriptions are in Section 4.2.8. Lightning ground rod considerations are discussed in Section 4.2.10.6.

Pedestal Electrical J-Box

The pedestal electrical J-box is the central termination point for both heliostat receiver and collector field network cables. There are two configurations of the pedestal electrical J-box; one has both a F/C and H/C packaged within it, the other contains only a H/C. There will be approximately 74 of the former version and 1,686 of the latter in the Pilot Plant collector field.

The electrical J-box contains terminal strips to terminate power and data network cables; a circuit breaker to provide overload and fault protection; and a heliostat microprocessor to accept instructions from a field controller, provide feedback information to a field controller, accept feedback information from the heliostat encoders and sensor, and process all information for the purpose of controlling the heliostat motor switching circuits. It also contains triacs to switch motor AC power on and off and a power supply to provide semiconductor, integrated circuit, microprocessor, sensor and encoder DC power. As mentioned previously, every 24th electrical J-box contains a field controller. The electrical J-box is mounted on the heliostat pedestal as shown in Figure 4-69.

Low-risk packaging techniques will be employed in the electrical J-box to meet environmental and service-life requirements. Emphasis has been placed upon low unit cost, low maintenance, and high reliability through judicial component selection and thermal management. The J-box housing will be a NEMA 3 or 3R enclosure for protection against dust, rain, and water. Cable entry will be connectorless with bulkhead seals for cables without armor and appropriate terminators for the armored cables. The J-box cover will be removable. All electronics will be mounted on a removable panel. Figure 4-70 shows the basic layout of the enclosure. The heliostat controller is composed of three printed circuit boards, a multilayer microprocessor, a two-sided triac switching, and a two-sided power supply board. The microprocessor will be in a shielded enclosure to minimize electromagnetic interference problems. The field controller is a multilayer printed circuit board (possibly two boards) which will also be

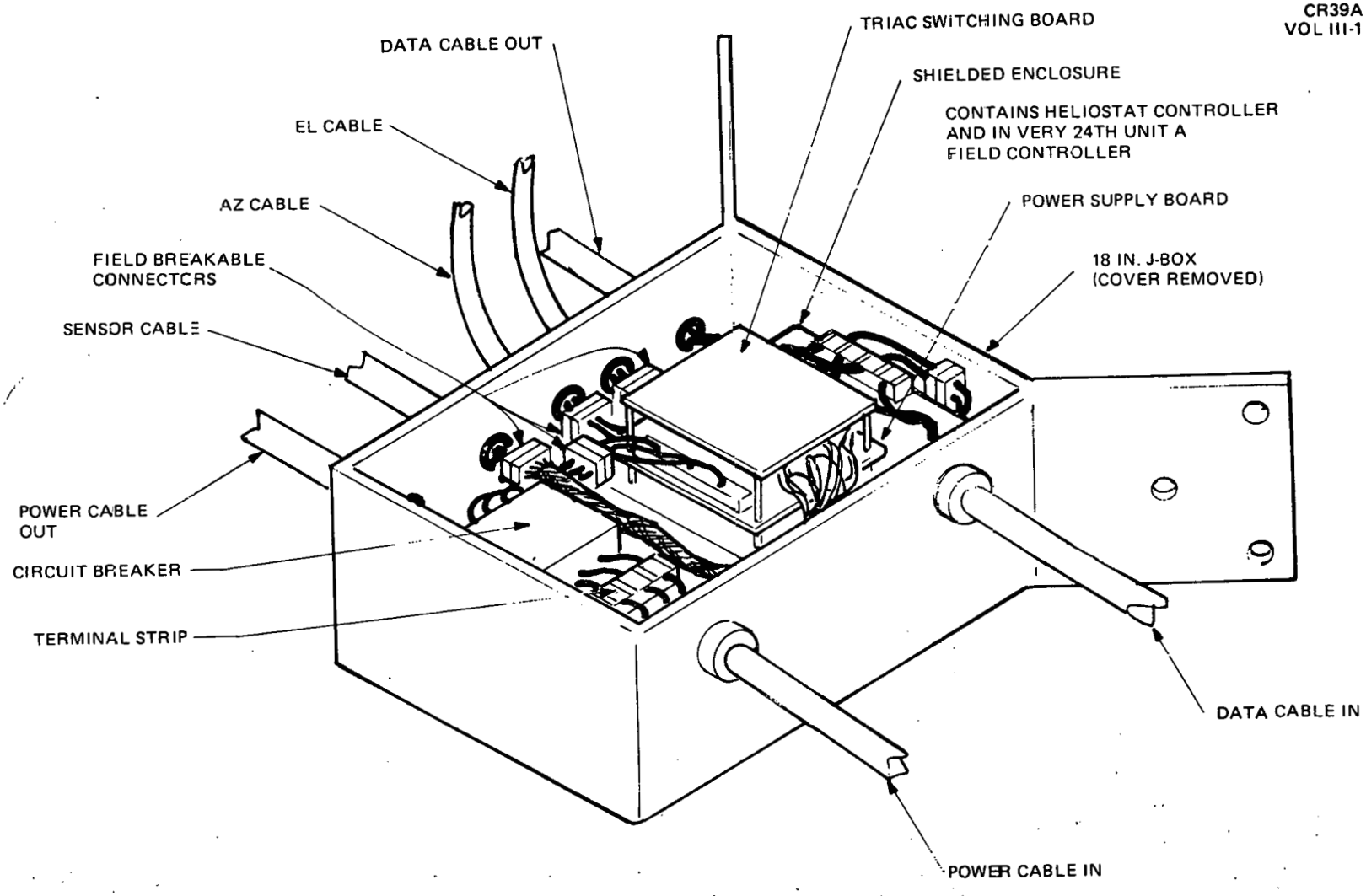

Figure 4-70. Pedestal Electrical J-Box

located in the shielded enclosure. Connectors will be provided as shown in Figure 4-70 to allow for efficient field installation and hookup and to provide a means of interfacing the heliostat with electrical troubleshooting and maintenance equipment (see Section 5.2.2).

No attempt will be made to prevent the enclosure from breathing during daily thermal cycling. To avoid internal moisture buildup over a period of time, as a result of the expected breathing, a screened drain hole or holes will be installed. Clearance between the housing bottom and any electronics will be provided to avoid moisture contamination. Natural convective cooling is planned which has the advantages of long-maintenance-free life, low cost, no moisture or dust contamination, no filtering, and no part replacement requirements.

Heliostat Cables

There are three heliostat cables for sensor, motor, and encoder operation. They will be simple cables without armor with a sun-resistant PVC or neoprene jacket. The azimuth and elevation motor encoder cable will contain 4 No. 20 AWG and 10 No. 22 conductors. The sensor cable will contain 12 No. 20 AWG conductors. A rigid conduit at grade level will be used for the sensor cable run from the sensor pole to the heliostat pedestal. Connectors will be used at cable terminations in the electrical J-box. The connectors will be of the low-cost, environment-proof, field-servicable, and one-piece molded body type. Power to a heliostat and data exchange between heliostat, field controller, and master control, are encompassed by the collector field network (see Section 4.2.10).

4.2.10 Collector Field Interconnecting Cable Network

The collector field interconnecting cable network provides the electrical command, control, communication, and power link between the central receiver area of the site and the distributed heliostats and field controllers. This network presented some unique engineering problems resultant from the large land area associated with the collector field installation and the large number of hardware items to be interconnected. The network is subdivided into two sections: a power-distribution network and a data-distribution network. The power network provides 240V 60 Hz AC power to

each heliostat for drive motor operation. The data network contains the command, control, and communication functions.

4.2.10.1 Power-Distribution Network

The power-distribution network provides 240V 60 Hz power to heliostat drive motors. Each motor draws about 1.1 amps per phase under slewing conditions. When all 1,760 heliostats are simultaneously slewed, the power distribution network is approximately 4,000 amps. This load has been used to size the power-distribution network. To deliver this current in a cost-effective manner, several key variables which influence the distribution network were investigated. Among them were: wire gage, transmission voltage, allowable voltage drop, wire layout, cable design, and installation technique.

Wire gage, transmission voltage, and voltage drop are variables which must be treated together because they are dependent upon each other. Some practical limits were placed on these variables; however, in order to keep the situation manageable. Wire gage was limited to 750 MCM, and transmission voltage was limited to 5,000V. The gage and voltage limitations are largely due to an effort to minimize installation, handling, and safety problems. Above 750, MCM cables are difficult to handle and operations above 5,000V introduce additional hazards due to the high voltage which should be avoided unless mandatory. Voltage drop limits between 2 and 10% were considered with 2% used for cost-comparison purposes. With these groundrules, several ways of distributing power were investigated, from a 240V transmission system directly from the power plant to heliostats and field controllers to a high-voltage transmission system with transformers at each location where 240V is required. A 240V transmission system would require large gages to satisfy current requirements within line drop limits and also reach distant points in the collector field. In addition to the expense of large cable, it became apparent that single cables could not handle the load and redundant long cable runs to the same general location would be needed. This concept quickly became unreasonable. A network which transmits at a higher voltage and then steps this voltage down where it is needed makes more sense. Increasing voltage allows a smaller wire gage to be used which in turn reduces unit cost of the cable plus installation

and handling costs. Surveys of 480V, 600V, and 2,400V networks showed the 2,400V transmission network to be the most cost-effective. It was more than half the cost of the equivalent network operating at 240V. It is conceivable that one could go to 5,000V, but with the present loads and line lengths, the advantages would be minimal, if any. The 2,400V portion of the power distribution network which will be designated as the primary feeder will originate at the central power plant and terminate at 225 kVA transformers. Eight primary feeders are planned for the collector field. The transformer secondaries will be 240V and another power distribution network, secondary feeders, will distribute power to the 74 groups of 24 heliostats each. Figure 4-71 shows this network in block diagram form. The primary feeders will be four conductors, No. 4 AWG, rated at 5,000V; the secondary feeders will be four conductors, No. 4 AWG, rated at 600V. A distribution panel will be located at each transformer location to provide a disconnecting means for the secondary feeders and to provide secondary feeder overcurrent protection.

The final distribution of power is the distribution of 240 VAC among a group of 24 heliostats. This distribution scheme is dependent upon several issues, the most important being the physical location of motor power switching. Two basic motor switching concepts were considered: (1) route 240V power and perform switching (triac operation) in the field controller (as in SRE) and then distribute the switched power to designated heliostats, (2) route 240V power to all heliostats and perform switching function at each individual heliostat. In the latter concept, a 240V bus as shown in Figure 4-72 distributes power to field controllers and heliostats. TRIACS for switching purposes are located at each heliostat. This concept uses the minimum quantity of wire. In the former concept, since switching occurs in the field controller, individual cables from the field controller to each heliostat are required for distribution (see Figure 4-72B). This concept uses the maximum quantity of wire and cable. For a cell which consists of one F/C and 24 heliostats, the bus concept uses less than one-half as much total length of cable as the other concept; in addition, it takes a cable with one-third the number of wires for the bus concept. In fairness, the bus cable uses wire of larger gage since it feeds 24 units as opposed to one unit (No. 4 vs No. 12 AWG). The bottom line, however, shows the field controller/heliostat network cost for the bus concept, for a 24-heliostat cell, saves about 40%. As

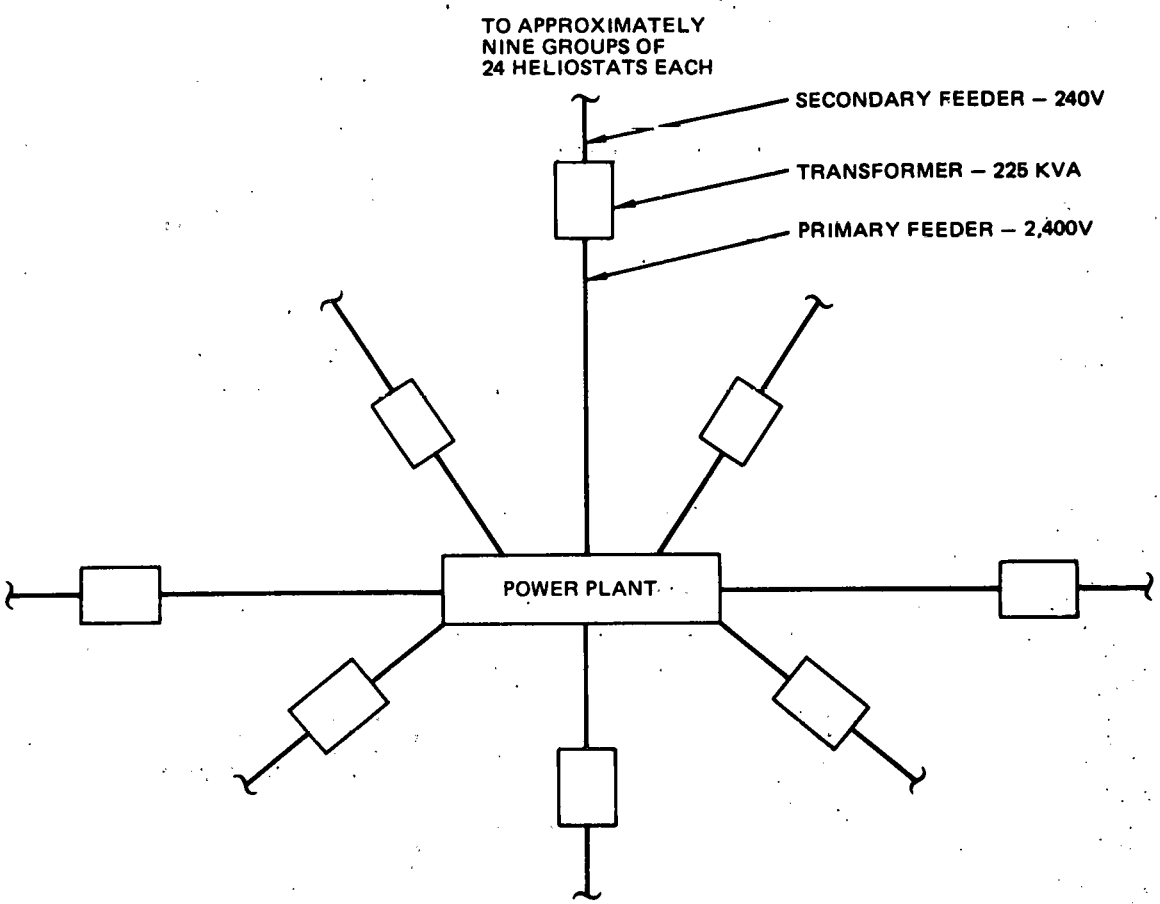

Figure 4-71. Power Distribution Network

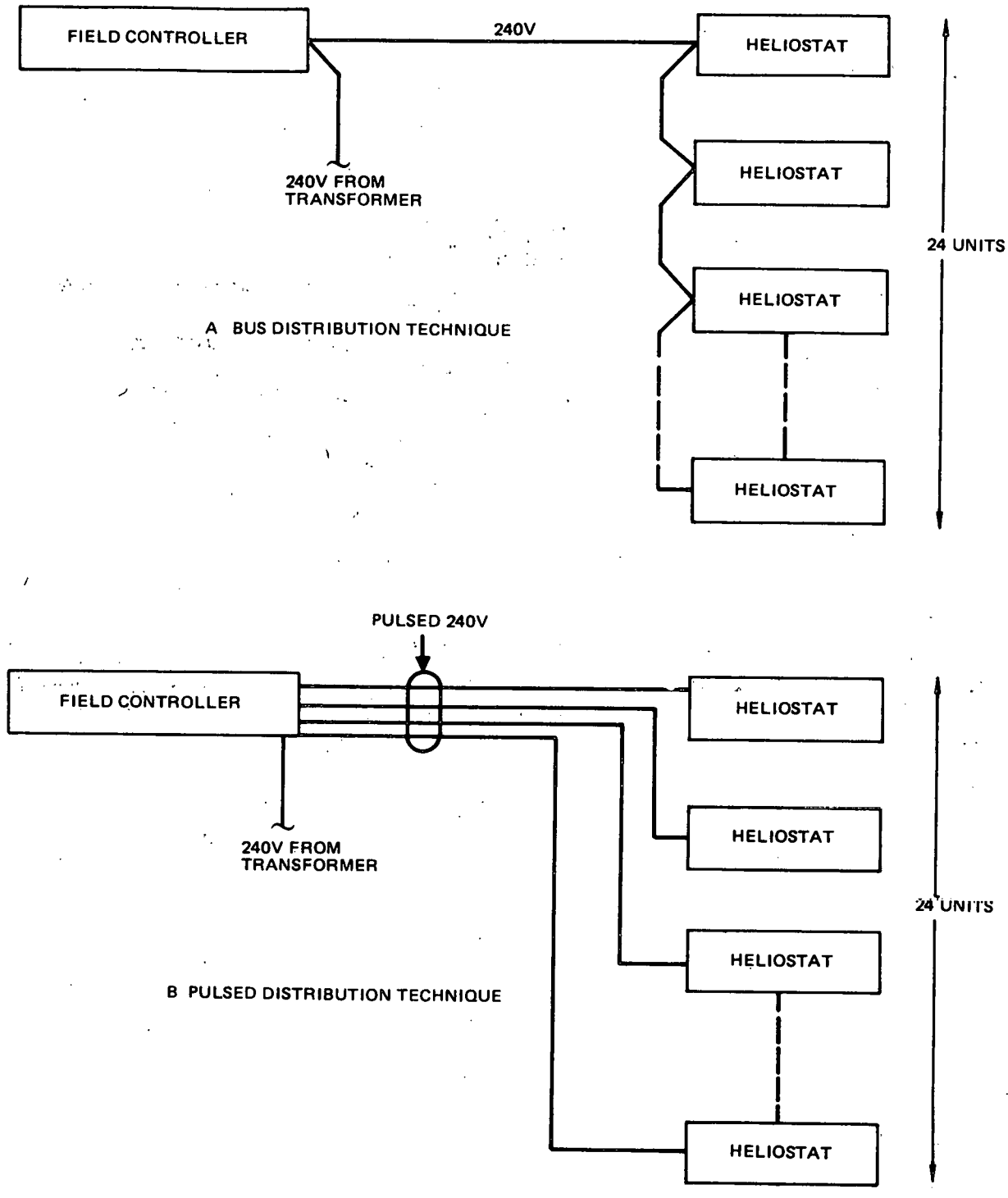

Figure 4-72. Field Controller to Heliostat Distribution Techniques

the number of heliostats in a cell increases, the bus concept becomes even more advantageous. Figure 4-73 shows the relative cost of the pulsed 240V AC distribution network normalized to the cost of a bus concept, as a function of the number of heliostats in a cell.

4.2.10.2 Data Distribution Network

The data distribution network provides for communication, command, and control between the central computer and the field controllers and between field controllers and heliostats. The central computer to FC network will be a 2-conductor bustype network. The F/C to heliostat network on the other hand can be either a digital (2-wire bus) or an analog-type network. The latter uses more wires, as many as 14, and also requires point-to-point distribution; i.e., one unique cable from each heliostat to its field controller. Figure 4-74 shows the relative costs of the analog vs the digital configuration. The data network is a low-voltage low-current system; therefore, wire gage, voltage drop, and line length are not critical considerations. Electromagnetic interference is an important consideration; however, the effects of heliostat motor switching noise and other electrical noise generators on and around the site must be minimized. The data network cabled will use twisted shielded pairs to accomplish this objective.

4.2.10.3 Network Cable Construction

Selection of network cables involved the assessment of numerous variables associated with cable construction; i.e., conductor insulation, jacket type, armor, no armor, etc. Information had to be evaluated relative to direct burial, cable tray, conduit, and above-ground installation as well as rodent protection, code acceptability, environmental protection, installation and handling, and cost. A substantial effort was made to survey the market place, consult with suppliers, and make a cost-effective choice.

An attempt was made to identify a first-class cable type and a marginally acceptable cable type; then compare costs. An example of a first-class cable type for the collector field application is the Okonite type C-L-X cable (Figure 4-75). The cable has a continuous corrugated aluminum sheath which provides maximum moisture and mechanical and rodent protection while avoiding the cost of installation of a metallic conduit system and pulling

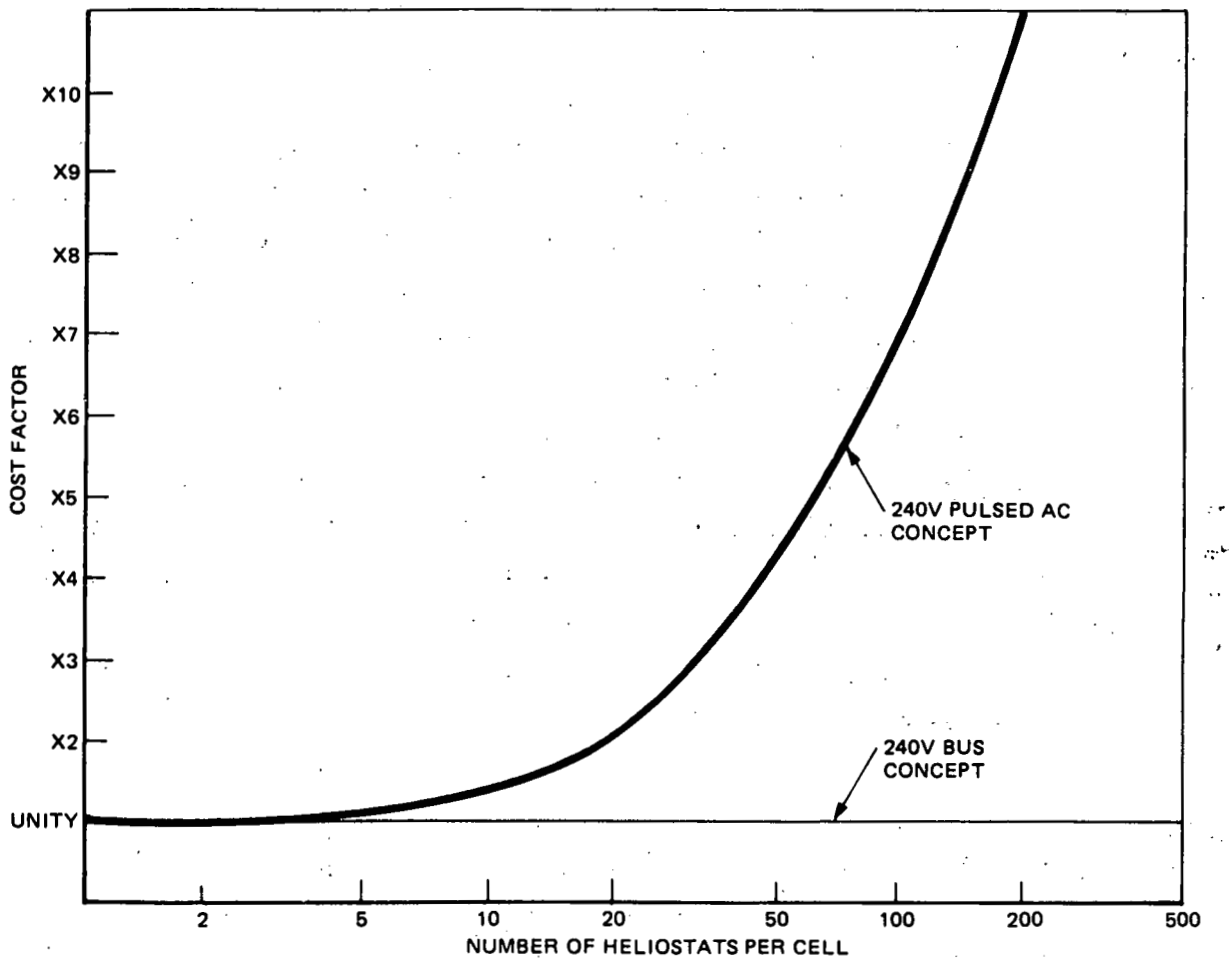

Figure 4-73. Field Controller to Heliostat Power Distribution Costs

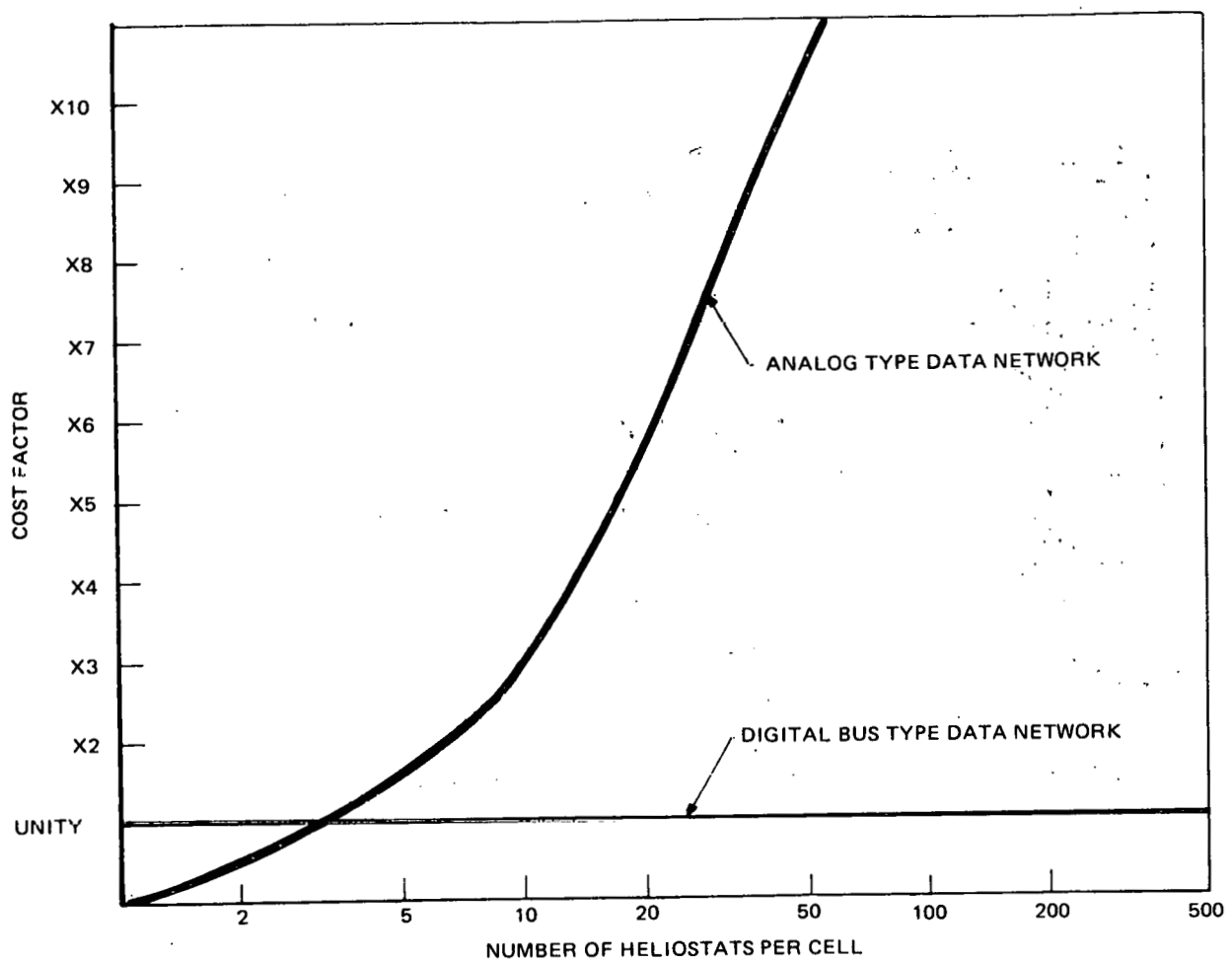

Figure 4-74. Field Controller to Heliostat Data Distribution Costs

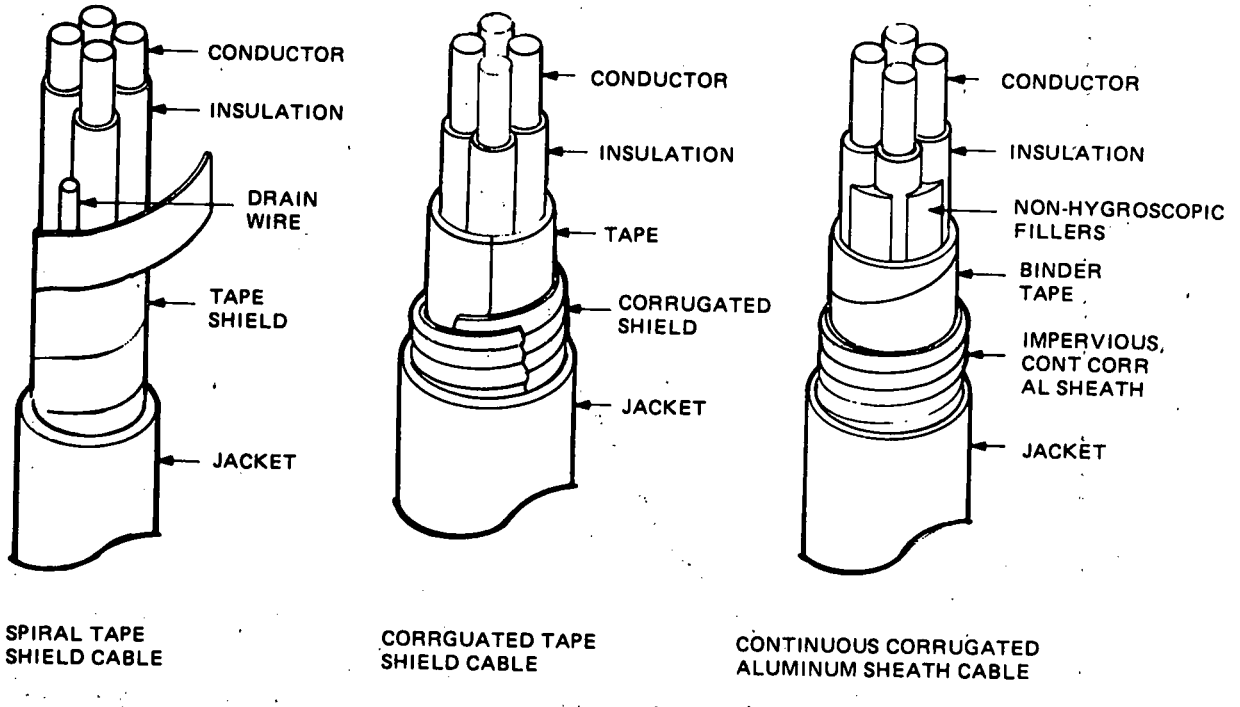

Figure 4-75. Cable Constructions

cable. It is recommended by the manufacturer for both exposed and direct burial application; it is constructed to the typical industry standards (UL, NEC, IPCEA, NEMA), and its aluminum sheath provides some shielding protection. The conductors are insulated with thermoset cross-linked polyethylene.

For comparison purposes, a cable without armor, with sun-resistant PVC outer jacket (neoprene would be better), and with thermoplastic polyethylene (not as good as cross-link) insulated conductors was investigated. This cable was expected to be substantially less expensive than the continuous aluminum sheath cable. As it turned out, it was only 13% less expensive. A step above this non-armored cable was a cable with a corrugated sheath that is not continuous (see Figure 4-75). This cable is more expensive than the continuous sheath cable by 20%. The traditional shielded cable with a spiral tape (see Figure 4-75), is more expensive yet. Neoprene jacket would add even more. The suppliers explain that reduced manufacturing processes account for the cost advantage for the continuous aluminum sheath cable.

Cables of the continuous corrugated aluminum sheath type are planned for use in the collector field. These cables are cost-effective and acceptable for direct burial, and are flexible, mechanically tough, and rodent proof. They provided some EMI protection and, in addition, the aluminum sheath may be used as the grounding conductor (equipment ground or green wire) providing for inherent grounding safety.

4.2.10.4 Network Installation Technique

The cost of installation of the collector field network has been a key concern during this design definition activity. A cursory look at installation costs showed they could be several times the cost of the cable material alone. The alternatives considered were: direct burial, buried conduit, concrete trench, above ground in metal cable tray, above ground in fiberglass cable tray, and above ground with no cable tray.

Direct burial is the least expensive of the buried approaches. It is the least acceptable technique, however, from a maintainability and accessibility point

of view. Experience during SRE wherein cable accessibility has not been required; the relatively low operating voltage of the network and the restricted access nature of the collector field somewhat counterbalance the usual maintainability/accessibility arguments against direct burial. The preferred practice for burying cables directly in the ground usually includes laying the cable in a bed of soft sand or stone-free earth plus some kind of mechanical protection like galvanized wire fencing or redwood planks above the cable. The need for these precautions can be reduced or possibly eliminated with an attendent cost saving by consideration of the rugged continuous metallic sheath cable discussed in Section 4.2.10.3.

Buried conduit is a common installation technique. It involves essentially the same costs as the direct burial installation; i.e., excavation and back-fill, plus the additional costs of the conduit, its installation, and pulling of the cable. A cable of lower quality may be used in this installation but the saving in cable costs is outweighed by added conduit costs. This technique also suffers from the same maintainability and accessibility problems as direct burial.

Concrete trench is an attractive installation technique. It is unusually appropriate from maintainability and accessibility considerations. It is typically precast and buried flush at grade level with removable covers made of concrete or wood. Cables can be easily laid in the trench; no cable pulling is required. They key disadvantage of the concrete trench is cost; it is an order of magnitude more expensive than rigid conduit, for instance. In a small, localized situation, this cost penalty may be small compared to other system costs, and the cost advantages for access may be substantial over the system lifetime. The collector field network requires approximately 100,000 ft of trench. To use precast or poured-in-place concrete trench, even in small widths of 9 in. to 18 in., involves large cost penalties relative to other installation methods, i.e., it is not cost-effective.

All above-ground network installations are less attractive than buried installations in three key areas: safety, convenience, and esthetics. The very fact of having something laying on the ground creates at the very least a situation where someone can fall or somehow cause cable damage (like

driving over a cable), thus creating a safety hazard. Cables laying on the ground, whether in cable trays or not, limit the vehicular accessibility in the collector field and in general produce an inconvenience. Lastly, an above-ground network will cause the collector field to look cluttered, especially without the use of some kind of cable organizer like a tray. Open cable trays, closed cable trays, ladder-type trays, solid-type trays, and fiberglass trays were investigated. In general, cable tray material cost (6 in. wide) is about twice the cost of excavation and backfill for direct burial. Cable installation in the tray is no more expensive than cable installation in a trench; the tray installation itself is an added expense.

Direct burial is the preferred technique for installation of the collector field network. Table 4-32 summarizes the various techniques investigated and their relative cost impact.

4.2.10.5 Network Layout

As a result of the trade studies discussed in the preceding paragraphs, a tentative network definition has been created for the collector field. This definition uses a minimum number and length of conductors. A bus-type wiring scheme has been adopted for both power and data with all cables buried directly and all cables of the rugged continuous aluminum sheath type.

The layout of the cable network for the collector field is shown in block diagram form in Figure 4-76. Indicated cable lengths are the total lengths required to interconnect the entire field. Heliostat cables, sensor, motor and encoder are discussed in Section 4.2.9. It has been assumed here that one field controller interfaces with 24 heliostats; it should be noted, however, that this has little effect upon the total wire lengths.

The Pilot Plant network will require 74 branches to cover the collector field. One of these branches is shown in Figure 4-77 in block diagram form and in Figure 4-78 superimposed on the site plan.

4.2.10.6 Lightning Considerations

The Barstow area is not an area of high lightning activity; however, the probability of a lightning strike to the receiver tower and to the collector

Table 4-32

CABLE INSTALLATION TECHNIQUE COMPARISONS

Cable Installation Technique	Relative Installed Cost ($/ft)	Comments
On Surface of Ground	Unity	Cluttered Appearance, Unprotected Cable, Safety Hazard
Above Ground Metal Cable Tray		
Ladder-Type 6 in. Wide, No Cover	x 6.1	Somewhat Cluttered Appearance, Possible Safety Hazard
Ladder-Type 6 in. Wide, Covered	x 8.6	Somewhat Cluttered Appearance, Possible Safety Hazard
Oil-Tight 6 in. Wide	x 24	Somewhat Cluttered Appearance, Possible Safety Hazard
Above-Ground Fiberglass Cable Tray	x 36	Somewhat Cluttered Appearance, Possible Safety Hazard
Precast Concrete Trench, Buried to Grade Level with Concrete Cover	x 25	Very Neat Appearance, Good Accessibility, Easy Installation
Buried Conduit	x 10	Requires Pulling Wire
Direct Burial		
Minimum Care in Backfill	x 4.7	Recommended Technique
Maximum Care in Backfill	x 8	Not Required with Rugged Continuous AL Sheath Cable

field has been estimated. Assuming that a lightning strike occurs, various traditional protection schemes have been investigated for their applicability to the collector field installation.

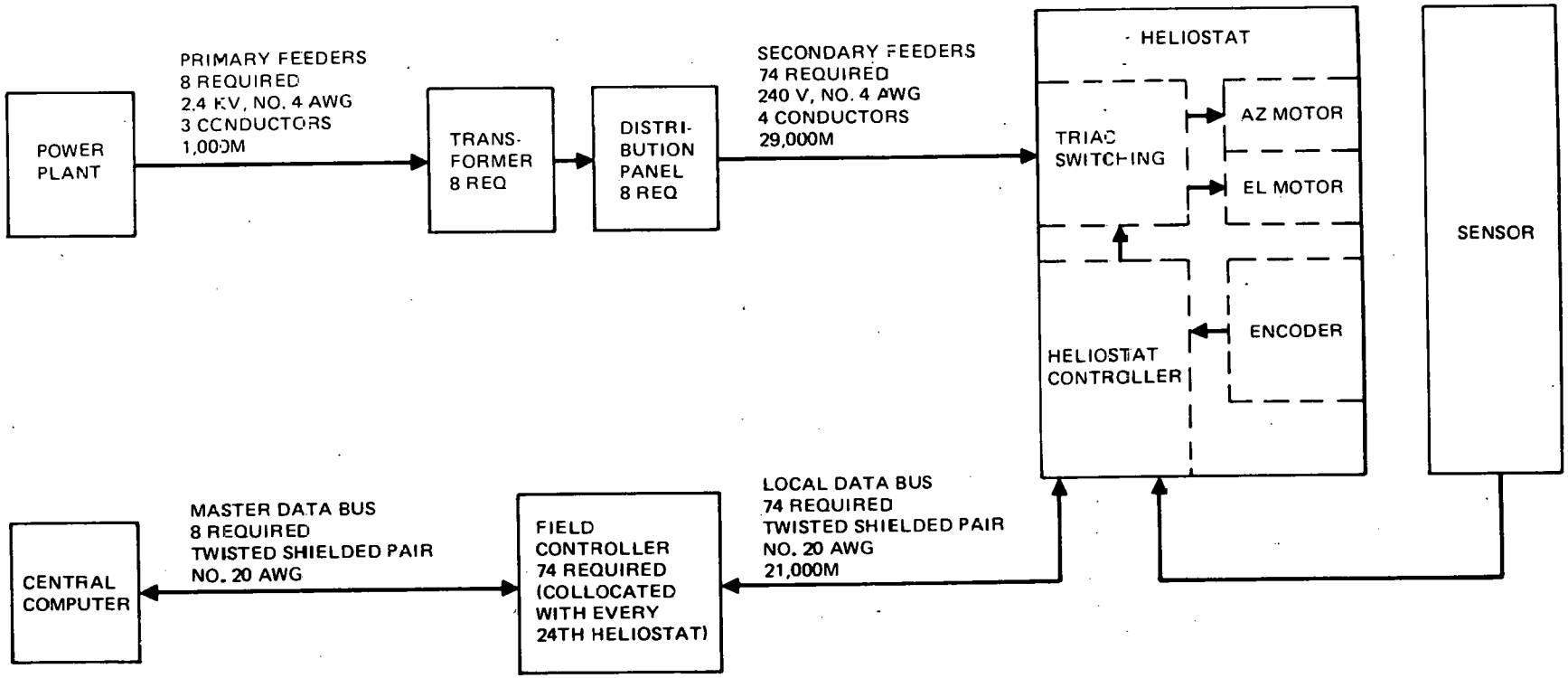

Figure 4-76. Power and Data Distribution — Collector Field Network

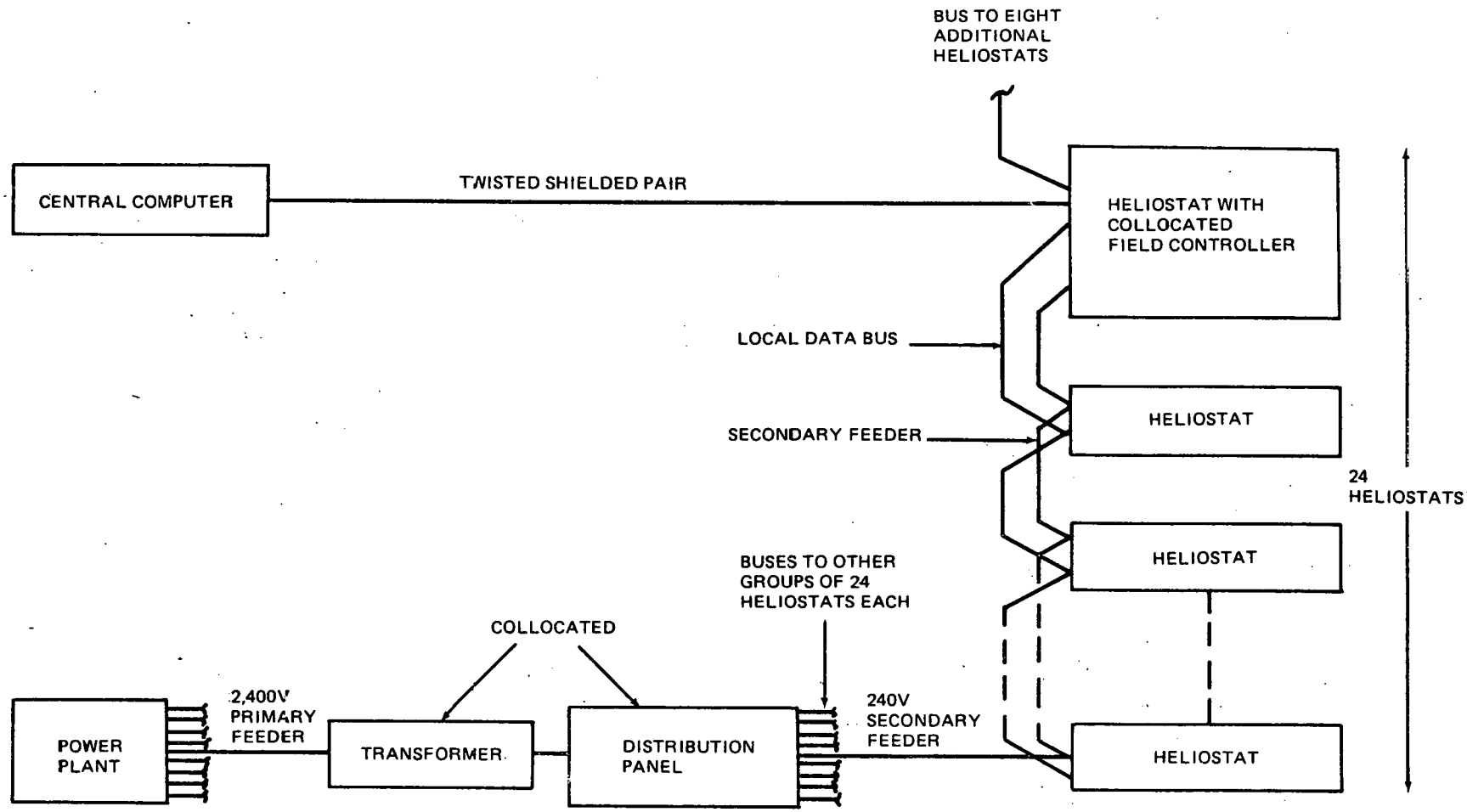

Figure 4-77. Branch-Collector Field Network

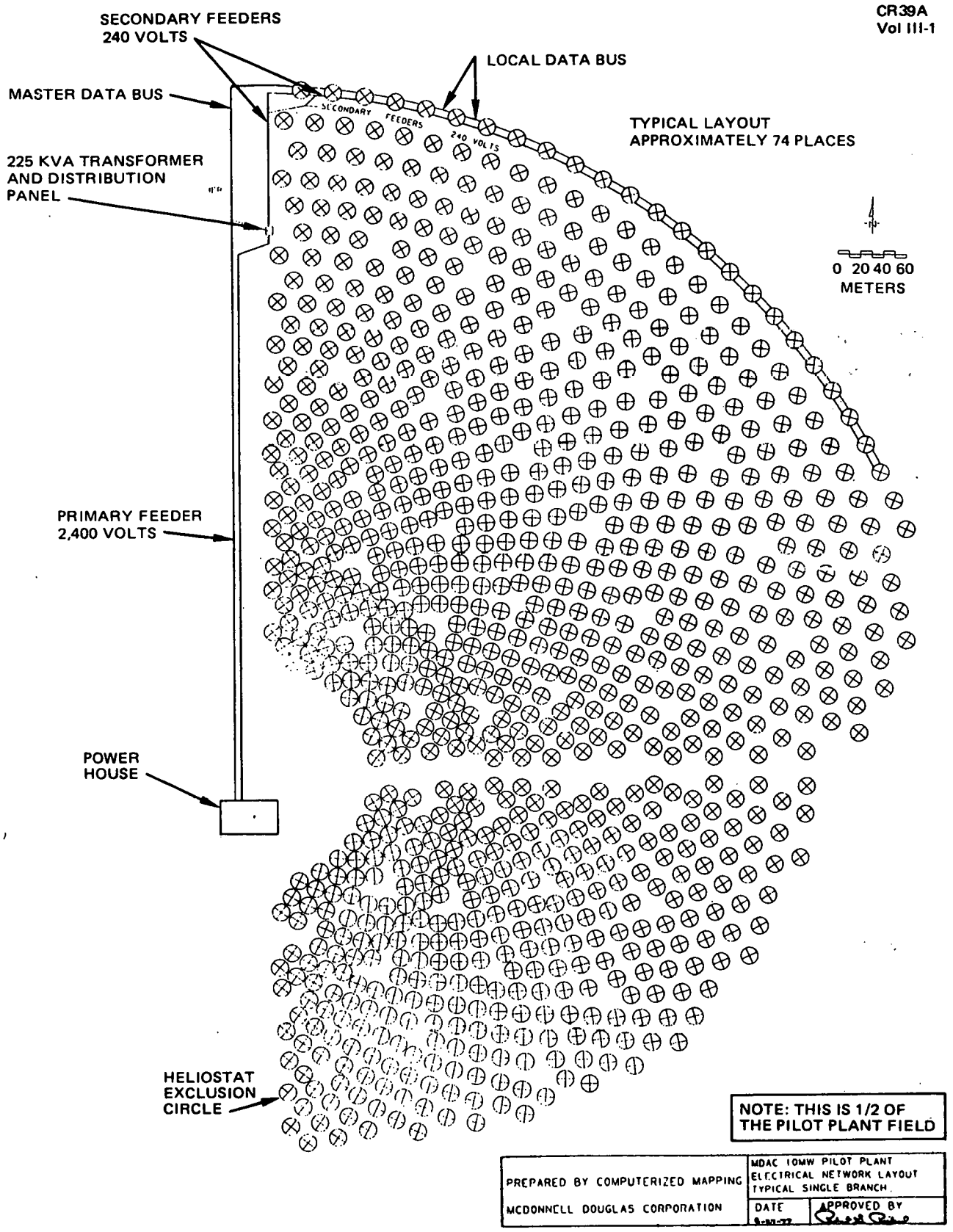

Figure 4-78. Network Layout, Single Branch, Circle No. 32

Probability of Direct Strike

The number of flashes to a given area of earth per year is given by

$$N = \sigma_y \rho A \text{ (Ref. 1)*}$$

where σ_y is the number of lightning flashes per Km^2 per annum, ρ is the proportion of discharges which go to ground and A is the attractive area of the site in question. From Figure 4-79 it will be assumed that there are 12 thunderstorm days per year in Barstow. In Reference 1, a relationship is developed between thunderstorm days and lightning flashes per Km^2. Approximately two flashes/Km^2/year can be expected in Barstow. Not all the flashes will be to earth, however. The proportion which go to earth depends on geographical latitude. Barstow is at latitude 32° 54' N; the proportion of flashes to earth is 0.24. Since the Pilot Plant facility is 527 meters square, its attractive area is 0.278 Km^2, therefore

$$N = 2(0.24)(0.278) = 0.133$$

The annual flash occurrence is about 0.13. Thus, the facility should expect a lightning strike about once every 92 mo or once every 8 yr. This analysis assumes flat terrain. The receiver tower may be more receptive to a lightning strike than a surface area of 0.278 Km^2. The attractive area of a tall structure is given by

$$A_a = \pi r_a^2$$

where r_a is an attractive range or radius given in meters by

$$r_a = 80 \sqrt{h} \left(e^{-Ah} - e^{-Bh}\right) + 400 \left(1 - e^{-Ch^2}\right)$$

where h is the structure height in meters and A, B, and C are constants with values 2×10^{-2}, 5×10^{-2}, and 10^{-4}, respectively. Assuming an overall tower height of 100m, the attractive area, A_a, of a receiver tower would be 0.366 Km^2. The tower presents a slightly larger target for a lightning

*A Ground Lightning Environment for Engineering Usage, August 1972, Stanford Research Institute Project Number 1834.

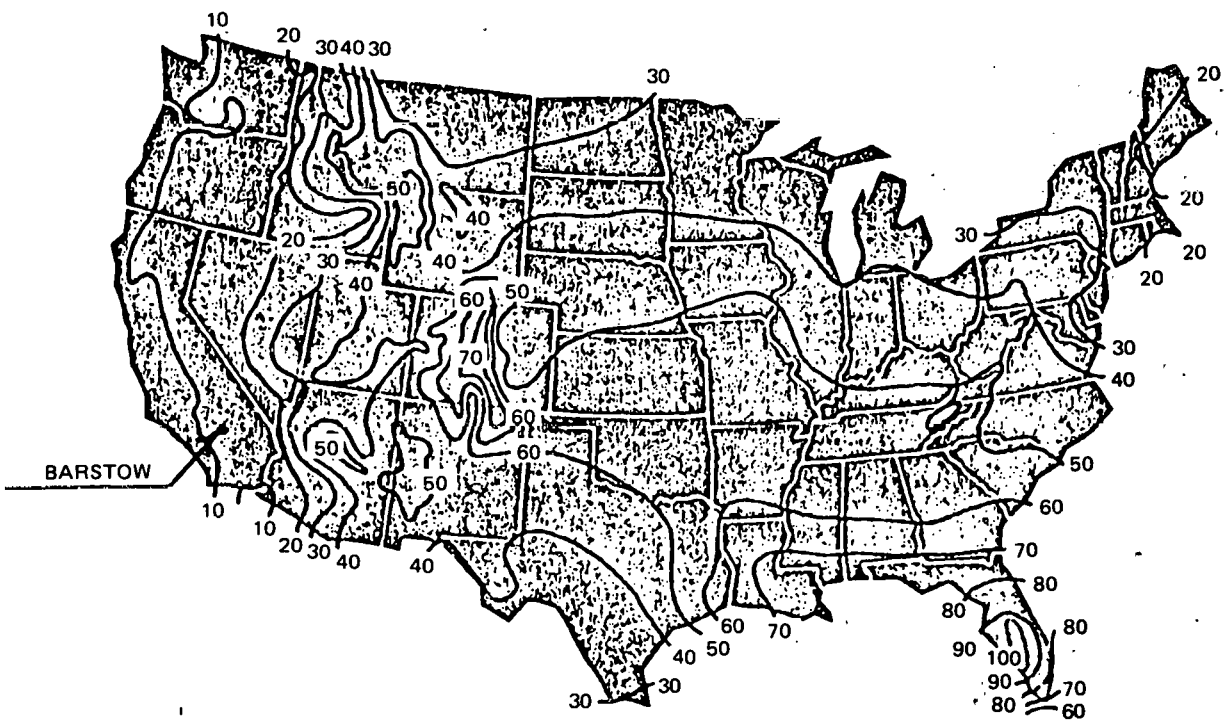

Figure 4-79. Mean Annual Number of Days With Thunderstorms in the United States

strike than the facility surface area. In Reference 1, an additional contribution to the lightning hazard for high structures, self-triggering, is considered. A high structure can trigger lightning, thus increasing its effective attractive area; the factor F_T is therefore applied to A where

$$F_T = 1 + 2^{(9- 1,500/h)}$$

F_T is negligible for structure heights, h, less than 100m and becomes significant above 150m. A receiver tower of 100m should not self-trigger lightning; in fact, F_T is found to be equal to 1.02. Taken together, the annual flash incidence to a receiver tower is

$$N_{RT} = \sigma_y \rho A_a F_t$$

$$= 2(0.24)(0.366)(1.02)$$

$$= 0.18$$

The receiver tower should not trigger lightning because of its height, but it should be expected that it will be struck by lightning about every 67 mo, or once every 5-1/2 yr.

One last refinement of these probabilities can be made if one excludes from the surface area of the collector field that area protected by the tower "cone-of-protection." Objects with a circle of radius equal to the tower height may be considered "effectively protected" from a lightning strike. With a tower height of 100m, the area under the cone-of-protection is 0.031 Km^2. This is subtracted from the site attractive area, A, and N is recalculated.

$$N = 2(0.24)(0.247) = 0.118$$

The site, with the exception of the tower area, should expect a lightning strike about once every 101 mo, or about once in 8-1/2 yr.

Lightning Protection Schemes

A lightning flash produces two basic effects which require attention. The first is the direct strike effect wherein large currents must be conducted to earth by the structure struck by lightning. This effect is usually taken care of by air terminals (lightning rods) which harmlessly conduct the lightning current to ground. No direct strike protection is planned for the heliostats in the collector field, however, for two primary reasons: the Pilot Plant location has a very low probability of lightning incidence, and the high costs associated with protection. Protection would take the form of several (10 to 20) tall (100 ft) poles or individual air terminals for the heliostat field. These methods are costly and may possibly interfere with heliostat views of the receiver. If precautions are taken to avoid the indirect effects of lightning described below, the risk taken with no direct strike protection involves the possible repair or replacement of a struck heliostat. Taking this risk is the cost-effective approach to follow.

The second effect requiring attention is an indirect effect. The indirect effect is a result of electromagnetic coupling which causes the development of extremely high lightning-induced voltages and currents across and within electrical equipments. These voltages and currents present a hazard to personnel and electronics. Grounding, shielding, terminal protection, and maintaining all equipment at the same potential are the prime considerations for elimination of the hazards.

Proper grounding is probably the most important element of any lightning protection system. The huge currents in a lightning stroke (20,000 to 200,000 amps) produce huge voltage across small resistances.

Consider a piece of grounded equipment; in fact, consider it grounded with a properly installed driven ground rod. There is a small but real resistance between the "grounded equipment" and true earth ground. The resistance is dependent upon ground resistivity and the characteristics of the ground rod (length, diameter, material). The least resistance to true ground one can achieve with a single ground rod is on the order of 5 to 10 ohms. If 20,000 amps flows through 5 ohms, a voltage of 100,000v is developed. Thus, this piece of equipment is 100,000V above true earth ground and any

other equipment or personnel at true earth ground. (Any person or equipment remote from the site of the lightning strike will be at true earth ground.) This situation is crudely illustrated in Figure 4-80. These voltages can cause uncontrolled arcing at Points A, B, C, and D. A similar condition exists along the surface of the earth; two points separated by a distance have a voltage drop between them dependent upon resistance and current flowing in the earth. This is the situation especially harmful to people and animals. The best way to reduce the voltages is to have multiple paths to ground, thus effectively reducing ground resistance. Multiple ground paths are typically accomplished by the use of many ground rods and/or a buried counterpoise (a matrix of buried bare conductors). Both of these approaches have been investigated. With the low incidence of lightning at the Pilot Plant location, it was assumed one or the other approach, ground rods or counterpoise, would suffice. It was found that ground rods are more cost-effective than a counterpoise. The installed cost of a ground rod is approximately $30 each; with 1,760 heliostats, the total site cost would be about $53,000. The installed cost of a No. 2 AWG bare copper wire is approximately $1/ft; with 100,000 ft (to interconnect all heliostats), the total cost is about $100,000. Although No. 2 AWG is typically used for a counterpoise, it is possible to use a smaller gage wire, say a No. 6 AWG; for this installation, the ground rod and the counterpoise costs are equal. Closely associated with the low resistance to ground problem is the need to keep all equipment at same voltage potential. This is usually accomplished by tying all equipment to the counterpoise. In this case, however, it will be accomplished at the Pilot Plant by use of the continuous aluminum sheath on the power and data cables (which is there for other reasons; see Section 4.2.10). The cables connect all collector field equipment and the sheath is bonded to structure at all cable termination points. Because a counterpoise seems more costly than a ground rod installation for the collector field application, and since the collector field cable network already performs a key function of a counterpoise, it is recommended that each heliostat use a driven ground rod for lightning protection. The ground rod will be bonded to the heliostat pedestal near the pedestal electrical J-Box.

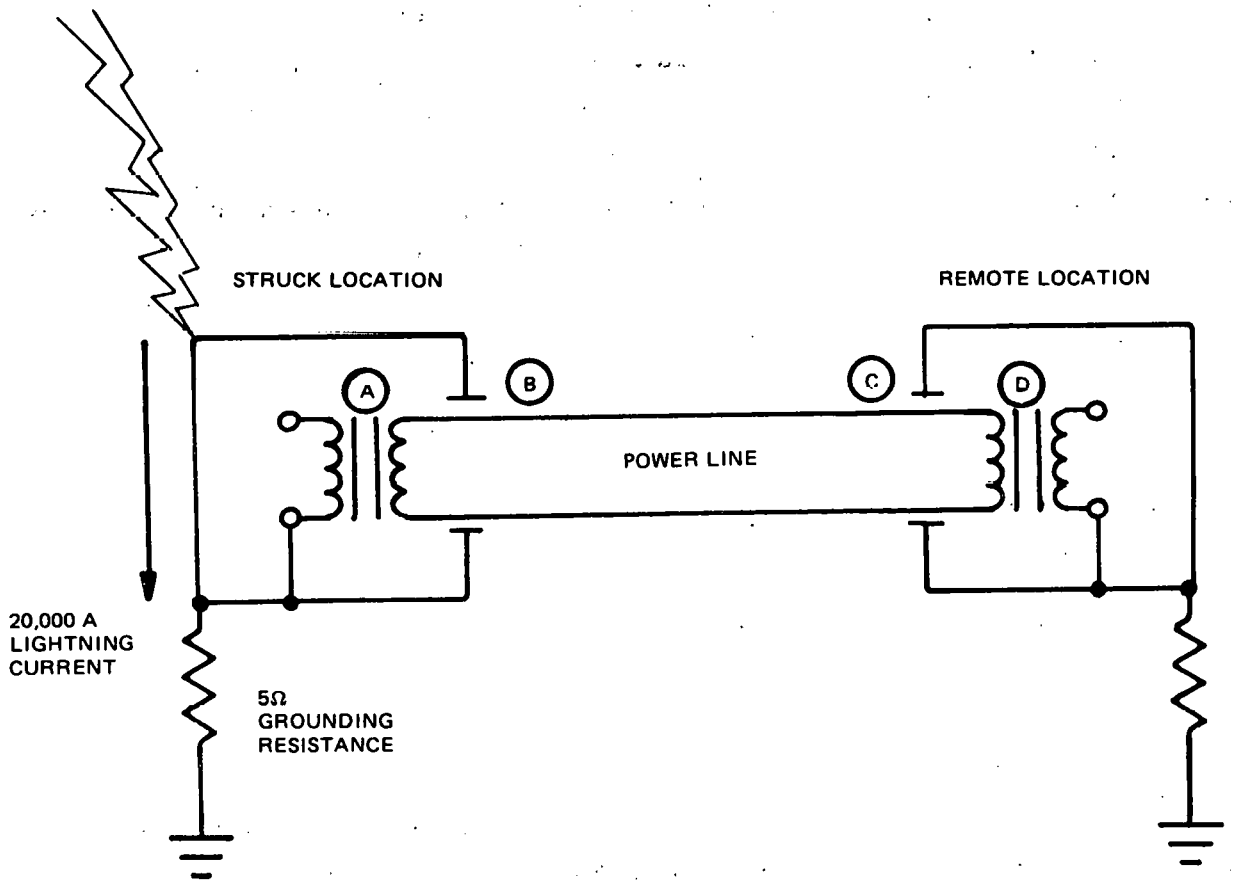

Figure 4-80. Lightning Induced Voltages

Where sensitive electronics are involved, lightning-protection design studies usually demand that all wiring between different locations should be carried in shielded cables, with shields grounded at both ends. In addition, twisting is usually recommended. With the use of the cables discussed in Section Section 4.2.10, these requirements are being met.

The last line of defense to protect electronics against induced lightning voltages and currents is at the circuit level where terminal protection can be provided. Terminal protection can be in the form of spark gaps, gas tubes, capacitors, filters, diodes, varistors, and zener diodes. The particulars; choice of device, installation, etc; are dependent on the circuit application, i.e., the circuit being protected. Circuit criticality, device selection, and terminal protection design will be performed as details of the collector field electronics design become firm.

4.2.11 Safety Provisions

The safety requirements or criteria for the 10-MW Pilot Plant collector subsystem include the conventional industrial safety and the special safety problems associated with a solar thermal power plant.

The applicable Federal OSHA and the California OSHA regulations will apply as discussed in Volume II, Section 4.10.3.2. In addition, other safety codes such as Sections 70 (National Electric Code) and Section 78 (Lightning Protection Code) of the National Fire Protection Association (NFPA) and the American National Standards Institute (ANSI) Code No. ANSI-C2, the National Electrical Safety Code, are also applicable.

Specific potential safety problems unique to a solar thermal plant include the fact that the heliostats are under either remote control from the central computer or in a closed-loop mode and therefore can move in a vertical or azimuthal direction without notice. Therefore, when maintenance is being performed on an individual heliostat, the heliostat must be in a local manual control and the remote control and the closed-loop control must be locked out in a positive manner.

There are many specific safety design criteria that will be applied to the electrical and electronic components of the heliostat and field controllers, including criteria on cables and connectors, test points, controls, insulations, circuit breakers, and grounding. These criteria would be listed in detail in a Safety Design Criteria document.

The major safety problem associated with the collector subsystem is the concentrated solar beam from individual or multiple heliostats. A summary of the hazards considered is shown in Table 4-33. The potential hazards from these beams include injury to the eyes and skin of personnel, damage to equipment, distraction due to eye glare, and possible brush fires. The hazards to personnel can be to personnel on the ground (both operating personnel and the general public) and to members of the public in aircraft, gliders, or helicopters above the collector field.

Table 4-33
COLLECTOR BEAM HAZARDS

Condition	Hazards Evaluated
Single Canted Focus	Ground Personnel
Heliostat	Skin Burn
	Retinal Burn
	Structures
	Brush, Etc
	People in Air Space
	Skin Burn
	Retinal Burn
Multiple Heliostats in Transit to or from Receiver	Air Space Exclusion Defined
Heliostat Stowage	Air Space Exclusion Defined
Multiple Failures	Probability of Multiple Heliostat Intersections Defined

A detailed discussion on the damage mechanism to personnel is given in Volume II, Section 4.10.3.3. The discussion in Volume II showed that the damage mechanism to the eye is retinal burns caused by a temperature rise on the retina. The amount of temperature rise is a function of the power density and the size of the retinal image. For example, the incident retinal irradiance (power density) due to the sun is a maximum of about 7.9 Watts/ cm^2 with a retinal image size of 158 micrometers. These retinal parameters due to looking at the sun can be dangerous but the normal inherent mechanisms of the eye (blink reflex, etc) protect the eye and allow us to live safely in our

one-sun atmosphere. The incident retinal irradiance, which results from a person looking at the reflection of the sun in the MDAC Pilot Plant heliostat, is the irradiance of the sun reduced by the reflectance of the heliostat mirror, or about 6.98 Watts/cm^2. However, size of the retinal image developed by looking at the heliostat while standing at the focal point (350m from the heliostat) is due largely to the canting of the six segments which produce focusing characteristics. As shown in Volume II, the maximum retinal image effective diameter (taking into account that the heliostat has a square configuration and is not completely covered by the sun's image) is 323.5 micrometers. As discussed above, and in Volume II, the hazard to the retina is a function of the irradiance and the retina image size. The threshold levels for retina damage have been under study and are reported in the literature, but a safe level or Maximum Permissible Exposure (MPE) has not been established for visible light as it has for laser radiation. However, a MPE has been proposed by the Army Environmental Hygiene Agency (discussed in Volume II) for absorbed retinal irradiance which is shown in Figure 4-81.

Using the above data and the respective image diameters (158 μm and 324 μm) the two points can be plotted on Figure 4-81.

It can be seen that the individual MDAC Pilot Plant heliostat is marginal with respect to this proposed criterion. It can be pointed out that this criterion has a safety factor of 12 as discussed in Volume II.

The potential skin damage is also discussed in Volume II and the results are shown in Figure 4-82. The maximum theoretical skin irradiance (at the focal point) from one Pilot Plant heliostat is about 0.37 Watts/cm^2, or about 3.3 times the irradiance of the sun as shown on Figure 4-82. The threshold time for injury at this irradiance is about 80 sec. A person would have to stand at the focal point of a mirror for 80 sec and ignore the heat before an injury could occur. The skin irradiance from the unfocused MDAC commercial heliostat is about 0.11 Watts/cm^2 with a larger threshold injury time.

The conclusion from the above discussion is that there are no hazards to personnel from the solar beam of an individual heliostat.

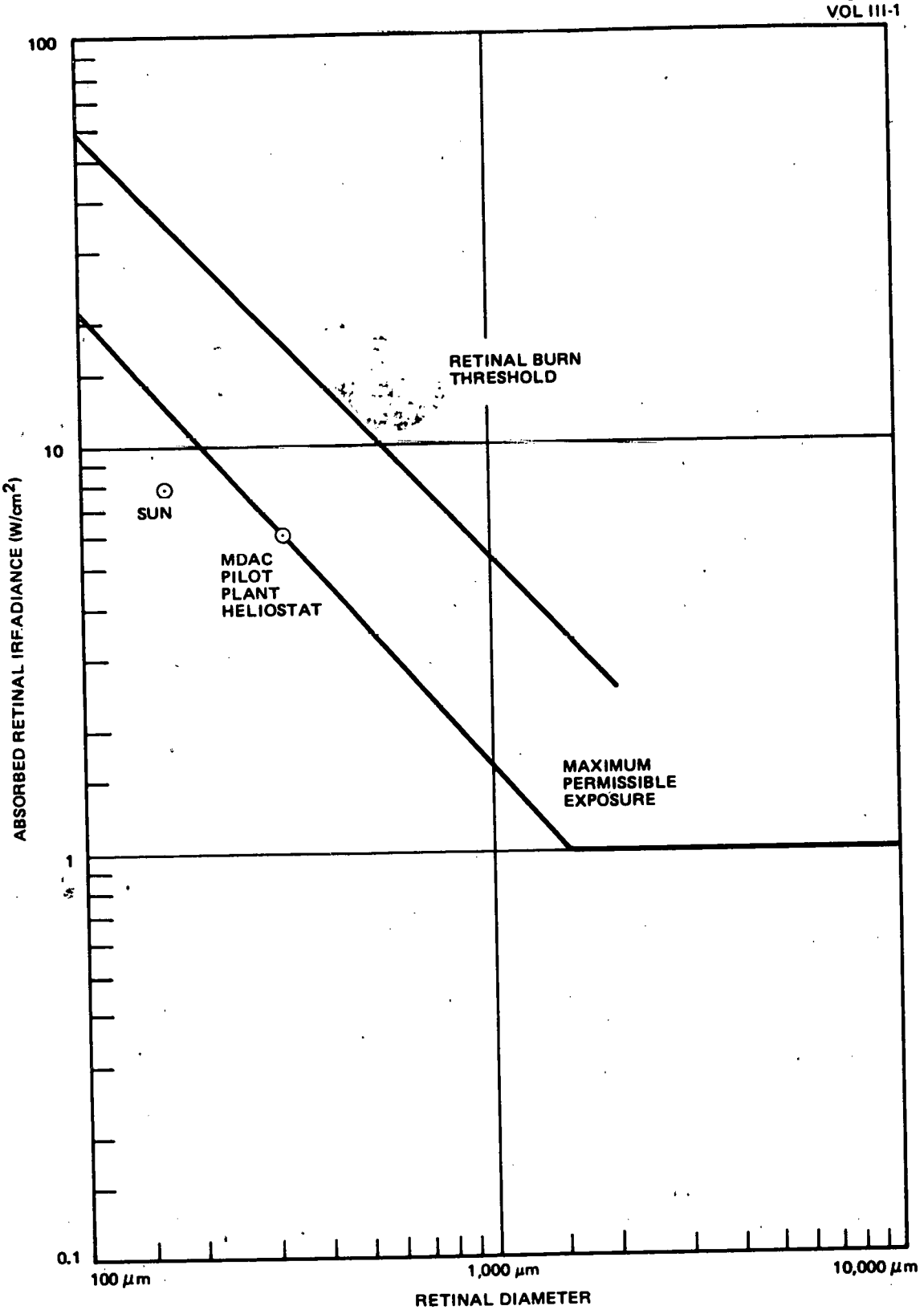

Figure 4-81. Retinal Burn Threshold Safety Exposure

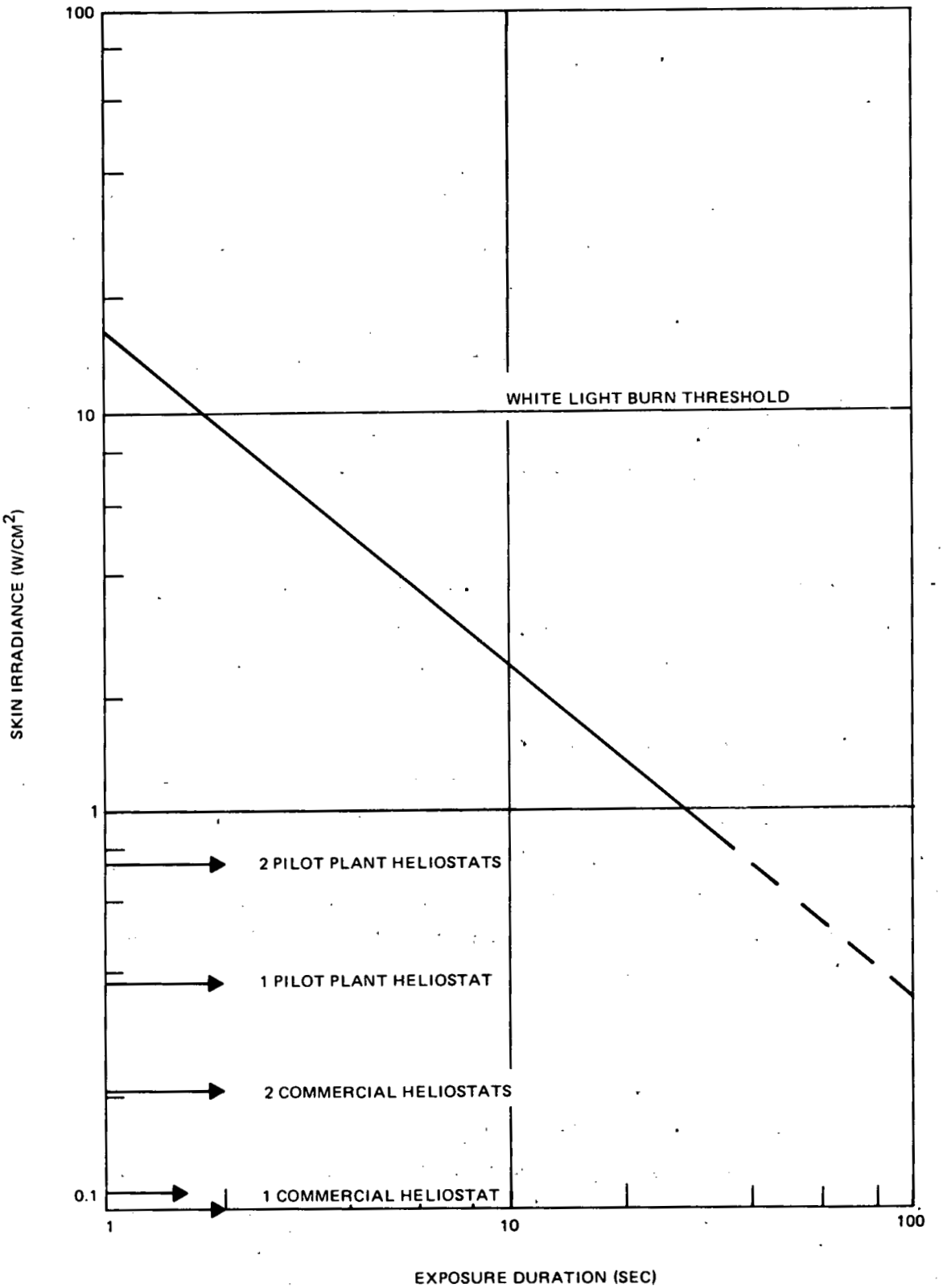

Figure 4-82. Pig Skin Injury Data

It has been estimated that an irradiance of over 5 suns (0.55 Watts/cm^2) is required to initiate combustion in a brush. The maximum irradiance from the MDAC heliostats is only about 3.3 suns (0.37 Watts/cm^2); therefore, a single MDAC heliostat should not present a brush fire hazard.

The hazards from multiple heliostats are potentially more severe, but operational procedures and suitable personnel exclusion areas will eliminate the hazards or reduce them to acceptable levels.

Two potential problems include:

A. Personnel or equipment situated at a point on the ground where multiple beams intercept.

B. The possibility that an aircraft will appear at a point above the collector field and intercept the solar beam from a number of heliostats.

Either or both of the problems can occur during normal operations as the heliostat field is activated or deactivated, or during heliostat storage operations, or as a result of heliostat failures.

When the collector field is activated in the morning (or after a cloud passage) and deactivated in the evening, the heliostats will be controlled by Master Control in such a way that the focal point of the several heliostats will move in a controlled and safe manner. For example, the focal point can be designated as a point on the ground (in a personnel exclusion area) and then moved to the receiver on a path which does not intercept any equipment. This should preclude any hazards to personnel or equipment on the ground and thus solve the first problem.

The second problem has two aspects: The first considers the normal tracking operation of the heliostats. The airspace affected was determined by a brief analytical study. An observer looking down at the receiver location (looking toward the collector field) would see sunlight reflected from a small number of heliostats. At an altitude equal to twice the tower height (2 times 80m) the average flux density would be at one sun. Above that level, less than one sun is seen at any location. Peak flux density

occurs when looking down at the closest-in heliostat at an angle of about 52.2^{o}. The peak flux density at any altitude above the tower can be calculated by

$$E_p = \frac{2A_p \quad \dot{q}}{(1.27h)^2 \pi \theta}$$

where

Ap = area of heliostat ($3.19m^2$)

θ = sun angle (9.3 mr)

h = source altitude

$\dot{q}$ = irradiance (1,000 Watts/m^2)

which gives a result of 2.14 suns at 200m and 0.94 suns at 300m.

The second aspect is concerned with heliostat stowage. If the heliostats are stowed face down, there is no possibility of a reflection of the sun. The only possibility of a potential problem when the heliostats are stowed in a vertical position is when the sun is at zero-degree elevation, and the irradiance then is very low. A computer study of stowage in a face-up position showed that the maximum solar irradiance, under any condition, at 305m (1,000 ft) from one heliostat is 0.231 Watts/cm^2 or about 2.1 suns. With accurately controlled stowage position, the laws of optics will preclude the observer seeing the sun in more than one mirror at any instant of time at this altitude. To ensure that the heliostat beams do not intersect, a divergent stowage orientation with the divergence between adjacent heliostats greater than the stowage orientation error will be used if face-up stowage is used. Hence, the only crossing beams will be from widely separated heliostats. The effect of one heliostat with this solar magnification was shown to be safe in the discussion above for both skin burn and retinal burn. At higher altitudes, one can see the sun in more than one heliostat, but the irradiance will drop because of (1) divergence of the light past the focal point of a central focus heliostat, and (2) open spaces between heliostats. Either effect is sufficient to ensure continued safety with increased altitude.

As stated earlier, there is no established criteria for the maximum permissible exposure (MPE) to visible light. In lieu of a specific criteria or standard, it would appear that the airspace above 305m (1,000 ft) should be safe under all conditions and the airspace above 152m (500 ft) should be safe for all normal conditions except face-up stowage. These altitudes are consistent with FAA regulations 14 CFR 91.79.

To further examine the potential hazard presented by multiple heliostat reflected beams converging at a single point, let us consider first the cases involving the failure of one or more elements of the collector.

If, during the course of normal tracking, a portion of the collector field is disabled, the heliostats will remain in their last commanded position. Solar drift will cause the heliostat reflected beams to move off the target. The effects of off-axis abberation will cause a gradual defocusing of the heliostats to a line of focus within the normal air space exclusion area of the Pilot Plant until it is dispersed to a low concentration level. Hence, loss of control to one or more heliostats during normal tracking is not considered to create an unsafe condition.

Consider next a failure mode in which one or more heliostats are oriented at a random orientation. Failure of a single heliostat has already been shown not to result in an unsafe condition.

It is possible, however, for a heliostat failure condition to produce a situation where two or more heliostats will have a common focus point. The failure probability for one heliostat is about 5.9 (10^{-5}) per hour as discussed in Section 4.2.12. The longest repair time for any heliostat is about 3 hours (Table 4-34). If two heliostats are about 10 heliostats apart, we can assume that they are independent from a retina image standpoint. This means about 64 heliostats would be dependent.

Table 4-34 (Page 1 of 2)

COLLECTOR AVAILABILITY ANALYSIS

Item	Component	MTBF (Hrs)	MTTR (Hrs)	Pilot Plant		Commercial	
				Failures Per Yr	Unavailable Hrs/Yr	Failures Per Yr	Unavailable Hrs/Yr
1	Transformer	$1.2(10^6)$	7.96	0.02	0.16	0.27	2.15
2	Power Cables to Transformers	$9.3(10^6)$	3.11	0.003	0.009	0.04	0.23
3	Distribution Panels	$2.9(10^5)$	1.51	0.09	0.14	1.2	1.8
4	Field Controllers	$1.2(10^5)$	1.29	2.10	2.7	27.1	35
5	Cables to Field Controllers	$9.3(10^6)$	3.11	0.03	0.09	0.33	1.03
6	Field Controller Junction Box	$2.9(10^5)$	1.84	0.81	1.49	10.8	20
7	Heliostat Controller	$2.1(10^5)$	1.04	27.5	28.6	359	373
8	Cables to Heliostat	$9.3(10^6)$	1.50	1.22	1.80	16.0	24
9	Heliostat Circuit Breaker	$5.7(10^5)$	1.66	10	16.6	129	214
10	Azimuth Drive Motor	$5(10^5)$	2.15	11.6	25.0	151	325
11	Elevation Drive Motor	$5(10^5)$	1.54	11.6	17.9	151	233
12	Azimuth Position Sensor	$8.3(10^5)$	1.62	7.0	11.4	91	147
13	Elevation Position Sensor	$8.3(10^5)$	1.10	7.0	7.7	91	100
14	Azimuth RPM Counter	$7.4(10^5)$	1.33	7.8	10.4	102	136
15	Elevation RPM Counter	$7.4(10^5)$	1.05	7.8	8.2	102	107

Table 4-34 (Page 2 of 2)

COLLECTOR AVAILABILITY ANALYSIS

Item	Component	MTBF (Hrs)	MTTR (Hrs)	Pilot Plant		Commercial	
				Failures Per Yr	Unavailable Hrs/Yr	Failures Per Yr	Unavailable Hrs/Yr
16	Azimuth Primary Compudrive	$9.6(10^4)$	2.15	60	129	786	1690
17	Azimuth Secondary Compudrive	$1.3(10^5)$	2.68	44	118	575	1540
18	Elevation Primary Compudrive	$9.6(10^4)$	1.54	60	92	786	1211
19	Elevation Secondary Compudrive	$1.3(10^5)$	2.43	44	107	575	1396
20	Sun Sensor	$2(10^6)$	1.12	3	3.36	38	42
21	Mirror Panels	$1(10^6)$	1.12	35	39.2	454	508
22	Pedestal	$10(10^6)$	1.49	0.58	0.86	7.56	11.3
23	Reflector Structure	$2(10^6)$	2.96	2.9	8.58	38	112
24	Sun Sensor Pedestal	$10(10^6)$	1.01	0.58	0.59	7.6	7.6
	Total Failures Per Year			344.63		4498.90	
	Total Failures Per Day			1.04		13.63	
	Total Heliostat Outages Per Day			1.32		17.30	

The probability of two simultaneous failures (within the repair time) is about $7\ (10^{-5})$. This must be multiplied by the probability that both heliostats would fail in such a way that both beams are pointed at the same spot (1×10^{-5}) and the probability that someone would be in this spot at that time. It can be seen that this probability is at least less than 7×10^{-12} and thus extremely low.

Analysis has shown that there are no hazards to ground-based personnel which cannot be controlled by proper procedures and that there are no hazards above an altitude of about 300m. Both conclusions are subject to further analysis and the acceptance of an MPE for visible light.

Since it has been shown that heliostat failures are most unlikely to produce an unsafe condition, it is concluded that redundant power cables to individual heliostats are not required. Power cables to components which control multiple heliostats (transformers, field controllers, master control)should be redundant. Redundant heliostat cables would prevent only 0.36% of the heliostat failures (1.25 failures per year out of 345). Also, automatic stowage of a failed heliostat, communication link, or power supply is not required. It is much more cost-effective to stow a failed heliostat by use of a mobile test set. The test set can stow or repair a failed heliostat within 3 hr, regardless of the nature of the failure. If the heliostat is completely inoperable, an opacifying solution can be applied to prevent specular reflection from the heliostat. Other procedures available include commanding stowage through the field controller or heliostat controller, providing manual stowage through an auxiliary power supply direct to the drive motors, and direct drive of the drive unit through an auxiliary motor (1/2-in. drill applied to the input shaft).

With the procedures indicated, MDAC believes that the operation of the Pilot Plant will present no undue hazards, and the cost impact would be minimal.

4.2.12 Pilot Plant Availability

The predicted failure characteristics of the Pilot Plant collector subsystem are shown in Table 4-34. Also shown in Table 4-34 is the estimate of the repair characteristics generated using actual data from the SRE test program. Unavailability is the combination of the component failures and their effect on system operations and the time it takes to recover from these failures. In effect, it is the percentage of the total possible operating time that a component or a system is not available for operation. Availability is then one minus unavailability or the percentage of time that a component or system is available for operation. A detailed discussion on the availability characteristics of the entire Pilot Plant system is given in Volume II, Section 4.10.2.

The results of the initial availability analysis are shown in Table 4-34. The individual component failure rates or mean time between failures (MTBF) were obtained, in general, from historical data on other but similar systems. Some of these were obtained from Reference 4.2.12-1 (listed at the end of Section 4.2.12), which was a study to determine the accident probabilities in commercial nuclear powerplants. Data in the source were obtained from reference handbooks, reports, and commercial powerplant experience (both fossil and nuclear) and were considered for the applicable environment of standard operational Power Plant conditions. The compilation is particularly useful because it performs the analyses required to incorporate data from different reporting sources and different operational and environmental conditions, and reports a median value and a 90% likelihood range for each component. The compilation is also useful for a solar power plant because it was performed for a Commercial Plant. Other data used included the FARADA data (Reference 4.2.12-2), the BIDEP data (Reference 4.2.12-3), and the electronic failure rate data in Reference 4.2.12-4.

The determination of the mean time to repair (MTTR) is discussed in detail in Section 5.2.3.

The component with the largest failure rate (smallest MTBF) is the Compudrive actuator, and a search of historical data on this component was

negative. Therefore, data on similar components (linear actuators, variable speed drives, constant speed drives, gear boxes, etc) were used to make an estimate. A failure rate value of 10.4 per 10^6 hours was assigned to the primary mechanism and a value of 7.6 per 10^6 hours to the larger secondary drive. The larger failure rate was applied for the primary drive because of the smaller sizes of bearings and expected higher contact stress on the lobe interface rollers.

The next largest failure item is the heliostat electronics where the failure rate was established by a part count and failure rates from Reference 4.2.12-3. The failure rates for the drive motors were obtained from Reference 4.2.12-1.

The results show that the predicted overall heliostat failure rate is 59 per 10^6 hours or an MTBF of 17,000 hr. The estimated yearly operating time is 3,300 hr based on a calculated average of 10 hr/day and a 330-day year. This assumes the system will be unavailable for 35 days per year due to inclement weather. The results for a collector field of 1,760 heliostats show that we can expect 342 heliostat failures per year, or 1.035 failures per day.

The failure rate for the field controllers was estimated at 8.6 per 10^6 hours by a parts count. This value, plus the estimated failure rate of the cables, gives an MTBF of 83,056 hours and three failures per year or one failure per 110 days for the 74 field controllers in the Pilot Plant field.

There are eight transformers to provide power for the collector subsystem with an estimated failure rate of 0.8 per 10^6 hours. This value, plus the failure rates for the cables and the distribution panel, gives an expected failure rate of 0.11 per year.

A loss of a field controller will cause a loss of 24 heliostats and a loss of a power transformer will cause a loss of 220 heliostats. Therefore, as shown in Table 4-34, while the expected failure rate for heliostats is 1.035 per day, the expected heliostat outage due to failures of all components (heliostats, field controller, and transformers) is 1.32 per day or 437 per year.

Any reliability improvement effort, on the heliostats, would logically be accomplished by installing components with a higher reliability, for example, Hi-Rel electronics components. It would be impractical to provide redundancy because much redundancy is already provided (1, 760 heliostats) and the loss of one (or 10) heliostats does not materially affect system performance. In fact, the loss of a field controller, with the attendant loss of 24 heliostats, only causes an average reduction of 1.36% in system power level. However, the loss of a transformer will cause a reduction of 12.5% in system power.

The accepted definitions of availability and forced outages, discussed in Volume II, Section 4.10.2 and Reference 4.2.12-5, do not count a forced outage of less than 2% as unavailable time. Therefore, the loss of three to four heliostats or a field controller will not affect system availability, but the loss of a transformer will.

Therefore, while the component unavailabilities are as shown in Table 4-34, the only three items that affect system unavailability are the transformer, the distribution panels, and the power cables to the transformer (Items 1, 2, and 3). This gives an unavailability of 0.309 hr per year or 0.0094%.

The results for the Commercial system collector field are also shown in Table 4-4. It was assumed that the MTBF and MTTR values for the individual components would be the same for the Commercial field and the Pilot Plant. However, the number of components change. The Pilot Plant collector field has 1,760 heliostats, and the Commercial field has 22,914 heliostats. The Pilot Plant field has 74 field controllers and eight power transformers, the Commercial field 955 field controllers and 104 power transformers. Therefore, the failures per year and the unavailable hours per year are scaled up by the ratio of components. The results show that we can expect to have 4,460 heliostat failures, 38 field controllers, and 1.5 transformer failures per year, or a total of 13.6 failures per day for the entire field.

References for Section 4.2.12

4.2.12-1 WASH-1400, Reactor Safety Study. An assessment of accident risks in US Commercial Nuclear Power Plants, USAEC.

4.2.12-2 Government-Industry Data Exchange Program (GIDEP). Summaries of Failure Rate Data and Summaries of Replacement Rate Data.

4.2.12-3 Failure Rate Data Handbook (FARADA). Naval Weapons Station, Corona, Calfiornia.

4.2.12-4 MIL-HDBK-217B, Reliability Stress and Failure Rate Data for Electronic Equipment.

4.2.12-5 Report on Equipment Availability for the 10 Year Period, 1964-1973. Edison Electric Institute, EEI-74-57.

4.2.13 Collector Susbsystem

In this section, preliminary concepts are presented covering the support requirements for a 10-MWe solar thermal Pilot Plant. The concepts are compatible, to the extent feasible, with those developed for a Commercial Plant, as described in Section 3.3.3. During the Pilot Plant construction and test operations, application of these concepts, which will be revised and expanded as hardware development progresses, will prove their validity and adequacy. Concepts which may prove to be inadequate will be improved and tested to the extent feasible during the Pilot Plant program, and necessary changes will be incorporated into the Commercial Plant support concepts. The following Pilot Plant support concepts are of a preliminary nature and subject to modifications caused by design changes, program direction, and other influencing factors.

The following descriptions of Pilot Plant support functions address only the differences between Pilot Plant and Commercial Plant requirements. This approach is used to keep repetition and redundancy in this report to a minimum.

4.2.13.1 Site Activation, Installation, and Checkout

During Pilot Plant equipment installation and checkout, the Commercial Plant support concepts will be applied except where there are significant differences between the two programs.

Transportation, Handling, and Packaging

Description is similar to Commercial Plant, except for lower quantities (See Section 3.3.3).

Facilities

There is no foreseeable requirement to augment planned permanent site facilities. A temporary structure for assembling heliostats will also serve as headquarters for installation and checkout operations. The immediate area surrounding the assembly building will be used for storage and parking. The assembly building will be close to the heliostat field to minimize transportation problems.

Support Equipment

Support equipment will be designed and selected with economical and expeditious objectives in view. When the installation and checkout phase is completed, the equipment will be usable for maintenance operations during testing. Description is similar to that of Commercial Plant support equipment in Table 3-8.

Maintenance

Maintenance activities during installation and checkout of the collector subsystem will be responsive to:

- Protecting installed equipment from environmental effects.
- Repairing equipment damaged during installation and checkout operations.
- Discovering discrepant items.
- Scheduled requirements.

Periodic maintenance will be scheduled for inspection and recertification of support equipment, inspection of installed equipment, and operations such as washing reflector surfaces and lubricating mechanical equipment.

Corrective maintenance will be accomplished by removal and replacement of damaged or discrepant items. Repair of items will be accomplished at the appropriate manufacturer's facility. See Section 3.3.3 for detailed requirements.

Spares Supply

Approved quantities of consumables and low-cost spares and repair parts, as defined by maintenance data analyses, will be acquired and delivered to support installation and checkout operations and maintenance tasks.

High-cost spares such as reflector panels and field controllers will not be acquired. If the need arises for this type of spare, the item will be diverted from the production line. Then a spare will be ordered and turned over to the production line as a replacement. This concept reduces investment in high-cost spares and ensures completion of installation and checkout.

Technical Documentation

Technical documentation requirements will be satisfied by providing low-cost instructions for installation, checkout, and maintenance of the collector subsystem. Simple, commercially acceptable methods will allow quick-reaction preparations and reproduction of instructions.

Installation and checkout instructions will be similar to the site activation kit work order, which MDAC used successfully during installation of the Army Safeguard Spartan missile subsystem. Initial procedures will be validated during preproduction buildup and testing of one complete heliostat, sensor, and field controller at MDAC-Huntington Beach. At site, MDAC personnel will use the approved procedures to accomplish installation, checkout, and buyoff activities.

Maintenance procedures will be prepared in consonance with development of maintenance data analyses for subsystem logistics requirements. Maintenance data analyses will define preventive and corrective maintenance, fault detection, inspection, alignment, lubrication, and repair requirements.

Technical data, such as diagrams, repair, and fault isolation, which cannot be validated, will be verified at meetings attended by MDAC and customer personnel.

Final instructions will be updated, as required, to reflect equipment modifications and procedural improvements.

Training

A training program will be developed in accordance with tasks necessary for successful completion of installation and checkout operations. Data pertaining to collector subsystem requirements for manpower, crew size, tasks, maintenance, and personnel skills will be evaluated, and then compared with existing personnel classifications anticipated on site.

Primary method will be on-the-job or on-equipment training with supervision by a knowledgeable training engineer.

The training program will be time-phased to ensure a smooth and effective operation at the onset of site activation.

4.2.13.2 Operations

The customer will assume responsibility for operations and maintenance of the Pilot Plant at the end of installation and checkout. Support concepts could be totally implemented during the testing phase, and carried over into the Commercial operations phase. MDAC could furnish technical support to the customer until full operations and maintenance capabilities are established.

Transportation, Handling, and Packaging

Description is similar to that of the Commercial Plant discussion in Section 3.3.3.

Facilities

There is no foreseeable requirement to augment planned permanent facilities on site. The temporary structure used for assembly of heliostats during installation and checkout phase will serve as a distribution and storage facility until other permanent arrangements can be made.

Support Equipment

Description is similar to Commercial Plant support equipment (see Section 3.3.3).

Maintenance

Maintenance activities identified during the installation and checkout phase will continue and will be responsive to:

- Protecting equipment from environmental effects.
- Repairing damaged equipment.

Periodic maintenance will continue on a scheduled basis for inspection and recertification of support equipment, inspection of installed equipment, and operations such as washing reflector surfaces and lubricating mechanical equipment.

Results of the testing program (described in detail in Section 6.4) indicate that the heliostat reflective surfaces can be effectively washed using pressure spray nozzles and the following application technique:

A. Apply approximately 1 gal of wash solution (5% cleaning concentrate, 95% deionized water) in approximately 1 min to heliostats oriented with surfaces near vertical.
B. Allow approximately 1 min dwell time for the wash solution to act on surface contaminants.
C. Rinse with approximately 5 gal of deionized water applied in approximately 2 min.

The washing operation should be conducted with the heliostat surfaces facing away from the sun, prefereably during predawn and early morning hours. This procedure takes advantage of the cleaning action afforded by any dew which may have formed and avoids premature drying of wash solution or rinse water.

The selected approach for implementing the technique for the Pilot Plant operation involves use of a tanker truck (Figure 4-83) which carries both the wash solution and rinse water. The truck is fitted with the necessary

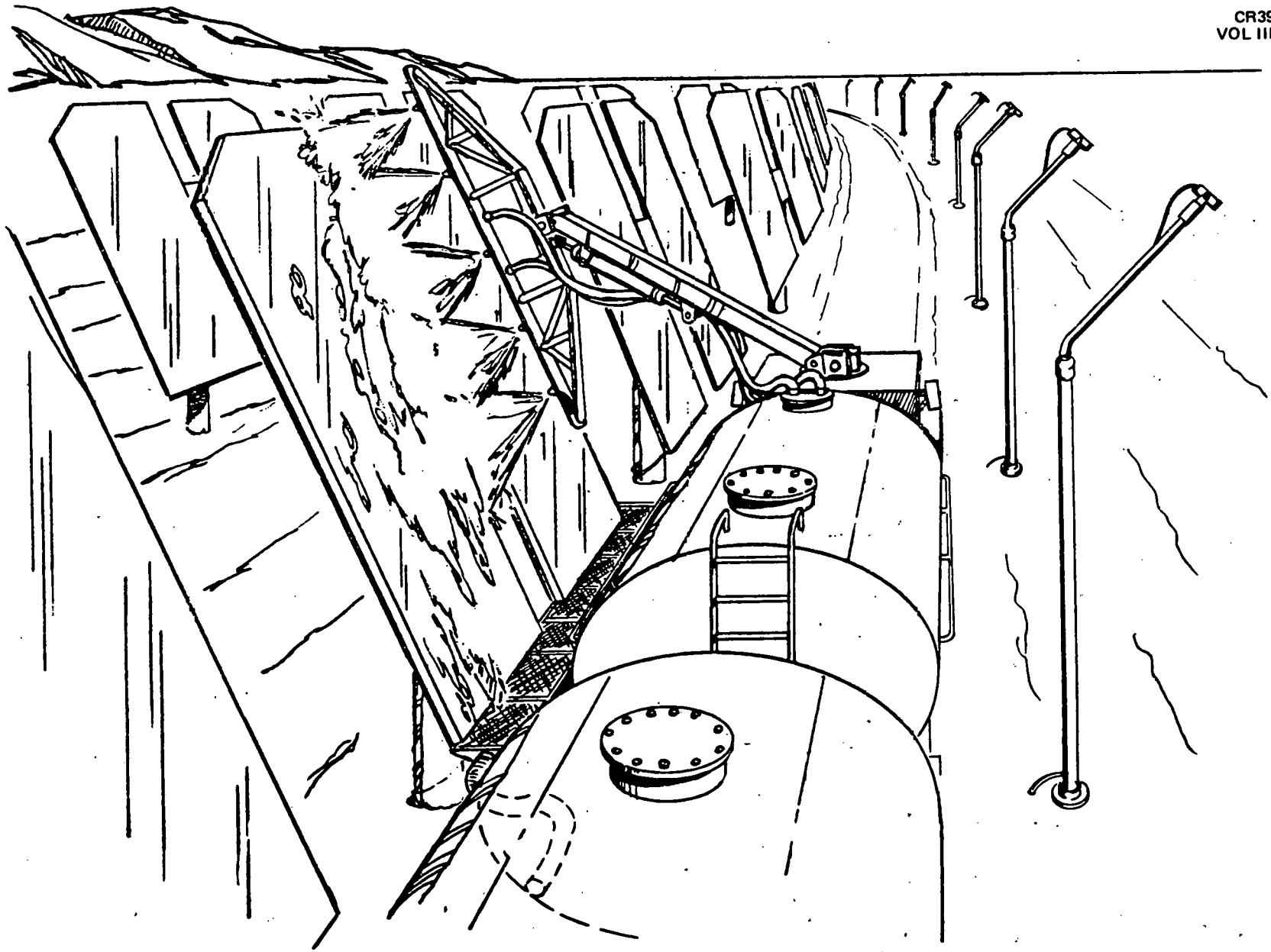

Figure 4-83. Heliostat Cleaning

valving, controls, and pressurization system for fluid application at the flow rates indicated. Fluid is applied by a multiple nozzle array which extends from the side of the truck and provides the controlled spray patterns necessary for both wash and rinse functions. A fluid catch basin extends from the truck and is positioned under the heliostat to retrieve the wash solution and rinse water. This recently identified requirement to prevent spillage of wash solution and rinse water was a significant factor in selecting this approach over other promising alternative methods.

The conclusion has been drawn that the best approach for Pilot Plant maintenance is to schedule the reflector field cleaning on a 30-day basis rather than accomplishing as corrective maintenance. This approach permits realistic washing equipment quantity, sizing, and manpower estimates with the least risk of error. Variable weather conditions are the most important factor in determining when cleaning is required; however, the data obtained during the limited test period tends to indicate that a 30-day frequency is a reasonable approach. The scheduled maintenance concept requires two tanker trucks (each operated by two men) for approximately 4 hr to clean 88 mirrors each day. Cleaning will be done in the early morning hours and will require 20 working days to complete the entire field. At this rate, the total field could be cleaned in 80 working hours should adverse weather degrade field reflectivity below acceptable limits.

It should be recognized that only limited data has been obtained to date for heliostat washing and reflectivity degradation under field conditions. The above maintenance approach is based on these data and the relative merit of alternative concepts to provide an acceptable cleaning technique. The concept and maintenance procedures may be directly applicable to the Commercial Plant; however, the decision should be delayed until additional testing has been accomplished and experience gained during Pilot Plant operation. A more detailed study based on comprehensive test results and experience data is certainly warranted. For example, the reduction of washing time

for a heliostat by 1 min results in a savings of 8,800 manhours/year for a 22,000-heliostat Commercial field:

$$\frac{22,000 \text{ heliostats} \times 1 \text{ min} \times 2 \text{ men} \times 12 \text{ washings}}{60 \text{ min}} = 8,800 \text{ hr}$$

It is also interesting to note that rough calculations indicate the value of increasing reflectivity by 1% is equal to $\$0.30/ft^2$ compared with an estimated cost for washing Pilot Plant heliostats of $\$0.08/ft^2$.

A life-cycle cost study including definition of initial equipment investment and recurring costs for time, materials, and labor is recommended to determine the best possible approach for the Commercial plant.

Additional field test data is required to fully define reflectivity degradation rates, especially for seasonal effects and severe weather conditions. Natural cleaning resulting from dew, frost deposits, rain, and snow must be further evaluated. The optimum heliostat orientation during various weather conditions needs to be identified to minimize reflectivity degradation or take advantage of natural cleaning.

Another consideration which apparently has not been fully resolved is the requirement to collect and retrieve the washing solution and rinse water. The Pilot Plant cleaning method is based on full compliance, and modification or relaxation of this requirement could result in a considerable cost saving. An attractive approach being considered prior to identification of this requirement involved a "drive through" washing concept using one or more pairs of trucks. Washing would be done while driving slowly past the heliostat (or pausing only briefly), rinsing by a following truck in a similar manner. Apparent advantages of this concept were effectively negated by the requirement to collect both wash solution and rinse water since the trucks would have remained at the heliostat for a much longer period. A system of drainage trenches and sumps to trap runoff could be installed during site construction; however, a detailed evaluation and cost analysis is required to determine the feasibility and economics of such an approach.

orrective maintenance will be accomplished by removal and replacement of damaged items. Repair of items will be accomplished at the appropriate manufacturer's facility. (Refer to Section 3.3.3 for detailed requirements.)

Spares Supply

Description is similar to Commercial Plant supply support (Section 3.3.3).

Technical Documentation

Use of approved procedures will continue. These procedures will define preventive maintenance, fault detection, inspection, alignment, lubrication, and repair requirements.

Instructions will be updated, as required, to reflect equipment modifications and procedural improvements.

Training

A formal training program is not required. Replacement technicians will be trained on-the-job or on equipment, with supervision by experienced technicians.

4.3 PILOT PLANT COLLECTOR PRELIMINARY DESIGN

This section presents the MDAC Pilot Plant collector preliminary design. The design package consists of foldout drawings and descriptions of the hardware. The following major components are shown and discussed: reflector, reflector support structure, drive unit, pedestal/foundation, and heliostat electronics and controls. Finally, the collector heliostat assembly is described, together with a typical field installation layout.

4.3.1 Reflector

The reflector (Figure 4-84 and 4-85) is composed of six rectangular sandwich panels, each 85 x 114 in. Two of the panels have 45-deg scarfed corners to allow closer heliostat field spacing when the reflectors rotate in an azimuth direction. The front face of each panel is a 0.125-in. second-surface float glass mirror; the core is 2 lb/ft^3 polystyrene foam 2-in. thick, and the back

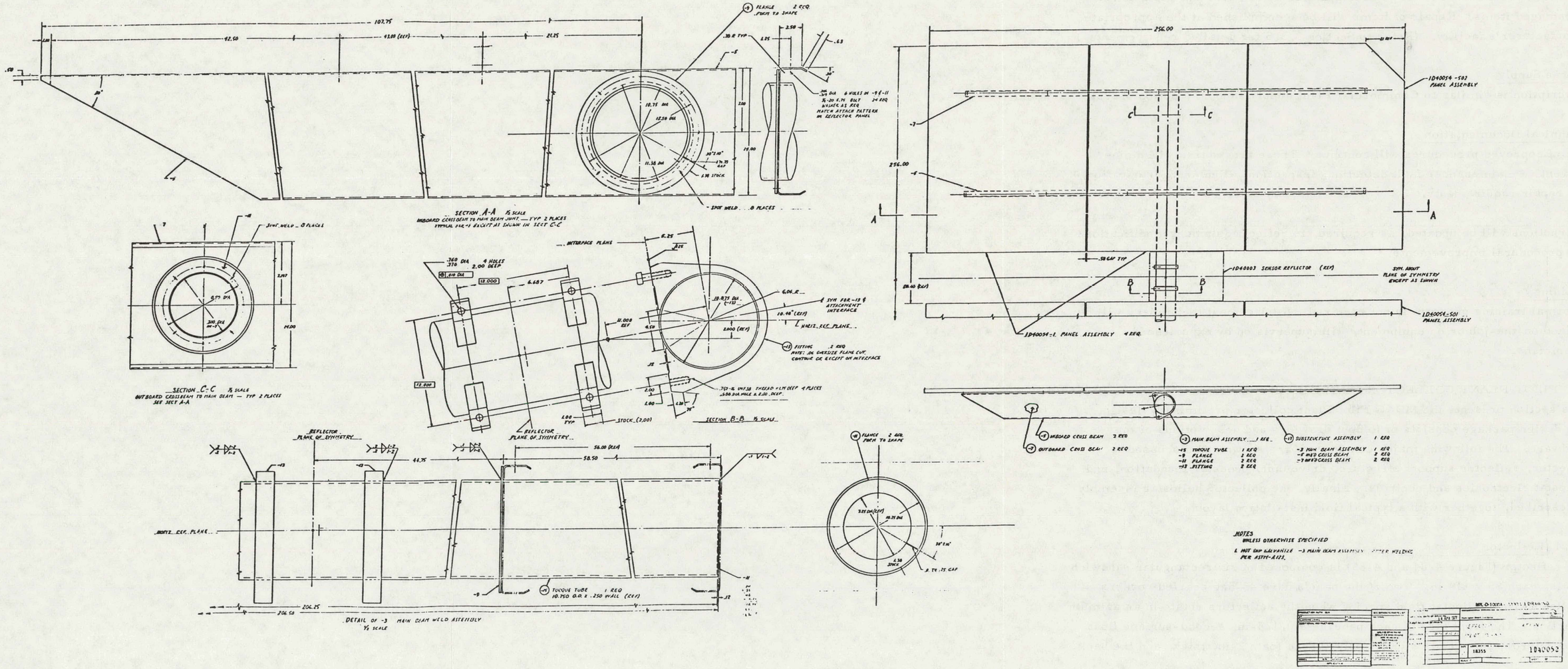

Figure 4-84. Refector-Installation — Pilot Plant

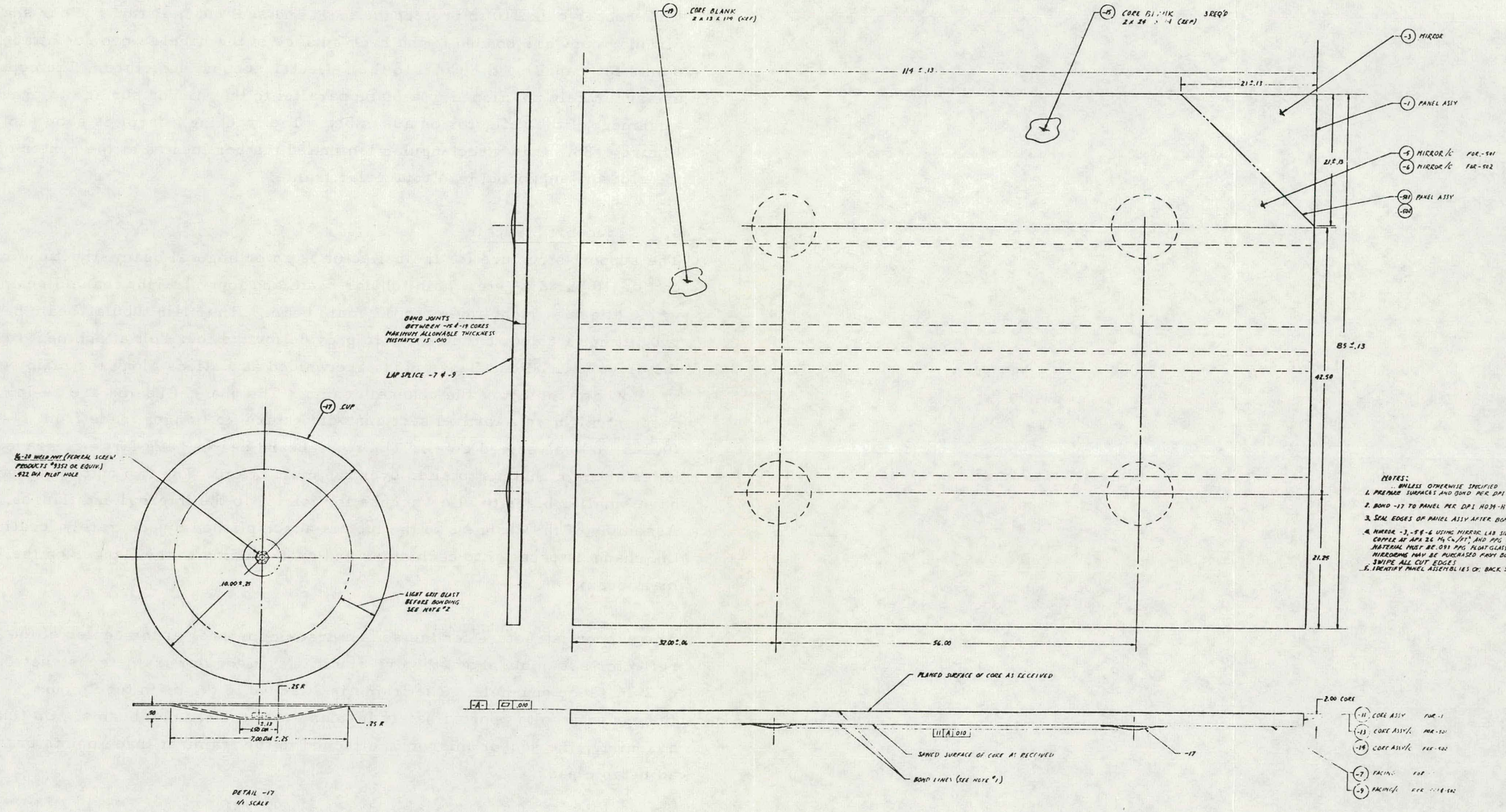

MIL-D-1000A LEVEL 1 DRAWING

18355 1040054

Figure 4-85. Panel Assembly — Pilot Plant

face is 0.022-in. thick galvanized steel sheet. The panel is bonded with a polyurethane adhesive. After bonding, the edges of the foam are sealed with PRC rubber calk 210 to protect the foam and seal out moisture. Four shallow circular cups are bonded to the back surface of the panel to provide attach points for mounting the panel to the reflector support structure. The cups are accurately positioned in a plane parallel to the mirror surface to provide alignment of the reflector on assembly. The tracking mirror is shown in Figure 4-86. It is a rectangular laminated mirror located at the center of the slot and supported by a triangular frame.

4.3.2 Support Structure

The support structure for the reflector is an orthogonal beam structure made up of a 10-in. diameter main tubular beam and four straight channel beams which attach at right angles to the main beam. The main tubular beam has two fittings welded at the center to provide for the four bolt attachment to the drive unit. Four flange rings are welded at stations along the main beam to allow attachment of the channel beams. The channel beams are 14-in. deep, straight roll-formed sections with return lip flanges made from 11-gage (0.123 in.) galvanized steel. The two inboard beams have large clearance holes at their centers to slide over the main beam. The two outboard beams have smaller holes to allow access for joining to the internal end flanges. Assembly of the channels to the tube is accomplished by accurately locating the channels parallel to each other and spot-welding to the flanges on the main beam.

The support structure for the sensor tracking mirror at the center of the reflector assembly above the drive unit is a triangular frame constructed of 2-in. deep channels. The frame is attached to the main tube mount fittings with bolts approximately in-plane with the channel beams. On final assembly, the sensor mirror is attached to the frame at three points by adjustable pads.

4.3.3 Drive Unit Description

Figure 4-87 shows the drive unit assembly. It consists of similar two-stage reducers for both the azimuth and elevation drives with input torque provided

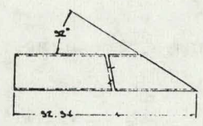

DETAIL OF -17 BAR - FULL SIZE
SAME STOCK AS -15, -15

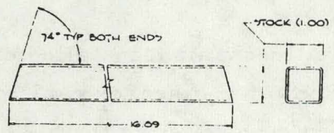

DETAIL OF -13 BAR - FULL SIZE

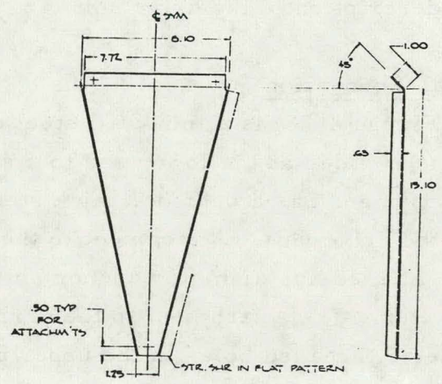

DETAIL OF -9 BRACKET
.12 BEND R

SYM ABOUT PLANE OF SYMMETRY EXCEPT AS SHOWN

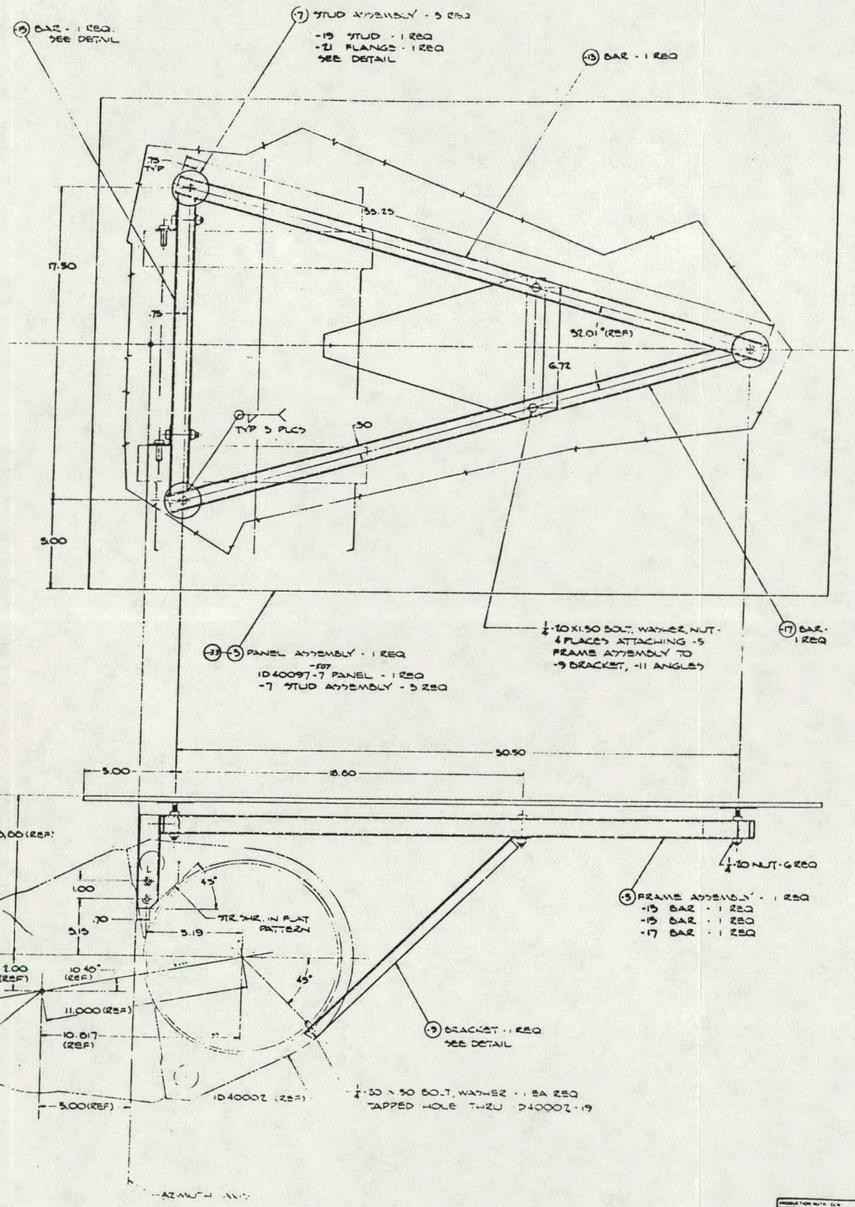

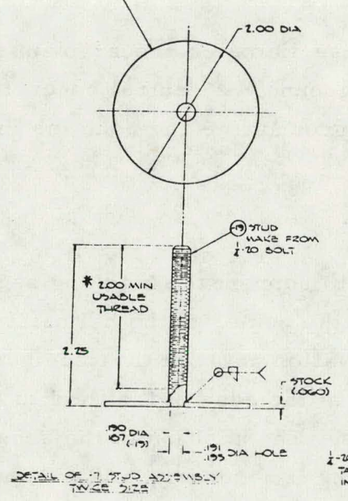

DETAIL OF -7 STUD ASSEMBLY
TWICE SIZE

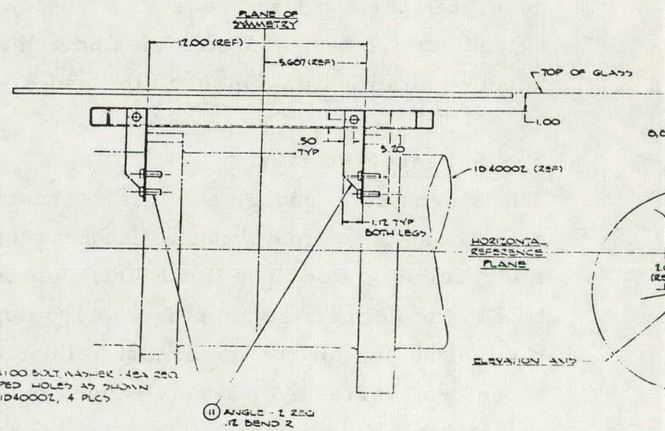

1/4-20 X 1.00 BOLT, WASHER - 4 EA REQ TAPPED HOLES AS SHOWN IN ID40002, 4 PLCS

(11) ANGLE - 2 REQ .12 BEND R

NOTES:
UNLESS OTHERWISE SPECIFIED:

1. FOR BONDING -5 PANEL ASSEMBLY -
   A. PREPARE GLASS SURFACE PER DPS 5000 - 7.13
      1) WITHIN 2 TO 4 HRS, PRIME PREPARED GLASS WITH PR-506 (DPN 4758)
      2) DRY FOR 8 HRS MAX AT ROOM TEMP
   B. PREPARE STEEL SURFACE AS FOLLOWS
      1) WIPE WITH METHYL ETHYL KETONE (DPN 5355)
      2) GRIT BLAST SURFACE W/ AO 100 GRIT ALUMINUM OXIDE (DPN 1150-5)
      3) WITHIN 24 HRS, PRIME W PR-420M (DPN 4720) PER DPI HO28 PARA 2.2.2
   C. BOND MATING SURFACES AS FOLLOWS:
      1) MIX ADHESIVE MASONITE X109411 (DPN 4755) AT 100 PARTS PART B WITH 50 PARTS PART A (HARDENER) BY WEIGHT. REMOVE ENTRAPPED AIR WITH VACUUM (29 IN. HG) FOR 5 MINUTES MINIMUM AFTER FOAM COLLAPSE. CAUTION: ASSEMBLE PARTS WITHIN ONE HR AFTER MIXING ADHESIVE
      2) APPLY .50 DIA. ADHESIVE FILLET ON PRIMED GLASS TO SUPPLY A .05 MIN BOND LINE.
      3) ALIGN & MATE PARTS. CURE WITHOUT MOVEMENT FOR 8 HRS MIN AT 72°±5°F, 60% MAX REL HUMIDITY.
2. HOT DIP GALVANIZE -5 FRAME ASSEMBLY
3. CAD PLATE -7 STUD ASSEMBLY PER QQ-P-416 OR EQUIVALENT
4. .339/.291 (9/32) DIA. ATTACHMENT HOLES FOR .25 DIA BOLTS IN -5, -9, & -11
   DRILL IN ASSEMBLY OR REF SEQ

MIL-D-1000A LEVEL 1 DRAWING

		SIZE 18355	1040003

Figure 4-86. Sensor Reflector Installation

by two electric motors. The elevation drive housing has four bolt holes which serve as attach points for the reflector structure.

A mechanism installed on the azimuth drive base feeds the elevation drive power and sensor cable onto the azimuth drive housing which acts as a cable stowage reel as the heliostat rotates plus and minus 270 deg. A cover protects the cable from direct exposure to the elements. See Section 4.2.4 for a detailed description of the drive unit.

4.3.4 Pedestal/Foundation

The pedestal (Figure 4-88) is a thin-wall steel column, 20 in. in diameter and 108 in. long, welded at the lower end to a standard weld neck pipe flange. The upper end has a 0.75-in. thick steel plate welded in place for attachment of the drive unit. Attachment to the concrete foundation is provided by eight 1.25-in. diameter anchor bolts equally spaced on a circle of 27-in. diameter. The attachment to the drive unit is by means of eight 0.50-in. diameter threaded holes in the upper plate.

The foundation (Figure 4-89) is a 96-in. base diameter precast reinforced concrete cone, with the base 45 in. below ground. A central concrete column extends up from the pad to 3 in. above the ground line and contains the eight anchor bolts for attachment to the pedestal.

4.3.5 Sensor Pole

The sensor pole (Figure 4-90) is designed to support the tracking sensor at a location approximately on a line between the center of the heliostat and the receiver. For the Pilot Plant, the elevation angle of the receiver relative to the heliostats varies from 11.5 deg at the edge of the field to a maximum of 50 deg for the innermost heliostats. The position of the sensor, therefore, varies over a wide range, making it necessary to have both height and lateral adjustments. A thin-wall tube 5 in. diameter and 0.120 in. wall, located 190 in. from the heliostat centerline, is used for the vertical column. A tubular steel boom 3 in. diameter x 0.120 in. wall with a 45-deg bend at the lower end is attached to the vertical column with a standard swage

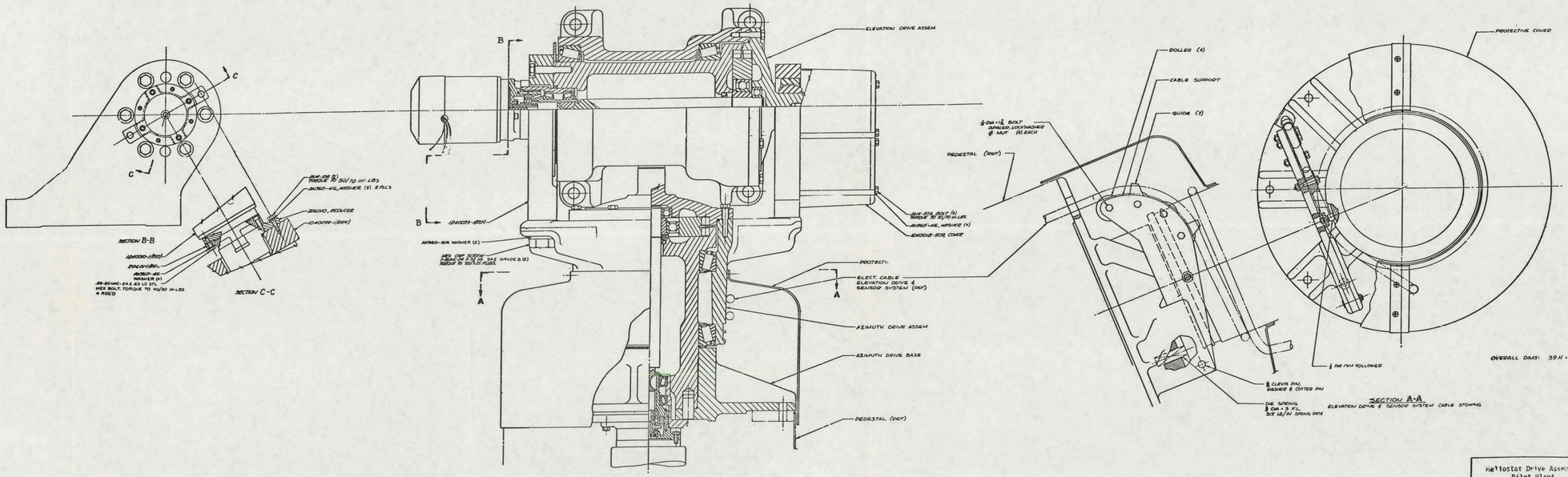

Heliostat Drive Assembly
Pilot Plant

Figure 4-87. Heliostat Driver Assembly — Pilot Plant

THIS PAGE

WAS INTENTIONALLY

LEFT BLANK

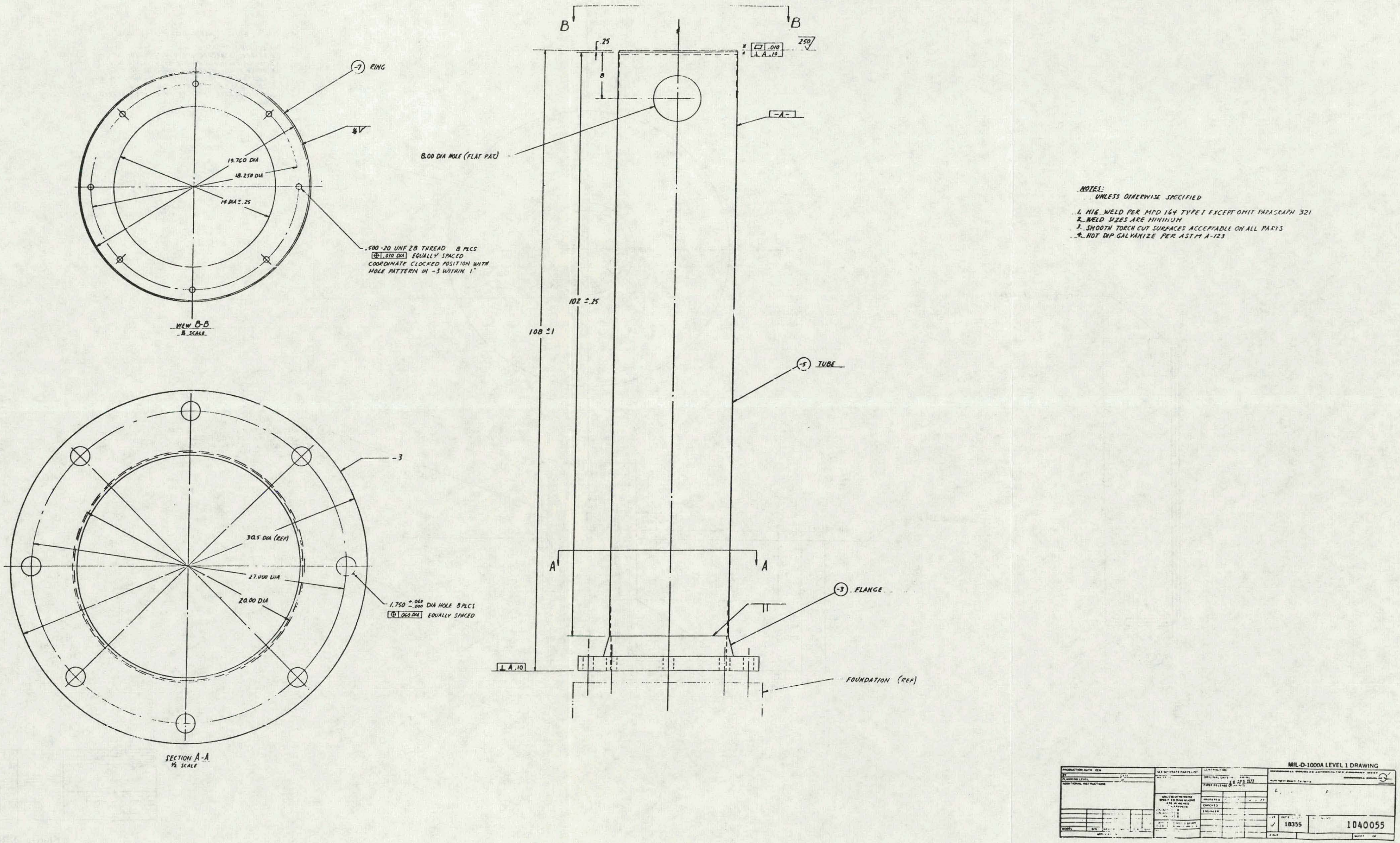

Figure 4-88. Pedestal – Pilot Plant

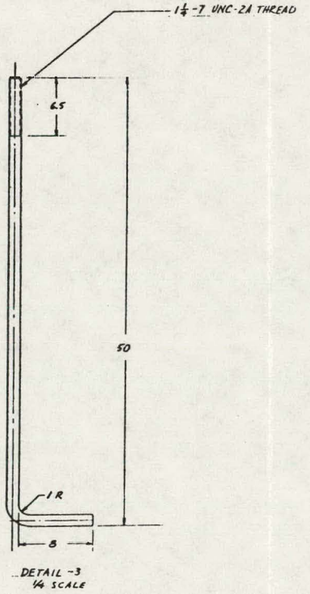

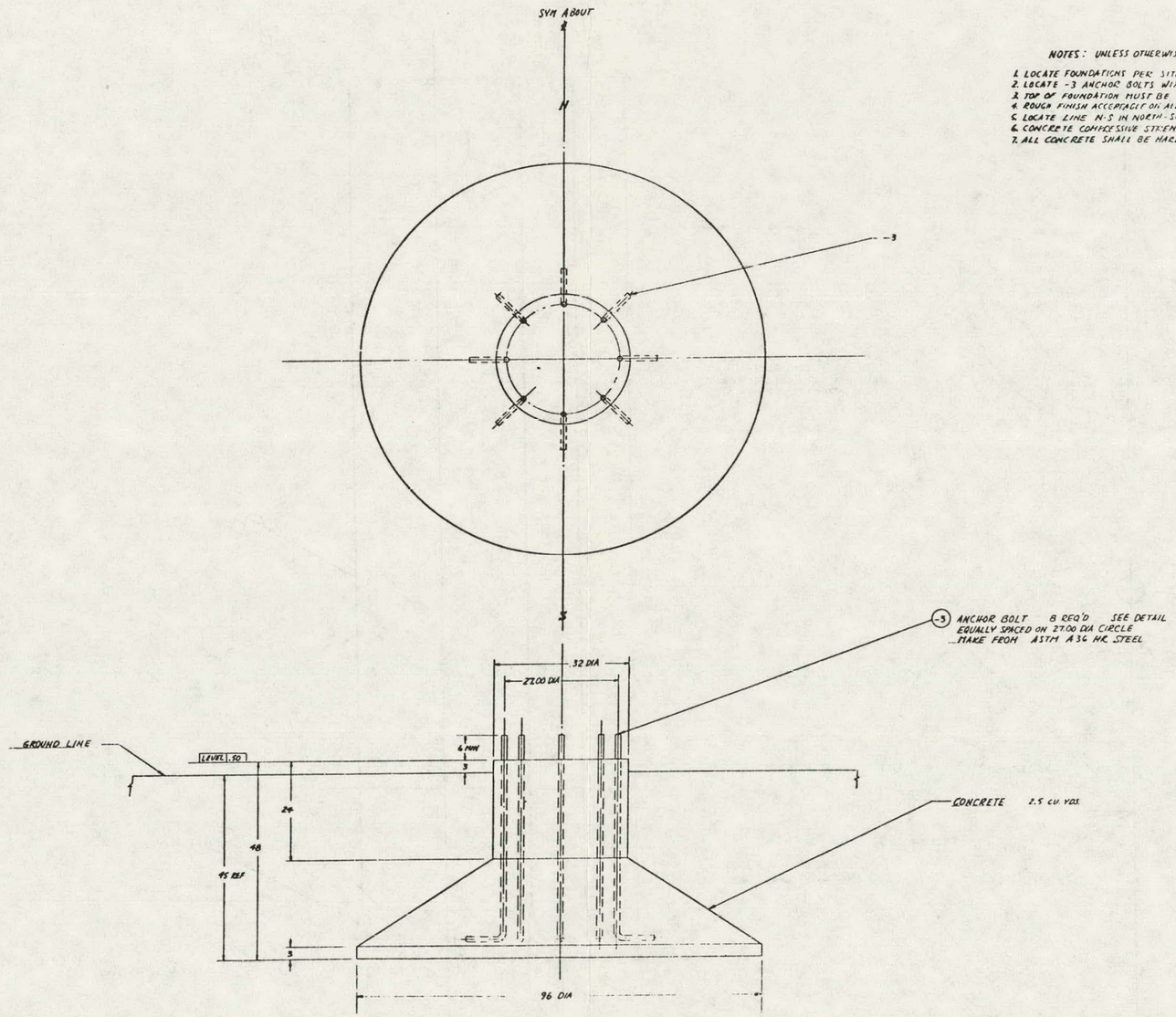

NOTES: UNLESS OTHERWISE SPECIFIED

1. LOCATE FOUNDATIONS PER SITE PLAN
2. LOCATE -3 ANCHOR BOLTS WITHIN .150 OF TRUE POSITION
3. TOP OF FOUNDATION MUST BE LEVEL WITHIN .50 INCH
4. ROUGH FINISH ACCEPTABLE ON ALL SURFACES
5. LOCATE LINE N-S IN NORTH-SOUTH DIRECTION WITHIN 1°
6. CONCRETE COMPRESSIVE STRENGTH TO BE 2500 PSI OR GREATER AFTER 28 DAYS
7. ALL CONCRETE SHALL BE HARD ROCK CONCRETE USING PORTLAND CEMENT TYPE I

MIL-D-1000A LEVEL 1 DRAWING

SIZE	CODE IDENT NO.	DWG NO.	
	18355	104C	
SCALE			SHEET OF

Figure 4-89. Foundation – Pilot Plant

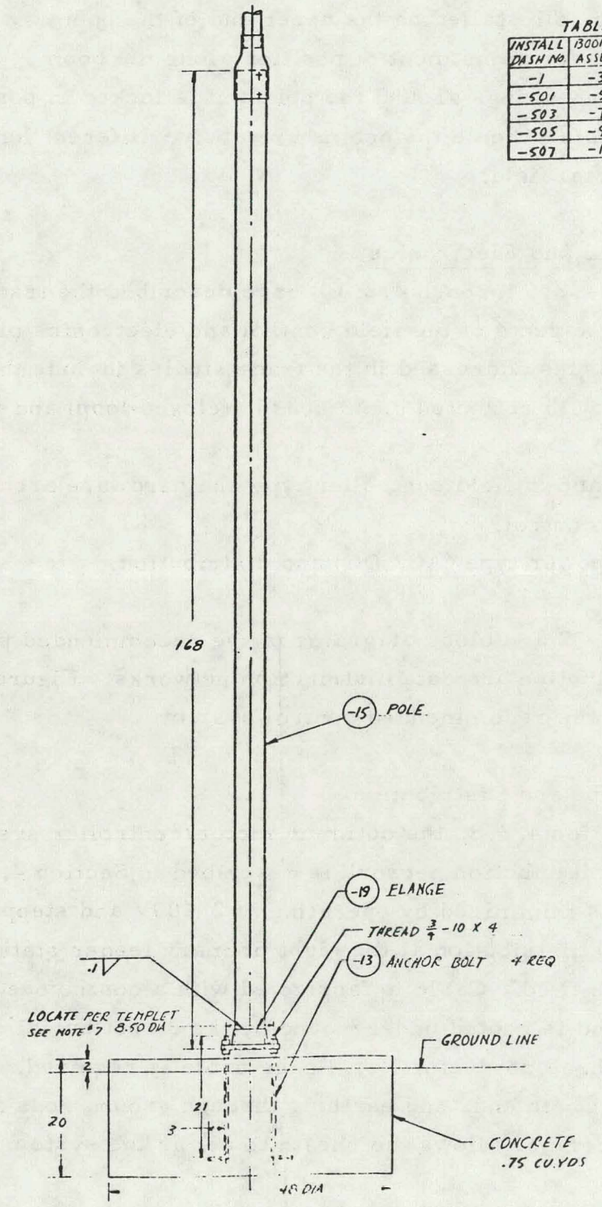

TABLE I

INSTALL DASH NO	BOOM ASSEM	DIM A	TUBE DASH NO
-1	-3	5	-19
-501	-5	30	-21
-503	-7	55	-23
-505	-9	80	-25
-507	-11	105	-27

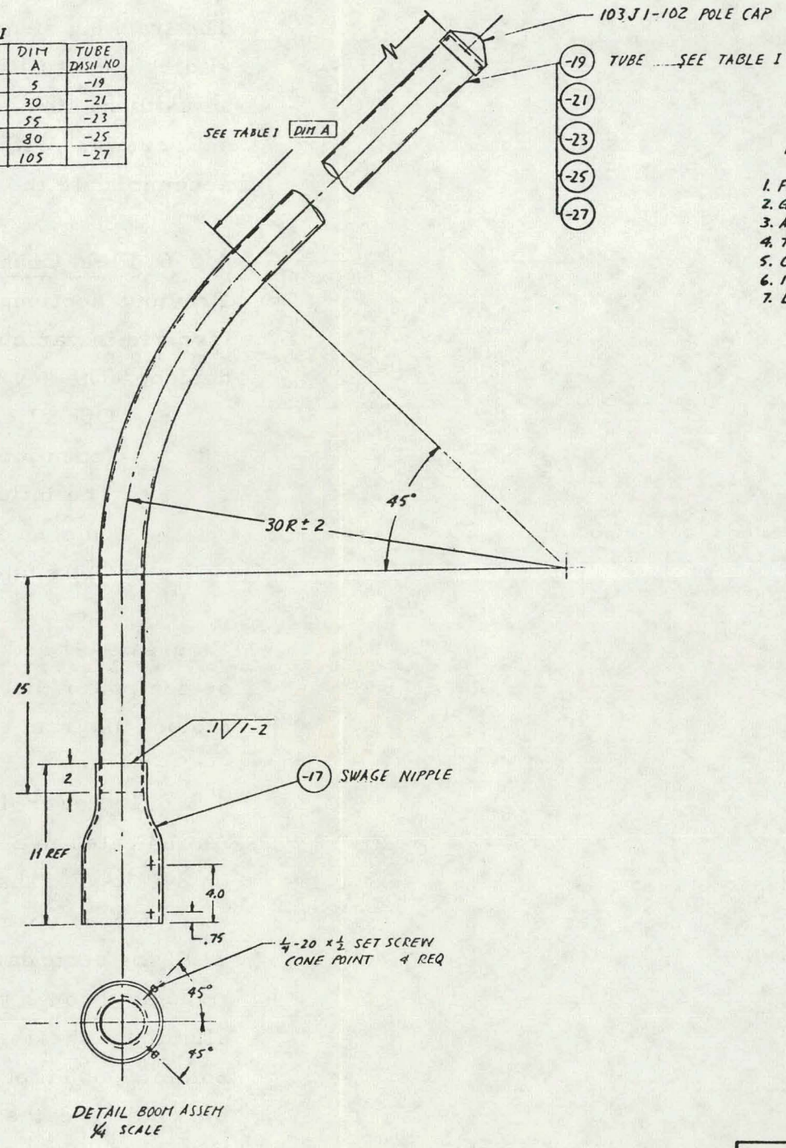

DETAIL BOOM ASSEM
1/4 SCALE

NOTES: UNLESS OTHERWISE SPECIFIED

1. FUSION WELD PER AWS SPEC D1.0-69
2. GRIT BLAST AS REQUIRED FOR PAINT ADHESION
3. APPLY 2 COATS DMS 2104 PRIMER PER DPS 4.50-139 1.9-2.4 MIL THICK
4. TOP COAT PER DPS 4.50-163 WITH DMS 2112-DN 9338 WHITE 1.5-2.0 MIL THICK
5. CONCRETE MINIMUM COMPRESSIVE STRENGTH 2000 P.S.I AFTER 28 DAYS
6. INSTALL POLES VERTICAL WITHIN 1°
7. LOCATE -13 ANCHOR BOLTS WITHIN .060 PER TEMPLET

-507	-505	-503	-501	-1	-11	-9	-7	-5	-3	PART OR IDENTIFYING NO.	NOMENCLATURE OR DESCRIPTION	CODE IDENT NO.	STOCK SIZE	MATERIAL DESCRIPTION	MATERIAL SPECIFICATION	FIND NO.	ZONE
				1		1				-27	TUBE		3" O.D. X .120 WALL X 143.6	LC STL TUBE	ASTM A-513 GRADE 1010		
					1					-25	TUBE		3" O.D. X .120 WALL X 118.6				
						1				-23	TUBE		3" O.D. X .120 WALL X 93.6				
								1		-21	TUBE		3" O.D. X .120 WALL X 68.6				
									1	-19	TUBE		3" O.D. X .120 WALL X 43.6	LC STL TUBE	ASTM A-513 GRADE 1010		
1	1	1	1	1						1031J1-102	POLE CAP		3.0 TO 3.5 D POLE SIZE	MAY BE PURCHASED FROM UNION METAL MFG. CO.			
4	4	4	4	4							SET SCREW		SQ HEAD 1/4-20 X .50	CONE POINT CAD STL	COMM'L		
1	1	1	1	1						-19	FLANGE		5 DIA WELD NECK PIPE FLANGE	FORGED STL ASA 150#	ASTM A-181		
					1	1	1	1	1	-17	SWAGE NIPPLE		5" TO 3" NOM DIA X 10+	ASA STD PIPE SWAGE NIPPLE	LC STL C-1018		1 thru 249
1	1	1	1	1						-15	POLE		5" O.D. X .120 WALL X 168	LC STL TUBE	ASTM A-513 GRADE 1010		
4	4	4	4	4						-13	ANCHOR BOLT		.750 DIA X 24	CARBON STL BAR	ASTM A-36 HR		
1										-11	BOOM ASSEM						
	1									-9	BOOM ASSEM						
		1								-7	BOOM ASSEM						
			1							-5	BOOM ASSEM						
				1						-3	BOOM ASSEM						

LIST OF MATERIALS

QUANTITY REQUIRED PER NOTED ASSY

DASH NUMBERS OF THIS DRAWING: ODD DASH NUMBERS SHOWN; EVEN DASH NUMBERS OPPOSITE

MIL-D-1000A LEVEL 1 DRAWING

FINISH

UNLESS OTHERWISE SPECIFIED
DIMENSIONS ARE IN INCHES.
TOLERANCES
FRACTIONS ± 1/8
DECIMALS ± .10
ANGLES ± 1°

MATL | WT CHK | STR CHK | CHECK | PROJ ENGR | C.S ENGR | QUALITY ENGR | PREP BY

DOUGLAS AIRCRAFT COMPANY, INC SANTA MONICA, CALIFORNIA

INSTALLATION
PILOT PLANT

SEE ENGINEERING RECORDS FOR USAGE DATA

FIRST RELEASE OF PRINTS | DESIGN ACTIVITY APPROVAL

ORIGINAL DATE OF DRAWING 18 APR '67 | CUSTOMER APPROVAL

CODE IDENT NO. 18355 | SIZE D | 1D40057 | SCALE | SHEET 1 OF 1

Figure 4-90. Sensor Pole Installation — Pilot Plant

reducing pipe nipple. The nipple is welded to the boom and clamped to the vertical pole with four set screws to maintain a rigid position.

The tracking sensor is installed on the upper end of the boom by means of a sliding mount fitting for adjustment of position along the boom. For lateral adjustment, the boom swings around the pole and is locked in position by four set screws. With this scheme the booms are of five different lengths to accommodate the total field.

4.3.6 Field Control and Electronics

Previous sections (4.2.6 through 4.2.10) have described the tradeoffs involved in various aspects of the field control and electronics preliminary design. The key issues addressed in the trade studies include the following:

- Operation with reflected beam sensor (closed-loop) and without (open-loop).
- The influence of field controller type and hardware architecture on cost of control.
- Optimum power type (AC, DC) and distribution.

Figures 4-91 and 4-92 are block diagrams of the recommended preliminary design power distribution and data distribution networks. Figure 4-93 is a block diagram of the recommended control system.

4.3.6.1 Power Type and Distribution

As indicated in Section 4.2.8, the optimum motor/controller system operates on 240 VAC. The distribution network is described in Section 4.2.10. Primary feeder cost is minimized by operating at 2,400V and stepping down to 240V for secondary distribution at the eight primary feeder stations distributed through the field. Cable is fabricated with a continuous corrugated aluminum sheath and is routed underground by the direct burial method. Some 39,000m of three conductor No. 4 gage cable is required. Bonding of the cable sheaths at both ends and earthing through ground rods at each heliostat and transformer allows the sheath to act as the system ground plane.

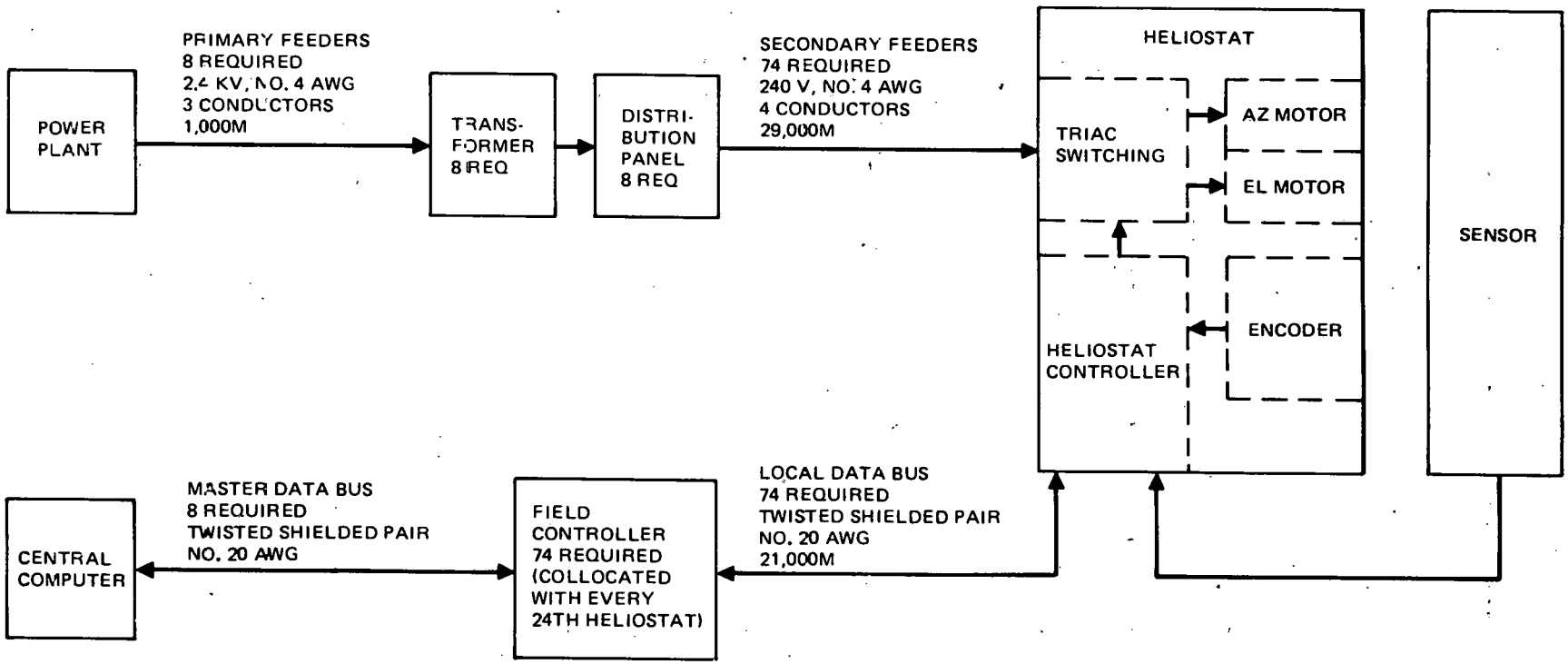

Figure 4-91. Power and Data Distribution — Collector Field Network

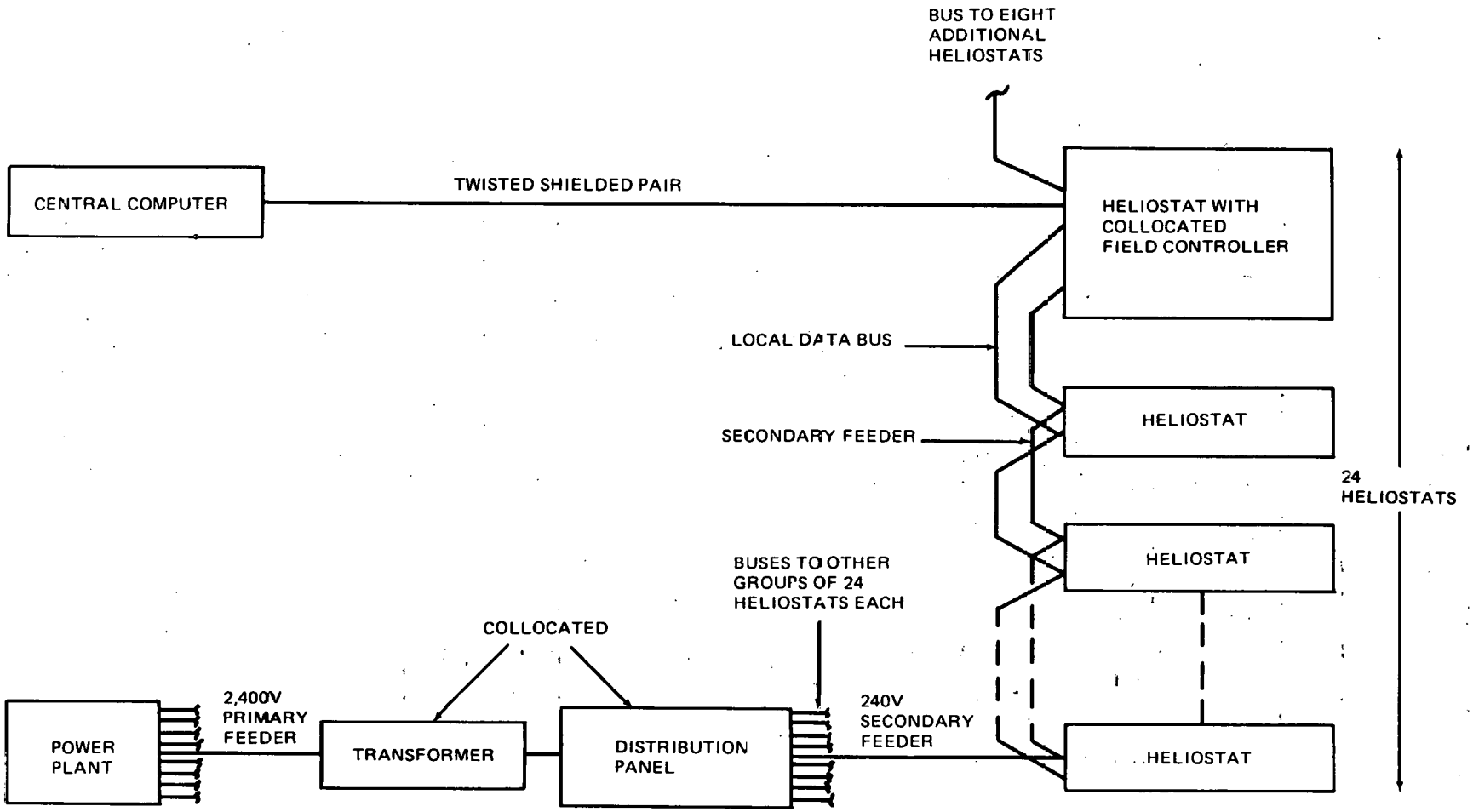

Figu 2. Branch-Collector Field Network

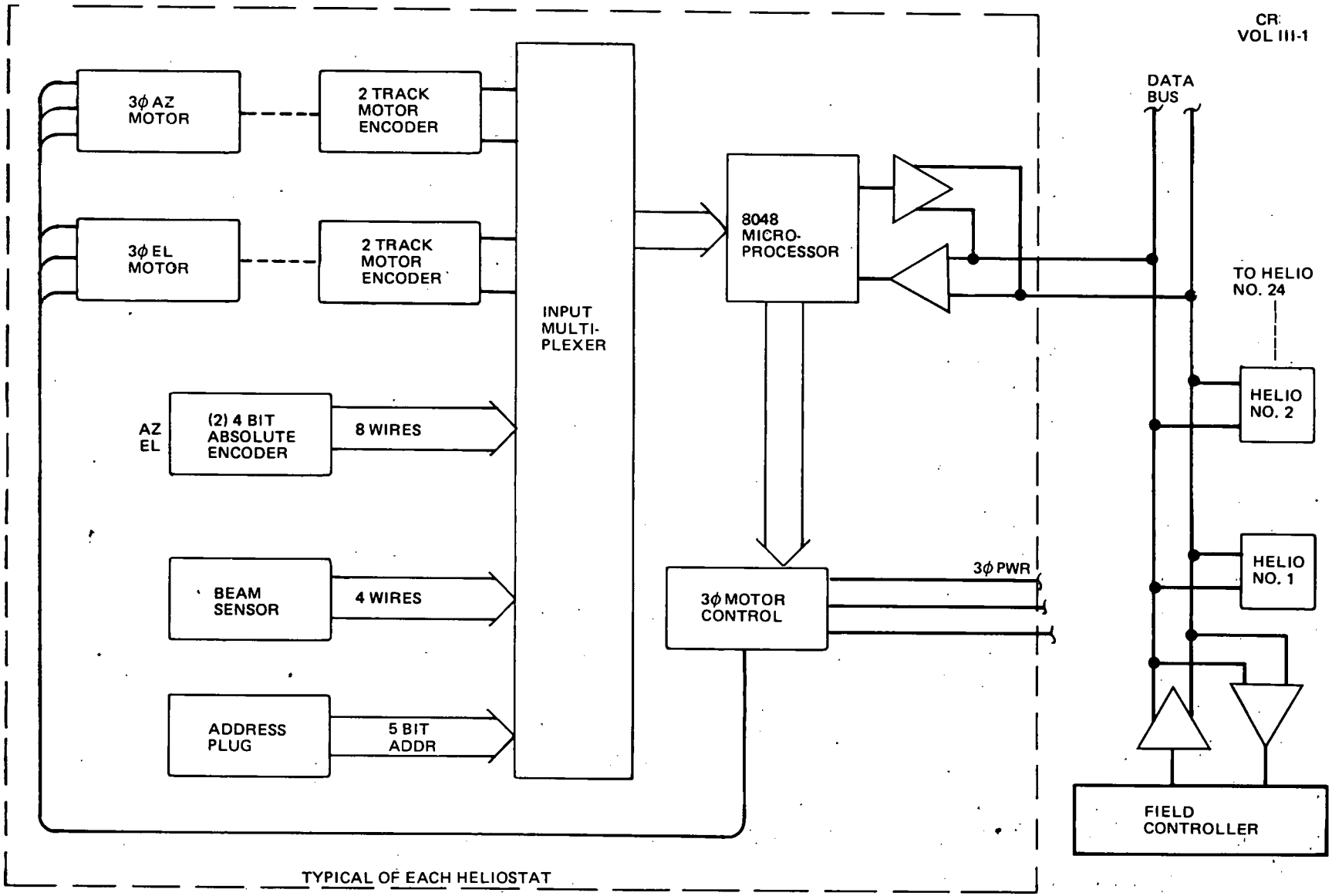

Figure 4-93. Control Electronics Block Diagram – Closed Loop

4.3.6.2 Controller Type and Architectur

Section 4.2.8 discusses analog and digital controllers and concludes digital control is optimum. Sections 4.2.10 and 4.2.8 discuss the influence of the hardware architecture on network cost and conclude that the optimum configuration places some control at each heliostat. A small controller, which communicates with the field controller and with the heliostat control sensors, and also controls the AC motor operation, is located in the pedestal electrical junction box at each heliostat. The field controller communicates with the heliostat controller and the master control and is mainly concerned with coordinate transformation directing the heliostat controller in motor control operation. One pedestal electrical junction box in 24 contains a field controller.

The resulting secondary distribution network with this hardware configuration, as shown in Figure 4-91, is a bus serving a set of heliostats associated with a field controller, resulting in significant savings in cable.

4.3.6.3 Sun Tracking

The recommended preliminary design of the field control and electronics is based on operation with a reflected beam sensor (closed loop) to guide positioning of the reflected solar beam on the receiver. A tradeoff study evaluated the relative merits of closed-loop and open-loop operation. Section 4.2.6 discusses the error sources and predicted performance as it affects cost. A summary chart has been included in this book to indicate the potential engineering trade study cost differences between closed and open loop. While Section 4.2.6 discusses two open-loop implementations, only one, the shaft sensor version, is discussed here because the gimbal sensor version does not cost trade effectively with closed loop. Section 4.2.8 discusses the hardware differences. A summary of these findings is presented in Table 4-35.

Figure 4-94 is the block diagram of the control electronics for the open-loop system. Comparison with Figure 4-91 indicates the main difference in the two systems is removal of the beam sensor. The network for both is identical.

Table 4-35

OPEN/CLOSED-LOOP TRADE SUMMARY

Item	Closed Loop	Open Loop	Comments
Basic Control Accuracy	Better		See Section 4.2.6.
Environmental Effects	Minimal	Wind Problems	Wind is problem in a minimum-cost open-loop system (Section 4.2.6)
Power Loss		Greater	(Section 4.2.6)
Design Costs	Same	Same	
Hardware Cost	Greater		Large potential cost savings for open loop because of less hardware.
Installation Cost	Somewhat Greater		Installation of pole and sensor alignment of closed-loop system is more labor intensive than alignment of open-loop system.
Maintenance	Same	Same	More frequent realignment requirements of open-loop balanced by sensor maintenance of closed loop.
Total Cost	Greater		Primarily due to lower hardware cost of open loop.

4.3.7 Collector Assembly

The heliostat assembly is shown in Figure 4-95. The major components and overall dimensions and clearances are shown. The beam sensor pole is 190 in. from the center of the pedestal and approximately in line with the receiver tower. The beam sensor is installed on the pole and positioned on a line between the center of the receiver and the center of the heliostat within a 2-in. radius to maintain sight of the sun in the tracking mirror as

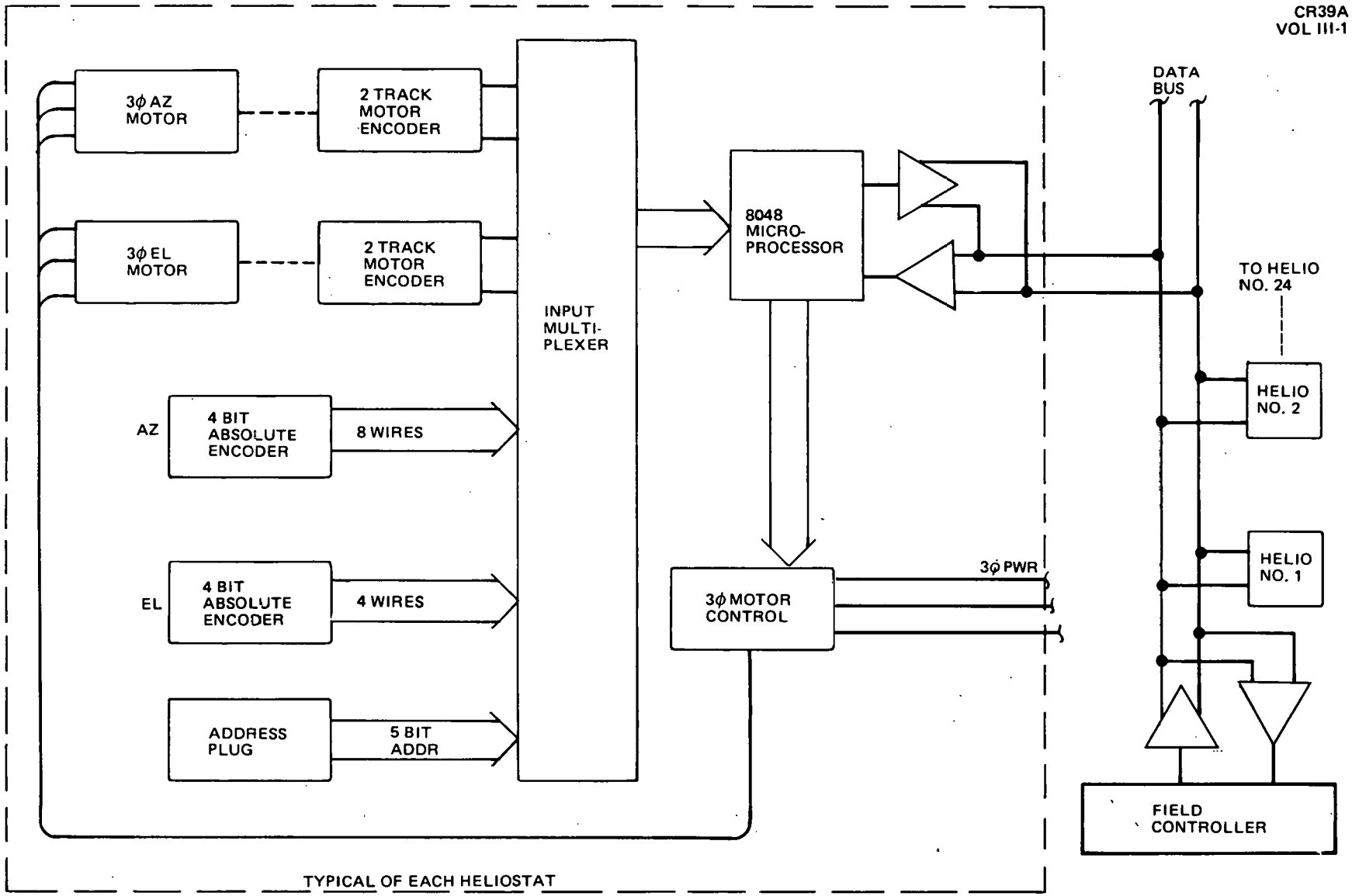

Fi 94. Control Electronics Block Diagram — Open Loop

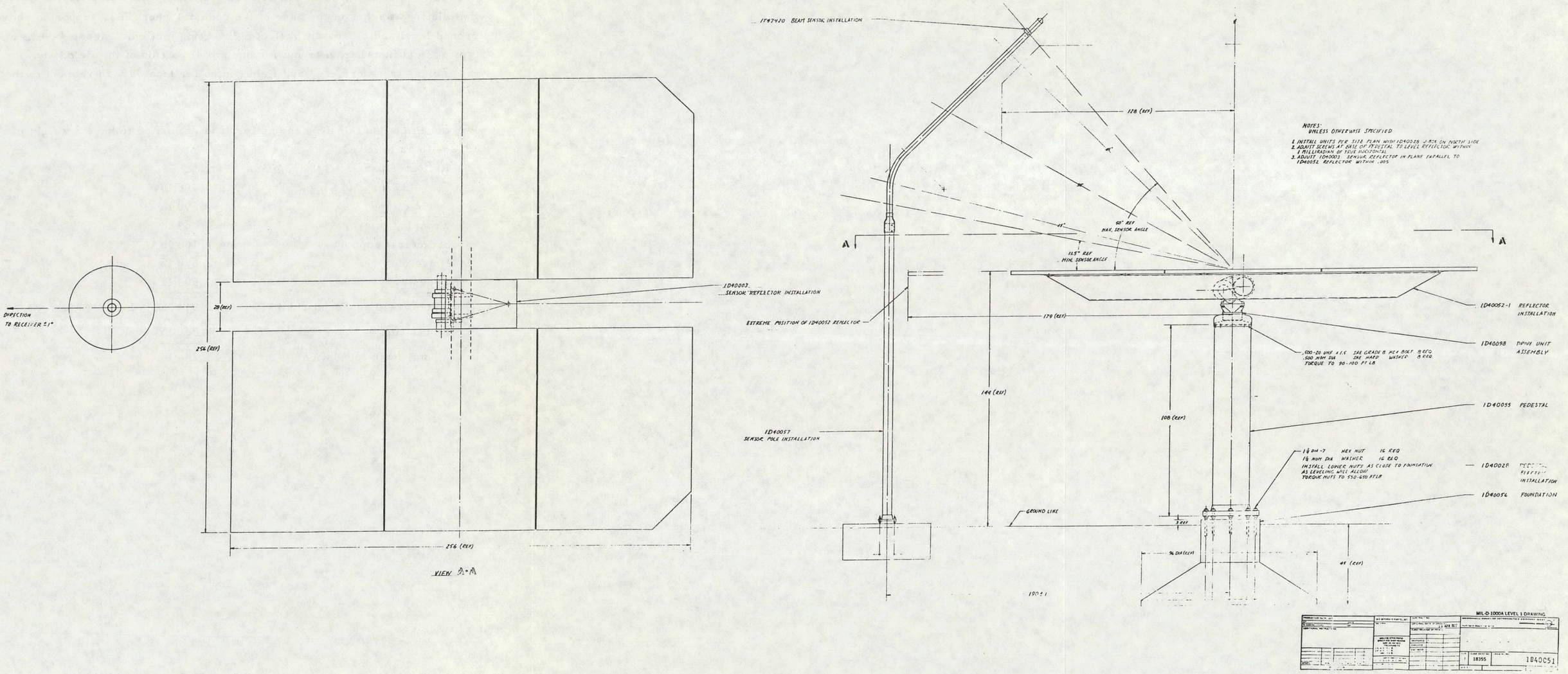

Figure 4-95. Heliostat Assembly — Pilot Plant

the heliostat rotates. The junction box (not shown) for the pedestal electrical installation attaches at the base of the pedestal where it is supported above ground level and clears the reflector inverting motion. Figure 4-96 is a typical field installation layout for one small portion of the field, showing the cables, transformers, and field controller located with respect to the heliostats.

For the Pilot Plant design, the heliostat is estimated to have a weight of 13, 264 lb as follows:

Reflector panels: (1/8 in. glass)	
4 85 in. x 114 in.	798 lb
2 clipped	390 lb
Tracking mirror	39 lb
Structural support	1, 108 lb
Drive unit	670 lb
Pedestal	509 lb
Total (without foundation)	3, 514 lb
Foundation	9, 750 lb
Total (with foundation)	13, 264 lb

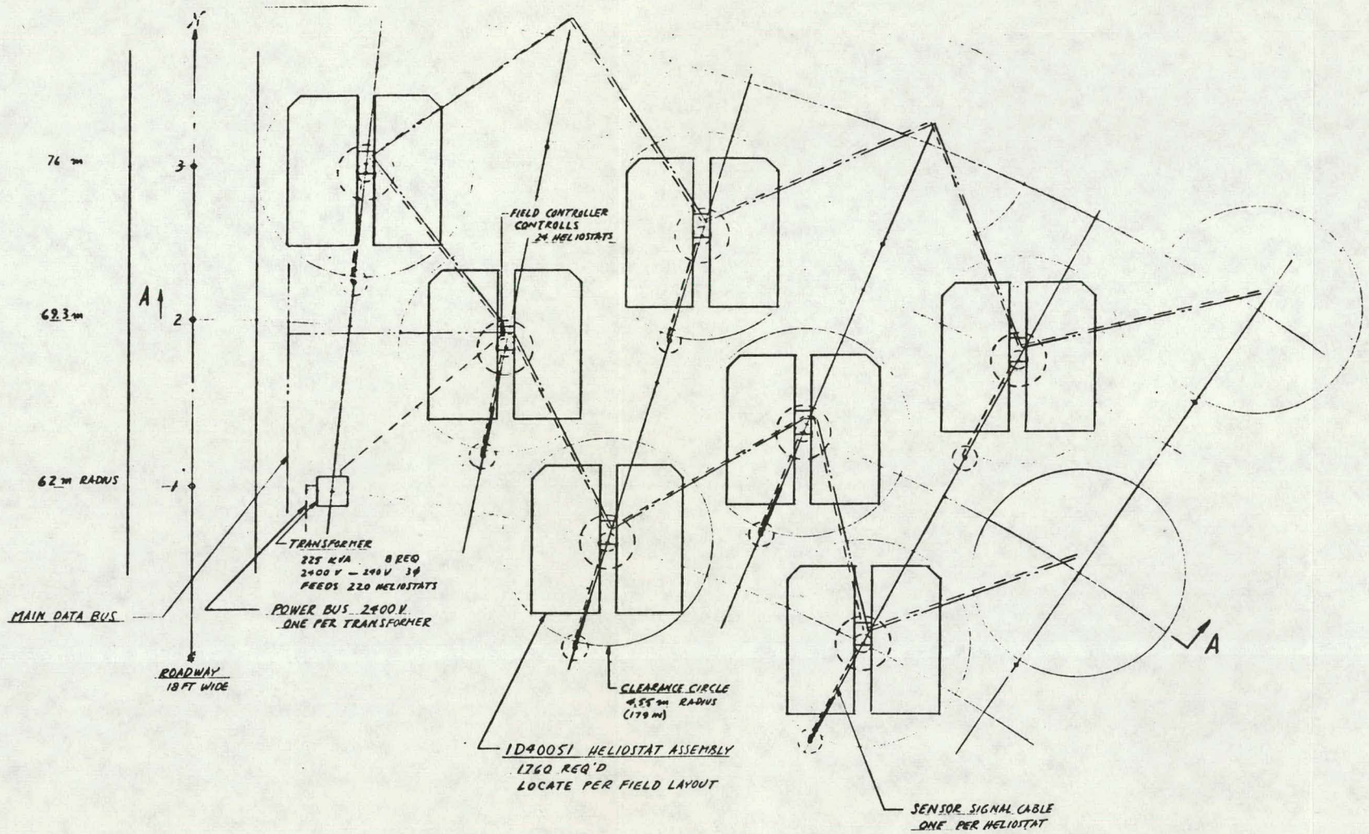

SECTION A-A

MIL-D-1000A LEVEL 1 DRAWING

FINISH	UNLESS OTHERWISE SPECIFIED, DIMENSIONS ARE IN INCHES TOLERANCES 2 PLACE DEC ± 3 PLACE DEC ± ANGLES ±	SEE SEPARATE PARTS LIST	
		CONTRACT NO.	MCDONNELL DOUGLAS ASTRONAUTICS COMPANY HUNTINGTON BEACH, CALIFORNIA MCDONNELL DOUGLAS
		ORIGINAL DATE OF DRAWING 30 APR '977	FIELD INSTALLATION - PILOT PLANT
		FIRST RELEASE OF PRINTS	
ODD DASH NUMBERS SHOWN EVEN DASH NUMBERS OPPOSITE	MATERIAL	PREPARED [illegible]	
		APPROVED	
PART OR IDENT NO.		CHECKED	SIZE D · CODE IDENT NO. 18355 · DRAWING NO. 1D40050
		DESIGN ACTIVITY APPROVAL	
FOR USAGE DATA SEE ENGINEERING RECORDS		CUSTOMER APPROVAL	SCALE [illegible] · SHEET 1 OF

Figure 4-96. Field Installation — Pilot Plant